

ERDC TR-03-4

Engineer Research and
Development Center



**US Army Corps
of Engineers®**
Engineer Research and
Development Center

Condition Assessment of Levees, U.S. Section of the International Boundary and Water Commission

Report 5

Flood Simulation Study of Retamal Levee, Lower Rio Grande Valley, Texas, Using
Seismic and Electrical Geophysical Models

Joseph B. Dunbar, José L. Llopis, George L. Sills, Eric W. Smith,
Rick D. Miller, Julian Ivanov, and Robert F. Corwin

January 2007

Condition Assessment of Levees, U.S. Section of the International Boundary and Water Commission

Report 5

**Flood Simulation Study of Retamal Levee, Lower Rio Grande Valley, Texas, Using Seismic
and Electrical Geophysical Models**

Joseph B. Dunbar, José L. Llopis, George L. Sills, and Eric W. Smith

*Geotechnical and Structures Laboratory
U.S. Army Engineer Research and Development Center
3909 Halls Ferry Road
Vicksburg, MS 39180-6199*

Rick D. Miller and Julian Ivanov

*Kansas Geological Survey
1930 Constant Avenue
Lawrence, KS 66047*

Robert F. Corwin

*SP Surveys
406 Sea View Drive
El Cerrito, CA 94530*

Report 5 of a series

Approved for public release; distribution is unlimited.

Abstract: In November 2004, a team from the U.S. Army Engineer Research and Development Center conducted a ponding test on a reach of the Retamal levee in the Lower Rio Grande Valley to simulate performance of the levee during a flood event. The work was performed for and with the assistance of the International Boundary and Water Commission, U.S. Section, on a levee reach with a significant number of surface cracks. Surface cracking of the levee was caused primarily by drought conditions as they affected expansive clay soils where total annual rainfall, in south Texas, was less than 20 in. (0.5 m) for several years between 1998 and 2003. Geophysical monitoring of the levee provided important information about levee performance during a maximum flood event and measured changes in moisture in clay soils in the levee. Various types of state-of-the-art electrical and seismic methods were appraised to monitor seepage caused by floodwater ponded against the levee. Seismic methods are especially attractive for levee screening, as velocity data from shear and body waves correlate directly to engineering properties that measure shear strength of soils. Seismic data indicated the higher rainfall in 2004 positively affected the core of the levee. Measurable increases in the seismic velocity of both body and shear waves were observed in 2004, compared with conditions in 2003, near the end of the drought period. Velocity values prior to the flood test in 2003 were much lower, likely caused by a levee core that was internally cracked and caused slower P- and S-wave velocities. Shear-wave velocity measured by multi-channel analysis of surface waves increased slightly and was the property most significantly affected by the increased water content, and the material property most sensitive to changes occurring during the levee-ponding experiment. Electrical methods were valuable for monitoring changes in soil moisture and possible seepage through the levee and the foundation. Self-potential surveys indicate that there was no measurable seepage through internal cracks in the levee or the foundation. Instead, electrical resistivity measurements identify a gradual change in soil moisture in the levee from a wetting front. This front increased soil conductivity along the riverside levee crest, but did not extend much beyond the landside crest or mid-slope. Surveys were performed using ground penetrating radar but did not penetrate beyond 1 to 2 m because of the soil conductivity. Results of the field testing of a flood event against the Retamal levee are favorable from an engineering perspective. The levee performed as designed, without any through-seepage or piping.

DISCLAIMER: The contents of this report are not to be used for advertising, publication, or promotional purposes. Citation of trade names does not constitute an official endorsement or approval of the use of such commercial products. All product names and trademarks cited are the property of their respective owners. The findings of this report are not to be construed as an official Department of the Army position unless so designated by other authorized documents.

DESTROY THIS REPORT WHEN NO LONGER NEEDED. DO NOT RETURN IT TO THE ORIGINATOR.

Contents

List of Figures	v
List of Tables.....	vii
Preface.....	viii
Conversion Factors, Non-SI to SI Units of Measure.....	x
Acronyms and Abbreviations.....	xi
Executive Summary	xiii
1—Introduction	1
Background	1
Purpose and Scope.....	1
Study Area.....	3
Approach	3
2—General Setting.....	5
Introduction	5
Floodplain Setting	5
Retamal Levee Construction	5
Borrow Pits and the Soils for Levee Construction	7
Original Land Surface Beneath the Retamal Levee	7
Annual Rainfall Data in the LRGV	7
Monthly Rainfall Data in the LRGV	12
Observations on Levee Desiccation	14
3—Geotechnical Data	15
Floodplain Geology.....	15
Geotechnical Borings	18
Laboratory Soil Testing.....	18
Physical Soil Test Results and Properties	21
Clay Mineralogy.....	23
Chemical Soil Test Results.....	26
4—Geophysical Methods.....	28
Introduction	28

Test Pond.....	29
Introduction	29
Site preparation.....	29
Test duration.....	30
Instrumentation of test pond.....	31
Airborne Conductivity Surveys.....	31
Introduction	31
General theory and equipment.....	33
Retamal levee signatures	33
Focused studies of different conductivity signatures	35
Seismic Methods	35
Introduction	35
Data collection efforts	35
Seismic wave types and properties.....	36
Objectives in levee screening by seismic methods.....	36
Seismic equipment.....	38
Seismic results and levee conditions in December 2003.....	39
Seismic results and levee conditions in November 2004	42
Seismic data summary	44
Self-Potential (SP) Methods.....	47
Introduction	47
Data collection and equipment	48
SP monitoring results	50
Resistivity Methods.....	58
Introduction	58
Data collection and equipment	59
Resistivity results	60
Other Geophysical Methods.....	74
5—Conclusions and Recommendations.....	78
Summary and Conclusions	78
Recommendations	80
References	82
Appendix A: Summary Trip Report on Trench at Retamal Levee.....	A1
Appendix B: ERDC Drilling Logs for Sampling of Levee Test Sites.....	B1
Appendix C: Drash Laboratory Soil Test Results	C1
Appendix D: Pettiet Soil Chemistry Results	D1
Appendix E: Seismic Test on IBWC Levees: Weslaco, TX	E1
Appendix F: Report on SP Surveys.....	F1
Appendix G: Resistivity Time Plots for Levee Crest, Face, and Toe.....	G1
Report Documentation Page	

List of Figures

Figure 1.	Map of general study area along the U.S. and Mexican border showing nearby towns, IBWC floodway levees, and local study area.....	2
Figure 2.	Location of test pond along the upstream end of the Longoria Banco, Number 39, which was cut from Mexico in 1872	4
Figure 3.	View of Retamal levee looking east toward test pond site	6
Figure 4.	View looking west at landside toe of levee	6
Figure 5.	Construction drawing No. 19382 for Retamal levee test pond area showing original ground surface, sources of borrow material, and boring data from the borrow areas	8
Figure 6.	Detailed view of construction drawing 19382, showing Borrow Area 2 location, borings made in the pit, and soil types identified on the boring log	9
Figure 7.	Retamal levee construction photo from October 1973 with view looking west.....	10
Figure 8.	Historic rainfall record for Brownsville, TX, from 1871 to 1999	11
Figure 9.	Annual rainfall for Brownsville, TX, between 1990 and 2004	12
Figure 10.	Regional geologic map of the study area showing abandoned channels and courses, limits of point bar deposits, flood basin deposits, and Beaumont Formation	16
Figure 11.	Geologic cross section across Retamal levee and the Main Floodway	17
Figure 12.	Atterberg Limits for samples from Retamal levee and Main Floodway	24
Figure 13.	Photos of test pond showing (A) preparation of foundation, (B) bladder before being filled with water, (C) filled bladder and the staff gages in empty pond, and (D) pond at full pool	30
Figure 14.	Flood inundation curve for levee test pond study.....	31
Figure 15.	Sketch of pond test site showing position of pond, riverside of levee.....	32
Figure 16.	Relative conductivity map of the the IBWC levees at the 25-kHz frequency in the San Juan East area as determined by airborne survey in 2001.....	34
Figure 17.	Different types of seismic waves used in engineering investigations of the shallow subsurface	37
Figure 18.	Seismic equipment used during investigations of IBWC levees	38
Figure 19.	Refraction tomography solutions for the pond site in December 2003: (a) P-wave, (b) S-wave, and (c) V_p/V_s ratio.....	40

Figure 20.	Rayleigh-wave dispersion curve analysis of phase-velocity versus frequency in units of ft/sec	41
Figure 21.	Phase velocities of levee at 20-Hz vibrator monofrequency, Rayleigh-wave velocity V_R is different for original levee, levee trench backfill, and area of levee core infiltrated by water from ponding test in October 2003	42
Figure 22.	Rayleigh-wave dispersion curve analysis of phase-velocity versus frequency in units of ft/sec for November 2004 data collection at site 2.....	43
Figure 23.	MASW V_s solutions for seven time slices at 12-hr intervals after the start of the test for the south seismic line	45
Figure 24.	V_p solutions for seven time slices estimated at 12-hr intervals after the beginning of the test at the south seismic line	46
Figure 25.	Installation of SP line along landside crest of levee	48
Figure 26.	View of SP line looking upstream (west).....	49
Figure 27.	Data recorders used to measure voltages on each SP line of electrodes.....	49
Figure 28.	SP monitoring data for Line C (upstream face).....	51
Figure 29.	SP monitoring data for Line D (upstream crest).....	52
Figure 30.	SP monitoring data for Line A (downstream crest).....	53
Figure 31.	SP monitoring data for Line B (downstream face).....	54
Figure 32.	SP profile plots with pond empty (before filling).....	55
Figure 33.	SP profile plots with pond full (el 93.7 ft).....	56
Figure 34.	SP difference profile plots (full pond at el 93.7 ft – empty pond)....	57
Figure 35.	A dipole-dipole electrical resistivity profile array.....	59
Figure 36.	Resistivity measurement station behind RV during the flood test.....	61
Figure 37.	Time lapse comparison of resistivity data from the levee crest at the start (time 1) and end (time 9) of flood test	62
Figure 38.	Time lapse comparison of resistivity data from the levee face at the start (time 1) and end (time 9) of flood test	63
Figure 39.	Time lapse comparison of resistivity data from the levee toe at the start (time 1) and end (time 9) of flood test	64
Figure 40.	Cone penetrometer log SJ-15-2 pushed 10 December 2002 at levee center line near pond	65
Figure 41.	Percent change in model resistivity for levee crest	68
Figure 42.	Percent change in model resistivity for levee face	69
Figure 43.	Percent change in model resistivity for levee toe	70
Figure 44.	Time series plots of resistivity at the riverside levee crest	71

Figure 45. Time series plots of resistivity at the landside levee face.....	73
Figure 46. Time series plots of resistivity at the landside levee toe.....	75
Figure 47. GPR record from riverside crest with 50-MHz antenna, view looking south with section extending east to west	77
Figure 48. GPR record from riverside crest with 100-MHz antenna, view looking south with section extending from east to west.....	77

List of Tables

Table 1. Monthly Precipitation Data for Brownsville, TX, Weather Station from January 1975 to December 2004.....	14
Table 2. Engineering Properties of Levee Soils Determined from Laboratory Soil Testing	19
Table 3. Relative Percentage of Clay Minerals in Soil Samples from Borings Identified in Figure 1.....	21
Table 4. Chemical Test Data by Pettiet Soil Testing Laboratory.....	21
Table 5. Comparison of Soil Types by Grain Size Diameter and U.S. Standard Sieve Size	22
Table 6. Atterberg Limits of Selected Clay Minerals and Major Cations.....	25
Table 7. Vp/Vs Ratios from Refraction Tomography Within the 3.6- to 4.5-m Depth Range for Five LRGV Levee Sites Studied in December 2003.	39
Table 8. Resistivities of Common Unconsolidated Sediments	66

Preface

The study reported herein was authorized by the U.S. Section of the International Boundary and Water Commission (USIBWC) under Memorandum of Understanding IBM 01-12 with the U.S. Army Engineer Research and Development Center (ERDC), Vicksburg, MS. This investigation was funded by the USIBWC under Individual Work Order No. 4 in September 2002. Steve Smullen, Engineering Services Division, USIBWC, El Paso, TX, was the technical point of contact for this study. Joseph B. Dunbar, Engineering Geology and Geophysics Branch (EGGB), Geotechnical and Structures Laboratory (GSL), ERDC, Vicksburg, MS, was the technical point of contact at ERDC.

The report of investigation was prepared by Joseph B. Dunbar, José L. Llopis, George L. Sills, and Eric W. Smith of Geosciences and Structures Division (GSD), GSL. Work was performed between September 2003 and August 2005. A trench study at Retamal levee was made by Dunbar and Robert F. Ballard, Soils Engineering and Geophysics, Inc. (SE&G), Clinton, MS, in October 2003 with personnel from the USIBWC. Drilling in support of this investigation was performed in September and December 2003 by Dunbar and personnel from Omega Drilling, San Antonio, TX. Seismic studies were performed by Drs. Rick Miller and Julian Ivanov of the Kansas Geological Survey (KGS) and the University of Kansas and by Ballard of SE&G in December 2003 and November 2004. Laboratory soils testing and analyses were performed by Drash Soil Testing, Pharr, TX; by the Geology Department, University of Southern Mississippi, Hattiesburg, MS; and by Pettiet Soil Testing Laboratory, Leland, MS.

Geophysical fieldwork at the test pond site was performed by EGGB personnel in November 2004 and involved Dunbar, Llopis, and Smith. Individuals providing support to ERDC geophysicists at the test pond were Dr. Robert F. Corwin, SP Surveys, El Cerrito, CA; Ballard, SE&G; and Drs. Miller and Ivanov, KGS. Geophysical data reduction and analysis were performed by Llopis, Smith, and Dunbar, EGGB. Geologic mapping and development of geographic information system layers were performed by Dunbar. Sarah Jackson, EGGB, assisted with data reduction and preparation of various illustrations. Tina Grau, EGGB, provided logistical support to the contractors in this study, as well as project management support.

Special thanks are extended to personnel from the USIBWC Mercedes Project Office for their support during this study and for assisting the ERDC field team. Their support and assistance made the Retamal levee flood test a success.

Work was performed under the supervision of Dr. Lillian D. Wakeley, Chief, EGGB; Dr. Robert L. Hall, Chief, GSD; Dr. William P. Grogan, Deputy Director, GSL; and Dr. David W. Pittman, Director, GSL.

COL Richard B. Jenkins was Commander and Executive Director of ERDC. Dr. James R. Houston was Director.

Conversion Factors, Non-SI to SI Units of Measure

Multiply	By	To Obtain
cubic feet	0.02831685	cubic meters
cubic feet per day	28.32	liters per day
cubic feet per minute	28.32	liters per minute
degrees (angle)	0.01745329	radians
degrees Fahrenheit	(F-32)/1.8	degrees Celsius
feet	0.3048	meters
feet per day	0.0003528	centimeters per second
feet per minute	0.508	centimeters/second
gallons (U.S. liquid)	3.785412 E-03	cubic meters
gallons per day	3.785	liters per day
gallons per day per foot	12.42	liters per day per meter
gallons per minute per foot	12.42	liters per minute per meter
inches	0.0254	meters
miles (U.S. statute)	1,609.347	meters
parts per billion	1.0	micrograms per liter
parts per million	1.0	milligrams per liter
pounds (force)	4.448222	newtons
pounds (force) per square inch	6.894757	kilopascals
square feet	0.09290304	square meters
square feet per day	0.0929	square meters per day
square miles	2.589998 E+06	square meters

Acronyms and Abbreviations

ArcIMS	Arc Internet Mapping Service
ASCII	American Standard Code for Information Interchange
CD	compact disc
CD-ROM	compact disc, read-only memory
cm	centimeter(s)
CPT	cone penetrometer technology
DEM	Digital Elevation Model
DIGHEM	Digital Helicopter Electromagnetic
DOQQ	digital orthophoto quarter quadrangle
DRG	Digital Raster Graphics
EM	electromagnetic
EMI	electromagnetic induction
ERDC	Engineer Research and Development Center
ESRI	Environmental Systems Research Institute
FDEM	frequency-domain electromagnetic
ft	feet
FY	fiscal year
GIS	geographic information system
GPR	ground penetrating radar
GPS	global positioning system
Hz	hertz (unit of electromagnetic frequency)
IBWC	International Boundary and Water Commission
in.	inch
kHz	thousand hertz (unit of electromagnetic frequency)
LIDAR	light detection and ranging
LRGFCP	Lower Rio Grande Flood Control Project
LRGV	Lower Rio Grande Valley
MASW	multi-channel analysis of seismic shear wave data
M	million
m	meter
mSm	millisiemens/meter (measure of conductivity)
MrSID	Multi-resolution Seamless Image database
NAD	North American Datum
OD or O.D.	outside diameter
QA	quality assurance
SARIS	Scintrex Automated Resistivity Imaging System
SCAPS	Site Characterization and Analysis Penetrometer System (cone penetrometer system for measure soil type and electrical properties)

sec	second(s)
SP	spontaneous potential or self-potential
TDEM	time-domain electromagnetic
TIFF	Tagged Image File Format
USCS	Unified Soil Classification System
USGS	United States Geological Survey
UTC	Universal Coordinated Time
XYZ	a three-coordinate data point or file
μm	micron (one millionth of a meter)
V _p	P-wave or primary-wave velocity
V _s	S-wave or shear-wave velocity

Executive Summary

The performance of Retamal levee, Lower Rio Grande Valley, was tested by simulating a flood against the levee using a man-made temporary pond. The levee segment chosen for this test had given anomalous geophysical signatures during airborne surveys, suggesting that the segment was constructed of highly permeable materials. Ground-truthing had proven that the segment was constructed appropriately of clay-rich soil but that the levee was extensively cracked by shrinkage of the soil during an 11-year drought.

The simulated flood test demonstrated not only that the levee segment performed as designed during flood conditions, but also that the cracks effectively “healed” when the water content of levee soils was increased. The simulated flood test was monitored during this study by use of several ground-based geophysical techniques. These techniques also were evaluated for their potential for rapid ground-based assessment of levee condition.

Significant differences were noted in the physical conditions of Retamal levee between October 2003, when a trench was cut for ground-truthing, and November 2004, when the ponding study was completed. In October 2003, surface cracking in some reaches of Retamal were visible and extensive. Results of the airborne electromagnetic conductivity survey data, the trench study, and seismic baseline surveys indicated the Retamal levee contained sections that were internally desiccated, with significant surface cracking. Surface cracks at Retamal levee were observed to be concentrated primarily in areas where soils from borrow pits in abandoned Rio Grande oxbows were used. Besides the link to borrow pits and the geologic environment, surface cracking may result, in part, from the higher fill volumes needed to build across these topographically low areas, or from their softer levee foundations. This condition was caused by regional drought in the Lower Rio Grande Valley (LRGV).

Surface cracking of levee soils (which were expansive clays) was caused primarily by drought conditions in the LRGV, where total annual rainfall was less than 20 in. Drought conditions began in the LRGV in 1998, and ended in the latter part of 2003. Airborne geophysical surveys of LRGV levees, trenching at Retamal levee, and preliminary seismic surveys were performed at the end of this drought cycle. Normal rainfall conditions resumed in late 2003, and continued throughout 2004, with annual rainfall above 25 in. Prior to the levee-ponding study in November 2004, ample rainfall hydrated the clay soils in the levee, and effectively “healed” the surface cracking problem that was visible in late 2003. Annual rainfall below 20 in. in the LRGV is considered problematic for levee soils, especially if drought conditions persist over several years.

Geophysical monitoring of the flood cycle provided important information about levee performance during a maximum flood event. Several state-of-the-art

electrical and seismic methods were appraised. Seismic methods are especially attractive for levee screening, as velocity data from shear and body waves correlate directly to engineering properties that are related to the shear strength of soils. Seismic data indicate the higher rainfall in 2004 improved the structural integrity of the core of the levee by closing desiccation cracks. Measurable increases in the seismic velocity of both body and shear waves were observed in 2004 as compared with 2003 data. Velocity values from 2003 surveys were much lower, likely caused by a levee core that was internally cracked, resulting in slower P- and S-wave velocities.

Results of the seismic data indicate the higher rainfall in 2004 increased the shear strength of the levee soils as determined by MASW (multi-channel analysis of surface waves) analyses of Rayleigh waves. Shear-wave velocity calculated from surface-wave energy using the MASW method was sensitive to changes in soil moisture in the levee. Filling of the test pond caused slight increases in V_s values initially, probably as a result of hydration of the clay levee with a corresponding increase in soil density. The V_s measured by MASW was the property most significantly affected by the increased saturation and the material property most sensitive to changes occurring during the levee-ponding experiment. The property V_p was least sensitive to changes in water height during the ponding experiment.

Results of LRGV studies using seismic methods indicate that use of towable land streamers is more time efficient than installing geophones for rapid seismic assessment. However, better understanding of the near-surface seismic data from the LRGV is required before data acquisition using land streamers is possible in a production-type collection effort. Ultimately, this rapid method of data acquisition will be able to provide cost efficiency in sampling and data processing for the number of levee miles surveyed.

Electrical methods were valuable for monitoring changes in soil moisture and possible seepage through the levee and the foundation during the controlled ponding of water against the levee. An automated self-potential monitoring system, using four lines of detectors, identified no measurable fluid flow through the levee or in the upper foundation. SP data did not indicate significant seepage through the levee or in the foundation through internal cracks. Surface cracks were healed at the beginning of the flood test as described above from ample rainfall prior to the test. Surface cracks that were visible during the previous calendar year were potential pathways for seepage into the levee and into the levee core.

Electrical resistivity measurements identify a gradual change in levee soil moisture during a maximum flood cycle. Resistivity measurements identify a wetting front that caused a decrease in the soil resistivity in the levee nearest the pond face. Resistivity data from the upstream crest line clearly identify an increase in conductivity or a decrease in resistivity with time from increased soil moisture across the levee that is associated with the rise in water height. This change in electrical resistivity extends to the landside midslope, and is observed only at the levee foundation. The decrease in resistivity caused by a wetting front at the base of the levee does not extend into the levee embankment at the midslope or beyond at the levee toe. The wetting front produced an increase in the soil density and levee shear strength as measured by the seismic shear-wave data.

Ground penetrating radar surveys were performed during the flood test, but the method was unable to penetrate beyond 1 to 2 m into the levee because of the conductive nature of the levee soils. Consequently, this survey technique did not identify or resolve any large-scale cracks that might be located in the body of the levee.

1 Introduction

Background

The U.S. Section of the International Boundary and Water Commission (IBWC) and the U.S. Army Engineer Research and Development Center (ERDC) undertook a condition assessment of 270 miles of the Lower Rio Grande Valley (LRGV) levee system in 2001 (Dunbar et al. 2003). Results of this study and field studies to determine the properties of levee soils indicated anomalous conditions for the Retamal levee (Dunbar et al. 2004). An exploratory trench into the Retamal levee (Figure 1) in October 2003 showed a levee that had undergone drying and internal desiccation of soils as a result of 11 years of drought in the LRGV (Dunbar and Ballard 2003; Appendix A). These conditions are consistent with the geophysical signatures that were obtained from earlier airborne surveys.

Results of the trench study prompted the IBWC to perform an experiment that involved building a pond against a 50-ft reach of Retamal levee to simulate flooding, and simultaneously monitor the levee for internal seepage using several geophysical methods over the entire flood cycle. The flood simulation or ponding experiment was designed to replicate a maximum flood event against the levee to determine the behavior of the levee and to determine how flooding affects the properties of the levee soils. The flood-simulation test was performed during the period 8 to 16 November 2004.

Purpose and Scope

This report describes the results of a flood-simulation study conducted against the Retamal levee during the period 8 to 16 November 2004. Major questions addressed by the flood-simulation study concerned the performance and stability of the levee under flood conditions in view of the magnitude of drought-induced cracking over the past 11 years. The reach of levee selected for testing was considered representative of general conditions along Retamal levee. Specific questions to be addressed by the test were these: (a) will the levee hold water as designed, (b) will the flood cause seepage, (c) will the cracks within the body of the levee heal themselves as the clay soils hydrate with the introduction of floodwater, (d) will piping of levee soils occur, and (e) how does water move through the levee during flooding? To answer these questions, geophysical

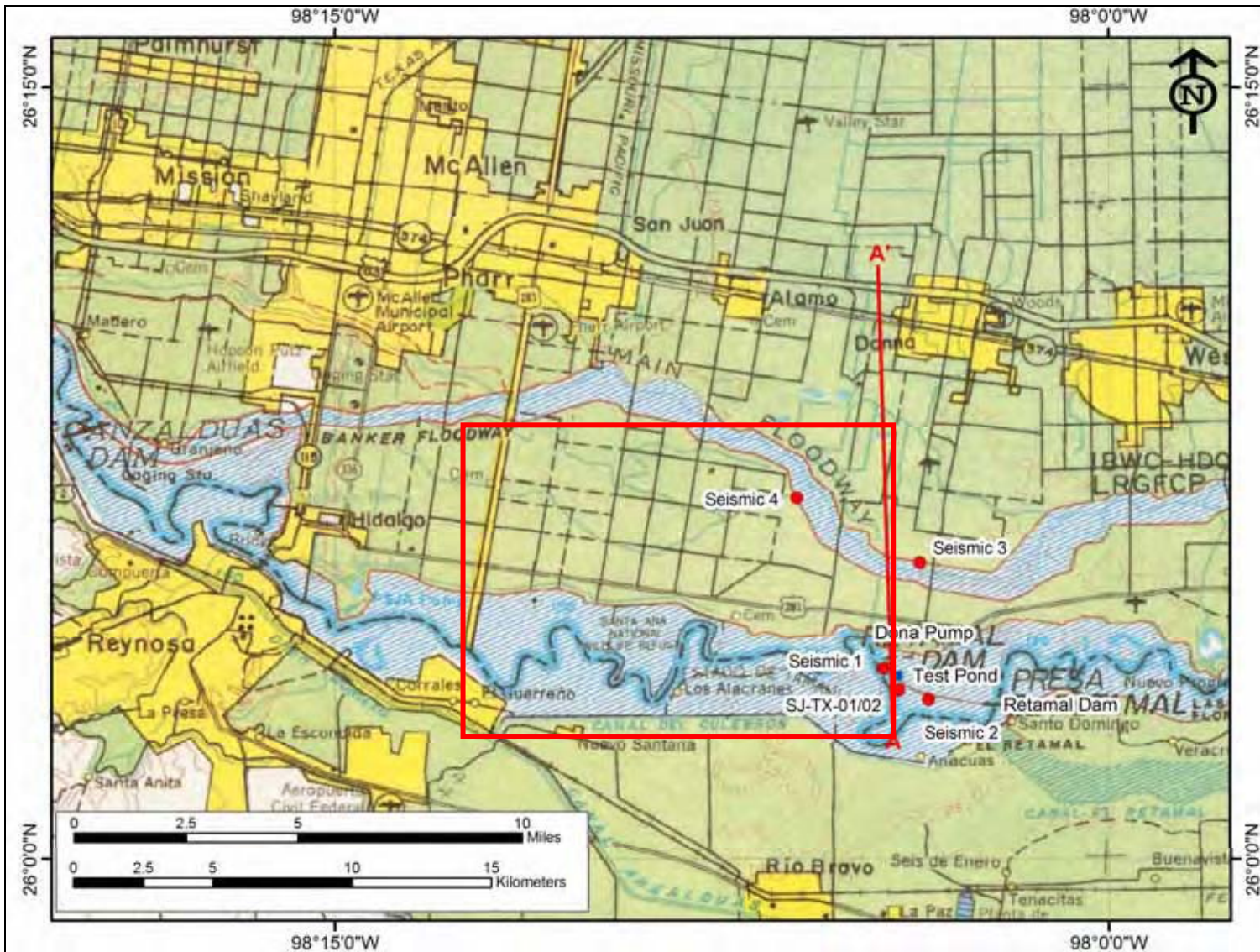


Figure 1. Map of general study area along the U.S. and Mexican border showing nearby towns, IBWC floodway levees, and local study area (red rectangle). Within the local study area are boring locations (red circles) and test pond (blue rectangle). Trench cut into Retamal levee was located at SJ-TX-01 and SJ-TX-02 (see Appendix A for details)

monitoring of a test reach at the Retamal levee was conducted during the rise and fall of a design flood. Raising and lowering of the flood stage was based on a design hydrograph for this event. Activities performed during this study include geological site characterization, various types of geophysical surveys in the study area, reduction and analyses of data, and preparation of a report documenting study methods and findings.

Study Area

The study area is located in Hidalgo County, TX, on the San Juan SE, TX, 7-1/2-min USGS topographic map. Work during this study was performed only on the U.S. side of the Rio Grande, and mainly on the Retamal levee (Figure 1). Retamal levee extends from Dona Pump to Retamal Dam. During this study, stratigraphic and seismic data were collected from five areas: two areas located along the north and south levees of the Main Floodway, and three areas at Retamal levee (Figure 1). Data from the Main Floodway (i.e., Seismic 3 and 4) were obtained for comparison with similar data collected from Retamal levee, which are identified as the Test Pond site, Seismic 1, and Seismic 2.

A trench across the Retamal levee is located at SJ-TX-01/02 (see Figure 1). A trip report describing methods and findings from the trench study across the Retamal levee at this location is presented as Appendix A (Dunbar and Ballard 2003). Locations selected for study in Figure 1 were based on data obtained from airborne geophysical surveys, particularly soils conductivity measurements made from helicopter electromagnetic induction surveys of the levee. These data indicated that the Retamal levee soils were anomalous, as they showed low conductivity signatures for levees constructed mainly of clay (which normally has high conductivity characteristics).

Approach

A primary consideration for locating the test pond was to select a severely desiccated reach, and simulate a design flood against the levee at this location to test the integrity of the levee. Site selection for the test pond was performed by ERDC and IBWC in December 2003 following the results of the trench study. A visual inspection of the Retamal levee was performed, based on the airborne conductivity data, to select possible sites for the test pond. Three locations at Retamal levee were selected as candidates for possible testing. Geotechnical borings were drilled at each location identified in Figure 1 to obtain soil samples for laboratory testing to determine specific engineering properties of the soils, and seismic surveys were performed to characterize the bulk physical properties of the levee at each area. A final site was selected in June 2004, near the location of the trench, and a pond was built by the IBWC in November 2004, approximately 1.5 km (0.96 mile) downstream of Dona Pump (Figure 1 and Figure 2). During the ponding phase of the study, concurrent geophysical monitoring was performed, which involved different types of electrical methods and seismic surveys.



Figure 2. Location of test pond along the upstream end of the Longoria Banco, Number 39, which was cut from Mexico in 1872 (from IBWC survey records and maps of Rio Grande Bancos, 10 March 1910)

2 General Setting

Introduction

General background data about the Retamal levee were collected and evaluated to better understand the characteristics of the levee system, to determine the physical properties of the levee, and to accurately interpret the results of the investigation. Information on the geologic setting of the floodplain, levee construction, surface topography, and climate history was collected and is presented in this section to document the levee conditions prior to and during the time of the airborne geophysical survey, and at the time when the flood-simulation study was conducted.

Floodplain Setting

The test site is located within the Rio Grande floodplain (blue area along river in Figure 1). It is located at the upstream arm of a historic Rio Grande oxbow (i.e., Longoria Banco, No. 39) that was cut from Mexico in 1872 (Figure 2). The levee was built across this oxbow as shown by Figure 2 (center). Land on the riverside of the levee is actively farmed where the old Rio Grande channel once flowed, and which has been subsequently filled with sediment (Figure 2). The oxbow serves as water storage for irrigation and recreation. Retamal dam and levee derive their name from the Ratamal Banco (No. 105), located downstream from Longoria Banco (Figure 2), cut from Mexico in 1919 under the Treaty of 1905. Throughout historic time, the Rio Grande has actively migrated across this part of its floodplain. Retamal levee is located in point bar deposits that are intersected by numerous abandoned Rio Grande channels.

Retamal Levee Construction

Retamal levee is approximately 4.3 m (14 ft) tall at the test pond site. Levee slopes are defined by the ratio of one vertical to three horizontal (1V:3H), pictured in Figure 3 and Figure 4. Retamal levee and dam were constructed in 1973 to 1974, after Hurricane Beulah struck the south Texas coast in September 1967. Retamal levee and dam were constructed to divert 40 percent of a design flood into the Mexican Floodway, and limit the discharge of a design flood to only 20 percent into the Rio Grande channel below the dam. Banker and



Figure 3. View of Retamal levee looking east toward test pond site (approximate location of semi-truck)



Figure 4. View looking west at landside toe of levee. Location corresponds to test pond site. Levee is approximately 4.3 m (14 ft) tall at this location

Main Floodways on the U.S. side are regulated by Anzalduas Dam (see Figure 1 for location), and remove 40 percent of a design flood from the Rio Grande and discharge this volume into the Gulf via the Arroyo Colorado and North Floodway. No floodwaters have been held against the surface of Retamal levee since its construction in the 1970s.

Borrow Pits and the Soils for Levee Construction

Soils to build the levee were derived from nearby borrow pits as shown by IBWC construction drawings no. 19381 through 19386 (Figure 5 and Figure 6). Old Rio Grande oxbows and natural levees along the right-of-way were a primary source for borrow material to build the levees. The reach of levee at the test pond site was built from soils obtained from Borrow Areas 2 and 3 (Figure 6), which is within the Longoria Banco. Construction drawings Nos. 19381 through 19386 identify the locations of the different borrow pits used to build the levee along its right-of-way, and identify soil types from shallow borings made in the pits. According to construction drawing no. 19382, the levee at the test pond reach was built mainly of CH soils (Unified Soils Classification System, USCS). A construction photograph is presented as Figure 7.

Original Land Surface Beneath the Retamal Levee

In addition to showing the borrow pit locations and soil types, the drawing in Figure 5 identifies the original land surface topography, and the height that the levee was raised over the abandoned channel. The abandoned channel was filled nearly 21.5 ft, from elevation (el) 75.0 at the lowest point in the old channel along the levee center line, to about el 96.5 ft at its design height. The old channel was approximately 10 to 12 ft lower in elevation than the surrounding land surface. The width of the old channel from the profile data shown in Figure 5 was approximately 400 ft.

Annual Rainfall Data in the LRGV

Drought conditions were reported by IBWC during the 11 years preceding 2004 for the LRGV to account for the severe cracking and desiccation of their levees. Rainfall records are presented over the long and short term in Figure 8 and Figure 9 for the Brownsville area, a location that is representative of the LRGV, and which contains long-term historic rainfall data. Figure 8 presents a 128-year record, dating back to 1871 (from the National Oceanic and Atmospheric Administration (NOAA), National Weather Service Forecast Office (NWS), 2005; see <http://www.srh.noaa.gov/bro/>). Figure 9 presents a 14-year record beginning with 1990. Historically, the average annual rainfall for the Brownsville area has been 26.71 in./year.

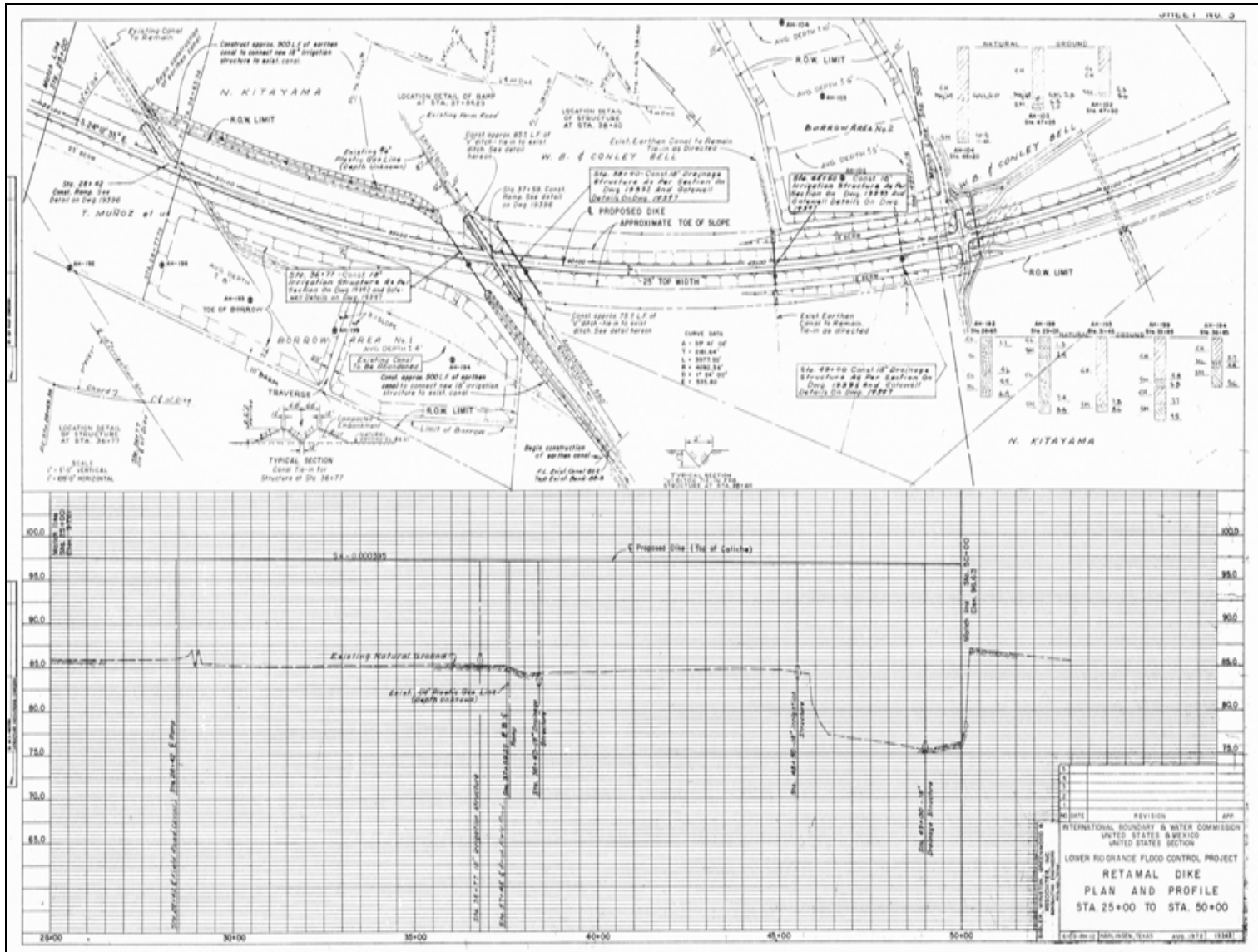


Figure 5. Construction drawing No. 19382 for Retamal levee test pond area showing original ground surface, sources of borrow material, and boring data from the borrow areas. Test pond site is located at approximately station 47+00, at midpoint of levee intersection with Borrow Area 2 (or Longoria Banco, No. 39)

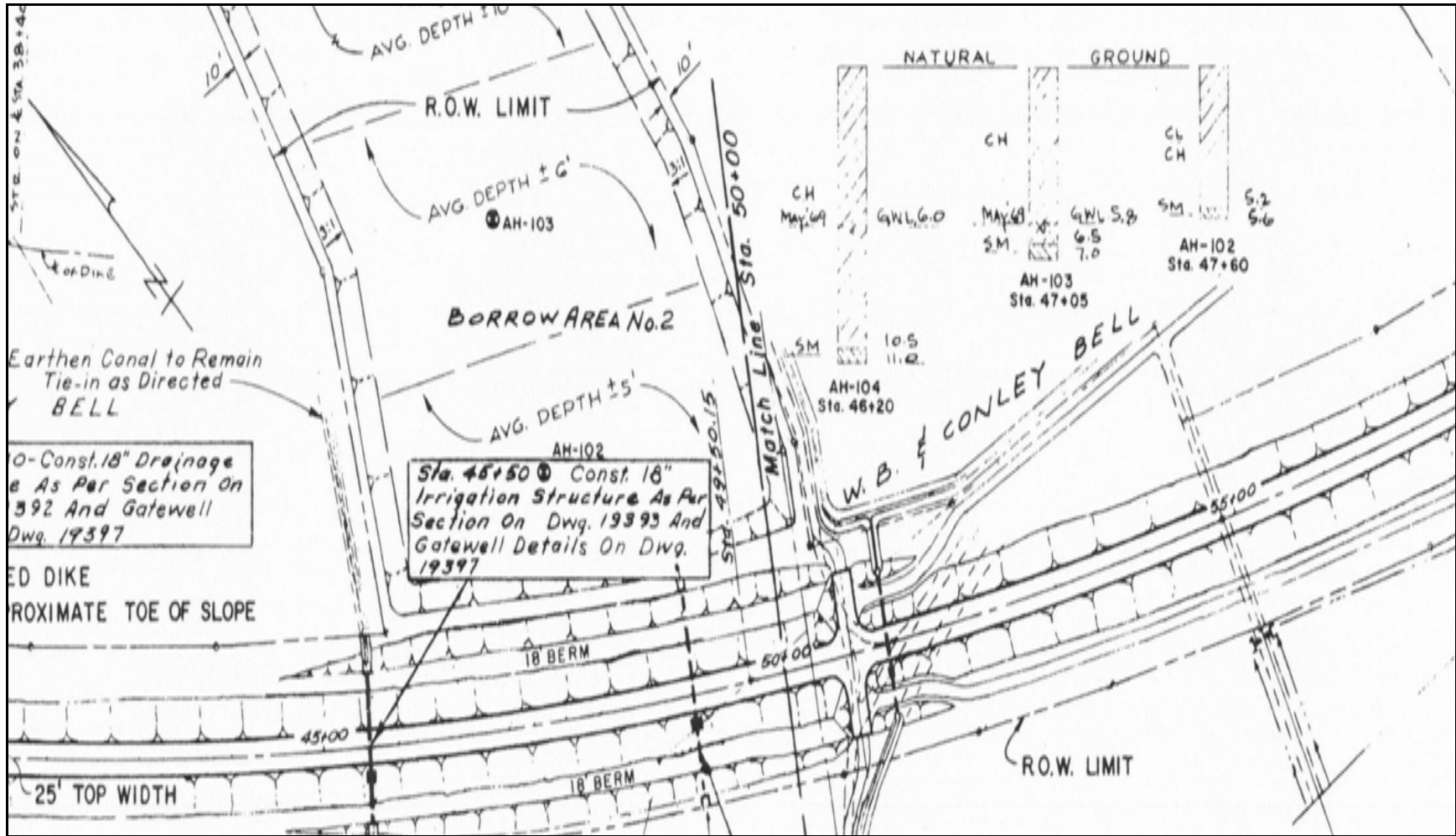


Figure 6. Detailed view of construction drawing 19382, showing Borrow Area 2 location, borings made in the pit, and soil types identified on the boring log



Figure 7. Retamal levee construction photo from October 1973 with view looking west

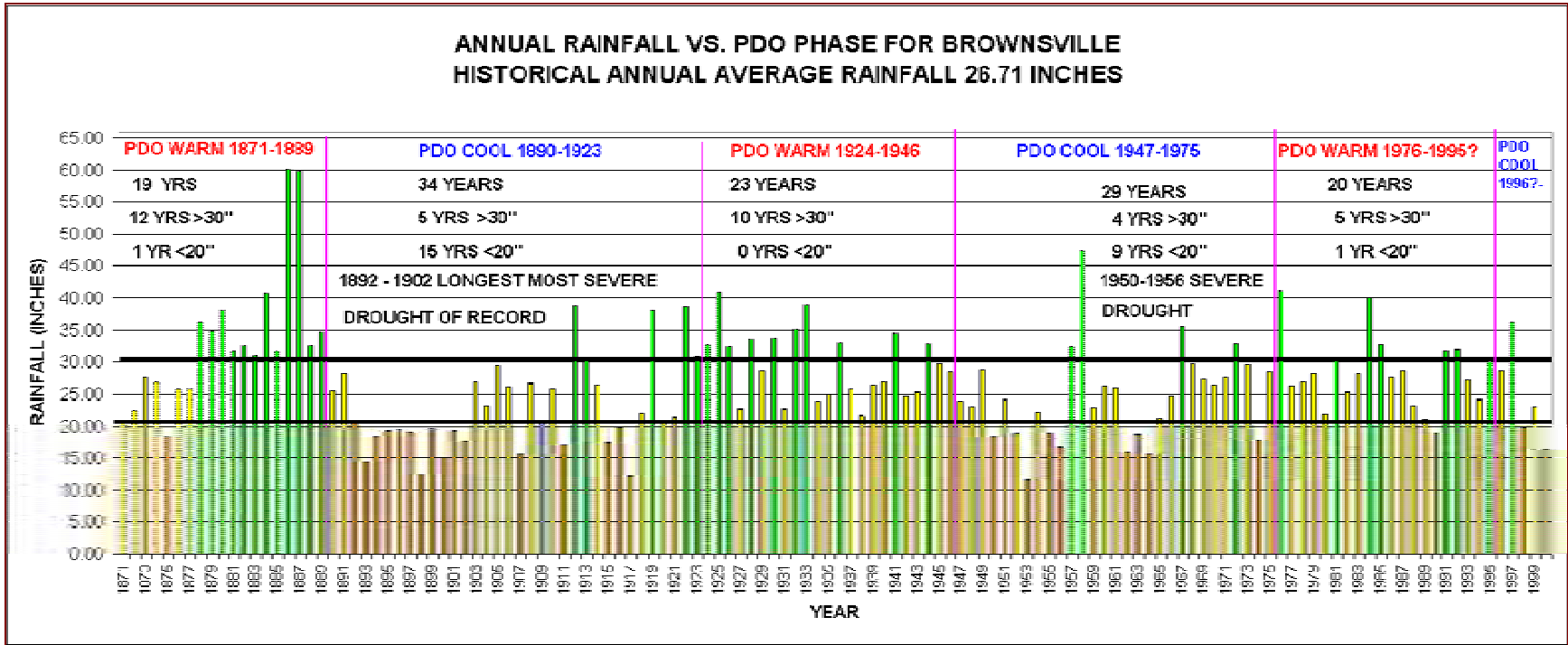


Figure 8. Historic rainfall record for Brownsville, TX, from 1871 to 1999 (from http://www.srh.noaa.gov/bro/brolcd_locked.htm)

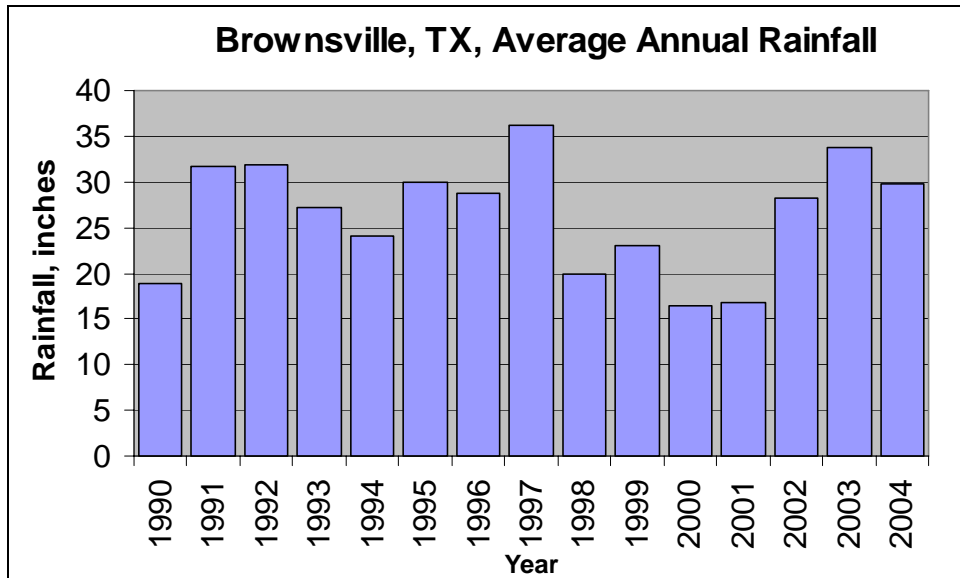


Figure 9. Annual rainfall (in inches) for Brownsville, TX, between 1990 and 2004. PDO cool cycle that began in 1996 (see Figure 8) contains 3 years with rainfall below 20 in., and 1 year below 25 in. (data from NOAA, NWS 2005)

Examination of the 128-year annual rainfall record in Figure 8 identifies variable annual rainfall during historic times and a possible new climate trend, caused by the warm and cool phases associated with the Pacific Decadal Oscillation (PDO). The PDO is a recently discovered, decades-long (i.e., 20- to 30-year length) oscillation in surface water temperatures in the Pacific Ocean. Results of the multidecade-long fluctuation in surface water temperature cause impacts to climate over the continents (Hagan 2005). It has been suggested by climatologists that the PDO in the Brownsville area is shifting toward the cool phase, which results in overall warmer winter temperatures and a corresponding increase in drought for the southwestern United States. Since 1871, there have been 27 years during which the total yearly rainfall was less than 20 in., and 24 of those years occurred when the PDO was in the cold phase (Hagan 2005).

As shown by Figure 9, rainfall data after 1996 contain 3 years that were below 20 in. (i.e., 1998, 2000, and 2001), 1 year was between 20 and 25 in. (in 1999), and the remaining years were above 25 in. In summary, during the cool phase of the PDO, rainfall has been 20 percent less than during the warm phase, with an average annual rainfall at Brownsville during the cold phase at 24.07 in., and 29.79 in. during the warm phase (Hagan 2005).

Monthly Rainfall Data in the LRGV

Airborne geophysical surveys to support the condition assessment of IBWC levees in the LRGV were flown in late June and early July 2001, which corresponds to a dry year in Figure 9. Additionally, the survey was flown at the end of a 4-year period with lower than average rainfall. Low conductivity signatures

were generally associated with the recently constructed (early 1970s) Retamal levee reach. This reach includes levees constructed of clay soils that were cracked and desiccated, according to ground-truth borings and trenching conducted in late 2003. This physical condition of the levees is likely responsible for the low conductivity signatures associated with the airborne survey of the Retamal reach. Trenching across Retamal levee was performed in October 2003, during a wet year (see Figure 9), and it was observed that surface cracking was severe and had extended into the body of the levee (see Appendix A for information). However, during the construction of the pond, and during the test of levee performance in November 2004, it was observed that surface cracking was less severe than had been reported in 2003.

Monthly rainfall data from the LRGV were examined to help resolve the difference in apparent soil moisture conditions, and the impact to the levee. Specifically, cracked conditions were noted for Retamal levee during the airborne survey and during the trench study (Appendix A). However, surface cracking was generally absent during the flood-simulation study. Monthly rainfall totals for the Brownsville area are presented in Table 1 for the past 29 years. Monthly rainfall in 2004 was generally evenly distributed, compared with the preceding years. It is concluded, based on data presented in Table 1, that abundant rainfall in 2004 had hydrated the levee soils to heal the surface cracks that were present in October 2003. During 2004, rainfall amounts were above the 134-year average for 5 months (i.e., Jan, Mar, Apr, May, Jun), 2 months were almost the same (i.e., Nov, Dec), and 5 months were slightly below (i.e., Feb, Jul, Aug, Sep, Oct).

Information presented in Table 1 suggests that the soil hydration process for the surface cracks (as well as the body of the levee) was not rapid, but may have taken place over several months. It is noteworthy that, 1 month prior to the trench being cut at Retamal levee in October 2003, Brownsville recorded 15.13 in. of rainfall for the month of September 2003, almost 10 in. above the 134-year average for this month (Table 1). Two major rainfall events occurred in September 2003 during two separate 24-hr periods: 3.60 in. on 14 September 2003 and 5.24 in. on 19 September 2003. The trench was cut less than 3 weeks after the second major rainfall event. The trench was cut on 7 October 2003, and still contained some surface and internal cracking. However, it was observed during the trenching study that the upper 30 cm (~1 ft) of the levee was not as severely cracked as the body of the levee.

Table 1 indicates that rainfall was above the average after June 2003, and generally continued to the time of the flood test in November 2004, especially during the winter months of 2004. In contrast, between January 1996 and June 2003, there were 66 months during which rainfall was below the average monthly rainfall amount. During this period, there were only 25 months that were above the average. As shown by Table 1 and Figure 9, the time period between 1998 through June 2003 was an extremely dry interval with low monthly rainfall totals recorded.

**Table 1
Monthly Precipitation Data for Brownsville, TX, Weather Station from January 1975 to December 2004**

Precipitation (in.) 2004 Brownsville, TX (BRO)													
Year	Jan	Feb	Mar	Apr	May	Jun	Jul	Aug	Sep	Oct	Nov	Dec	Annual
1975	0.60	0.09	0.01	0.01	2.22	2.19	4.78	9.56	4.77	0.51	1.66	2.17	28.57
1976	0.48	0.03	1.28	5.71	4.95	0.80	9.43	3.35	2.85	8.45	2.49	1.32	41.14
1977	1.24	1.37	0.12	6.62	0.76	4.72	0.27	1.27	2.84	2.87	4.07	0.14	26.30
1978	1.94	1.29	0.01	2.39	T	2.25	0.39	3.20	8.28	4.45	0.82	1.86	26.88
1979	1.43	1.10	0.14	3.91	0.59	1.52	2.10	5.25	8.84	1.18	0.12	2.04	28.22
1980	1.05	1.74	0.28	0.01	1.78	0.02	1.46	7.29	1.48	2.26	2.50	1.90	21.77
1981	1.79	0.76	3.47	0.34	5.88	2.29	2.65	4.47	5.05	2.47	0.33	0.75	30.25
1982	0.04	0.75	0.19	4.08	9.12	0.18	T	1.04	2.42	1.63	3.11	2.70	25.26
1983	1.10	2.62	0.61	T	1.41	1.78	6.11	2.34	8.61	2.53	0.52	0.48	28.11
1984	4.79	0.42	0.13	T	6.18	2.44	1.59	1.80	20.18	0.93	0.02	1.85	40.33
1985	1.49	0.54	0.40	1.91	4.21	6.47	4.18	2.10	6.04	4.04	1.02	0.42	32.82
1986	1.07	0.21	T	0.87	2.89	3.72	0.35	2.14	1.71	4.61	7.69	2.42	27.68
1987	2.46	2.26	0.58	1.39	1.52	4.78	1.64	0.73	4.70	4.44	3.83	0.42	28.75
1988	3.97	1.53	1.42	T	0.25	2.86	1.00	2.56	7.48	1.80	0.14	0.07	23.08
1989	1.94	0.08	0.17	3.83	1.23	2.35	2.13	1.25	2.46	3.06	0.93	1.73	21.16
1990	0.58	0.56	0.81	1.55	2.72	1.08	1.53	2.87	3.90	2.29	0.91	0.05	18.85
1991	0.47	2.50	0.02	10.35	2.97	1.93	2.26	0.89	5.57	3.33	0.15	1.18	31.72
1992	3.50	1.99	0.12	4.15	5.55	1.50	0.40	3.71	3.62	0.85	5.61	0.85	31.85
1993	1.79	2.86	1.68	0.34	3.64	6.72	T	0.04	1.93	4.69	1.25	2.29	27.23
1994	2.01	0.44	1.84	0.71	1.25	3.32	0.15	3.39	4.09	3.91	1.42	1.59	24.12
1995	0.64	0.57	0.64	0.13	0.17	5.82	0.07	8.25	2.12	8.82	1.83	0.98	30.04
1996	0.06	0.15	T	0.50	0.08	0.01	0.65	5.77	8.57	11.49	0.66	0.77	28.71
1997	0.61	0.42	5.94	4.78	2.06	1.47	T	1.80	4.77	13.03	0.87	0.46	36.21
1998	0.37	1.72	0.62	0.04	T	0.30	T	1.36	7.82	3.59	3.72	0.29	19.82
1999	0.26	1.49	3.01	0.14	3.59	2.30	1.86	2.61	3.99	0.69	2.77	0.32	23.03
2000	0.85	0.19	2.89	0.39	1.87	0.85	0.28	4.29	0.66	2.71	0.41	1.10	16.49
2001	0.48	1.43	0.36	1.10	0.49	2.21	1.81	1.80	3.25	0.36	2.42	1.02	16.73
2002	0.09	0.98	0.22	0.64	1.96	1.88	0.84	1.87	6.04	8.31	4.22	1.24	28.29
2003	0.69	0.55	0.56	0.41	0.19	3.24	2.58	2.74	15.13	6.90	0.44	0.31	33.74
2004	1.84	0.79	3.63	2.85	5.37	3.19	0.38	2.35	4.05	1.98	1.82	1.46	29.71
POR= 134 yr	1.37	1.29	1.07	1.53	2.56	2.73	1.76	2.65	5.54	3.40	1.80	1.47	27.17

WBAN : 12919

Observations on Levee Desiccation

Historic rainfall data examined in this study indicate that, prior to the test pond experiment in November 2004, the LRGV area had experienced severe drought conditions, especially during the period between 1996 and the end of 2003. A primary consideration for locating sites for seismic testing, as well as the selection of the test pond area in December 2003, was to select a severely desiccated reach to test. Surface cracks were confined primarily to the reach of Retamal levee that had been constructed of soils obtained from the borrow pits that were located within abandoned Rio Grande oxbows. Levees built of natural-levee soils, such as the reach of levee built from Borrow Area 1, were generally not as severely cracked. It is likely that higher plasticity soils, differences in clay mineralogy between natural-levee soils and those obtained from Rio Grande Oxbows, and/or perhaps increased thickness of fill across deep oxbow reaches may have contributed to the increase in desiccation, compared with other reaches along the Retamal levee. Engineering properties of the levee soils are examined in the next section to address these questions and better understand the levee desiccation observed in some areas and not others.

3 Geotechnical Data

Floodplain Geology

A basic summary of the floodplain geology is important for evaluating the engineering properties of the levee soils and for understanding the reasons for selecting locations for geotechnical borings. A geologic map and cross section is presented in Figure 10 and Figure 11. The cross section extends across the Rio Grande floodplain, from Retamal levee and northward to Dona, TX (see Figure 1 and Figure 10 for section location). This geologic section extends across the Main Floodway. The river's floodplain contains Holocene-age deposits (less than 10,000 years) and deposits of Pleistocene age (between 10,000 and 2 million years old) formed by the Rio Grande. Retamal levee is located upon point bar deposits, while the Main Floodway is located on flood basin deposits. Bordering the floodplain to the north at Dona are terrace deposits, which represent an older floodplain surface that occurs at a higher elevation than the present floodplain.

Point bar deposits are formed by the migration of the river across its floodplain. LRGV boring data in the San Juan East area identify typical point bar deposits as containing a fine-grained (silt and clay) top-stratum, between 5 and 10 ft thick, and a much thicker, coarse-grained (fine to coarse sand and gravel) substratum that extends to the depth of the river that formed these deposits (Dunbar et al. 2003). Substratum deposits generally become finer grained upward, because of the decrease in capacity of the river to transport larger grain sizes in the channel. The cross section in Figure 11 shows the difference in thickness between the top stratum and the thicker substratum based on available boring data. Additionally, the section shows the difference in top stratum thickness between point bar and flood basin deposits. Flood basin deposits in Figure 10 are significantly thicker than point bar deposits.

Flood basin deposits accumulate in low areas that border the river, and receive fine-grained (clay) sediments during major flood events, when the river overtops its banks and carries these sediments to the distal portions of its floodplain. Present within the floodplain are abandoned channels and courses of the Rio Grande that were cut from the main channel by river migration or by human activity (Figure 10). Natural-levee deposits occupy that portion of the floodplain that is adjacent to the main channel, and form as a consequence of overbank deposition during floods. These deposits form prominent banks near the edge of

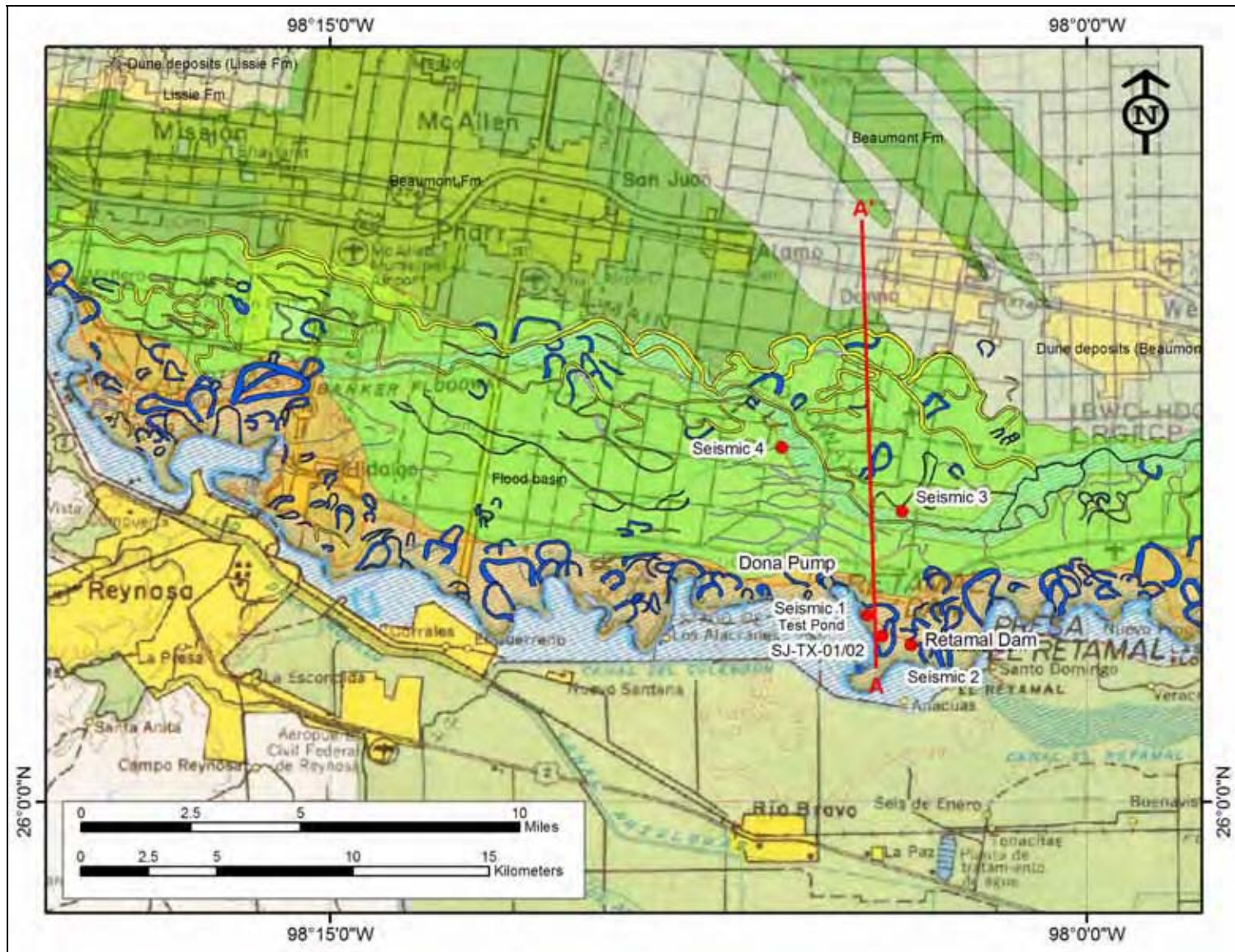


Figure 10. Regional geologic map of the study area showing abandoned channels and courses, limits of point bar deposits (orange), flood basin deposits (light green), and Beaumont Formation (dark green). Dunes deposits (grey) are present in northern part of area covering the Beaumont and Lizzie Formations

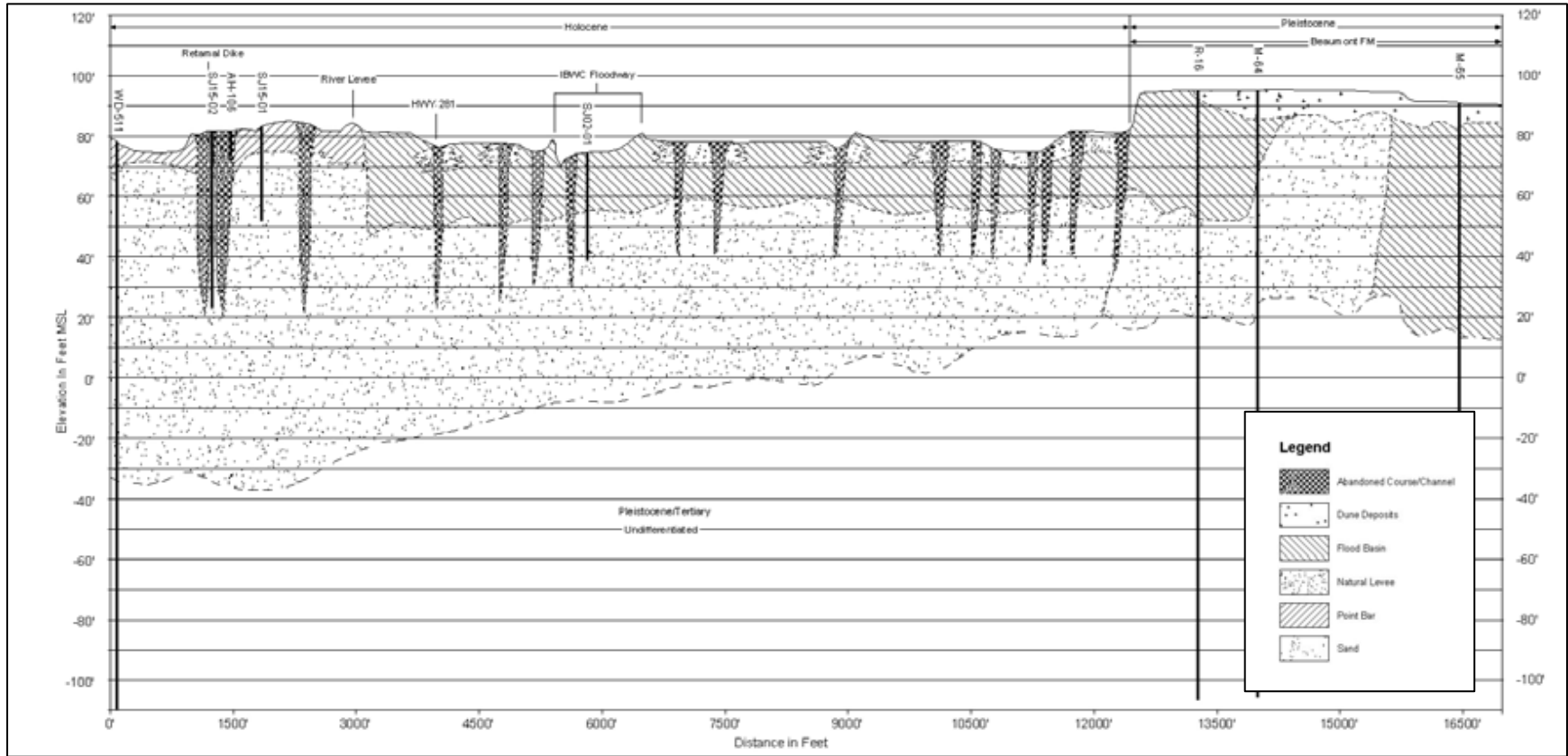


Figure 11. Geologic cross section across Retamal levee and the Main Floodway (from Dunbar et al. 2003)

the river channel, are usually coarser grained (silt and fine sand), and become finer grained (silt and clay) with distance from the river. Borrow material to build the levees that form the IBWC flood-control system was derived locally from these different depositional settings.

Geotechnical Borings

Identified on Figure 1 are the locations of six borings that were drilled in support of geophysical and geologic studies for the Retamal levee. Two borings were drilled on the north and south levee of the Main Floodway (identified as Seismic 3 and 4), and four borings were drilled at Retamal levee. Two of the four borings drilled at Retamal levee were in support of the trench study. Borings were drilled by Alpha and Omega, San Antonio, TX, with an ERDC geologist logging the soils and identifying samples to be submitted for laboratory testing. Borings at the trench site (SJ-TX-01 and 02) were drilled on 7 October 2003, while the remaining four borings were drilled on 2 December 2003. Field boring logs from the six borings that were drilled for this study are presented in Appendix B.

Laboratory Soil Testing

Selected soil samples from five borings were submitted for laboratory soil testing. Only samples from the one trench-site boring (SJ-TX-02) were submitted for laboratory soil testing. Laboratory soil testing involved determination of the physical or engineering properties, clay mineralogy, and soil chemistry. Three laboratories were used to determine soil properties and report test results.

Laboratory testing for the engineering properties was performed by Drash Consulting Engineers, Inc., Pharr, TX, a Corps of Engineers-certified soils testing laboratory. Soil test results are summarized in Table 2 and presented in Appendix C. Seventy soil samples were submitted for testing. Soil test results are reported using the USCS and American Society for Testing and Materials (ASTM) standards. Testing involved determination of USCS soil classification (ASTM D 2487), natural moisture content (ASTM D 2216), Atterberg Limits (ASTM D 4318), particle size analysis (ASTM D 421 and D 422), and density of soil in-place by the drive cylinder method (ASTM D 2937). Lithology logs for each boring, along with the laboratory test values are presented in Appendix B (Note: Boring B1, B2, B3, and B4 corresponds to Seismic 1, 2, 3, and 4, respectively.)

Determination of the clay mineralogy of levee soils was performed by Dr. David Patrick and Patrick Bourne from the Geology Department, University of Southern Mississippi (USM), Hattiesburg, MS, using X-ray diffraction (XRD) procedures. Clay mineralogy affects the engineering properties of fine-grained soils by causing volume changes under different moisture states.

Sample Identification	Sample Depth (ft)	Moisture Content (%)	Unit Dry Weight (pcf)	Liquid Limit (%)	Plastic Limit (%)	Plasticity Index (%)	Fraction Passing No. 200 Sieve (%)	Silt Fraction (%)	Clay Fraction (< 0.005 mm) (%)	USCE Soil Classification
B-1, S-1	1	13	114							LEAN CLAY (CL)
B-1, S-2	2	13								LEAN CLAY (CL)
B-1, S-3	3	11	118	35	20	15				LEAN CLAY (CL)
B-1, S-4	4	15	113	34	18	16	96	48	38	LEAN CLAY (CL)
B-1, S-5	4.5	13								LEAN CLAY (CL)
B-1, S-6	5	14	110	32	19	13				LEAN CLAY (CL)
B-1, S-7	5.8	15								LEAN CLAY (CL)
B-1, S-8	6.8	15	106	41	20	21				LEAN CLAY (CL)
B-1, S-9	7.4	12								LEAN CLAY (CL)
B-1, S-10	8.1	12	113	42	19	23	95	47	48	LEAN CLAY (CL)
B-1, S-11	10	16								LEAN CLAY (CL)
B-1, S-12	10.7	12	106	34	19	15				LEAN CLAY (CL)
B-1, S-13	11.5	11					94			LEAN CLAY (CL)
B-1, S-14	12.3	11	110				29			SILTY SAND (SM)
B-1, S-15	13.2	10					12			SILTY SAND (SM)
B-1, S-16	13.7	6								SILTY SAND (SM)
B-1, S-17	14.3	8								SILTY SAND (SM)
B-1, S-18	15.3	5					41			SILTY SAND (SM)
B-2, S-1	1	21	107							LEAN CLAY (CL)
B-2, S-2	1.6	21								LEAN CLAY (CL)
B-2, S-3	3	20	105	40	20	20	96	45	49	LEAN CLAY (CL)
B-2, S-4	5	21					29			LEAN CLAY (CL)
B-2, S-5	5.7	10								SILTY SAND (SM)
B-2, S-6	7	25	102	54	25	29	97	40	57	SILTY SAND (SM)
B-2, S-7	8.6	22								CLAY (CH)
B-2, S-8	9.2	18	100	45	20	25				CLAY (CH)
B-2, S-9	9.7	20								CLAY (CH)
B-2, S-10	10.6	21	104	56	24	32				CLAY (CH)
B-2, S-11	10.9	23								CLAY (CH)
B-2, S-12	11.5	15	109							LEAN CLAY (CL)
B-2, S-13	12.4	14								LEAN CLAY (CL)
B-2, S-14	12.9	17								LEAN CLAY (CL)
B-2, S-15	14.6	17	104	55	25	30	97	36	61	CLAY (CH)
B-2, S-16	16.2	28		54	23	31				CLAY (CH)
B-2, S-17	16.9	30								CLAY (CH)
B-2, S-18	17.4	28	94							CLAY (CH)

(Continued)

Sample Identification	Sample Depth (ft)	Moisture Content (%)	Unit Dry Weight (pcf)	Liquid Limit (%)	Plastic Limit (%)	Plasticity Index (%)	Fraction Passing No. 200 Sieve (%)	Silt Fraction (%)	Clay Fraction (< 0.005 mm) (%)	USCE Soil Classification
B-3,S-1	1	27	97							CLAY (CH)
B-3,S-2	2.2	26								CLAY (CH)
B-3,S-3	3.5	19	111	63	26	37				CLAY (CH)
B-3,S-4	5	15	113	71	24	47	99	13	86	CLAY (CH)
B-3,S-5	7.7	20	102	65	25	40				CLAY (CH)
B-3,S-6	8.8	20								CLAY (CH)
B-3,S-7	9.8	16	107	64	24	40	98	20	78	CLAY (CH)
B-3,S-8	10.8	23								CLAY (CH)
B-3,S-9	11.8	19	106	66	24	42				CLAY (CH)
B-3,S-10	12.7	18								CLAY (CH)
B-3,S-11	13.5	19	105	65	24	41	99	19	80	CLAY (CH)
B-3,S-12	14.8	24								CLAY (CH)
B-3,S-13	15.8	25								CLAY (CH)
B-3,S-14	16.8	19	103	68	23	45				CLAY (CH)
B-4,S-1	1	21								CLAY (CH)
B-4,S-2	1.9	22	101	71	25	46				CLAY (CH)
B-4,S-3	3.5	24								CLAY (CH)
B-4,S-4	5.1	21	102	68	26	42				CLAY (CH)
B-4,S-5	6.7	22								CLAY (CH)
B-4,S-6	8.5	20	104	63	25	38	99	15	84	CLAY (CH)
B-4,S-7	9.5	21								CLAY (CH)
B-4,S-8	10.6	19								CLAY (CH)
B-4,S-9	11.6	22								CLAY (CH)
B-4,S-10	12.5	21	105	68	25	43				CLAY (CH)
B-4,S-11	13.5	22								CLAY (CH)
B-4,S-12	14.5	23								CLAY (CH)
B-4,S-13	15.5	24								CLAY (CH)
B-4,S-14	16.5	25								CLAY (CH)
B-4,S-15	17.5	24								CLAY (CH)
B-4,S-16	18.5	26	100	70	24	26				CLAY (CH)
SJ-TX-02, S-1	3	19		74	24	50				CLAY (CH)
SJ-TX-02, S-2	5	17		58	20	38	99	32	67	CLAY (CH)
SJ-TX-02, S-3	9	21		75	27	48				CLAY (CH)
SJ-TX-02, S-4	17	23		65	23	42				CLAY (CH)

Sample	Smectite	Illite	Kaolinite
Seismic 1-5: (4.5 - 5.0')	53%	27%	21%
Seismic 1-8: (6.75' - 7.5')	45%	35%	20%
Seismic 2-4: (7.0' - 7.4')	56%	32%	12%
Seismic 3-4: (7.7' - 8.3')	45%	36%	19%
Seismic 4-4: (7.0' - 7.4')	33%	35%	32%
SJ-TX-02-2 (3' - 5')	32%	34%	34%
SJ-TX-02-5 (9' - 11')	20%	49%	31%
SJ-TX-02-7 (13' - 15')	34%	39%	27%

NOTE: The sample identification contains the boring number, sample number, and depth.

Soil chemistry was performed by Pettiet Soil Testing Laboratory, Leland, MS. An important property of clay soils that can affect the stability of levees is their dispersive character, whereby clay minerals in the presence of water become suspended in the fluid without agitation or scouring against the levee surface. Basic soil chemistry tests can help determine whether clay soils are susceptible to dispersion. Eight samples were submitted for soil chemical analyses. Reported results of this analysis are presented in Table 4.

Bore-spl No	Depth (ft)	Ca (ppm)	Mg (ppm)	Na (ppm)	CEC (% base sat.)	ESP (meq/100g)	SAR (meq/L)
Seismic-1-5	4.5-5.0	16589	391	162	18	3.91	0.82
Seismic-1-8	6.75-7.3	13809	576	250	27.3	3.98	1.48
Seismic-2-4	7.0-7.9	14069	622	313	34.7	3.92	1.81
Seismic-3-4	7.7 - 8.3	26729	735	1276	42	13.21	3.98
Seismic-4-4	7.0-7.4	28269	833	1760	44.1	17.36	5.18
SJ-TX-02	3.0-5.0	14409	698	392	39	4.37	2.20
SJ-TX-02	9.0-11.0	14169	721	331	38.6	3.73	1.88
SJ-TX-02	13.0-15.0	14249	754	268	39.1	2.98	1.51

NOTE: CEC = cation exchange capacity. ESP = exchangeable sodium percentage. SAR = sodium absorption ratio. (See text for discussion.) Values of ESP and SAR in boldface identify possible dispersive soils.

Physical Soil Test Results and Properties

Soils are classified by the particle size of the individual components as shown in Table 5 (Rollings and Rollings 1996). Fine-grained soils are those passing the No. 200 sieve (<0.075 mm). Soils reported in Table 2 are classified using the USCS, which is based on U.S. Standard Sieve sizes and the Atterberg Limits for separation of fine-grained soils into the silt and clay categories.

A comparison of the laboratory soils data among the five borings drilled provides some indication of the range in physical properties, as well as the general moisture conditions of the levee soils at each site at the time the samples were obtained (see Table 2). Variations occur in soil moisture, the unit weight,

Table 5 Comparison of Soil Types by Grain Size Diameter (mm) and U.S. Standard Sieve Size (from Rollings and Rollings 1996)				
Soil Component	U.S. Standard Sieve		Size (mm)	
	Passing	Retained On	Maximum	Minimum
Cobbles	--	3 in.	--	75
Gravel	3 in.	No. 4	75	4.75
Coarse gravel	3 in.	3/4 in.	75	19
Fine gravel	3/4 in.	No. 4	19	4.75
Sand	No. 4	No. 200	4.75	0.075
Coarse sand	No. 4	No. 10	4.75	2.00
Medium sand	No. 10	No. 40	2.00	0.425
Fine sand	No. 40	No. 200	0.425	0.075
Fines	No. 200	--	0.075	--
Silt	--	--	0.075	0.005
Clay	--	--	0.005	--

Plasticity Index (PI), and USCS soil types among the five sites represented by the borings in Table 2 and Figure 1. Variations occur because of geology, both horizontally over the floodplain and with depth. Soils data in Table 2 also permit comparison of physical properties between soils in the levee and the foundation. Lithology logs in Appendix C identify the base of the levee on the drilling log as determined from LiDAR survey data performed in 2001 by airborne geophysics.

Soil samples from the different levee borings are derived from different borrow pits. Soils in borings B-1 (Seismic 1), B-2 (Seismic 2), and SJ-TX-02 were derived from borrow pits adjacent to Retamal levee numbered 1, 4, and 2, respectively. Retamal levee soils from borrow pit 1 are from natural-levee deposits, while borrow pits 2 and 4 are in abandoned Rio Grande channels. Borings B-3 and B-4 (Seismic 3 and 4, respectively) are from the Main Floodway, where these soils were obtained by scraping borrow from the interior surface of the floodway, or from the central pilot channel that was cut. These soils represent flood basin deposits and were formed by overbank deposition of fine-grained sediments during major flood events.

Discernible variations occur in soil types and physical properties among the five levee sites in Table 2. The majority of fine-grained samples submitted for testing classified as highly plastic clay (CH). Soils at Retamal levee location B-1 (Seismic 1) are composed of lean clay (CL). They are derived from natural-levee deposits (i.e., overbank deposits adjacent to the main channel) and contain silty sand (SM) at the base of the levee (i.e., ~14-ft depth). Moisture content values (percent by weight) for boring B-1 for the clay soils are some of the lowest values (less than 15 percent) identified in Table 2. Abandoned channel soils from SJ-TX-02 and B-2 (Seismic-2) from Retamal levee had water contents slightly near or above 20 percent and were mainly CH (borrow pits 2 and 4). Soils from the Main Floodway borings are mainly CH with water contents that were slightly higher than those from Retamal levee. Unit soil weights are generally similar among the five areas for samples measured.

A plot showing the Atterberg Limits for fine-grained soil samples that were tested is presented as Figure 12. The Atterberg Limits are an important index engineering property and represent the water content boundaries between the

semi-liquid or liquid limit (LL) and plastic limit (PL) states. Laboratory procedures to determine these two states of consistency are described in engineering and soils testing references (ASTM D 4318) and are not covered in this report. The PI is the difference between the two ranges in water contents ($PI = LL - PL$). The graph in Figure 12 contains a limited number of samples. Not all sites contain an equal representation of samples, but the distribution of points indicates there are distinct variations and clusterings of soils by PI and LL among the sites represented. Soils at the upper end of the PI and LL plot correspond to an abandoned channel (i.e., Borrow Area 2, on Retamal levee) and flood basin deposits from the Main Floodway. The lowest values shown are from natural-levee deposits (Borrow Area 1, Retamal levee). At the middle part of the plot are soils from an abandoned channel (Borrow Area 4, Retamal levee).

Clay Mineralogy

Clay mineralogy influences the volumetric properties of clay soils because certain clay minerals can incorporate large amounts of water into their lattice. Changes in the water content of clay soils can significantly affect soil volume by expansion from addition of water, or by contraction upon drying. This expansive character of clay soils can have a significant impact in engineering and construction, especially in building foundations and for levees in flood control systems.

Clay soils as defined in engineering use implies a soil in which the majority of particles will pass the No. 200 sieve (i.e., <0.075 mm) and plot above the A-line (Figure 12) whereas, in geology, a clay soil is defined as one in which the grain size diameter for the majority of particles is less than $1/256$ mm or 0.0039 mm. In either case, clay soils are generally a mixture of more than one clay mineral. The different clay minerals classify into one of three clay families or groups, based on their internal molecular structure. This molecular structure relates to the stacking of sheet or plate-like aluminosilicate minerals, and associated cations within these sheet structures. Detailed information about clay mineralogy lattice structure is beyond the scope of this study. The three major clay mineral groups are kaolinite, illite, and smectite. The clay mineral montmorillonite is in the smectite group. Also, bentonite is a form of smectite that is used exclusively in drilling muds, because of its thixotropic properties.

Results of laboratory clay mineralogy by XRD analyses for selected IBWC soil samples are presented in Table 3 (see Figure 1 for sample locations). XRD analysis identifies the relative percent of clay minerals in the sample to each other, and not the volume of clay in the sample. Samples submitted for testing are representative of the different borrow pits and depositional settings, as previously discussed. Laboratory results indicate clay mineralogy is a mixture of the three clay groups among the tested samples. Smectite is generally the dominant clay mineral in the samples from among borings 1, 2, and 3. Illite is the dominant

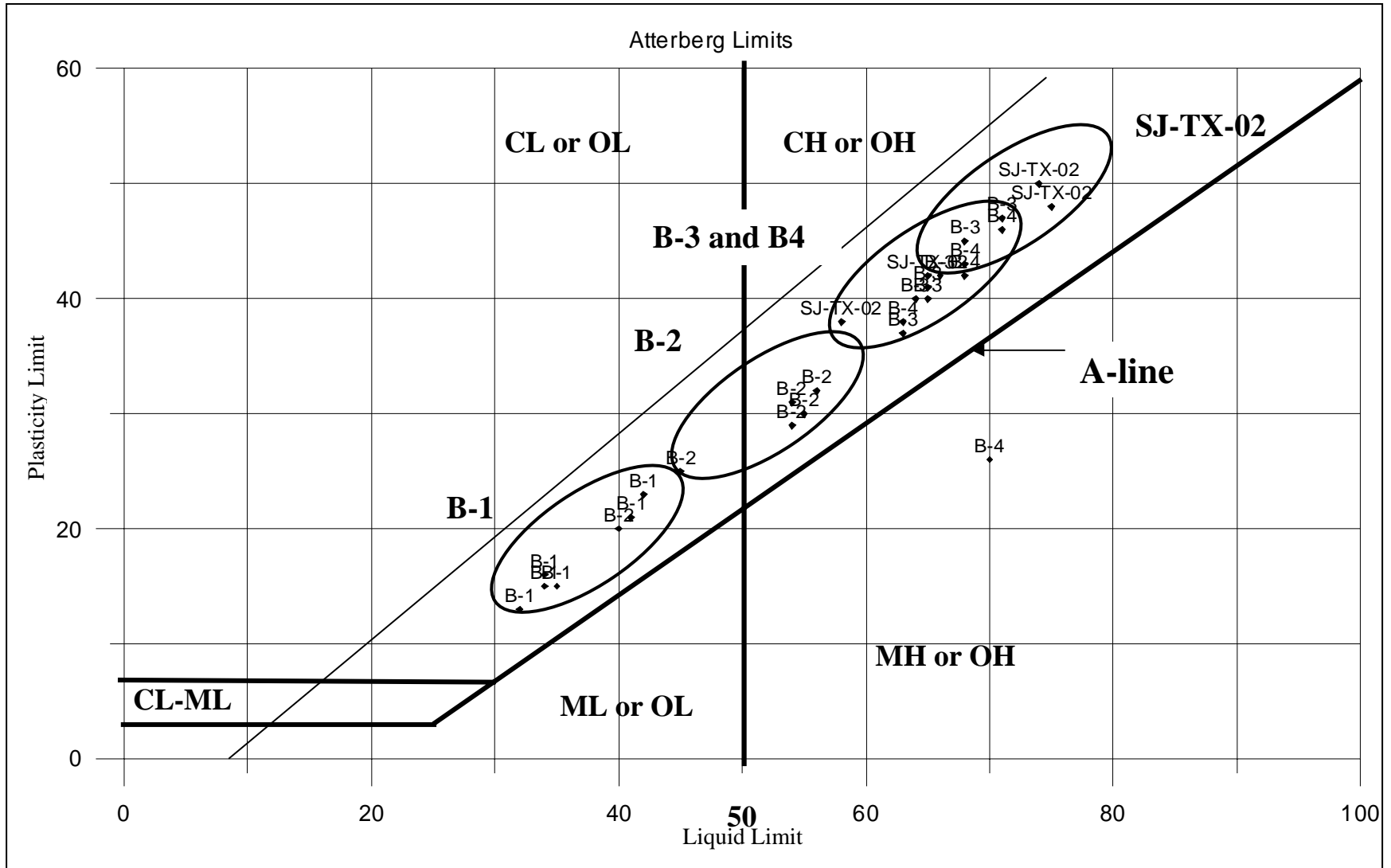


Figure 12. Atterberg Limits for samples from Retamal levee and Main Floodway

mineral in the test pond and trench site (SJ-TX-02). And last, in boring number 4, the three clay groups are generally equally represented. Laboratory data suggest that the geologic setting has some bearing on the mineralogy. These data suggest that flood-related environments or overbank type deposits (i.e., natural-levee and flood basin deposits) contain a slightly higher percentage of smectite minerals. Abandoned channel settings (i.e., borings SJ-TX-02 and Seismic 2) contain a majority of either smectite or illite minerals. The dominance of either mineral is perhaps dependent upon the energy conditions under which these sediments were deposited. Since the exact location in the borrow pit and the depth from which the soils was removed from the abandoned channel to construct the levee is unknown, no generalizations can be made regarding clay mineralogy with respect to position and depth in the abandoned channel setting.

Clay mineralogy can significantly impact the Atterberg Limits as shown by Table 6 (Rollings and Rollings 1996). Montmorillonite or smectite type clay can have the highest LL and PI values. The cation that is present in the lattice also affects the Atterberg Limits as identified by Table 6. The clay minerals carry an electric charge that attracts both water and ions known as exchangeable ions. Kaolinite has the lowest range of PI values, while illite is midway these two clay groups. Data shown in Table 5 are for individual clay minerals. Clay minerals that have small particle size, such as smectite group minerals, have a much higher volume expansion as they are able to incorporate more water per unit of surface area.

Clay Mineral	Exchangeable Ion	Liquid Limit (%)	Plastic Limit (%)	Plasticity Index (%)
Montmorillonite	Na	710	54	656
	K	660	98	562
	Ca	510	81	429
	Mg	410	60	350
	Fe	290	75	215
	Fe ¹	140	73	67
Illite	Na	120	53	67
	K	120	60	60
	Ca	100	45	55
	Mg	95	46	49
	Fe	110	49	61
	Fe ¹	79	46	33
Kaolinite	Na	53	32	21
	K	49	29	20
	Ca	38	27	11
	Mg	54	31	23
	Fe	59	37	22
	Fe ¹	56	35	21
Attapulgite	H	270	150	120

¹ After five cycles of wetting and drying.
SOURCE: *Soil Mechanics*, W. T. Lambe and R. V. Whitman. Copyright © 1969. Table reprinted by permission of John Wiley and Sons.

A soil containing a mixture of the different clay minerals can cause notable variations in the Atterberg Limits from the values shown in Table 6. The composition and relative abundance of each mineral can affect the engineering properties. LRGV lab test results in Figure 12 are quite different from trends shown in Table 6. Some of the highest values for PI in Figure 12 are samples where illite was the dominant clay mineral in the sample (Table 3). Samples from the trench boring (abandoned channel) and those from the Main levee (flood basin deposits) had the highest PI values, but intermediate to low abundance of smectite compared with the illite.

Mineralogy data presented in Table 3 represent the relative percentages of the clay minerals compared with one another, and not the relative percentage of sample where the clay grain size diameter is less than 0.005 mm in the sample. The ratio of silt to clay, as well as other inert minerals in the sample (i.e., quartz, calcite, and detrital parent material) can affect the influence on mineralogy for causing bulk volume changes in the sample with the loss or gain of water. Included in Table 2 is the ratio of silt to clay (particles <0.005 mm diameter) for selected samples. Generally, samples with higher overall clay content are more expansive, with smectite and illite minerals contributing between 66 and 80 percent of the clay minerals in the sample. As shown in Table 6, these two minerals have properties that can affect the behavior of the Atterberg Limits.

The influence of the depositional setting plays an important role in predicting soil behavior. Proximity to the main river channel and energy conditions under which the sediments are deposited is a contributing factor to clay content over the floodplain. Therefore, natural-levee soils may contain an abundance of smectite minerals, but the overall clay content of the sample is the lowest of all the samples measured because of the higher turbulence associated with this depositional setting. Low-energy environments, such as flood basin and abandoned channels, are generally apt to contain a higher percentage of fine-grained soils. The geologic cross section in Figure 10 clearly identifies this trend by the distribution of the top stratum and substratum deposits and their thickness across the floodplain. Abandoned channels and flood basin deposits contain fine-grained soils (CH) that are thick (i.e., generally greater than 20 ft). Point bar top stratum and natural-levee deposits are usually found in combination and are generally less than 10 ft thick, slightly coarser grained, and contain lean clays (CL).

Chemical Soil Test Results

Analyses of soil chemistry were performed to determine whether the levee soils under study were dispersive (Table 4) and could cause levee failure during flooding. A soil is considered dispersive when clay in the presence of water becomes suspended in the fluid without agitation. Removal of soil material from the levee can cause seepage and piping and eventual failure by loss of mass. Dispersion can cause a void to form that extends headward to the water side of the levee under a seepage force, and causes eventual failure of the embankment. Generally illite and smectite clays are likely to exhibit this property.

Chemical laboratory tests to determine if a clay soils is dispersive are values of exchangeable sodium percentage (ESP) and sodium absorption ratio (SAR) of pore water (Knodel 1991). The general formula for ESP is

$$\text{ESP} = (\text{exchangeable sodium}/\text{cation exchange capacity}) \times 100$$

Soils with ESP greater than 10 are subject to having free salts leached by seepage or relatively pure water and are considered dispersive (Knodel 1991). ESP less than 7 is nondispersive, and values between 7 and 10 are classified intermediate. Table 4 presents ESP values for levee soils with values ranging from about 3 to 17. Only the Main Floodway levee tested above 10, and these soils are considered dispersive.

Another parameter used to classify whether a soil is dispersive is the SAR of the pore water when free salts are present. The SAR method is not applicable if no free salts are present (Knodel 1991). Soil chemistry by Pettiet Soil Testing Laboratory reported that LRGV samples contained an abundance of free salts (see Appendix D). The general formula for SAR is

$$\text{SAR} = \text{NA} / 0.5 (\text{Ca} + \text{Mg}) \text{ with units of meq/L}$$

Use of the SAR is based on the fact that the soils in nature are in equilibrium with their environment, and there is a relationship between electrolyte concentration of the soil pore water and the exchangeable ions in the clay absorbed layer. SAR values of greater than 2 are considered dispersive. Table 4 presents SAR values that range from less than 1 to greater than 5.

Chemical test results by ESP and SAR identify flood basin soils with high sodium values and having dispersive properties. Retamal levee soils contained lower salts and were not dispersive, except one sample near surface at the trench site.

4 Geophysical Methods

Introduction

Several geophysical methods were employed during this study to compare different levee reaches to one another, to select the flood test site based on geophysical signatures and associated physical characteristics, and to determine changes in the levee properties during the flood-simulation phase of the investigation. Geophysical surveys consisted of seismic and electrical methods. Seismic surveys were performed at each location identified in Figure 1. Focused two-dimensional (2-D) and 3-D seismic studies were performed at Seismic 1 (Site 1) and at SJ-TX-01/02 (Site 2) before the final selection of the pond location was made. Various electrical methods were used during the flood-simulation portion of this study. Electrical techniques involved resistivity, spontaneous potential, electromagnetic induction, and ground penetrating radar surveys.

Various kinds of seismic surveys were performed to determine which technique was diagnostic of unstable soils and to develop procedures to easily measure and detect signatures associated with unstable reaches. Seismic surveys were performed to measure changes in the bulk physical properties of the levee soils as they underwent hydration during the flood test. Seismic surveys were performed prior to the flood test and repeatedly throughout the rise and fall of the test flood. Similarly, electrical methods were used because of their sensitivity to changes in soil electrical conductivity as the levee soils hydrate during the flood test. Changes in soil conductivity are likely to occur as water moves into the levee core along potential desiccation cracks that may be present.

ERDC geophysicists were responsible for conducting the resistivity and GPR surveys. Supporting the ERDC research team during this study were nationally known experts in their respective fields. Contractors supporting seismic field activities were Drs. Rick Miller and Julian Ivanov, geophysicists, with the Kansas Geological Survey; Robert Ballard, retired ERDC geophysicist and consultant, Clinton, MS; and Dr. Bob Corwin, a geophysicist specializing in spontaneous potential monitoring, with SP Surveys, El Cerrito, CA. A report of the seismic study by Drs. Miller and Ivanov is presented as Appendix E. A report of the SP survey by Dr. Corwin is presented as Appendix F. These two reports describe in detail the respective approach of each method, study methods involved, equipment used, data processing procedures, results observed, and conclusions obtained.

The focus of this chapter is to summarize the results of the geophysical methods that were used during this study. A detailed examination of the theory and application of each geophysical method used is beyond the scope of this study. Detailed information about the different methods is described in Reynolds (1997) and in Engineer Manual (EM) 1110-1-1802 (U.S. Army Corps of Engineers, USACE 1995). Geophysical methods used in this study are described at a level of detail to provide a general understanding of the techniques and associated results obtained by each method. Supporting data are presented in the appendixes to this report for more in-depth examination of each method as it was applied to the IBWC levees. The order of presentation of the geophysical data in this section is based on their use in this study.

Test Pond

Introduction

Before the different geophysical methods and results are discussed, information about the test pond and instrumentation used to measure the different electrical and seismic properties is presented. Generally, all the geophysical testing involved monitoring the rise and fall of the simulated maximum flood event against the levee and the saturation of the levee soils. Because of the infrequency of major flooding in the LRGV, historic performance data are lacking for newly constructed areas of the IBWC flood control system. To permit full-scale testing of their levee system, IBWC purchased a movable bladder to hold water against the levee face for the duration of a maximum flood event.

Site preparation

The site preparation involved construction of a test pond against the levee using a portable cofferdam or water-filled bladder. Construction and filling of the bladder was performed during the period 27 October 2004 to 5 November 2004. IBWC personnel from the Mercedes field office prepared the pond site at the Retamal levee (Figure 1 and Figure 2) and installed the bladder against the levee (Figure 13). Preparation of the site involved constructing a suitable foundation to raise the ground surface for the bladder to reach the top of the levee crest. The bladder manufacturer was onsite to assist with the installation and filling of the bladder.

To ensure that the bladder did not leak on the riverside other than along the levee surface, a polyvinyl chloride liner was laid over the bladder and all liner joints were sealed with a heat-activated adhesive to prevent unwanted leakage (Figure 13, photo C). Upon completion of the test pond, only the earthen face of the levee was exposed to the floodwater. A staff gage was placed in the test pond to monitor water levels. Controlled raising and lowering of the water elevation was performed with pumps. IBWC provided the pumps (2-in. and 4-in.) and fuel. ERDC personnel maintained the water level in the pond during the test.



A



B



C



D

Figure 13. Photos of test pond showing: (A) preparation of foundation, (B) bladder before being filled with water, (C) filled bladder and the staff gages in empty pond, and (D) pond at full pool (11.5 ft, el 93.7 ft NGVD)

Water for the pond and the bladder was obtained from the nearby abandoned Rio Grande oxbow on the Bell Brother's property (see Figure 2). IBWC had obtained permission for water rights prior to the conduct of the test.

Test duration

The test began at 10 a.m., Monday, 8 November 2004, and ended at 3 p.m., 16 November 2004. The test ran for 197 hr and involved filling the pond to a height of 11.5 ft. ERDC personnel maintained a presence at the site 24 hr each day for the duration of the test. A flood hydrograph (Figure 14) for the test was provided by Dr. Raymundo Aguirre, IBWC, El Paso, TX, and required raising (and lowering) the water level every hour by a specified amount, usually 1 or 2 tenths of a foot on the staff gage in the pond. Maximum flood height allowed for 3 ft of freeboard from the levee crest.

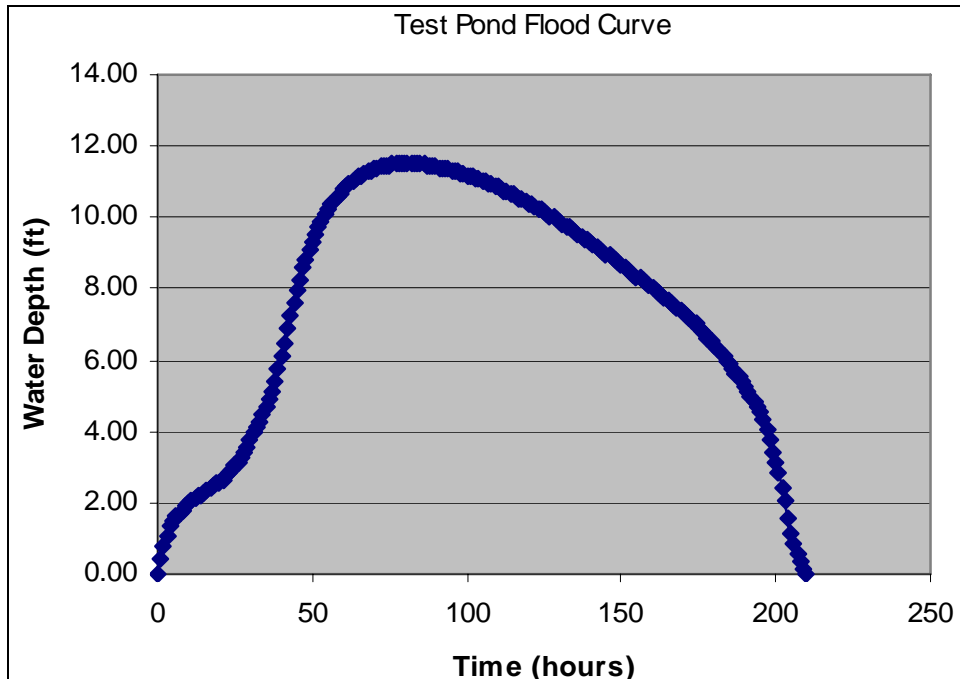


Figure 14. Flood inundation curve for levee test pond study. Water depth is in feet with 3 ft of freeboard remaining after maximum flood depth of 11.5 ft (el 93.7 ft NGVD). Flooding of the test pond was conducted from 8 to 16 November 2004

Instrumentation of test pond

Instrumentation of the pond site occurred between 3 and 7 November 2004 and involved installation of seismic geophones and resistivity and SP electrodes across the levee surface and at the toe. Two lines of geophones were placed at the riverside and landside crest (Figure 15). Three 80-m-long resistivity lines with 2-m spaced electrodes were installed along the riverside crest (labeled crest), landside midslope (labeled face), and landside toe (labeled toe) of the levee. Four lines of SP electrodes (20 per line, 2.5-ft spacing) were installed along the riverside midslope (line C), riverside crest (line D), landside crest (line A), and landside midslope (Line B). Individual leads for both resistivity and SP electrode were run to a common point outside of the flooded area. A recreation vehicle (RV) served as the common point where measurements were made on both the resistivity and SP arrays. Seismic lines were run to a separate mobile location for collection and initial processing of data.

Airborne Conductivity Surveys

Introduction

Fugro Airborne Surveys Inc., Mississauga, Ontario, flew an airborne conductivity survey over 270 miles of IBWC levees in the LRGV in June and July 2001.

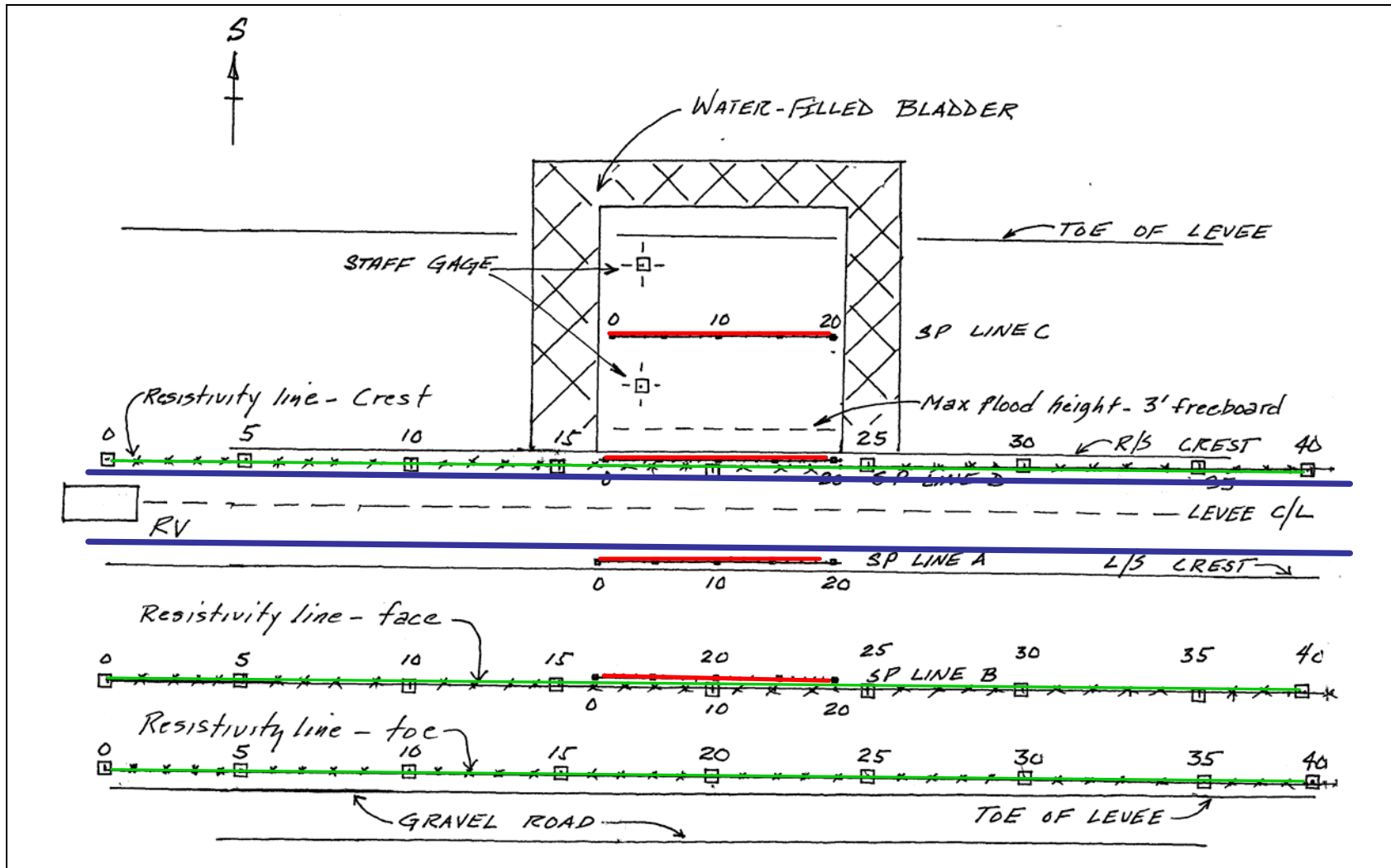


Figure 15. Sketch of pond test site showing position of pond, riverside (R/S) of levee. View is facing south. SP lines are highlighted red and labeled A, B, C, and D. Resistivity lines are highlighted green and are located on R/S crest and landside ((L/S) face and toe of levee. (Geophone lines are in blue)

The survey was flown near the end of a drought period, as noted in Section 2. Airborne conductivity measurements of the IBWC levees were made with a helicopter-towed EMI system. Detailed information about the airborne survey of LRGV levees and the survey results are presented in Dunbar et al. (2003). A brief overview of the EMI method and theory is presented below to allow a better understanding of the reasons for using the different geophysical methods in this study to characterize levee properties.

General theory and equipment

The airborne EMI system flown for the IBWC levee condition assessment contains five pairs of transmitter and receiver coils. Each set of transmitter-receiver coils in the sensor system broadcasts an alternating electromagnetic signal at a fixed frequency. The EM signal from the transmitter induces weak currents to the underlying ground, which in turn causes a secondary magnetic field to form within the soil and/or around nearby conductive objects (McNeill 1980). The receiver coils within the survey instrument then measure the secondary field as a voltage, which is related to the soil resistivity (or its reciprocal conductivity). Thus, multiple transmitter and receiver coils in the sensor system permit rapid measurements of the ground conductivity over multiple frequencies. The range of frequencies used in the airborne EM survey of IBWC levees is between 380 Hz and 102,000 Hz.

An advantage of multi-frequency EM survey systems, compared with single-frequency systems, is their ability to measure the conductivity of the subsurface at different depths of investigation, with depth dependent on the frequency. Higher EM frequencies are able to measure the near-surface conductivity, while lower frequencies measure to greater depths. Apparent-conductivity measurements of IBWC levees were made at five frequencies: at 102, 25, 6.2, 1.5, and 0.38 kHz. The specific depth of investigation in airborne surveys is related mathematically to the conductivity and frequency, and can be determined by the formula for calculating skin depth (Reynolds 1997). Normal depths range from 1 m to 30 m (approximately).

Retamal levee signatures

Relatively low conductivity signatures (Figure 16) were associated with the Retamal levee reach. This reach was constructed in the 1970s (Figure 7). The 25-kHz frequency corresponds to about 3- to 5-m depth of investigation, or about the base of the levee. Relationships between the signatures for apparent conductivity (identified by the legend in Figure 16) and soil types are based on ground-truth data obtained from LRGV geotechnical and cone-penetrometer (CP) borings (Dunbar et al. 2003; 2004). The condition assessment of the IBWC levees in the LRGV was based primarily on the 102- and 25-kHz frequencies of apparent conductivity. Relatively low apparent-conductivity signatures occur along the western half of the Retamal levee reach for the 102- and 25-kHz frequencies. Low conductivity signatures at Retamal levee were considered anomalous, as CP and borrow pit borings identified the levee and near surface as

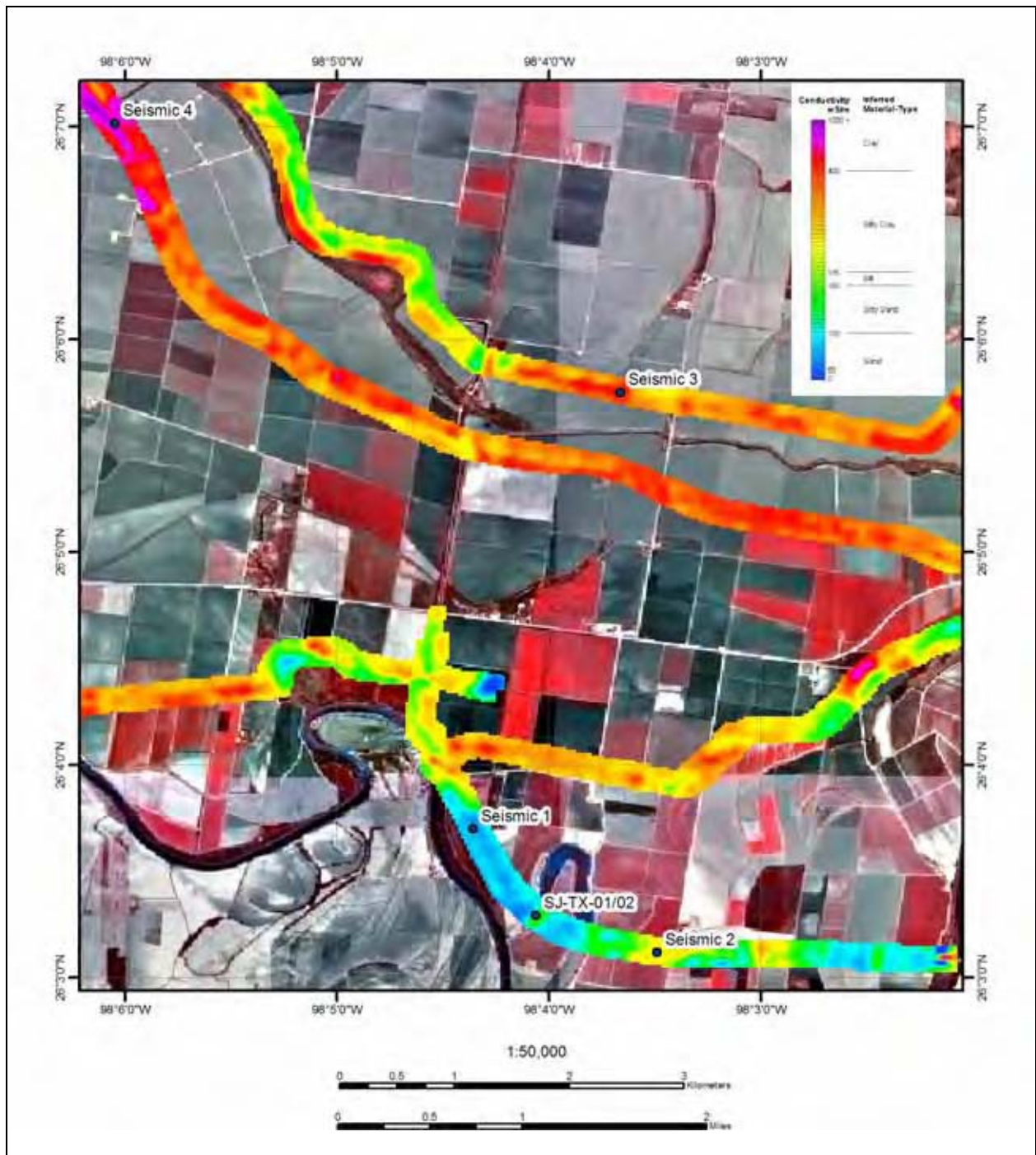


Figure 16. Relative conductivity map of the IBWC levees at the 25-kHz frequency in the San Juan East area as determined by airborne survey in 2001. The 25-kHz frequency shown corresponds to about 3- to 5-m depth of investigation or about the base of levee. Five sites studied contain different conductivity signatures and inferred soils. Relationship between conductivity signatures and soil type is based on empirical relations from ground-truth data from LRGV geotechnical and cone borings

being constructed of clay soils. These phenomena were probably caused by air within the cracks in the body of the levee.

Focused studies of different conductivity signatures

Five sites identified in Figure 16 were further evaluated by drilling geotechnical borings and performing seismic surveys. Selection of these sites was based primarily on their respective conductivity signatures, and in part on their depositional setting on the floodplain. Comparison of geotechnical and seismic properties for these five sites was an underlying goal of this investigation in addition to monitoring the levee during the flood-simulation study. The five sites are all representative of different soil conductivities and conditions as described in Section 2.

Seismic Methods

Introduction

Seismic methods were incorporated into the study of IBWC levees because of their engineering application in determining the in situ elastic moduli or elastic constants. Elastic parameters in engineering use are the shear modulus (μ), Young's modulus (E), and Poisson's ratio (σ). These values relate to index properties of soil or rock strength and can be derived by measuring the compressional- (V_p) and shear-wave (V_s) velocities of elastic body waves that pass through homogeneous isotropic media. Numerous publications describe the derivation of these values by seismic methods, including Ballard and McLean (1975), Chang and Ballard (1973), Reynolds (1997), Sharma (1986), and USACE (1995). Cross sections or profiles of V_p/V_s can be produced for levees that are surveyed by seismic methods. Generally, the larger the V_p/V_s ratio becomes, the material is considered weaker from a ripability or shear strength perspective (see Appendix E).

Data collection efforts

Seismic surveys over IBWC levees were performed on two separate data collection efforts in the LRGV by personnel from KGS. A report of investigation is presented in Appendix E by Drs. Rick Miller and Julian Ivanov for the seismic study of LRGV levees. Seismic data from IBWC levees were collected between 4 and 12 December 2003 at the five study sites (Figure 1 and Figure 16). Subsequently, data were collected at the Retamal levee pond site during the period 8 to 13 November 2004 during the flood-simulation study. During this same period, seismic surveys were performed at levee sites 1, 2, and 4 previously surveyed (December 2003) for comparison purposes.

Seismic wave types and properties

To better understand the types of seismic surveys that were conducted at locations identified in Figures 1 and 16, a brief review of seismic waves and their general characteristics is presented before examination and discussion of survey results. Two major classes of seismic waves occur: body waves and surface waves (Figure 17). Body waves are the fastest of all seismic waves and consist of compressional (also known as pressure or primary) or P-waves, and shear (also known as secondary or transverse) or S-waves. P-wave motion is extension (dilation) and compression along the path of propagating. S-waves are directly dependent on the shear modulus, travel slower than P-waves, have particle motion perpendicular to the direction of propagation, and can have both a horizontal and vertical component. S-waves do not exist in liquids or gases, as these types of media have no shear strength.

Surface waves exist only at the surface or at interfaces and travel slower than body waves. There are two types of surface waves: Love and Rayleigh waves (Figure 17). Love waves have particle motion only in a horizontal direction and are similar to horizontal shear waves. Rayleigh waves have a retrograde elliptical motion in the direction of propagation. Additional information about the different wave forms and their properties is presented in introductory seismic texts (e.g., Reynolds 1997) and in EM 1110-1-1802 (USACE 1995). Seismic surveys were used to measure the soil and foundation properties of IBWC levees using the four types of seismic waves identified in Figure 17.

Objectives in levee screening by seismic methods

A major goal for using seismic methods was to determine if existing technologies could be used to rapidly screen IBWC levee reaches for anomalous soil strength based on measurements of V_p and V_s velocities and calculated values of the in situ moduli. Additionally, examination of all known seismic collection methods was performed as part of this study to identify any procedures and methods that would be diagnostic of levee reaches with potential stability problems.

Primary objectives of the seismic work were to measure the P-wave and S-wave velocities at the five study sites identified in Figure 1 and Figure 16. These measurements were obtained during the first data collection effort in December 2003. During the flood-simulation part of the study, seismic measurements were repeated every 12 hr for the duration of the flooding to evaluate subsequent changes in these initial velocity measurements, as well as changes caused by soil saturation of the levee and foundation soils.

Various types of seismic methods were appraised and associated data processing performed by the KGS study team. Methods include refraction (P- and S-wave), tomography (P- and S-wave refraction with both 2-D turning ray and 3-D straight ray through levee), surface-wave propagation, and surface-wave (Rayleigh and Love wave) dispersion curve analysis (also known as multi-channel analysis of surface waves, MASW). Data sampling and processing procedures used for the two data collection efforts in the LRGV were identical to avoid any

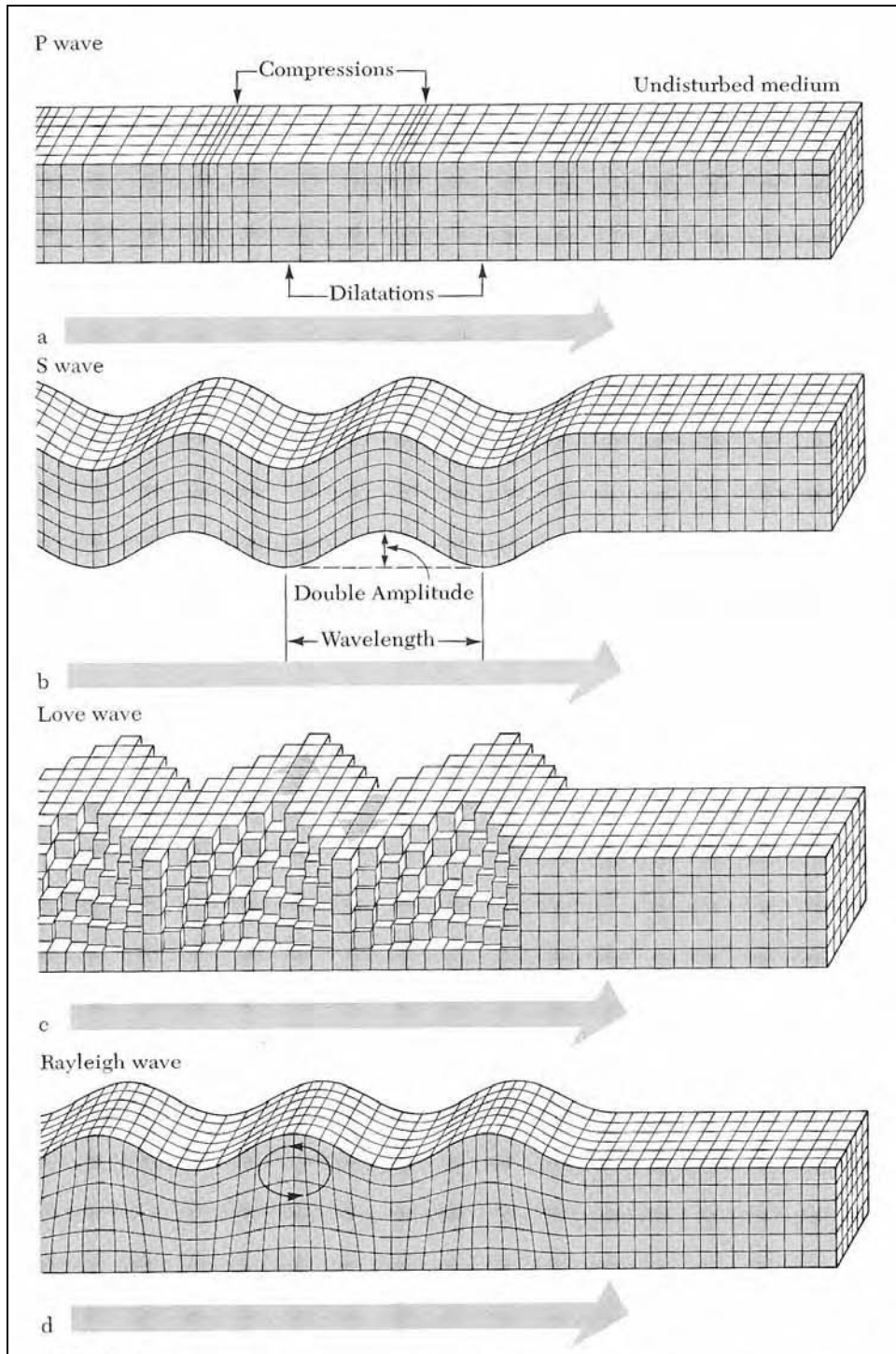


Figure 17. Different types of seismic waves used in engineering investigations of the shallow subsurface (from Bolt 1978). P- and S-waves are body waves, while Love and Rayleigh waves are surface waves. Note the characteristic ground motion for each wave type

potential changes in results due to sampling or processing issues. Information about the different data processing methods is detailed in Appendix E.

Seismic equipment

State-of-the-art seismic equipment was used to survey and measure the different levee areas (Figure 18). Fixed geophones and a land streamer containing a towed geophone array were evaluated. Seismic sources that were tested included various sizes of sledge hammers and a mechanical weight drop, each impacting metal striker plates. Additionally, a vibratory source was used to develop harmonic oscillation at different frequencies to develop Rayleigh waves. Equipment used was identical for the two data collection efforts in the LRGV. Information about the different equipment used is presented in Appendix E.



Figure 18. Seismic equipment used during investigations of IBWC levees: (A) seismic recording cart, (B) close-up view of seismographs in recording cart, and (C) seismic source for producing surface waves, (D) towed land streamer or geophones in fire-hose for rapid seismic surveying capabilities and fixed geophones (in blue, foreground) were evaluated

Seismic results and levee conditions in December 2003

Seismic screening of the five sites shown in Figures 1 and 16 was performed in December 2003 and produced surprising results in both the body- and surface-wave data (Ivanov et al. 2004). Unconsolidated sediments typically have V_p/V_s ratios that range from 3 to as much as 8, but LRGV sites studied had values below 3. First-arrival velocity analysis of sites studied identified V_p/V_s ratios that are in the 2.1 to 2.6 range for the shallower portion (3.6- to 4.5-m depth) of the levee (Table 7). V_p/V_s values at depths greater than 6 m increase to between 4 and 10, which is more consistent with the reported literature and laboratory measurements (Ivanov et al. 2004). Exceptions were sites 4 and 5 (seismic 3 and 4), which have higher V_p and V_s in view of soils and conductivity. Levee soils have slightly lower densities, which may account for lower values as determined from laboratory analysis of soils data.

Table 7
 V_p/V_s Ratios from Refraction Tomography Within the 3.6- to 4.5-m Depth Range for Five LRGV Levee Sites Studied in December 2003 (See Figure 1 and Figure 16 for locations of sites. Velocity values are in units of meters/second (m/s). Locations of areas shown in Figure 1.)

Site	Location	V_p (m/s)	V_s (m/s)	V_p/V_s
1	Seismic 1	397.71	167.15	2.38
2	SJ-TX-01/02	409.27	160.58	2.54
3	Seismic 2	440.51	173.39	2.54
4	Seismic 3	334.29	154.96	2.16
5	Seismic 4	326.48	142.15	2.30

A refraction tomography profile of V_p , V_s , and V_p/V_s is presented as Figure 19 for the pond site (Site 2), near SJ-TX-01/02 (Figure 1 and Figure 16), for December 2003 conditions. This profile is representative of conditions at all five sites that were surveyed in December 2003. It was concluded by the KGS team that the values for V_s were erroneous, and caused by possible mode conversions of P-waves into S-waves (Ivanov et al. 2004). Mode conversions in seismic energy occur at interfaces, where part is refracted as a compressional wave and part as a shear wave. It was interpreted by the KGS team that, because of the mode conversion, energy wavelets arrive with an apparent velocity higher than the actual shallow shear-wave velocity, but lower than compressional velocity, and were yielding higher values for V_s than was expected.

In addition to the body-wave data, anomalous results and/or levee conditions were recognized in the surface-wave data from the December 2003 surveys. Advanced MASW analyses of Rayleigh waves identified deficiencies in frequencies above 15 Hz for the fundamental mode (Figure 20). The KGS team applied a variety of processing techniques to extract higher frequencies, but the data indicated the fundamental mode energy is concentrated between 8 and 12 Hz (Ivanov et al. 2004 and Appendix E). Exact causes for the body- and surface-wave anomalies are uncertain. It was initially concluded by the KGS team that the geometry of the levee, the construction, the material properties, or a combination of these factors was responsible for the observed conditions. Further clues are

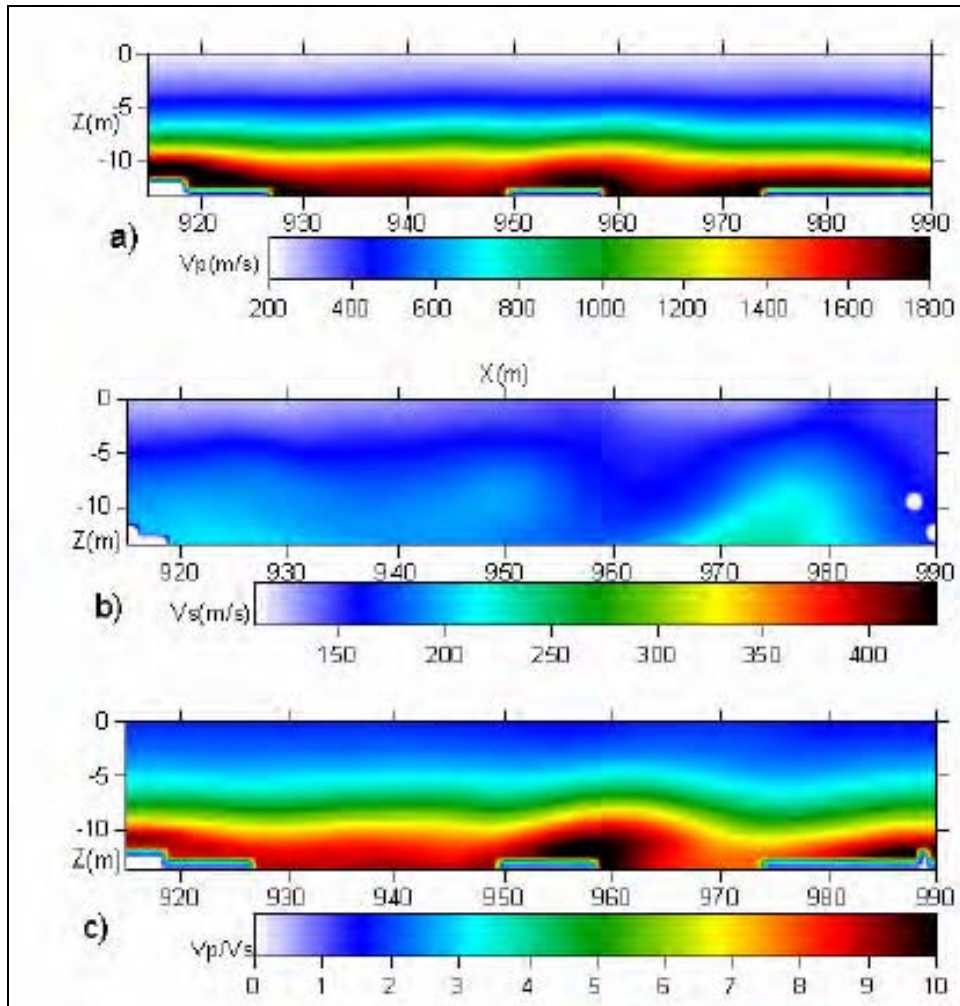


Figure 19. Refraction tomography solutions for the pond site in December 2003: (a) P-wave, (b) S-wave, and (c) V_p/V_s ratio (Ivanov et al. 2004). (Velocities are in meters/second)

contained in the second set of seismic data that were collected and processed in November 2004 to fully understand specific causes responsible for these characteristics.

Before examining the November 2004 data collection, a final characteristic of the December 2003 data is noted for Retamal levee reach. Seismic experiments identified an interesting phenomenon in the trench area and vicinity. Experiments with vibrator sweeps at selected frequencies were performed on the levee crest to determine variations in phase velocities from Rayleigh waves as a function of the input frequency. Dwell or mono-frequency tests involved a vibratory source located upon the levee crest, producing an impact to the levee at a fixed frequency, and the geophone array recording the resultant seismic waves, from which velocity calculations are possible. The geophone array included the reach of the levee previously trenched and the levee area impacted by a small-scale ponding test.

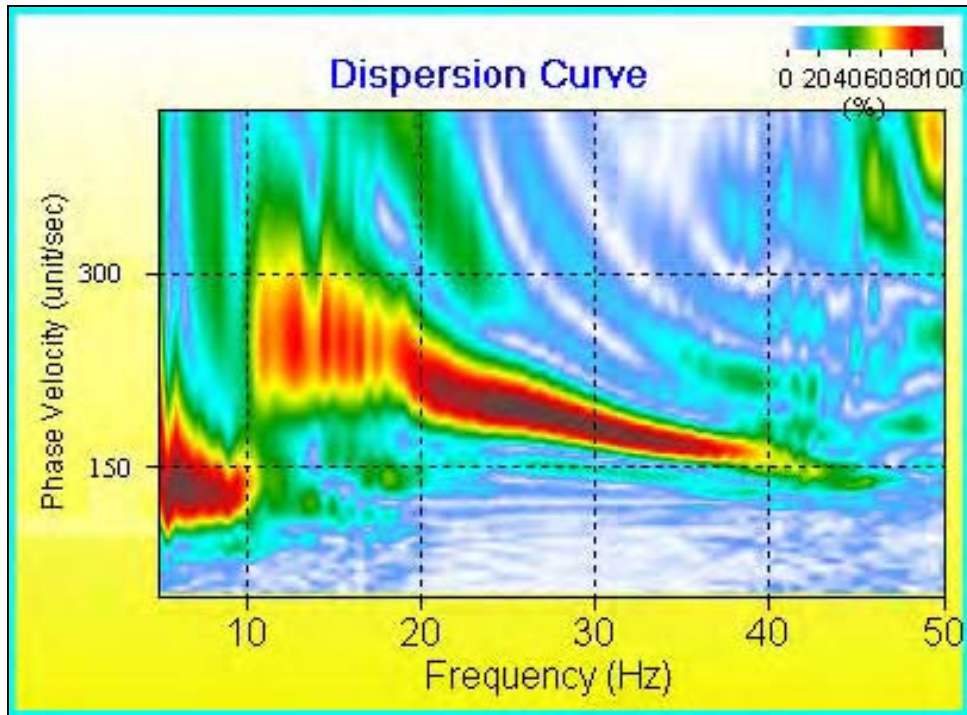


Figure 20. Rayleigh-wave dispersion curve analysis of phase-velocity versus frequency in units of ft/sec (Ivanov et al. 2004)

A ponding experiment was conducted as part of the October 2003 trench study, whereby the trench was filled with water to determine the ability of the levee core to absorb water and provide an estimate of soil permeability. Expansion of levee soils by clay hydration occurred following the small-scale ponding test as determined from surface cracks along the levee crest in the upstream direction. (See Appendix A for information about the trench and ponding results.) The geophone array spanned the reach containing the trench, the adjacent area of the levee that was impacted by water that had infiltrated the levee core, and nondisturbed levee reaches upstream and downstream of the trench. It was observed that the Rayleigh-wave velocities (VR) at 20 Hz were different along the Retamal levee reach, depending on distance from the trench (Figure 21). Generally, the part of the levee where hydration of the core had occurred, because of the October 2003 ponding experiment, had phase velocities that were significantly higher (VR = 1,740 to 2,100 ft/s) than the trench fill (VR = 600 ft/s) or the undisturbed levee reaches (VR = 750 ft/s). Hydration of the levee core by the ponding in October 2003 had increased VR between 2.2 and 2.8 times compared with the original levee upstream and downstream of the trench.

However, it should be noted that the increase in phase velocity in this reach occurred only when the vibratory was located at the upstream end of the array (Figure 21). When the vibrator was located at the midpoint or downstream end of the geophone array, the changes in phase velocity were less pronounced, and were thus not diagnostic, but were dependent on the location of the vibrator.

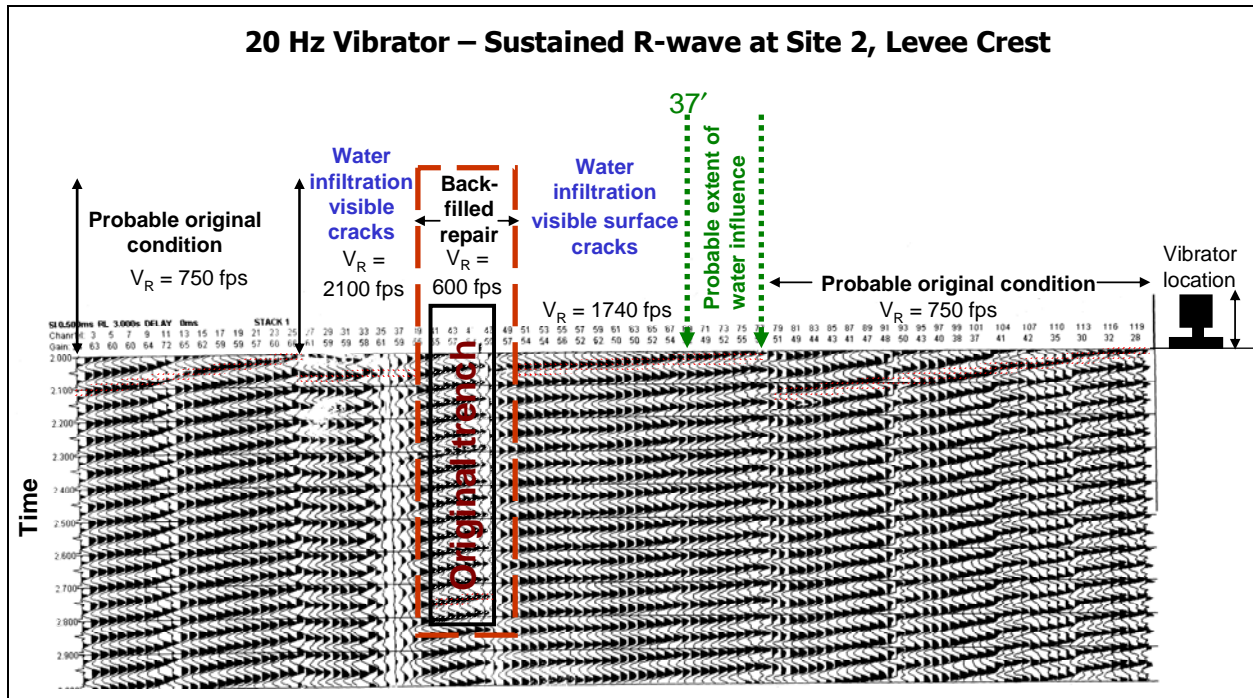


Figure 21. Phase velocities of levee at 20-Hz vibrator monofrequency, Rayleigh-wave velocity V_R is different for original levee, levee trench backfill, and area of levee core infiltrated by water from ponding test in October 2003. Seismic line contains 119 geophones at 3-ft spacing. Vibratory source at western or upstream end of levee and produces approximate 2000 ft-lb at 20 Hz

Hydration of the levee was more concentrated in the upstream direction and may have significantly impacted the propagation of wave energy when the vibrator was located at the upstream end of the levee reach. Specific details about dwell tests are described in Appendix E.

Seismic results and levee conditions in November 2004

Seismic data collected during the second trip exhibit notable differences in characteristics compared with those observed during the first trip, nearly a year previously (Appendix E). Sites 1, 2, and 4 were surveyed again in November 2004, and results were compared with those obtained in 2003. Highlights of these differences are described below. Detailed examination and discussion of the differences are presented in Appendix E.

Generally, the 2004 seismic-frequency spectra were much broader, and the waveforms propagated much easier through the levee among the three sites and produced a higher signal-to-noise ratio. These differences between the two data collection events are attributed to the change in near-surface properties of the levee soils from increased rainfall, compared with the previous year (Appendix E). Sites 1, 2, and 4 contained measurable differences in V_p in 2004, compared with measurements made in 2003. Refraction-tomography V_p analysis in 2004 identified a similar overall velocity structure compared with the 2003 data

(Figure 19). However, the primary difference between the two data sets is a 3- to 8-percent increase in V_p values for the top 5 to 8 ft, and about a 3-percent increase at 30-ft depths in 2004 compared with 2003. Identical survey locations, equipment, methods, and processing were performed. A primary difference between the two surveys has been the increased rainfall and probable hydration of levee soils. As noted previously, surface cracking of the levees was absent in the November 2004 survey period, supporting the assessment that higher rainfall during the preceding months likely hydrated the levee soils (see Section 2) and changed the seismic properties.

Velocity measurements using S-wave refraction tomography were not performed during the second seismic data collection in November 2004 because of earlier problems linked to mode conversions due to possible levee geometry. Instead, the MASW method was considered to be more reliable for estimating V_s . MASW analyses of Rayleigh waves identified frequencies above 15 Hz for the fundamental mode in November 2004, whereas the 2003 data were deficient above this frequency value. The fundamental mode of the surface wave was well defined in 2004, with a wide frequency range from 5 to about 50 Hz (Figure 22). Again, identical sample locations, equipment, survey methods, and data processing were performed for the two collection dates.

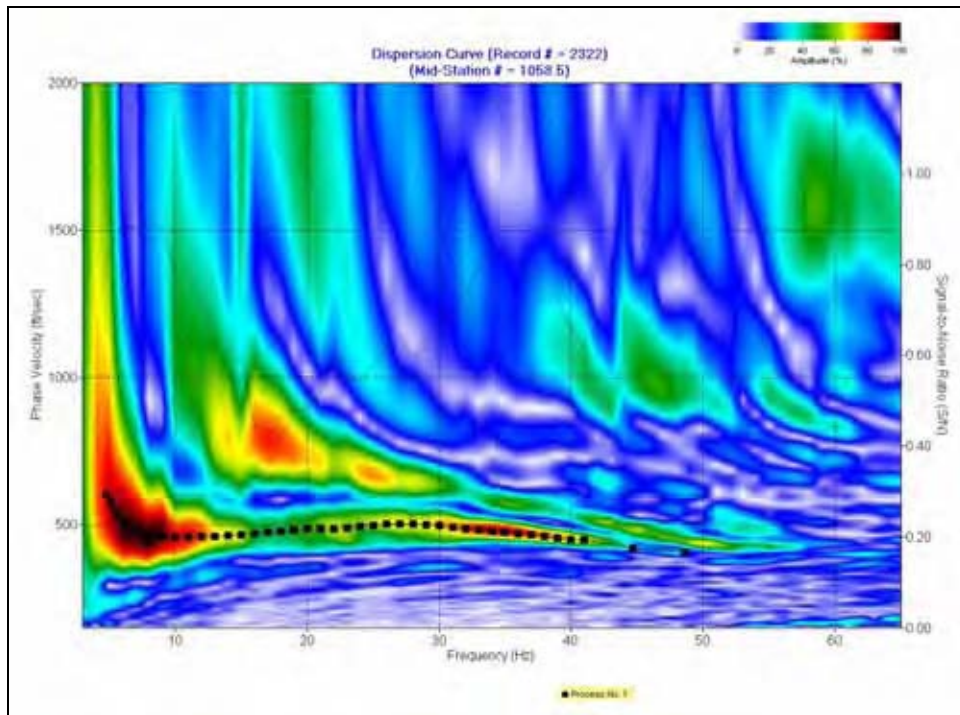


Figure 22. Rayleigh-wave dispersion curve analysis of phase-velocity versus frequency (in units, ft/sec) for November 2004 data collection at site 2 (Ivanov et al. 2005)

During the flood-simulation study at Site 2, seismic measurements were performed prior to the flood test, and at 12-hr intervals for the duration of the test. MASW V_s solutions for seven time periods are presented in Figure 23, and these

correspond to the first 84 hr of the test. Comparison of V_s properties 24 hr after the start of the water fill shows a noticeable change in the shear-wave properties about 5 m below the levee surface, at about horizontal location 950 m. (Note that the pond is located at stations 946 to 961 in Figure 23.) After 26 hr (see Figure 14 for flood curve and water depth), the shear-wave velocity of the levee core (2 to 4 m below the surface) starts to increase between horizontal locations 950 and 955 m. After 48 hr, the water level in the pond is about two-thirds full, and the previously low-velocity zone has reached a shear-wave velocity similar to other parts of the levee. A possible explanation for the observed phenomena is that the water flooding into the relatively drier clay section of the levee caused the clays to expand and fill in the existing cracks, which in turn increased the stiffness of the levee-core material and its shear-wave velocity. During the next three measurement cycles (i.e., 60, 72, and 84 hr, respectively, Figure 23), as the water level approaches maximum pool, no significant changes in levee properties are observed. No further seismic data were collected beyond the sixth day as no changes were apparent.

Refraction-tomography analysis was performed to detect relative changes in the V_p properties due to the flooding experiment (Figure 24). There were no significant changes in V_p due to the flooding and associated soil saturation from the ponded water. Refraction-tomography V_p analysis of the south line suggests that compressional-wave velocity is not sensitive to the material changes from the ponding.

Seismic data summary

Various types of state-of-the-art seismic equipment and methods were appraised and associated data processing performed by the KGS study team. Both fixed geophone arrays and land streamers were tested to determine their use in measuring the seismic properties of levees. A land streamer containing multiple geophones permits rapid collection of seismic data, since the geophone array can be rapidly pulled along the levee surface without having to couple individual geophones to the ground surface. However, land streamers are not as sensitive to high frequencies as fixed geophone arrays because of poor coupling with the levee road surface. Land streamers can be efficiently used with seismic methods emphasizing the low frequencies (MASW), or avoided when high frequencies are of major significance for the survey (i.e., reflection methods). Results of LRGV studies indicate seismic methods by land streamers are possible, but better understanding of the near-surface seismic data from the LRGV is required before land streamer data acquisition is possible in a production-type collection effort. Ultimately, this rapid method of data acquisition will be able to provide cost efficiency in sampling, data processing, and levee distance surveyed.

Levee geometry influences the ability to measure V_s of body waves in the near surface by refraction tomography methods because of mode conversions in the S-waves. Shear-wave velocity measurements calculated from refraction methods of LRGV levees are slightly higher than the actual values and yield erroneously lower V_p/V_s ratios than expected for these soils. Further study and analysis is needed to resolve these near-surface data.

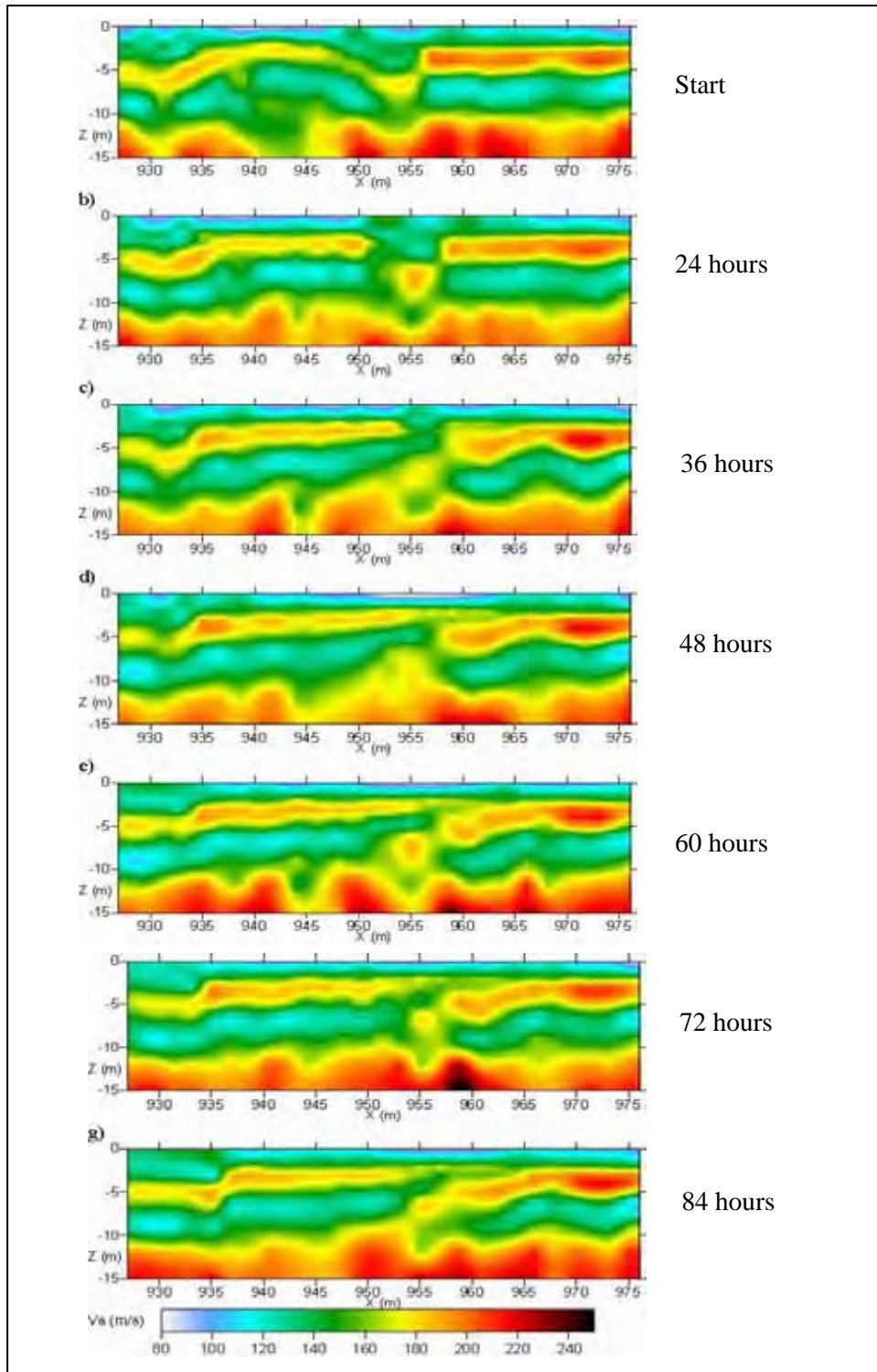


Figure 23. MASW Vs solutions for seven time slices at 12-hr intervals after the start of the test for the south seismic line (i.e., closest line to pond, see Figure 15). Pond is located between stations 946 and 961. View is velocity profile with depth, with view looking approximately due north. Levee base is at about 5 m (15 ft)

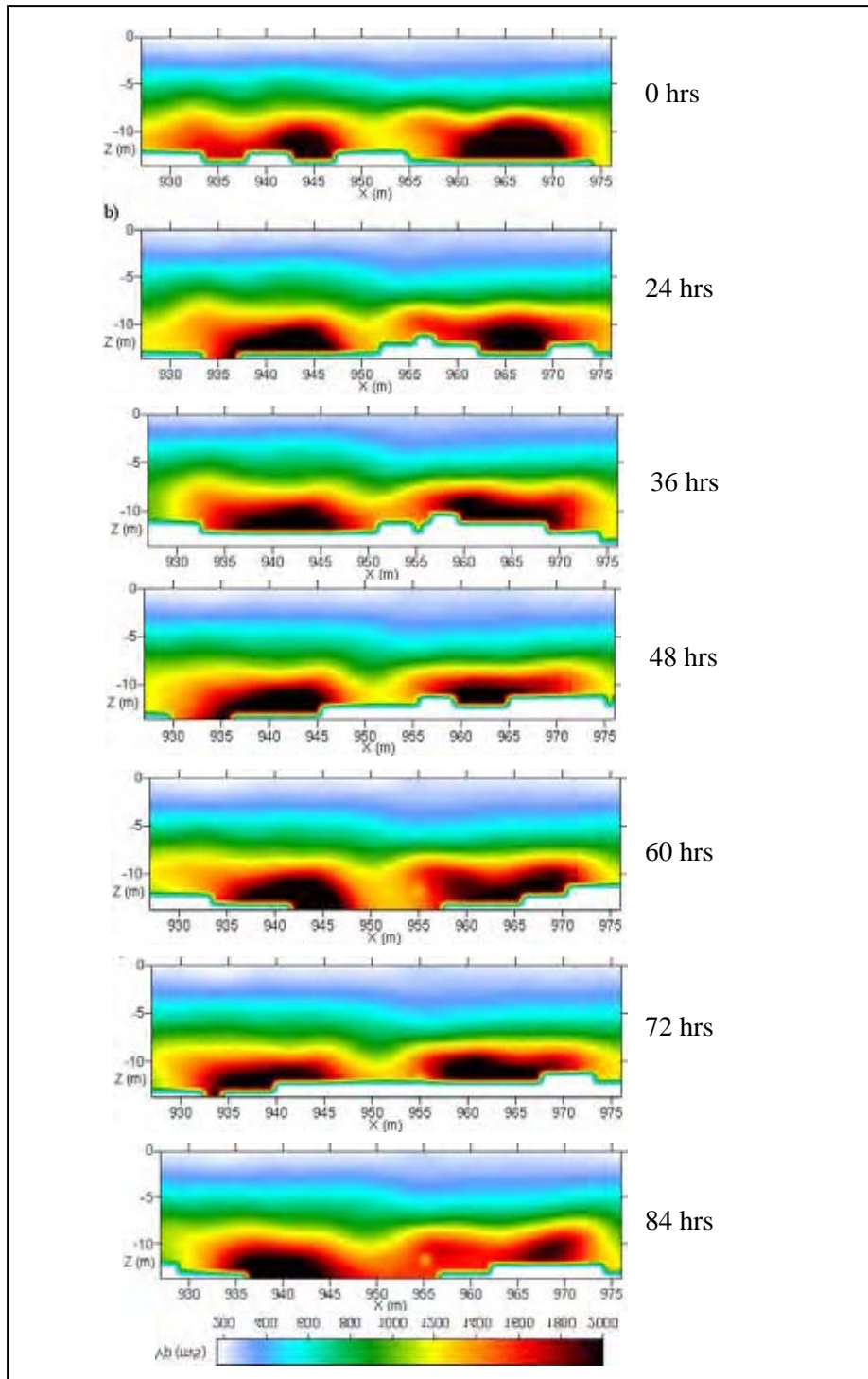


Figure 24. Vp solutions for seven time slices estimated at 12-hr intervals after the beginning of the test at the south seismic line (i.e., closest line to pond, see Figure 15). Pond is located between stations 946 and 961. View is velocity profile with depth looking approximately due north. Levee base is at about 5 m (15 ft)

Shear-wave velocity calculated from surface-wave energy using the MASW methods is sensitive to changes in soil moisture in the levee. Levee soil moisture between the December 2003 and November 2004 seismic surveys was noticeably different. Filling of the test pond caused slight increases in V_s values initially, probably because of the hydration of the clay levee with a corresponding increase in soil density. V_s measured by MASW was the property most significantly affected by the increased saturation and the material property most sensitive to changes occurring during the levee-ponding experiment.

V_p measurements by refraction tomography methods were less sensitive to changes in levee soil moisture. V_p values between the December 2003 and November 2004 surveys were less than 8 percent different between the two survey periods. Changes in levee soil moisture caused no measurable changes in V_p values with rising water levels during flood simulation. This lack of change may be attributed in part to hydration of the levee prior to the second survey because of rainfall and sealing of the small cracks in the outer levee surface and/or core that were present during the trench in October 2003 (Appendix A).

Self-Potential (SP) Methods

Introduction

Self-potential or SP methods were incorporated into the design of the ponding experiment to monitor the movement of the wetting front into and through the levee caused by the flood-simulation test. Because of the deep surface cracking that was observed in October 2003, SP methods were considered to be an ideal method to monitor the movement of water in real time through the levee and its core. ERDC contracted with Dr. Robert Corwin, SP Surveys, El Cerrito, CA, to install an automated SP monitoring system across the levee test area. A report by Dr. Corwin describing the SP instrumentation, survey methods, and results is presented as Appendix F.

SP anomalies are generated by flows of heat, fluid, and ions in the earth (Corwin 1990). A common factor among the various processes thought to be responsible for self-potentials is groundwater (Reynolds 1997). These potentials are generated by the flow of water, by water acting as an electrolyte, and as a solvent of different minerals. Various types of potentials are recognized and are described by Reynolds (1997) and USACE (1995). A streaming potential involves the movement of water through earth materials, causing electrons to be stripped from the mobile atoms within the fluid. Seepage flow typically generates SP anomalies (or changes in voltage (in mV) among the detectors), which show negative polarity associated with the upstream portion of the seepage flow path and positive polarity associated with the downstream portion. Buried near-surface electrodes containing an electrolyte solution can measure the flow of water through earth materials as changes in voltage. Analysis of the shape and wavelength of the SP anomalies can help to determine the depth and configuration of seepage flow paths.

Data collection and equipment

Four lines of SP electrodes were installed against the riverside and landside face of the levee at the midslope and on the edge of the crest as shown by Figure 25 and Figure 26. (See Figure 15 for location of SP lines.) Each SP line contained 20 Farwest electrodes (Model SP-150) at 2.5-ft spacing, which use a plaster filling material saturated with copper-copper sulfate electrolyte. These electrodes are designed for stable, long-term measurement of SP values for corrosion and seepage monitoring applications.



Figure 25. Installation of SP line (line A) along landside crest of levee. See Figure 15 for location of line A

Each electrode array was connected to an automated data acquisition system (Figure 27). Measurements were made every 2 min, starting about 36 hr prior to the test and throughout the duration of the test. Measurements were made between each electrode and a common ground electrode (E3), located 160 ft due east of electrode A20 on the levee crest (Appendix F, Figure 2). Each set of measurements was recorded to a separate data file and involved voltage measurements on a total of 84 electrodes, that is, 80 electrodes in lines A, B, C, and D, plus 1 common electrode (E3), and 3 auxiliary electrodes (E1, E2, and E4) (see Appendix F, Figure 2). Detailed information about the SP equipment, recording interval, data formats, and processing of the different data files is presented in Appendix F.



Figure 26. View of SP line (line A) looking upstream (west). Electrodes spacing is 2.5 ft, total length of line is 50 ft



Figure 27. Data recorders used to measure voltages on each SP line of electrodes

SP monitoring results

SP data processing involved merging the individual SP data files, recorded every 2 min, into a master data file, which was then separated into a series of individual files and data plots according to the different SP lines. SP data were evaluated by Dr. Corwin to identify noise in the data (i.e., solar storms, abnormal telluric currents, etc.), remove erroneous data, perform subsequent analyses, and identify any temporal trends. These data were summarized for final presentation. One source of noise in the SP data was created when resistivity measurements were performed by the ERDC team. Current was injected into the ground as part of the resistivity measurement process and affected the SP record. Resistivity affected records were removed from the SP files wherever possible to better observe the time-related trends in the data.

SP data are summarized and displayed both as time series and as spatial profiles (Figure 28 to Figure 34). Time series plots of selected electrodes (i.e., 0, 5, 10, 15, and 20) are presented in Figure 28 to Figure 31 and span the SP monitoring period from 6 through 16 November 2004. These five electrodes are representative of the levee reach and show the general trend and changes in voltage observed during the duration of the test. A graph of the flood height is included in each of these figures to compare the flood stage height with any associated changes in voltages. The graphs identify cyclic changes in the data. Sources of external SP variations are diurnal temperature changes and telluric voltages generated by geomagnetic activity. Temperature variations are responsible for the approximate 24-hr periodicity of up to a few mV amplitude visible on all the profiles. However, temperature-induced variations should not obscure longer term seepage-related trends (Corwin 2005).

Dr. Corwin reports the presence of an extremely powerful magnetic storm in the data between 7 and 12 November. The effects of this storm are evident in Figure 28 to Figure 31 as a higher short-period noise level for the SP readings during the period of 7 to 12 November, compared with those after 12 November. This noise is especially evident on the generally quieter downstream lines (A and B). Large SP deviations on 7 November are considered by Dr. Corwin to result from a combination of magnetic storm onset and electrode stabilization effects.

The most notable feature observed in the time series profiles is the large positive jump that occurred on 10 November in the riverside (upstream) line C (Figure 28). This jump was caused by submersion of the electrodes beneath the water surface, and the resulting saturation of the soil, when the pond elevation reached Line C at an elevation of 90.7 ft. Analyses of the SP data in the time series plots from lines D, A, and B (Figure 29 to Figure 31, respectively) by Dr. Corwin indicate no specific trends in the data that indicate anomalous conditions attributed to seepage (Appendix F).

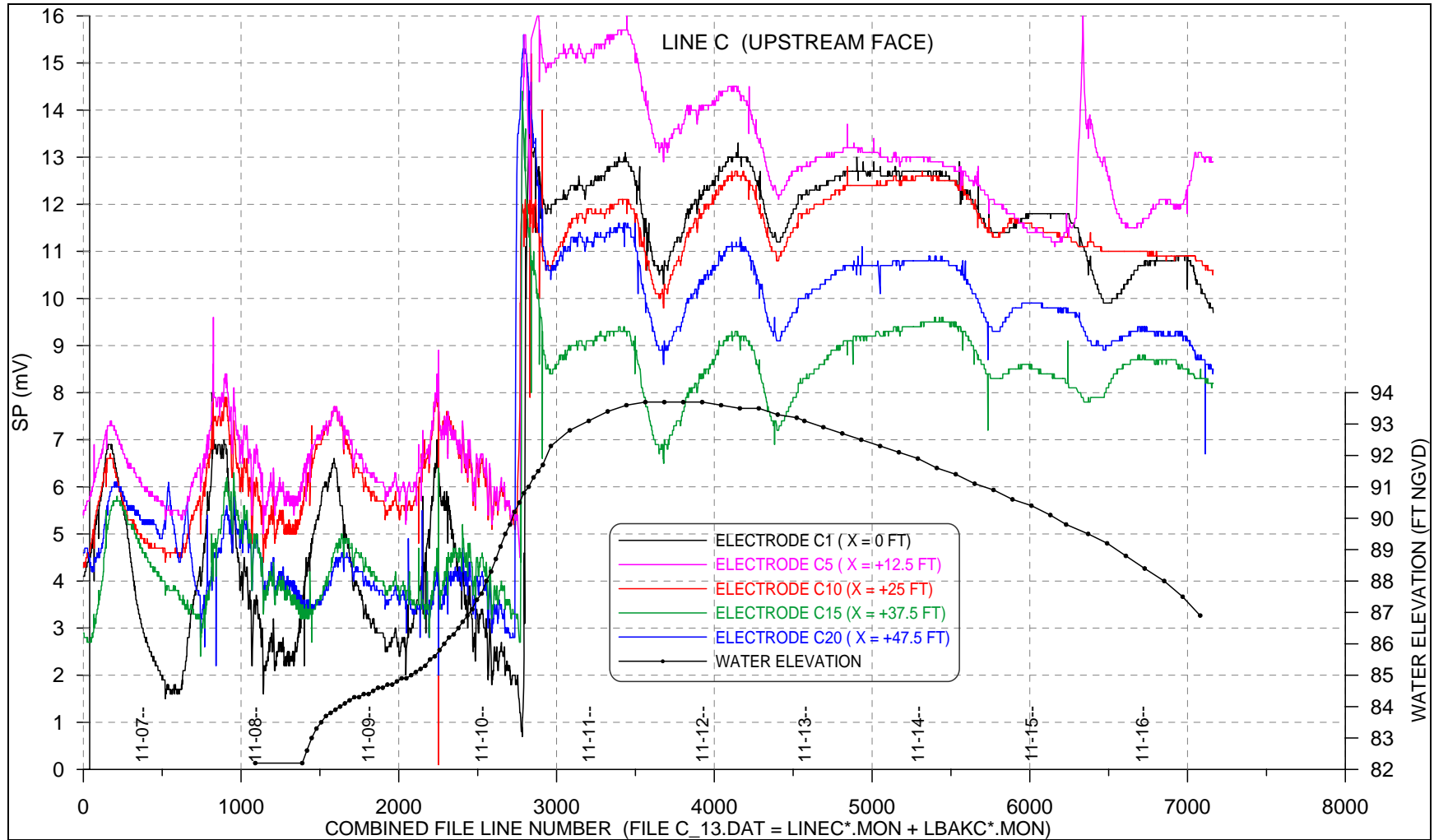


Figure 28. SP monitoring data for Line C (upstream face). Note that electrodes are submerged approximately midway during test, causing sharp increase in voltage

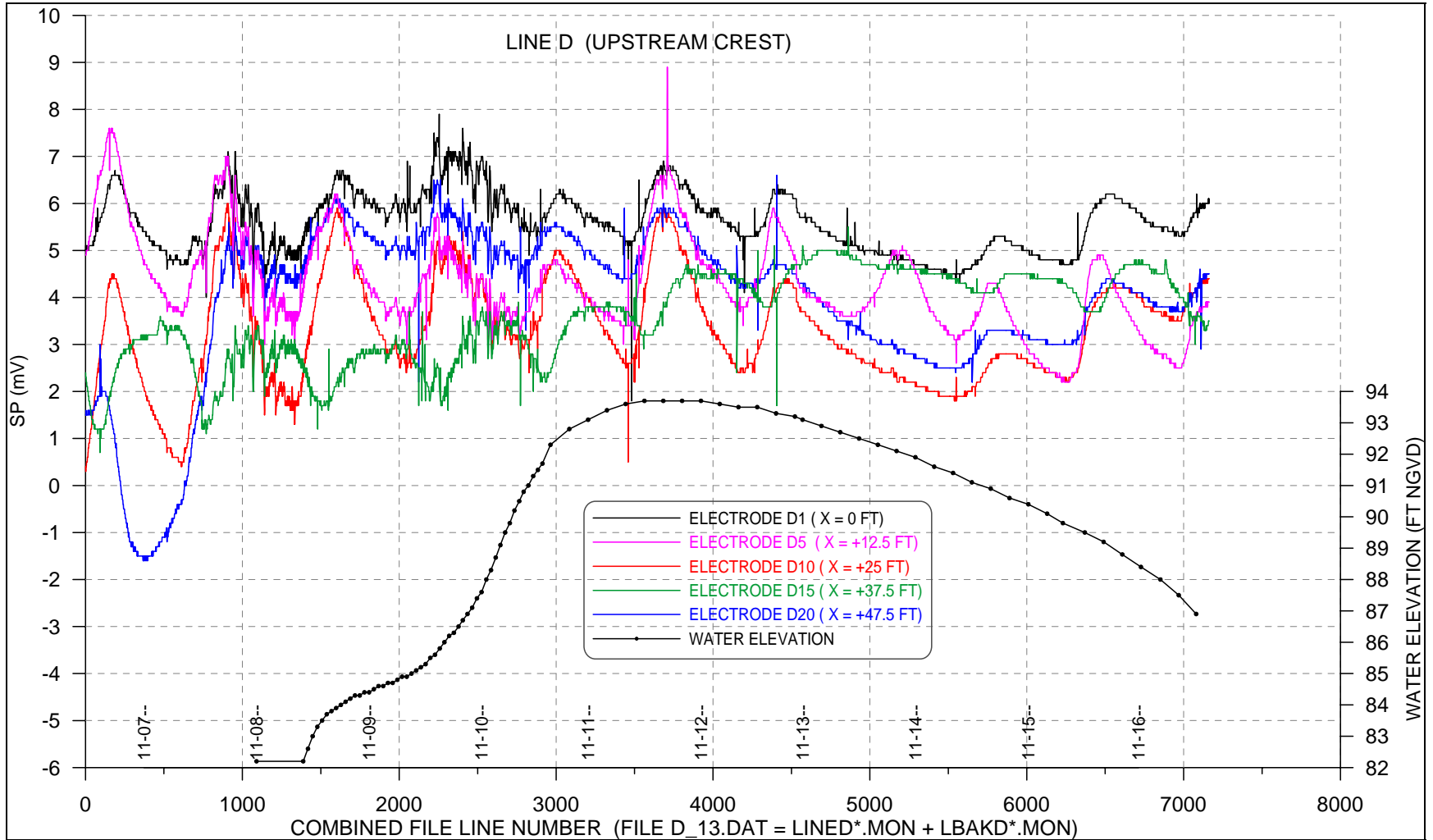


Figure 29. SP monitoring data for Line D (upstream crest)

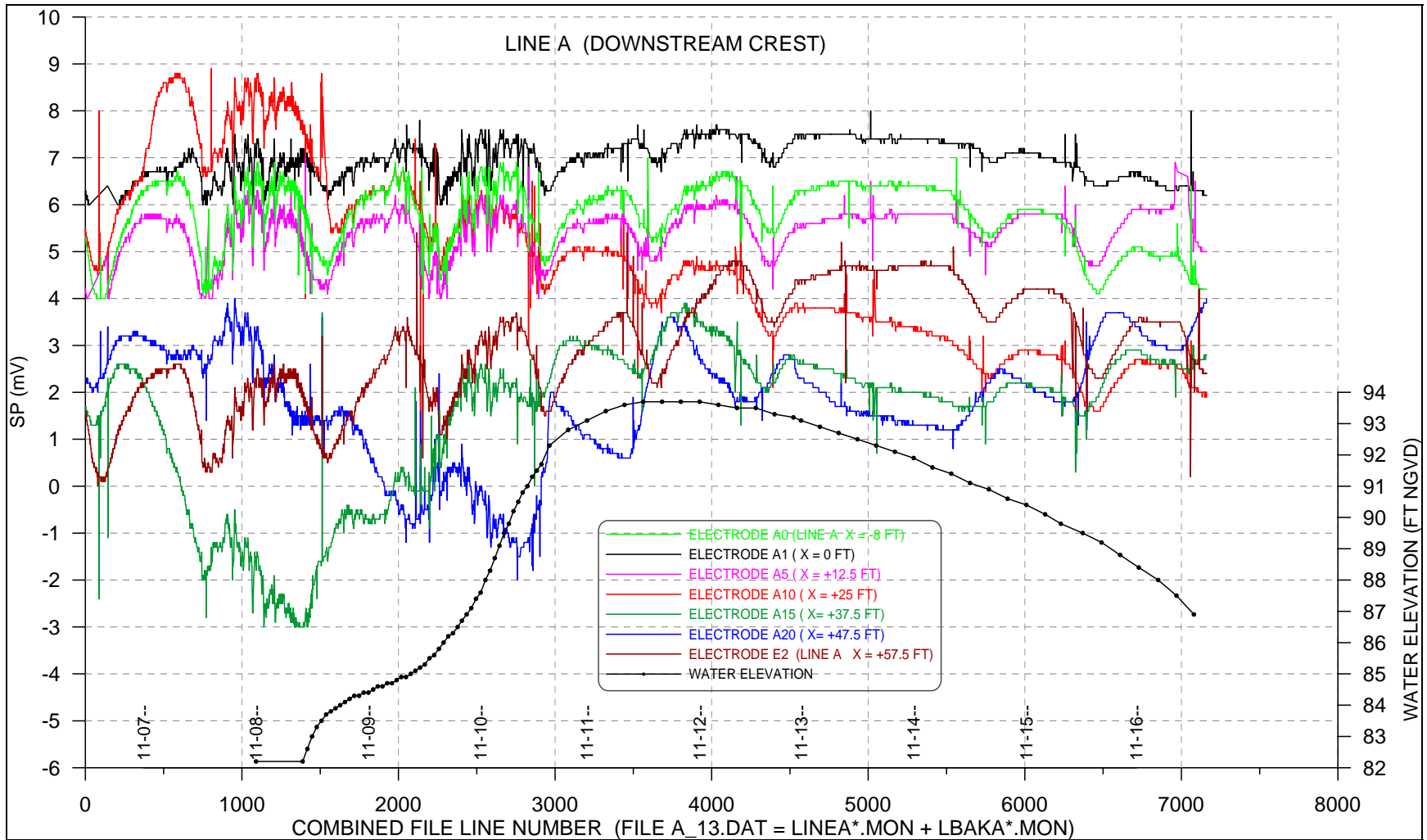


Figure 30. SP monitoring data for Line A (downstream crest)

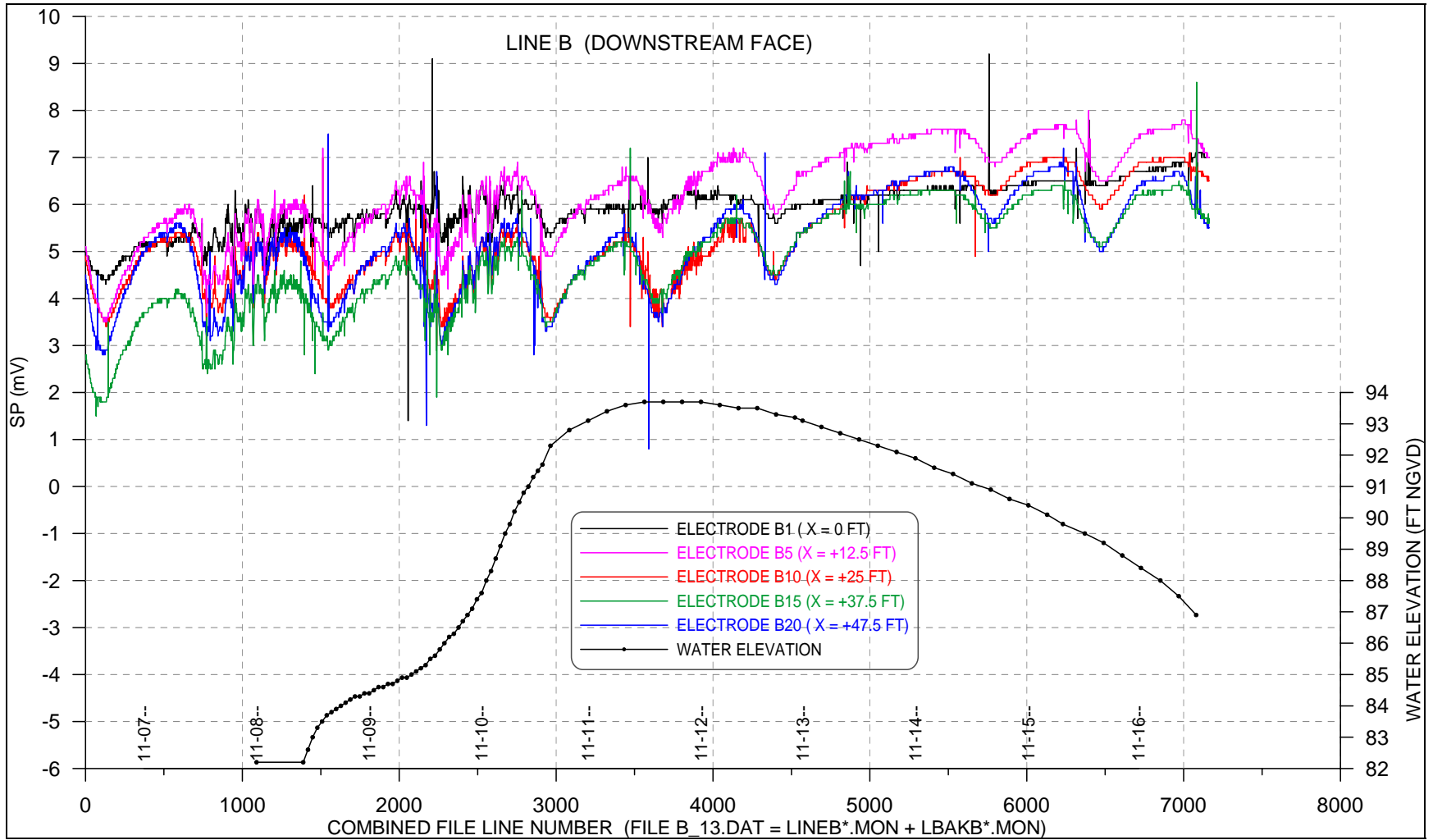


Figure 31. SP monitoring data for Line B (downstream face)

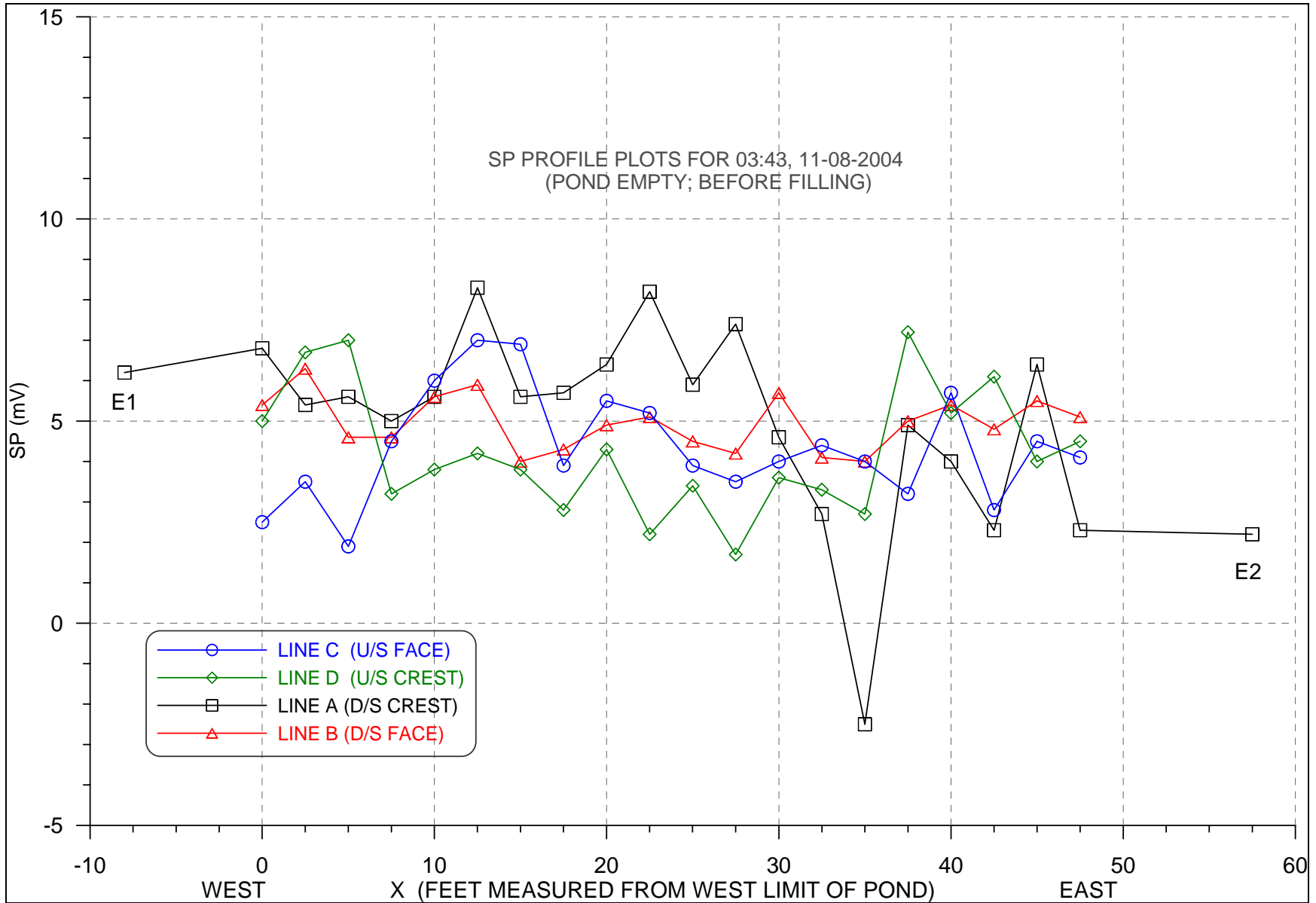


Figure 32. SP profile plots with pond empty (before filling)

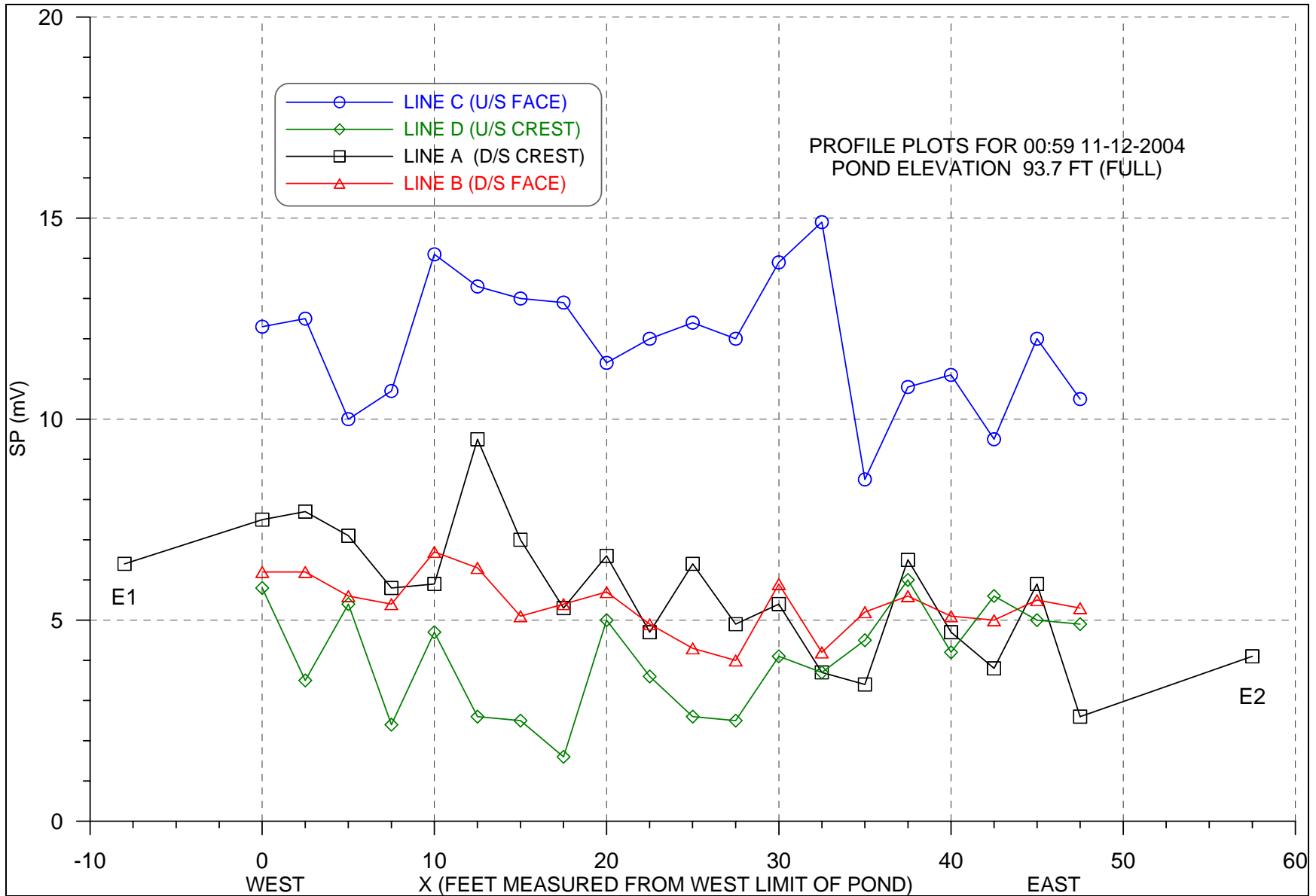


Figure 33. SP profile plots with pond full (el 93.7 ft)

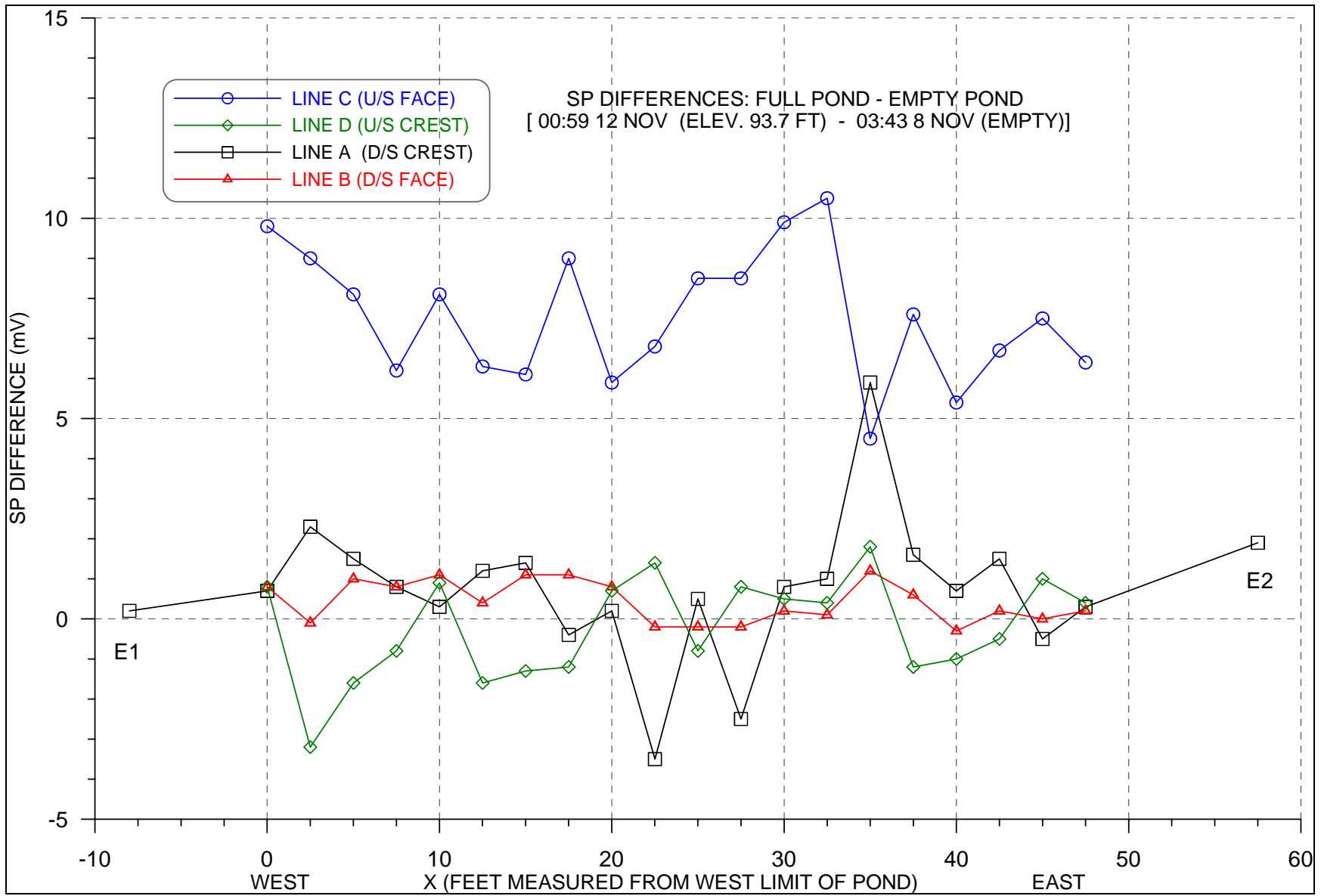


Figure 34. SP difference profile plots (full pond at el 93.7 ft – empty pond)

Another summary view of the data compares all the electrodes along a single monitoring line (A, B, C, and D) at a given instant of time. Times selected for comparison were the empty pond, full pond, and the difference between these two states (Figure 32 to Figure 34, respectively). A full pond would be expected to affect the SP profiles if seepage were occurring along the levee face, especially if the levee surface contained appreciable cracking. Concentrated seepage would be expected to produce a negative anomaly near the affected electrodes and a positive anomaly above the electrode at the downstream flow path. No anomalous conditions are observed in the profile plots of these data. Other plots of the electrode data are presented in Appendix 2 in Dr. Corwin's report (see Appendix F), as well as complete descriptions and analyses of the data.

In summary, SP data were inspected by Dr. Corwin in the form of both time series (plots of individual electrode readings versus time) and spatial profiles (plots of the readings for all the electrodes along a given monitoring line at a single point of time). None of the data showed any obvious indication of the development of either uniform or concentrated seepage flow within the embankment in response to changing water levels within the pond. These results suggest that the embankment soil was of very low permeability, and that there were no cracks or other features that allowed significant water flow through the embankment.

Resistivity Methods

Introduction

Resistivity measures how well the soil conducts an electrical current. Factors that directly affect the electrical resistivity of a soil are its grain size (soil type), water content, porosity, and the presence of conductive minerals in the soils, or ions in the fluids between the individual soil grains. Resistivity measurements were included as part of the flood-simulation study to identify any seepage pathways that occur through or under the levee related to the flood test. Seepage beneath or through the levee soils would be expected to produce a change in the soil resistivity along the flow path. Measurements were made at the start of the flood test to determine background values, and daily throughout the test to monitor changes in soil resistivity from possible seepage. Resistivity monitoring measures changes in soil moisture in the levee as it influences the electrical properties of the soil, whereas self-potential methods (described above) measure potential differences as water moves through the soil column.

Resistivity measurements used for this study incorporated direct ground contact methods, as compared to the electromagnetic-induction methods used in the airborne surveys of LRGV levees, or the ground-based EM surveys used to assess San Diego levees (Dunbar and Llopis 2005). Resistivity is the reciprocal of conductivity. Airborne conductivity measurements were made in June 2001 and indicated the Retamal levee soils displayed low conductivity (or high resistivity) characteristics. Recall that these signatures were considered anomalous based on the available engineering and boring data from the Retamal levee, which indicated the levees were composed of clay soils, and should have

measured much higher conductivity (lower resistivity) values. Resistivity methods used in the levee flood test are at a much higher resolution than previous EM surveys, and measure true resistivity as opposed to apparent resistivity.

Variations in resistivity can occur from changes in the physical conditions at a site, and because of different survey methods and geophysical instruments that are used to measure this property. In practice, different geophysical methods and instruments measure an apparent resistivity (or conductivity), rather than a true resistivity. Characteristics of each geophysical instrument, the survey methods that are used, and the volume of earth material that is actually being measured by these different instruments and techniques will affect the measured values. Because of these differences, variations can occur in the actual resistivity values that are measured. Therefore, resistivity surveys will usually measure an apparent resistivity and require an inversion of these data to calculate the true resistivity. The relationship between apparent and true resistivity is complex and requires a mathematical analysis using advanced computer processing techniques (inversion) to derive a true resistivity profile of the subsurface.

Data collection and equipment

Resistivity surveying involves injecting direct current into the ground through two current electrodes (C1 and C2) and measuring the resulting voltage difference at two potential electrodes (P1 and P2), as shown in Figure 35. A dipole-dipole array was used for this study since it is sensitive to measuring lateral resistivity changes. Various arrangements and spacing of the current and potential electrodes are possible in performing resistivity surveys. Advantages and disadvantages of the different electrode configurations are described by Reynolds (1997) and USACE (1995).

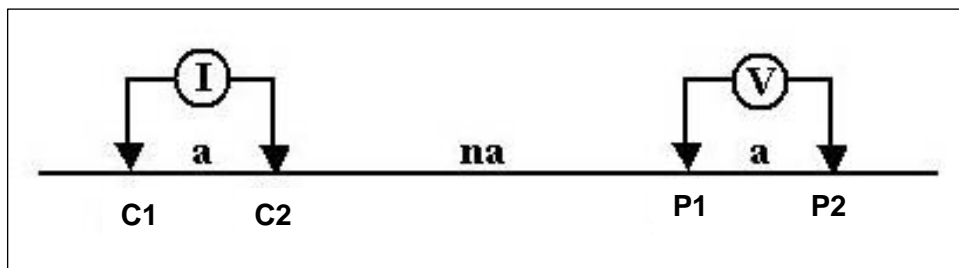


Figure 35. A dipole-dipole electrical resistivity profile array (I = current, V = voltage, C1 and C2 are current electrodes, P1 and P2 are potential electrodes, a = spacing between electrodes, and n = the ratio of the distance between the C1 and P1 electrodes to the C1-C2 (or P1-P2) dipole separation) (USACE 1995)

The dipole-dipole method involves a series of measurements along the electrodes in each line, based on the “ a -spacing” (Figure 35). To increase the depth of investigation into the subsurface, the distance between the current and potential electrode pairs is systematically increased by a distance or factor of “ n .” The value of n increases by a multiple of the a -spacing, where n is the ratio of the distance between the C1 and P1 electrodes to the C1 and C2 (or P1 and P2)

separation distance. Increasing the distance between the current and potential electrodes allows for measurements of a larger volume of the ground. The n-factor was increased to six times the a-spacing for the Retamal levee. Measurements are repeated for each new n value, until all the electrode combinations have been sampled.

Three 80-m-long resistivity lines, with 2-m spaced electrodes, were installed along the riverside crest (labeled crest), landside midslope (labeled face), and landside toe (labeled toe) of the levee. (See Figure 15 for location of resistivity lines.) The center of the resistivity array corresponds to midpoint of the pond (Figure 15). Electrodes used during the test are 1/2-in.-diameter steel rods driven about 2 ft into the ground with several inches above ground to connect a wire lead. Wire leads from each electrode were run to a common measuring point behind the RV that was used as the command-post for the flood experiment (Figure 36). Two resistivity cables were daisy-chained together to connect the 40 electrodes in each line to the automated resistivity meter and measuring system. Electrodes were connected to the meter at the cable in a numbered order each time the survey was repeated. Surveys were performed daily during the test on each line.

A Scintrex, Ltd., automated resistivity imaging system (SARIS) was used in this investigation (Figure 36). The Scintrex meter has a series of programmable data menus and inputs that automates the sequence of measurements to be performed. Information entered in the setup includes the type of array to use (dipole-dipole, Wenner, Schlumberger, etc.), electrode spacing, n-factor, and other survey parameters (such as the current to use). A program in the meter then automatically selects the appropriate electrodes for each measurement, and a roll-along measurement method is used to advance the profile line. Measurements are taken in a systematic manner by the SARIS system, until all possible combinations of measurements in each line are recorded. These data were transferred to a computer at the end of the survey day for computer processing using RES2DINV by Geotomo Software, Penang, Malaysia, for inversion of the resistivity measurements.

Resistivity results

Daily resistivity measurements were processed by the RES2DINV software to develop resistivity depth section of the subsurface to evaluate any changes that occurred from controlled ponding of water against the levee. Daily time series resistivity profiles are presented in Appendix G for the levee crest, face, and toe, respectively. These profiles show changes occurring between time 1 and succeeding time intervals (i.e., time 1 vs. time 2, time 1 vs. time 3, time 1 vs. time 4, etc.). Comparisons of summary resistivity profiles are presented in Figure 37 to Figure 40, corresponding to changes between time 1 and the last time (time 9) for the crest, face, and toe, respectively. The lower profile in Figure 37 and Figure 38 (and in Appendix G) represents the percent change that occurred between time 1 and the time period identified by each profile.



Figure 36. Resistivity measurement station behind RV during the flood test. (Electrodes in each resistivity line were connected to blue cable at numbered take-out locations. Numbered electrodes from each line were connected to a specific location on the blue cable. Blue cable plugs into the SARIS automated electrical resistivity meter, which records voltage measurements between the potential electrodes to data files, and automatically advances the measurement location along the electrode array by a specified distance. Resistivity profiles of the subsurface along each line are produced by inversion of these data by computer programs)

Additionally, the center point of the resistivity array corresponds to the midpoint of the pond, with the pond extending roughly 8 m (~25 ft) on each side of station 40, and extending from station 32 to 48 (see Figure 15, Figure 37 and Figure 38).

Resistivity values and contours in the profiles are ohm-m units. Note that the color range is different for each line (crest, face, and toe), but is consistent among succeeding time intervals for each line. Different color tables were used to enhance resistivity data among the different lines and the range of data in each line. A time series view, with subsequent data compared to time 1, was considered to be an easy and efficient method to present the resistivity data. The profiles showing percentage change use a consistent color table among all the illustrations to easily compare subsequent changes.

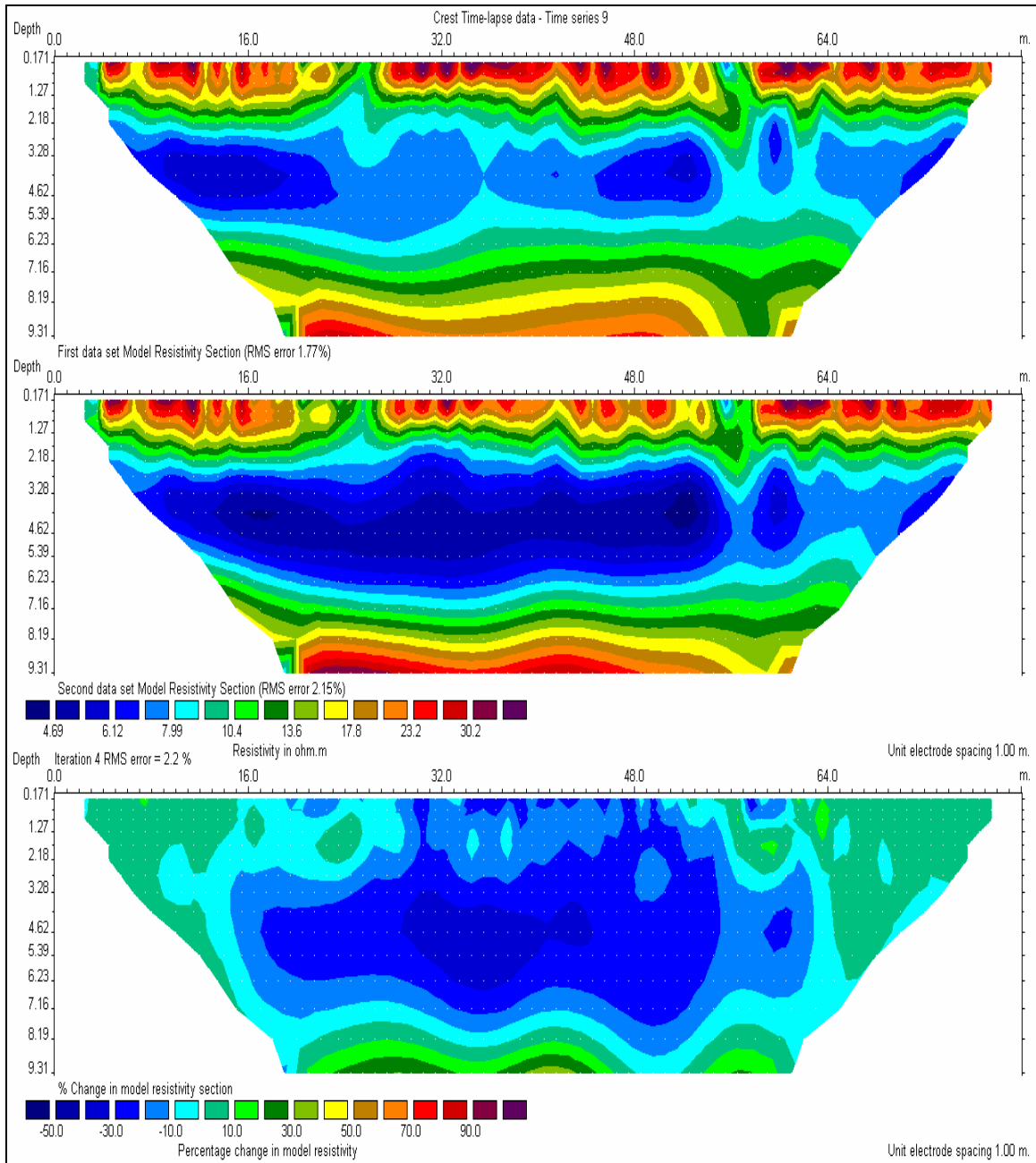


Figure 37. Time lapse comparison of resistivity data from the levee crest at the start (time 1) and end (time 9) of flood test. (Upper profile represents a resistivity model of levee and foundation after inversion of the resistivity data at the beginning of the test. Middle profile is a resistivity model of levee and foundation at the end of the flood test, 193 hr and 40 min later. Lower profile represents the percent change between the two profiles. Appendix G contains a complete set of profiles for the crest for each day to review daily changes. Pond located between stations 32 and 48)

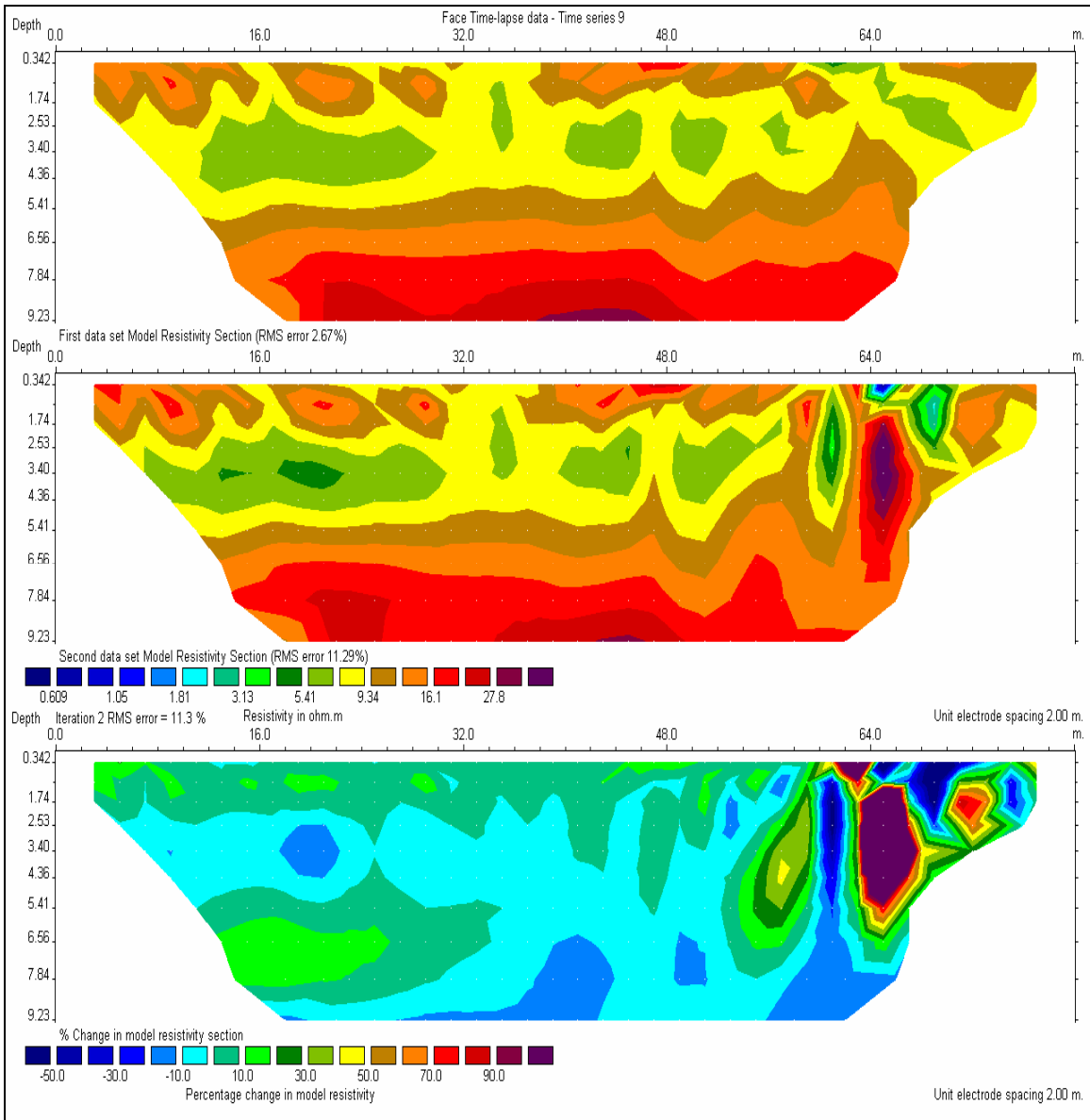


Figure 38. Time lapse comparison of resistivity data from the levee face at the start (time 1) and end (time 9) of flood test. (Upper profile represents a resistivity model of levee and foundation after inversion of the resistivity data at the beginning of the test. Middle profile is a resistivity inversion model of levee and foundation at the end of the flood test, 195 hr and 39 min later. Lower profile represents the percent change between the two profiles. Appendix G contains a complete set of profiles for the face for each day to review daily changes. Pond located between stations 32 and 48. Note that color scale and range are different from Figure 37 and Figure 39)

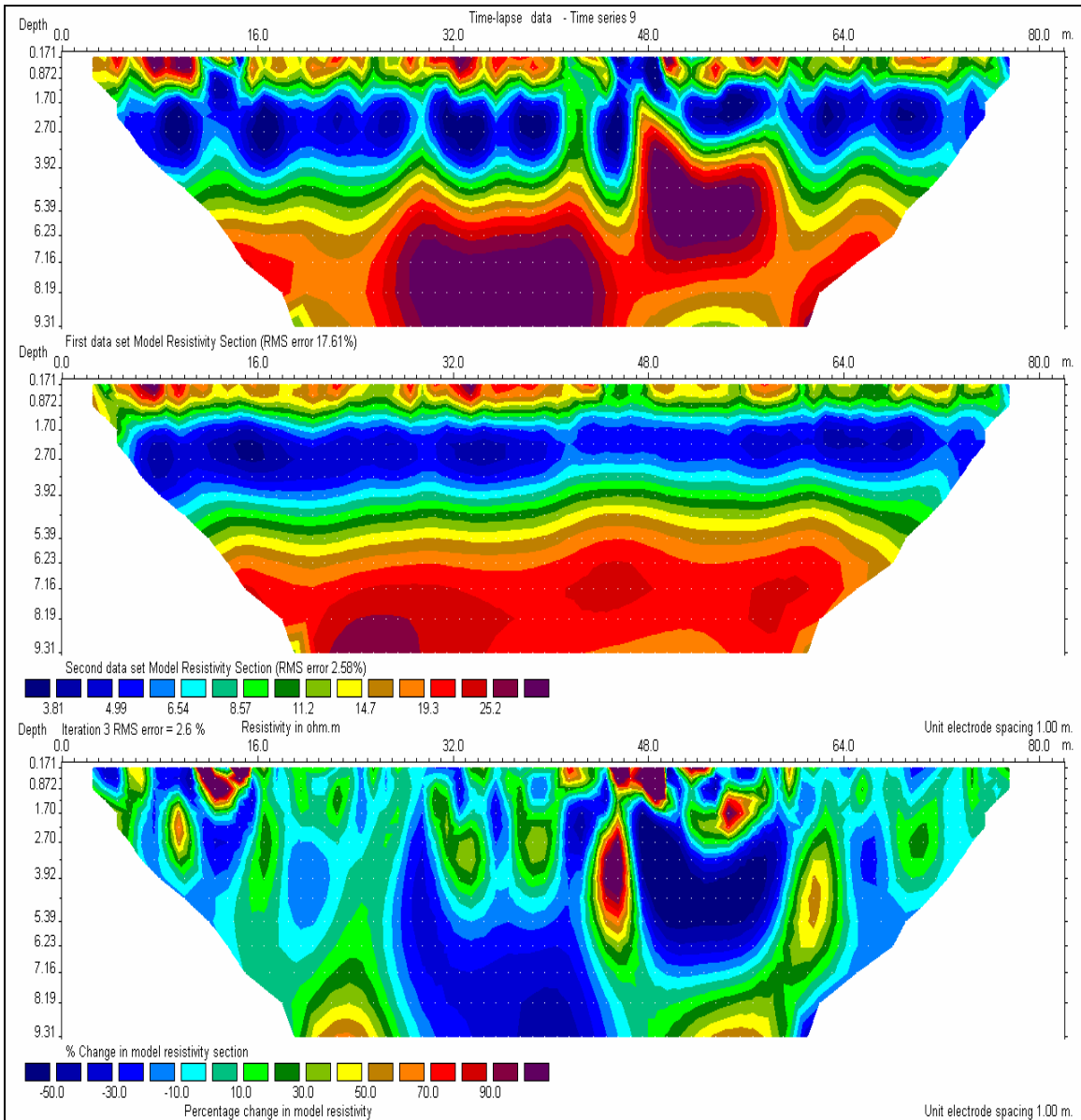


Figure 39. Time lapse comparison of resistivity data from the levee toe at the start (time 1) and end (time 9) of flood test. (Upper profile represents a resistivity model of levee foundation after inversion of the resistivity data at the beginning of the test. Middle profile is a resistivity inversion model of levee foundation at the end of the flood test, 191 hr and 47 min later. Lower profile represents the percent change between the two profiles. Appendix G contains a complete set of profiles for the face for each day to review daily changes. Pond located between stations 32 and 48. Note that color scale and range are different from Figure 37 and Figure 38)

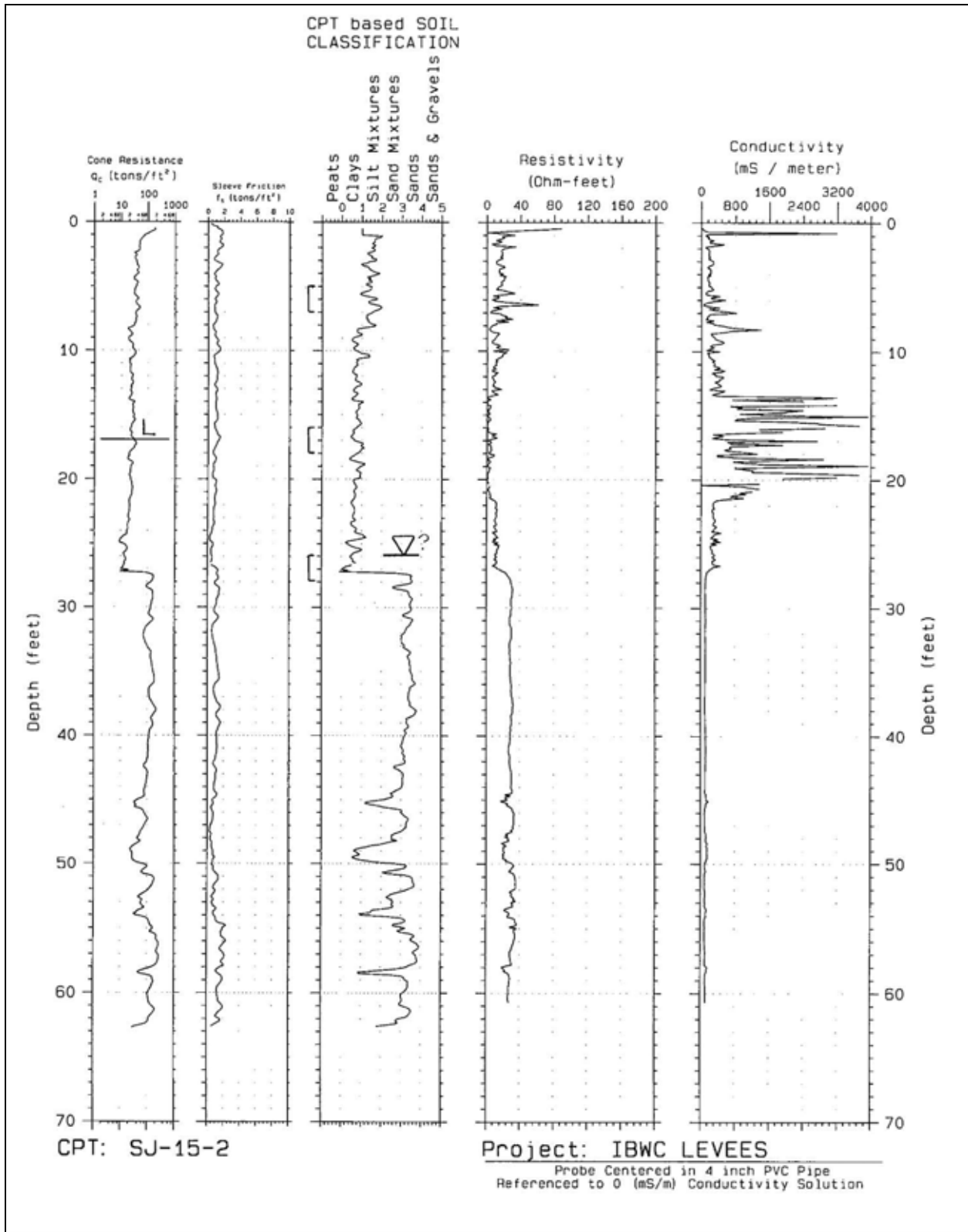


Figure 40. Cone penetrometer log SJ-15-2 pushed 10 December 2002 at levee center line near pond

Comparison of resistivity profiles in Figure 37 to Figure 39 and Appendix G indicates that the general range in values extends from about 5 to 30 ohm-m. All the resistivity sections extend to a depth of about 9 m (29.5 ft) and generally identify an increase in values with depth. For comparison purposes, Table 8 presents resistivity values for some common soils (Reynolds 1995). Values above 25 ohm-m probably correspond to coarser soils as determined from existing boring logs and geologic data (Figure 11).

Table 8 Resistivities of Common Soils and Unconsolidated Sediments (Reynolds 1997)	
Material	Nominal Resistivity (Ohm-m)
Clays	1 – 100
Alluvium and sand	800 – 1000
Soil (40 percent clay)	8
Soil (20 percent clay)	33
Top soil	250 – 1700
Clay (very dry)	50 – 150
Gravel (dry)	1400
Gravel (saturated)	100
Quaternary/Recent sands	50 – 100
Dry sandy soil	80 – 1050
Sandy clay/clayey sand	30 – 215
Sand and gravel	30 – 225

The resistivity models in Figure 37 to Figure 39 and Appendix G are consistent with geological information previously collected from this reach. Boring data from this study (Appendix A) and from a deeper cone-penetrometer boring taken at this location in December 2002, presented in Figure 40 (from Dunbar et al. 2003), show the base of the levee occurs at a depth of between 13 and 17 ft, the base of the top-stratum (upper clay unit) is at 28 ft, and below this depth are the substratum sands, which extend to depths in excess of 100 ft (Figure 11). Resistivity sections clearly identify the top of the substratum sands at about 8 m along the crest section (Figure 37), about 7 m along the landside face section (Figure 38), and about 5 m at the toe section (Figure 39). Above the top-stratum sands, low resistivity clay soils are identified in all the sections for the top-stratum and overlying levee. Resistivity values are consistent for clay soils (see Table 8). Furthermore, their vertical distribution generally corresponds to their position in the available boring data. A higher resistivity layer occurs at surface to about the upper 1 m, probably because of gravel incorporated into roadway and upper levee soils. This resistivity picture is generally consistent with the geophysical and boring data from this reach.

Included in the 2001 boring data are electrical measurements of soils that were performed as part of the verification studies of airborne EM signatures (Dunbar et al. 2003). Identified in Figure 40 are point resistivity values from an instrumented cone that was used to verify the texture of the underlying levee soils, to measure electrical properties, and to correlate these soils to both airborne EM signatures and point resistivity measurements. Values of resistivity (ohm-feet) measured by this down-hole instrument are generally below 20 ohm-ft, with local variations due to sand, silt, and clay layers. Resistivity values increase to 30 ohm-ft at 27 ft below surface, corresponding to the top of the substratum deposits.

Comparison of the upper and middle profiles in Figure 37 to Figure 39 identifies changes in levee and foundation resistivity caused by the flood pond. Cumulative changes in levee resistivity between the initial and end states are identified by the lower sections in Figure 37 to Figure 39. The resistivity profiles for the crest (Figure 37) and toe (Figure 39) indicate resistivity decreased (conductivity increased) in the levee and upper foundation (top-stratum) over the course of the rise and fall of the levee pond. Also, the resistivity profile at the levee toe shows localized variations in resistivity, especially at station 46, at 3- to 4-m depth. It is possible that temperature effects and/or contact problems with this electrode could be responsible for the higher resistivity values. The resistivity profile for the landside levee face also shows significant changes along the western (upstream) edge of the profile. This area is nearly 12 m upstream from the edge of the pond.

To better resolve observed changes in resistivity, especially for the higher resistivity areas noted, daily changes in the resistivity model are compared with time 1 in Figure 41 to Figure 43 for the crest, landside face, and toe, respectively. Additionally, resistivity profiles for each line are presented in Figure 44 to Figure 46 to permit comparison between contiguous measurement periods. The series of illustrations showing percent change (Figure 41 to Figure 43) is highly revealing. Significant changes occur in resistivity along the levee crest during the flood cycle (Figure 41). Resistivity generally decreases between 30 and 40 percent during the flooding, and the shape of the area that is impacted increases in size and volume over the course of the flood cycle. The peak of the flood stage occurs between 90 and 120 hr (see Figure 14) and is generally reflected by these profiles. These data are consistent with clay soils that become wetter, and the electrical conductivity increases or the resistivity decreases, because of changes to the soil moisture in the levee. Localized high resistivity changes are present at about 120 hr, but disappear in later measurements.

A similar trend is identified in the profile for the landside face in Figure 42, but the difference is not as significant as changes occurring to the crest. A low resistivity zone occurs at the base of the profile starting about 75 hr after the start of the test. This low resistivity zone is constant throughout the flood cycle, and generally does not increase in size or volume. A poor ground contact at the western (upstream) end or a localized anomaly is present that is consistent for all the measurements shown. This series of profiles indicates the flood cycle has caused only minor changes in resistivity at the landside face.

Profiles depicting change at the landside levee toe in Figure 43 are complex and difficult to interpret, but are generally consistent over the entire measurement cycle when compared with time 1. The shape and position of the various anomalies are constant except for measurements at about 95.75 and 145.5 hr. This trend disappears during the final two measurements, with resistivity closer to the earlier time intervals. Because the percent change is based on the initial set of measurements, this first profile was examined closer in Figure 39, Figure 43, and Figure 46. The most significant differences between times 1 and 9 are the higher resistivity zones at around stations 32 and 50. Both of these zones diminish in

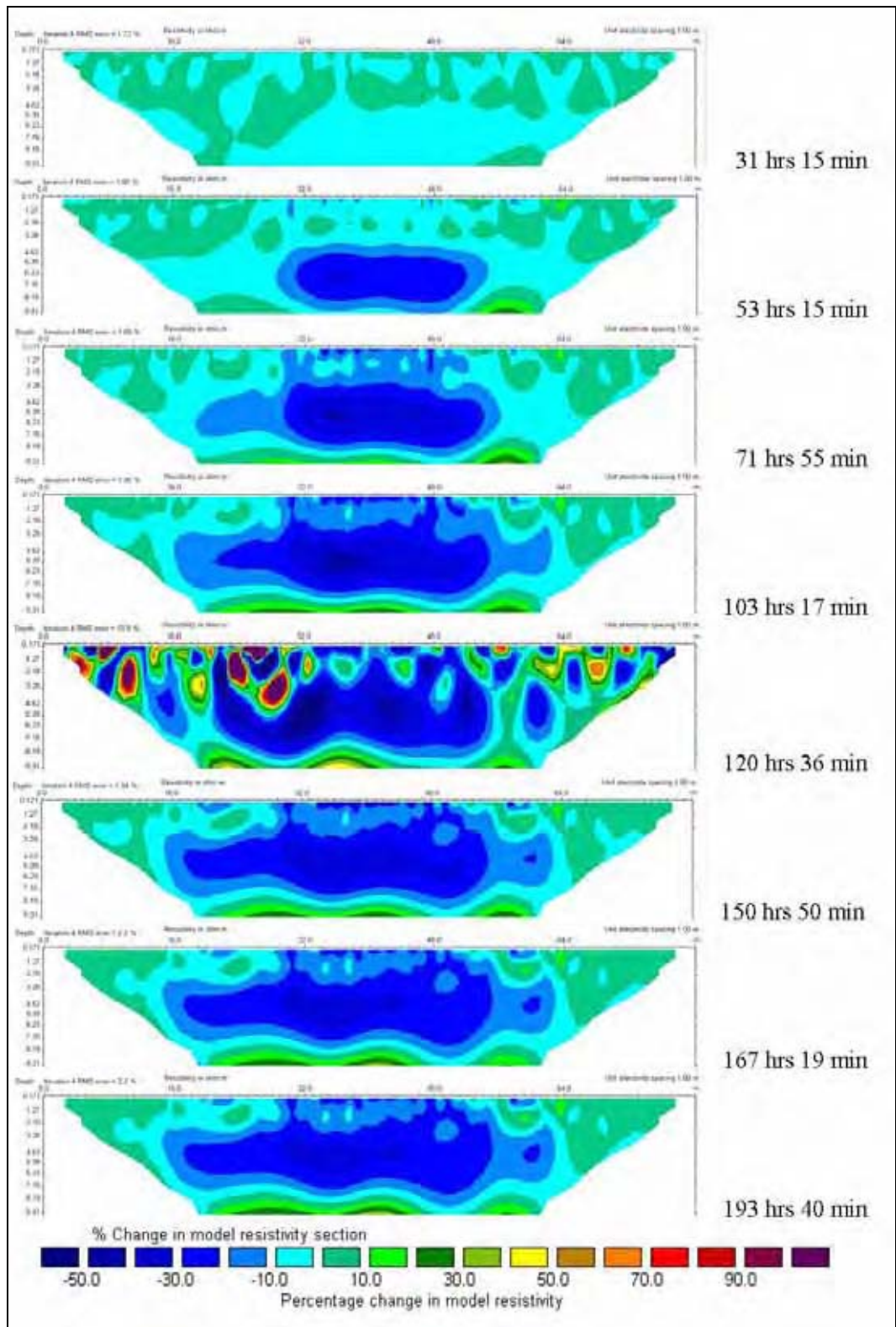


Figure 41. Percent change in model resistivity for levee crest

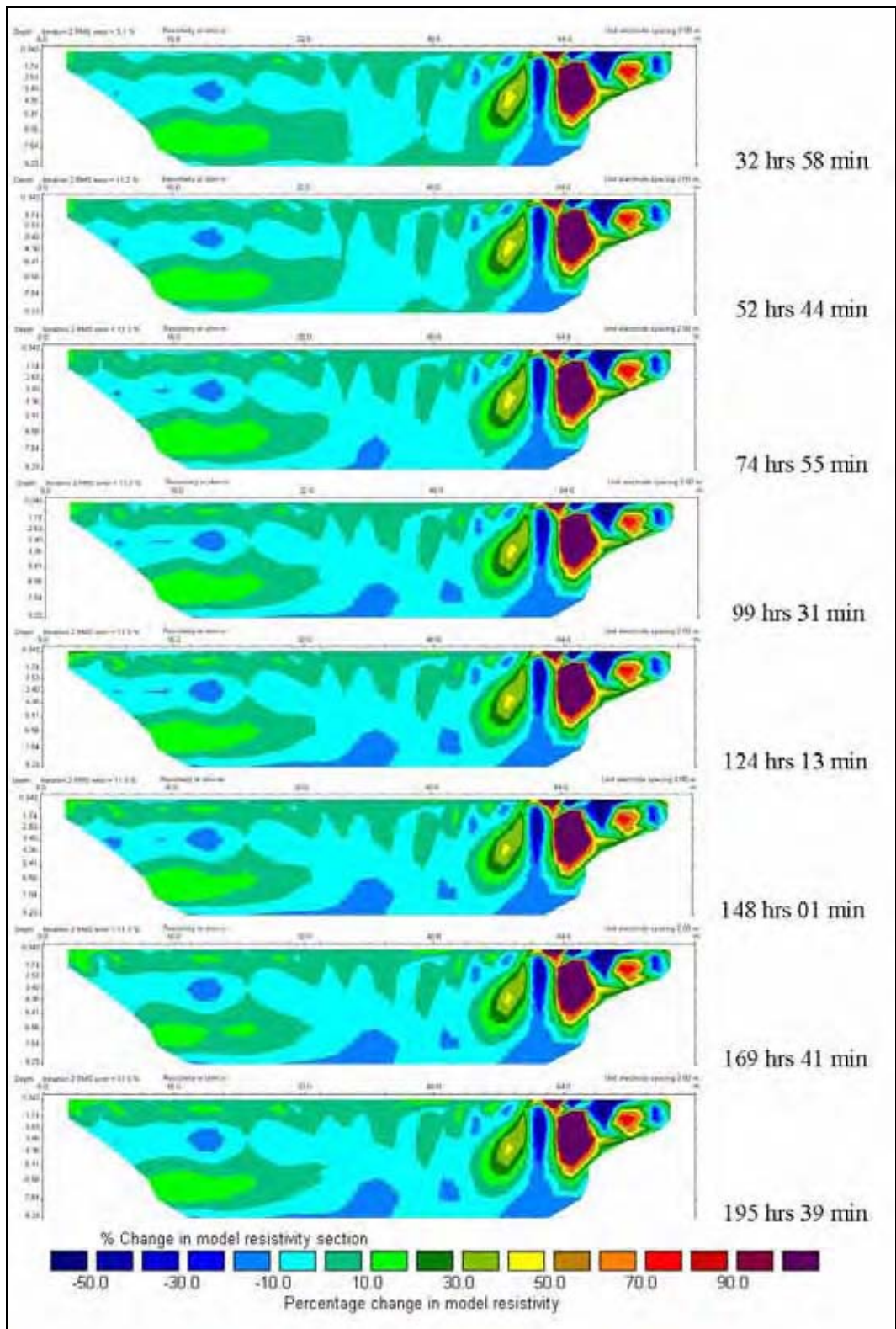


Figure 42. Percent change in model resistivity for levee face

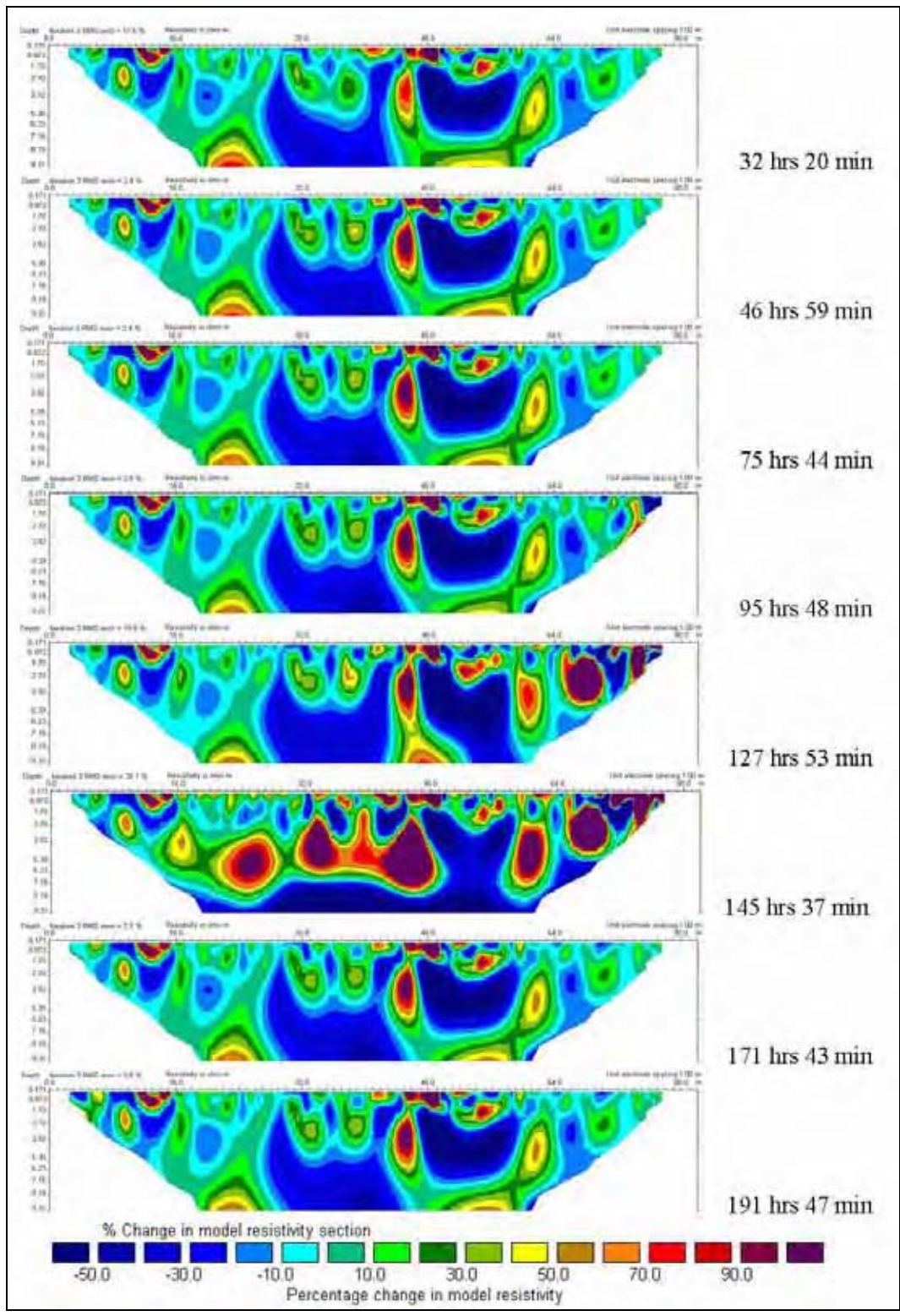


Figure 43. Percent change in model resistivity for levee toe

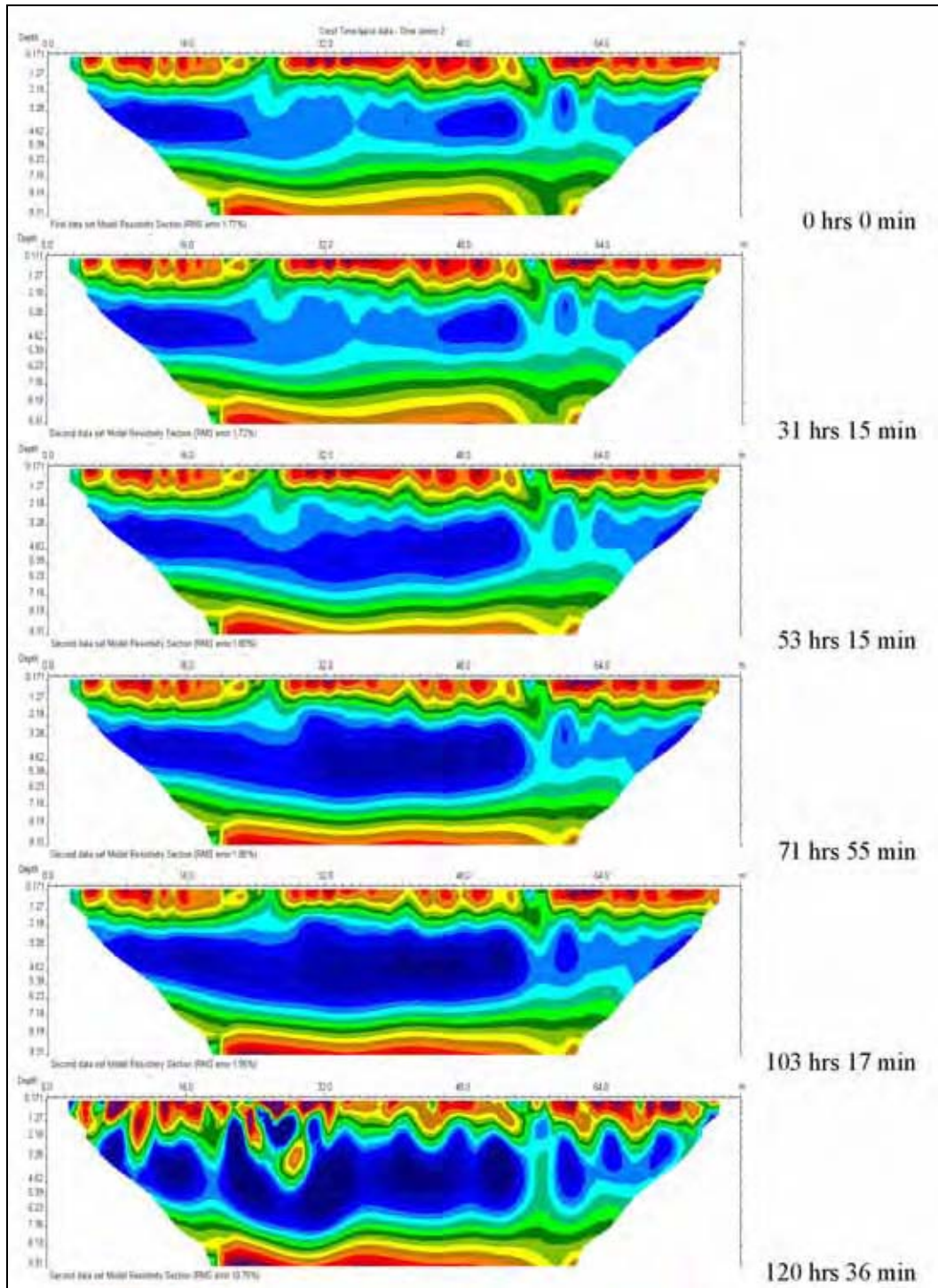


Figure 44. Time series plots of resistivity at the riverside levee crest (Continued)

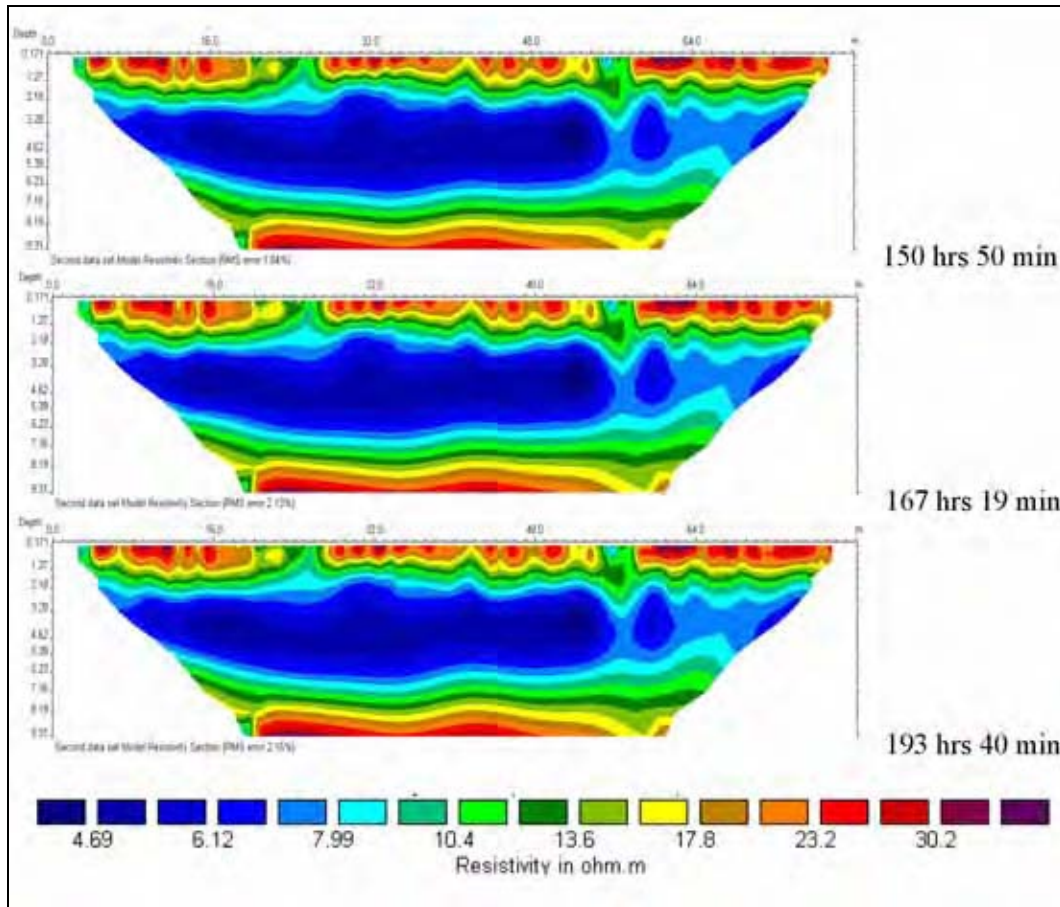


Figure 44. (Concluded)

importance at time 9. However, during the second set of measurements (see Figure 46 and Appendix G, p G18), these higher resistivity trends have generally all disappeared, and are more consistent with the final time interval. These data seem to suggest there were probably coupling issues with the electrodes initially, possibly explaining the erratic results in Figure 43 (127 hr) and Figure 46 (127-143 hr). One possible explanation for the erratic values is the rainfall that occurred during the test, corresponding to this event. Subsequent measurements are generally more consistent to the second set of data as shown in Figure 46.

In summary, resistivity data obtained during the ponding study indicate soil moisture in the levee soils increased along the riverside edge during the simulated flood. The change in soil moisture along the riverside crest of the levee decreases the soil resistivity as shown by Figure 37, Figure 41, and Figure 44. Additionally, increases in soil conductivity are observed along the landside face of the levee (Figure 45) from wetting of the levee soils in the foundation or near the levee base. No significant resistivity changes are observed at the toe that are directly associated with changes in water levee in the riverside pond. Possible temperature effects and or electrode coupling are believed responsible for localized anomalies observed in the data, especially at the levee to toe.

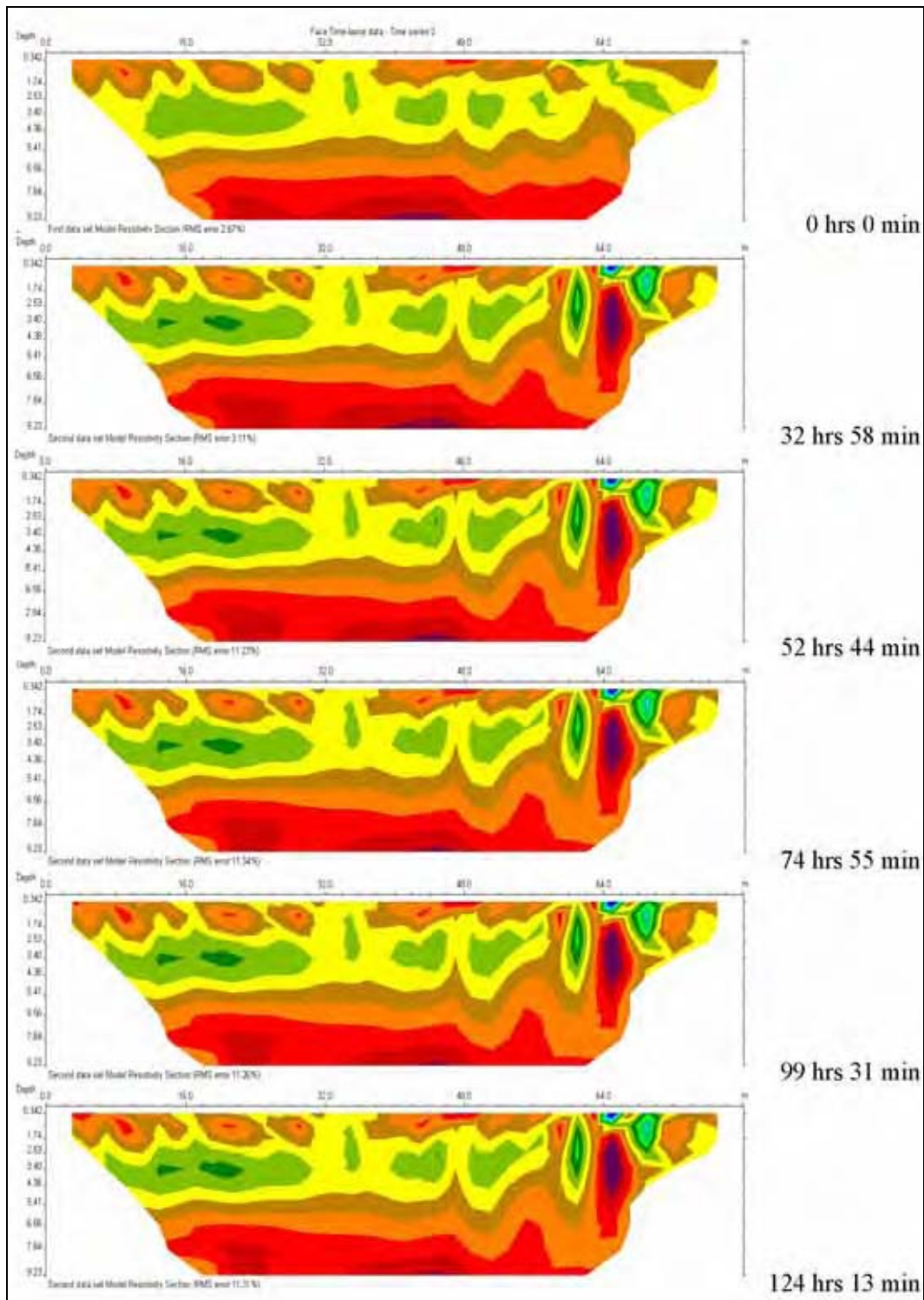


Figure 45. Time series plots of resistivity at the landside levee face (Continued)

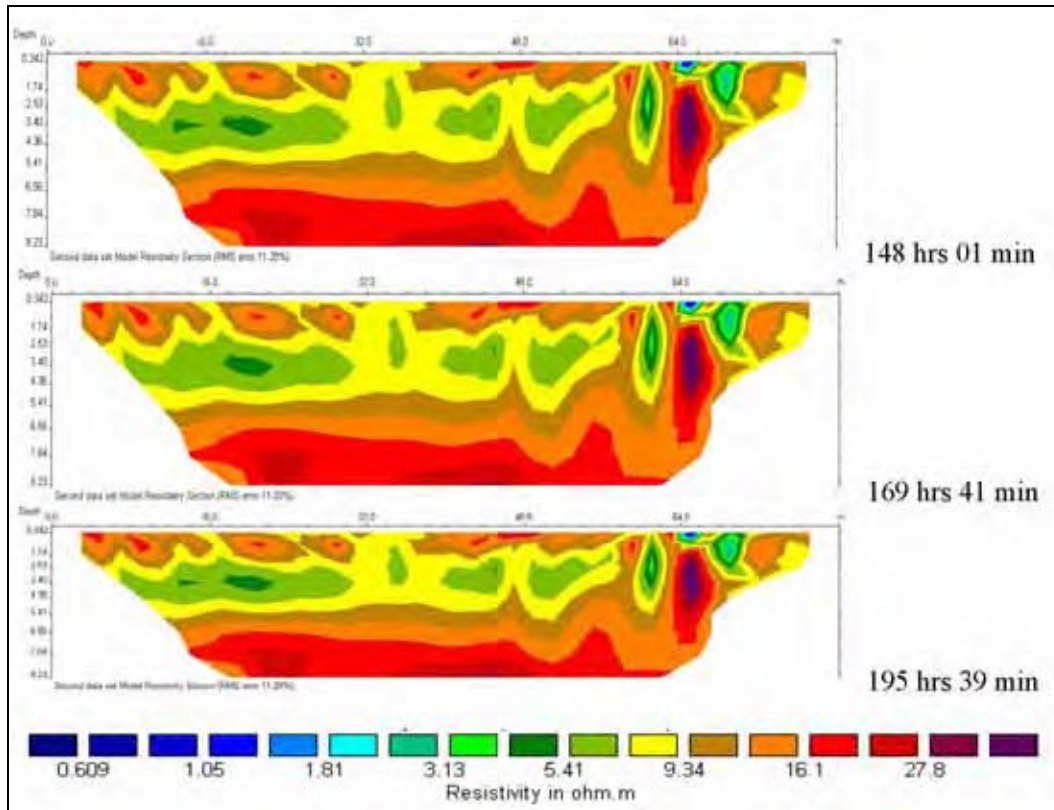


Figure 45. (Concluded)

Other Geophysical Methods

A GPR survey was conducted prior to the flood test to image the levee. GPR surveys have been successfully used in various types of engineering and geologic projects to define subsurface stratigraphy and identify buried objects. A high-frequency electromagnetic pulse in the megahertz (MHz) or microwave frequency range is transmitted into the ground by a radar antenna that is coupled to the ground to image the subsurface for variations in soil and stratigraphy. Transmitted radar pulses are reflected back to a receiver antenna that detects interfaces or other horizons where the electrical properties of the underlying material are different.

A pulse EKKO 100 (PE-100), manufactured by Sensors and Software, Inc., Mississauga, Canada, was used to image the Retamal levee at the pond site. The PE-100 is a bistatic (separate transmitter and receiver antenna) radar system connected to a digital data recorder. A common offset profiling mode was used, where the transmitter and receiver antennas are spaced apart at 1 m over the length of the survey line. GPR antennas used in the levee survey were 50 and 100 MHz. The antennas are mounted to a fiberglass cart at a fixed transmitter and receiver spacing of 1 m. Both the receiver and transmitter antennas are matched to one another for proper coupling and system operation. The PE-100 system was moved along the levee center line. The radar transmitter and receiver are connected to a data recorder by fiber optic cables.

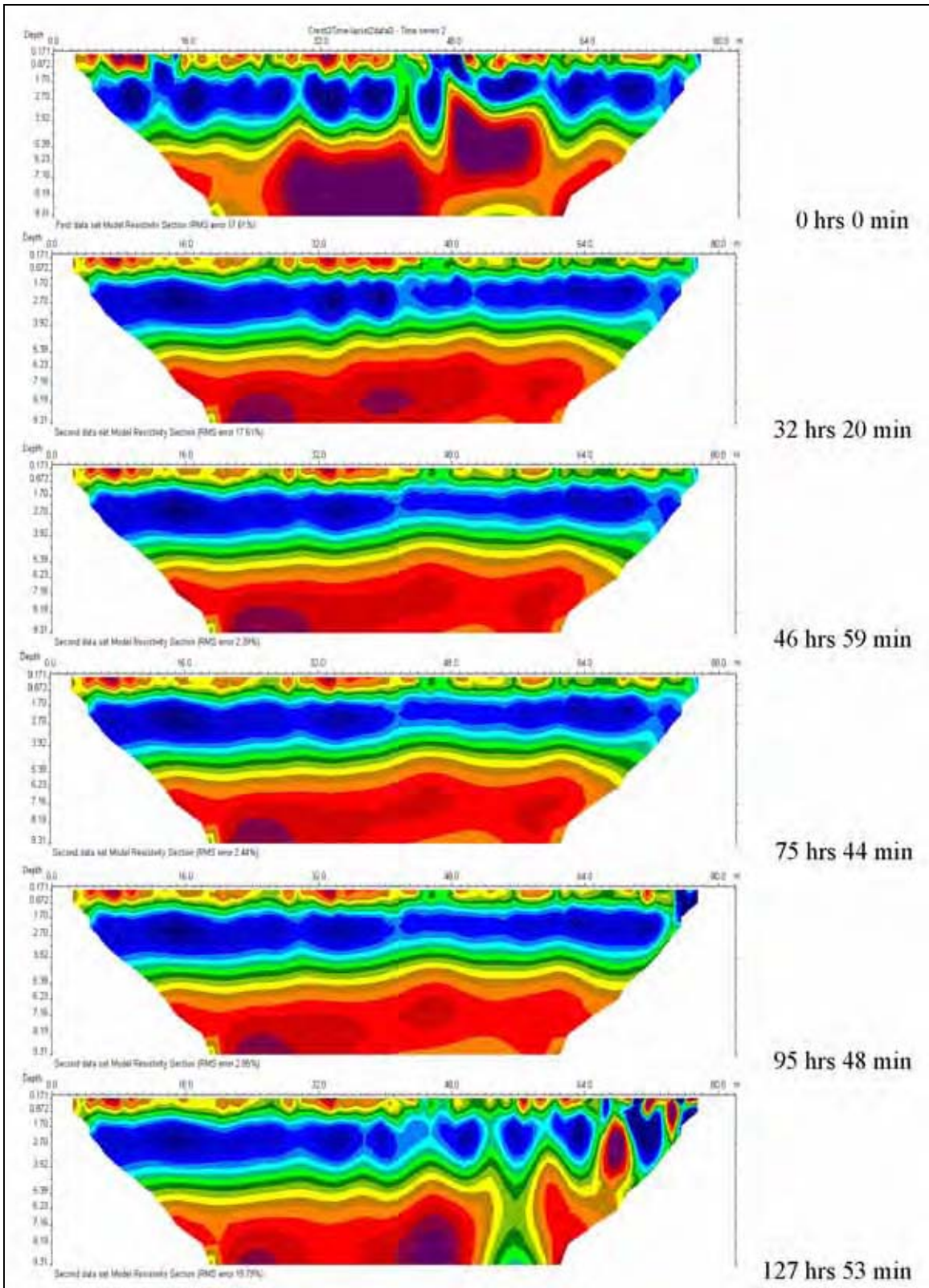


Figure 46. Time series plots of resistivity at the landside levee toe (Continued)

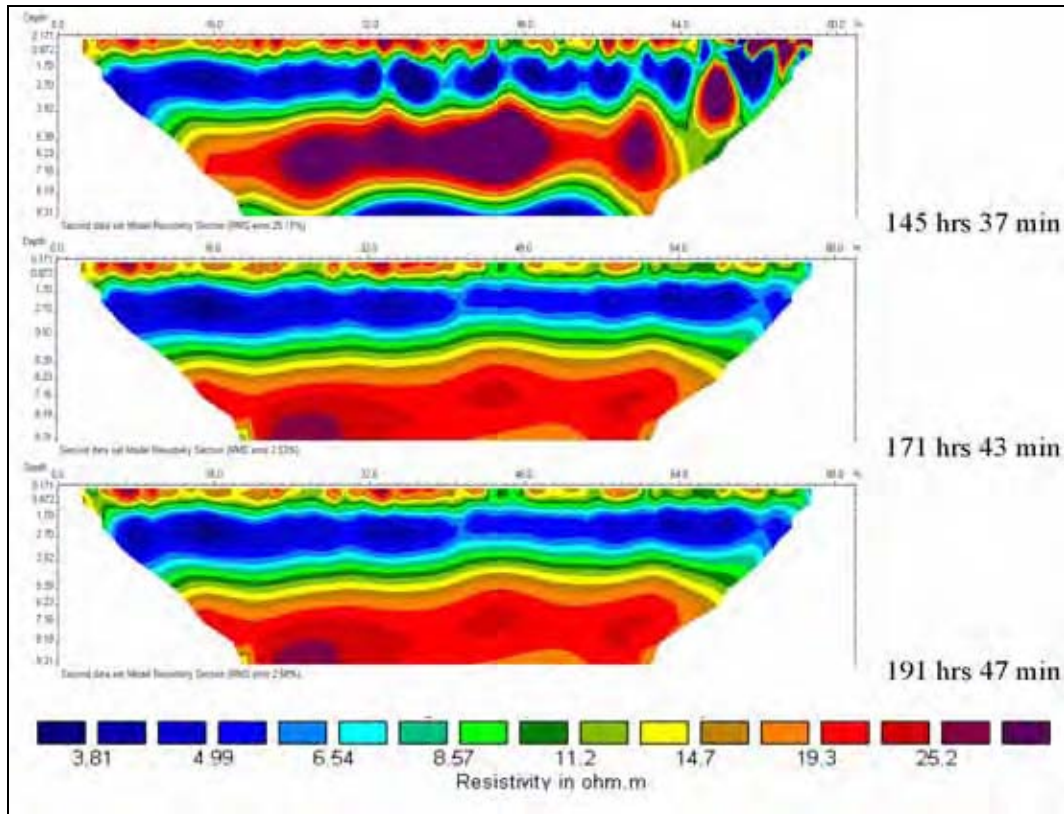


Figure 46. (Concluded)

In order for the radar receiver to detect a change in the underlying material, a contrast in the electrical properties of two soil horizons must occur. Different types of earth materials have contrasting electrical properties, which influence the ability of the GPR system to image the subsurface. Differences in the electrical properties influence the propagation, attenuation, and reflection of radar waves in the subsurface (Reynolds 1997). As previously mentioned, the electrical properties of earth materials are influenced by mineralogy, grain size, bedding, porosity, and the degree of fluid saturation. Important electrical properties in GPR surveys are the dielectric constant (i.e., capacity of a material to store electrical charge) and the soil conductivity. Both of these parameters affect the attenuation of the source energy and influence the amplitude of the reflection back to the receiver.

Loss of signal strength in GPR surveys occurs by geometrical spreading, attenuation of energy by the material properties, and scattering. In highly conductive soils, the transmitted signal is rapidly attenuated, which results in low depth penetration of the signal, and leads to corresponding loss of resolution of the subsurface features. Because of the conductive nature of the levee soils at the pond site, the penetration into the levee by GPR methods was limited to about 1 m (see Figure 47 and Figure 48). Consequently, GPR surveys were discontinued as part of the flood test as the depth of investigation did not contribute to understanding levee seepage.

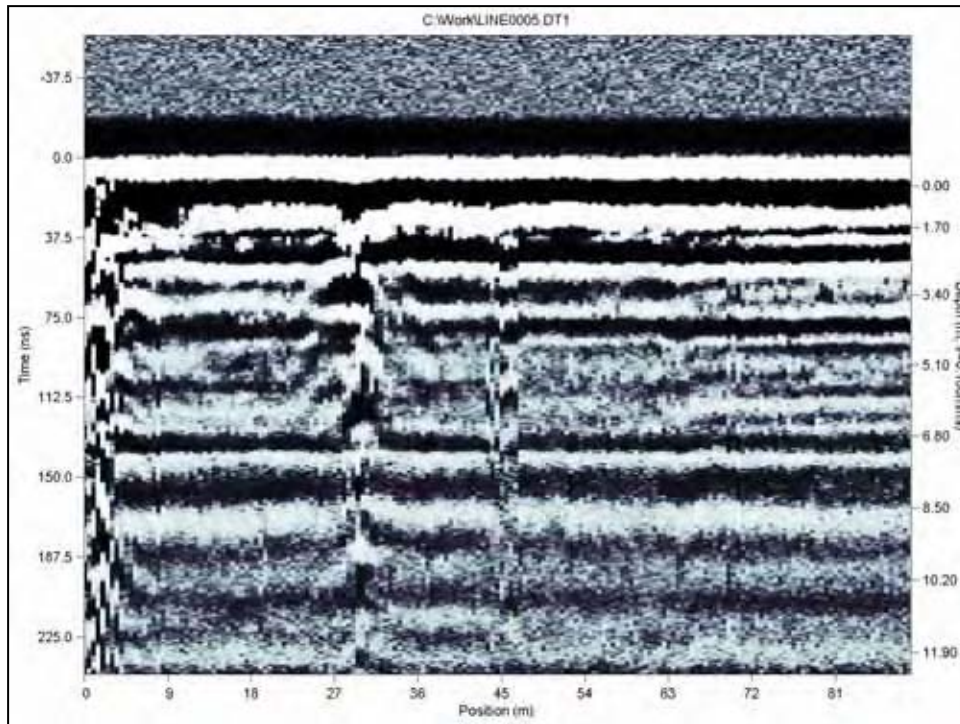


Figure 47. GPR record from river side crest with 50-MHz antenna, view looking south with section extending east to west

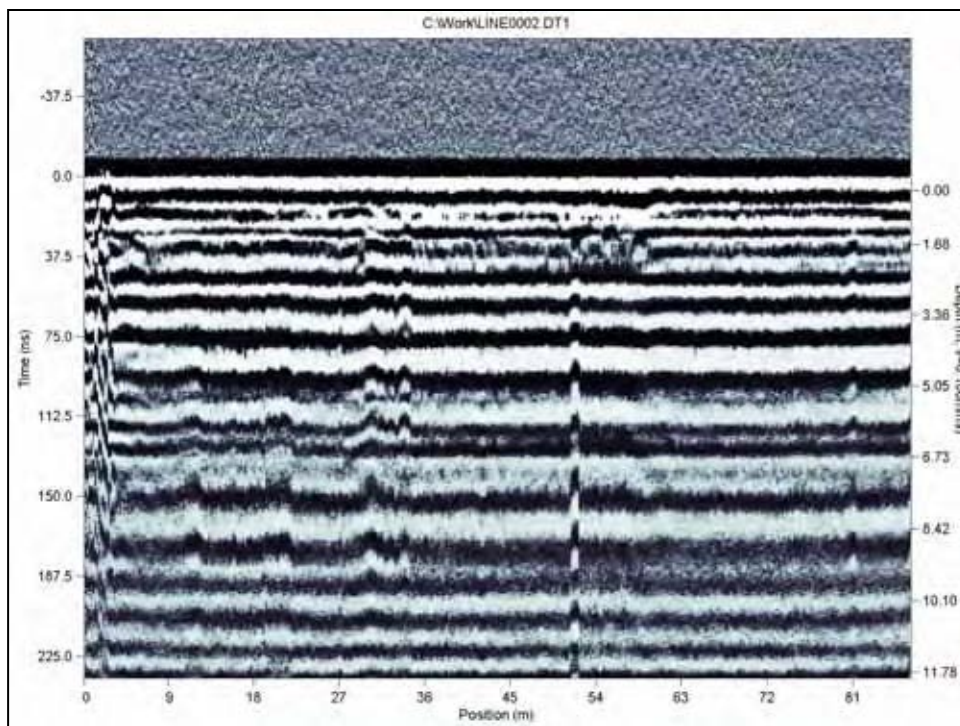


Figure 48. GPR record from river side crest with 100-MHz antenna, view looking south with section extending from east to west

5 Conclusions and Recommendations

Summary and Conclusions

A ponding test of the Retamal levee was completed successfully along with the geophysical monitoring of the simulated flood cycle. Personnel from the Mercedes Office did an excellent job in preparing the site and supporting the ERDC field study. Overall, results of the field testing of a maximum flood event against the Retamal levee are favorable from an engineering perspective.

Significant differences were noted in the physical conditions at Retamal levee between October 2003, when the trench was cut, and November 2004, when the ponding study was completed. In October 2003, surface cracking in some reaches of the Retamal were visible and extensive. Results of the airborne EM conductivity data, the trench study, and seismic baseline surveys indicated the Retamal levee contained sections that were internally desiccated, with significant surface cracking. Surface cracks at Retamal levee were observed to be concentrated primarily in areas where soils from borrow pits in abandoned Rio Grande oxbows were used. Besides the link to borrow pits in this geologic environment, surface cracking may result, in part, from the higher fill volumes needed to build across these topographically low areas, or because of their softer levee foundations. This condition was enhanced by regional drought in the LRGV.

Surface cracking of levee soils was caused primarily by drought conditions in the LRGV, where total annual rainfall was less than 20 in. Drought conditions began in the LRGV in 1998, and ended in later part of 2003. Airborne geophysical surveys of LRGV levees, trenching at Retamal levee, and preliminary seismic surveys were performed at the end of this drought cycle. Normal rainfall conditions resumed again in late 2003, and continued throughout 2004, with annual rainfall above 25 in. Prior to the levee ponding in November 2004, ample rainfall had hydrated the levee clay soils and effectively “healed” the surface cracking problem that was visible in late 2003. Annual rainfall below 20 in. in the LRGV is considered problematic for levee soils, especially if drought conditions persist over several years.

Geophysical monitoring of the levee flood cycle provided important information about levee performance during a maximum flood event. Various types of

state-of-the-art electrical and seismic methods were appraised. Seismic methods are especially attractive for levee screening as velocity data from shear and body waves correlate directly to engineering properties that measure shear strength of soils. Seismic data indicate the higher rainfall in 2004 positively affected the core of the levee. Measurable increases in the seismic velocity of both body and shear waves were observed in 2004, compared with 2003 data. Measurable increases in data quality were also noted. Velocity data from 2003 surveys were much lower, likely caused by a levee core that was internally cracked, resulting in slower P- and S-wave velocities.

Results of the seismic data indicate the higher rainfall in 2004 increased the shear strength of the levee soils as determined by MASW analyses of Rayleigh waves. Shear-wave velocity calculated from surface-wave energy using the MASW methods was sensitive to changes in soil moisture in the levee. Filling of the test pond caused slight increases in V_s values initially, probably due to hydration of the clay levee with a corresponding increase in soil density. V_s measured by MASW was the property most significantly affected by the increased saturation and the material property most sensitive to changes occurring during the levee-ponding experiment. V_p was the property that was least sensitive to changes in water height during the ponding experiment.

Results of LRGV studies using seismic methods indicate land streamers are possible, but better understanding of the near-surface seismic data from the LRGV is required before land streamer data acquisition is possible in a production-type collection effort. Ultimately, this rapid method of data acquisition will be able to provide cost efficiency in sampling and data processing for the amount of levee miles surveyed.

Electrical methods were valuable for monitoring changes in soil moisture and possible seepage through the levee and the foundation during the controlled ponding of water against the levee over a maximum flood cycle. An automated self-potential monitoring system, using four lines of detectors, identified no measurable fluid flow through the levee or in the upper foundation. SP data indicate significant seepage through the levee or in the foundation through internal cracks did not occur. Surface cracks were healed at the beginning of the flood test as described above from ample rainfall prior to the test. Surface cracks that were visible during the previous calendar year were potential pathways for seepage into the levee and into the levee core.

Electrical resistivity measurements identify a gradual change in levee soil moisture during a maximum flood cycle. Resistivity measurements identify a wetting front that caused a decrease in the soil resistivity in the levee nearest the pond face. Resistivity data from the upstream crest line clearly identify an increase in conductivity or a decrease in resistivity with time from increased soil moisture across the levee that is associated with the rise in water height. This change in electrical resistivity extends to the landside midslope, and is observed only at the levee foundation. The decrease in resistivity caused by a wetting front at the base of the levee does not extend into the levee embankment at the midslope or beyond at the levee toe. The wetting front produced an increase in the soil density and levee shear strength as measured by the shear-wave data associated with the seismic surveys.

GPR surveys were performed during the flood test, but were unable to penetrate beyond 1 to 2 m into the levee because of the conductive nature of the levee soils. Consequently, this survey technique did not identify or resolve any large-scale cracks that might be located in the body of the levee. High soil conductivity effectively limited this geophysical technique from further use.

Recommendations

Based on results of this investigation, the following recommendations are made:

- a.* Institute a program of monitoring surface cracks when annual rainfall is below 25 in. to document the occurrence of cracked areas, and the soil types that are prone to cracking. Locations should be accurately located with GPS technology for further study of these areas. Rainfall below 20 in. annually will be a cause for concern, and cracked areas need to be documented and studied to better predict their occurrence in the LRGV. Personnel from the Mercedes Project Office working and maintaining the levees can report problem areas if made aware of the importance of this information. Surface cracks may be related to other factors besides drought conditions and need to be documented for better understanding.
- b.* Perform an engineering analysis of levees to determine their stability when rainfall conditions are below 20 in. annually for many years (say greater than 5 years) and levee soils have become cracked and desiccated. IBWC levees have generally not been evaluated for stability and underseepage for different floodplain characteristics involving geology, top stratum thickness, and loading. These levees were design-built according to standard levee sections. A work plan for conducting geotechnical investigations of selected areas was developed by ERDC to address these engineering studies (Dunbar and Sills 2004).
- c.* Perform further studies on the healing of major surface cracks. Maintenance of cracked levees by the IBWC in the past has involved filling the cracks with water to hydrate the soils and maintain the levee integrity. This process may lead to loss of shear strength in the levees, and the levees developing shallow slides in the levee section (Sills 1983, 1984). The hydration process needs to be studied and quantified further to determine the rate at which this process occurs and the associated change in engineering properties that is involved with this process. The available information indicates that a “healing” process occurs, but the exact rate is unknown. A possible worst-case condition to the levees involves several years of drought, and the threat of a Gulf hurricane whose rainfall falls mainly over the headwaters area in Mexico. This threat should be evaluated for changes in soil moisture and potential loading of the levees.
- d.* Perform additional development of the land-streamer technique for rapid condition assessment of levees. Airborne geophysical methods, especially multi-frequency electromagnetic surveys, had been shown

previously to identify anomalies based on differences in levee material type. The airborne method revealed the levee segment that was heavily cracked by desiccation of the soil. However, airborne methods are not universally applicable, and a rapid land-based geophysical technique is critically important for levee condition assessment.

References

- Ballard, R. F., and McLean, F. G. (1975). "Seismic field methods for in situ moduli; Final report," Miscellaneous Paper S-75-10, U.S. Army Engineer Waterways Experiment Station, Vicksburg, MS.
- Bolt, B. A. (1978). *Earthquakes, a primer*. W. H. Freeman and Company, San Francisco, CA.
- Chang, F. K., and Ballard, R. F., Jr. (1973). "Rayleigh-wave dispersion technique for rapid subsurface exploration," Miscellaneous Paper S-73-20, U.S. Army Engineer Waterways Experiment Station, Vicksburg, MS.
- Corwin, R. F. (1990). "The self-potential method for environmental and engineering applications." *Geotechnical and Environmental Geophysics*, Investigations in Geophysics No. 5. Stanley Ward, ed. Society of Exploration Geophysicists, Tulsa, OK. 127-146.
- Dunbar, J. B., and Ballard, R. F. (2003). "Trip report: Levee trench study, Retamal Levee, San Juan, TX, 6 to 10 October 2003," U.S. Army Engineer Research and Development Center, Vicksburg, MS.
- Dunbar, J. B., and Llopis, J. L. (2005). "Condition assessment of levees, U.S. Section of the International Boundary and Water Commission; Report 4, Tijuana River Levees, San Diego, California," Technical Report ERDC TR-03-4, U.S. Army Engineer Research and Development Center, Vicksburg, MS.
- Dunbar, J. B., and Sills, G. L. (2004). "Geotechnical investigation work plan of selected areas, Lower Rio Grande Valley Flood Control Project, South Texas," Letter Report, U.S. Army Engineer Research and Development Center, Vicksburg, MS.
- Dunbar, J. B., Ballard, R. F., and Murphy, W. L. (2004). "Condition assessment of levees, U.S. Section of the International Boundary and Water Commission; Report 3, Supplement to condition assessment of Lower Rio Grande Valley Levees, South Texas, Mercedes to Brownsville," Technical Report ERDC TR-03-4, U.S. Army Engineer Research and Development Center, Vicksburg, MS.

- Dunbar, J. B., Ballard, R. F., Murphy, W. L., McGill, T. E., Llopis, J. L., Peyman-Dove, L. D., and Bishop, M. J. (2003). "Condition assessment of levees, U.S. Section of the International Boundary and Water Commission; Report 1, Lower Rio Grande Valley Levees, South Texas; Vols I and II," Technical Report ERDC TR-03-4, U.S. Army Engineer Research and Development Center, Vicksburg, MS.
- Grim, R. E. (1968). *Clay mineralogy*. McGraw-Hill, New York.
- Gromko, G. (1974). "Review of expansive soils," *Journal of the Geotechnical Engineering Division, ASCE*, 667-87.
- Hagan, R. (2005). "What is the Pacific Decadal Oscillation (PDO) and should we be concerned?" <http://www.srh.noaa.gov/bro/pdo.htm>.
- Ivanov, J., Miller, R. D., Ballard, R. F., and Dunbar, J. B. (2004). "Interrogating levees using seismic methods in southern Texas," Letter Report, Kansas Geological Survey, The University of Kansas, Lawrence, KS.
- Ivanov, J., Miller, R. D., Dunbar, J. B., and Smullen, S. (2005). "Interrogating levees using seismic methods in southern Texas," Letter Report, Kansas Geological Survey, The University of Kansas, Lawrence, KS.
- Knodel, P. C. (1991). "Characteristics and problems of dispersive clay soils," Report R-91-09. U.S. Bureau of Reclamation, Denver, CO.
- McNeill, J. D. (1980). "Electromagnetic terrain conductivity measurement at low induction numbers," Technical Note TN-6, Geonics, Ltd., Mississauga, Ontario, Canada.
- National Weather Service. (2005). "Annual rainfall versus PDO phase for Brownsville, historical annual average rainfall 26.71 in.," <http://www.srh.noaa.gov/bro/>.
- Reynolds, J. M. (1997). *An introduction to applied and environmental geophysics*. John Wiley and Sons, New York.
- Rollings, M. P., and Rollings, R. S. (1996). *Geotechnical materials in construction*. McGraw Hill, New York.
- Sharma, P. V. (1986). *Geophysical methods in geology*. Elsevier, Amsterdam.
- Sills, G. L. (1983). "Long-term strength reduction and slough slides in Mississippi River levees," Unpublished Technical Report, U.S. Army Corps of Engineers, Vicksburg, MS.
- Sills, G. L. (1984). "Long-term failure in compacted clay slopes." *International conference on case histories in geotechnical engineering*, University of Missouri at Rolla, St. Louis.

U.S. Army Corps of Engineers. (1995). "Geophysical exploration for engineering and environmental investigations," Engineer Manual 1110-1-1802, Washington, DC.

Appendix A

Summary of Trip Report on Trench at Retamal Levee



ERDC-WES
3909 Halls Ferry Road
Vicksburg, MS 39180

21 October 2003

Trip Report: Levee Trench Study, Retamal Dike, San Juan, TX, 6 to 10 October 2003



Prepared by

**Joe Dunbar and Robert Ballard
Engineering Geology and Geophysics Branch
Geotechnical Laboratory**

Memorandum for Record

Subject: Trip Report to Mercedes, TX, to perform trench study at Retamal Dike, San Juan Quadrangle

1. **Background.** Retamal Dike, located in the San Juan, Texas Quadrangle, was constructed during the early 1970s. Construction was performed using materials obtained from borrow pits in the near vicinity. Materials consisted primarily of clays (probably expansive – to be determined by laboratory testing) interspersed with sand. Compaction was mechanically performed using accepted techniques. It is assumed that optimum moisture content was maintained during the construction phase. Construction was completed before the mid 1970s and the levee remained in a dormant state, never having been subjected to flood waters to this date. During the period 1992-2003 a drought condition existed in the Lower Rio Grande Valley. The 11-year draught period affected the materials contained within the interior core of the levee through a slow drying and shrinkage process.

2. In 2000, the IBWC undertook a condition assessment of its 270-mile Lower Rio Grande Valley levee system. During this process, a variable frequency electromagnetic survey was conducted using helicopter-borne transmitters and receivers. These data, obtained along three passes above every levee reach, revealed conductivities of the levee materials from near the surface to depths of 100 ft. In-depth analysis of the EM data revealed anomalously low conductivities for most of the Retamal Dike. (Clays are usually highly conductive materials). Further, in situ cone penetrometer conductivity tests and soil sampling tended to verify the hypothesis that voids might exist within the body of the levee. Grout losses in the sample holes were also noted. In order to verify the true condition of Retamal Dike, a plan was devised to perform a reconnaissance trenching experiment. If this verification experiment was deemed to be successful, further testing will be necessary to establish the integrity of Retamal Dike and determine if remediation will be necessary. This report describes findings of the trenching reconnaissance undertaking.

3. **Purpose for Visit and Study.** The purpose for the site visit was to determine the bulk composition and integrity of the levee at the test location. Major questions to be addressed by the trench study were a) soil moisture conditions, b) whether the levee was cracked and permeable, as indicated by the airborne conductivity survey and SCAPS borings, c) the feasibility of performing a levee ponding experiment, and d) what procedures and methods will be needed if a ponding experiment is warranted. The following letter report contains a description of activities performed during the course of this study, a summary of findings, and a discussion and recommendations on future activities and tasks.

Monday, 6 October 2003

4. **Travel.** Traveled from Vicksburg, MS, to Harlingen, TX. Stopped at US IBWC office in Mercedes to pick up gate key and coordinate trenching activities with Chris Anzaldua. Drove to Pharr, TX, and met with Tony Adamo, Drash Engineering, to coordinate location and time for drilling crew to meet on the levee. Drove to Retamal Dike to site borings and trench at location where SCAPS boring (SJ-15-02) indicated high grout take and intermittent near-zero conductivities in the levee (geographic coordinates: 26.05471N lat, 98.06771 W long).

Tuesday, 7 October 2003

5. **Drilling.** Two borings were drilled at location SJ-15-02. Borings were drilled at the south and north levee crest (i.e., south crest is SJ-TX-01 and north crest SJ-TX-02, respectively, see Figure 1). Borings were sampled with a split-spoon (SJ-TX-01) and with a 3-in. Shelby-tube (SJ-TX-02) to compare sampling methods and results. Drilling logs are presented in Appendix A. Borings were drilled to the levee base (depth of 19 ft). Sampling was continuous and cleanout between samples was with a 3.5-in. flight auger. Soil samples were bagged for later analysis and laboratory testing (soil moisture and clay mineralogy). Following completion of the falling head test described below, the borings were grouted with a portland cement and bentonite slurry.

6. **Soils.** Levee soils are primarily dry to slightly moist, stiff to hard, clay with numerous silt/sand lenses and thin silt/sand beds (< 6-in.). Soil moisture was determined in the field using a soils-moisture-test device. Soil moisture for boring SJ-TX-01 is as follows: 9.6% (by weight) at 2 ft, 10% at 3.5 ft, 9.8% at 5.0 ft, 13% at 6.5 ft, 12% at 10 ft, 11.4% at 11.5 ft, and 13.5% at 18.5 ft (see boring log SJ-TX-01 in Appendix A).

7. **Clay Mineralogy.** Three soil samples from boring SJ-TX-02 have been submitted for laboratory analysis of clay mineralogy by X-ray diffraction to Dr. Dave Patrick at the University of Southern Mississippi, Hattiesburg, MS. Mineralogy sample depths are identified on the boring log in Appendix A.

8. **Falling Head Tests.** Both borings were filled with water following completion to determine whether the levee was permeable. Boring SJ-TX-01 took about 12 to 15 gallons to fill and was relatively stable.

9. Two efforts were made to fill boring SJ-TX-02 but it would not maintain a constant head. Approximately 200 gallons of colored (green) water were poured into the borehole. The water level stabilized at approximately 10.3 ft below the levee surface during both filling efforts. Water is escaping through cracks and/or permeable sand zones within the body of the levee. No visible signs of leakage were detected on the levee surface.

Wednesday, 8 October 2003

10. **Levee Trench** . A 2 ft wide trench was cut into the levee with a backhoe, beginning at the landside toe of the levee, extending through the levee centerline, to about the riverside crest of the levee at station RS 10 (Figure 2). The levee trench did not cut through to the riverside toe, because soils data recorded from the limits of the trench opening shown in Figure 2 answered the basic research questions and objectives defined in paragraph 2 above.

11. **Soil Profiles**. Soil profiles were logged at 5 ft stations along the axis of the levee trench, beginning at landside station 30, and continuing to the riverside crest (see Figure 2 for station locations). Soil profile descriptions are presented in Appendix B along with photographic descriptions of physical features at each station. Because of personnel safety in unsupported trenches, the deeper part of the trench was only logged from visual inspection and soil scrapings using a shovel. A generalized cross-section of the levee profiles is presented in Figure 3. The trench did not identify any evidence for the presence of colored water or grout associated with the borehole falling head tests.

12. **Levee Condition**. Examination of soil profiles along the axis of the trench defines a variable range in soil moisture. Overall, the levee soils are on the dry side. Cracking is readily visible as small, blocky cracks (Figure 4) to vertical cracks (Figure 5). The vast majority of cracks are the small blocky cracks forming angular clay clumps. Cracking is extensive throughout the body of the levee, especially within the main core of the levee as shown by the photos of the centerline profile in Appendix B. Extensive cracking has caused the low conductivity values as determined by the airborne geophysical survey. Two 4 to 6 in., very fine-grained sand seams are present within the trench. The deeper sand layer is continuous as shown by the cross-section in Figure 3.

13. **Ponding Experiment**. The landside toe of the trench was backfilled to the crest to permit a ponding experiment (see photograph front cover). The initial volume for the pond measured 22 x 2 x 11 ft (length, width, depth, respectively) or 484 cubic ft (3,620 gals). Two filling cycles were performed and the water level was monitored to determine the rate of leakage into the levee cracks. The average leakage rate was about 1 in./min or 27.4 gals/min as determined from monitoring the decline in water level against a measuring tape. About 7,000 gals was used to fill the levee pond during the two filling cycles. The water level was permitted to settle overnight from its 1600 hr level of about 8 ft. below the levee crest. Significant slumpage of the trench side walls occurred during and after the ponding experiment.

Thursday, 9 October 2003

14. **Levee Cracks**. Visited trench site during early morning (0800 hrs) to view water level in trench. Water had leaked and/or been absorbed overnight by the levee soil. Trench had slumped to about 6 to 8 ft below the levee crest. Significant cracking was visible on the surface of the levee road as shown by the sketch of cracks in Figure 6. Longitudinal tension cracks were present on the west side of the trench to about 36 ft

from the west wall of the trench. Because of the dirt that was stockpiled on the eastern side of the trench, significant cracking was not observed except for a large crack adjacent to and parallel to the trench. No cracks were observed on either the river- or land-side slopes of the levee, however, vegetation may have prevented that observation.

15. **Causes for Cracking.** Possible causes for the pronounced cracks on the west side of the trench involve a) loss of core material by piping of soil through cracks and internal collapse and slumping, b) hydration and expansion of the clay as water passed through the body of the levee and was absorbed, and c) a combination of these two factors. Cracks parallel to the trench are due to saturation of core soils and gravity slumping of soil blocks or masses into the trench opening. Cracks located along the axis of the levee road, or perpendicular to the trench, are judged to be from clay hydration and a volume expansion of the clay.

16. The significance of these cracks is their overall distance from the trench. Water was able to pass through the body of the levee to about 36 ft from the edge of the trench as shown by Figure 6. Cracks are not only extensive, but are permeable to significant distances as indicated by Figure 6. No evidence of colored water was detected in the trenching from the falling head test conducted as part of the borings, suggesting that the westerly flow path may have a higher permeability than the eastern flow path. Further, it must be stated that no water leakage was observed on either slope. It is possible that recent rainfall during the past month may have caused a “healing process” in the upper 18 inches of surface material, thus containing the trench-injected water to find the path of least resistance along the dry, cracked interior of the levee core.

17. **Seismic Survey Boreholes.** Located 6 lithology borings for the upcoming seismic survey of the selected levee sites by Mr. Rick Miller of the Kansas Geological Survey. The survey will be performed in November and will be monitored by Mr. Robert Ballard.

18. **LiDAR Survey Elevations.** A discussion was held with Mr. Chris Anzaldua and the IBWC surveyor regarding the system wide difference in elevation values between the LiDAR survey (Horizontal NAD 83, Vertical, NAVD 88) and the IBWC survey datum (Horizontal, NAD27, Vertical, NGVD 1929). I explained the conversation I had with Mr. Blain Thibideaux, from John Chance Land Surveys, Inc. the week before about the elevation difference between the two survey datums and obtaining their control data from John Chance that was used to calibrate their survey. This data will be sent to Chris and their surveyor will set up on the John Chance Control Points to determine the systematic difference between the two surveys. A local correction will need to be applied to the survey data, providing the survey error is systematic throughout the LRGV area. I subsequently spoke to Mr. Blain Thibideaux about a conference call to assist the IBWC folks in Mercedes to solve the problem with the elevation difference. The control data was subsequently copied and it was FedX to the Mercedes Office on 20 October 2003. According to Mr. Thibideaux, a copy of the control data was sent to the IBWC office in El Paso as part of the data deliverable.

Friday, 10 October 2003

19. **Travel.** Traveled from Harlingen, TX, to Vicksburg, MS

20. **Summary.** The site visit and experiments performed on the Retamal levee were highly successful. Airborne geophysical data suggested that the clay levee was cracked because of the low conductivity values measured for this reach. Trenching of the levee and ponding of a pool of water in the trench confirmed the interpretation of the conductivity data.

21. Levee soils are primarily clay. These soils are generally dry to slightly moist. Water content ranges from 9.6 to 13.5% by weight as determined from field measurements of borehole samples and examination of trench soils. Cracking of the levee ranges from mainly small cracks that create 1-in. to 6-in. clay blocks or fragments, to the occasional, vertical cracks of at least 2 ft in length. Cracking is present in the core of the levee to about a depth of 9 ft. Two layers of fine sand were found in the levee with the lower layer being continuous across the levee trench.

22. Ponding of water in the trench confirmed the interconnectivity of the cracks and high permeability of the cracks. Seven thousand gallons of water filled the trench on two filling cycles and was readily absorbed and flowed through the body of the levee. Cracks were visible to at least 36 ft from the face of the trench indicating movement of water through the core. Permeability is variable as evidenced by the majority of cracks on the west side of the trench. No exit leakage was observed on the levee surface along either slope. Cracks along the axis of the levee would suggest the clays have the ability to hydrate and cause a significant volume expansion.

23. **Discussion and Recommendations** A fundamental question that the trenching experiments raise is whether the levee can hold a project flood for a 2 to 3 week period as designed. Does cracking significantly impact the strength of the soil to withstand the flood and seepage forces? Will the cracks in the clay soil hydrate and seal themselves should a flood occur? If hydration and sealing occurs, how long does it take for the clay cracks to partially or fully heal themselves? Do the cracks create potential pathways for water flow through the levee, and permit piping of core soils, thereby creating voids, and causing the possible collapse of the levee under flood conditions? What experiments can be conducted, both in the short and long term to evaluate these questions? And last, what are the possible fixes to strengthen and safeguard the levee system against the threat of major flooding should cracking impact levee stability.

24. Before fixes or solutions should be considered, it is recommended that the planned seismic surveys, external ponding tests, and geophysical tests associated with full scale ponding should be conducted for the Retamal levee. Seismic surveys will be performed initially to provide base-line data about the levee, provide a basis for comparison of the Retamal levee to other levee segments within the IBWC system, and possibly relate seismic velocities within the levee body to condition, material type, and electrical characteristics.

25. A major purpose for the trench study described above was to determine whether it was necessary to perform a full-scale ponding test, and what is the best design method for the test. Two alternatives were initially proposed for the ponding, excavate a trench within the body of the levee to hold the water (i.e., an internal impoundment along the axis of the levee), or build an external impoundment of water against the river side face of the levee. From results of the reconnaissance trench experiment, it is recommended that an external impoundment be constructed because it will best simulate true flooding conditions.

26. Reasons for not conducting an internal impoundment were discovered from the trenching study. A potential problem with the internal levee impoundment is maintaining the steep vertical slopes of the internal excavation. The current trenching experiment demonstrated the problems of sidewall slumping into the unsupported excavation. Furthermore, the current trench study identified the core was already cracked, and water will pass rapidly through the body of the levee. The core is highly permeable because of internal cracking and the presence of some sand lenses.

27. Added benefits of building an external impoundment are seeing whether the levee will fail. Additionally, an external test will factor the recent rainfall in the LRGV and show whether it has moistened the levee surface, thereby possibly sealing surface cracks. A major question is whether the surface and subsurface cracks will hydrate and seal themselves against infiltration and seepage with time. Geophysical testing planned as part of the ponding study may help answer some of these basic questions and help determine what changes in levee properties occur over the flood duration.

28. Following the ponding test, a seismic line will be re-run over the levee reach under study as currently planned to note changes in velocity as a result of the pond test. It is suggested that a second levee trench be cut in the ponded area to evaluate the levee core and compare the physical differences between the soils in the two trenches.

29. Results of the ponding and geophysical test results should provide additional data to determine the stability of the levee and what fixes or solutions are warranted.



Figure 1. Soil sampling of levee at location SJ-TX-02. Boring SJ-TX-01 is located 10 ft to left on south levee crest.

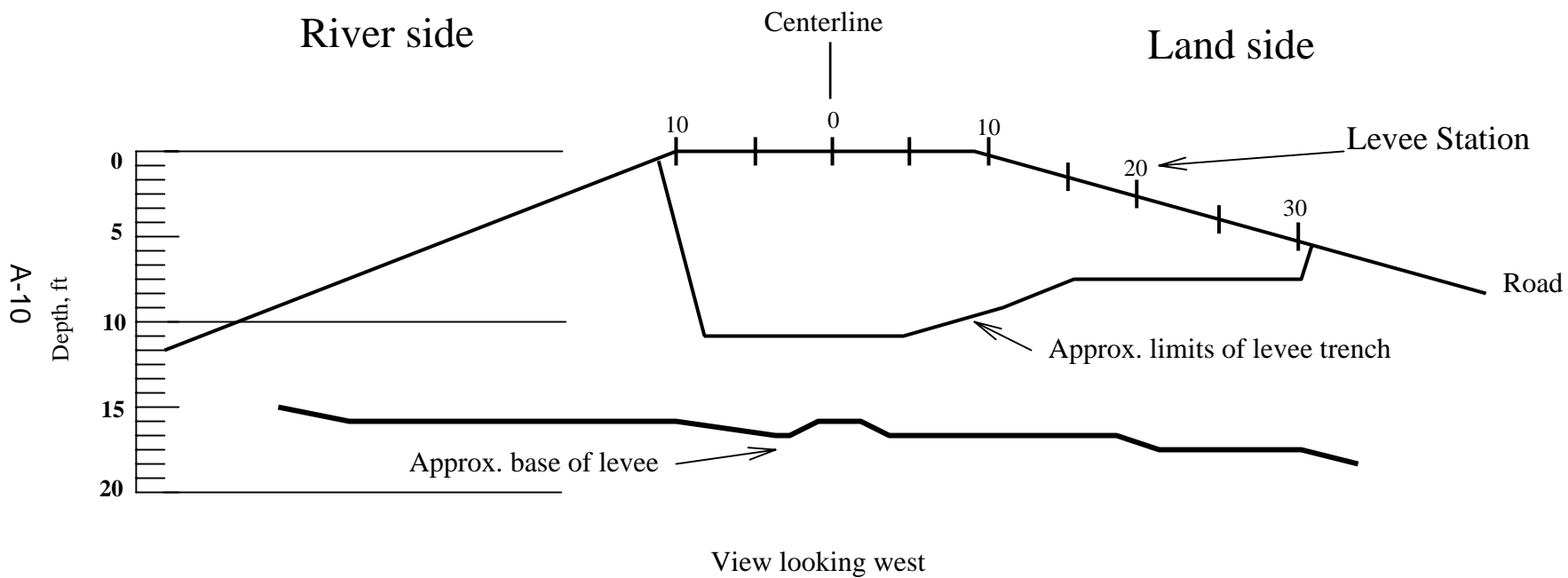


Figure 2. Profile view of levee with soil profile stations and approximate trench outline

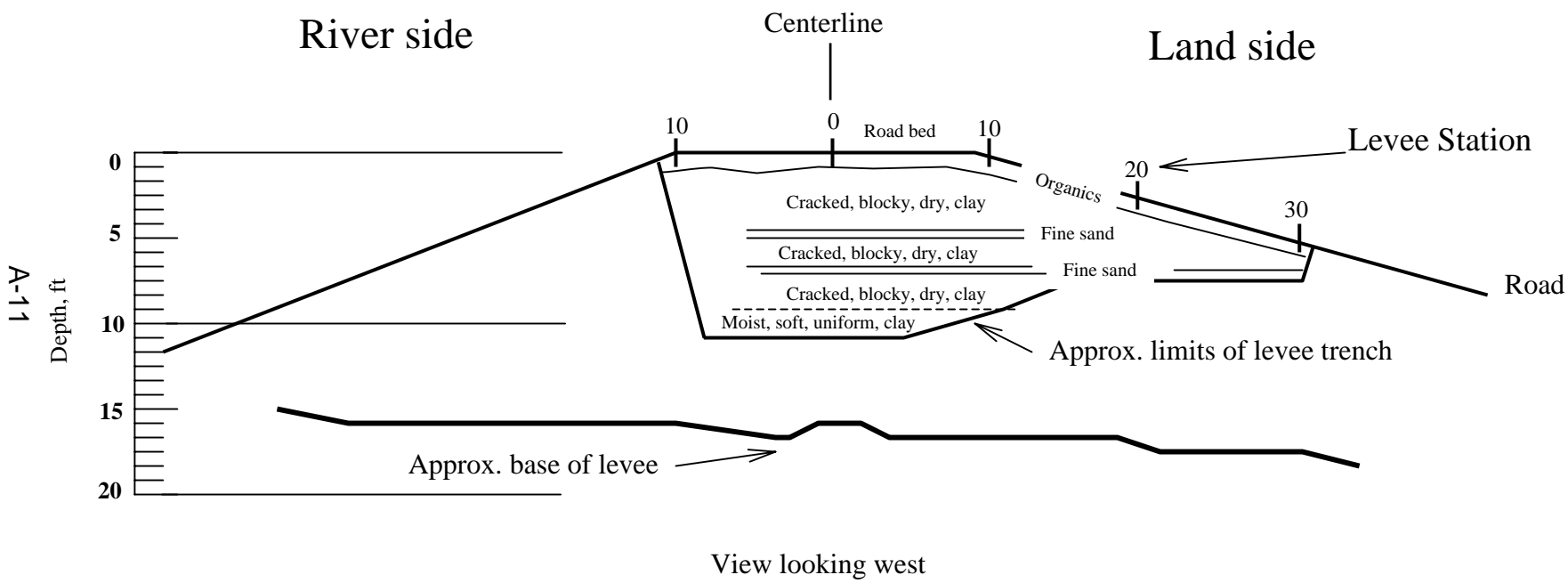


Figure 3. Profile of levee stratigraphy and soil texture



Figure 4. Close-up view looking west at cracked, blocky clay texture at RS 5, depth from about 2 to 3 ft.



Figure 5. View looking west at profile LS 25 showing crack extending from 2.2 to 3.7 ft,note trowel in vertical crack ranging from ¼ to ½ in. wide.

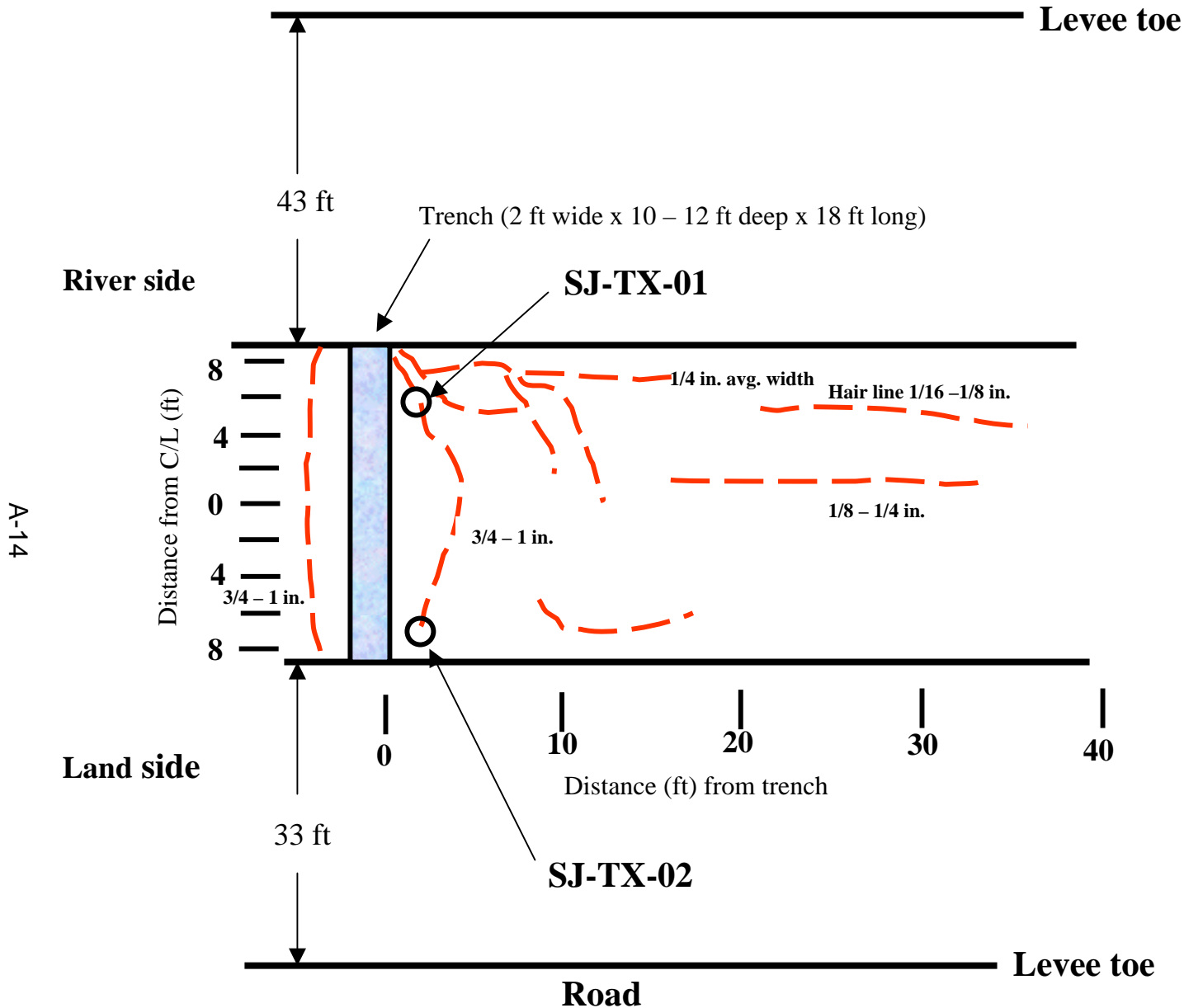


Figure 6. Sketch of cracks on levee road following ponding experiment after 16 hours

Appendix A: Boring Logs from Retamal Trench Area

**BORING LOG
FIELD DATA**

Page 1

Project HSFBWC Levee Trench Study Site Retamal Dike Date 10-7-03
 Location Retamal Dike, San Juan Quad, South Side Levee
 Drill Rig _____ Inspector Danbar Operator Maitia Surface El _____ Job No. _____
 Boring No. SJ-TV-01

SAMPLE NUMBER	DATE TAKEN	STRATUM		DRIVE		SAMPLE		TYPE OF SAMPLER	Blows	Bag	CLASSIFICATION AND REMARKS
		FROM	TO	FROM	TO	FROM	TO				
1	10-7	0.0	0.6	0.0	0.5	0.0	0.5	Standard Split Spoon	25	1	Gravel / Levee Road
		0.6		0.5	1.0	0.5	0.7	(SSS)	19		Clay (CC) brown (10YR5/3)
				1.0	1.5	Rec.	30.7		14		stiff, dry, mottled
				0.0	1.5			3 1/2 Auger			3 1/2 Auger - Cleanout
2	10-7			1.5	2.0	1.5	3.0	SSS	10	2	Clay (CC-CN); brwn (10YR5/3)
				2.0	2.5	Rec.	1.0 ft		11		stiff, dry, w. sand
				2.5	3.0				11		partings. Rec ~ 1.0 ft.
				1.5	3.0			3 1/2 Auger			Cleanout [Moist ~ 9.6%]
3	10-7			3.0	3.5	3.0	4.5	SSS	9	3	Clay (CC-CH), w. silt/sand
				3.5	4.0	Rec.	0.6'		11		partings, dry stiff, crumbles
				4.0	4.5				12		Rec ~ 0.6 ft.
				3.0	4.5			3 1/2 Auger			Cleanout [Moist ~ 10.0%]

A-16

BORING LOG
FIELD DATA

Page 2

Project _____ Site _____ Date 10-7-03
 Location _____ Job No. _____
 Drill Rig _____ Inspector _____ Operator _____ Surface El _____ Boring No. SJ-TX-01

SAMPLE NUMBER	DATE TAKEN	STRATUM		DRIVE		SAMPLE		TYPE OF SAMPLER	Blows	Bag	CLASSIFICATION AND REMARKS
		FROM	TO	FROM	TO	FROM	TO				
4	10-7		4.6	4.5	5.0	4.5	6.0	SSS	11	4	clay (same)
		4.6	5.0	5.0	5.5				9		Silt/F. sand (ML-SP)
		5.0		5.5	6.0				10		Clay (CL); brown (10YR 5/3) soft, slightly moist, will roll [Moist = 98%]
				4.5	6.0			3 1/2 Auger			Cleanout
5	10-7			6.0	6.5			SSS	9	5	Clay (CL-CH) brown (10YR 5/3)
				6.5	7.0				9		stiff, dry, mottled (5YR 4/6)
			2.5	7.0	7.5				9		dense, Rec. 0.65' [Moist = 13%]
				6.0	9.5			3 1/2 Auger			Cleanout
6	10-7	9.5		9.5	10.0			SSS	9	6	Clay (CL-CH), brown (10YR 5/3)
				10.0	10.5				8		soft, dense, dry to moist,
				10.5	11.0				12		no cracks, grades to silty/sandy

A-17

**BORING LOG
FIELD DATA**

Page 3

Project _____ Site _____ Date 10-7-03
 Location _____ Job No. _____
 Drill Rig _____ Inspector _____ Operator _____ Surface El _____ Boring No. ST-TX-01

SAMPLE NUMBER	DATE TAKEN	STRATUM		DRIVE		SAMPLE		TYPE OF SAMPLER	Blows	Bag	CLASSIFICATION AND REMARKS
		FROM	TO	FROM	TO	FROM	TO				
											Clay (SC). [Moist. 12.0%]
				9.5	11.0			3 1/2 Auger			Cleanout
	10.7	1		11.0	11.5			SSS	8	7	Clay (CL-CH) same - brown grey, soft - moist, uniform dense, no crks. [Moist 11.4%]
				11.5	12.0				11		
				12.0	12.5				16		
				12.5	18.0						Cleanout
	10.7			18.0	18.5			SSS	8	8	Clay (CL-CH), drk Olive grey (5% R 4%), soft, moist, mottled (v. l. brown - 10% R 6/B) < 10% (Moist. 13.5%)
				18.5	19.0				11		
				19.0	19.5				15		
<p>Notes: Filled borehole in water, low infiltration - Approx 2.0 hrs had declined 19 ft from top or about 1.24 gals in 2 hrs = 0.62 gals/hr. Borehole took approx 10-15 gals.</p>											

A-18

$\uparrow r^2 \cdot d =$

BORING LOG
FIELD DATA

Page 1

Project MSFBWC Levee Trench Study Site Retamal Dike Date 10-7-03
 Location Retamal Dike; SAN JUAN Quad; North Side Levee Job No. _____
 Drill Rig _____ Inspector Dunbar Operator Martin Surface El _____ Boring No. SJ-TX-02

SAMPLE NUMBER	DATE TAKEN	STRATUM		DRIVE		SAMPLE		TYPE OF SAMPLER	Sample #	CLASSIFICATION AND REMARKS
		FROM	TO	FROM	TO	FROM	TO			
<i>Sampling</i>				0.0	1.0			<i>Auger</i>	-	<i>Road/gravel (NO SAMPLE)</i>
				1.0	3.0			<i>3" Shelby</i>	1	<i>Rec. 0.9'</i>
				3.0	5.0	<i>Clay Min Spl</i>		<i>"</i>	2	<i>Rec. 0.9'</i>
				5.0	7.0			<i>"</i>	3	<i>Rec. 0.85'</i>
				7.0	9.0			<i>"</i>	4	<i>Rec. 0.7'</i>
				9.0	11.0	<i>Clay Min Spl</i>		<i>"</i>	5	<i>Rec 1.05'</i>
				11.0	13.0			<i>"</i>	6	<i>Rec. 1.30'</i>
				13.0	15.0			<i>"</i>	7	<i>Rec. 1.47'</i>
				15.0	17.0	<i>Clay Min Spl</i>		<i>"</i>	8	<i>Rec. 1.35'</i>
				17.0	19.0			<i>"</i>	9	<i>Rec. 1.40'</i>
<i>Lithology</i>		0.0	1.0							<i>Road/Levee surface</i>
		1.0	1.5						1	<i>Clay w. f. gravel (lms), hard dry, difficult to break.</i>
		1.5	6.0						2	<i>Clay (CC-CH); hard, dry difficult to break, v. cohesive uniform</i>

A-19

BORING LOG
FIELD DATA

page 2

Project _____ Site _____ Date 10-7-03
 Location _____ Job No. _____
 Drill Rig _____ Inspector _____ Operator _____ Surface El _____ Boring No. SF-IX-02

SAMPLE NUMBER	DATE TAKEN	STRATUM		DRIVE		SAMPLE		TYPE OF SAMPLER	Bag	CLASSIFICATION AND REMARKS
		FROM	TO	FROM	TO	FROM	TO			
		6.0							3-4	Mixed clay (CL) with v. fine sand (SP)/silt (ML); 50-50% sand/silt is fine powder, clay is dry, stiff-hard
		9.8							5	clay (CL), drk. brown (104R 3/3), dense, dry, stiff-hard, with silt/f. sand partings, competent core, no visible cracks.
		12.0							6-8	clay (CL): Olive grey (5YR 4/1) stiff, slightly moist, uniform. Oxidized zone @ 13.5 ft where break occurred. Presence of weak mottling (10YR 6/8) Sand lens @ 15.6-15.7 (approx.)
		17.0								clay (CL): olive grey (5YR 4/1) w. high mottling 10-20% light

Water loss at
 ~ 10.3 ft from
 falling head test.
 (~ 200 gals. - void
 or crack at 10.3 ft.)

A-20

APPENDIX B
SOIL PROFILES OF LEVEE TRENCH
LOCATION SJ-15-2

Station: LS 30
Depth: 3.8 ft

Depth (ft)	Description
0.0 – 1.6	Clay (CL-CH), damp–moist, brown (10YR3/3) , organics upper 0.8 ft, cracked, minor fine sand, slight to moderate cohesion,
1.6 – 3.0	Clay (CL-CH), brown (10YR3/3) to olive grey (5Y3/2), mottled (7.5YR5/6), dense, moist (makes weak tread), soft to stiff
3.0 – 3.8	Fine sand (SP), lt grey (5YR7/1),

Photograph of profile LS 30 (see Figure 2 for profile location), view looking west into trench to about 3.8 ft.



Station: LS 25
Depth: 4.6 ft

Depth (ft)	Description
0.0 – 1.6	Clay (CL-CH), damp, brown (10YR3/3) , organics to 0.8 ft
1.6 – 1.9	Clay (CL-CH), brown (10YR3/3) to olive grey (5Y3/2), mottled (7.5YR5/6), dense, moist (makes weak tread), soft to stiff
1.9 – 4.4	Clay (CL-CH), d brown (10YR3/3), ry, mottled (7.5YR5/6), contains sand partings, crumbles very easily, brittle, crack from 2.2 to 3.7 ft (½ to ¾ in. wide), see photo below
4.4 – 4.65	Fine sand (SP), lt grey (5YR7/1)

Photograph of LS 25 showing crack from 2.2 to 3.7 ft, note trowel in crack and close-up of crack below. View looking west



Close up of crack, note blocky texture of soil, and fine sand partings between blocks

Station: LS 20
Depth: 6.0 ft

Depth (ft)	Description
0.0 – 1.4	Clay (CL-CH), damp, brown (10YR3/3), organics, with carbonate films, slight cohesion
1.4 – 3.0	Clay (CL-CH), brown (10YR3/3), mottled (7.5YR5/6), moist, soft to stiff
3.0 – 6.0	Clay (CL-CH) w. sand (SP) partings, crumbles very easily, brittle, clay ~80-90%, sand ~10-20%, mottled (7.5YR5/6), blocky texture w. sand/silt partings, cracked



Station LS 20, photograph from 5. to 6 ft, crack near base of trench, note the blocky texture, soil is generally brittle and dry

Station: LS 15
Depth: 7.0 ft

Depth (ft)	Description
0.0 – 1.3	Clay (CL-CH), organics and roots, slight cohesion,
1.3 – 3.0	Clay (CL-CH), brown (10YR3/3), mottled (7.5YR5/6), damp to moist, soft to stiff
3.0 – 7.0	Clay (CL-CH) w. sand (SP) partings, crumbles very easily, brittle, clay ~80-90%, sand ~10-20%, mottled (7.5YR5/6), blocky texture w. sand/silt partings, cracked



Surface to about 2 ft



Bottom 2 ft of profile (~ 5 to 7 ft)

Station: LS 10
Depth: 10.0 ft

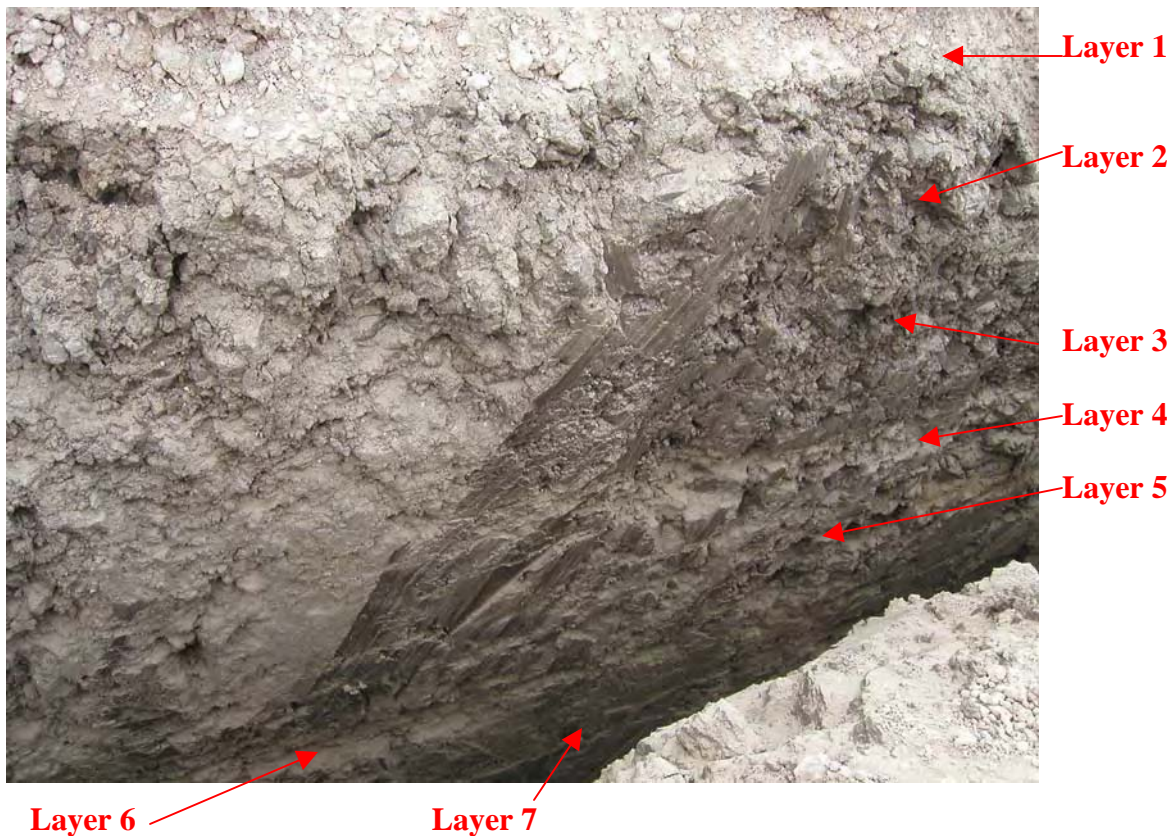
Depth (ft)	Description
0.0 – 0.75	Roadway gravel
0.75 – 2.5	Clay (CL-CH), organics and roots, damp, slight cohesion, will roll
2.5 – 5.5	Clay (CL-CH), brown (10YR3/3), mottled (7.5YR5/6), damp, soft to stiff
5.5 – 8.0	Clay (CL-CH), same, blocky zone with sand/silt partings, mottled
8.0 – 10.0	Clay (CL-CH), same, damp



Note blocky zone at about
5.5 to 8.0 ft

Stations: Levee Core, LS 5, C/L, RS 5, RS 10 (see Figure 2 of report)
Depth: 11.0 ft

Depth (ft)	Description
0.0 – 1.2	Roadway, gravel - Layer 1
1.2 – 1.8	Clay (CL-CH), brown (10YR3/3), mottled (7.5YR5/6), damp, dense – Layer 2
1.8 – 4.5	Clay (CL-CH), brown (10YR3/3), mottled (7.5YR5/6), blocky, brittle, crumbles, dry - Layer 3
4.5 – 5.0	Sand (SP) – Layer 4
5.0 – 7.0	Clay (CL-CH), brown (10YR3/3), mottled (7.5YR5/6), blocky, brittle, crumbles, dry – Layer 5
7.0-7.5	Sand (SP) - Layer 6
7.5 –11	Clay (CL-CH), brown (10YR3/3) - Layer 7 cracked to 9 ft, moist below 9.0 ft



Station: RS 5



Top photo: view of profile RS 5 from surface to about 4.5 ft. Corresponds to northwest portion of above photo showing different layers in levee core. Note the blocky texture and individual clay pieces or pedon surfaces.

Bottom photo: close-up view of blocky clay texture at RS 5, ~ 2 to 3 ft



Appendix B ERDC Drilling Logs for Sampling of Levee Test Sites

**BORING LOG
FIELD DATA**

Project Seismic Study of IBWC levee Site Retamal Dike, San Juan TX Date 2 Dec 03
 Location Retamal Dike, San Juan, TX Job No. _____
 Drill Rig Alpha/Omega Inspector J. Dunbar Operator Martinez Surface El 296.97 Boring No. Seismic 1

SAMPLE NUMBER	DATE TAKEN	STRATUM		DRIVE		SAMPLE		TYPE OF SAMPLER	Bag	CLASSIFICATION AND REMARKS
		FROM	TO	FROM	TO	FROM	TO			
	2 Dec	0.0	1.0	0.0	1.0			3 1/2 Auger		Cleanout - Roadbase
1	"	1.0		1.0	1.95	1.0	1.7	3" Shelby Tube	1	Silt (ML): brown, sandy dry, stiff, refusal at 1.95 ft
2	"		3.0	2.0	3.0	2.0	2.85	3" Shelby	2	Silt/clay (CL-ML) dry, stiff.
3	"	3.0		3.0	4.0	3.0	3.75	3" Shelby	3	Clay (CL-ML) dry, stiff, brown, w. silt partings
4	"			4.0	4.5	3.85	4.5	3" Shelby	4	Refusal @ 4.5' - stiff. Dry stiff clay (CL), w. silt partings (XRD)
5	"			4.5	5.0	4.5	5.0	3" Shelby	5	Soft to 5.0' / Refusal @ 5.0 ft Dry stiff, clay (CL) w. silt partings & sand (V.F.G).

B-2

BORING LOG
FIELD DATA

Project _____ Site _____ Date 2 Dec 03
 Location _____ Job No. _____
 Drill Rig _____ Inspector _____ Operator _____ Surface El _____ Boring No. 1

SAMPLE NUMBER	DATE TAKEN	STRATUM		DRIVE		SAMPLE		TYPE OF SAMPLER	Bag	CLASSIFICATION AND REMARKS
		FROM	TO	FROM	TO	FROM	TO			
6	2 Dec.			5.0	5.75	5.0	5.70	3" Shelby	6	Silt/clay (ML-CL): brown stiff, dry w. sand/silt partings.
7	"			5.75	6.75	5.75	6.45	"	7	Silt/clay (ML-CL) slightly damp soft-stiff, w. sand/silt partings, brown
8	"			6.75	7.4	6.75	7.3	"	8	clay-silt (CL-ML) slightly damp, soft to stiff, brown
9	"			7.4	8.1	7.4	8.1	"	9	Silt (ML) slightly damp, soft to brittle, brown
10	"			8.1	9.7	8.1	9.0	"	10	Clay (CL) damp, soft, brown will roll, plastic, w. silt/sand partings.

CLAY XRD

B-3

**BORING LOG
FIELD DATA**

Project _____ Site _____ Date 2 Dec 03
 Location _____ Job No. _____
 Drill Rig _____ Inspector _____ Operator _____ Surface El _____ Boring No. 1

SAMPLE NUMBER	DATE TAKEN	STRATUM		DRIVE		SAMPLE		TYPE OF SAMPLER	Bag	CLASSIFICATION AND REMARKS
		FROM	TO	FROM	TO	FROM	TO			
11	2 Dec			9.7	10.5	9.7	10.5	3" Shelby	11	clay (cl): brown, damp, plastic, w. silt/sand parting
12	"		11.0	10.5	11.5	10.5	11.3	"	12	clay (cl): brown, slightly damp to dry, w. silt - grades to silt
13	"			11.5	12.3	11.5	12.25	"	13	silt (ml) dry, brittle, core cracks along horie planes 1/8 - 1/4" brown, grades to coarse gm downward - sand.
14	"			12.25	13.2	12.25	13.0	"	14	Sand (SP-SM) v. fine, brown cracks along planes as above dry,
15	"		13.8	13.2	14.3	13.2	14.0	"	15	Sand (SP): lt brown, v. f. grained, river sand - Base of levee @ 13.8 ft

B-4

BORING LOG
FIELD DATA

Project Seismic Study of IBWC Levee Site Retamal Dike, San Juan, Tx Date 2 Dec 03
 Location Retamal Dike, San Juan, Tx Job No. _____
 Drill Rig Alpha/Omega Inspector J. Dunbar Operator Martinez Surface El ~93.91 Boring No. Seismic 2

SAMPLE NUMBER	DATE TAKEN	STRATUM		DRIVE		SAMPLE		TYPE OF SAMPLER	Bag	CLASSIFICATION AND REMARKS
		FROM	TO	FROM	TO	FROM	TO			
	2 Dec	0.0	1.0	0.0	1.0			3 1/2 Auger		Cleanout Roadway
1	"	1.0		1.0	3.0	1.0	2.4	3" Shelby	1	Clay: (CL-CH): uniform, damp, stiff, drk brown
2	"		5.7	3.0	5.0	3.5	3.6	3" Shelby	2	Same
3	"	5.7		5.0	7.00	5.0	5.7	3" Shelby	3	(SP) Sand: Lt. brown, v. fine grad.
			7.0			5.7	6.0		3B	crumbles.
4	"	7.0		7.0	8.7	7.1	8.15	3" Shelby	4	(CL) Clay w. Sand/Silt partings; slightly damp, stiff, cohesive, mottled dark brown (XRD)
5	"			8.7	9.7	8.6	9.2	3" Shelby	5	Clay (CL) w. Sand - damp
						9.2	9.6		B	clay, cohesive, mottled dark brown

B-6

BORING LOG
FIELD DATA

Project _____ Site _____ Date 2 Dec 03
 Location _____ Job No. _____
 Drill Rig _____ Inspector _____ Operator _____ Surface El _____ Boring No. 2

SAMPLE NUMBER	DATE TAKEN	STRATUM		DRIVE		SAMPLE		TYPE OF SAMPLER	Bag	CLASSIFICATION AND REMARKS	
		FROM	TO	FROM	TO	FROM	TO				
6	2 Dec			9.7	10.85	9.7	10.8	3" Shelby	6	Clay (CL): damp, brown, cohesive, mottled, w. sand - silt partings	
						9.7-10.55			B		
						10.55-10.8					
7	"			10.85	12.4	10.85	12.2	3" Shelby	7	Clay (CL) damp, brown, cohesive	
			12.5			10.85-11.5			B	sand/silt lense (2") @ 11.8, mottled	
						11.5-12.2				stiff, grades to ML/SP at base	
8	"	12.5	13.25	12.4	14.6	12.4	13.45	3" Shelby	8	Silt (ML): oxidized, sandy	
		13.25	16.7			12.4	12.9		B	CLAY (CL): dark grey, organics damp. Reducing below 13.25, oxidized above w. heavy mottles	
						12.9	13.4				
				Base of Levee @ 13, 25 ft depth							
9	"			14.6	16.2	14.6	15.4	3" Shelby	9	Clay (CL): dark grey w. organics, damp, will roll, cohesive, plastic; environment poorly drained swamp.	
10	"	16.7	16.95	16.2	18.25	16.2	17.9	3" Shelby	10	clay (CL): same as above	
						16.2	16.9 (A)		B	Silt (ML) wet from 16.7-16.95	
						16.9	17.35 (B)			dark grey	
						17.35-17.8 (C)					

B-7

**BORING LOG
FIELD DATA**

Project Seismic Study of IBWC Levees Site North Levee, PUNN, Tx Date 2 Dec 03
 Location North levee, Main Floodway Job No. _____
 Drill Rig _____ Inspector J.B. Dunbar Operator Martinez Surface El 288.94 Boring No. Seismic 3

SAMPLE NUMBER	DATE TAKEN	STRATUM		DRIVE		SAMPLE		TYPE OF SAMPLER	Bag	CLASSIFICATION AND REMARKS
		FROM	TO	FROM	TO	FROM	TO			
	2 Dec	0.0	1.0	0.0	1.0			3 1/2 Auger		Cleanout - Rdway
1	"	1.0		1.0	3.5	1.0	2.15	3" Shelby Tube	1	Clay (CL): moist, cohesive brown, w. silt partings
2	"			3.5	5.0	3.5	4.2	3" Shelby	2	Clay (CL): dense, dry, brown v. hard to stiff.
3	"			5.0	7.7	5.0	5.75	3" Shelby	3	Clay (CL) dense dry brown v hard to stiff, silt partings & small lenses throughout.
4	"			7.7	8.6	7.7	8.3	3" Shelby	4	Clay (CL): brown, dense, dry, stiff to v hard. Clay mineral 7.0-7.4

XRD

B-9

**BORING LOG
FIELD DATA**

Project _____ Site _____ Date 2 Dec 03
 Location _____ Job No. _____
 Drill Rig _____ Inspector _____ Operator _____ Surface El _____ Boring No. 3

SAMPLE NUMBER	DATE TAKEN	STRATUM		DRIVE		SAMPLE		TYPE OF SAMPLER	Bag	CLASSIFICATION AND REMARKS
		FROM	TO	FROM	TO	FROM	TO			
5	2 Dec			8.8	9.8	8.8	9.45	3" Shelby	5	Clay-SLW (CL-ML): brown, dry - slightly damp, stiff. brittle, w. rattling
6	"			9.8	10.8	9.8	10.45	3" Shelby	6	Clay (CL) brown - same
7	"			10.8	11.8	10.8	11.55	3" Shelby	7	Clay (CL): brown - same
8	"			11.8	12.7	11.8	12.55	3" Shelby	8	Clay (CL): brown - same
9	"			12.7	13.8	12.7	13.50	3" Shelby	9	Clay (CL) brown - same

B-10

BORING LOG
FIELD DATA

Project _____ Site _____ Date _____
 Location _____ Job No. _____
 Drill Rig _____ Inspector _____ Operator _____ Surface El _____ Boring No. 3

SAMPLE NUMBER	DATE TAKEN	STRATUM		DRIVE		SAMPLE		TYPE OF SAMPLER	Bag	CLASSIFICATION AND REMARKS
		FROM	TO	FROM	TO	FROM	TO			
10	2 Dec			13.5	14.8	13.5	14.3	3" Shelby	10	Clay (CL): brown - same
11	"			14.8	15.8	14.8	14.65	3" Shelby	11	Clay (CL) brown - same
12	"			15.8	16.8	15.8	16.65	3" Shelby	12	Clay (CL): brown - same
13	"			16.8	17.8	16.8	17.7	3" Shelby	13	Clay (CL): brown - same
Very uniform throughout - base of levee approx 12 ft. below crest based on LIDAR data.										

B-11

BORING LOG
FIELD DATA

Project Seismic Study of IBWC Levee Site _____ Date 2 Dec. 03
 Location South Levee Main Floodway 3.57 miles West Hwy 493 Job No. _____
 Drill Rig Alpha/Durga Inspector J. Dunbar Operator Martinez Surface EI ~95.85 Boring No. SEISMIC 4

SAMPLE NUMBER	DATE TAKEN	STRATUM		DRIVE		SAMPLE		TYPE OF SAMPLER			CLASSIFICATION AND REMARKS
		FROM	TO	FROM	TO	FROM	TO				
—		0.0	1.0					3 1/2 Auger			Cleanout - Road base
1	2 Dec	1.0		1.0	1.9	1.0	1.7	3" Shelby	1		Clay (CL): Brown moist stiff, plastic, uniform, mottled
2	"			1.9	3.5	1.9	2.4	3" Shelby	2		Clay (CL): brown - same
3	"			3.5	5.1	3.5	4.35	3" Shelby	3		Clay (CL): brown; stiff, damp plastic, uniform, some mottles, cohesive dense
4	"			5.1	6.65	5.1	5.7	3" Shelby	4		Clay (CL) Brown - same
5	"			6.65	8.5	6.65	7.4	3" Shelby	5		Clay (CL) Brown. same

B-12

BORING LOG
FIELD DATA

Project _____ Site _____ Date _____
 Location _____ Job No. _____
 Drill Rig _____ Inspector _____ Operator _____ Surface El _____ Boring No. 4

SAMPLE NUMBER	DATE TAKEN	STRATUM		DRIVE		SAMPLE		TYPE OF SAMPLER	Bay	CLASSIFICATION AND REMARKS
		FROM	TO	FROM	TO	FROM	TO			
				8.5	9.5	8.5	9.3	3" Shelby	6	Clay (CL): Brown - same
				9.5	10.5	9.5	10.2		7	Clay (CL): Brown - same
				10.5	11.5	10.6	11.3		8	Clay (CL): Brown + same
				11.5	12.5	11.5	12.4		9	"
				12.5	13.5	12.5	13.1		10	"
				13.5	14.5	13.5	14.1		11	"

B-13

BORING LOG
FIELD DATA

Project _____ Site _____ Date _____
 Location _____ Job No. _____
 Drill Rig _____ Inspector _____ Operator _____ Surface El _____ Boring No. 4

SAMPLE NUMBER	DATE TAKEN	STRATUM		DRIVE		SAMPLE		TYPE OF SAMPLER			CLASSIFICATION AND REMARKS
		FROM	TO	FROM	TO	FROM	TO				
				14.5	15.5	14.5	15.15	3" Shelby		12	Clay (CL) Brown, stiff, slightly moist, slightly plastic
				15.5	16.5	15.5	16.15	3" Shelby		13	CLAY (CL) Brown, stiff, moist uniform, plastic, dense
				16.5	17.5	16.5	17.2	3" Shelby		14	CLAY (CL) Brown, stiff, moist uniform, plastic, dense
				17.5	18.5	17.5	18.3	3" Shelby		15	CLAY (CL) Brown, stiff, dense moist, plastic, uniform
				18.5	19.5	18.5	19.2	3" Shelby		16	Clay (CL): Brown, stiff, moist, brown, plastic, uniform

B-14

BORING LOG
FIELD DATA

Page 1

Project USIBWC Levee Trench Study Site Retamal Dike Date 10-7-03
 Location Retamal Dike, San Juan Quad, South Side levee Job No. _____
 Drill Rig _____ Inspector Danbar Operator Martín Surface El _____ Boring No. SJ-TX-01

SAMPLE NUMBER	DATE TAKEN	STRATUM		DRIVE		SAMPLE		TYPE OF SAMPLER	Ebus	Bag	CLASSIFICATION AND REMARKS
		FROM	TO	FROM	TO	FROM	TO				
1	10-7	0.0	0.6	0.0	0.5	0.0	0.5	Standard Split Spoon	25	1	Gravel / Levee Road
		0.6		0.5	1.0	0.5	0.7	(SSS)	19		Clay (CC) brown (10x125/3)
				1.0	1.5	Rec	30.7		14		stiff, dry, mottled
				0.0	1.5						3 1/2 Auger
2	10-7			1.5	2.0	1.5	3.0	SSS	10	2	Clay (CC-CN); brwn (10x125/3)
				2.0	2.5	Rec	1.0ft		11		stiff, dry, w. sand
				2.5	3.0				11		partings. Rec ~ 1.0ft.
				1.5	3.0						3 1/2 Auger
3	10-7			3.0	3.5	3.0	4.5	SSS	9	3	Clay (CC-CH), w. silt/sand
				3.5	4.0	Rec	0.6'		11		partings, dry, stiff, crumbles
				4.0	4.5				12		Rec ~ 0.6ft.
				3.0	4.5						3 1/2 Auger

B-15

**BORING LOG
FIELD DATA**

Page 2

Project _____ Site _____ Date 10-7-03
 Location _____ Job No. _____
 Drill Rig _____ Inspector _____ Operator _____ Surface El _____ Boring No. SJ-TX-01

SAMPLE NUMBER	DATE TAKEN	STRATUM		DRIVE		SAMPLE		TYPE OF SAMPLER	Blows	Bag	CLASSIFICATION AND REMARKS
		FROM	TO	FROM	TO	FROM	TO				
4	10-7		4.6	4.5	5.0	4.5	6.0	SSS	11	4	Clay (same)
		4.6	5.0	5.0	5.5				9		Silt/F. Sand (ML-SP)
		5.0		5.5	6.0				10		Clay (CL); brown (10YR 5/3) Soft, slightly moist, will roll [Moist = 98%]
				4.5	6.0			3 1/2 Auger			Cleanout
5	10-7			6.0	6.5			SSS	9	5	Clay (CL-CH) brown (10YR 5/3)
				6.5	7.0				9		Stiff, dry, mottled (5YR 4/6)
			2.5	7.0	7.5				9		dense, Rec. 0.65' [Moist = 13%]
				6.0	9.5			3 1/2 Auger			Cleanout
6	10-7	9.5		9.5	10.0			SSS	9	6	Clay (CL-CH), brown (10YR 5/3)
				10.0	10.5				8		soft, dense, dry to moist,
				10.5	11.0				12		no cracks, grades to silty/sandy

B-16

**BORING LOG
FIELD DATA**

Page 3

Project _____ Site _____ Date 10-7-03
 Location _____ Job No. _____
 Drill Rig _____ Inspector _____ Operator _____ Surface El _____ Boring No. ST-TX-01

SAMPLE NUMBER	DATE TAKEN	STRATUM		DRIVE		SAMPLE		TYPE OF SAMPLER	Blows	Bag	CLASSIFICATION AND REMARKS
		FROM	TO	FROM	TO	FROM	TO				
											Clay (SC). [Moist ₂ 12.0%]
				9.5	11.0			3 1/2 Auger			Cleanout
	16.7	1		11.0	11.5			SSS	8	7	Clay (CL-CH) same - brown
				11.5	12.0				11		grey, soft - moist, uniform
				12.0	12.5				16		dense, no crks. [Moist 11.4%]
				12.5	18.0						Cleanout
	16.7			18.0	18.5			SSS	8	8	Clay (CL-CH), drk Olive
				18.5	19.0				11		grey (5YR 4/1), soft, moist,
				19.0	19.5				15		mottled (Vlw. brown - 10YR 6/8)
											< 10% (Moist. 13.5)
Note: Filled borehole w water, low infiltration - Approx 2.0 hrs had declined 1.9 ft from top or about 1.24 gals in 2 hrs = 0.62 gals/hr. Borehole took approx 10-15 gals.											

B-17

$\pi r^2 d =$

98° 04' 03.756"
26° 03' 16.956"

BORING LOG
FIELD DATA

Page 1

Project USIBWC Levee Trench Study Site Retamal Dike Date 10-7-03
 Location Retamal Dike; SAN JUAN QUAD; North Side Levee Job No. _____
 Drill Rig _____ Inspector Dunbar Operator Martin Surface EI _____ Boring No. SJ-TX-02

SAMPLE NUMBER	DATE TAKEN	STRATUM		DRIVE		SAMPLE		TYPE OF SAMPLER	Sample #	CLASSIFICATION AND REMARKS
		FROM	TO	FROM	TO	FROM	TO			
<i>Sampling</i>				0.0	1.0			<i>Auger</i>	-	<i>Road/gravel (NO SAMPLE)</i>
				1.0	3.0			<i>3" Shelby</i>	1	<i>Rec. 0.9'</i>
				3.0	5.0	<i>Clay Min Spl</i>		<i>"</i>	2	<i>Rec. 0.9'</i>
				5.0	7.0			<i>"</i>	3	<i>Rec. 0.85'</i>
				7.0	9.0			<i>"</i>	4	<i>Rec. 0.7'</i>
				9.0	11.0	<i>Clay Min Spl</i>		<i>"</i>	5	<i>Rec 1.05'</i>
				11.0	13.0			<i>"</i>	6	<i>Rec. 1.30'</i>
				13.0	15.0			<i>"</i>	7	<i>Rec. 1.47'</i>
				15.0	17.0	<i>Clay Min Spl</i>		<i>"</i>	8	<i>Rec. 1.35'</i>
				17.0	19.0			<i>"</i>	9	<i>Rec. 1.40'</i>
<i>Lithology</i>		0.0	1.0							<i>Road/Levee surface</i>
		1.0	1.5						1	<i>Clay w. f. gravel (ins); hard dry, difficult to break.</i>
		1.5	6.0						2	<i>Clay (CL-CH); hard, dry difficult to break, v. cohesive</i>
<i>2</i>						3.0	3.5	<i>Drash</i>		<i>uniform</i>

B-18

**BORING LOG
FIELD DATA**

page 2

Project _____ Site _____ Date 10-7-03
 Location _____ Job No. _____
 Drill Rig _____ Inspector _____ Operator _____ Surface El _____ Boring No. SJ-TX-02

SAMPLE NUMBER	DATE TAKEN	STRATUM		DRIVE		SAMPLE		TYPE OF SAMPLER	Bag	CLASSIFICATION AND REMARKS
		FROM	TO	FROM	TO	FROM	TO			
3		6.0				5.0	5.5	Drash	3-4	Mixed clay (CL) with v. fine sand (sp)/silt (ul); 50-50%. sand/silt is fine powder, clay is dry, stiff-hard
5		9.8	9.8			9.0	9.5	Drash	5	clay (CL), drk. brown (104R 3/3), dense, dry, stiff-hard, with silt/f. sand partings, competent core, no visible cracks.
		12.0								Water loss at 2 10.3 ft from falling head test, (2 200 gals. - void or crack at 10.3 ft.)
		12.								
										6-8 clay (CL): olive grey (5Y4/1) stiff, slightly moist, uniform, oxidized zone @ 13.8 ft where break occurred. Presence of weak mottling (10YR 6/8)
										Sand lens @ 15.6-15.7 (approx.)
9		17.0	17.0			17.0	17.5	Drash		clay (CL): olive grey (5YR 4/1) w. high mottling 10-20% slightly

B-19

Appendix C

Drash Laboratory Soil Test Results



Geotechnical • Construction Materials • Environmental • Forensic

January 23, 2004

Mr. Joe Dunbar
U. S. Army Corps of Engineers
Engineer Research and Development Center
Waterways Experiment Station
3909 Halls Ferry Road
Vicksburg, Mississippi 39180

SUBJECT
Soils Classification Testing
Rio Grande River Levee Study –
Task 1
Rio Grande Valley, Texas
Contract N^o DACW42-03-P-0321
DCE Project N^o 203G2082

Dear Mr. Dunbar:

We have completed the requested soils analysis on the 70 soil samples you delivered to our lab during the first week of December 2003. The requested tests were performed in general accordance with the ASTM standards listed on the attached page B-1. The attached Table 1 summarizes the results of the tests performed on the provided samples. The test results are graphically depicted in the attached logs of borings and graphs for all tested samples.

We appreciate this opportunity to be of service to you on this project. If you have any questions regarding the information presented in this letter or the attached tables and figures, please do not hesitate to contact the undersigned.

Very Truly Yours,
Drash Consulting Engineers, Inc.

Maria O. Flores
Maria O. Flores, E.I.T.
Project Manager
Geotechnical Engineering Division



Anthony F. Adamo
Anthony F. Adamo, P.E.
Manager
Rio Grande Valley Office
1/23/04

Attachments: Table 1 – Soil Test Summary
Logs of Borings A-1 thru A-5
Laboratory Testing Program B-1
Atterberg Limits Results B-2 and B-3
Gradation Curves B-4 thru B-18

MOF/AFA/yl
Rio Grande Valley
1506 Mid-Cities Drive • Pharr, Texas 78577 • (956) 283-8254
(888) 298-7103 • Fax: (956) 283-8279

E-mail: drash@drashce.com
San Antonio • Laredo • Rio Grande Valley

**Table 1
Soil Test Summary
Army Corps of Engineering
Rio Grande River Levee Study
Contract No. DACW42-03-P-0321
Hidalgo County, Texas**

Sample Identification	Sample Depth (ft)	Moisture Content (%)	Unit Dry Weight (pcf)	Liquid Limit (%)	Plastic Limit (%)	Plasticity Index (%)	Fraction Passing No. 200 Sieve (%)	Silt Fraction (%)	Clay Fraction (< 0.005 mm) (%)	USCS Soil Classification
B-1, S-1	1	13	114							LEAN CLAY (CL)
B-1, S-2	2	13								LEAN CLAY (CL)
B-1, S-3	3	11	118	35	20	15				LEAN CLAY (CL)
B-1, S-4	4	15	113	34	18	16	96	48	38	LEAN CLAY (CL)
B-1, S-5	4.5	13								LEAN CLAY (CL)
B-1, S-6	5	14	110	32	19	13				LEAN CLAY (CL)
B-1, S-7	5.8	15								LEAN CLAY (CL)
B-1, S-8	6.8	15	106	41	20	21				LEAN CLAY (CL)
B-1, S-9	7.4	12								LEAN CLAY (CL)
B-1, S-10	8.1	12	113	42	19	23	95	47	48	LEAN CLAY (CL)
B-1, S-11	10	16								LEAN CLAY (CL)
B-1, S-12	10.7	12	106	34	19	15				LEAN CLAY (CL)
B-1, S-13	11.5	11					94			LEAN CLAY (CL)
B-1, S-14	12.3	11	110				29			SILTY SAND (SM)
B-1, S-15	13.2	10					12			SILTY SAND (SM)
B-1, S-16	13.7	6								SILTY SAND (SM)
B-1, S-17	14.3	8								SILTY SAND (SM)
B-1, S-18	15.3	5					41			SILTY SAND (SM)
B-2, S-1	1	21	107							LEAN CLAY (CL)
B-2, S-2	1.6	21								LEAN CLAY (CL)
B-2, S-3	3	20	105	40	20	20	96	45	49	LEAN CLAY (CL)
B-2, S-4	5	21					29			LEAN CLAY (CL)
B-2, S-5	5.7	10								SILTY SAND (SM)
B-2, S-6	7	25	102	54	25	29	97	40	57	SILTY SAND (SM)
B-2, S-7	8.6	22								CLAY (CH)
B-2, S-8	9.2	18	100	45	20	25				CLAY (CH)
B-2, S-9	9.7	20								CLAY (CH)
B-2, S-10	10.6	21	104	56	24	32				CLAY (CH)
B-2, S-11	10.9	23								CLAY (CH)
B-2, S-12	11.5	15	109							LEAN CLAY (CL)
B-2, S-13	12.4	14								LEAN CLAY (CL)
B-2, S-14	12.9	17								LEAN CLAY (CL)
B-2, S-15	14.6	17	104	55	25	30	97	36	61	CLAY (CH)
B-2, S-16	16.2	28		54	23	31				CLAY (CH)

C-3

C-4

Sample Identification	Sample Depth (ft)	Moisture Content (%)	Unit Dry Weight (pcf)	Liquid Limit (%)	Plastic Limit (%)	Plasticity Index (%)	Fraction Passing No. 200 Sieve (%)	Silt Fraction (%)	Clay Fraction (< 0.005 mm) (%)	USCS Soil Classification
B-2, S-17	16.9	30								
B-2, S-18	17.4	28	94							CLAY (CH)
B-3, S-1	1	27	97							CLAY (CH)
B-3, S-2	2.2	26								CLAY (CH)
B-3, S-3	3.5	19	111	63	26	37				CLAY (CH)
B-3, S-4	5	15	113	71	24	47	99	13	86	CLAY (CH)
B-3, S-5	7.7	20	102	65	25	40				CLAY (CH)
B-3, S-6	8.8	20								CLAY (CH)
B-3, S-7	9.8	16	107	64	24	40	98	20	78	CLAY (CH)
B-3, S-8	10.8	23								CLAY (CH)
B-3, S-9	11.8	19	106	66	24	42				CLAY (CH)
B-3, S-10	12.7	18								CLAY (CH)
B-3, S-11	13.5	19	105	65	24	41	99	19	80	CLAY (CH)
B-3, S-12	14.8	24								CLAY (CH)
B-3, S-13	15.8	25								CLAY (CH)
B-3, S-14	16.8	19	103	68	23	45				CLAY (CH)
B-4, S-1	1	21								CLAY (CH)
B-4, S-2	1.9	22	101	71	25	46				CLAY (CH)
B-4, S-3	3.5	24								CLAY (CH)
B-4, S-4	5.1	21	102	68	26	42				CLAY (CH)
B-4, S-5	6.7	22								CLAY (CH)
B-4, S-6	8.5	20	104	63	25	38	99	15	84	CLAY (CH)
B-4, S-7	9.5	21								CLAY (CH)
B-4, S-8	10.6	19								CLAY (CH)
B-4, S-9	11.6	22								CLAY (CH)
B-4, S-10	12.5	21	105	68	25	43				CLAY (CH)
B-4, S-11	13.5	22								CLAY (CH)
B-4, S-12	14.5	23								CLAY (CH)
B-4, S-13	15.5	24								CLAY (CH)
B-4, S-14	16.5	25								CLAY (CH)
B-4, S-15	17.5	24								CLAY (CH)
B-4, S-16	18.5	26	100	70	24	26				CLAY (CH)
SJ-TX-02, S-1	3	19		74	24	50				CLAY (CH)
SJ-TX-02, S-2	5	17		58	20	38	99	32	67	CLAY (CH)
SJ-TX-02, S-3	9	21		75	27	48				CLAY (CH)
SJ-TX-02, S-4	17	23		65	23	42				CLAY (CH)

LOG OF BORING

PROJECT: Rio Grande Levee Study - Task 1 near the Donna Pump Hidalgo County, Texas CLIENT: U.S. Army Corp of Engineers Vicksburg, Missouri	<table style="width: 100%; border-collapse: collapse;"> <tr> <td style="border: none;">PROJECT NO.</td> <td style="border: none;">203G2082</td> </tr> <tr> <td style="border: none;">BORING NO.</td> <td style="border: none;">B-1</td> </tr> <tr> <td style="border: none;">DATE</td> <td style="border: none;">12/02/03</td> </tr> <tr> <td style="border: none;">SURFACE ELEVATION</td> <td style="border: none;"></td> </tr> </table>	PROJECT NO.	203G2082	BORING NO.	B-1	DATE	12/02/03	SURFACE ELEVATION	
PROJECT NO.	203G2082								
BORING NO.	B-1								
DATE	12/02/03								
SURFACE ELEVATION									
PAGE 1 OF 1									

SOIL SYMBOL	FIELD DATA		LABORATORY DATA								DRILLING METHOD(S):	
	DEPTH (FT)	SAMPLES N: BLOWS/FT P: TONS/SQ FT T: TONS/SQ FT PERCENT RECOVERY/ ROCK QUALITY DESIGNATION	ATTERBERG LIMITS (%)			DRY DENSITY (POUNDS/CU FT)	COMPRESSIVE STRENGTH (TONS/SQ FT)	FAILURE STRAIN (%)	CONFINING PRESSURE (POUNDS/SQ IN)	MINUS NO. 200 SIEVE (%)	GROUNDWATER INFORMATION:	
			LL LIQUID LIMIT	PL PLASTIC LIMIT	PI PLASTICITY INDEX						Subsurface water was not encountered either during or upon completion of the drilling operations.	
											DESCRIPTION OF STRATUM	
											FILL: road base	
	13				114						LEAN CLAY (CL); brown	
	13											
	11		35	20	15	118						
	15		34	18	16	113			96			
	13											
	14		32	19	13	110						
	15											
	15		41	20	21	106						
	12											
	12		42	19	23	113			95			
	16											
	12		34	19	15	106						
	11								94			
	11					110				29	SILTY SAND (SM); brown	
	10								12		- grades to light brown	
	6										Base of Levee at 14 feet	
	8											
	5								41			
											Boring Terminated at 16 Feet	

This Log is not valid if separated from original report.

LOG OF BORING 203G2082 - TASK 1.GPJ DRASH.GDT 01/23/04



Drash Consulting Engineers, Inc.
 1506 Mid-Cities Drive
 Pharr, Texas
 (956) 283-8254

FAX (956) 283-8279

REMARKS

LOG OF BORING

PROJECT: Rio Grande Levee Study - Task 1
near the Donna Pump
Hidalgo County, Texas

CLIENT: U.S. Army Corp of Engineers
Vicksburg, Missouri

PROJECT NO. 203G2082
BORING NO. B-2
DATE 12/02/03
SURFACE ELEVATION _____

PAGE 1 OF 1

SOIL SYMBOL	FIELD DATA			LABORATORY DATA							DRILLING METHOD(S):	
	DEPTH (FT)	SAMPLES	N: BLOWS/FT P: TONS/SQ FT T: TONS/SQ FT PERCENT RECOVERY/ ROCK QUALITY DESIGNATION	ATTERBERG LIMITS (%)			DRY DENSITY (POUNDS/CU FT)	COMPRESSIVE STRENGTH (TONS/SQ FT)	FAILURE STRAIN (%)	CONFINING PRESSURE (POUNDS/SQ IN)	MINUS NO. 200 SIEVE (%)	GROUNDWATER INFORMATION:
				LL	PL	PI						Subsurface water was encountered at 23 feet during the drilling operations.
DESCRIPTION OF STRATUM												
												FILL: roadway
	21					107						LEAN CLAY (CL); dark brown
	21											
	20			40	20	20	105				94	
5	21											SILTY SAND (SM); light brown, very fine grained
	10										29	
	25			54	25	29	102				97	FAT CLAY (CH); dark brown with sand/silt partings
	22											
	18			45	20	25	100					- lean clay from 9 to 10 feet
10	20											
	21			56	24	32	104					
	23											
	15						109					LEAN CLAY (CL); brown
	14											
	17											Base of Levee at 13.25 feet
15	17										97	FAT CLAY (CH); dark gray with organics
	17			55	25	30	104					- with silt
	28			54	23	31						
	30											
	28						94					
20												
												Boring Terminated at 23.5 Feet

LOG OF BORING 203G2082 - TASK1.GPJ DRASH.GDT 01/23/04 This Log is not valid if separated from original report.



Drash Consulting Engineers, Inc.
1506 Mid-Cities Drive
Pharr, Texas
(956) 283-8254
FAX (956) 283-8279

REMARKS

LOG OF BORING

PROJECT: Rio Grande Levee Study - Task 1
near the Donna Pump
Hidalgo County, Texas

CLIENT: U.S. Army Corp of Engineers
Vicksburg, Missouri

PROJECT NO. 203G2082
BORING NO. B-3
DATE 12/02/03
SURFACE ELEVATION

PAGE 1 OF 1

SOIL SYMBOL	FIELD DATA				LABORATORY DATA							DRILLING METHOD(S):		
	DEPTH (FT)	SAMPLES	N: BLOWS/FT P: TONS/SQ.FT T: TONS/SQ.FT PERCENT RECOVERY/ ROCK QUALITY DESIGNATION	MOISTURE CONTENT (%)	ATTERBERG LIMITS (%)			DRY DENSITY (POUNDS/CU FT)	COMPRESSIVE STRENGTH (TONS/SQ.FT)	FAILURE STRAIN (%)	CONFINING PRESSURE (POUNDS/SQ.IN)	MINUS NO. 200 SIEVE (%)	GROUNDWATER INFORMATION:	
					LL	PL	PI						DESCRIPTION OF STRATUM	
													Dry augered from 0 to 18 feet.	
													Subsurface water was not encountered either during or upon completion of the drilling operations.	
													FILL: roadway	
													FAT CLAY (CH); brown - with silt partings to 3.5 feet	
													- with silt partings from 5 to 7 feet	
													- with silt seam	
													Base of Levee at 12 feet	
													Boring Terminated at 18 Feet	

LOG OF BORING 203G2082 - TASK 1.GPJ DRASH.GDT 01/23/04 This Log is not valid if separated from original report.



Drash Consulting Engineers, Inc.
1506 Mid-Cities Drive
Pharr, Texas
(956) 283-8254

FAX (956) 283-8279

REMARKS

LOG OF BORING

PROJECT: Rio Grande Levee Study - Task 1
 near the Donna Pump
 Hidalgo County, Texas

CLIENT: U.S. Army Corp of Engineers
 Vicksburg, Missouri

PROJECT NO. 203G2082
BORING NO. SJ-TX-02
DATE _____
SURFACE ELEVATION _____

PAGE 1 OF 1

FIELD DATA		LABORATORY DATA							DRILLING METHOD(S):		
SOIL SYMBOL	DEPTH (FT)	SAMPLES N: BLOWS/FT P: TONS/SQ FT T: TONS/SQ FT PERCENT RECOVERY/ ROCK QUALITY DESIGNATION	MOISTURE CONTENT (%)	ATTERBERG LIMITS (%)			DRY DENSITY (POUNDS/CU FT)	COMPRESSIVE STRENGTH (TONS/SQ FT)	FAILURE STRAIN (%)	CONFINING PRESSURE (POUNDS/SQ IN)	MINUS NO. 200 SIEVE (%)
				LL	PL	PI					
				LIQUID LIMIT	PLASTIC LIMIT	PLASTICITY INDEX					
GROUNDWATER INFORMATION: Subsurface water was not encountered either during or upon completion of the drilling operations.											
DESCRIPTION OF STRATUM											
											FAT CLAY (CH); brown
	5		19	74	24	50					
			17	58	20	38				99	
	10		21	75	27	48					
	15		23	65	23	42					
											Boring Terminated at 18 Feet
 Drash Consulting Engineers, Inc. 1506 Mid-Cities Drive Pharr, Texas (956) 283-8254										REMARKS	
LOG OF BORING 203G2082 - TASK 1.GPJ_DRASH.GDT 01/23/04 This Log is not valid if separated from original report.										FAX (956) 283-8279	

LABORATORY TESTING PROGRAM

General

Soil mechanics laboratory tests procedures are performed in accordance with accepted geotechnical engineering practice. These procedures are described in detail in the most current edition of the American Society for Testing and Materials (ASTM) book titled Annual Book of ASTM Standards or as outlined in the book titled: Soil Testing for Engineers, by T. William Lambe.

Testing Program

The laboratory-testing program was directed towards evaluating the physical and engineering properties of the soils. The tests performed for this study consisted of the following:

Laboratory Test

Applicable Test Standards

Moisture Content of Soil

ASTM D 2216

Liquid Limit, Plastic Limit & Plasticity Index of Soil

ASTM D 4318

Particle Size Analysis for Soils

ASTM D 421 & D 422

Density of Soil In-Place by the Drive Cylinder Method

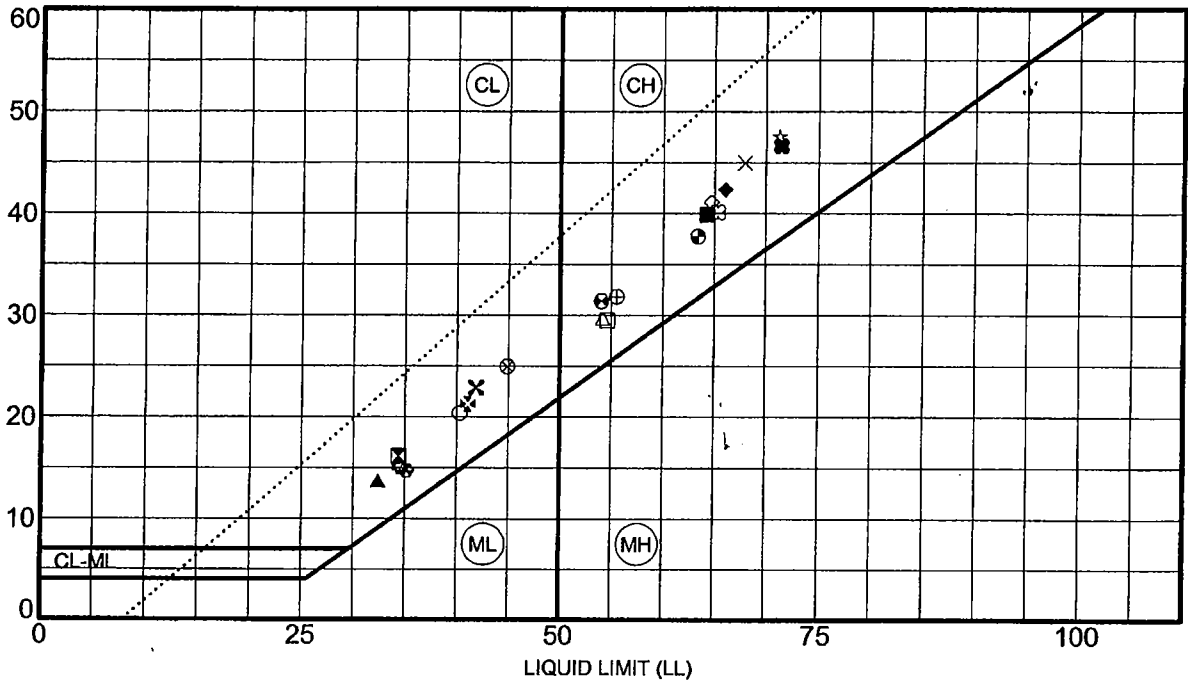
ASTM D 2937

The laboratory test results are tabulated on attached sheets that follow. Laboratory test results were used to classify the soils encountered in substantial accordance with the Unified Soil Classification System (ASTM D 2487).

Sample Disposal

All samples were returned to our laboratory. The samples not tested in the laboratory will be stored for a period of 60 days subsequent to submittal of this report and will be discarded after this period, unless other arrangements are made prior to the disposal period.

PLASTICITY INDEX



Symbol	Specimen Identification	LL	PL	PI	Fines	MC%	Classification
⊕	B-1	3.0	35	20	15	11	
⊠	B-1	4.0	34	18	16	96	LEAN CLAY(CL)
▲	B-1	5.0	32	19	13	14	
⊗	B-1	6.8	41	20	21	15	
×	B-1	8.1	42	19	23	95	LEAN CLAY(CL)
⊕	B-1	10.7	34	19	15	12	
○	B-2	3.0	40	20	20	94	LEAN CLAY(CL)
△	B-2	7.0	54	25	29	97	FAT CLAY(CH)
⊗	B-2	9.2	45	20	25	18	
⊕	B-2	10.6	56	24	32	21	
□	B-2	14.6	55	25	30	97	FAT CLAY(CH)
⊕	B-2	16.2	54	23	31	28	
⊕	B-3	3.5	63	26	37	19	
☆	B-3	5.0	71	24	47	99	FAT CLAY(CH)
⊗	B-3	7.7	65	25	40	20	
■	B-3	9.8	64	24	40	98	FAT CLAY(CH)
◆	B-3	11.8	66	24	42	19	
◇	B-3	13.5	65	24	41	99	FAT CLAY(CH)
×	B-3	16.8	68	23	45	19	
⊗	B-4	1.9	71	25	46	22	

PROJECT Rio Grande Levee Study - Task 1 - near the Donna Pump

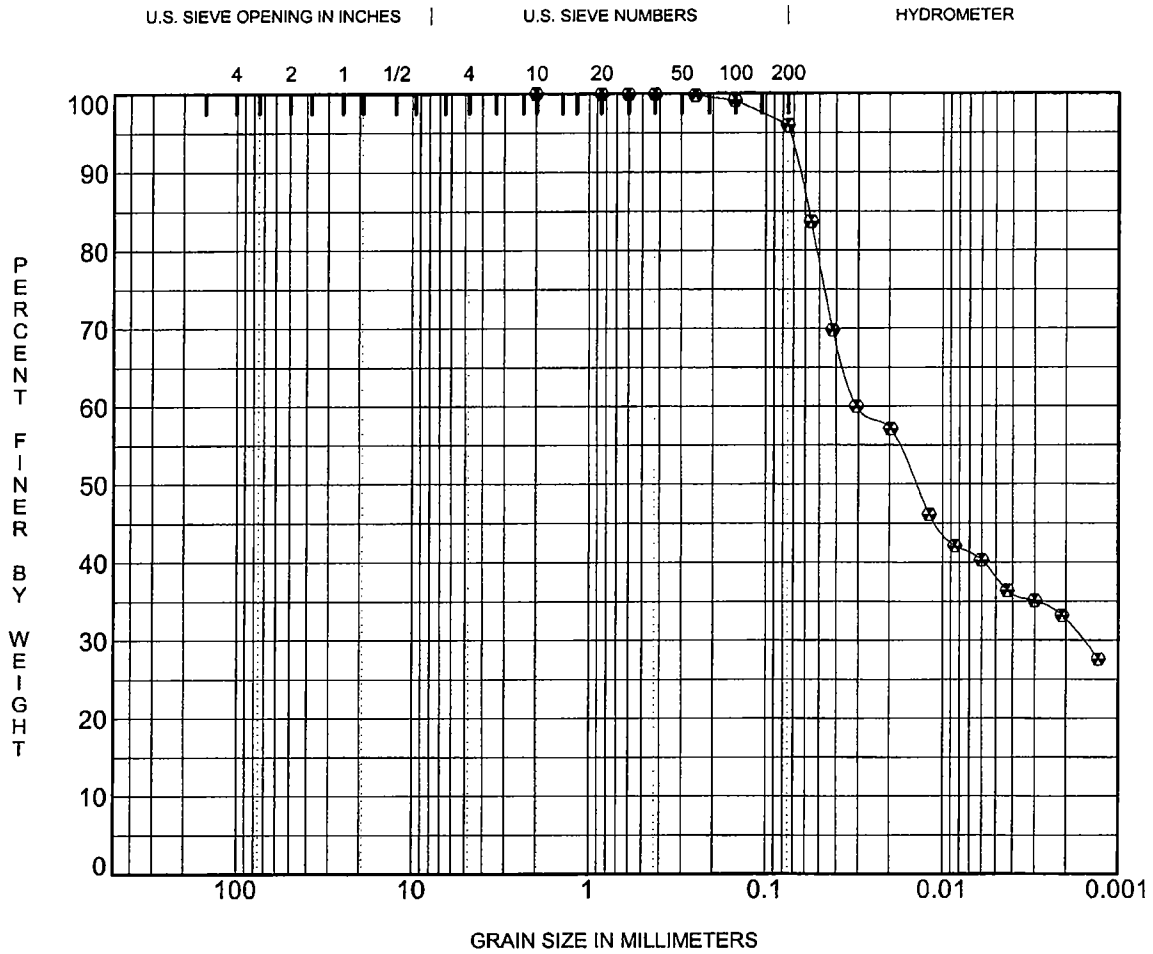
JOB NO. 203G2082

ATTERBERG LIMITS RESULTS



DRASH
CONSULTING ENGINEERS, INC.

B-2



COBBLES	GRAVEL		SAND			SILT OR CLAY
	coarse	fine	coarse	medium	fine	

Specimen Identification	Classification	MC%	LL	PL	PI	Cc	Cu
⊗ B-1 4.0	LEAN CLAY(CL)	15	34	18	16		

Specimen Identification	D100	D60	D30	D10	%Gravel	%Sand	%Silt	%Clay
⊗ B-1 4.0	2.00	0.03	0.002		0	4	58	38

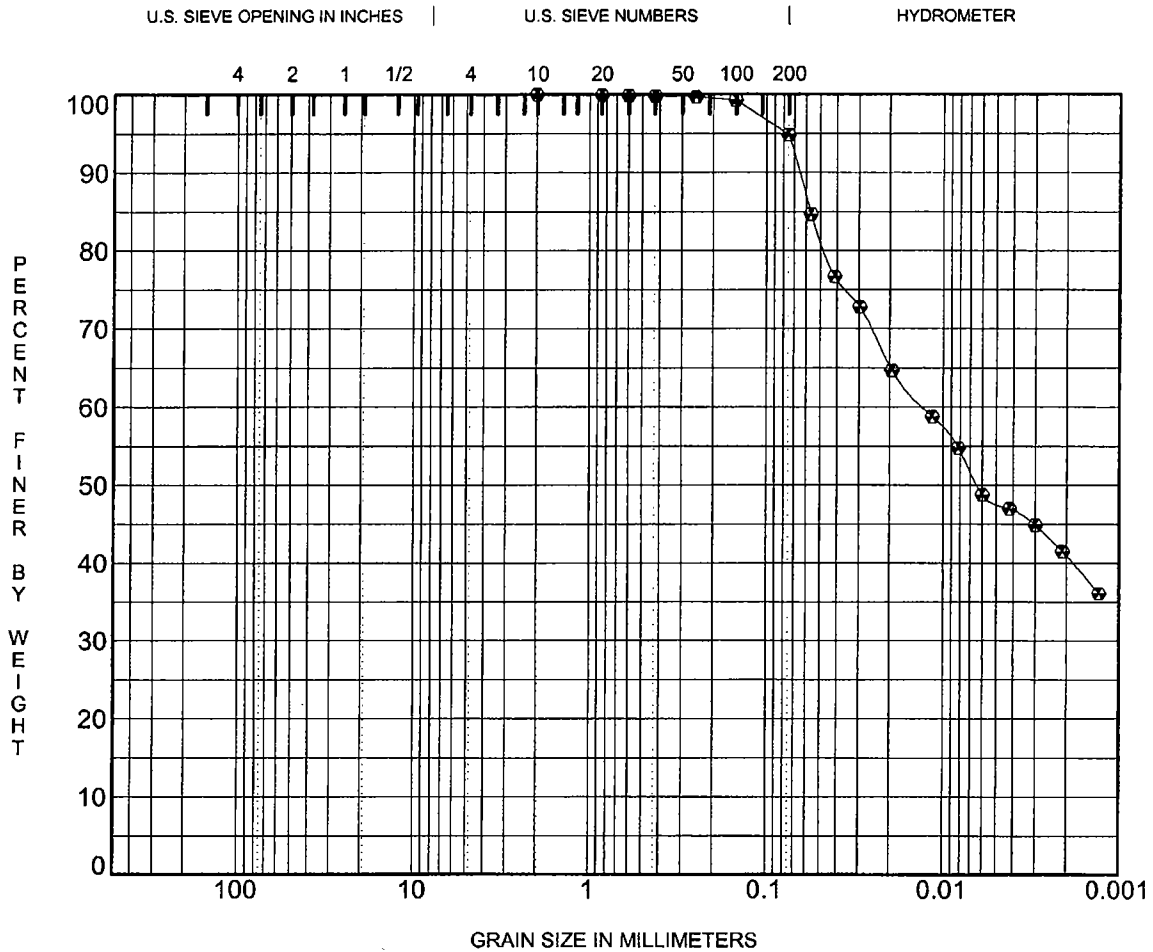
PROJECT **Rio Grande Levee Study - Task 1 - near the Donna Pump** JOB NO. **203G2082**

GRADATION CURVES



DRASH CONSULTING ENGINEERS, INC.

SIEVE 203G2082 - TASK 1.GPJ DRASH.GDT 1/23/04



COBBLES	GRAVEL		SAND			SILT OR CLAY
	coarse	fine	coarse	medium	fine	

Specimen Identification	Classification	MC%	LL	PL	PI	Cc	Cu
⊕ B-1 8.1	LEAN CLAY(CL)	12	42	19	23		

Specimen Identification	D100	D60	D30	D10	%Gravel	%Sand	%Silt	%Clay
⊕ B-1 8.1	2.00	0.01			0	5	47	48

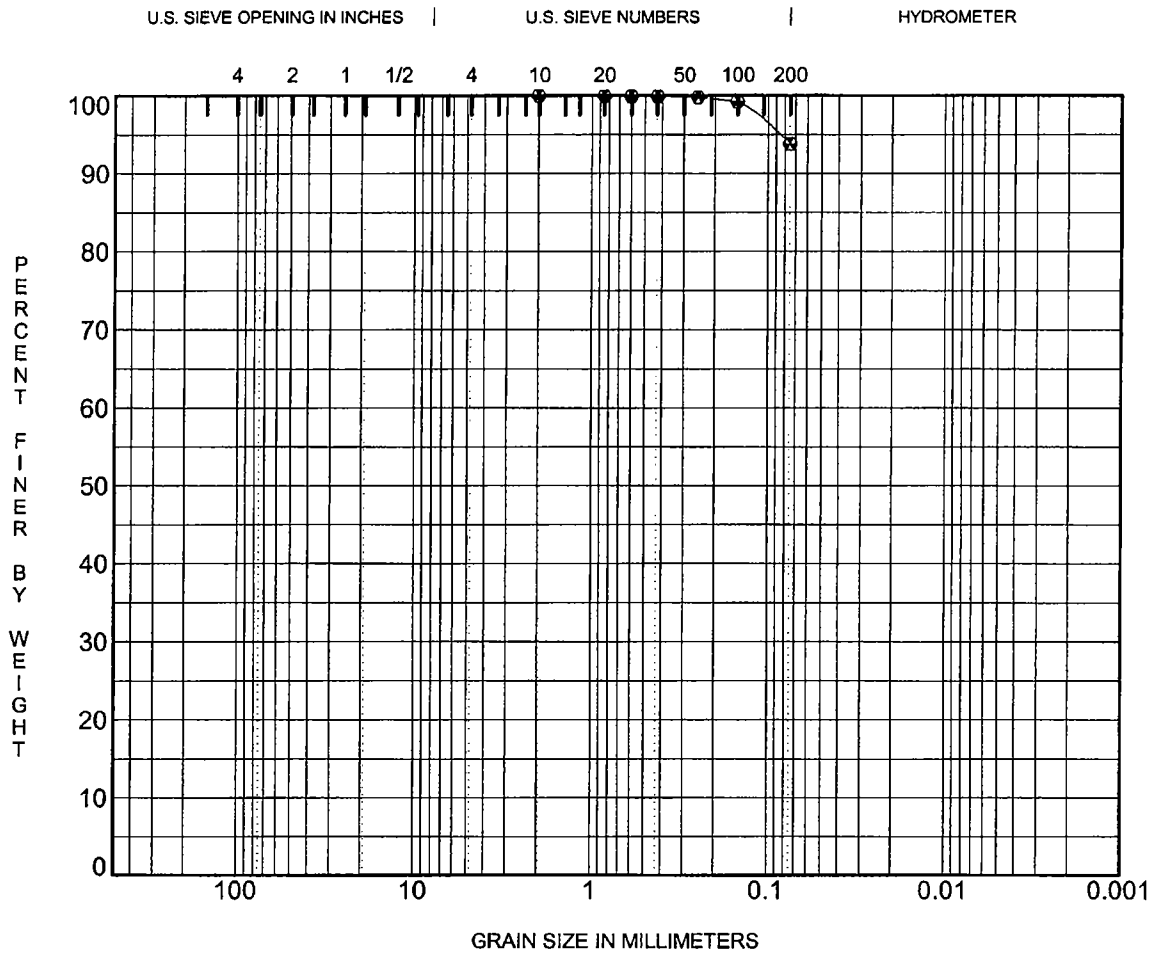
PROJECT **Rio Grande Levee Study - Task 1 - near the Donna Pump** JOB NO. **203G2082**

GRADATION CURVES



DRASH CONSULTING ENGINEERS, INC.

SIEVE 203G2082 - TASK 1.GPJ DRASH.GDT 1/23/04



COBBLES	GRAVEL		SAND			SILT OR CLAY
	coarse	fine	coarse	medium	fine	

Specimen Identification	Classification	MC%	LL	PL	PI	Cc	Cu
⊕ B-1 11.5		11					

Specimen Identification	D100	D60	D30	D10	%Gravel	%Sand	%Silt	%Clay
⊕ B-1 11.5	2.00				0	6	94	

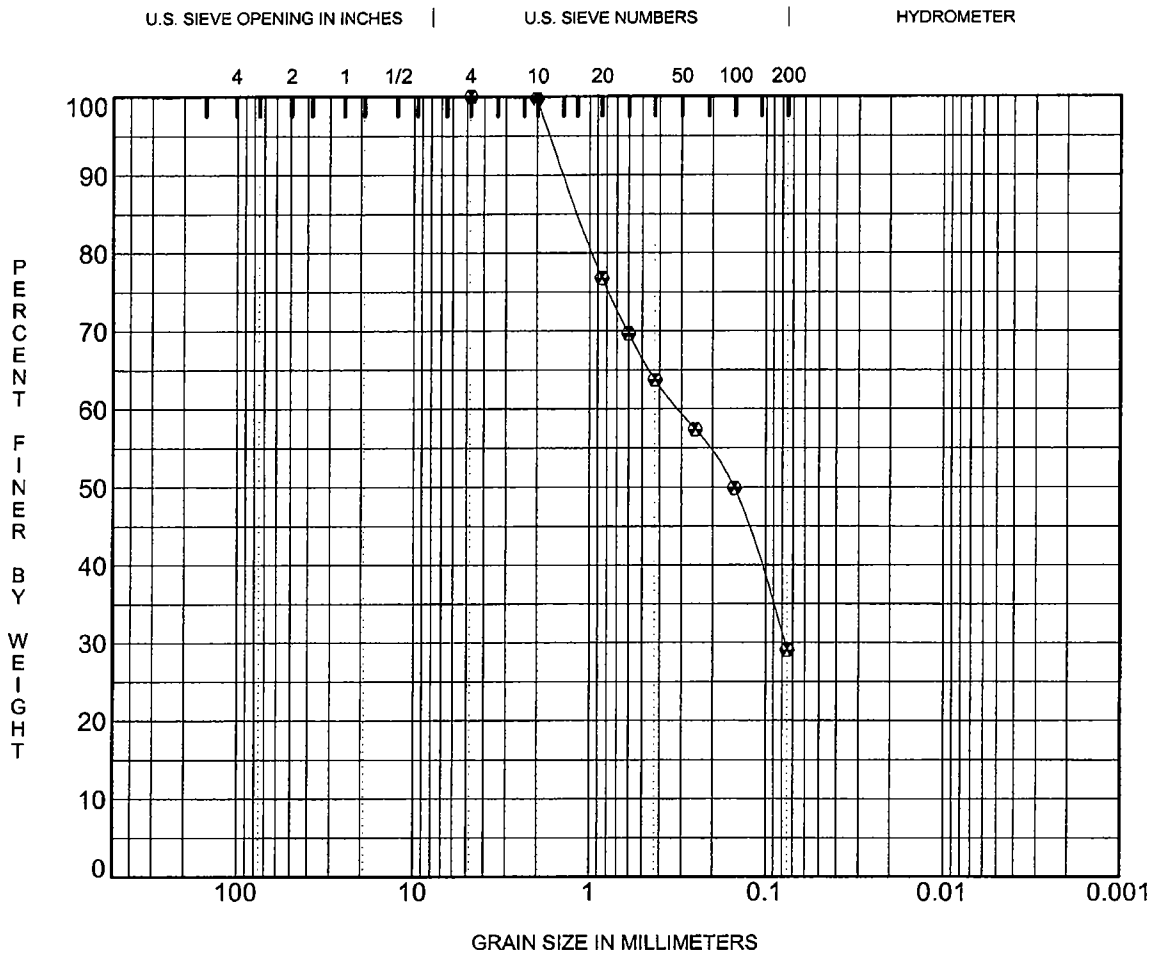
PROJECT **Rio Grande Levee Study - Task 1 - near the Donna Pump** JOB NO. 203G2082

GRADATION CURVES



DRASH CONSULTING ENGINEERS, INC.

SIEVE 203G2082 - TASK 1.GPJ DRASH.GDT 1/23/04



COBBLES	GRAVEL		SAND			SILT OR CLAY
	coarse	fine	coarse	medium	fine	

Specimen Identification	Classification	MC%	LL	PL	PI	Cc	Cu
⊗ B-1 12.3		11					

Specimen Identification	D100	D60	D30	D10	%Gravel	%Sand	%Silt	%Clay
⊗ B-1 12.3	4.75	0.31	0.077		0	71	29	

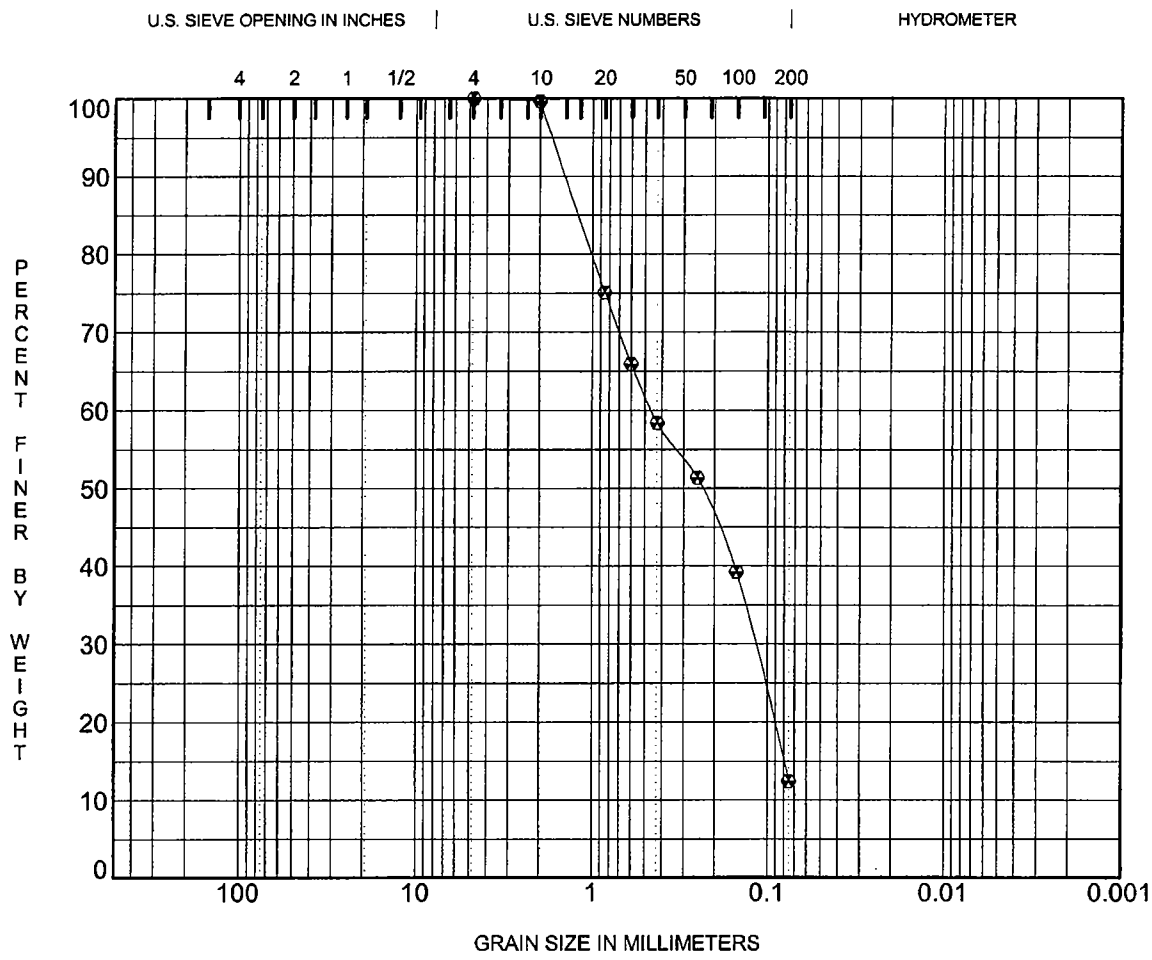
PROJECT **Rio Grande Levee Study - Task 1 - near the Donna Pump** JOB NO. **203G2082**

GRADATION CURVES



DRASH CONSULTING ENGINEERS, INC.

SIEVE 203G2082 - TASK 1.GPJ DRASH.GDT 1/23/04



COBBLES	GRAVEL		SAND			SILT OR CLAY
	coarse	fine	coarse	medium	fine	

Specimen Identification	Classification	MC%	LL	PL	PI	Cc	Cu
⊕ B-1 13.2		10				0.43	6.5

Specimen Identification	D100	D60	D30	D10	%Gravel	%Sand	%Silt	%Clay
⊕ B-1 13.2	4.75	0.46	0.118		0	88	12	

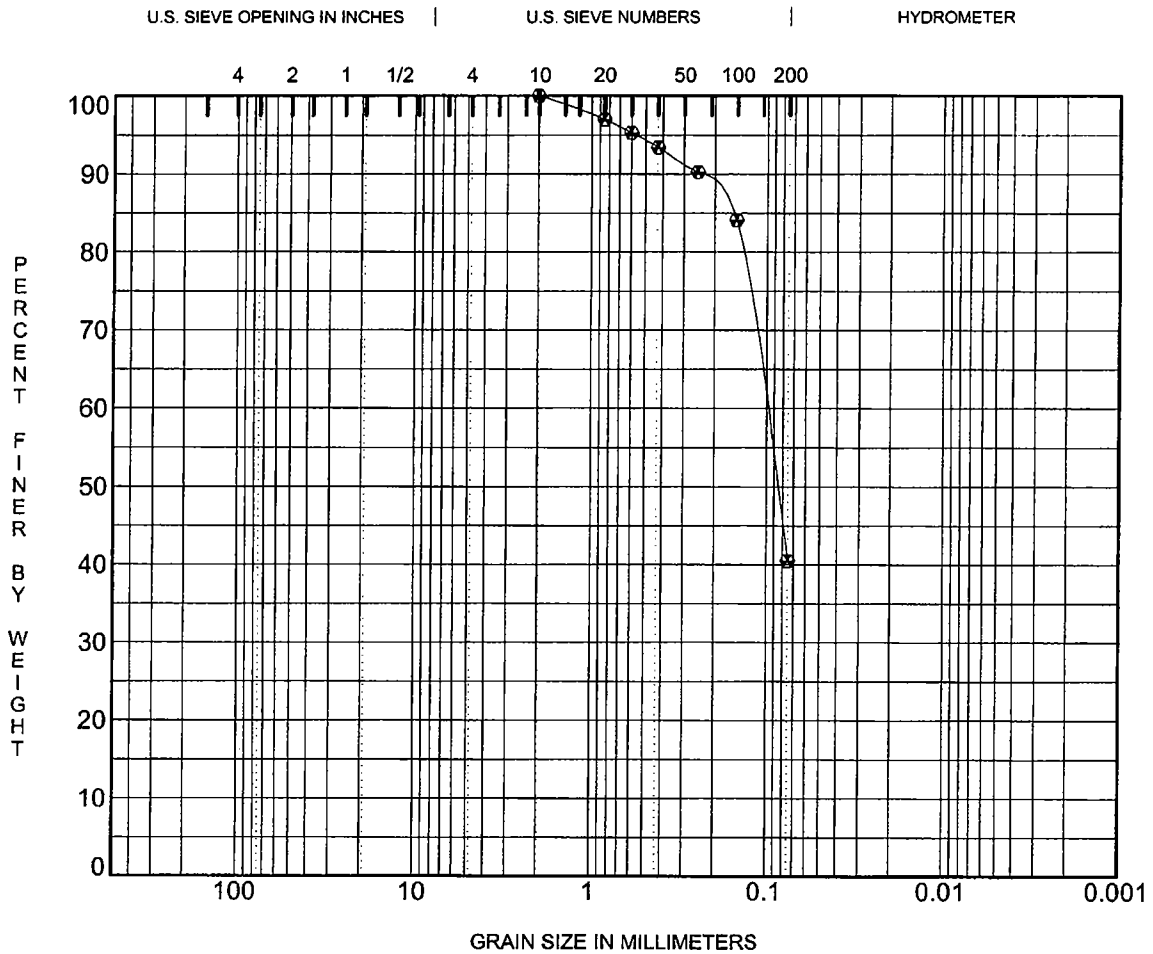
PROJECT **Rio Grande Levee Study - Task 1 - near the Donna Pump** JOB NO. **203G2082**

GRADATION CURVES



DRASH CONSULTING ENGINEERS, INC.

SIEVE 203G2082 - TASK 1.GPJ DRASH.GDT 1/23/04



COBBLES	GRAVEL		SAND			SILT OR CLAY
	coarse	fine	coarse	medium	fine	

Specimen Identification	Classification	MC%	LL	PL	PI	Cc	Cu
⊕ B-1 15.3		5					

Specimen Identification	D100	D60	D30	D10	%Gravel	%Sand	%Silt	%Clay
⊕ B-1 15.3	2.00	0.10			0	59	41	

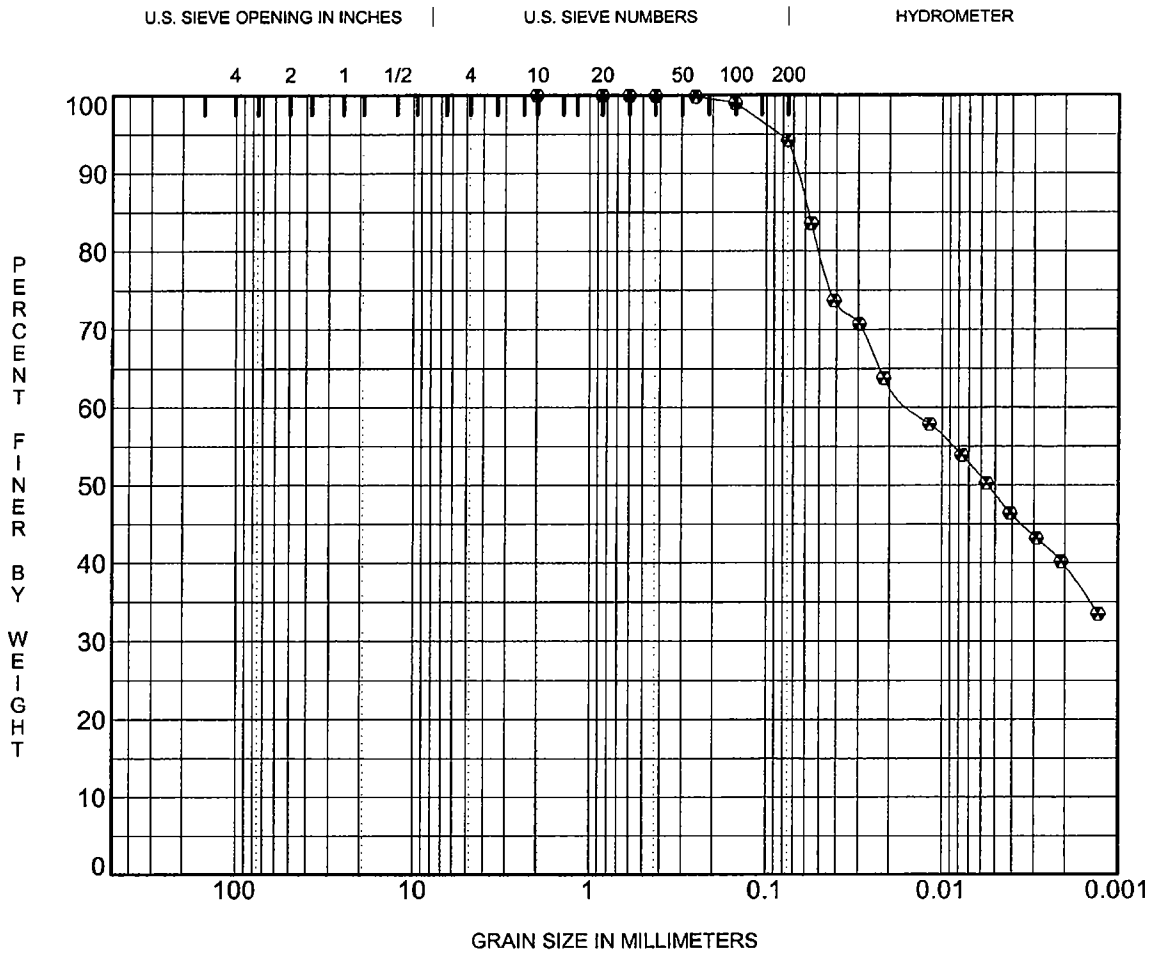
PROJECT Rio Grande Levee Study - Task 1 - near the Donna Pump JOB NO. 203G2082

GRADATION CURVES



**DRASH
CONSULTING ENGINEERS, INC.**

SIEVE 203G2082 - TASK 1.GPJ DRASH.GDT 1/23/04



COBBLES	GRAVEL		SAND			SILT OR CLAY
	coarse	fine	coarse	medium	fine	

Specimen Identification	Classification	MC%	LL	PL	PI	Cc	Cu
⊕ B-2 3.0	LEAN CLAY(CL)	20	40	20	20		

Specimen Identification	D100	D60	D30	D10	%Gravel	%Sand	%Silt	%Clay
⊕ B-2 3.0	2.00	0.01			0	6	45	49

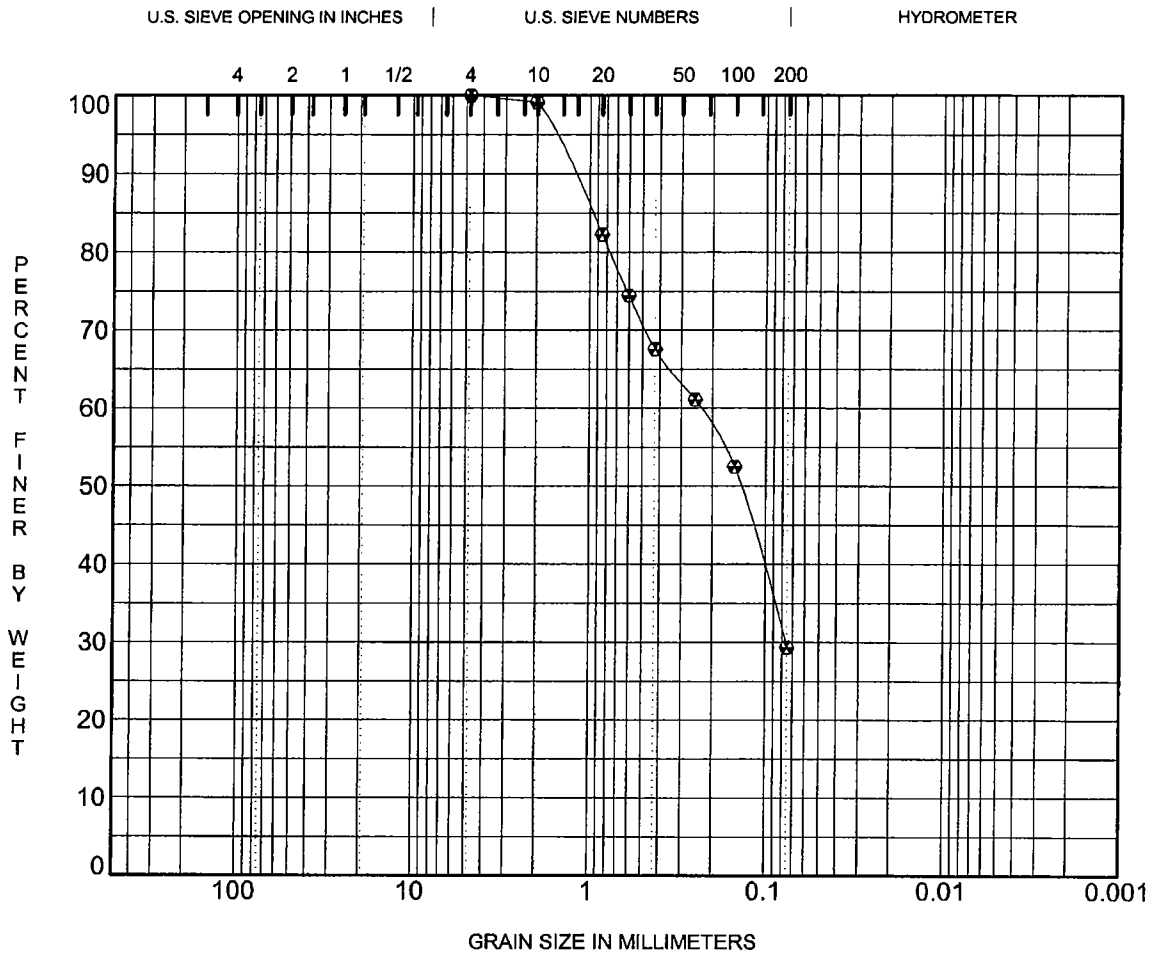
PROJECT Rio Grande Levee Study - Task 1 - near the Donna Pump JOB NO. 203G2082

GRADATION CURVES



DRASH CONSULTING ENGINEERS, INC.

SIEVE 203G2082 - TASK 1.GPJ DRASH.GDT 1/23/04



COBBLES	GRAVEL		SAND			SILT OR CLAY
	coarse	fine	coarse	medium	fine	

Specimen Identification	Classification	MC%	LL	PL	PI	Cc	Cu
⊕ B-2 5.0		21					

Specimen Identification	D100	D60	D30	D10	%Gravel	%Sand	%Silt	%Clay
⊕ B-2 5.0	4.75	0.23	0.077		0	71	29	

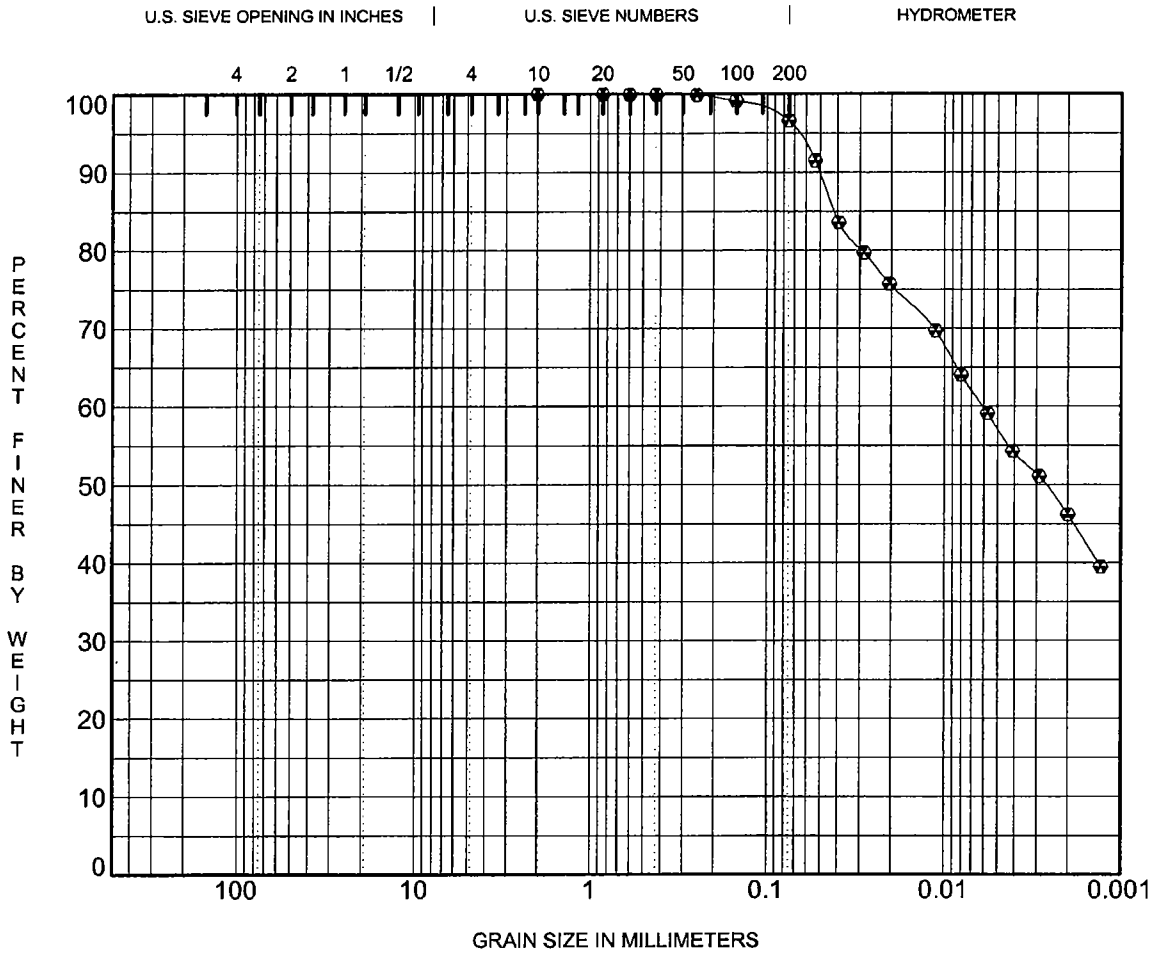
PROJECT **Rio Grande Levee Study - Task 1 - near the Donna Pump** JOB NO. **203G2082**

GRADATION CURVES



DRASH CONSULTING ENGINEERS, INC.

SIEVE 203G2082 - TASK 1.GPJ DRASH.GDT 1/23/04



COBBLES	GRAVEL		SAND			SILT OR CLAY
	coarse	fine	coarse	medium	fine	

Specimen Identification	Classification	MC%	LL	PL	PI	Cc	Cu
⊕ B-2 7.0	FAT CLAY(CH)	25	54	25	29		

Specimen Identification	D100	D60	D30	D10	%Gravel	%Sand	%Silt	%Clay
⊕ B-2 7.0	2.00	0.01			0	3	39	57

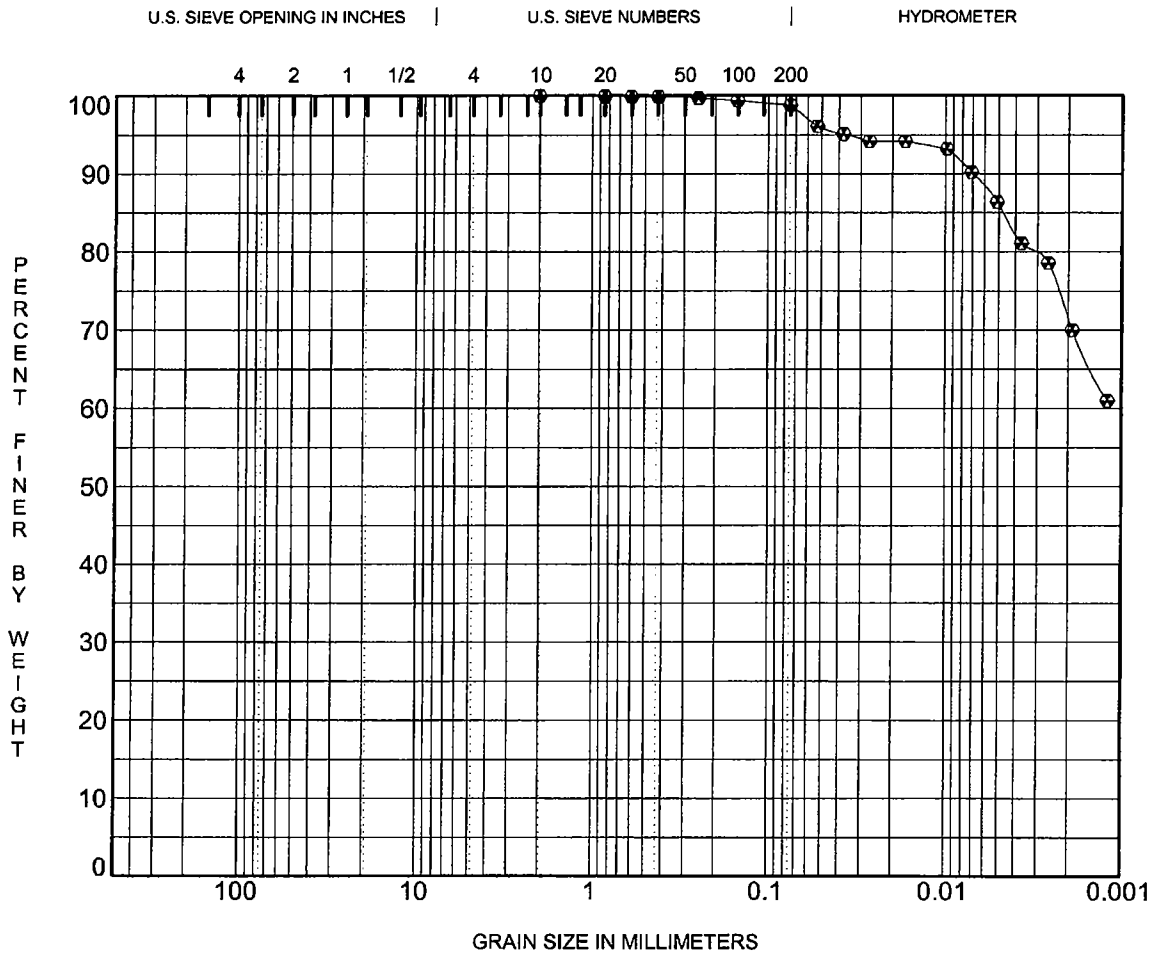
PROJECT **Rio Grande Levee Study - Task 1 - near the Donna Pump** JOB NO. **203G2082**

GRADATION CURVES



DRASH CONSULTING ENGINEERS, INC.

SIEVE 203G2082 - TASK 1.GPJ DRASH.GDT 1/23/04



COBBLES	GRAVEL		SAND			SILT OR CLAY
	coarse	fine	coarse	medium	fine	

Specimen Identification	Classification	MC%	LL	PL	PI	Cc	Cu
⊕ B-3 5.0	FAT CLAY(CH)	15	71	24	47		

Specimen Identification	D100	D60	D30	D10	%Gravel	%Sand	%Silt	%Clay
⊕ B-3 5.0	2.00				0	1	13	86

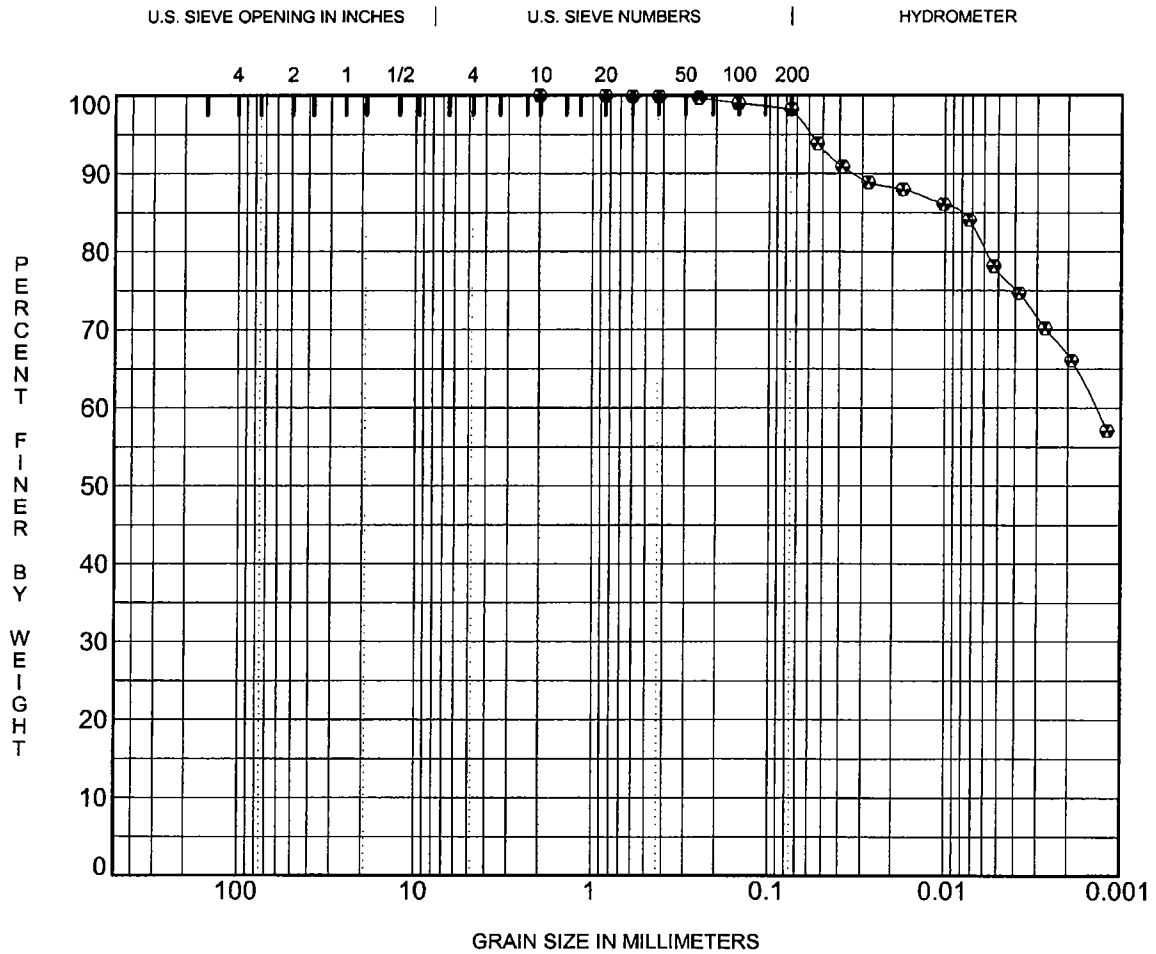
PROJECT **Rio Grande Levee Study - Task 1 - near the Donna Pump** JOB NO. **203G2082**

GRADATION CURVES



DRASH CONSULTING ENGINEERS, INC.

SIEVE 203G2082-TASK1.GPJ DRASH.GDT 1/23/04



COBBLES	GRAVEL		SAND			SILT OR CLAY
	coarse	fine	coarse	medium	fine	

Specimen Identification	Classification	MC%	LL	PL	PI	Cc	Cu
⊗ B-3 9.8	FAT CLAY(CH)	16	64	24	40		

Specimen Identification	D100	D60	D30	D10	%Gravel	%Sand	%Silt	%Clay
⊗ B-3 9.8	2.00	0.00			0	2	21	78

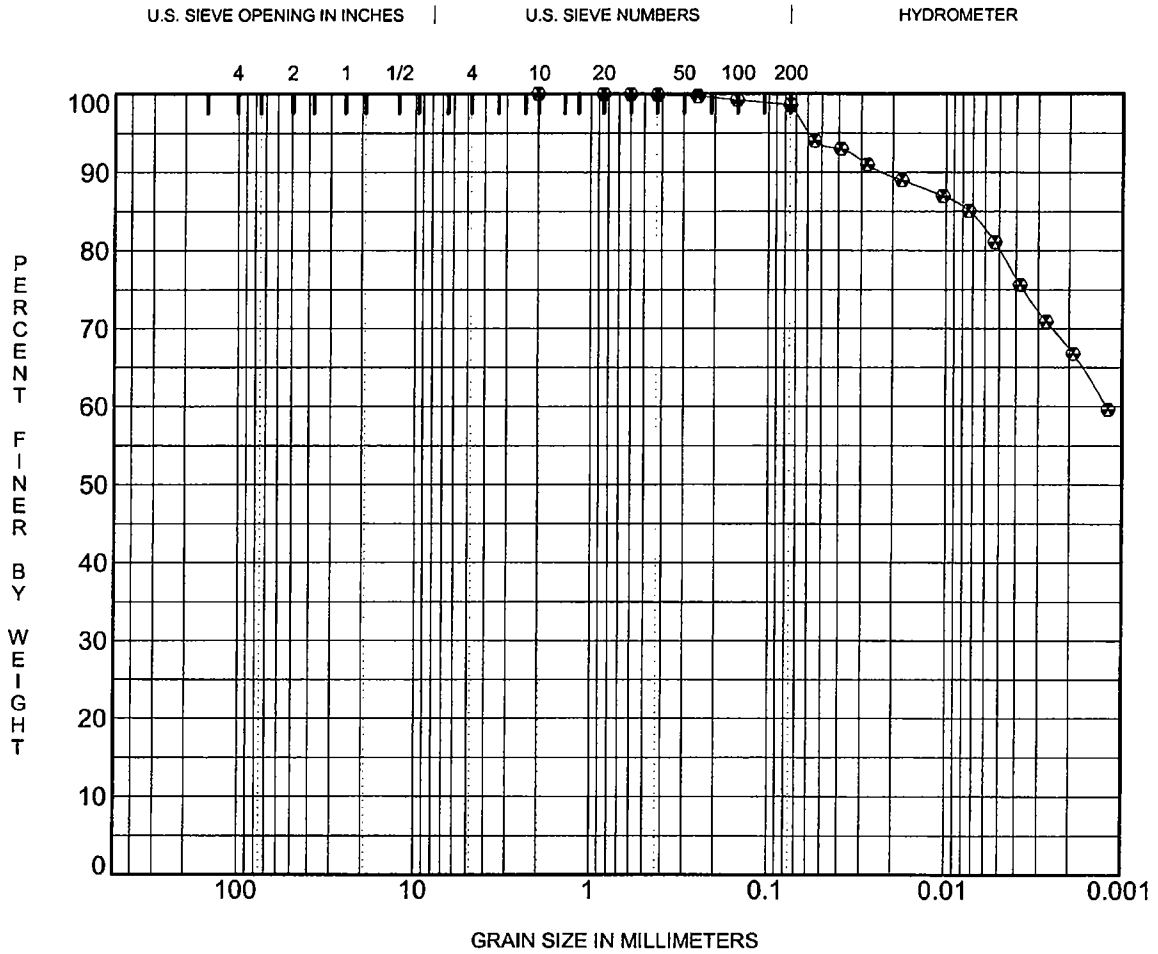
PROJECT Rio Grande Levee Study - Task 1 - near the Donna Pump JOB NO. 203G2082

GRADATION CURVES



**DRASH
CONSULTING ENGINEERS, INC.**

SIEVE 203G2082 - TASK 1.GPJ DRASH.GDT 1/23/04



COBBLES	GRAVEL		SAND			SILT OR CLAY
	coarse	fine	coarse	medium	fine	

Specimen Identification	Classification	MC%	LL	PL	PI	Cc	Cu
⊕ B-3 13.5	FAT CLAY(CH)	19	65	24	41		

Specimen Identification	D100	D60	D30	D10	%Gravel	%Sand	%Silt	%Clay
⊕ B-3 13.5	2.00	0.00			0	1	18	80

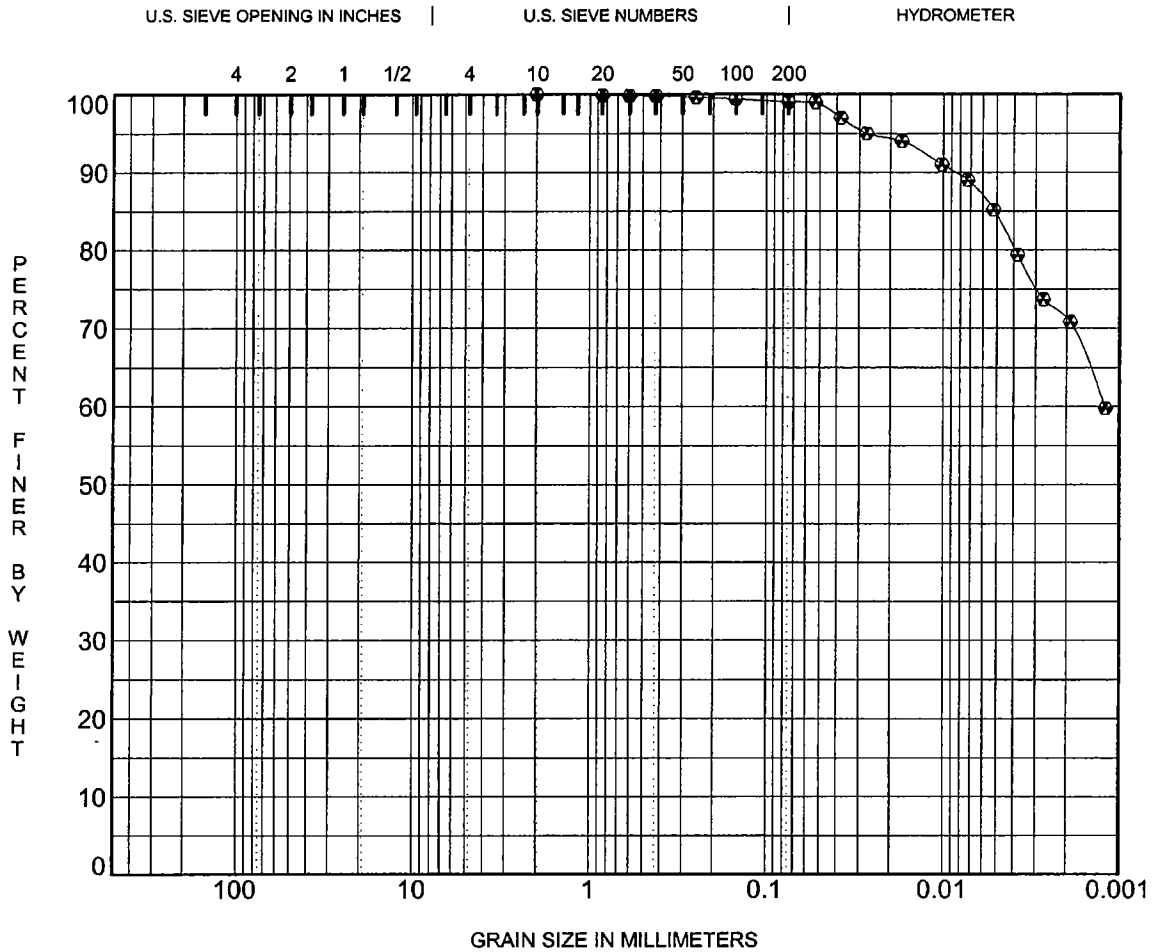
PROJECT **Rio Grande Levee Study - Task 1 - near the Donna Pump** JOB NO. **203G2082**

GRADATION CURVES



DRASH CONSULTING ENGINEERS, INC.

SIEVE 203G2082 - TASK 1.GPJ DRASH.GDT 1/23/04



COBBLES	GRAVEL		SAND			SILT OR CLAY
	coarse	fine	coarse	medium	fine	

Specimen Identification	Classification	MC%	LL	PL	PI	Cc	Cu
⊕ B-4 8.5	FAT CLAY(CH)	20	63	25	38		

Specimen Identification	D100	D60	D30	D10	%Gravel	%Sand	%Silt	%Clay
⊕ B-4 8.5	2.00	0.00			0	1	15	84

PROJECT **Rio Grande Levee Study - Task 1 - near the Donna Pump**

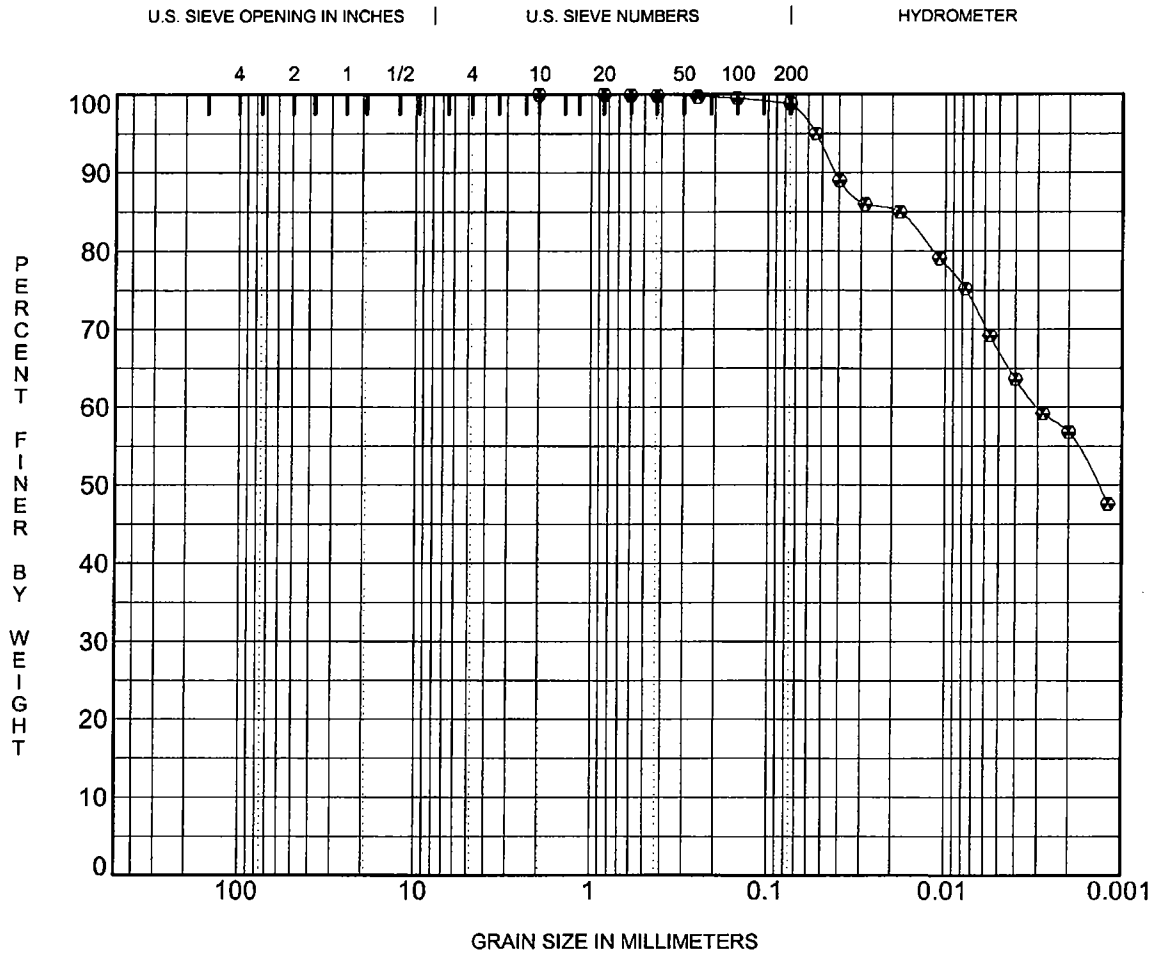
JOB NO. **203G2082**

GRADATION CURVES



DRASH CONSULTING ENGINEERS, INC.

SIEVE 203G2082 - TASK 1.GPJ DRASH.GDT 1/23/04



COBBLES	GRAVEL		SAND			SILT OR CLAY
	coarse	fine	coarse	medium	fine	

Specimen Identification	Classification	MC%	LL	PL	PI	Cc	Cu
⊕ SJ-TX-02 5.0	FAT CLAY(CH)	17	58	20	38		

Specimen Identification	D100	D60	D30	D10	%Gravel	%Sand	%Silt	%Clay
⊕ SJ-TX-02 5.0	2.00	0.00			0	1	32	67

PROJECT **Rio Grande Levee Study - Task 1 - near the Donna Pump** JOB NO. **203G2082**

GRADATION CURVES



DRASH CONSULTING ENGINEERS, INC.

SIEVE_203G2082 - TASK 1.GPJ DRASH.GDT 1/23/04

Appendix D

Pettiet Soil Chemistry Results

Pettiet Agricultural Services, Inc.

Soil Testing & Plant Analysis Laboratory

105 Old Highway 61S - P.O. Box 838

Leland, MS 38756

Phone: (662) 686-9473 Fax: (662) 686-7579

Joe V. Pettiet, Ph.D.....President

Clinton Pettiet, M.A.....Agronomist

February 10, 2004

Mr. Joe Dunbar
ERDC
3909 Halls Ferry Road
Vicksburg, MS 39189

Dear Joe:

Soil test results of 15 soil samples brought to the Lab last week are included in this report. You requested our regular soil test that included exchangeable sodium and cation exchange capacity of soils. These data are shown in our Soil Test Analyses - Fertilizer recommendation (green) sheets.

The following laboratory procedures were used in the analyses:

pH	Glass pH electrode measure of a 1:2 soil to water mixture.
Total Acidity	Glass pH electrode measure of a 1:2 soil to buffer mixture using the single SMP lime solution.
P, K, Ca Mg, Na, S, & Zn	Using the Mehlich 3 soil extract* (0.2N CH ₃ COOH; 0.25N NH ₄ NO ₃ ; 0.01N NHF; 0.013N HNO ₃ ; 0.01M EDTA). All elements were determined by an inducely coupled argon plasma emission spectrophotometer (ICP).
CEC, % Base sat.	Calculated by summation of the base nutrients and acidity shown by the lime test.
Organic Matter	Based on loss-on-ignition, proposed by M. J. Donkin.**

* Mehlich, 1984. Mehlich 3 Soil Test Extractant: A modification of Mehlich 2 Extractant. Comm. Soil Sci. and Plant Anal. 15(12), 1406-1416.

**Modified procedure of M. J. Donkin, 1991 Loss-On-Ignition as an Estimator of Soil Organic Carbon in A-Horizon Forestry Soils. Comm. Soil Sci. and plant anal. 22(3,4) pp 233-241.

We usually determine cation exchange capacity by summation of base nutrient concentrations (Ca, Mg, K) and exchangeable acidity (in Me/100g soil). However, your soil samples contained high sodium and free calcium carbonate salts that were extracted and measured by our soil test. The high salt content nullifies the CEC measure based on summation of exchangeable bases. As a result, we measured the clay content in soil samples and calculated CEC based on the high correlation equation of clay content and CEC for soils in this area ($r^2=.98$).

For your information, the corrected CEC values are shown in red in the Soil Analyses (green) sheets. CEC values based on cation summation are shown below the red values. You had more free salt than exchangeable bases.

The calcium concentrations in samples were above the range of our computer generated calculations, so I have corrected calcium, CEC, and base saturation values based on sum of bases.

We did not have enough soil to run the percent organic matter and organic sulfur content. The values shown are calculated values from organic matter - clay and organic matter - organic sulfur correlations. Your samples will most likely have higher organic matter and organic sulfur values. Soluble sulfur values are shown in red below calculated organic sulfur (in ppm).

The identification of sampling sites are shown on a separate sheet in this report. The majority of soil samples are clay soils with high calcium, sodium and soluble sulfur concentrations.

I hope this information is helpful. Call or come by the Laboratory if you have questions. We appreciate your business.

Respectfully,



Joe V. Pettiet
Agronomist

Enclosures:

SOIL AND CROPPING HISTORY-INFORMATION SHEET

RECORD NUMBER _____

Farmer's name: JOE DUNBAR USCE waterway site

Date: 1-28-04

Address: ERDC-WAS 3909 HALL'S FERRY RD VICKSBURG, MS 39189

Phone: 1-800-522-6937 ext. 3315
601-634-3315

Type of services needed: DETAILED ANALYSIS (GREEN SHEETS) in cooperation w/ PATRICK ROYNE @ USM

NO - RECOMMENDATIONS

Identification: Sample number	<u>SMPLE ID</u>	Primary Crop this year	Secondary Crop this Year	Special information..	<u>SMPLE ID</u>
EB-06-01-01	1			3-4: 7.7' - 8.3'	6
EB 07-01-01	2			4-4: 7.0' - 7.4'	7
MC 03-01-02	3			SJ TX-02: 3'-5'	8
MC 06-01-01	4			SJ TX-02: 9'-11'	9
MC 09-01-02	5			SJ TX-02: 13'-15'	10
D 4				RETAMAL 1-8: 6.75' - 7.3'	11
				RETAMAL 1-5: 4.5' - 5.0'	12
				RETAMAL DIKE 2-4: 7.0' - 7.9'	13
				WB-02-01-02: 15.8' - 16.0'	14
				WB-04-01-02: 13.0' - 13.5'	15

PETTIER AGRICULTURAL SERVICES
SOIL TESTING LABORATORY
P. O. BOX 838 LELAND, MS 38756
601-686-9473

Cost of services should be billed to:

Name: Joe Dunbar

Address: _____

Signature: _____

SEND TO Joe Dunbar
 ERDC 3909 Halls Ferry Rd. Vicksburg, MS 39189

SOIL TEST ANALYSES - FERTILIZER RECOMMENDATIONS

Pettier Agricultural Services, Inc.
 105 Old Highway 61 S. - P. O. Box 838 - Leland, MS 38756

RECOMMENDED BY: *Joel Pettier*

LAB. NO. 24514

DATE: February 10, 2004

SOIL TEST ANALYSES (ppm and level)

SITE NUMBER	pH	ACIDITY (Me/100 g)	PHOS-PHORUS	EXCHANGEABLE BASES			ORGANIC MATTER (%)	ORGANIC SULFUR	ZINC	SODIUM	CATION EXCHANGE CAPACITY (Me/100g)	BASE SATURATION (%) Ca-Mg-K-Acid	FERTILIZER RECOMMENDATIONS			
				POTASSIUM	MAGNESIUM	CALCIUM							CROP	LIME (T/A)	N-P ₂ O ₅ -K ₂ O (#/A)	OTHER
1	7.64	0.0 v1	12 m	359 h	1215 h	13379 h	2.8 h	185 h	0.8 l	2214	40.7 77.9	86-13- 1- 0				
								769								

2	7.67	0.0 v1	14 m	451 h	1282 h	14569 h	3.0 h	195 h	1.7 m	2524	43.6 84.7	86-13- 1- 0				
								975								

3	7.97	0.0 v1	15 m	345 h	1017 m	27649 v1	3.0 h	195 h	1.4 m	3695	44.4 147.6	94-5-1-0				
								729								

4	7.78	0.0 v1	24 m+	426 h	772 h	11299 h	2.4 h	166 h	1.0 l	1317	34.1 64.0	88-10- 2- 0				
								464								

5	7.68	0.0 v1	37 h	463 h	1132 h	15899 h	3.0 h	195 h	2.3 h	2568	43.5 90.1	88-10- 1- 0				
								357								

D-5

Joe Dunbar
 SEND TO ERDC 3909 Halls Ferry Rd. Vicksburg, MS 39189

SOIL TEST ANALYSES - FERTILIZER RECOMMENDATIONS

Petriet Agricultural Services, Inc.
 105 Old Highway 61 S. - P.O. Box 838 - Leland, MS 38756

RECOMMENDED BY: JLD

DATE: February 10, 2004

LAB. NO. 24514

SOIL TEST ANALYSES (ppm and level)

SITE NUMBER	pH	ACIDITY (Me/100 g)	PHOS-PHORUS	EXCHANGEABLE BASES			ORGANIC MATTER (%)	ORGANIC SULFUR	ZINC	CATION EXCHANGE CAPACITY (Me/100g)	BASE SATURATION (%) Ca-Mg-K-Acid	FERTILIZER RECOMMENDATIONS				
				POTASSIUM	MAGNESIUM	CALCIUM						CROP	LIME (T/A)	N-P ₂ O ₅ -K ₂ O (#/A)	OTHER	
6	7.78	0.0 vl	17 mt	381 h	735 m	26729 vh	2.9 h	190 h	1.4 m	1276	42.0 140.7	95-4-1-0				
								683								

7	7.90	0.0 vl	20 mt	389 h	833 m	28269 vh	3.0 h	195 h	1.9 m	1760	44.1 149.2	95-4-1-0				
								528								

8	8.13	0.0 vl	13 m	446 h	698 m	14409 h	2.7 h	180 h	2.7 h	392	39.0 79.0	91-7-1-0				
								256								

9	8.10	0.0 vl	15 m	428 h	721 m	14169 h	2.7 h	180 h	2.6 h	331	38.6 78.0	91-8-1-0				
								245								

10	8.18	0.0 vl	13 m	458 h	754 m	14249 h	2.7 h	180 h	2.3 m	268	39.1 78.7	91-8-1-0				
								228								

D-6

SEND TO Joe Dunbar
 ERDC 3909 Halls Ferry Rd. Vicksburg, MS 39189

SOIL TEST ANALYSES - FERTILIZER RECOMMENDATIONS

Pettiet Agricultural Services, Inc.
 105 Old Highway 61 S. - P. O. Box 838 - Leland, MS 38756

RECOMMENDED BY: JUP

LAB. NO. 24514

DATE: February 10, 2004

SOIL TEST ANALYSES (ppm and level)

SITE NUMBER	pH	ACIDITY (Me/100 g)	PHOS-PHORUS	EXCHANGEABLE BASES			ORGANIC MATTER (%)	ORGANIC SULFUR	ZINC	CATION EXCHANGE CAPACITY (Me/100g)	BASE SATURATION (%) Ca-Mg-K-Acid	FERTILIZER RECOMMENDATIONS				
				POTASSIUM	MAGNESIUM	CALCIUM						CROP	LIME (T/A)	N-P ₂ O ₅ -K ₂ O (#/A)	OTHER	
11	8.07	0.0 v1	14 m	343 h	576 m	13809 h	2.0 h	147 h	4.2 h	250	27.3 74.7	92- 6- 1- 0				
								229								

12	8.22	0.0 v1	9 m	212 m	391 l	16589 h	1.4 m	118 m	2.1 m	162	18.0 86.7	96- 4- 1- 0				
								255								

13	8.06	0.0 v1	11 m	378 h	622 m	14069 h	2.4 h	166 h	2.4 h	313	34.7 76.5	92- 7- 1- 0				
								241								

14	8.26	0.0 v1	4 l	261 m+	881 m	26429 v1	2.7 h	180 h	1.0 l	1470	39.4 140.1	94-5- 1- 0				
								441								

15	7.84	0.0 v1	7 l	315 h	825 m	24929 v1	2.9 h	190 h	1.4 m	2795	42.2 132.3	94-5- 1- 0				
								494								

D-7

Appendix E

Seismic Test on IBWC Levees: Weslaco, TX

Seismic Tests on IBWC Levees: Weslaco, Texas

Richard D. Miller
Julian Ivanov

Kansas Geological Survey
1930 Constant Avenue
Lawrence, Kansas 66047



Final Report to

Joe Dunbar
U.S. Army Engineer R&D Center
Geotechnical and Structure Laboratory
3909 Halls Ferry Road
Vicksburg, Mississippi 39180

Open-file Report 2005-56

October 10, 2005

Seismic Tests on IBWC Levees: Weslaco, Texas

Richard D. Miller
Julian Ivanov

Kansas Geological Survey
1930 Constant Avenue
University of Kansas
Lawrence, Kansas 66047

Final Report to

Joe Dunbar
U.S. Army Engineer R&D Center
Geotechnical and Structure Laboratory
3909 Halls Ferry Road
Vicksburg, Mississippi 39180

Open-file Report No. 2005-56

October 10, 2005

Seismic Tests on IBWC Levees: Weslaco, Texas

EXECUTIVE SUMMARY

This applied research project evaluated the potential of a variety of seismic methods to characterize the condition of levee cores constructed in the 1970s as part of the International Boundary and Water Commission (IBWC) program in south Texas. Preliminary studies of levee cores in certain areas uncovered evidence of cracking in the expansive clays locally mined and used during construction of the core. Cracking of this nature is likely the result of more than eleven years of drought in south Texas and would increase the overall permeability and leak potential of the levees. This suggestion was made based on analysis of four different data sets: abnormally low conductivity determined by both airborne and surface geophysical surveys, abnormally high levels of grout intake during borehole plugging operations, and core samples intact when first removed from the ground and placed in plastic containment vessels showing marked shrinkage and visible cracking after one year in controlled storage.

Five levee sites were selected based on airborne geophysics and physical inspection to represent the range of conditions expected in levee cores during extended periods of drought in this area of south Texas. Lithology at each of these sites varied in sand and clay concentrations and types. Core materials for each levee site were locally mined at various locations within the river valley and therefore each possessed different physical properties as evident in core drill samples and electrical properties. Miles of airborne EM and LIDAR acquired in a continuous fashion over the levees in this area were instrumental in identifying and classifying each of these five very diverse sites.

Seismic methods have proven marginally successful identifying anomalies in levees on a few occasions. Most of these studies have focused on direct wave analysis, targeting areas with reduced seismic velocities. Lower seismic velocities are usually indicative of less strength or softer materials. Therefore, anomalously low velocities for a particular levee could be an early indicator of failure potential. Testing at each of these five sites was more extensive than any earthen structure study currently available in the scientific literature. The testing included compressional and shear first-arrival analysis (classic refraction, turning-ray tomography, and through-levee tomography), multi-channel surface-wave analysis, and vibration harmonics analysis. Tests were conducted both on the levee crest and at equivalent locations along the levee toe, with expanded studies at sites identified as good candidates for ponding experiments.

Tests were designed to evaluate both body waves and surface waves using well-documented methodologies specifically adapted to the levee problem. Due to the shallow depths of investigation, reflection was not considered a viable technique and therefore tests specifically designed to evaluate reflected arrivals were not undertaken. Seismic data were recorded using both horizontally polarized source and receivers and vertical source and receivers. Shots for the 2-D surveys were recorded at stations along the lines of receivers. A 3-D tomography experiment was conducted using shots on one side of the levee face recorded by receivers on the adjacent side. Data quality was method dependent, but in general most recorded data were good, possessing excellent signal-to-noise ratios and good-to-poor signal bandwidth and range of recorded frequency. Seismic velocities (compressional and shear) were estimated from measurements of first-arrival time/offset distances and inversion of surface-wave phase velocities as a function of frequency.

These investigations targeted seismic velocities, both absolute and relative (changes). Seismic velocities of levee materials were estimated and compared both site to site and within specific sites. A unique study of surface-wave phase velocities was conducted observing phase variations in the expected (for consistent material characteristics) uniform wavetrain at and near resonance (resonance in this case is

controlled by levee height and surface-wave velocity of the materials: wavelength). This surface-wave study was conducted in hopes of identifying anomalous zones where changes in phase velocity might be indicative of reduced or increased material strength. Seismic velocities were measured based on travel time between adjacent sets of receivers.

Body-wave propagation characteristics are unique to the material through which the seismic energy is traveling. Shear velocity is generally accepted as a relative measure of material strength or stiffness. Compressional velocity is a measure of both the rock matrix and pore materials. Therefore, increases in shear velocity will generally indicate stronger materials, while increases in compressional velocity in unconsolidated materials is a good indicator of increased saturation.

Compressional-wave velocities were for the most part within a “reasonable” range for this setting; however, shear-wave velocities were estimated to be significantly higher than expected based on both levee materials and equivalent compressional-wave velocities. Shear velocities were consistently measured with a V_p/V_s ratio around 2, which is generally more characteristic of consolidated rocks. Ratios for unconsolidated fill materials such as these are generally expected to fall in the 3 to 5 range. This higher-than-expected ratio could result in measuring mode-converted shear rather than the primary direct shear arrival. It is also possible this higher-than-expected shear velocity could be real and related to these earth materials and the mechanical compaction used to construct these levees.

Estimates of shear velocity using both refraction tomography and slope intercept methods provided shear velocities that were unrealistically high and with offset-dependent arrival patterns extremely consistent with the faster compressional-wave arrivals. Calculating shear-wave velocity from inverted surface waves was strongly dependent on bandwidth and percentage of higher-mode energy recorded. During the first survey, ground conditions were not conducive to producing and/or recording broadband surface waves. Therefore, no confident shear-wave velocity sections were produced. On the second trip near-surface conditions had sufficiently changed to allow sufficient broadband surface wave that a 2-D shear wave profile could be produced for the levee core.

Velocity anomalies within the levee were detected at each of the three Retamal levee sites. Distribution and range of values for these anomalies are consistent with variations in material types used during construction and the construction process itself. It is not clear that velocity information alone will be sufficient to identify areas with a high density of cracks, which could be present as a result of the dewatering during drought of the expansive clays used in some places during core construction. However, it does seem likely that reduction in the material stiffness of the levee core could be used to identify failure risk areas with a relatively high resolution. Discontinuities in the levees associated with cracks seem to interfere with the otherwise uniform propagation of surface waves through the levee. These disturbances, once fully understood, could provide relatively accurate locations of weak zones within the core material.

Problems and pitfalls associated with using seismic techniques to estimate velocities intended to help characterize levee competence do exist and require significant attention to detail and understanding of the seismic-wavefield arrival patterns ($t-x$) and significance of the spectral properties of each mode. In particular, mode converted shear-wave energy can lead to completely incorrect conclusions. Interpreting the propagation irregularities in surface-wave energy is not clearly understood and, therefore, is not yet ready for use as a routine tool in interrogating levees. It must also be kept in mind that the geometry of the levee and the proximity of its basal contact with native earth can result in refracted first arrivals dominating the majority of close-offset traces where direct waves are normally expected.

Rapid, precise seismic methods for identifying areas worthy of further investigation could be developed for specific levee geometries and construction materials. Monitoring is by far the most

confident and accurate application for seismic techniques on levees. Consideration must be given for changes in skin conditions due to seasonal variations in moisture. At the five sites studied on the Retamal and Main Levees, LRGV compressional-wave velocity estimations were most accurate for all conditions using refraction tomography. Shear-wave-velocity survey data were contaminated with mode-converted energy and therefore difficult to use to estimate material characteristics. Changes in near-surface conditions between the first and second survey resulted in an increase in recorded surface-wave bandwidth and therefore reasonably confident shear-wave velocity estimations within the levee. This change in surface conditions did not seem to change the arrival patterns observed on data recorded to capture first-order shear-wave first arrivals.

Infiltration of water into the levee skin was identified on seismic data during the ponding experiment conducted during the second site visit at site #2 (oxbow lake site). Notable changes in both compressional and shear velocity can be associated with the infiltration of water dammed against the south levee face. Compressional-wave data suggest percolation of water into the native river valley sediments beneath the levee. Shear-wave velocity change was rapid, occurring at the very beginning of the simulation, and was isolated to one area within the pond. The isolated nature of the infiltration on the shear data could be related to a fracture/crack system opened as a result of the years of drought and dewatering of the core. An alternate possibility is a possible material inconsistency resulting from construction practices and locally mined core material.

Considering the observations from the ponding experiment and five-site study, it is clear that the seismic tool can be used during flood events to detect more permeable areas where infiltration is active and the potential exists for failure. The most effective use of this tool would be as a monitoring system, where a baseline survey is acquired for all suspect areas, then during a flood event repeat surveys are run using differencing techniques to detect weak points pre-failure. Complications from mode conversions and near-surface dependent propagation characteristics will limit the use of this tool in some settings until more advanced processing capabilities have been developed. Clearly, more information is present in the seismic wavefield than we currently have the capability to meaningfully extract. Optimized future use of this tool will depend to some degree on acquisition of baseline data sets that will allow full wavefield processing once the methods have been fully developed. Current research in these areas is active and incrementally moving forward with providing solution to many problems encountered on this study.

Seismic Tests on IBWC Levees: Weslaco, Texas

1-INTRODUCTION

In support of the U.S. Army Corps of Engineers' strong commitment to dam and levee safety, new and/or adaptations of existing technologies need to be identified and evaluated at sites with both physical characteristics conducive to those technologies and a history of substandard dam or levee performance. Models used to predict dam or levee performance levels during earthquakes and floods are only as realistic as the material attributes (especially rigidity) incorporated into those simulations. Proven correlation between acoustic properties and material properties (especially stiffness/rigidity) is the basis for developing and implementing field-efficient, laterally continuous, non-invasive methods to accurately measure the seismic wave field.

Characterization of levees or dams in areas with liquefaction, core failure, or leakage potential would be enhanced if Poisson's ratio were calculated based on continuous, detailed, coincident, two- and three-dimensional measurements of compressional and shear-wave velocities for cells uniformly distributed throughout the dam or levee volume. Routine non-invasive appraisal of dam/dike core integrity could prove quite valuable if lateral variability in shear-wave velocities could be accurately measured and correlated to localized anomalous material zones. This would be especially significant if these anomalous zones were indicative of dissolution activity, non-uniform compaction/settling or fracturing/cracking from dewatering of expansive clays prior to surface subsidence, the formation of vertically extensive chimney features or piping, or fracture permeability through the core. Seismic techniques hold vast potential for imaging and measuring materials in a fashion suitable for evaluating levee integrity.

This applied research project was designed to evaluate the potential of several seismic methods to characterize the condition of levee cores built in the 1970s as part of the International Boundary and Water Commission (IBWC) program in south Texas. Preliminary studies of levee cores in certain areas uncovered evidence of cracking in the expansive clays mined locally and used extensively during construction of the core. Cracking of the nature suspected here is likely the result of more than a decade of drought in south Texas and would act to increase the overall permeability and leak potential of the levees. This suggestion was made based on previous analysis of four different data sets: abnormally low conductivity determined by both airborne and surface geophysical surveys, abnormally high levels of grout intake during borehole plugging operations, and change in intact core samples (shrinkage and visible cracking after one year in controlled storage).

By isolating and measuring changes or the effects of changes to physical earth properties using seismic methods it should be possible to both reduce the inherent problem of non-uniqueness and lower the threshold of physical property change currently necessary for seismic methods to uniquely and confidently detect a change. Correlating and quantifying known changes in physical properties with observed variations in seismic data attributes should provide the basis for accurate characterization of earth materials with no *a priori* information. For that reason, comparing two data sets acquired with identical techniques and geometries—one acquired when cracks in the core are most pronounced (dewatered clay) and a second when the clay core is fully watered, allowing the cracks to heal—is the most effective approach for evaluating the various methods' ability to detect and quantify these fractures. Contrasting seismic data before and after changes in core saturation should allow differences in data characteristics related specifically to core dewatering to be identified and quantified, with a template developed for use of seismic methods as a reconnaissance tool on levees.

Program Objectives

Geophysics used during site characterization routinely involves relatively noisy measurements of earth properties, qualitatively incorporated into working subsurface models with ground truth provided by observational data sets (e.g., drilling, outcrop studies, etc.). Near-surface seismic data are no exception to this generality. The primary objective or product of most surveys of this type is the qualitative assessment of subsurface layer topography (Clement et al., 1997; Pullan and Hunter, 1990; Lankston, 1990). Travel-time structure maps or two- or three-layer velocity maps are typical interpretation products of seismic surveys. These seismic interpretation maps are routinely merged into borehole derived geologic and hydrologic models based for the most part on highly subjective and very sparse data sets. These simplistic models are then used for ground-water monitoring and remediation, geologic hazard detection, or engineering design purposes in an intuitive, experience-based manner (Steeple and Miller, 1990; Miller and Xia, 1999).

Considering the wealth of information contained in the seismic wave field, seismic measurement or imaging data are routinely underutilized for site characterization (Steeple et al., 1995). Surface seismic techniques are generally limited to routine mapping and delineation of subsurface structures, layer topography, anomalies, and stratigraphic changes (Jongerius and Helbig, 1988; Miller et al., 1989; Goforth and Hayward, 1992; Miller et al., 1995; Shtivelman et al., 1998; Guo and Liu, 1999; Stokoe et al., 1994; Michaels, 1999). In many instances, several earth properties (V_p , V_s , Q_p , Q_s , layer orientation, and thickness) can be estimated from the seismic wave field, for each subsurface cell. Velocity is probably the parameter most consistently measured or estimated by all the seismic methods. A single seismic shot record has the potential to be divided into multiple modes or combinations of modes and processed uniquely for each mode and wave type. One data set could be uniquely processed focusing on at least four different energy types (body waves: refraction, reflection, and tomography; surface waves: shear velocity and Q).

This applied research project evaluated the applicability of several seismic techniques to identify, delineate, and estimate the physical characteristics or properties of materials within and beneath a representative expanse of IBWC levees south of Weslaco, Texas (Figure 1). It was important that some measure be established (qualitative if necessary) of the correlation between seismic measurements, conductivity measurements, and the physical condition (increased permeability zones related to fractures, joints, dissolution, or erosion) of the levee core. Several surface seismic measurements were made and analyzed using state-of-the art methods and equipment. As part of the phase II component of this study, a repeat survey was conducted immediately before, during, and after ponding and levee saturation. Methods evaluated include: (P & S) refraction, (P & S) tomography (both 2-D turning ray and 3-D straight ray through levee), surface-wave dwell, and surface-wave dispersion curve analysis (MASW) for shear-wave velocity.

- The delayed-time method of first arrival/refraction analysis was used along the 2-D profiles at the crest and toe of the levee to look for variations in layer velocities (V_p and V_s) at the core/pervious fill contact, core/native earth interface, and any discrete velocity contrast within the first 30 ft below the base of the core along both crest and toe profile lines (Scott, 1973).
- Turning-ray tomography was used to define V_p and V_s for subsurface cells filling the space between the levee/ground surface and 30 ft below the base of the levee along the crest and toe profile lines (Lanz et al., 1998). Conventional turning-ray tomography and joint analysis of surface waves and refractions (JARS) was done to appraise their relative accuracy when appropriate (Ivanov, 2002).

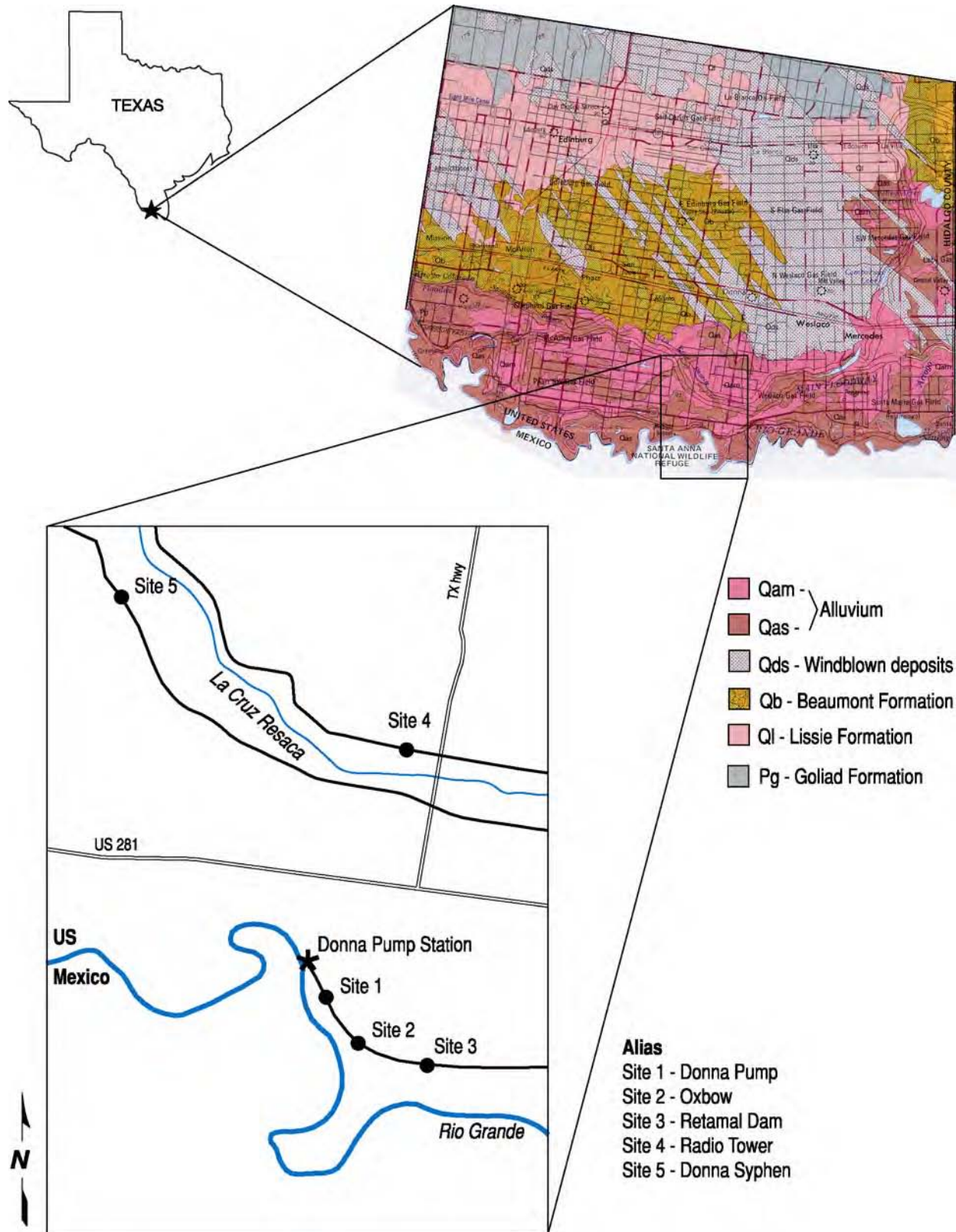


Figure 1. Maps of survey site near Weslaco, Texas (most detailed map from Texas Natural Resources Information System, www.tnris.state.tx.us).

- Through-levee tomography was completed for both compressional and shear energy along a 2-D surface grid designed with sources on one side and receivers on the other side of the levee deployed relative to the centerline road. Analysis relied on a relatively straightforward travel-time delay technique analogous to crosshole tomography (Gaffran et al., 1999).
- Multichannel surface-wave inversion techniques (MASW) have proven capable of detecting anomalous shear-wave velocity zones within and below fill materials (Miller et al., 1999). Application of this technique to differential fill and core integrity problems at levee sites with expansive clays provided key insights into and an increased awareness of areas with leak or failure potential.
- Frequency dwell experiments provided the opportunity to compare frequency-dependent changes in surface waves with physical properties and/or changes in properties. Monofrequency sweeps several seconds long were produced and recorded using the dependence of surface-wave spectra on depth of penetration and the shear-wave velocity (Xia et al., 1999).
- High-resolution seismic reflection data from the crest 2-D profiles was studied to determine the feasibility of coincidentally estimating V_p and V_s , sensitivity of reflection wavelet attributes returning from the base and/or beneath the levee to variations in core permeability (cracks), and travel time variations (static) associated with wavelet delays through cracked and/or clay core shrinkage within closely spaced subsurface cells for use in detailed mapping of levee core properties (Batzie et al., 1999; Berryman et al., 1999). Unfortunately, no usable reflection energy was recorded at any of the sites from within the levee.

Tests to determine field efficiency, resolution potential, cost effectiveness, interpretability (signal-to-noise), processing requirements, and measurement accuracy were integral to each of the individual seismic techniques studies. It was the intent of this study to acquire single-pass full-waveform compressional- and shear-wave data and to process the individual components of each mode using methodologies appropriate for the particular energy arrival. Therefore, minimal acquisition effort would yield several redundant measurements of seismic properties using different parts of the wavefield.

In summary, the primary objectives set out from the onset of this project were to determine compressional and shear velocity distribution within the body of the levee and any relationship to levee permeability. Measurements were made at several locations, each with unique physical and/or lithologic differences, while in their dry state to a depth approximately equal to the water table (geophysical tools used had at least a maximum depth of investigation extending 30 ft below the native ground surface or below the base of the levee). These measurements were followed some time later by an abbreviated comparison survey at one site after water had been introduced to the levee core/body to provide a time-lapse seismic view of the levee, studying seismic response as a function of changes in saturation. As a result, the potential of reconnaissance and high-resolution imaging using non-invasive seismic methods could be appraised.

2—SITE DESCRIPTION

Levees along significant expanses of the Rio Grande River in south Texas are currently the responsibility of the International Boundary Water Commission (IBWC). Many of these levees were designed and constructed to minimize or eliminate the threat of the statistically determined 100-year flood event. Newer (1970s era) reaches of IBWC levees were constructed, in some cases, using highly expansive clay materials. Materials used to construct the levees were generally mined from barrow pits in relative close proximity to the active construction area. Therefore, lateral variability in construction materials is common over distances of a mile or less. Average levee height in these areas is about 16 ft with slopes on the order of 1 to 3 (Figure 2).

With 11 years of prolonged drought conditions plaguing the McAllen-Brownsville corridor, soil moisture conditions reached the point that concern arose about internal levee conditions and its impact on the levees' design characteristics. It was postulated that in some areas moisture levels within the levee could have dropped to the point cracks formed in the impervious core, weakening the core to the point failure was possible under 100-year flood conditions. A series of field tests were devised to first determine if a non-invasive method existed that could measure a levee's internal strength properties sufficiently to diagnose if this problem existed, and secondly to classify levees in terms of core characteristics. These investigations included seismic, ground probing radar, resistivity, SP, drilling and sampling, and levee design-height (toe to within 3 ft of the levee crown) full-scale ponding tests. Data obtained prior to and after ponding tests were designed to assess differences at a single representative location that could be correlated to other sites with similar measured characteristics. This document is only intended to address seismic investigations undertaken by the Kansas Geological Survey.



Figure 2. Field site 1 with vibrator on south side of levee, crew working on north side, and semi parked on levee.

Preliminary studies focused on levees in south Texas between Brownsville and McAllen (Figure 1). Seismic investigations were conducted at five levee sites located in the San Juan Quadrangle (Figure 3). Three of the sites were immediately north of the Rio Grande River at low-conductivity locations along the Retamal dike and two were at levee sites on opposing sides of the La Cruz Resaca within the interior floodway. Of the two within the interior floodway, one location was at an intermediate-conductivity site and the other was at a high-conductivity site. These sites were chosen specifically based on observations from airborne and surface geophysical surveys and borehole data. To study the relationship between electrical conductivity, lithology, fracture permeability, seismic properties, and failure potential, it was necessary to study a range of sites with characteristics classified from average to extreme. Key factors in selecting these five sites were abnormally low EM conductivities determined from and consistent on both airborne and surface geophysical survey data, abnormally high grout intake while backfilling sampling boreholes, and marked shrinkage and visible cracks in year-old preserved cores.



Figure 3. Aerial photo with GPS locations of the end of the study areas for each site.

In general, these sites are within the main floodplain of the Rio Grande River and situated on unconsolidated alluvial sediments (Figure 1). Gravels present within the alluvium at these sites included sedimentary rocks from the Cretaceous and Tertiary and a wide variety of igneous

(including some agate) and sedimentary rocks from Trans-Pecos Texas, Mexico, and New Mexico. Surface materials at sites 1, 2, and 3 are in an area classified predominantly as silt and sand, while sites 4 and 5 are in areas dominantly mud. These distinctions could be important when considering the levees are generally constructed of locally farmed earth materials. Another noteworthy distinction between these two areas is the source of the alluvium: at sites 4 and 5, several miles north of the Rio Grande River, gravels are mostly local Tertiary rocks and chert derived from Uvalde gravel.



Figure 4. Cracks/fissures evident along the flanks at site 2.

Surface investigations of the slopes and crests at all five sites revealed more evidence of differences in material characteristics. At sites 1 and 2 the conductivity was notably low, and the core samples were clearly less competent than equivalent measurements and samples from sites 4 and 5. Surface investigations at site 1 indicated a much greater concentration of sand to clay than the other sites, a characteristic also evident in cores from this site. At site 2 a higher concentration of surface cracks or fissures were observed both on the crest and along the slopes than at any of the other four sites (Figure 4). A levee core percolation test at site 2 revealed extremely rapid movement of water into/through a trench cut into the levee core.

Sites 4 and 5 were in newer segments of levee with higher measured conductivity and clay cores showing little or no evidence of the dynamic properties characteristic of expansive clays (contract when dry and expand when wet) as suggested to be present at site 2.

Site 2 was selected for the percolation test based on the fairly extensive network of observed surface cracks and its relatively low conductivity. A trench was opened from the crest road down several feet into the core. The trench was then kept full of water with observations made as to the volume of water moving out of the trench and into the core. Beyond tracking the volume of water necessary to keep the trench full of water, this test was limited to surface observation of seepage along the levee sides. These surface observations were intended to determine the breadth and density of this apparent network of cracks and some qualitative idea as to flow potential within the core as a result of this likely higher than average permeability zone.

3—APPROACH (Program Components)

Refraction/Tomography

Direct and refracted P-wave and S-wave arrivals were analyzed using conventional methods (Palmer, 1981; Haeni, 1986; Lankston, 1990) and inversion techniques (Scott, 1977; Schneider et al., 1992; Ivanov et al., 2000). Use of direct and refracted arrivals for mapping distinct velocity contrasts between layers has been in routine use for everything from crustal seismic research (Steinhart and Meyer, 1961) to shallow ground-water studies (Haeni, 1978). It is an established, proven technique whose limitations are well documented (Soske, 1954; Sander, 1978). Methods to approximate solutions when physical conditions violate assumptions of the refraction method (Mooney, 1981; Redpath, 1973) are known. Recent research incorporating refraction inversion with shear-wave velocity calculations from surface-wave data has provided encouraging results that seem to be insensitive to the velocity reversal problem (Ivanov, 2002).

Tomography has a variety of applications in the subsurface, including: waste repository characterization (Peterson et al., 1985), engineering studies (Cottin et al., 1986), void detection (Lytle and

Dines, 1980), and mining (Kilty and Lange, 1990). The simplicity of acquisition and lack of computational intensity makes it especially applicable for velocity estimation using data acquired for surface-wave or refraction analysis. Using this approach in conjunction with multichannel surface-wave inversion allows anomalous features within the levees to be examined from toe to toe and all along the crest using shear and compressional waves. Study of through-levee compressional waves was important if for no reason other than to provide confidence in first-arrival interpretations on shear-wave tomograms. Processing data for tomographic analysis incorporated existing algorithms and standard curved-ray methodologies (Chiu et al., 1986).

Application of refraction (tomography) methods can be inaccurate due to the problem of non-uniqueness, meaning there are many possible solutions that can generate the same first-arrival values (Ivanov et al., 2005). The Joint Analysis of Surface Wave and Refractions (JASR) method, developed at the KGS (Ivanov, 2002), offers an approach for minimizing one of the main problems in refraction tomography: nonuniqueness. A general way to overcome nonuniqueness is the use of *a priori* information. Such information generally comes from direct observations (borehole, outcrops, etc.). The JASR method obtains *a priori* information from Multichannel Analysis of Surface Waves (MASW) where a two-dimensional shear-wave velocity (V_s) section is used to construct a two-dimensional compressional-wave velocity (V_p) initial model (*a priori* information for deterministic-type refraction tomography inversion). The validity of creating a V_p model from these V_s values is based on the common elastic and density parameters on which these two types of seismic velocities depend. Qualitatively this assumption is consistent with the frequently made observation that the general trend of V_s follows to the general trend of V_p . The JASR technique significantly improves the reliability of the final refraction-tomography inversion results (Miller et al., 2001; Ivanov et al., 2000; Ivanov, 2002).

It was necessary to understand the arrival patterns of the various compressional- and shear-wave modes during through-levee tomography. At one site two-component data were recorded from a 2-D grid of sources and receivers on opposing sides of the levee (Figure 5). Three-dimensional images highlighted areas within the body of the levee with anomalous velocity characteristics. Integrating the interpretation of the crest 2-D profile and the slope through-levee tomography provided consistent images and allowed confidence in the effectiveness of these techniques. While the emphasis of this effort is on data collection and analysis, modeling is necessary to ensure a thorough understanding of the principal features of the seismograms, and to target those features that are not clearly understood for continued investigation.



Figure 5. Shear-wave source operated along the north line at site 2 during the ponding test.

Surface Wave Inversion

Surface waves traditionally have been viewed as noise in multichannel seismic data collected to image targets for shallow engineering, environmental, and ground-water purposes (Steeple and Miller, 1990). Recent advances in the use of surface waves for near-surface imaging have combined spectral analysis techniques (SASW), developed for civil engineering applications (Nazarian et al., 1983), with multi-trace reflection technologies developed for near-surface (Schepers, 1975) and petroleum applications (Glover, 1959). The combination of these two uniquely different approaches to seismic imaging of the shallow subsurface permits non-invasive estimation of shear-wave velocities (within 10% of measured in many cases) (Xia et al., 2002) and delineation of horizontal and vertical variations in near-surface

material properties based on changes in these velocities (MASW) (Park et al., 1996; Xia et al., 1999; Park et al., 1999).

Extending this imaging technology to include lateral variations in lithology as well as tunnel and fracture detection, bedrock mapping, and subsidence/karst delineation has required a unique approach that incorporates SASW, MASW, and CDP methods. By integrating these techniques, 2-D continuous shear-wave velocity profiles of the subsurface can be generated. Estimating the dispersion curve from up to 60 receiving channels, spaced every 3 ft to 6 ft along the ground surface, enhances the signal and results in a unique, relatively continuous view of shallow subsurface shear-wave velocity properties. This highly redundant surface-wave method improves the accuracy of calculated shear-wave velocities and minimizes the likelihood that irregularities resulting from erratic dispersion curves will corrupt the analysis in comparison to the more traditional SASW approach.

Surface-wave analysis was performed on data acquired on the crest and toe of the levee and on adjacent crest lines during the ponding experiment. Each of the five profiles located at different places along the levee and the two profiles used for the water flood experiment used the same spread geometry (120 stations with both compressional and shear receivers located every 3 ft) and permitted correlation between the various processed data sets for each line and between the five different lines. Even with the unique broadband requirements of surface-wave measurements it was not necessary to use an accelerated weight drop source, a hammer was sufficient (broad enough bandwidth, low enough frequency, and high enough energy), but low frequency receivers and windowed processing was necessary to produce the highest quality results. Shear-wave velocity maps generated along each profile line were optimized for resolution and signal-to-noise. Several unique approaches were used to minimize smearing resulting from variable wavelength averaging.

Reflection

High-resolution P-wave or S-wave seismic reflection surveys did not produce reflections from the basal reflector (velocity-density contrasts) of the levee or top of water table estimated to be less than 50 ft below ground surface. It was our intent to concentrate on: 1) generating high resolution (>250 Hz P-wave and >120 Hz S-wave) signals; 2) optimizing acquisition and processing for 2-D imaging along crest and toe without compromising first-arrival analysis, which was a higher priority operation; 3) establishing equipment configurations and parameter settings to maximize signal-to-noise and resolution potential considering the first-arrival acquisition deployment; 4) correlating P-wave reflections with S-wave reflections as well as with the other seismic, EM, and drill/excavation data; 5) performing attribute analysis of reflection waveforms passing through core, as well as careful study of velocity distribution calculated from NMO curves; 6) tailoring processing flows for non-optimized acquisition equipment and parameters due to full wavefield acquisition approach; 7) correlating compressional- and shear-wave NMO velocities for specific reflector(s); and 8) integrating reflection data with other seismic data. Source spacing, geophone spacing, line orientations, imaging, interpolation requirements, and fiscal constraints were to also be addressed, but due to limitations imposed as a result of coincident acquisition of first-arrival and surface-wave data, it was not possible to optimize both. Parameter and signal requirements are markedly different between the methods. Well-established shallow high-resolution data acquisition methodologies, emphasizing correlation of modal data and optimized velocity control, were adhered to as closely as possible without compromising other seismic methods (Hunter et al., 1984; Knapp and Steeples, 1986; Steeples and Miller, 1990).

4—OVERALL PROGRAM: DATA ACQUISITION

Phase I (data acquired during trip 1 from December 4 to 12, 2003)

Initial studies at the five sites were intended to identify any seismic characteristics unique to—or that could be correlated with—specific material characteristics or conductivity readings. This research program was intended to evaluate as many seismic methods as possible and appropriate, both on the crest and on the toe, to determine the range and level of sensitivity the methods have to areas identified as susceptible to core erosion and levee failure. Single data sets were acquired with the intention of separating and processing the individual components of the wavefield with appropriate methods and portion of the seismograms.

Consistency in recording equipment and parameters was critical for site-to-site comparison and especially for time-lapse studies of the kind planned here. A Geometrics 240-channel StrataView seismograph system was used to record all the seismic data for this project (Figure 6). The system is mounted in a 6-wheel John Deere Gator for added mobility and minimal environmental impact (Figure 7). This 24-bit A/D recording system used a Geometrics StrataVisor controller for basic QC and data storage. Throughout the project the same recording system was used, configured appropriately for each data set, and configured consistently for each data type.



Figure 6. Geometrics 240-channel seismograph mounted in John Deere Gator.



Figure 7. Compressional-wave hammer survey.

An important consideration when designing and acquiring these data was the need to optimize and retain the potential to compare toe and crest data at each site. Comparing and contrasting data allowed levee-specific seismic characteristics to be identified and isolated. Consistency in acquisition from site to site was also a high priority that allowed broader assertions about the significance of the observed seismic differences and their relationship to the different physical characteristics and make-up of the levees at each site. Since it was not clear from the onset which method or levee property would prove to be most sensitive to or indicative of levee degradation potential associated with expansive clays and increased permeability that resulted after over a decade of dewatering, all seismic methods and data modes had to be evaluated.

- 1) Initial testing at site 2 was completed first to measure some of the basic seismic characteristics and define the optimum equipment and configuration for data recorded on and at the toe of these levee structures. Analysis of test data concluded that 10-Hz single geophones, a 16-lb sledgehammer, three impacts per station, and planted geophones were optimum for both the surface-wave and

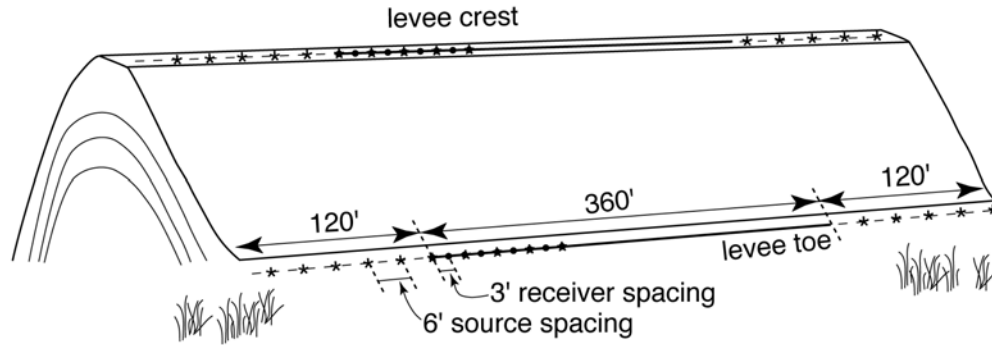


Figure 8. Crest and toe 2-D line deployments.

compressional-wave tomography. Included in the testing regimen was evaluation of land-streamer data, 12-lb and 20-lb sledgehammers, 4.5-Hz geophones, and a mechanical weight drop.

- 2) At each site, one 2-D, 2-C profile was acquired along the crest and at the toe of the levees (Figure 8). Receiver station spacing was 3 ft with two receivers at each location (10 Hz compressional-wave geophones and one 14 Hz shear-wave geophone) (Figure 9). Shear-wave receivers were oriented to be sensitive to motion perpendicular to the axis of the levee (transverse). A 16-lb sledgehammer impacting a striker plate of similar weight for compressional- and surface-wave data (Figure 10) and a 6" x 6" wood block outfitted with steel endplates and serrated earth-coupling teeth (Figures 11 and 12), were used for shear-wave data. The total spread length was 360 ft with 120 channels recording compressional and 120 channels recording shear signals. Source spacing through the spread varied, depending on data quality, from every 6 ft to every 24 ft. Each profile was acquired twice, once with the source in compressional-wave orientation and a second time with a shear-wave source orientation. Data were recorded from shear-wave phones when the shear-wave source was used and compressional-wave phones when the compressional-wave source was used. Stations (source and receiver) were located initially using analog measuring tapes/chain, followed by highly accurate (± 1 inch) x, y, and z measurement using a Trimble DGPS surveying system (Figure 13).



Figure 9. Both compressional and shear geophones were used at each station.



Figure 10. Compressional-wave survey along levee crest road.



Figure 11. A 1-m-long wood block with steel end plates held down by standing on top of the block was used to generate shear energy.



Figure 12. Steel teeth were forced into the ground to minimize source decoupling and sliding along ground surface.



Figure 13. Differential Global Position System (DGPS) was used to accurately locate all sources and receiver stations.

- 3) At levee sites 1 (Figure 14) and 2 (Figure 15), a 3-D through-levee tomographic study was conducted to investigate internal variations in levee conditions (physical properties) in three dimensions (Figure 16). A 240-receiver station grid was deployed on the south side of the levee at site 1 with each receiver station separated by 4 ft both parallel and perpendicular to the levee axis (Figure 17). Two geophones (one shear and one compressional) were connected to individual recording channels at each station of the grid on the receiver side of the levee. Two shots were fired and recorded at each of the 120 source stations on the north side of the levee at site 1 (one shear and one compressional) (Figure 18). The receiver grid included eight rows parallel to the levee axis and thirty stations per row. The source grid was made up of six rows of twenty stations per row with each row parallel to the levee axis. A unique directional source was used to record the appropriate data mode. The P-wave source was the 16-lb sledge and striker plate (Figure 19) and S-wave was the 16-lb sledge and shear block (Figure 20). Receivers were three 10-Hz Mark Products U2 digital-grade vertical geophones (Figure 21) and a single GS-11 GeoSpace horizontal geophone (Figure 22). All 240 channels were live for all shots. Channel 1 was used to extract the source signature. This single source wavelet receiver was placed approximately 5 ft from the source location for each shot, allowing measurement of as pure a source wavelet as possible. The grid was initially laid out using tape measures. Once the stations were flagged, highly accurate measurements of z, y, and x were made using a Trimble DGPS surveying system (Figure 14).



Figure 14. Through-levee receiver and source grids at site 1.



Figure 15. Through-levee receiver and source grids at site 2.



Figure 16. Source grid along north side of site 1 for through-levee study.

- 4) A second condensed through-levee tomography experiment was completed at site 2 (Figure 17b,c). Sources and receivers were the same as site 1 (item #3), but the deployment was reduced (Figure 23). A total of 120 receivers were deployed in a grid consisting of four lines of 30 receiver stations parallel to the levee axis. The source grid included three lines of 20 source stations each. After the data were recorded, a highly accurate DGPS survey was conducted to exactly locate each station (Figure 15).

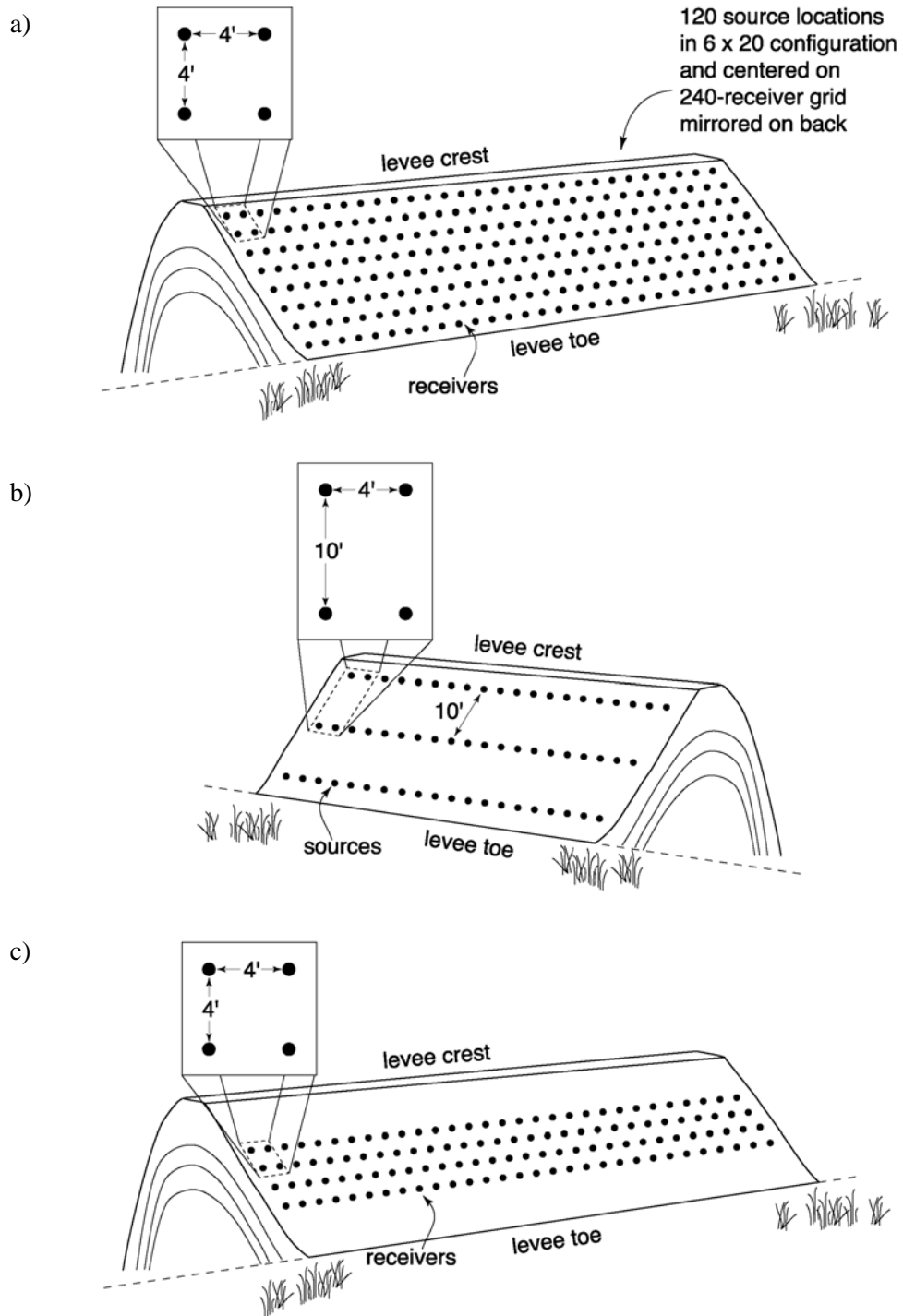


Figure 17. Deployment design for a) site 1 through-levee, b) site 2 source station design, and c) site 2 receiver location map.



Figure 18. Receiver deployment, site 1.



Figure 19. Compressional-wave data acquisition, site 1.



Figure 20. Shear-wave data acquisition, site 1.



Figure 21. Compressional-wave phones used for through-levee, site 1.



Figure 22. Shear-wave phone.



Figure 23. Compressional-wave survey, site 2.

- 5) Vibrator dwell experiments were run at sites 1 and 2. These experiments were designed to measure any non-uniformity in the surface-wave propagation that might relate to variable mechanical or hydrologic properties of the subsurface unique to each particular site. An IVI minivib1 was used as the source for experiments both at the crest and toe (Figure 24). Receivers used for the compressional-wave 2-D full wavefield recording (single 10-Hz GeoSpace geophones) were the same as used for the vibrator dwell experiments. Shot stations for the vibrator experiments were located immediate off each end of the 120-station receiver spread.

Phase II (data acquired during trip 2 from November 8 to 13, 2004)

6) The second trip focused on the ponding experiment carried out at site 2 (Figures 25 and 26), based on the analysis of data acquired during the first visit. A water-retention structure was built at site 2 to allow the simulation of a flood event across a portion of the levee suspected to be susceptible to internal erosion and potential failure. This experiment was intended to determine if fractures in the clay core, due to dewatering, would initiate and perpetuate piping. Site 2 was selected based on trenching, core drilling, conductivity measurements, and seismic properties. This phase of the project was designed as a time lapse experiment where differencing could be used to investigate change in seismic properties that might occur as a result of increased saturation of the permeable shell and changes in the material property as a result of piping on the core.



Figure 24. Vibrator at site 2 during dwell experiments.

7) Two survey lines were deployed along the north and south edges of the crest (Figure 27). Each receiver station has a 14-Hz shear-wave geophone (blue) and three 10-Hz compressional-wave geophones (Figure 28). Data from the appropriate receiver recorded for the source being used by physically changing the connection (Figure 29). Each mode and profile was recorded for a given survey time. A baseline survey was acquired prior to water being in contact with the levee sides (Figure 30). Surveys were acquired throughout the pool build up and retention of designed high pool (Figure 31). Day 1 baseline data included hammer compressional, transverse shear, and compressional-wave vibrator dwell on both the north and south lines (Figure 32). Day 2 water level was at 9.05 at the beginning of the data acquisition and the survey included hammer compressional (Figure 33), transverse shear (Figure 34), and vibrator dwell (Figure 35) for north and south profiles. Day 3 water was at simulated full pool (9.46) and data were recorded twice, once in the morning (hammer compressional, shear transverse, and vibrator dwell) for both lines, and compressional-wave hammer during the late evening/night. Day 4 full pool was maintained with hammer compressional, transverse shear, and vibrator dwell in the morning and hammer compressional in the late evening/night. On the morning of Day 5 the last seismic data were acquired, which included hammer compressional, transverse shear, and vibrator dwell on both the north and south lines.



Figure 25. Pond constructed to test flood simulation interrogations.



Figure 26. Water pumped into pond at rate consistent with model flood.



Figure 27. Seismic lines deployed along each side of crest road at site 2.



Figure 28. Compressional and shear phones used for monitoring experiments.



Figure 29. Receiver station spacing was 3 ft.



Figure 30. Pond was incrementally filled to simulate rising water from Rio Grande flood.



Figure 31. Pond nearing full.



Figure 32. Pool monitored with water added about once an hour.



Figure 33. Compressional-wave survey during full pool.



Figure 34. Shear-wave survey during full pool.



Figure 35. Vibrator on-line and ready to begin dwell experiment at various pool stages.



Figure 36. Night acquisition was necessary to capture water at key levels.

- 8) For all data acquired with the sledgehammer, each shot station and energy mode retained the field operator from beginning to completion. Three different hammer operators rotated off in a set order and at consistent shot stations. Comparison of recorded amplitudes was possible through time for a given configuration and energy mode because of this uniformity in energy provided, in part, as a result of consistency in hammer operation. Maintaining a schedule with reasonable uniform survey intervals required some night operations (Figure 36).
- 9) Increased seismic velocities were observed on the baseline survey at site 2, which suggested the wetter than normal summer and fall of 2004 had sufficiently altered the ground moisture conditions to affect the seismic velocities and therefore possibly the material properties, such as stiffness. If this did occur then the response of the levee to ponding would not be as expected based on the material properties measured and observed during the fall and winter of 2003. This observed increase in seismic velocity was a result of weather events and not site-specific variability or inconsistency of methodologies prompted the investigation of site 4 and site 1, allowing direct comparisons with trip 1 measured velocities. Crest profiles for sites 1 and 4 were acquired using as near identical parameters and equipment as possible (Figures 37 and 38). Stations were located as closely as possible using landmarks and GPS locations established during the winter of 2003 survey. A 120-station hammer compressional-wave survey was conducted using single 10-Hz geophones on 4-ft intervals at sites 1 and 4 during the late fall 2004 campaign.



Figure 37. Compressional-wave survey, 2003 campaign.



Figure 38. Site 1 compressional-wave survey, 2004 campaign.

Summary of Acquisition

December 2003	mode	source	receivers	method	
Site 1	crest	P-wave	hammer/plate	single 10 Hz	refract/tomography & MASW tomography dwell mono frequencies 10-100 Hz refract/tomography & MASW tomography dwell mono frequencies 10-100 Hz 3-D tomography 3-D tomography 3-D tomography dwell mono frequencies 10-100 Hz
		S-wave	hammer/block	single 14 Hz	
		Surface wave	vibrator	single 10 Hz	
	toe	P-wave	hammer/plate	single 10 Hz	
		S-wave	hammer/block	single 14 Hz	
		Surface wave	vibrator	single 10 Hz	
	slopes	P-wave	hammer/plate	three 10 Hz	
		S-wave	hammer/block	single 14 Hz	
		Surface wave	vibrator	three 10 Hz	
Site 2	crest	P-wave	RAWD-testing	single 10 Hz	
		P-wave	hammer/plate	single 10 Hz	
		S-wave	hammer/block	single 14 Hz	
		Surface wave	vibrator	single 10 Hz	
	toe	P-wave	hammer/plate	single 10 Hz	
		S-wave	hammer/block	single 14 Hz	
	slopes	P-wave	hammer/plate	three 10 Hz	
		S-wave	hammer/block	single 14 Hz	
		Surface wave	vibrator	three 10 Hz	
	Site 3	crest	P-wave	hammer/plate	single 10 Hz
			S-wave	hammer/block	single 14 Hz
Surface wave			vibrator	single 10 Hz	
toe		P-wave	hammer/plate	single 10 Hz	
		S-wave	hammer/block	single 14 Hz	
Site 4	crest	P-wave	hammer/plate	single 10 Hz	
		S-wave	hammer/block	single 14 Hz	
		Surface wave	vibrator	single 10 Hz	
	toe	P-wave	hammer/plate	single 10 Hz	
		S-wave	hammer/block	single 14 Hz	

December 2003 (continued)

Site 5	crest	P-wave	hammer/plate	single 10 Hz	refract/tomography & MASW tomography
		S-wave	hammer/block	single 14 Hz	
		Surface wave	vibrator	single 10 Hz	
	toe	P-wave	hammer/plate	single 10 Hz	refract/tomography & MASW tomography
		S-wave	hammer/block	single 14 Hz	

November 2004

		mode	line/source	receivers	method
Site 1	crest	P-wave	S hammer/plate	single 10 Hz	refract/tomography & MASW
Site 2	crest				
	Time 1	P-wave	S hammer/plate	single 10 Hz	refract/tomography & MASW
		P-wave	N hammer/plate	single 10 Hz	
		Sh-wave	S hammer/block	single 14 Hz	
	Time 2	Sh-wave	S hammer/ block	single 14 Hz	refract/tomography & MASW
			N hammer/ block	single 14 Hz	
			Center vibrator	single 14 Hz	
		Sv-wave	S hammer/ block	single 14 Hz	refract/tomography & MASW
			Center vibrator	single 14 Hz	
		P-wave	S hammer/plate	single 10 Hz	refract/tomography & MASW
	N hammer/plate		single 10 Hz	refract/tomography & MASW	
	Time 3	P-wave	S hammer/plate	single 10 Hz	refract/tomography & MASW
			N hammer/plate	single 10 Hz	
			Center vibrator	single 10 Hz	
		Sh-wave	S hammer/block	single 14 Hz	refract/tomography & MASW
	N hammer/block		single 14 Hz	refract/tomography & MASW	
	Time 4	P-wave	S hammer/plate	single 10 Hz	refract/tomography & MASW
		P-wave	N hammer/plate	single 10 Hz	
	Time 5	P-wave	S hammer/plate	single 10 Hz	refract/tomography & MASW
			N hammer/plate	single 10 Hz	
			Center vibrator	single 10 Hz	
Sh-wave		S hammer/block	single 14 Hz	refract/tomography & MASW	
	N hammer/block	single 14 Hz	refract/tomography & MASW		
Time 6	P-wave	S hammer/plate	single 10 Hz	refract/tomography & MASW	
	P-wave	N hammer/plate	single 10 Hz		refract/tomography & MASW
Time 7	P-wave	S hammer/plate	single 10 Hz	refract/tomography & MASW	
		N hammer/plate	single 10 Hz		
		Center vibrator	single 10 Hz		refract/tomography & MASW mono 10-50 Hz
	Sh-wave	S hammer/block	single 14 Hz	refract/tomography & MASW	
N hammer/block		single 14 Hz	refract/tomography & MASW		
Site 4	crest	P-wave	S hammer/plate	single 10 Hz	refract/tomography & MASW

QA/QC

The data acquired and processed on this survey were managed to ensure the highest quality and most accurate acoustic representation possible at this geologic setting. Current state-of-the-art techniques were used in a fashion that was appropriate and verified with step-by-step QA/QC. The most important (possibly even essential) QC information are samples of shot gathers. Raw and processed shot gathers allow the geophysicist and geologist to make determinations as to the authenticity of processed seismic sections. Seismic processing software and techniques are very powerful tools that, if not used properly, can and most likely will result in unrealistic interpretations.

The equipment and recorded data were continuously monitored during acquisition to ensure the highest quality sections. Receiver response and sensitivity were monitored using a modified tap test performed after the planting of each geophone or group of geophones. The continuity and leakage of each active station was monitored prior to each shot. The system was subjected to a series of pre-acquisition tests designed to ensure consistency in system noise and precision in digitally stored data. Visual analysis of general signal-to-noise ratio, environmental noise, DC bias, and variations in the optimum recording window were performed on at least every fifth field plot. Preliminary in-field processing provided excellent insights into data quality and need for real-time parameter adjustments as well.

Data Storage

Data were recorded and stored initially on the seismograph controller hard drive in SEG2 format. At the conclusion of each day's work the data were downloaded via Ethernet to computer hard drives located in the Mobile Processing Center (MPC). Once on computers in the MPC at the field site, the data were converted and viewed to verify data were fully readable and error free, archived in SEG2 format on DVD media (media was read verified with two copies burned), and processed for preliminary infield analysis. Long term these DVD media are archived at the KGS in the seismic data library. Processing of the data required reformatting into a fixed modified SEG-Y format.

5-DATA PROCESSING

Overview of Processing Objectives

Trip 1 — December 4 to 12, 2003

Each data set was acquired with the intent of capturing a specific mode (compressional or shear) and positioned to target certain types of energy (Rayleigh wave, reflections, refraction, first arrivals, etc.) while focusing on a particular distribution of seismic characteristics (time-offset [t-x], frequency-wave number [f-k], frequency-phase velocity [f-v], frequency-amplitude [f-a], etc.). For each site there are two unique data sets for crest and two for the toe; there is a compressional-wave survey and coincident shear-wave survey following the same line. Unique to sites 1 and 2 are the through-levee tomography. Several experiments were run using cross-modal data sets. These include acquisition using shear-wave receivers and a compressional-wave source and vice versa. Some of these more obscure data sets were not processed during this initial round of processing but were scheduled for later, more advanced processing runs.

Through-levee tomography data were processed using a crosshole 3-D tomography approach. Delay times were the focus during the first processing pass. Wavelet extraction analysis would be possible in the future using the source signature recorded on channel 1. Methods such as deconvolution and cross correlation could be used on the recorded first arrivals looking for variations in wavelet attributes that might be indicative of lithology or compaction. More than 50,000 raypaths were processed for

each mode of seismic energy (P-wave and S-wave). Throughout the processing of the through-dam tomography data, reciprocity was assumed. It was also assumed that there would be no advantage to reverse shooting or processing reverse shots at either through-levee test site.

Trip 2 — November 8 to 13, 2004

Design and construction of the water retention pond used for the flood simulation experiments was physically located directly over the through-levee tomography receiver locations at the oxbow lake site (Figure 39). The location of the pond meant no through-levee tomography was possible to observe the seismic changes due to increased saturation. However, with the crest relatively clear, baseline and monitor surface seismic experiments were acquired and processed to distinguish changes in the velocity indicative of increase saturation. If piping did occur, the experiments were set up to study the seismic changes and characteristics immediately prior to failure of the levee. Failure never occurred, so it is not clear how significant the seismic changes observed were in terms of extrapolating changes to the point of failure and, therefore, it is not clear how good an indicator or early warning potential seismic data might be in this situation.



Figure 39. Key stations occupied during 2003 seismic investigation at site 2 with location of pond superimposed.

Data acquired along the south and north sides of the crest road were processed to enhance changes in seismic velocities that could be correlated to changes in saturation. If effective, this approach could provide a method of tracking zones of increased saturation and/or leakage through the levee as water pressures increase with increasing pool height. Processing flows for tomography and MASW were maintained as close to identical as possible from one time lapse to the next to ensure changes observed were from velocity and not processing parameter variations.

Processing Software

Several processing packages were used to analyze these data, each with an emphasis on a specific energy type or travel path. For surface-wave analysis a commercial program called *SurfSeis* developed at the Kansas Geological Survey for Multichannel Analysis of Surface Wave (MASW) processing was used. Turning-ray tomography data were analyzed and displayed using *TomoSeis*, a collection of algorithms under development at the Kansas Geological Survey for Joint Analysis of Surface Waves and Refraction (JARS) processing. Seismic reflection data processing was undertaken with *WinSeis*, also a commercial processing package developed by the Kansas Geological Survey. Through-levee tomography processing was accomplished using 3-D borehole tomography and defining all the source and receiver locations in 3-D, allowing *GeoTomCG* to analyze first arrivals based on 3-D rays. Both compressional- and shear-wave data for each method were processed following the same approach and using the same software.

Data Processing Methods

Surface Wave

The surface-wave component of the seismic data was processed to estimate shear-wave velocity using the MASW method. By analyzing the fundamental-mode Rayleigh waves, a shear-wave velocity profile (1-D and 2-D) is produced that can be used to evaluate material stiffness or anomaly detection of ground materials usually shallower than 30 m, both applicable for either engineering or geophysical projects.

The *SurfSeis* processing procedure consists of three steps:

1. Field setup—This encodes the surface location of seismic source and receivers into the field data.
2. Extraction of dispersion curves—Dispersion of the fundamental-mode Rayleigh wave is extracted from the seismic data.
3. Inversion for shear-wave velocity (V_s) profiles—Extracted dispersion curves are inverted for the V_s profiles, each of which depicts the V_s variation with depth at a particular surface location.

Processing surface-wave data for this project involved extraction of the optimum 30 or fewer traces from each 120-channel shot record, transformation to phase velocity-frequency domain, and inversion of the fundamental-mode dispersion curve to produce an estimate of the shear-wave velocity function relative to depth (Figure 40). These 30-or-fewer-trace gathers were analyzed using *SurfSeis*. Each shot gather generates one dispersion curve that is assigned a surface location corresponding to the middle point of the analyzed spread. Care was taken to ensure that the spectral properties of the t-x data (shot gathers) were consistent with the maximum and minimum $f-v_c$ values (v_c is the phase velocity of surface waves) contained in the dispersion curve. Shear-wave velocity maps generated along each profile line were optimized for resolution using several approaches, including deblurring and slope filtering. Wavefield maps have been generated based on optimized receiver-spread offset for depths of interest and data characteristics.

2-D First-arrival Analysis

First-arrivals were processed using the turning-ray tomography approach. This method uses continuous raypath reconstruction and inversion to define the optimum velocity field beneath and between the source and receiver locations. Each subsurface cell has an optimum compressional-wave velocity assigned such that when all the cells a ray penetrates between source and receiver are summed, the travel time is consistent with the time of the observed first arriving energy. For the work we present here a method called JARS was used to help eliminate problems of nonuniqueness inherent in most

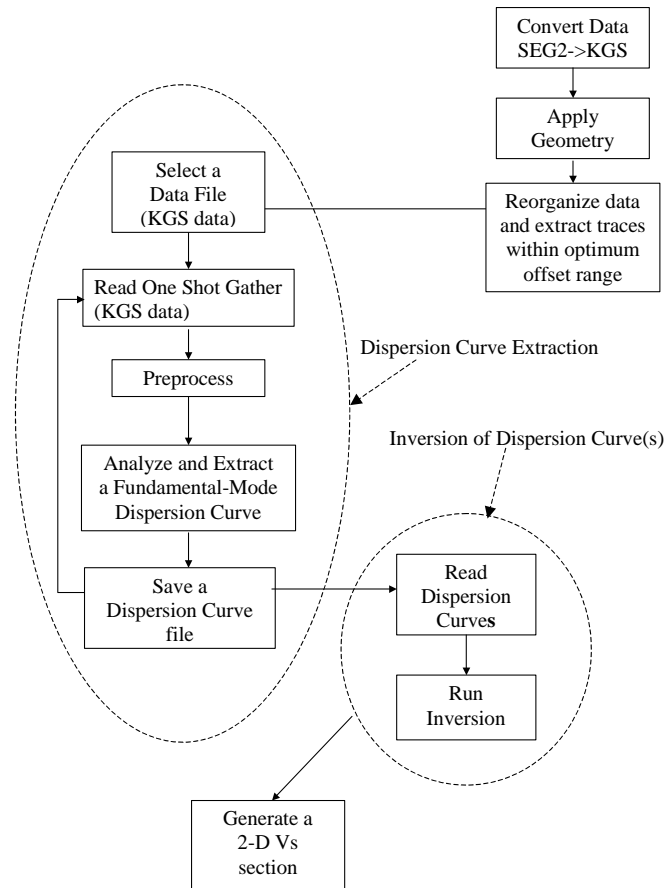


Figure 40. Processing flow for MASW data.

geophysical inversion problems. Incorporating the results of the surface-wave analysis permits *a priori* information to be included for construction of an initial model.

TomoSeis (under development at the KGS) analyzes first arrivals picked from seismic data that are collected along a single line and recorded by a single shot gather. First arrivals can be either direct or refracted seismic energy. Since propagation of seismic energy through the earth can be approximated by a ray traveling through multiple cells, each with unique velocity characteristics, each specific velocity set (all cells along a travel path) represent the geologic model consistent with the observed seismic shot gather. The inverse refraction traveltime problem can be solved by finding a velocity model whose first arrivals best match the observed first arrivals. However, the inverse refraction-tomography problem is nonunique and therefore many different velocity models can be valid solutions to the observed first-arrivals.

Two-dimensional V_s cross sections obtained from MASW analysis were used to generate an initial model for the tomographic inversion to V_p (Ivanov et al., 2000). Initial model optimization involves iterating an estimate of Poisson’s ratio until model-predicted first arrivals correlate with those on actual shot records. Convergence of inversion runs required several iterations of the initial model, each time modifying conditioning parameters in a fashion appropriate for this data set (Figures 41 and 42). Optimization of the initial model was most efficient when best-fit conditioning parameters were used during preliminary analyses. Considering the resolution requirements and redundancy in rays penetrating each subsurface cell within the depth interval of interest, it was necessary for first arrivals to be picked for all traces on every shot gather.

By analyzing the correlation between model and observed data, it was possible to use final inversion results for quality control of the first-arrival picking routines. In some instances, secondary first arrival analysis was necessary for convergence to a “good” solution. Additional quality control was achieved by verifying that the 2-D V_p/V_s data were reasonable. *TomoSeis* was used to provide both traditional and JARS solutions to the 2-D refraction-tomography problem.

3-D First-arrival Analysis

First-arrival analysis of through-levee seismic energy focused on discriminating intra-levee velocity anomalies, specifically, low-velocity zones potentially indicative of areas of structural weakness or unusual material properties. Processing the source/ receiver traveltime picks was undertaken using *GeoTomCG*, a commercial software package that was designed and written to perform 3-D tomographic analyses. Because of the universal design of *GeoTomCG* and the unique geometries associated with shooting on the levee slopes, it was possible to “fool” this borehole analysis software by using high-

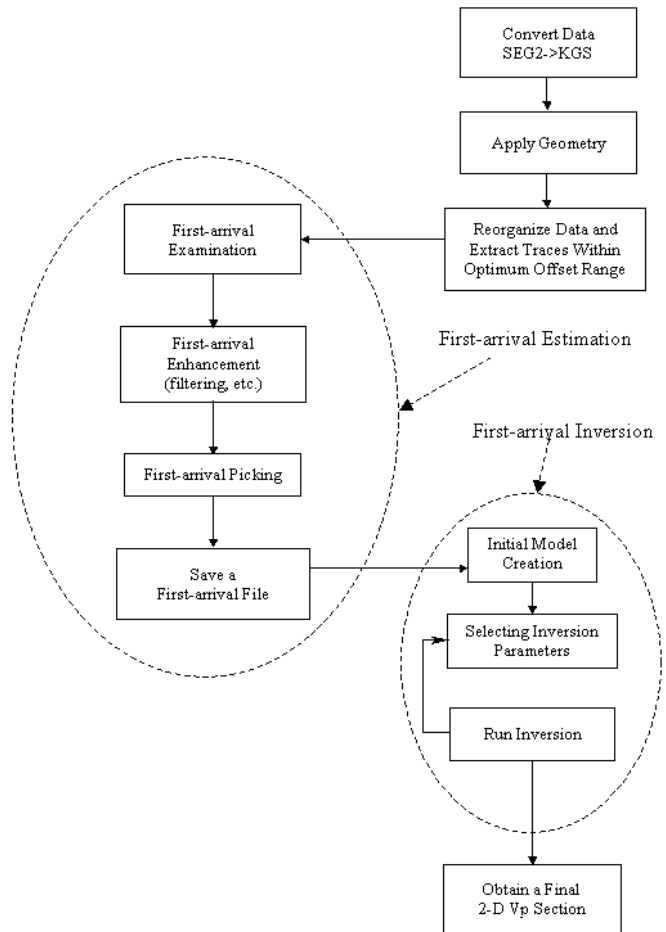


Figure 41. Processing flow for 2-D first-arrival analysis.

resolution land surveying to locate the shot and receiver lines, effectively making the lines simulate horizontal boreholes.

Key to any tomographic analysis is accurate and consistent first-arrival picking. First arrivals were picked using *TomoSeis* (the same software used for the turning-ray tomography). A total of 50,000 traces were analyzed with first arrivals automatically picked and manually inspected. From the first arrival pick a travel time between source and receiver is established and included in a grid to be inverted, iterating the inversion until convergence.

Source-to-receiver travel times can be analyzed to calculate velocities, or amplitudes can be analyzed to calculate attenuation coefficients. This method of through-levée tomography is extremely flexible, allowing source and receiver positions to be located anywhere around the study area in any configuration within a 3-D grid. The tomographic analysis calculates velocity and/or attenuation at points within the grid. Any point within the grid can be classified as having anisotropic characteristics. Raypaths between source and receiver can be straight or curved. The ability to perform 3-D analyses on data such as these is an important advantage in minimizing the problem of nonuniqueness prevalent in standard crosshole data.

Reflection

Reflections from within and immediately below the basal levee contact were of interest and were the focus of reflection processing. High-resolution seismic reflection data, by its very nature, lends itself to over-processing, inappropriate processing, and minimal involvement processing. Interpretations of high-resolution shallow reflection data must take into consideration not only the geologic information available, but also each step of the processing flow and the presence of reflection events on raw unprocessed data. Processing for the reflection portion of this study included only operations or processes that by their nature would enhance signal-to-noise-ratio and/or resolution as determined by evaluation of high confidence reflections interpreted directly on shot gathers.

Unfortunately, no primary reflection energy could be extracted from these data. With the focus of the acquisition more on first arrivals and surface waves, a very reflection-conducive setting would have been necessary for reflection returns from within the levee to be observed or enhanced through processing. For the most part, processing of high-resolution shallow reflection data is a matter of scaling down conventional processing techniques and methods; however, without extreme attention to details, conventional processing approaches will produce undesirable artifacts.

The basic architecture and sequence of processing steps followed during attempts to identify and enhance reflections was similar to conventional petroleum exploration flows (Yilmaz, 1987). The

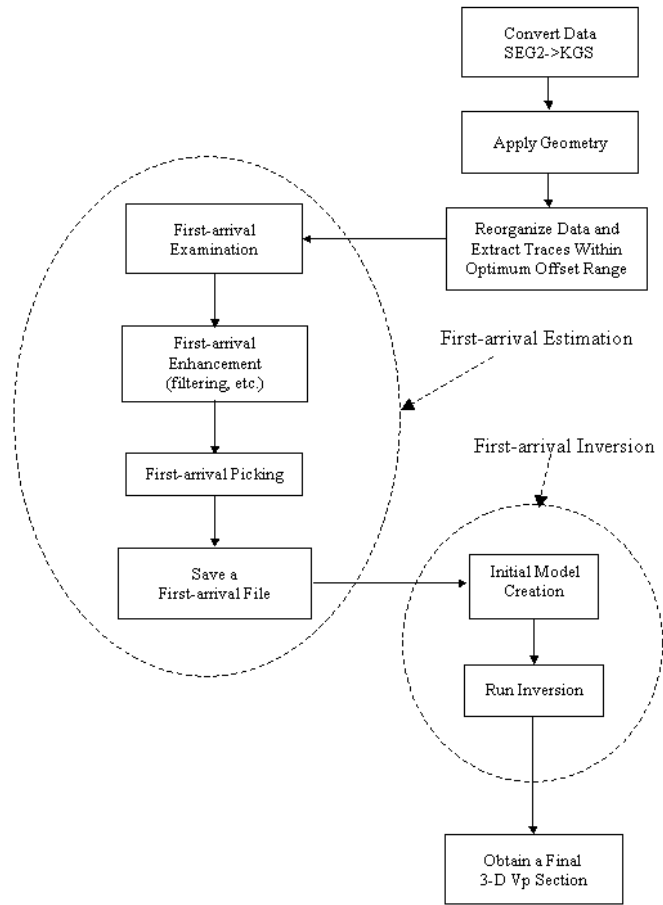


Figure 42. Processing flow for 3-D first-arrival analysis.

primary exceptions related to the step-by-step QC necessary for the highest confidence interpretations of shallow features and realization of full resolution potential (Miller et al., 1989; Miller et al., 1990; Miller and Steeples, 1991) (Figure 43). Specific distinctions related to the emphasis placed on avoiding processing techniques that through mixing, stacking, or filtering could either alias noise to appear as reflections or actually create artificial coherency. Data were processed using *WinSeis2* beta (next generation of *WinSeis*).

Display Formats and Presentation

Data are displayed in this report in a variety of formats, using several different scales and color schemes. Each of the various seismic methods has a preferred or “normal” display format. The use of color and scales is generally a data-specific designation. Color is used throughout this report to enhance the dimensionality of the numerical data sets and to improve the apparent resolution of the data by focusing on the signal portion of the data.



Figure 43. Processing flow for reflection data.

Seismic data are recorded as digital words (representing amplitude of deflection or velocity) stored in a time-sequential order with uniform sampling rates. Sound waves are only useful for imaging if they are recorded over a finite time duration (also known as record length or recording time). Considering that the velocity of sound in rock is generally several times to an order of magnitude or more greater than the velocity of sound in air, recording or listening times of fractions of a second are all that is necessary to fully capture the seismic wavefield from start (source impact/energy release) to finish (wavefield past the listening array). Analog display of seismic data is most commonly seen in what is referred to as wiggle-trace. In wiggle-trace format each sample is plotted as a function of time with a curve drawn through each sample forming a wiggle with the amount of deflection from the zero line equal to the amplitude of recorded signal.

Different components of the seismic wavefield are processed using very specific methods focusing on the particular characteristics of each different component. Initial surface-wave processing produces what is referred to as a dispersion curve. This curve is actually a trend in the data when displayed in frequency-phase-velocity space. A color scale indicative of degree of intensity or highest sample density is generally used to represent this pre-inversion data. Color contouring is a common display format for data that have gone through inversion. In this type of display, different colors represent different ranges of values; therefore, all areas with the same value will also have the same color. Velocity, as well, is generally represented using different colors for different ranges of values.

For most geologic applications, earth materials are generally considered to continuously change from one location to the next in a uniform and/or predictable manner. Since most seismic data are

processed in a cell-by-cell or discrete fashion, to represent earth materials as realistically as possible it is necessary to interpolate between discrete sample points or cells. This process basically makes the assumption that the values between sample points transition between those points in a predictable fashion. This process of interpolation results in a smooth curve or transition across a digital data set. In its most basic form, a digital data field or plot can be contoured such that all points of equal value are connected with curves. This process allows areas with a collection of highs or lows to be easily identified and some degree of continuity in data trends established.

Merging of colors through the spectrum is a way of indicating gradational changes or transitioning of certain earth properties across a survey area. Trends associated with inferred material properties can be established and equated to known values or ground truth. Color contoured (each color representing the same value or level for the mapped property) data provide an image sensitive to changes in the displayed property and therefore allow a greater awareness of difference across a site and from survey to survey (assuming each color is assigned a fixed value that is consistent for all data sets displaying a particular property).

Discussion of Data and Processing at Each Site: Trip #1

A generally consistent set of data was recorded for each site with data processing also following a flow that was relatively consistent for each site. However, each site did have slight differences in acquisition parameters and/or methods evaluated. As previously indicated, all sites had compressional and shear data acquired at the crest and toe; what was not mentioned is that source station spacing changed slightly for sites 3, 4, and 5 based on the findings at sites 1 and 2. Also, the low conductivity at sites 1 and 2 provided opportunities for testing not available at the other sites. For example, site 2 was the site of the percolation experiment with the dug trench.

Seismic-data processing was intended to provide accurate and precise V_p and V_s earth models for the crest and toe. These key seismic properties were used to search for anomalous zones within the levee core that might be indicative of weakening to a point the levee would not perform to construction specifications under the designed water load. As well, a V_p/V_s ratio map (reasonably consistent with a version of Poisson's ratio map) could be derived and used as an additional tool to look for areas of reduced strength within the levees. The larger the V_p/V_s , generally the weaker the material from a ripability or shear strength perspective. By comparing the crest data with the toe data from each site, contributions of native materials below the levee can be accurately characterized and allow separation of the energy traveling only in the levee. A second benefit to recording and processing data from both crest and toe is the potential to verify consistency in the measured native material values.

Site 1

Estimates of cross sectional V_s were obtained for both crest and toe using tomography and surface-wave inversion techniques. V_p information was extracted from P-wave data using first-arrival analysis (tomography) of seismic data collected along both toe and crest lines. Frequency dwell data were analyzed for amplitude variations as a function of frequency, specifically looking for changes in phase that could be related to changes in material seismic velocity. A full 240-channel through-levee traveltimes study was undertaken for both P- and S-wave energy. Data were acquired to allow the use of 3-D borehole tomography software to analyze first arrivals and generate a traveltimes delay volume focused within the core of the levee.

P-wave Velocity Distribution (foundation material vs. crest/levee material)

P-wave first-arrivals were picked from data acquired along the crest. In general, shot records possessed impulsive, relatively high signal-to-noise first breaks that were picked automatically with a small percentage requiring manual adjustments (Figures 44 and 45). There are two distinctively different

apparent first-arrival velocity trends from trace to trace on the P-wave data (Figures 44 and 45). From a basic refraction analysis overview perspective, the two distinctly different phase velocities observed in these data are likely from the material within the levee and the shallowest portion of the native earth (possibly the near-surface material [upper few feet of native sediments]). After selecting the first-arrival time for each trace on the P-wave data shot gathers from along the crest of the levee, a 2-D refraction-tomography Vp solution was obtained (Figure 46). In this case a 2-D solution represents a cross sectional slice of the levee, physically equivalent to cutting a trench parallel to the centerline (axis) of the levee and observing the material from some distance away either north or south (Figure 47). This solution was obtained with minimal model iterations and without any major discrepancies between the modeled and real first arrivals.

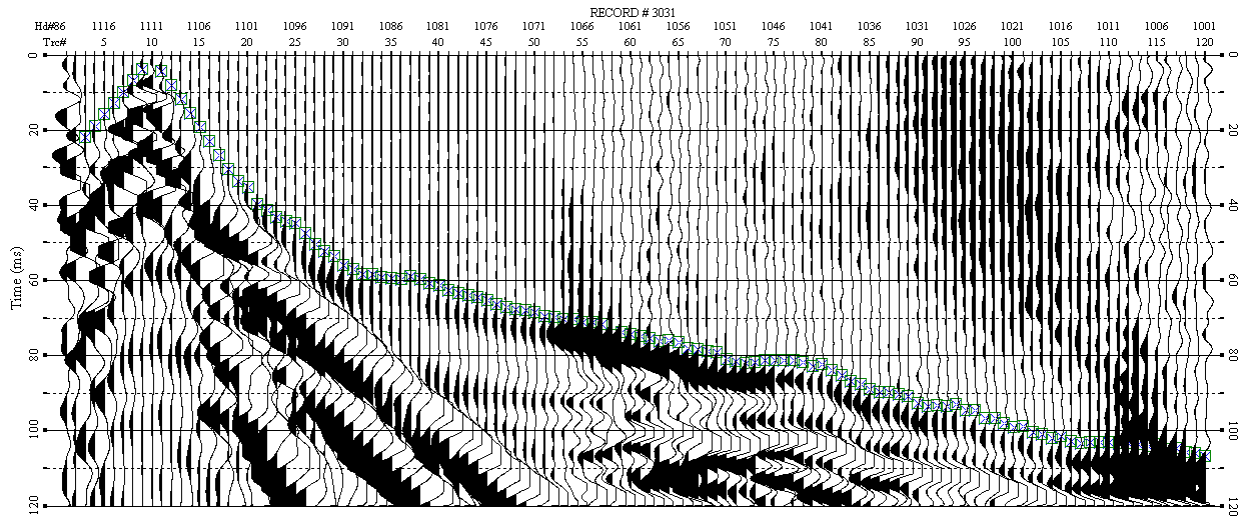


Figure 44. Estimation of first-arrivals times on a P-wave seismic data with source located at station 1111 (horizontal coordinate at 3333 ft).

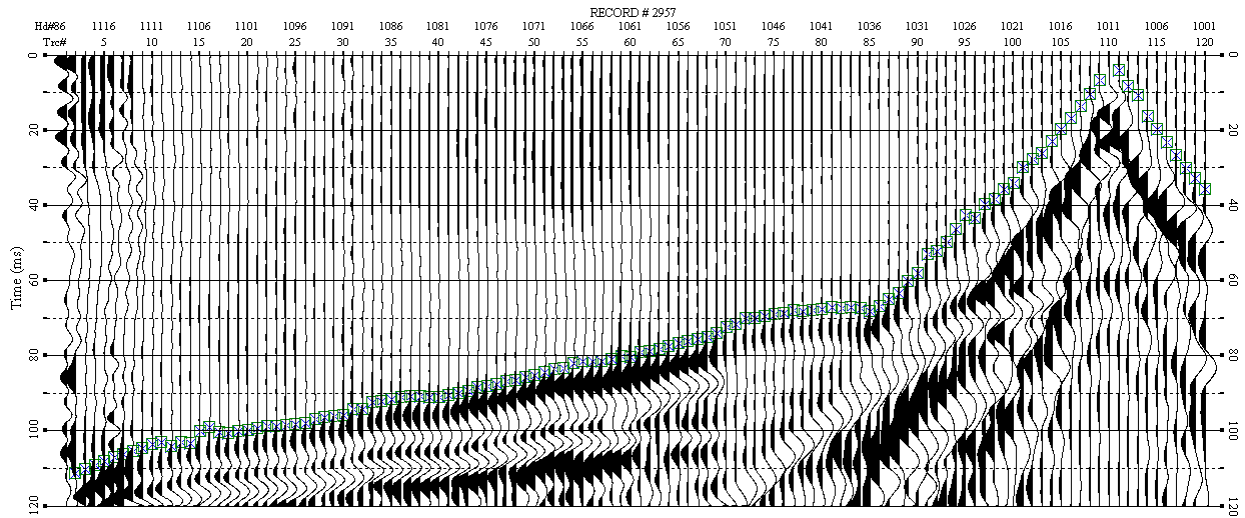


Figure 45. Estimation of first-arrivals times on a P-wave seismic data with source located at station 1011 (horizontal coordinate at 3033 ft).

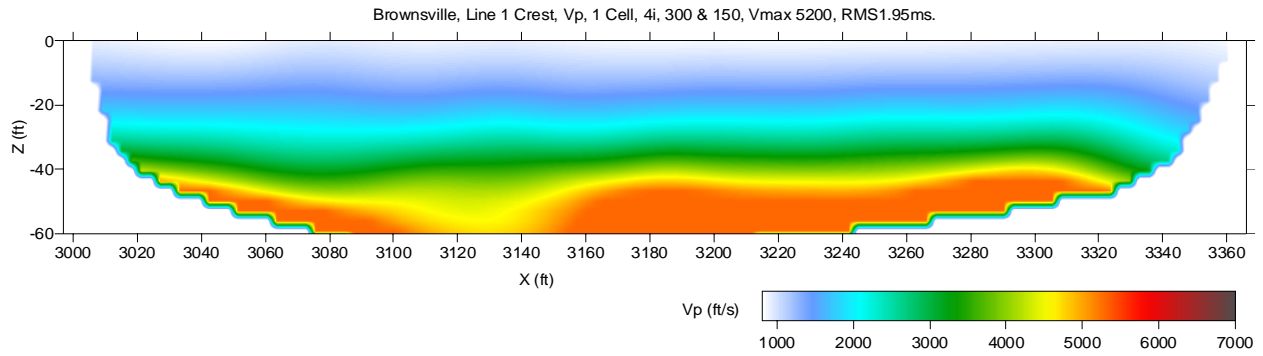


Figure 46. P-wave velocity model estimated for line 1 by analyzing P-wave-data first-arrival times using refraction-tomography software.

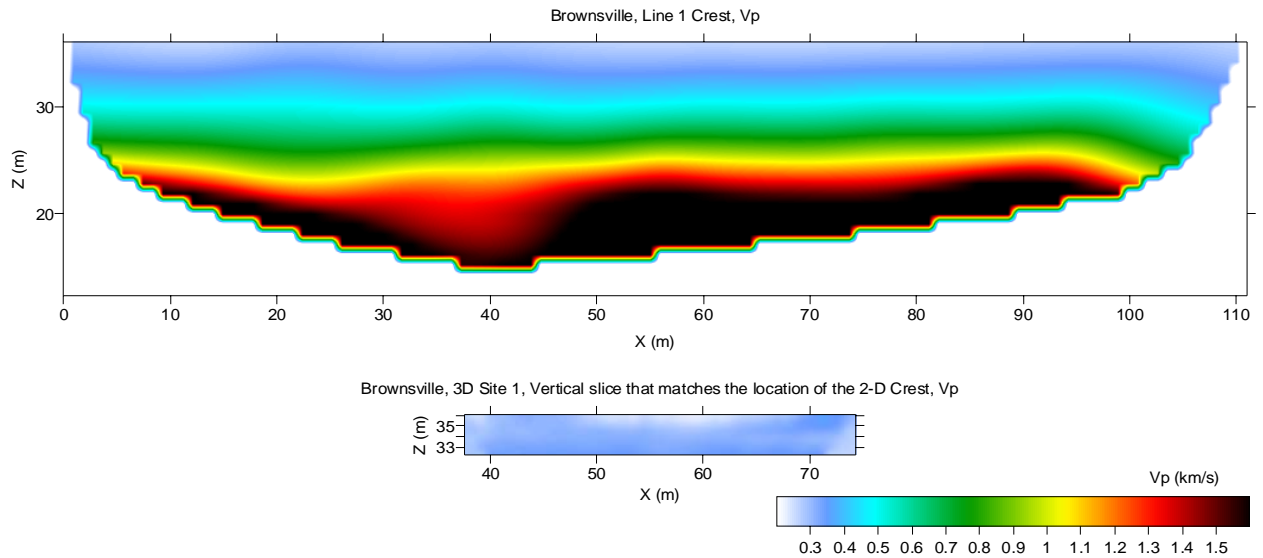


Figure 47. P-wave velocity model estimated for line 1 by analyzing P-wave-data first-arrival times using refraction-tomography software compared to a vertical slice from a 3-D P-wave velocity model estimated by analyzing 3-D through-levee P-wave-data first-arrival times using tomography software.

S-wave Velocity Distribution

S-wave first-arrivals were picked from data acquired along the crest site. Overall the first arrivals appeared a bit more irregular in wavelet character than observed on equivalent compressional-wave energy (Figure 48). As with the P-wave first-arrival pattern, when viewed as a function of source offset, the S-wave velocity structure appears to also support the interpretation that there are two unique velocity layers in the upper 10s of feet at site 1. However, unlike the equivalent compressional-wave data, the two different first-arrival slopes interpreted on the shear-wave data are not as pronounced with respect to consistent slope, clear cross-over, and trace-to-trace uniformity in arrivals. As expected with the slower shear velocities in the levee, the apparent shallower velocity is present on and interpreted from fewer traces within the near-offset range. As well, the velocity contrast between the two layers is relatively small so the change in slope representative of each layer's phase velocity is very subtle (Figure 48). Considering the apparent difference in the P- and S-wave first-arrival velocity trends, it would not be unexpected to have solutions for the two types of waves that were significantly different.

After picking the first-arrival times from the S-wave data shot gathers collected along the crest of the levee, a 2-D refraction-tomography V_s solution was obtained (Figure 49). In general, there is a wide range of equally possible solutions to the inverse refraction/tomography problem due to the

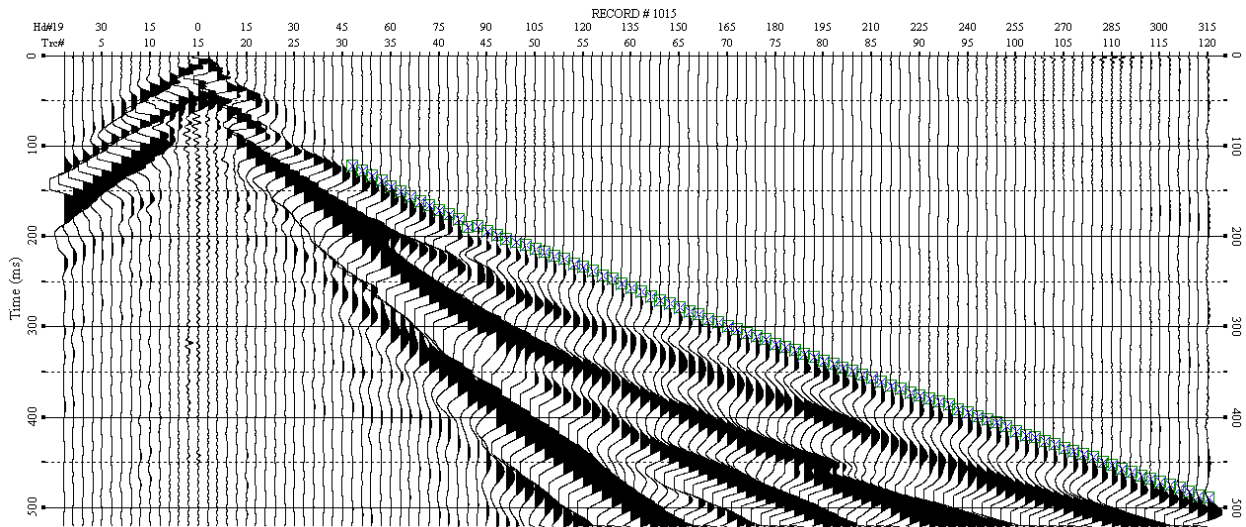


Figure 48. Estimation of first-arrivals times on an S-wave seismic data with source located at station 1111 (horizontal coordinate at 3333 ft).

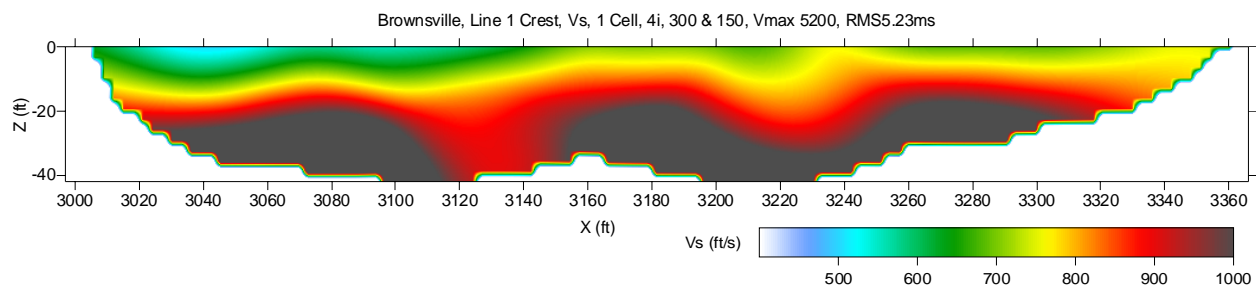


Figure 49. S-wave velocity model estimated for line 1 by analyzing S-wave-data first-arrival times using refraction-tomography software.

nonuniqueness of geophysical analysis. In addition, for the case of S-wave data, the nonuniqueness problem can be exacerbated due to the possibility of P-S wave conversions. In light of this mode conversion problem, the MASW method was preferred over the S-wave refraction/tomography analysis for estimating the Vs structure within the levee.

Rayleigh Wave

Two different methods were used to acquire and process Rayleigh-wave energy. Impulsive data were used for MASW analysis and sweep or variable frequency data were used for phase analysis. Comparisons of land-streamer data with traditional geophone coupling included comparisons of both body waves and surface waves. Surface-wave analysis of these comparative data sets was focused on dispersive data characteristics. Rayleigh-wave MASW analysis included two steps: estimation of dispersion curve, and inversion to shear velocity profile. The shear-wave velocity profile represents the geologically useful component of this analysis and therefore it was the primary emphasis of the processing and interpretations.

MASW Method at the Levee Crest

Dispersion-curve overtone analysis was used to optimize the picking of receiver-spread parameters that provide the best opportunity for recording the maximum frequency range of the surface-wave fundamental mode. Initially, all recorded traces from a fixed-spread shot gather were used to calculate the

dispersion curve, thereby allowing a general idea of the dispersive character of the surface wave at this particular site (Figure 50). The fundamental-mode energy ranges from 5 to 15 Hz at associated phase velocities from 650 to 500 ft/s. These surface-wave fundamental-mode energy characteristics were used to design the acquisition parameters and refine the dispersion-curve selection process. Two higher mode events were observed in the frequency range from 13 to 35 Hz and at velocities between 1300 to 600 ft/s (lower frequencies are sampling greater depths and therefore have higher velocities associated with them). Lower-amplitude higher-mode energy can be interpreted beyond 30 Hz and at phase velocities around 1000 ft/s. All higher-mode energy is considered noise for MASW analysis, which is designed to process fundamental-mode energy only.

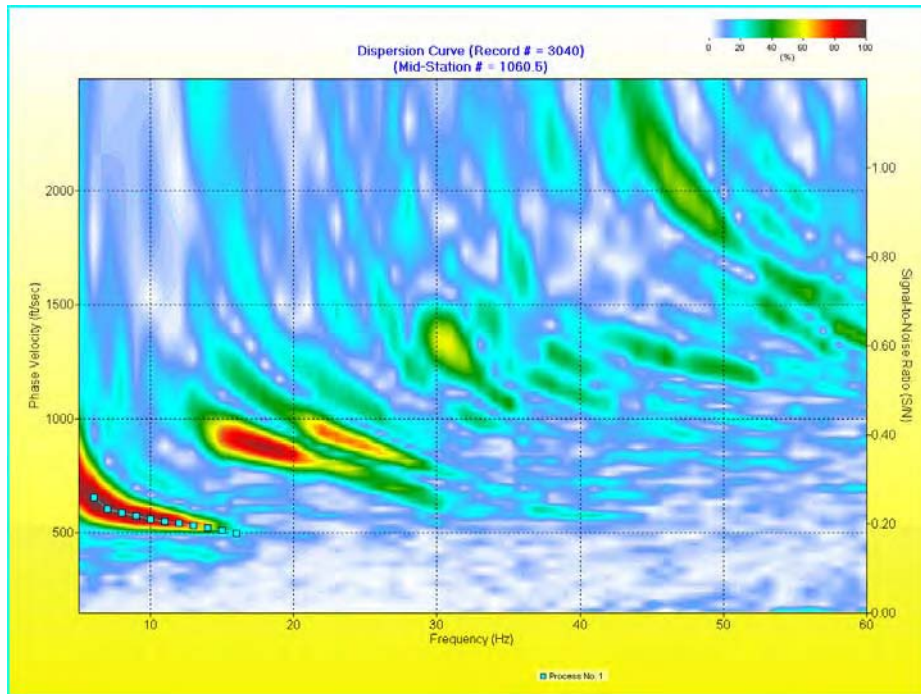


Figure 50. Dispersion-curve analysis of P-wave-data surface-wave using all 120 traces from shot record #3040.

To maximize the lateral resolution of the processed data the recording spread needs to be as short as possible and still provide adequate quality of the fundamental-mode dispersion-curve picking. Analysis of the first ten traces (Figure 51) demonstrates how a lack of far-offset traces does not allow the separation of fundamental and higher modes. This shorter spread also inhibits confident picking of fundamental-mode energy in the low-frequency range because these lower frequencies will not fully develop within the very near-offset ranges. With this short spread, close-offset data set, the fundamental and higher modes all interfere to form one dispersion curve that appears to possess a reverse trend (velocities increase with frequency).

Improvement in the separation between fundamental and higher modes is evident and identification of fundamental-mode dispersion properties at frequencies as low as about 7 Hz is possible when analysis includes the first twenty traces of the fixed spread (Figure 52). When analysis included the first forty traces (Figure 53), the high quality data were sufficient for fundamental-mode analysis of frequency as low as 4 Hz. Still troubling is the apparent lack of high frequencies in the fundamental-mode dispersion curve. The highest possible fundamental-mode frequencies identifiable on dispersion curves are between 13 and 18 Hz.

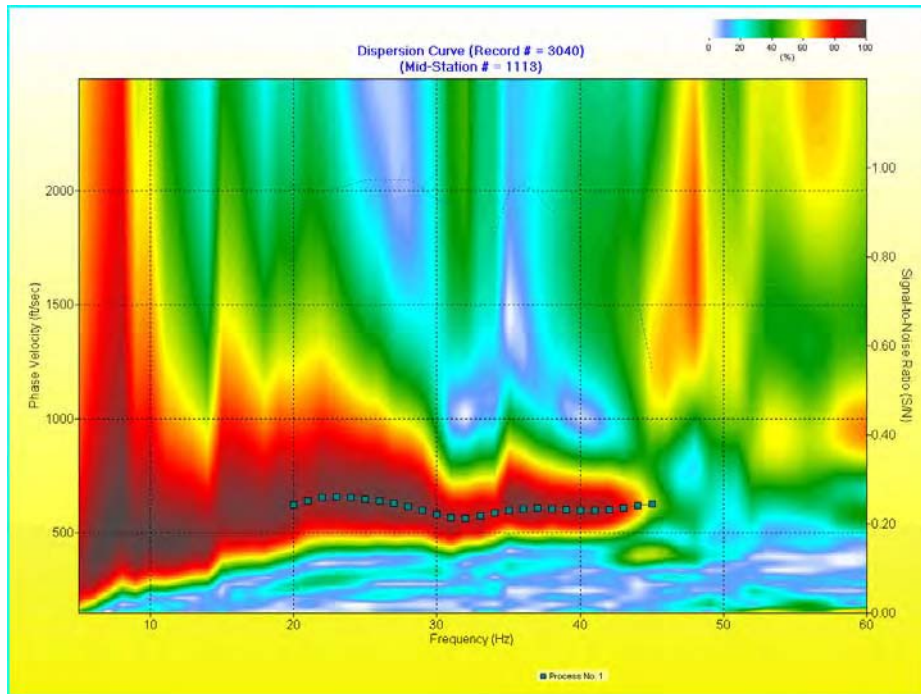


Figure 51. Dispersion-curve analysis of P-wave-data surface-wave using the first 10 traces from shot record #3040.

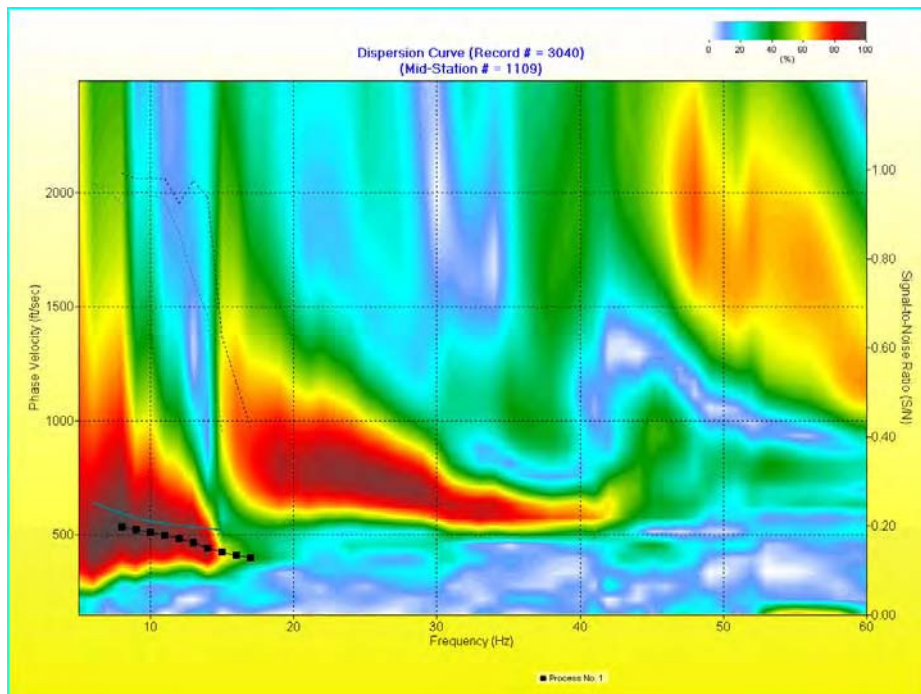


Figure 52. Dispersion-curve analysis of P-wave-data surface-wave using the first 20 traces from shot record #3040.

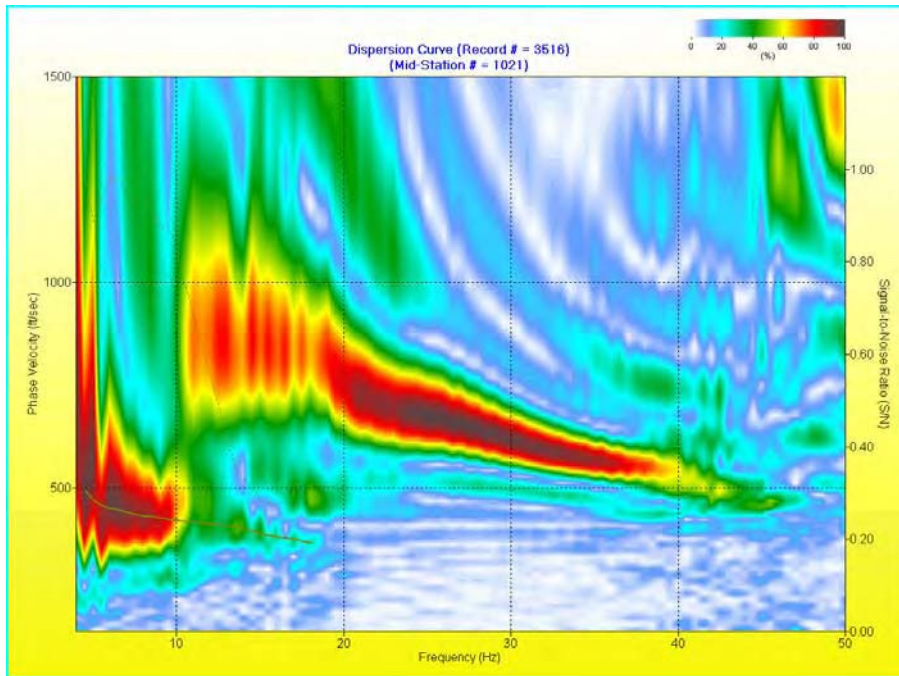


Figure 53. Dispersion-curve analysis of P-wave-data surface-wave using the first 40 traces from shot record #3040.

Using the first 40 traces and focusing spectral improvement on processing provided little in the way of significant improvements to the fundamental-mode dispersion events. Two different types of higher-mode filters were applied in an attempt to isolate any fundamental mode energy above 20 Hz (Figures 54 and 55). There appears to be no fundamental-mode energy propagating in the levee itself above 20 Hz. Energy observed on dwell experiments using the vibrator is all higher-mode energy.

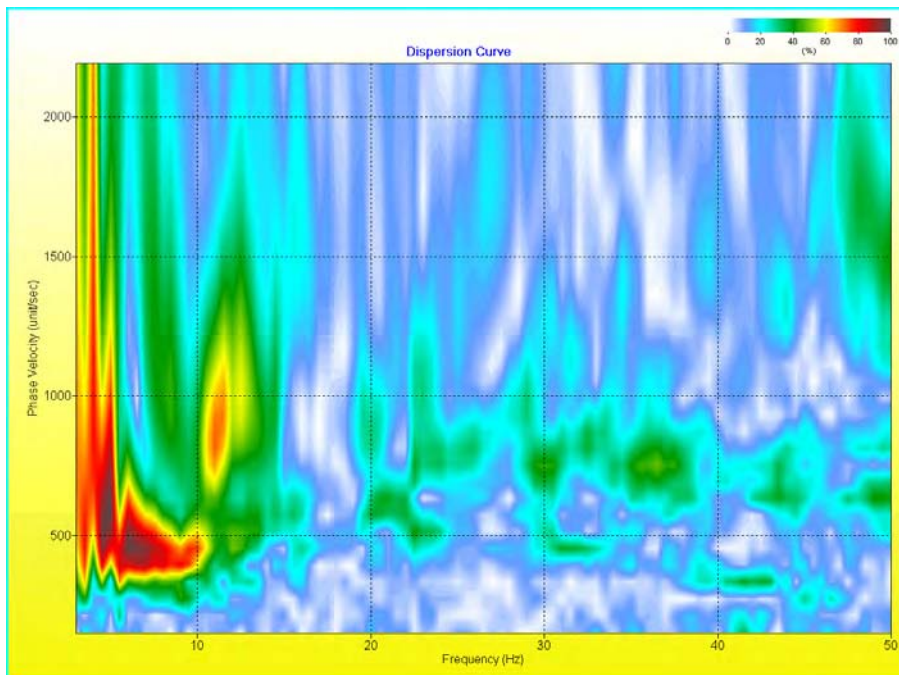


Figure 54. Dispersion-curve analysis of P-wave-data surface-wave using the first 40 traces from shot record #3040 after filtering the first higher mode (with interpolation).

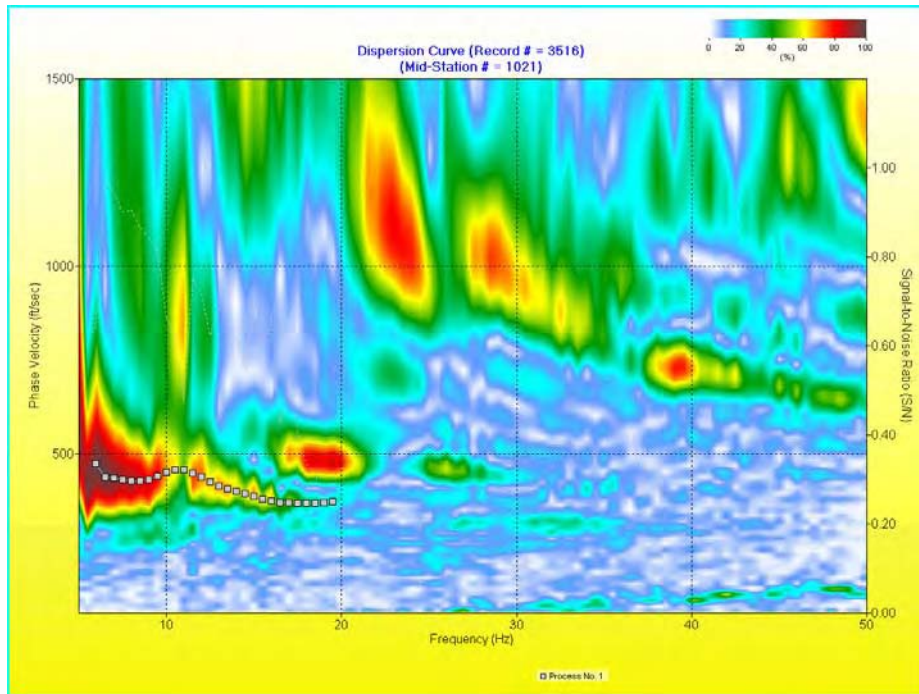


Figure 55. Dispersion-curve analysis of P-wave-data surface-wave using the first 40 traces from shot record #3040 after filtering the first higher mode (with no interpolation).

Too many traces included in fundamental-mode surface-wave analysis can result in frequency degradation and increased sample smearing of higher-frequency components of the surface-wave energy packet. An optimum number of traces should be determined based on uniformity of spectral properties across the entire proposed spread. A shot gather spectra from this site demonstrates the offset dependent nature of these seismic data (Figure 56). It is obvious that no significant energy exists above 20 Hz beyond trace 60. Thus, the largest usable spread to consider including in an image of the levee from the crest would include traces from 1 to 60.

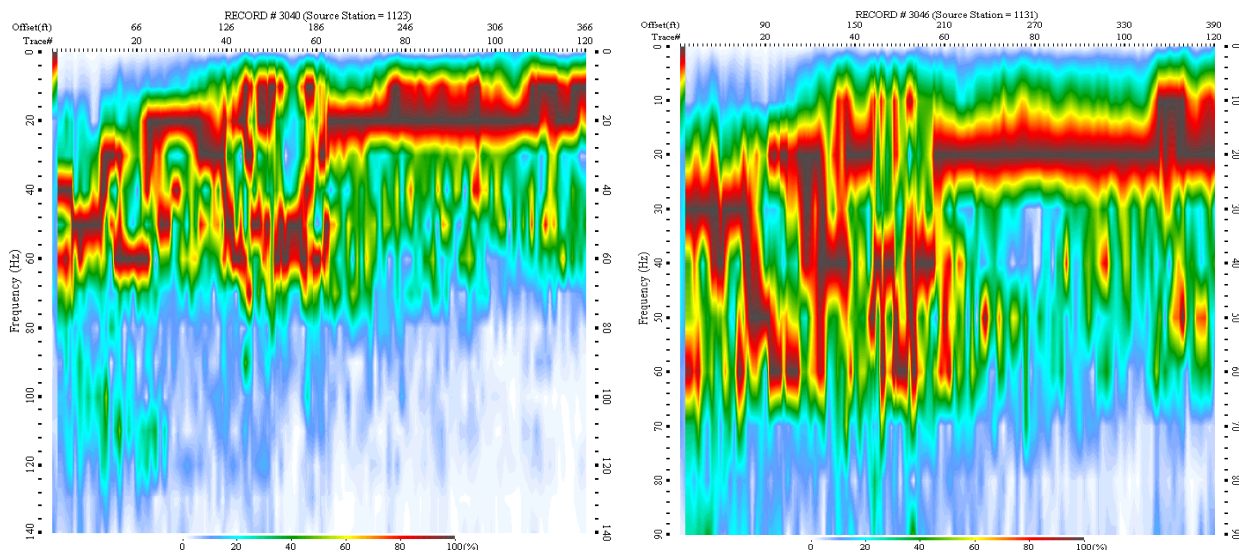


Figure 56. Amplitude spectral display of shot records 3040 and 3048.

MASW Vs Results

Even though no surface-wave fundamental mode energy above 20 Hz was recorded (and therefore no shallow Vs information, specifically no shear-wave velocity information was obtained that was isolated to the levee itself), the MASW method still provided an accurate overall estimation of the Vs from the crest to depths of between 25 ft and 70 ft below the crest of the levee (Figure 57). Even though changes in materials properties affecting velocity within the levee are not specifically sampled, lateral changes observed in lower frequency and therefore deeper penetrating energy could have remnant contributions from intra-levee properties.

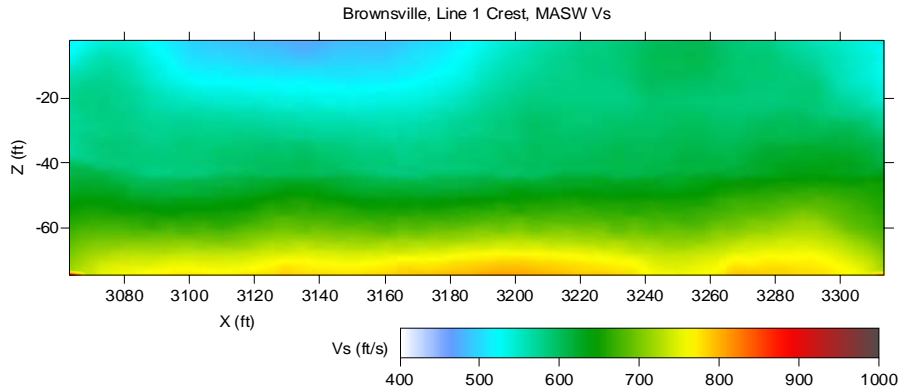


Figure 57. S-wave velocity model estimated for line 1 by analyzing P-wave-data surface-wave using MASW method.

Vibrator Dwell from Levee Crest

Frequency dwell experiments were run using a seismic vibrator to study resonance or phase abnormalities within the levees, possibly indicative of material property changes. Constant-frequency sweeps were recorded using the entire spread, allowing changes in phase velocity of the surface wave as a function of location to be studied. In particular, observations concerning interference and changes in phase velocity for the fixed-frequency energy were the primary target. Since surface-wave phase velocity is frequency dependent, any change in phase velocity for the selected frequency can be related to changes in material properties within an estimated depth range (which is dependent on the wavelength of the particular frequency of surface wave being produced). A combination of t-x and f-x analysis allowed any variations in the key seismic attributes of the surface waves to be identified.

More than 70% of all seismic energy is surface waves, therefore driving the ground with seismic energy at specific frequencies is an easy way to estimate sections of levee with laterally, and to a lesser degree vertically, inconsistent material composition. Unfortunately, in order to correlate surface-wave frequency with depth the surface-wave energy must be fundamental mode. Even using the high-energy vibrator, no fundamental-mode surface-wave energy above 20 Hz was observed on raw or processed shot gathers (Figure 58). This lack in higher frequency fundamental-mode surface-waves was a characteristic of all these sites. Of some interest was the much more chaotic and discontinuous nature observed on frequency dwell data at site 2 relative to the other sites. This phenomenon will be discussed in the section for site 2.

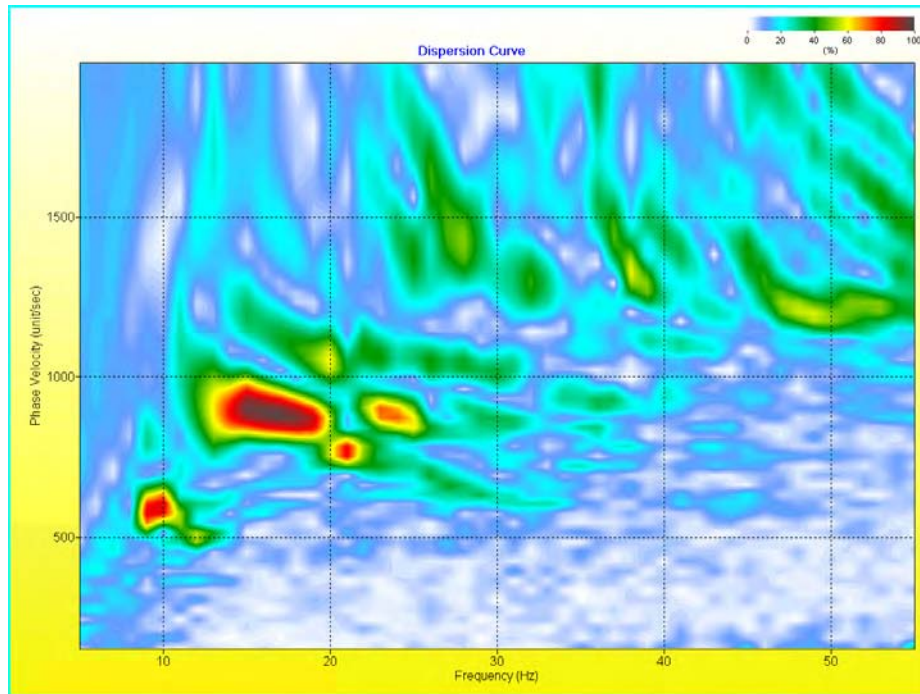


Figure 58. Dispersion-curve analysis of P-wave 10-100 Hz sweep vibrator-data surface wave using all traces from a shot.

Through-levee Tomography

First-arrival processing and analysis relies heavily on direct ray propagation paths between source and receiver and that the first-arriving energy at a receiver is primary, first order, non-mode-converted energy clearly distinguishable from any later arriving modes. For the 3-D through-levee tomography, at some stations refracted or mode-converted energy appears as the first arrival on a seismic trace. In these cases, the direct energy trails the refracted or mode-converted first arrival and with careful wavelet matching can be identified and selected for travel time analysis. This kind of meticulous and detailed trace-by-trace processing requires exorbitant amounts of time.

For the 3-D tomography, the geometry and overall dimensions of the levees significantly complicate event identification and analysis. With a low-velocity shell, medium-velocity core, and high-velocity base, a refracted source-receiver travel path was many times faster than direct or curved ray paths. As well, each of these interfaces represent an ideal source of mode-converted energy, and for shear through-levee tomography this becomes a significant hindrance to confident direct-ray identification. This complication is significant enough that several of the tomography analysis techniques will not provide accurate subsurface models or reliably converge on a high-confidence subsurface velocity model for levees of this type.

Visualization of tomographic images is best viewed in 3-D; however, with the source and receiver geometry deployed along the levees the most meaningful images come from 2-D slices, both longitudinal and transverse to the levee axis. Comparisons between through-levee 3-D velocity volumes and 2-D slices along the crest provide independent cross-checking of the general range of values and some level of precision possible with seismic type techniques. Considering the extreme geometry and potential for out-of-the-plane arrivals, some meaningful results can be deduced based purely on data quality.

P-wave 3-D Through-levee Tomography

Identification of P-wave Direct Arrivals

Most of the actual first-arrivals did not appear to have traveled a direct path through the levee. For example, first-arrival times for shots along the lowest-shot line on the levee face (closest to the toe of the levee) all had arrival times at the 120 lowest receivers in the spread (120 closest to the toe) within 6 ms of each other and a short travel time of 60 ms (Figure 59). Considering that the source-to-receiver-offset distance range was 22 to 38 m, if a straight line raypath was followed these first arrivals suggest a 40% change in velocity from one end of the spread to the other. This becomes even more unrealistic when the reverse shot depicts the same change in velocity with offset when assuming a straight-ray propagation path through the levee. All things considered, first arrivals from source and receiver locations near the toe are likely refractions from the basal contact. The velocity vs. offset trend is consistent with the suggestion that the first arrivals are refracted arrivals (Figure 60). The standard deviation of this data set is 52.23 m/s, reflecting the wide range of velocity values. The travel-time velocity is proportionally linearly dependent on the distance from the source, which is unlikely due to geology for a straight raypath model. More likely the first-arrivals are refracted energy.

Moving to greater time, the next set of arrivals have a time-offset relationship that is much more consistent with what would be considered a realistic direct-travelpath scenario for this site (Figure 59). Travel-time curvature of the second coherent event is consistent with the variable offset between the source and receivers. A travel-time velocity vs. distance relationship for the second coherent event contains velocity values that span a significantly smaller range, making them much more realistic candidates for direct waves (Figure 61). The standard deviation of this data set is 11.23 m/s and the velocity appears much less offset dependent. However, consistently picking the same wavelet and phase arrivals for an event from within the wavefield (that is, not the first arrival) is extremely difficult due to interference from all the other modes and coherent energy arriving at a receiver from a variety different travel paths.

Reversing the polarity of the data set greatly increases the confidence in picks of the initial onset of the direct traveling wave (Figure 62). Because the polarity is reversed, some adjustment was necessary to compensate for picks that were now being made on the second lobe of the direct-arriving wavelet.

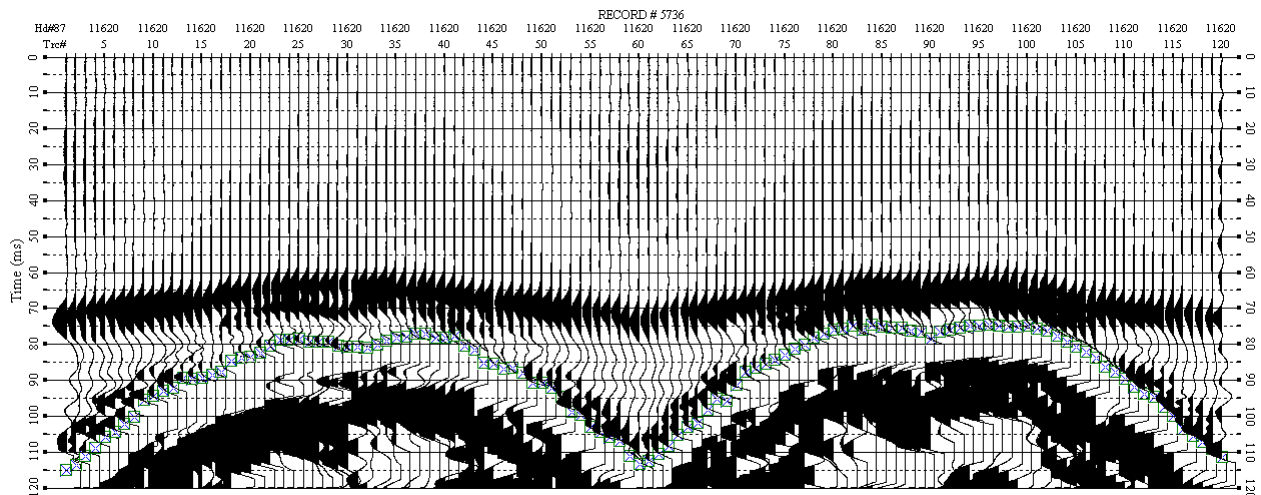


Figure 59. Estimation of first-arrival and secondary-arrival times on 3-D P-wave through-levee seismic data with source and receivers located at lowest altitude (closest to the toe), shot record 5736.

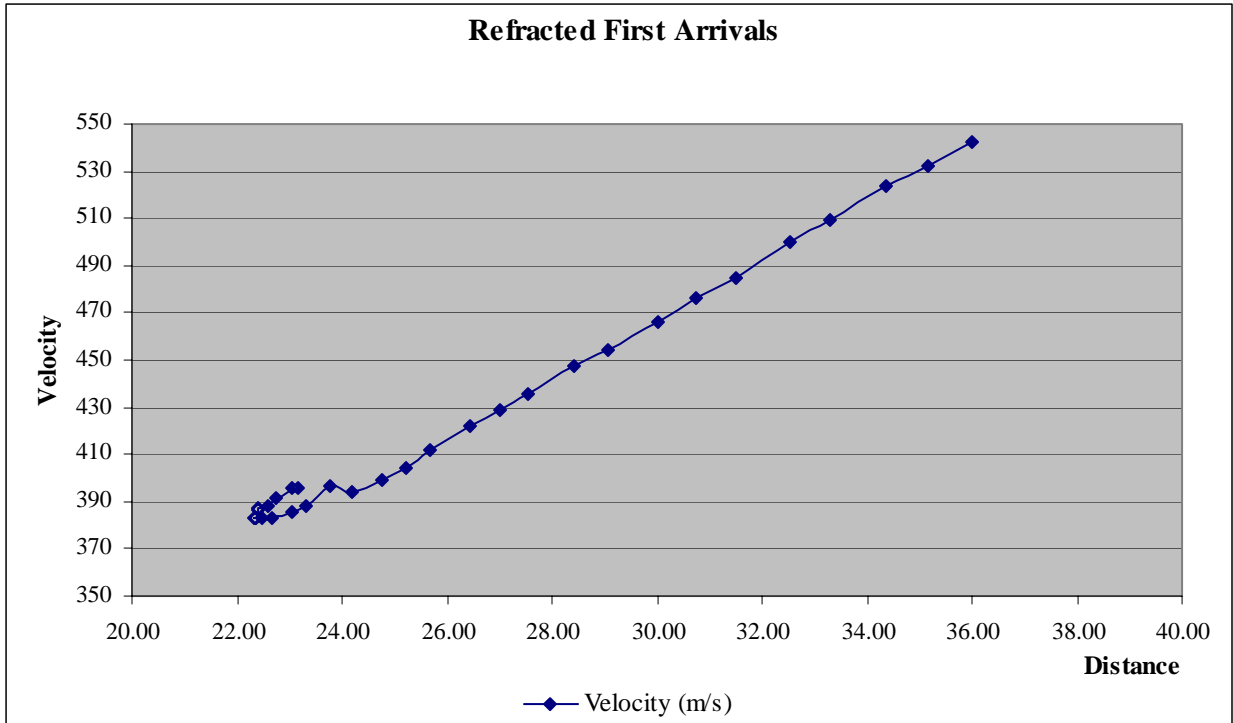


Figure 60. Through-levee first-arrival average velocity analysis versus distance.

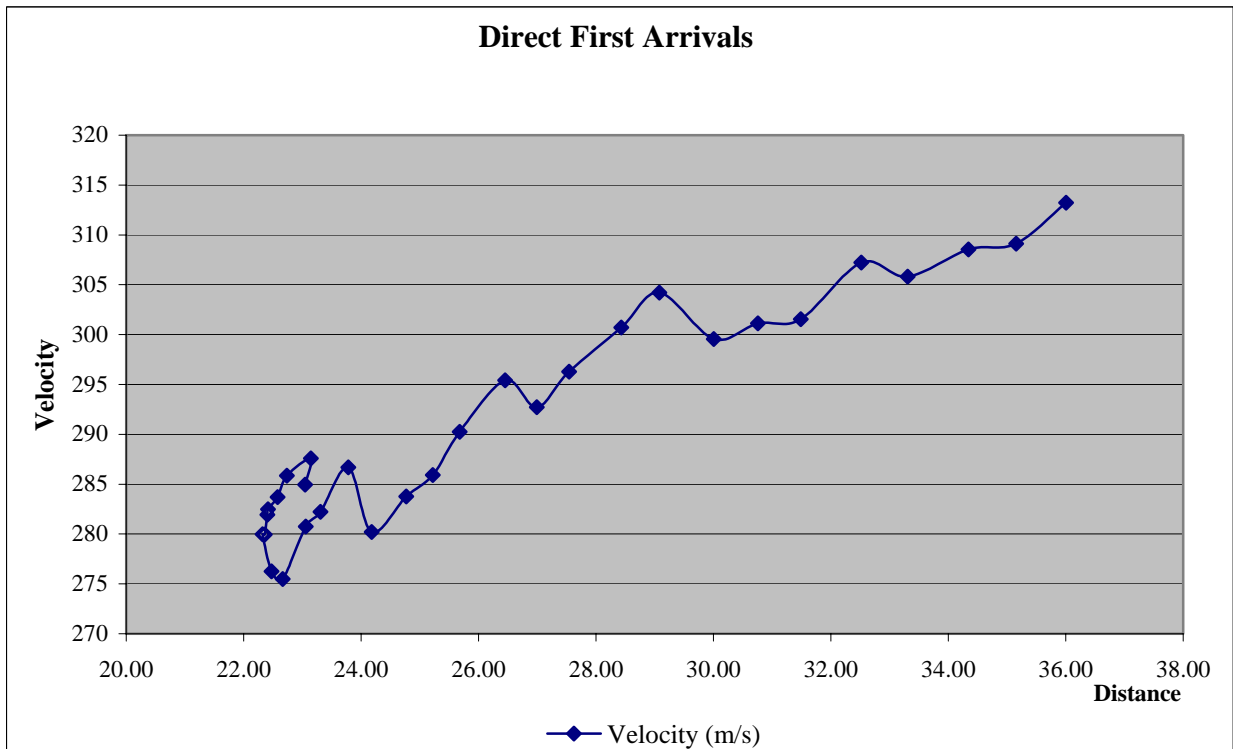


Figure 61. Through-levee secondary-arrival average velocity analysis versus distance.

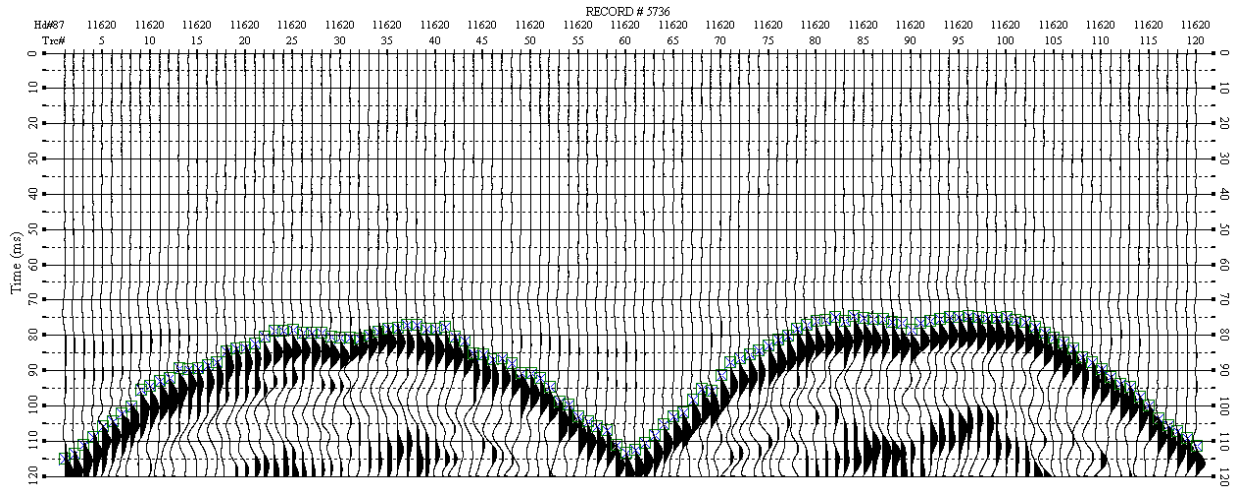


Figure 62. Estimation of direct-wave arrival times after reversing polarity of 3-D P-wave through-leeve seismic data with source and receivers located at lowest altitude (closest to the toe), shot record 5736.

Shot gathers with source and receiver locations near the top of the levee possessed first-arrival patterns consistent with traveltimes and velocity curves observed in the direct-wave arrivals interpreted from source and receiver stations near the toe of the levee, which, as mentioned earlier, arrived later in the wavetrain (Figure 63). Even with the source and receivers at the very top of the levee, direct-wave energy was not the first arrival on all traces. Refracted energy was again the source of the interference forcing the direct wave into a later position in the wavetrain. As with shot and receiver stations from near the bottom of the levee, it was easier to use the positive amplitude of the seismic wavelet and therefore polarity reversal was necessary (Figure 64). As a result, picking the zero crossing 180° out of phase from the actual onset of direct-wave energy, a constant 11 ms was calculated to be the difference between the actual direct through-leeve arrival (negative amplitude) and the picked positive amplitudes. Therefore, after all the first arrivals were picked on polarity-reversed traces, 11 ms was subtracted from the interpreted first-arrival time.

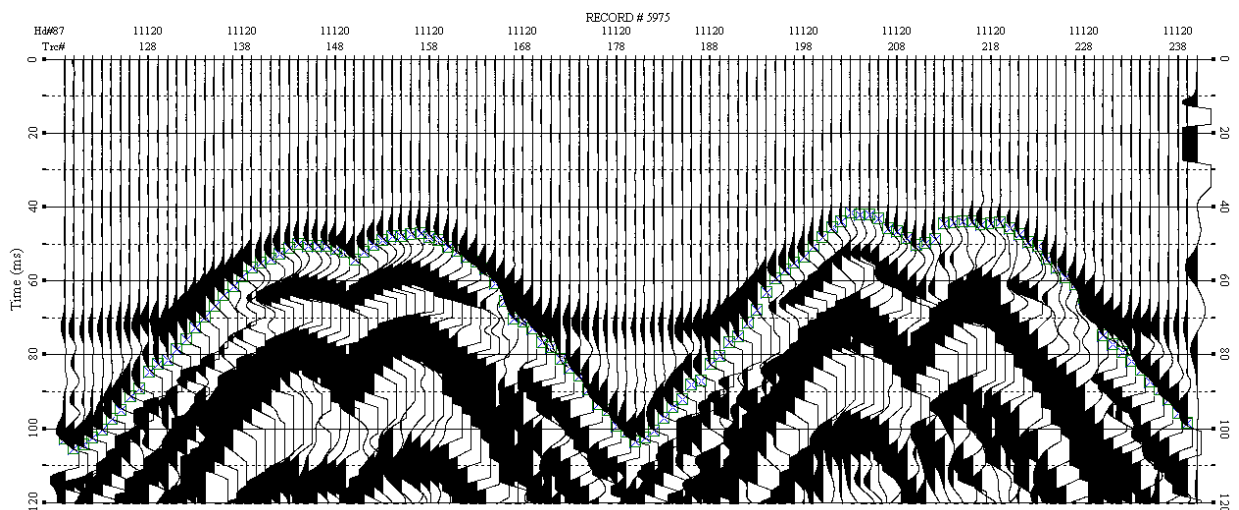


Figure 63. Estimation of direct-wave arrival times of 3-D P-wave through-leeve seismic data with source and receivers located at highest altitude (near the top of the levee), shot record 5975.

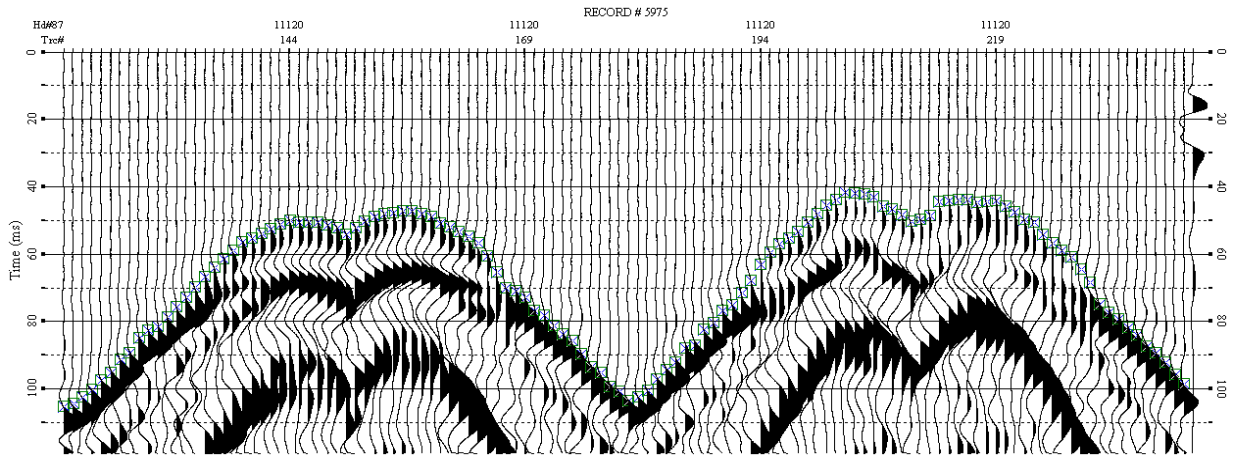


Figure 64. Estimation of direct-wave arrival times after reversing polarity of 3-D P-wave through-levee seismic data with source and receivers located at highest altitude (near the top of the levee), shot record 5975.

Results

All the data arrival times are plotted for quality control as a function of source-receiver separation (Figure 65a) and as a function of processing order supplied to the software (Figure 65b). Arrival times are clustered along a linear trend that represents the average velocity through the levee. Areas where the clusters of first arrivals deviate from the straight-line plot represent the range of velocities at a particular offset. Considering these scatter plots are not location dependent it is not possible to isolate areas with anomalous velocity zones, but areas with increased ranges of velocity for particular offsets and increased densities of first-arrival times at particular offsets are all related to the non-uniformity of the levee core.

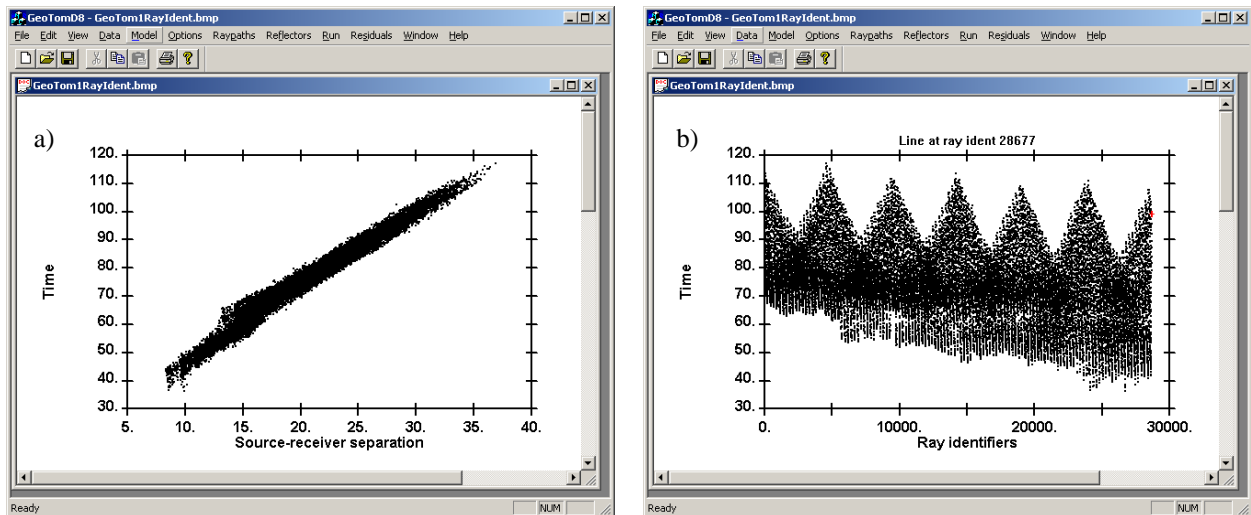


Figure 65. a) Plot of 3-D P-wave through-levee direct-wave arrival times versus source-receiver separation. b) Plot of 3-D P-wave through-levee direct-wave arrival times versus software order.

First-arrival time-offset pairs were inverted using *GeoTomCG* software with a residual RMS of 2.02 ms. The 3-D solution is presented using horizontal slices at elevation levels 32.29 m (Figure 66a), 33.05 m (Figure 66b), 33.81 m (Figure 66c), 34.57 m (Figure 66d), 35.32 m (Figure 66e), and 36.09 m (Figure 66f). A vertical slice along the levee volume was extracted (Figure 67) as noted by white circles (Figure 66f). The residuals from every raypath are plotted for quality control (Figure 68). An additional vertical slice was plotted that is consistent with the relative location of the 2-D MASW and refraction seismic lines (Figure 69).

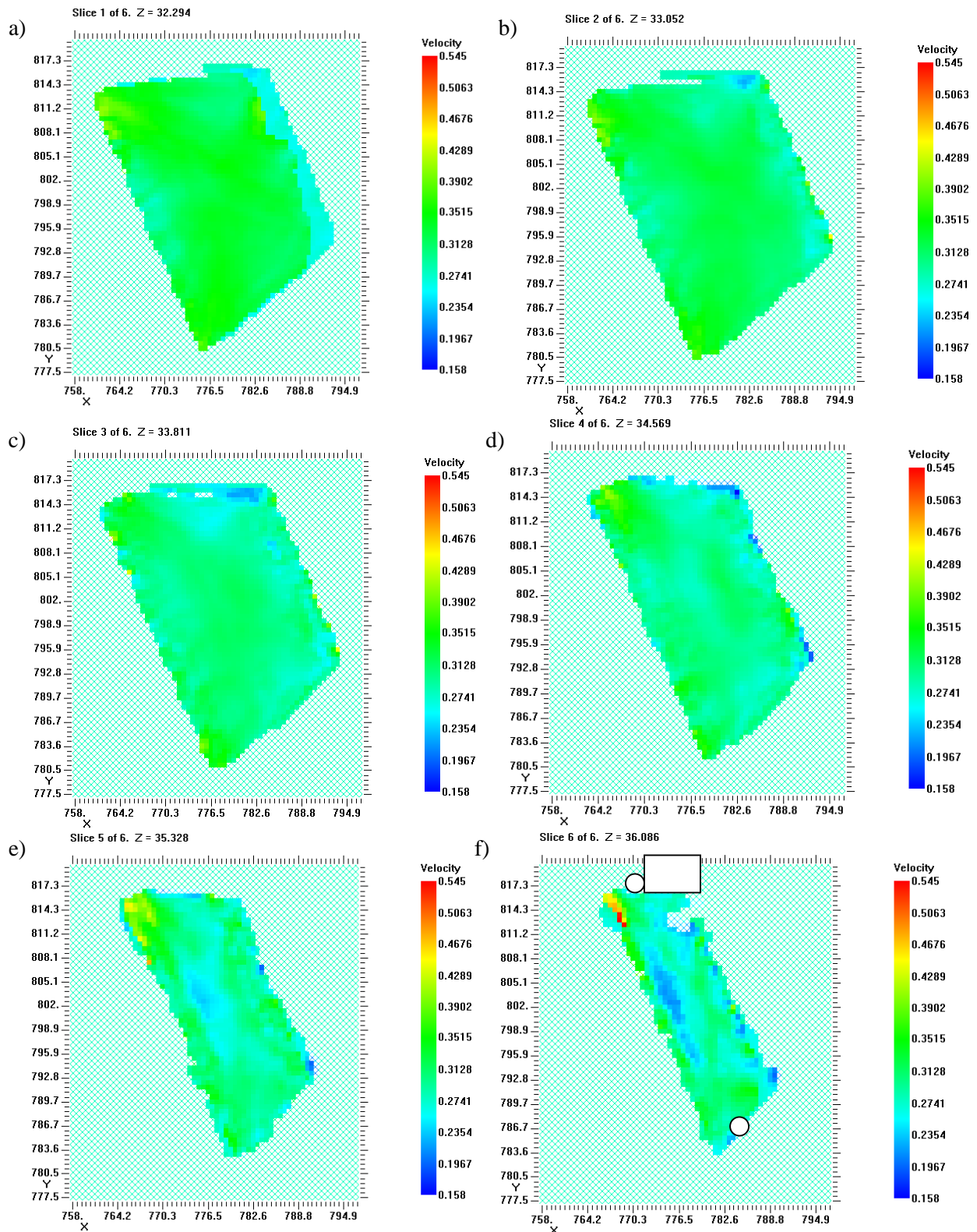


Figure 66. Horizontal slices extracted from the 3-D P-wave velocity volume obtained from inverting direct-wave arrivals. a) horizontal slice at elevation 32.29 m, b) horizontal slice at elevation 33.05 m, c) horizontal slice at elevation 33.81 m, d) horizontal slice at elevation 34.57 m, e) horizontal slice at elevation 35.32 m, and f) horizontal slice at elevation 36.09 m.

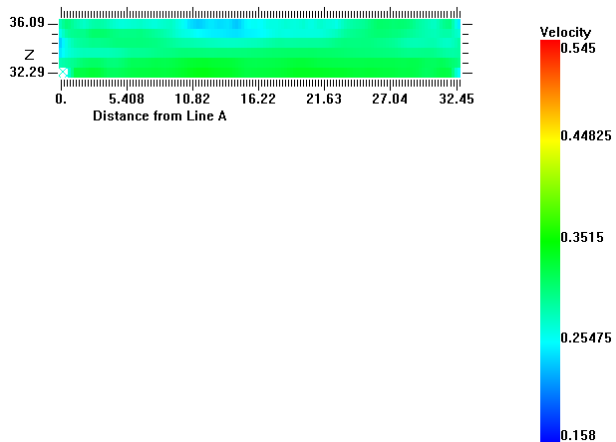


Figure 67. A vertical slice extracted from the 3-D P-wave velocity volume obtained from inverting direct-wave arrivals, coincident with the location of the 2-D P-wave seismic line.

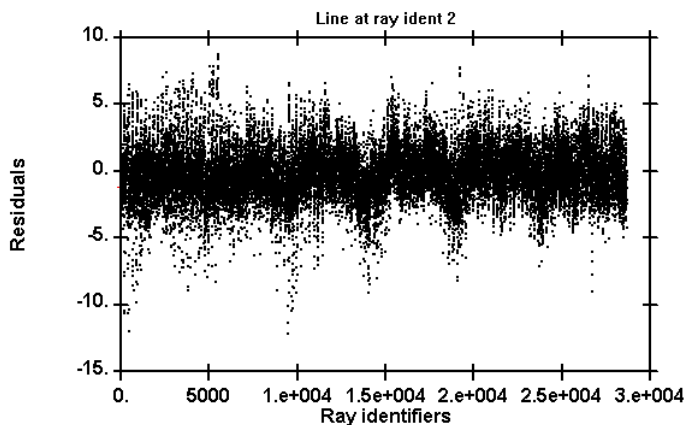


Figure 68. Residual error plot for all rays involved in the inversion. The sum of the residual errors is -4920 ms and the total RMS error is 2.02 ms.

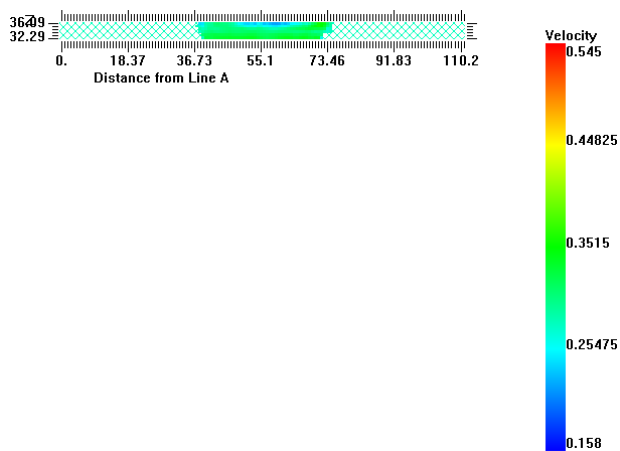


Figure 69. A vertical slice extracted from the 3-D P-wave velocity volume obtained from inverting direct-wave arrivals, compared with the extent of the 2-D P-wave seismic line.

S-wave 3-D Through-levee First-arrival Analysis

Identification of the direct-wave arrivals

In general the S-wave first arrivals should provide a picture of the subsurface that, in general, is consistent with that observed from P-wave first arrivals. Careful analysis and comparisons of the first-arrival wavelets proved beneficial for the P-wave through-levee tomography, so the same rigorous process was used for the S-wave data set. Adding to the complications resulting from refraction first arrivals on the P-wave data for S-wave data, the problems of mode conversions play a prominent role. Realistic velocities of shear-wave energy must be determined prior to trying to identify different arrivals on this kind of a shot gather. Because it is unlikely the direct S-wave will be the first arrival, problems similar to those encountered identifying direct energy on the P-wave through-levee shot gathers from the lower tier of receivers will be prevalent on all data.

For consistency and to minimize the number of variables in identifying direct shear energy, all analysis was completed on shot records where the source was located at station 610 (base of the slope, nearest the toe near the center of the grid). It is evident that there is a strong polarity, attenuation, or near-field problem that has left no consistency in the first-arriving wavelets along the top of the hyperbola that represents the closest receiver locations relative to the source (Figures 70 to 74). A lack of interpretable wavelets with consistent phase and amplitude characteristics at these close-offset receivers suggests a source problem (not generating sufficient shear energy with the appropriate polarity at close offsets) or a material characteristic (earth not conducive in the near-field to the production and propagation of shear-wave energy). This kind of a data characteristic would not be unexpected where a liquid or void was present with the appropriate dimensions and ratios. Another possibility is that the observed first-arrivals are refractions (from significantly faster underlying layers) instead of direct arrivals and closer offsets are less than the critical refracting offset distance.

If these longer-offset first arrivals are shear energy, they possess an apparent average velocity of about 300 m/s (1000 ft/s), which is much faster than the expected (200-300 ft/s). Velocities in this range are consistent with those observed on compressional-wave data sets. If these are near-receiver mode-converted waves, that would explain the apparent lack of arrivals at the nearest offset. These offsets would be only sensitive to energy polarized along the axis of the levee. Offsets further from the source will be at an angle relative to the axis and, due to orientation relative to the shear source, would be increasingly sensitive to compressional-wave energy with increasing angle from orthogonal relative to the source and levee axis.

Using the polarity sensitive nature of shear waves and the observations about energy recorded from non-orthogonal angles relative to the levee axis, arrivals immediate across the levee from the source are likely SH arrivals that have traveled through at least part of the levee. Using that assumption, the S-wave first-arrivals appear in the central part of each hyperbola, at about 80 ms, resulting in an average S-wave velocity of about 180 m/s (600 ft/s). This velocity is quite close to the MASW estimated shear velocity measured from the crest at depths from about 25 ft to 40 ft. Therefore, it is possible that the majority of the first-arriving shear-energy travel path was in that high-velocity zone.

Substantiating the suggestion that the greatest concentration of polarized shear arrivals are recorded at receivers in-line with the source relative to the levee axis can be accomplished by studying a record recorded with the source near the top of slope very near the crest and centered on the receiver grid (Figure 74). With the source location at station 310, the average velocity appears to be about 235 m/s (770 ft/s), which is still faster than the expected (200-300 ft/s), but not unreasonable for refracted energy traveling along the basal levee contact. As is clear with other through-levee data sets, wavelets arriving after the first arrival are strongly interfered with by the multitude of different types of energy and unique travelpaths that they follow between source and receiver. This also makes picking the true "direct arrival" from within the body of the wavetrain very speculative and inconsistent from record to record.

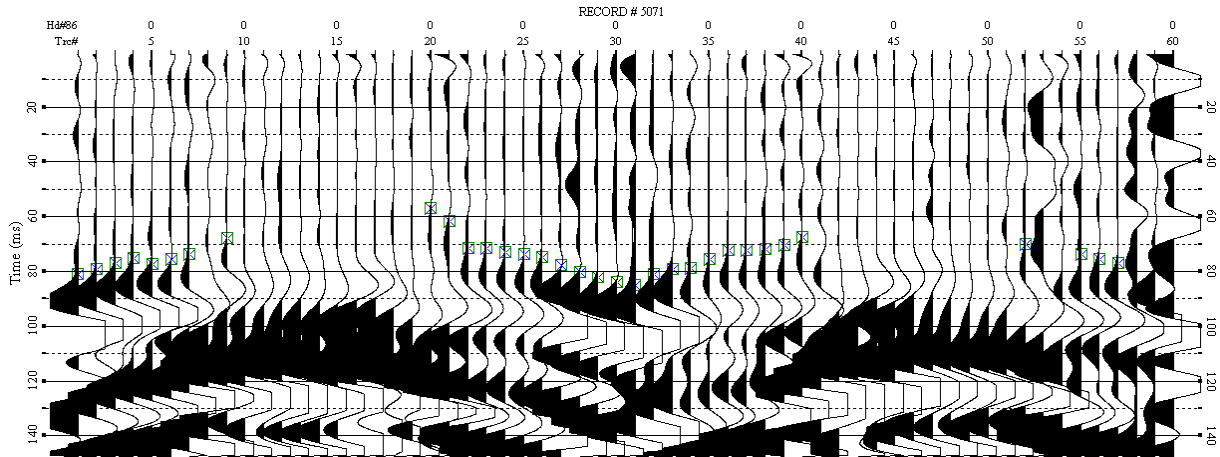


Figure 70. Estimation of first-arrival times on 3-D S-wave through-levee seismic data with source located at lowest altitude in the middle of the grid and receivers (from 0-60) located at the bottom two lines (closest to the toe) of the grid, shot record 5071.

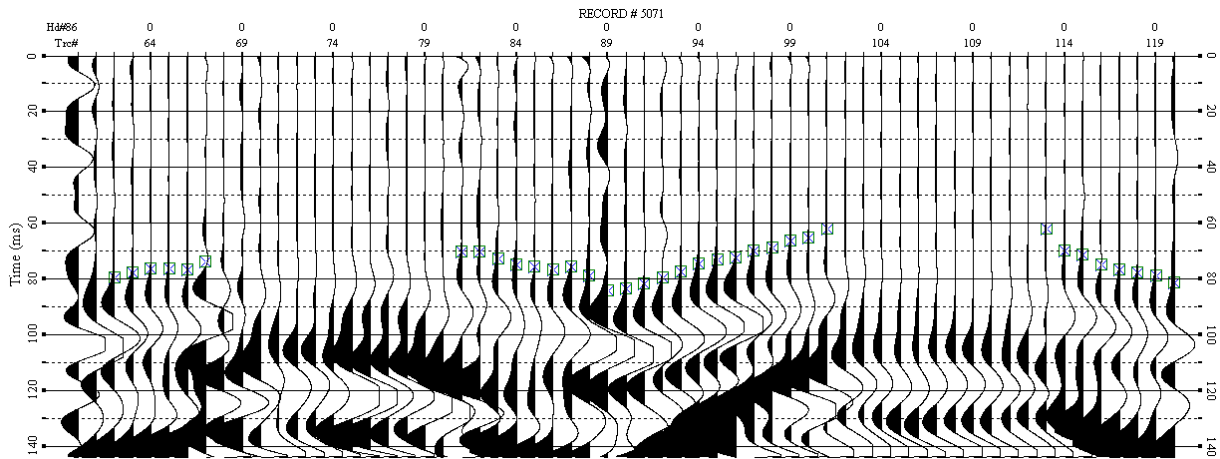


Figure 71. Estimation of first-arrival times on 3-D S-wave through-levee seismic data with source located at lowest altitude in the middle of the grid and receivers (from 61-120) located at two lines in the middle (closest to the toe) of the grid, shot record 5071.

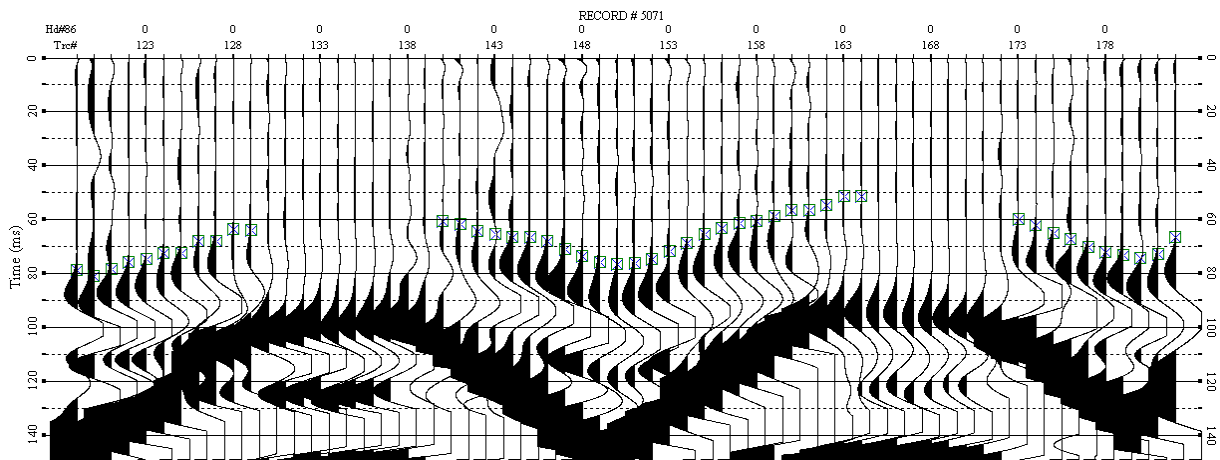


Figure 72. Estimation of first-arrival times on 3-D S-wave through-levee seismic data with source located at lowest altitude in the middle of the grid and receivers (from 121-180) located at two lines in the middle (closest to the top) of the grid, shot record 5071.

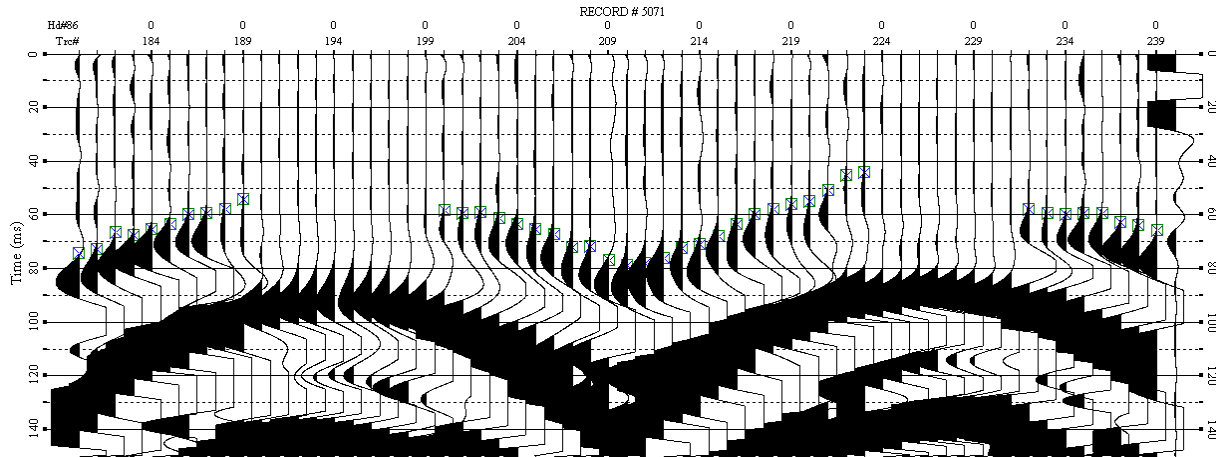


Figure 73. Estimation of first-arrival times on 3-D S-wave through-levee seismic data with source located at lowest altitude in the middle of the grid and receivers (from 180-240) located at the top two lines (closest to the top) of the grid, shot record 5071.

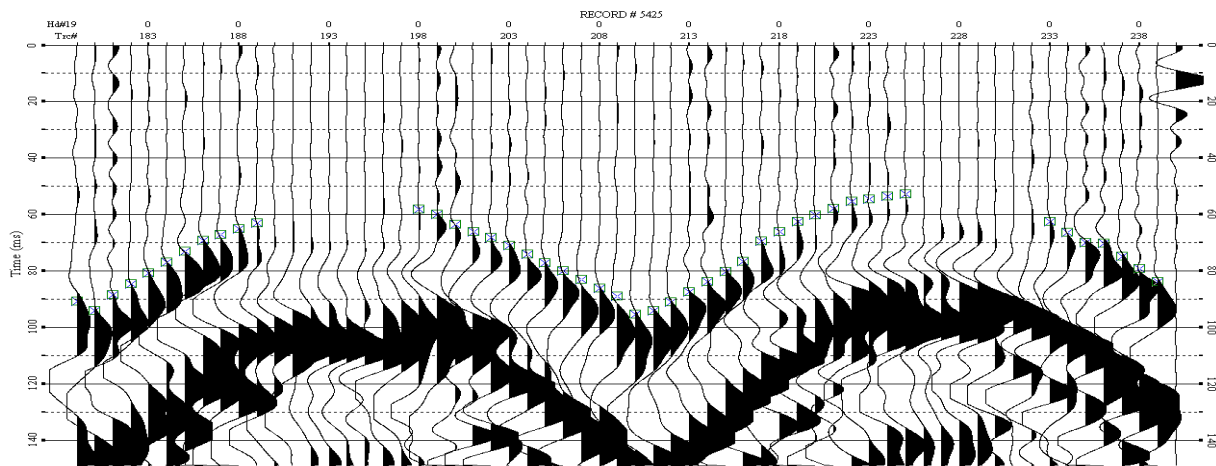


Figure 74. Estimation of first-arrival times on 3-D S-wave through-levee seismic data with source located at highest altitude in the middle of the grid and receivers (from 180-240) located at the top two lines (closest to the top) of the grid, shot record 5425.

P- and S-wave First-arrival Kinematic Comparison

A significant amount of effort was expended trying to compare and relate direct arriving and first-arrival wavelets interpreted on P-wave data (p-wave source and geophones) with the first arrivals observed on the S-wave data. To minimize the number of variables for this multi-modal comparison, shot records studied all have the source located at station 610 (the bottom of the slope, near the toe and at the center of the grid) and the receiver locations are the same for all (Figures 75 and 76). First-arrival times on P-wave cross-levee tomography shots (Figures 75 and 76) are (within experimental error) identical to equivalent S-wave cross-levee tomography shots (Figures 73 and 74). This observation is consistent with one of the previous suggestions that the S-wave phones recorded converted energy or the angle away from orthogonal between source and receiver relative to the crest axis was sufficient that the S-wave source and S-wave oriented phones were generating and recording P-waves. The similarity between P- and S-wave first-arrival kinematic patterns is highly suggestive and enforces the current thinking that first arrivals on S-wave data should not be considered and analyzed as pure S-waves.

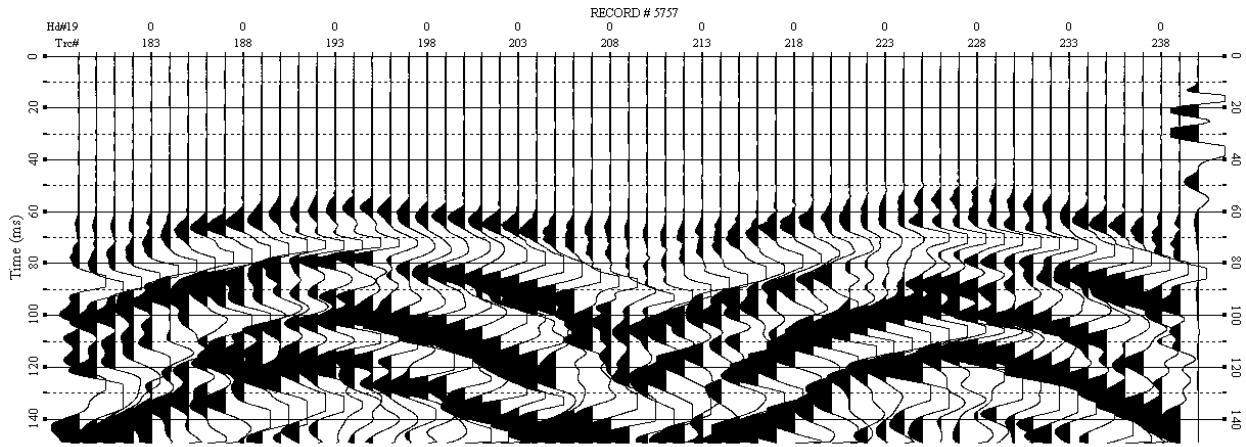


Figure 75. Estimation of first-arrival times on 3-D P-wave through-levee seismic data with source located at lowest altitude in the middle of the grid and receivers (from 180-240) located at the top two lines (closest to the top) of the grid, shot record 5757.

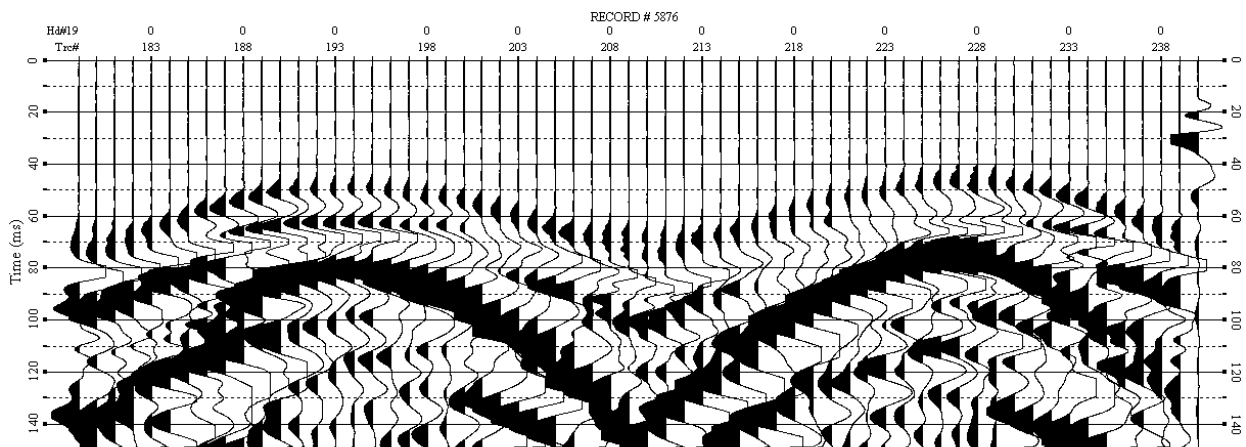


Figure 76. Estimation of first-arrival times on 3-D P-wave through-levee seismic data with source located at highest altitude in the middle of the grid and receivers (from 180-240) located at the top two lines (closest to the top) of the grid, shot record 5876.

S-wave Direct-raypath Search

Further study of S-wave data considered the possibility that other, non-first-arrival, energy arrival patterns could be the source of the observed S-wave first arrivals. The highest shot location (closest to the crest and at the center of the spread (station 310, Figure 77) was chosen as the spread geometry most likely to record shear-wave energy traveling directly from source to receiver; in effect, this geometry and these physical locations minimizes the possibility of recording refractions.

All the recorded wavelets examined had low dominant frequencies (15-20 Hz) and very limited bandwidth. These characteristics are consistent with the surface-wave energy observed on the recorded 2-D S-wave data at this same location (Figure 78). Picking consistent phase along a hyperbolic moveout pattern slow enough to be considered direct S-wave energy did not produce a velocity comparable with the distance divided by the direct arrival time. This inconsistency is suggestive of a propagation path that is not directly through the levee but either around the surface (such as a surface wave) or the result of multiple mode conversions and/or reflections/refractions from within the levee itself.

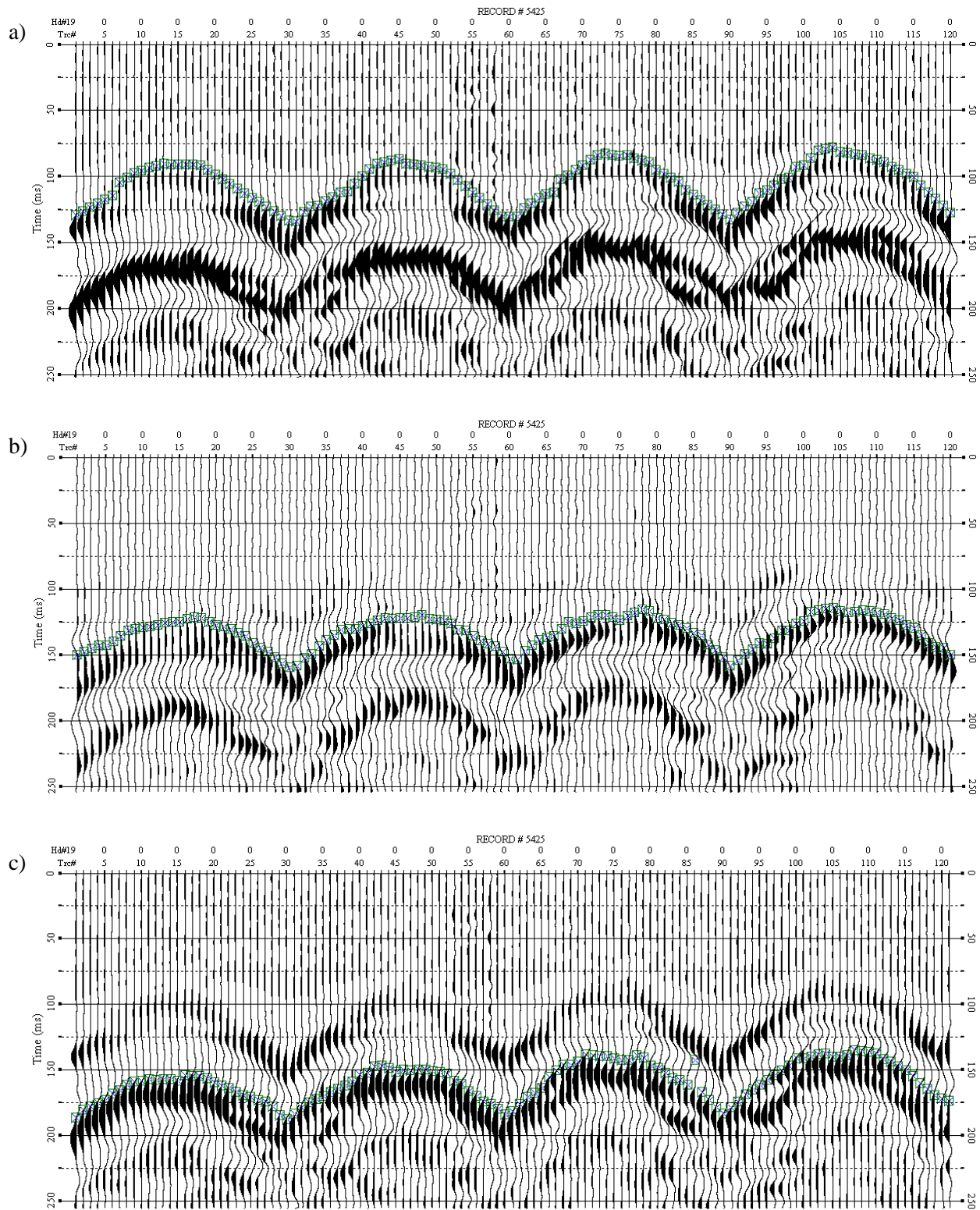


Figure 77. Possible S-wave refractions (direct-arrivals), which are not first arrivals. First-arrival events are hardly seen because of the lower gain. The average velocity of the first-arrivals of a) is about 600 ft/s (188 m/s); of b) is about 480 ft/s (143 m/s, reversed polarity traces); of c) is about 390 ft/s (119 m/s).

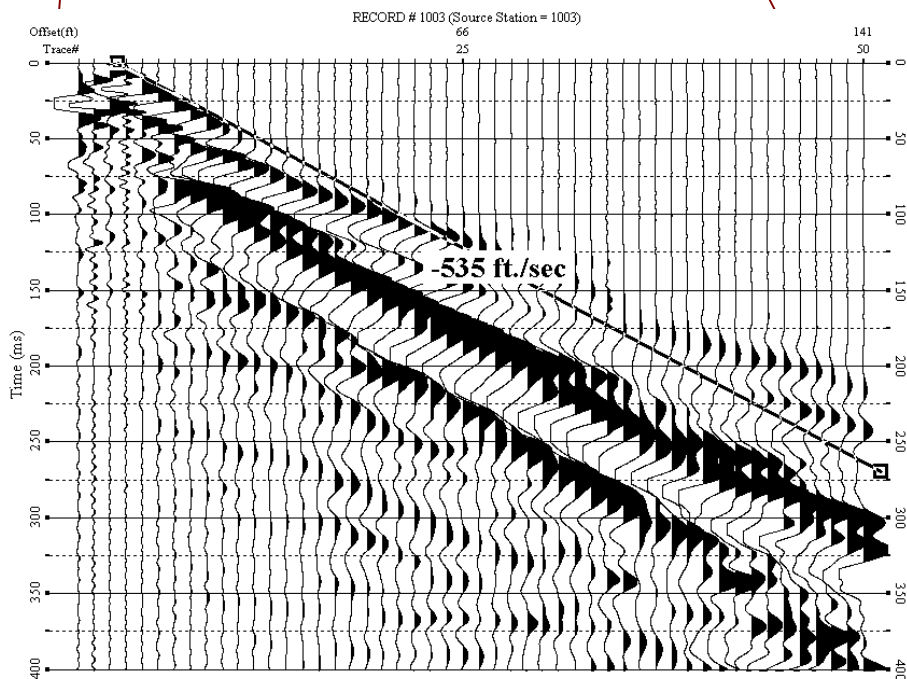
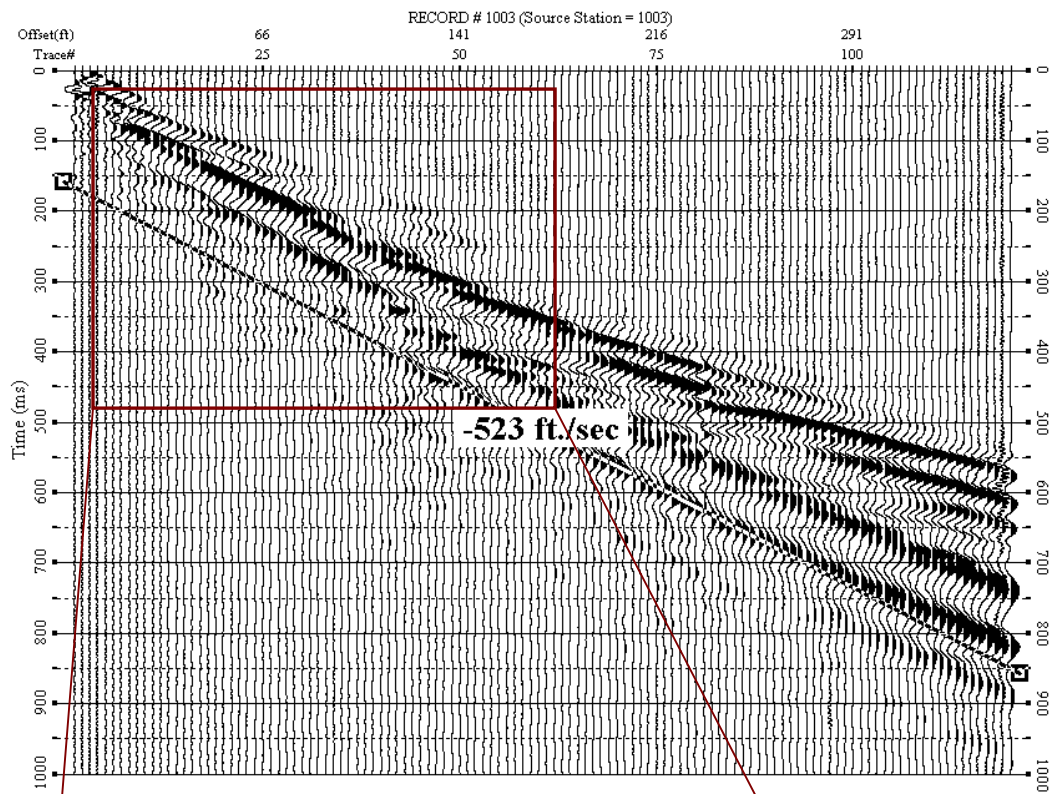


Figure 78. Seismic wavelet and apparent velocity observations on 2-D S-wave data record on top of the crest of the levee.

Love Wave

Unfavorable conditions present within the levee for the generation and detection of direct S-wave first-arrivals on 3-D through-levee data spurred a search for different ways to estimate Vs at the crest of these levees. Dispersion curve analysis of S-wave data produced very interesting results with a wide range of frequencies (6-30 Hz, Figure 79) detected in comparison to the previously analyzed P-wave surface-wave data (6-15 Hz, Figure 80). This wide range of dispersive frequencies observed in the S-wave surface-wave data was even more prominent when processing was limited to only the first 40 traces (Figure 81). With a phase velocity at 30 Hz of about 450 ft/s, the wavelength of the Love wave is equivalent to about 15 ft, providing a penetration depth of roughly 7.5 ft or half the wavelength. This observation demonstrates the potential of using Love waves to obtain shallow (upper 20 ft) Vs information. Unfortunately, algorithms and methods have not been sufficiently developed to allow confident and effective use of the dispersive attributes of Love waves to estimate seismic properties of earth materials.

After careful study of all data types and analysis methods, only the S-wave surface-wave (Love wave) possessed a sufficiently wide range of frequencies and sampling interval to provide Vs information from within the levees at a resolution that could potentially be used for long-term levee reconnaissance and differential characterization. A technique to invert Love waves is under development at several research institutes around the world. Even though it is currently not possible to invert the dispersive properties of Love waves, the dispersive properties can be used to identify zones within the subsurface that possess anomalous materials properties. A 2-D Love-wave dispersion display was generated from the top of the levee along the crest line (Figure 82). A gradient data set was calculated and filtered to emphasize potential anomalous zones (Figure 83). Clearly the characteristics of this filtered gradient data set are suggestive of real variability within the levee.

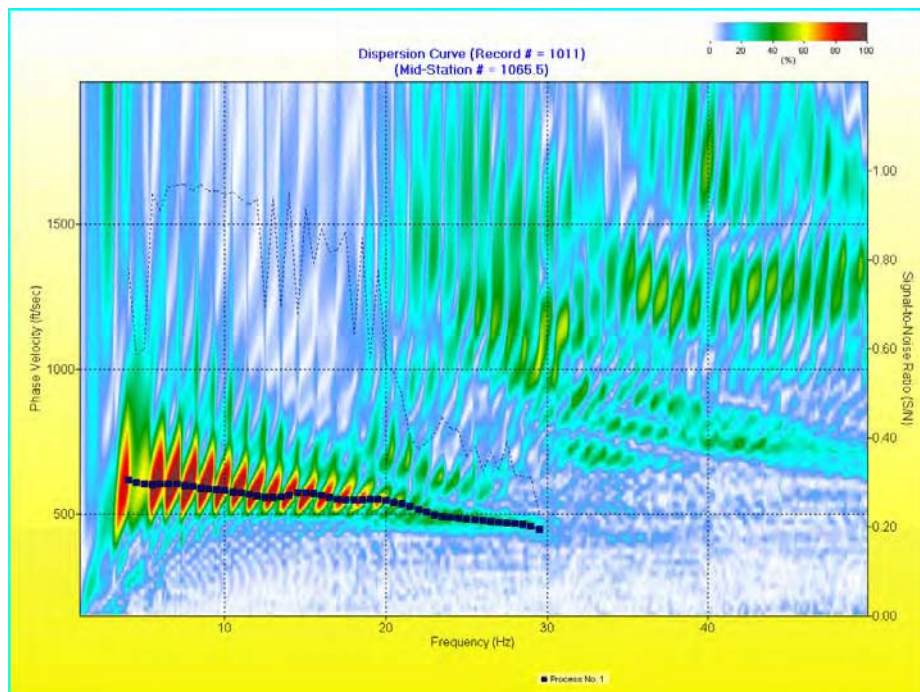


Figure 79. Dispersion-curve analysis of S-wave-data surface wave (Love wave).

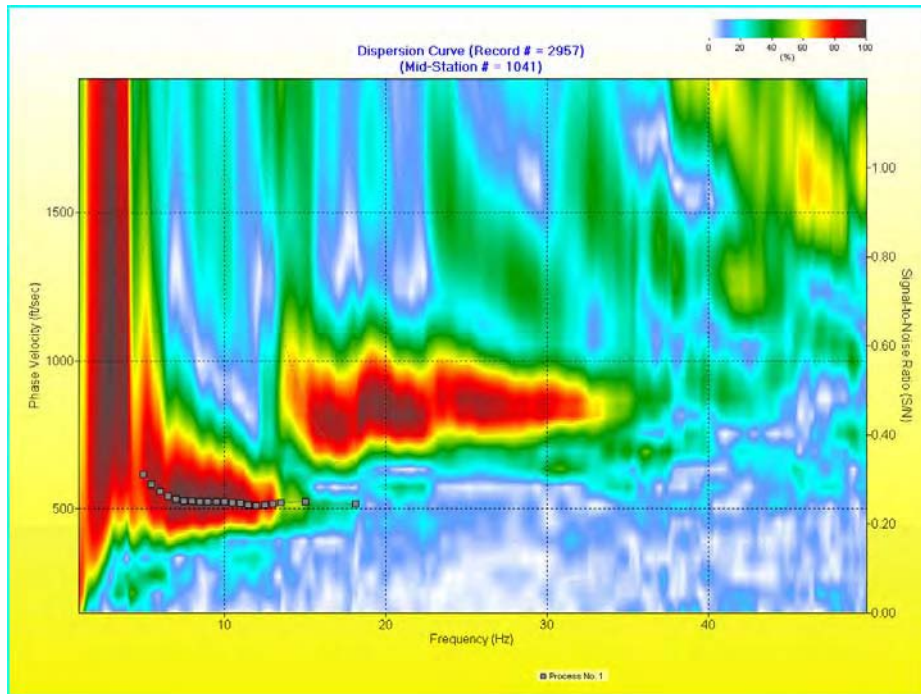


Figure 80. Dispersion-curve analysis of P-wave-data surface wave (Rayleigh wave).

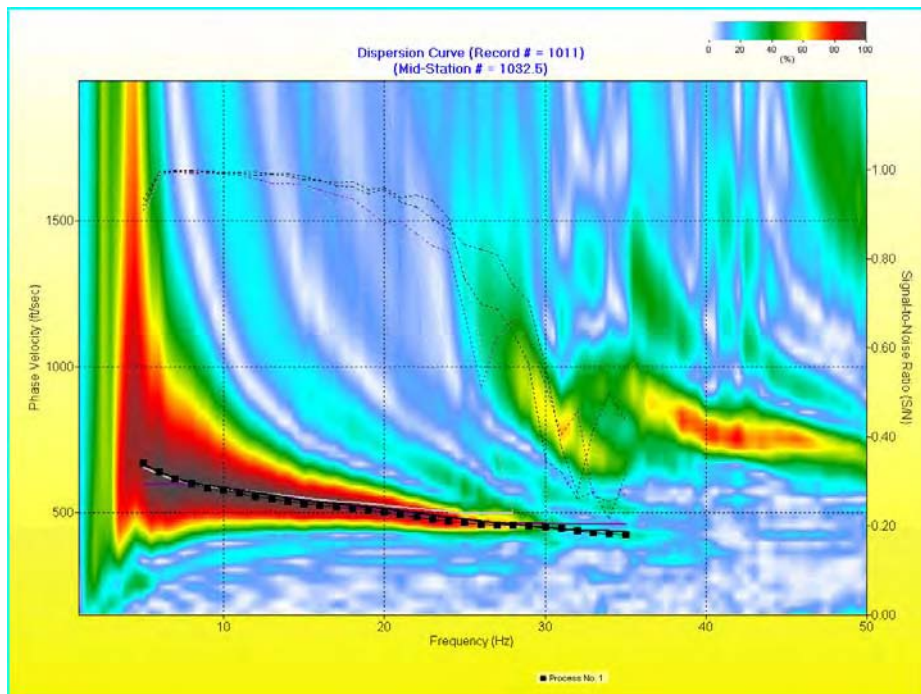


Figure 81. Dispersion curve analysis of first 40 traces of S-wave-data surface wave (Love wave).

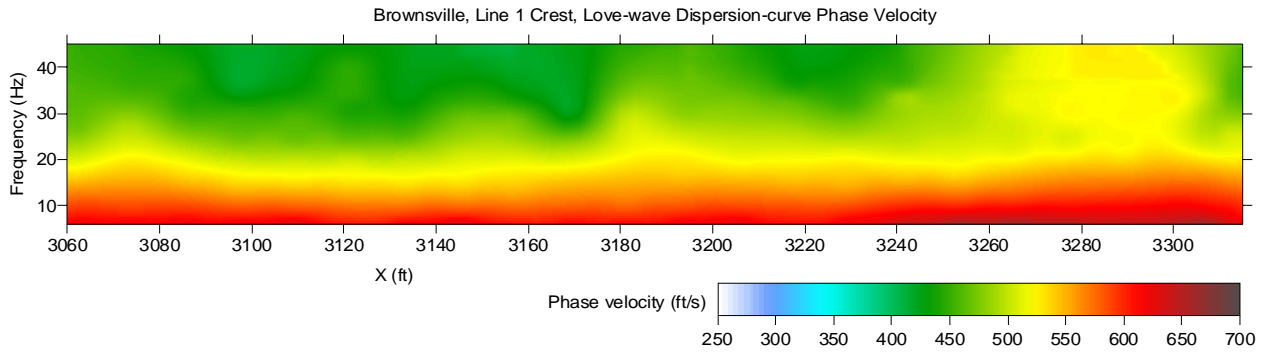


Figure 82. Love-wave dispersion-curve phase-velocity map estimated for line 1 by analyzing S-wave data.

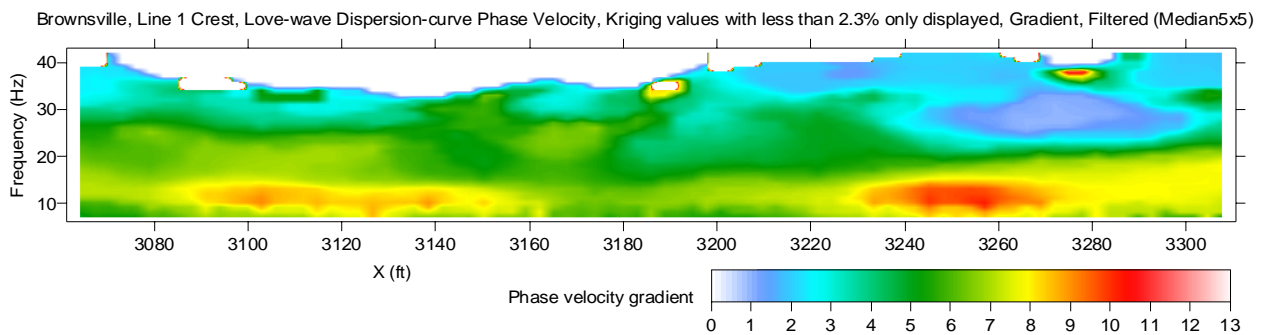


Figure 83. Love-wave dispersion-curve phase-velocity gradient map estimated for line 1 by analyzing S-wave data.

Site 2

Estimates of cross sectional V_s were obtained for both crest and toe using tomography and surface-wave inversion techniques. V_p information was extracted from P-wave data using first-arrival analysis (tomography) of seismic data collected along both toe and crest lines. Frequency-dwell data were analyzed for amplitude variations as a function of frequency, specifically looking for changes in phase that could be related to changes in material seismic velocity. A 120-channel through-levee travel-time study was undertaken for both P- and S-wave energy. This survey was much smaller in scope than the similar one undertaken for site 1. Data were acquired to allow the use of 3-D borehole tomography software to analyze first arrivals and generate a travel-time delay volume focused within the core of the levee.

Site 2 is unique with respect to its conductivity, surface fractures, and very shallow water table as evident by the oxbow lake just 100 ft north of the levee (Figure 3). Open fissures along the surface on the levee slopes at site 2 reinforced the suggestion that the core at this site was at least in part constructed of more expansive clay materials than likely present at other sites further north and that those clays were in a contracted state. Prior to the seismic study, a trench percolation test was performed to determine the velocity water would move through the core and therefore empirically appraise the permeability of the core. This site had several features and characteristics consistent with the suggestion that it would have the greatest failure potential in comparison to the other sites studied in this area.

Much of the data and many of the discussions pertinent and covered previously during site 1 reporting are also applicable to site 2. Unique data characteristics and observations that provide insight into the correlations between geology, construction, and geophysics will be discussed and displayed. Tests and data analysis that provided no unique information or did not allow for a meaningful discussion applicable to the purpose of this study were not expanded on in-site observations.

P-wave

First-arrival processing

First-arrival picking was accomplished in a fashion completely consistent with that used for site 1. Similar problems were encountered and remedies were also quite similar, yet unique for the specifics of data from this site. Each shot gather was run through an algorithm designed to automatically pick the first-arriving impulse of source-generated seismic energy. Once these initial picks were made, each one was manually inspected to ensure consistency and accuracy.

First-arrival time-offset pairs were used to construct a 2-D refraction-tomography V_p solution for the cross section of the levee beneath the crest P-wave profile (Figure 84). This velocity cross section represents a vertical slice along the levee with colors indicative of different velocities. These velocities in many cases can be directly related to material properties. Horizontal uniformity of the velocity field is, in general, indicative of a relatively layered geology with no significant change in material type. With compaction will generally come higher velocities, therefore a gradationally increase in velocity with depth is a natural byproduct of vertical material accumulation via natural deposition or anthropologic construction activities.

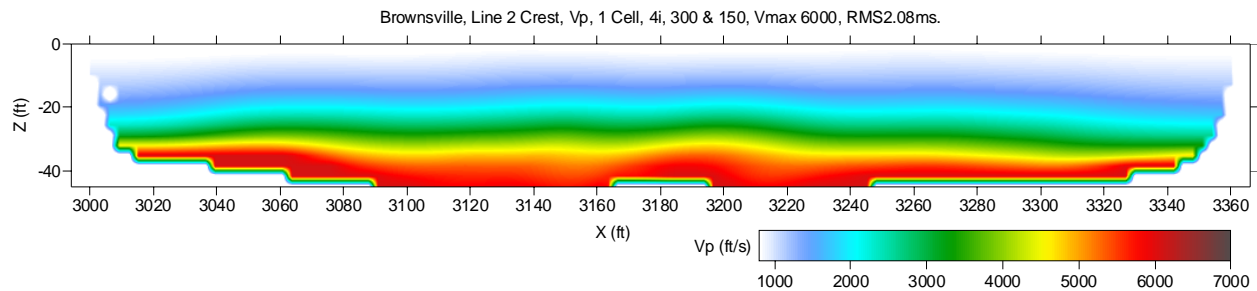


Figure 84. P-wave velocity model estimated for line 2 by analyzing P-wave-data first-arrival times using refraction-tomography software.

Vibrator dwell analysis at the crest

Dwell or mono-frequency vibrator sweeps were recorded at the center and each end of the levee along the crest P-wave profile at site 2. At each shot location a separate seismic sweep was recorded for each of the following frequencies: 12, 15, 20, 25, 30, 50, 75, and 100 Hz. Each mono-frequency sweep was analyzed to determine if there was any dependence of apparent phase velocity of the seismic-wave packet (predominantly surface waves) across the 350-ft range of consecutive traces that make up this spread. Changes in phase velocity could be indicative of changes in material properties. For each constant frequency sweep, the apparent phase velocity was estimated across distances between 10 and 100 ft depending on uniformity of the seismic data using consecutive traces. Each station was assigned a velocity for each frequency (which can be correlated to depth using the half-wavelength criteria) and then all velocity information was plotted as a cross section according to depth and surface station. This 2-D representation of the phase-velocity distribution as a function of both depth and surface location was generated while the source was at the start of line 2 (station 991) (Figure 85). Apparent phase-velocity information was extracted from wiggle-trace plots (Figures 86 and 87, examples for 15 and 25Hz).

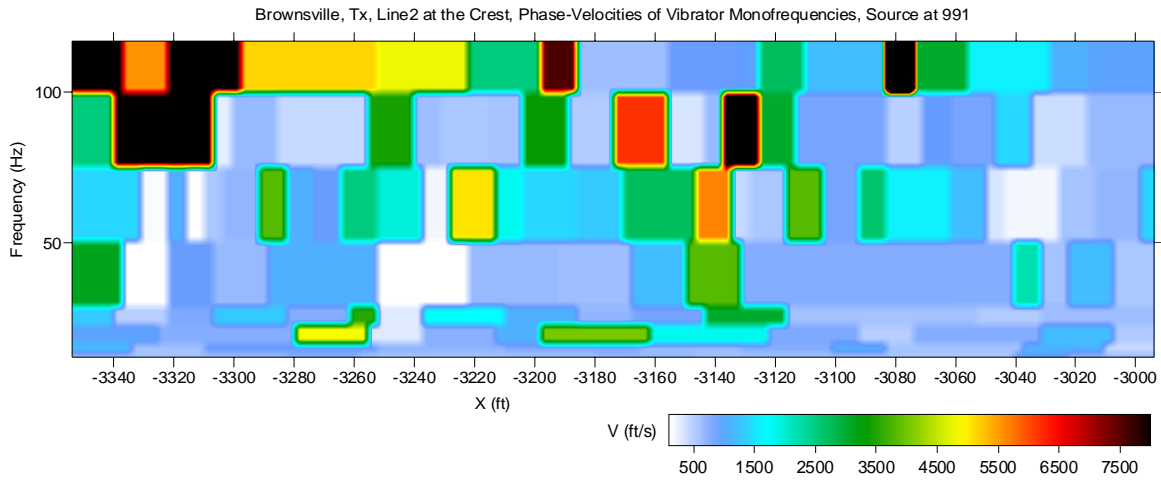


Figure 85. Rayleigh-wave apparent phase-velocity map estimated for line 2 by analyzing P-wave vibrator mono-frequency data.

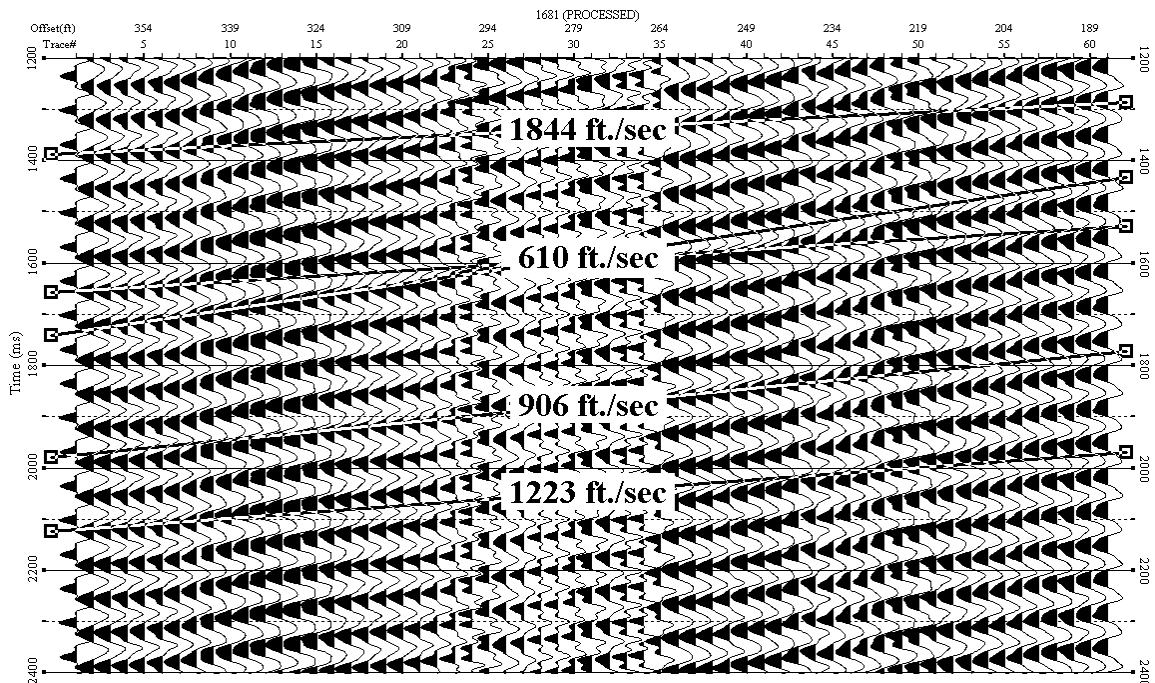


Figure 86. Apparent phase-velocity estimation of surface-wave propagation from 15 Hz mono-frequency vibrator data.

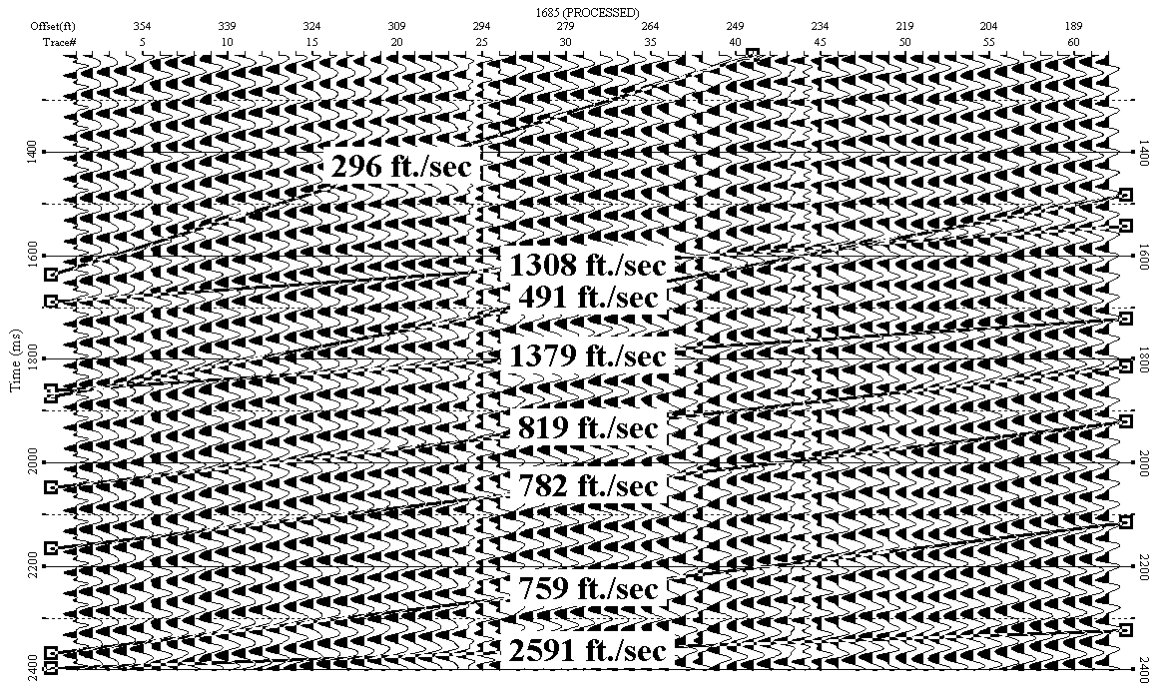


Figure 87. Apparent phase-velocity estimation of surface-wave propagation from 25 Hz mono-frequency vibrator data.

The same analysis was performed at the shot location from the other end of the line (station 1129). The very high frequency components (75 and 100 Hz) were not included with this analysis because penetration depths for these frequencies are only 2-3 ft below ground surface. These two directional opposing (source-to-receiver orientation) 2-D images (of measured phase velocity) did not provide similarities that could be confidently identified as anomalous zones within the levee where the seismic energy propagation characteristics were unique (Figure 88). A closer look at the low-frequency 2-D images did little to enhance the search of site-specific irregularities that might directly relate to material properties (Figure 89).

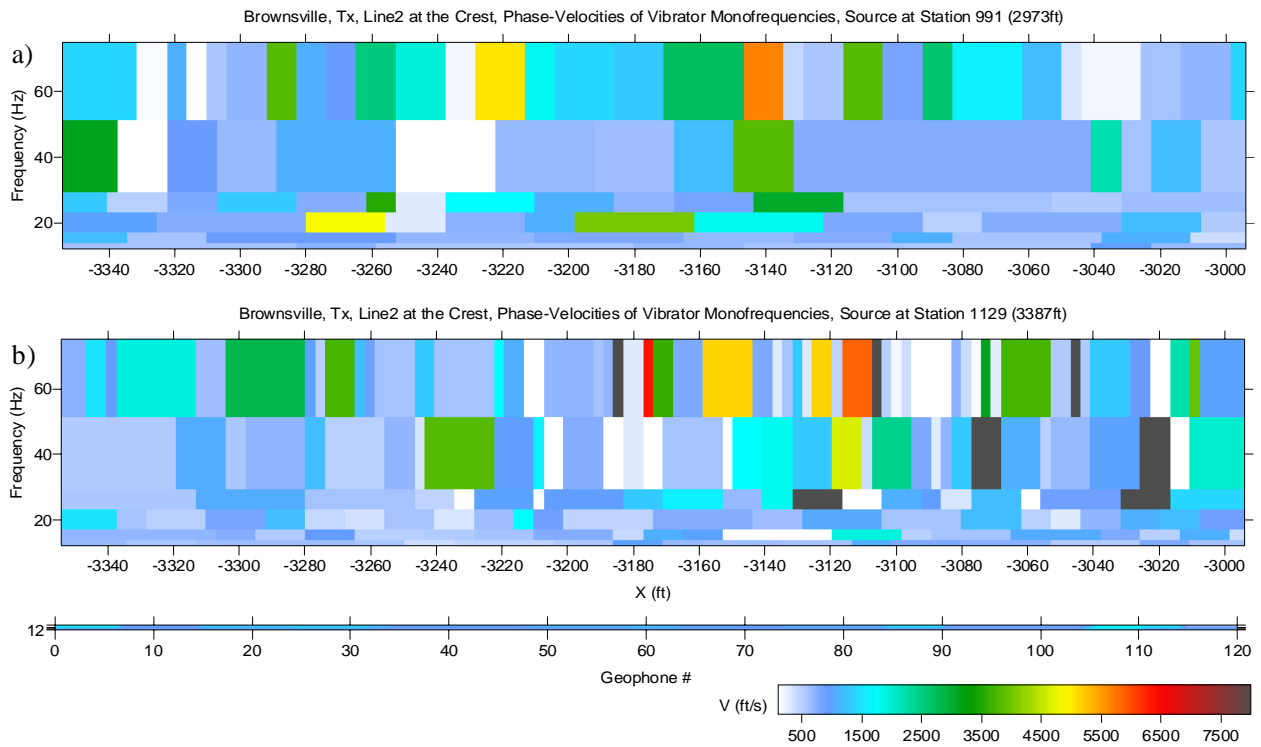


Figure 88. Rayleigh-wave apparent phase-velocity maps estimated for line 2 by analyzing P-wave vibrator monofrequency data, a) vibrator is located at station 991 (X=2973 ft), b) vibrator is located at station 1129 (X=3387 ft).

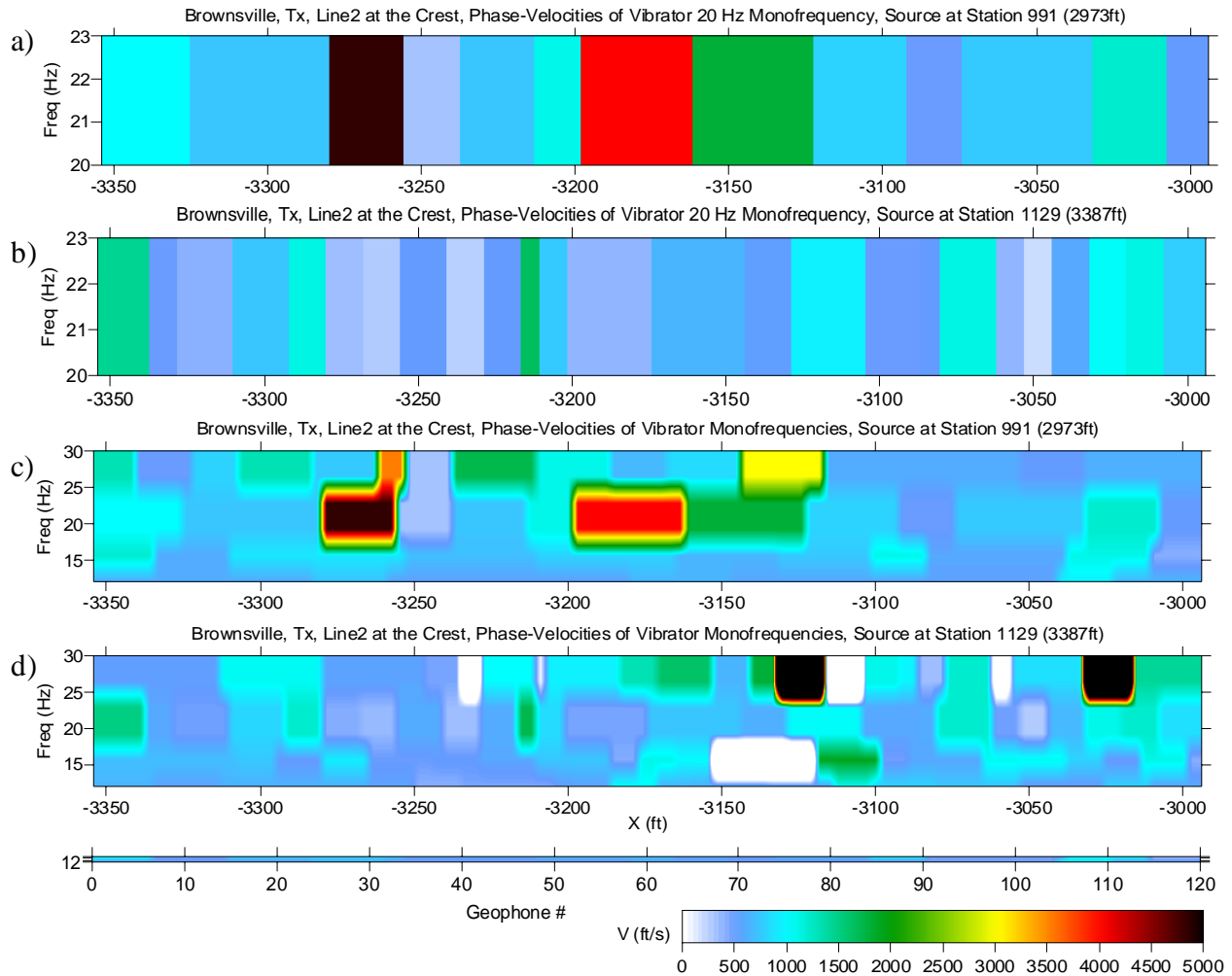


Figure 89. Rayleigh-wave apparent phase-velocity maps estimated for line 2 by analyzing P-wave vibrator monofrequency data, a) and c) vibrator is located at station 991 ($X=2973$ ft), b) and d) vibrator is located at station 1129 ($X=3387$ ft).

Of particular interest, both in the field at the time of acquisition and later in the laboratory during data analysis, the 20 Hz mono-sweep generated when the source was at station 991 had an apparent phase-velocity change at the location previous trenched, used for the percolation test, and then later back-filled with native soils. This correlation between seismic observations and physical site activities justified a much closer look at these data and the product of their analysis (Figure 90). Disturbing the levee by trenching and then back-filling that trench likely caused changes in material compaction and distribution that manifested itself as changes in the apparent phase-velocity. This change is evident when comparing the trace-to-trace phase velocity inside the trench area relative to similar comparisons outside the trench area.

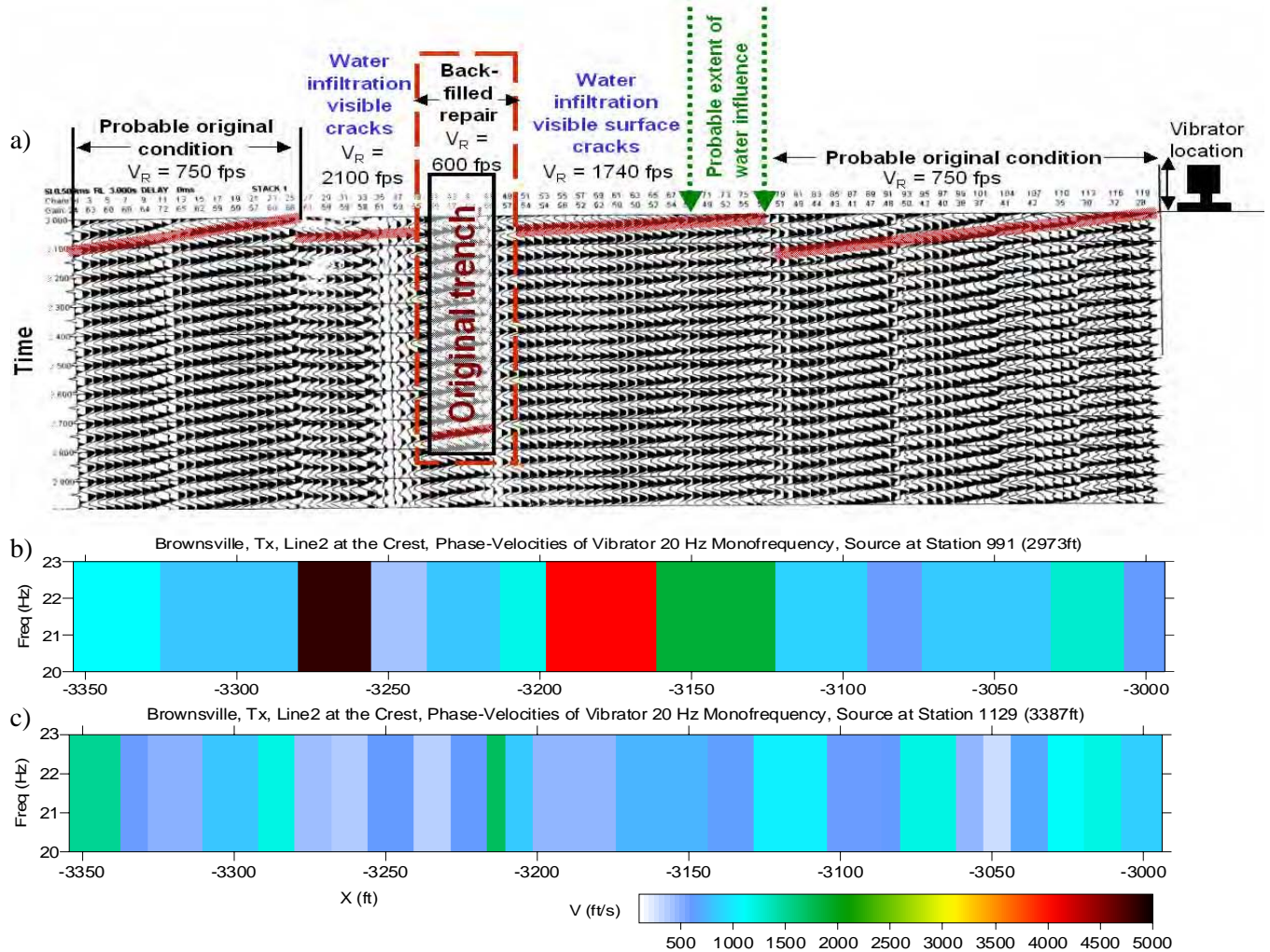


Figure 90. Rayleigh-wave apparent phase-velocity estimates for line 2 by analyzing p-wave vibrator 20 Hz monofrequency data, a) seismic data from vibrator located at station 991 ($X=2973$ ft), b) 2-D phase-velocity map when vibrator is located at station 991 ($X=2973$ ft), c) 2-D phase-velocity map when vibrator is located at station 1129 ($X=3387$ ft).

Generalizing to the point where this type of anomaly can be categorized as diagnostic of this type of ground disturbance is not feasible because when the source station was moved to the opposite end of the spread (station 1129) this same feature was not observed coincident with the trench. Similar analysis was undertaken for the 25-Hz sweeps when the source was at stations 991 and 1129. Data sets from both shot stations showed unique changes in phase velocity across the spread, but neither produced a pattern that could be clearly distinguished and categorized as diagnostic of a particular change in levee materials or condition (Figures 91 and 92).

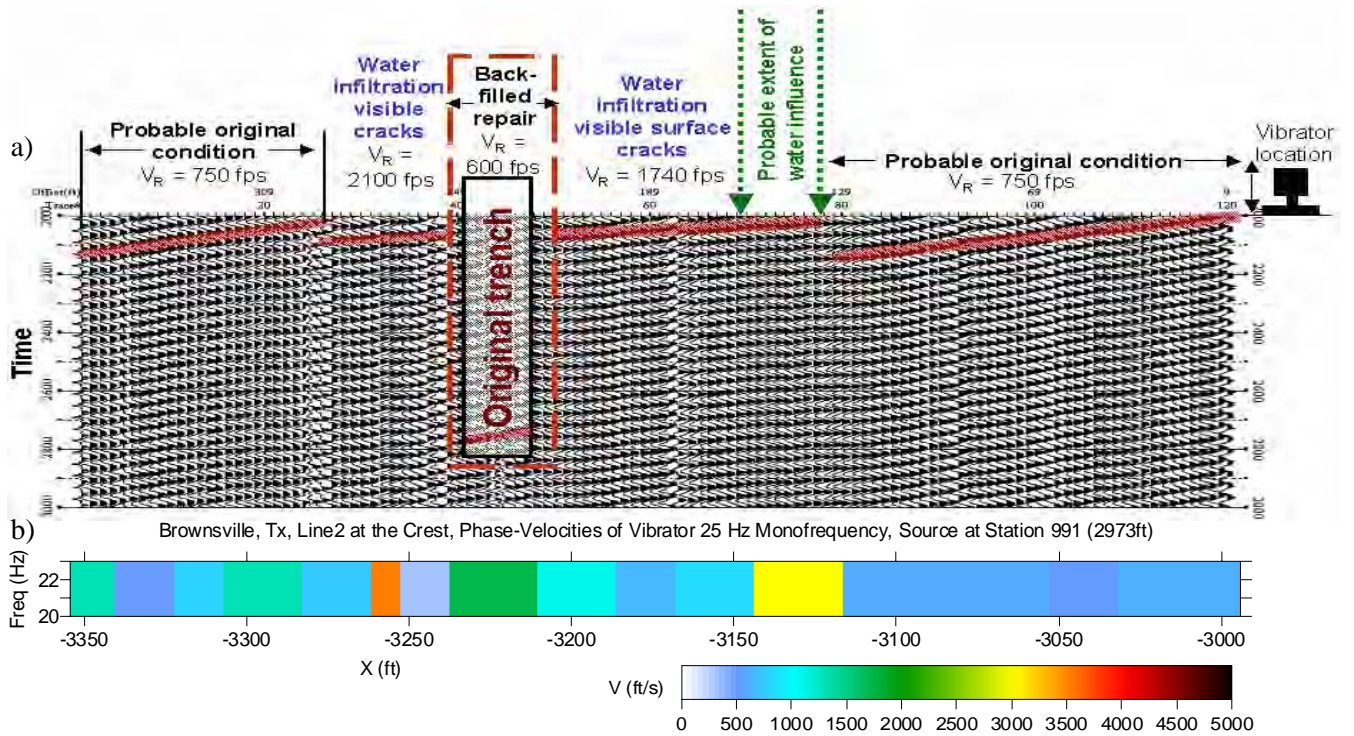


Figure 91. Rayleigh-wave apparent phase-velocity estimates for line 2 by analyzing P-wave vibrator 25 Hz monofrequency data, a) seismic data from vibrator located at station 991 ($X=2973$ ft), b) 2-D phase-velocity map of the same data.

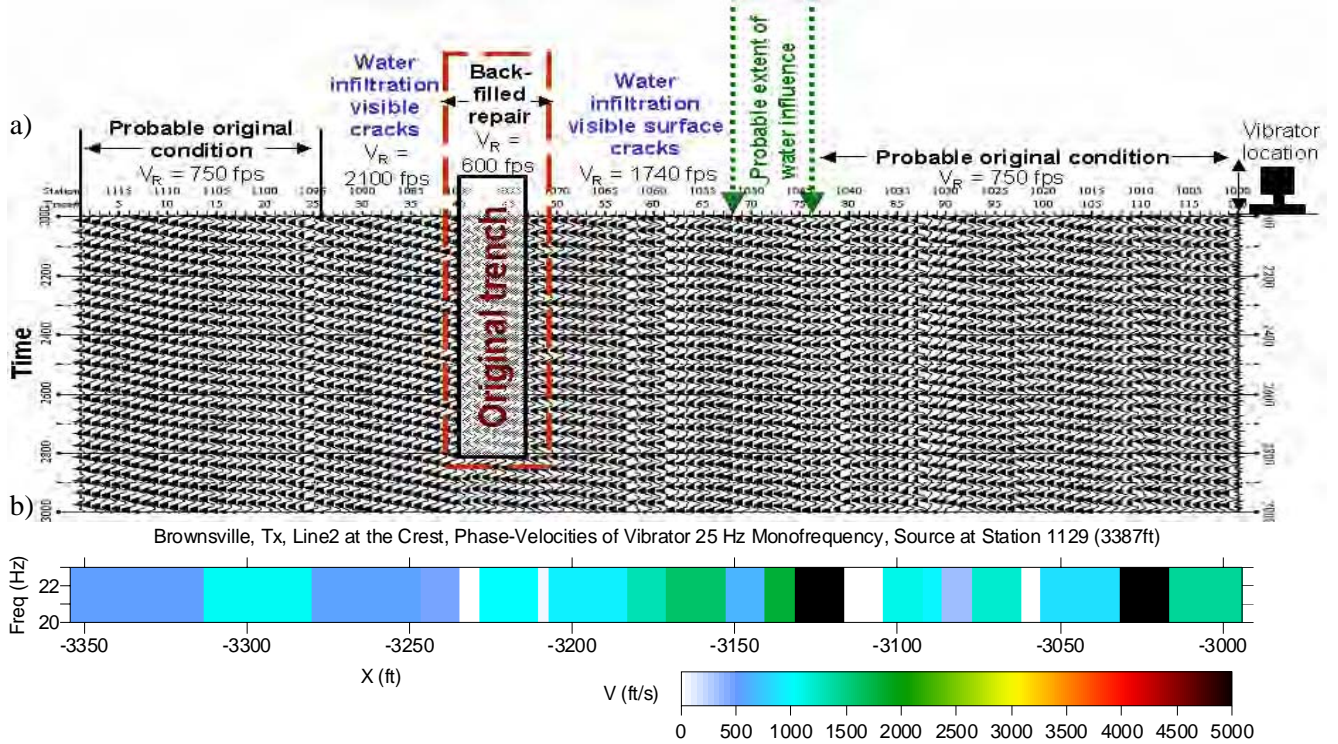


Figure 92. Rayleigh-wave apparent phase-velocity estimates for line 2 by analyzing P-wave vibrator 25 Hz monofrequency data, a) seismic data from vibrator located at station 1129 ($X=3387$ ft), b) 2-D phase-velocity map of the same data.

S-wave

First-arrival processing

Shear-wave first arrivals were automatically picked on shot gathers in the same fashion described for site 1. Each automatic first-arrival pick went through a manual inspection process to ensure the program had made “best” possible selection. First-arrival interference with noise of any kind can result in cycle skipping or pre-emergent selections. Most automatic first-arrival missed picks can easily be seen as well as the reason for the miscue identified. This allows a more confident manual pick to be substituted for the automatic selection. Shear waves are particularly difficult to analyze due to mode conversions, proximity to the surface wave (velocity of surface wave $\sim 0.9V_s$), compressional dispersive guided waves, and narrow band nature of wavelet.

First-arrivals selected for S-wave shot gathers, acquired along the crest of the levee at site 2 were fed into a 2-D refraction-tomography algorithm with a standard initial model for this area. A well-constrained V_s solution (Figure 93) with good convergence was produced, having what is considered a reasonable V_p/V_s for unconsolidated, unsaturated sediments. The presence of the oxbow lake north of site 2 leads to the suggestion that this meander cut off feature likely extends in the subsurface beneath the levee. Therefore, it is not unexpected to see what appear to be undulations in the velocity field consistent with the cut and fill of an ancient meander path of the river.

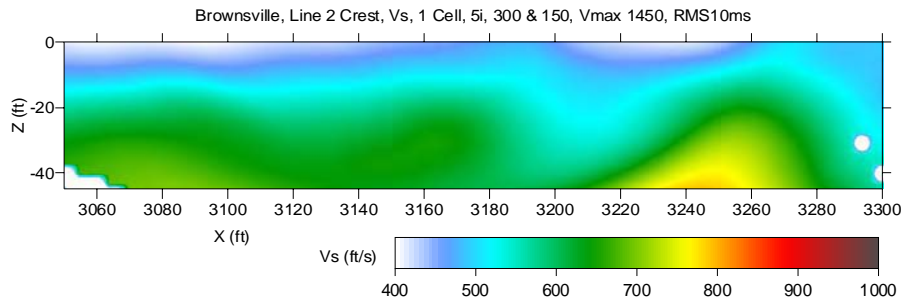


Figure 93. S-wave velocity model estimated for line 2 at the crest of the levee by analyzing S-wave-data first-arrival times using refraction-tomography software.

Shear-wave velocities within the depth range of the levee are between 400 ft/sec and 550 ft/sec. Considering the compressional-wave velocity in this same depth interval is 1000 ft/sec to 2000 ft/sec, the V_p/V_s is around 2.5 to 3 for the levee. This is a reasonable range for a compacted clay fill. The shallowest part of the levee (<10 ft) did not produce high confidence V_p or V_s values, making estimations of velocity ratios for those depths beyond these data.

Rayleigh Wave

Crest

Key to the extraction of shear-wave velocity information from surface waves is the presence of broadband fundamental-mode energy. Regardless of the source, receivers, or location, high-frequency fundamental-mode surface waves were just not recorded on these levees. It is our working hypothesis that the higher-frequency components of the surface wave were never produced due to near-surface (<2 ft) site conditions. An abundance of higher-mode energy was produced, but the current state-of-the-art in surface-wave analysis does not allow for incorporation of that type of energy into the inversion process. As the technology advances higher modes will allow key seismic characteristics of near-surface materials to be defined with reasonable confidence.

Although the fundamental mode of the surface wave lacked high frequencies (and thus did not provide shallow V_s information), the MASW method still provided an accurate overall estimation of the V_s between depths 25 ft and 85 ft at the crest of the levee (Figure 94). Interesting is the apparent

discrepancy between the MASW data (which appears to be representative between 25 ft and 85 ft) and the shear-wave velocity cross section generated using shear-wave tomography (Figure 93). Comparing the MASW Vs cross-section with the shear-wave tomography cross section along the same profile, a velocity discrepancy of about 15% to 20% is evident. Also notable is the exaggerated structure on the surface of bedrock interpretable on the Vs tomography cross section relative to the MASW cross section.

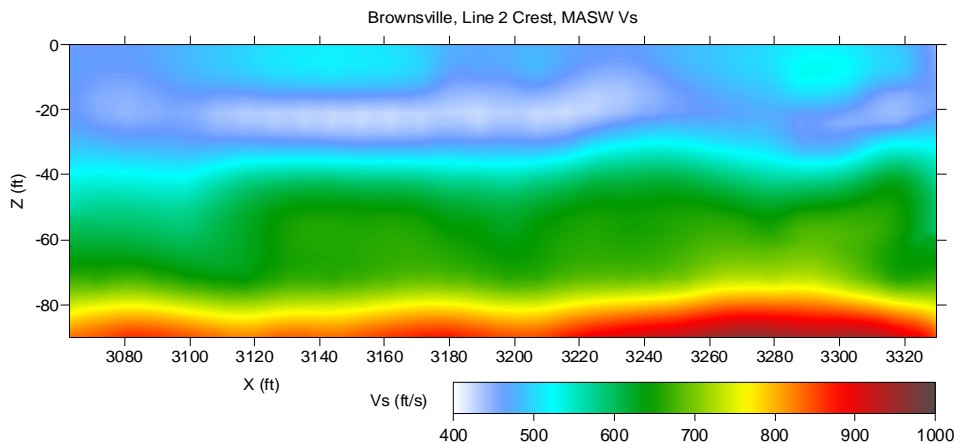


Figure 94. S-wave velocity model estimated for line 2 at the crest of the levee by analyzing P-wave-data surface-wave using MASW method.

Toe

Fundamental mode Rayleigh surface-wave energy possessed a sufficient broad range of frequency characteristics at the toe to avoid the high-frequency limitations observed on the crest data. The MASW method provided an accurate overall 2-D estimation of the Vs distribution at the toe of the levee (Figure 95a). Velocity and depth values matched reasonably well between MASW at the crest and MASW at the toe for the same absolute elevations (Figure 94). A subtle topographic west dip on the layer around 10 ft below ground surface on the toe data is not evident for the same layer when imaged from the crest.

Crest-Toe Comparison

All things considered the MASW-produced Vs images from the toe and the crest are reasonably similar (Figure 95). There is an up-going trend in the velocity contour from left to right at about -80 ft depth on both sections (for this report the levee crest is at elevation 0 at all sites). Greater detail observed in the toe image is probably due to the surface to boundary depth (that is, the boundary is about 20 ft closer to the surface at the toe in comparison to the crest), so there is less smearing and averaging of earth material by the surface wave along the toe line. A high-velocity lens-like anomaly location at range 3060 to 3120 ft on the toe MASW Vs, can not be interpreted on the crest MASW Vs image. One possibility is that it is a very local lens feature, evident on the higher-resolution data.

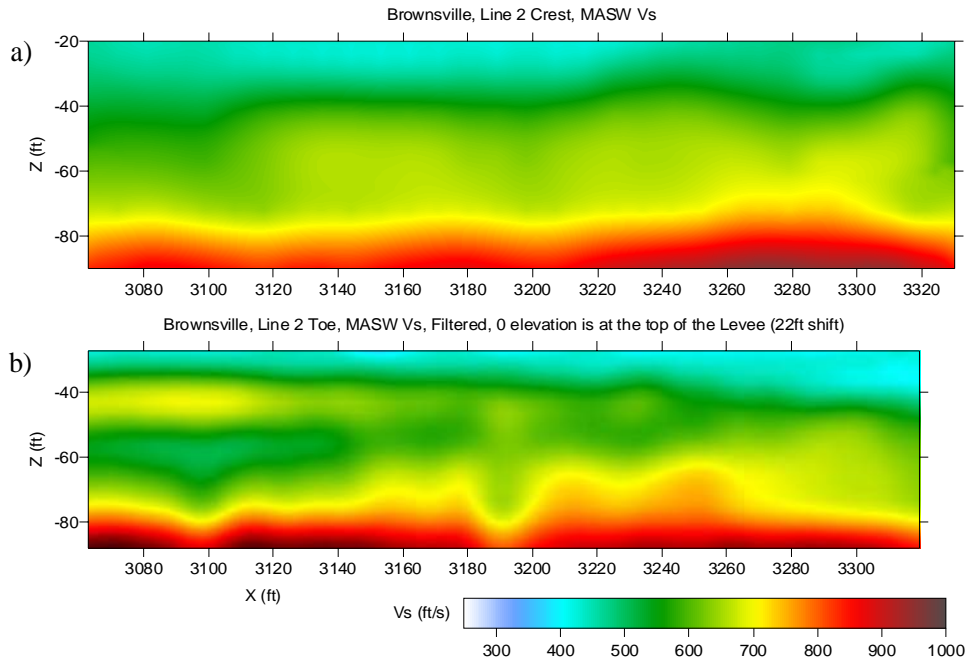


Figure 95. Line 2 S-wave velocity model estimates by analyzing P-wave-data surface-wave using MASW method, a) at the crest of the levee, b) at the toe of the levee.

Tomography

3-D Through-levee P-wave Direct Arrivals

First-arriving energy at site 2 was exclusively the result of refractions traveling in native materials below the basal contact of the levee (Figure 96). Differences in velocity with travel path, when calculated using the assumption of a straight ray path, are way outside what would be considered reasonable for any material fill of this nature. Clearly characteristics of the first arrivals as well as the next several tens of milliseconds of the wavetrain are consistent with that observed at site 1. However, unlike site 1, the direct-arriving energy is subdued by surface wave and guided waves. This interference was prevalent throughout these data.

Polarity reversing of shot gathers in a fashion identical to the process used to enhance direct arrivals on display of site 1 data was used on site 2 data but without the same benefits (Figure 97). A high-frequency arrival with a curvature consistent with that expected from the direct wave can be interpreted on the best through levee shot gathers from this site. However, their extremely low amplitude and lack of wavelet consistency made them impossible to both pick and confidently identify as the direct wave. Considering that when using the direct raypath distance the average velocity would be around 300 m/sec, it appears possible this arrival could be air-coupled wave. Therefore, it was only possible to pick with confidence the direct through-levee arrivals for site 1. On site 2 it was not possible to confidently separate direct-wave energy from secondary arrivals due to interference. One observation that can be made with reasonable confidence is the direct compressional-wave velocity through the levee at site 2 is slower than that observed at site 1.

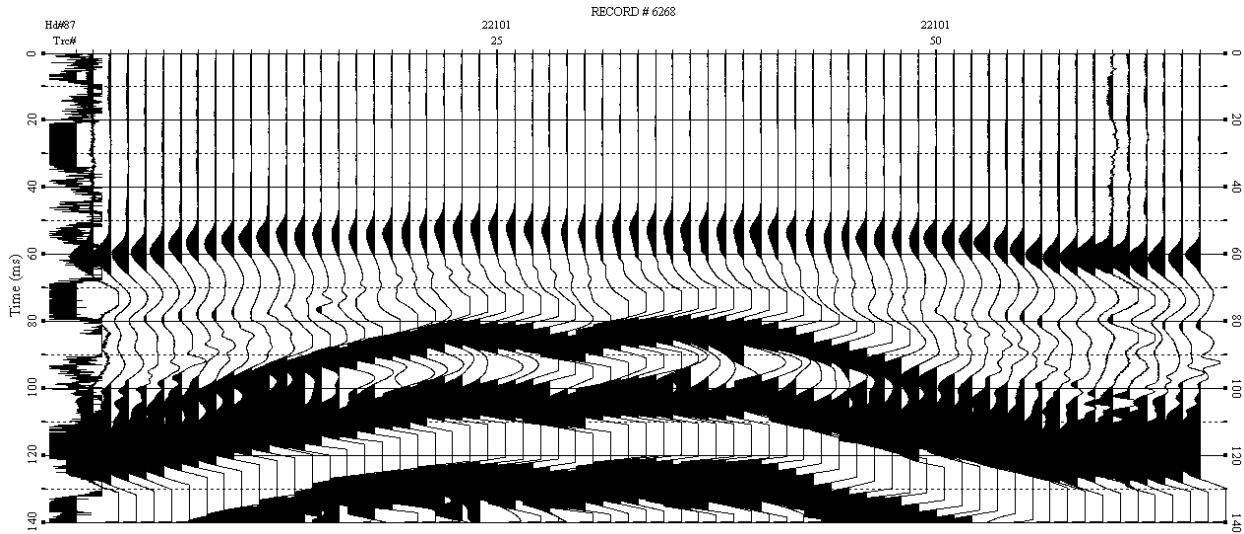


Figure 96. Estimation of first-arrival and secondary-arrival times on 3-D P-wave through-levee seismic data at site 2, shot record 6268.

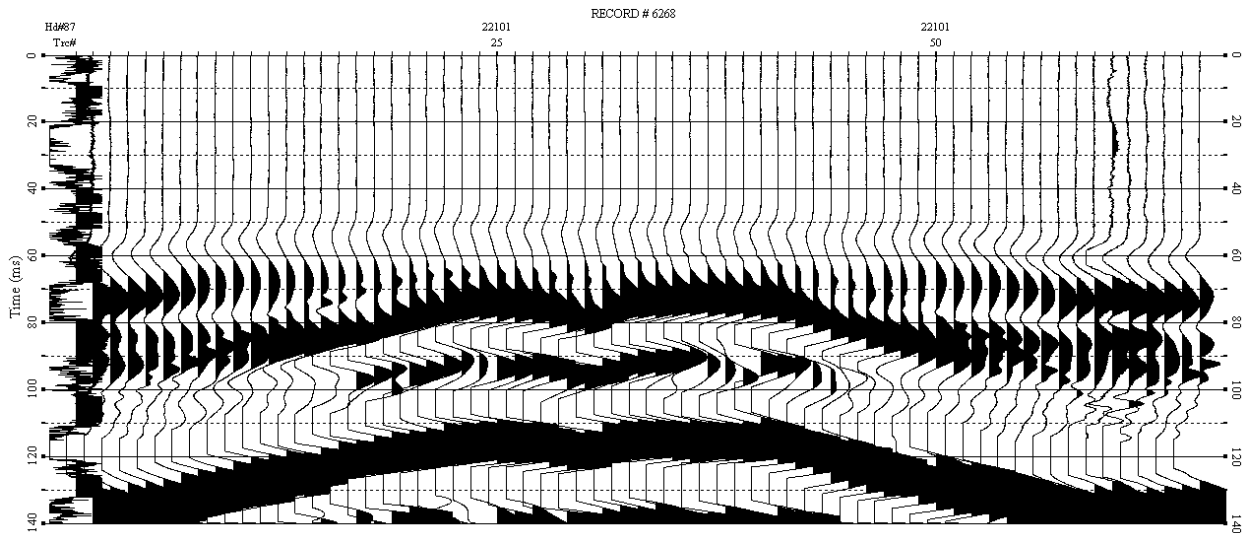


Figure 97. Estimation of first-arrival and secondary-arrival times after reversing polarity of 3-D P-wave through-levee seismic data at site 2, shot record 6268.

3-D Through-levee S-wave Direct Arrivals

Similar to site 1, it was not possible to identify S-wave direct through-levee arrivals on the S-wave data collected in the 3-D configuration. Many of the same anomalous arrival patterns were observed at this site consistent with site 1. Clearly, the orientation of source and receivers combined with the geometry of the levee adversely affected the recording of direct, polarized shear energy. With the exception of first arrivals on traces directly adjacent to the source relative to the levee axis, first-arriving energy was likely mode-converted compressional or S_v waves. This is based on the 3-D aspect of the receiver grid relative to the polarized source at wide angles, making receivers at greater offsets most sensitive to S_v and compressional-wave energy produced by the source.

Recorded wavelets within the first few cycles had relatively low dominant frequencies (15-20 Hz) and very limited bandwidth. These characteristics are consistent with surface-wave energy recorded on

2-D S-wave data at this same location. As with site 1, the inconsistency in first-arrival patterns is suggestive of a propagation path not directly through the levee but either around the surface (such as a surface wave) or the result of multiple mode conversions and/or reflections/refractions from within the levee itself.

Love Wave

Clearly the wave type with the apparent greatest potential for successfully and accurately measuring the shear-wave velocity field was the Love wave. The presence of a wide range of frequencies in the S surface wave (Love wave) is very suggestive of the potential depths of investigation possible with the Love wave. As with site 1, Love waves seem to have a great deal of potential interrogating the levee itself from the crest. This is true, of course, only if the same rules of thumb can be used with Love waves that appear to be applicable to Rayleigh waves. Critical to actualizing this potential is the development of a reliable, accurate, and meaningful technique for inverting Love waves to obtain a Vs model. For that reason only dispersion-curve analysis was performed on the Love-wave data in hopes of identifying areas that could represent anomalous zones within the levee. From 2-D Love-wave dispersion curves from the top of the levee (Figure 98) a gradient map was calculated and filtered to emphasize potential anomalous zones (Figure 99).

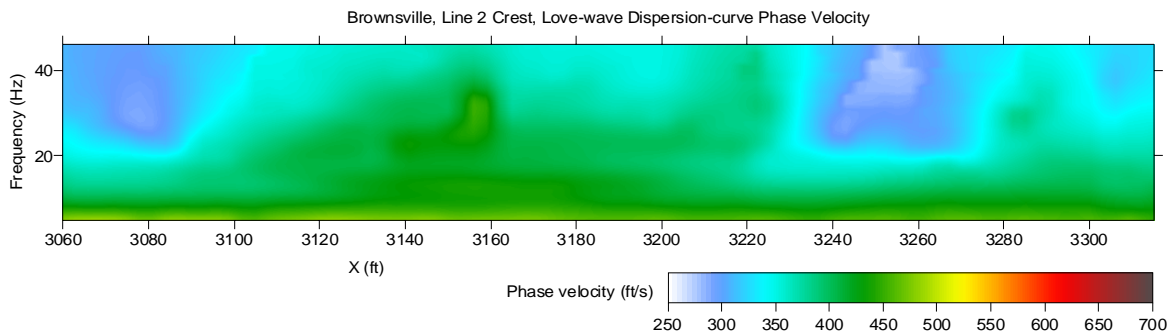


Figure 98. Love-wave dispersion-curve phase-velocity map estimated for line 2 by analyzing S-wave data.

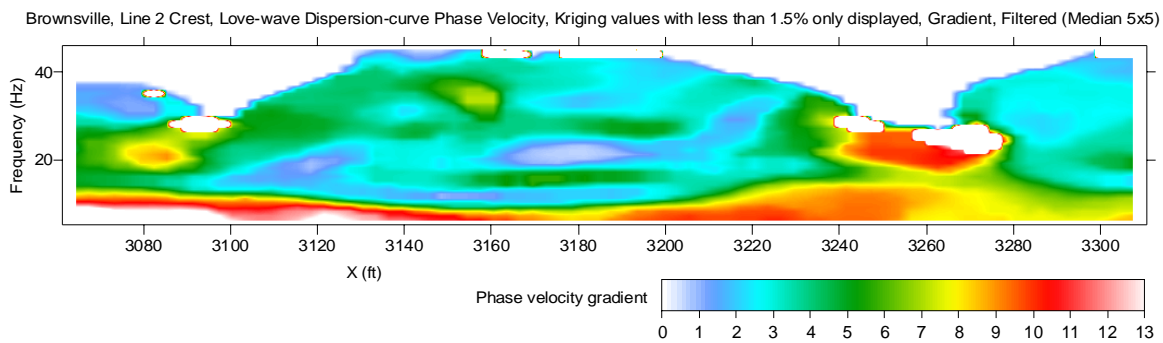


Figure 99. Love-wave dispersion-curve phase-velocity gradient map estimated for line 2 by analyzing S-wave data.

Sites 3, 4, and 5 were studied to provide background information important for establishing the seismic characteristics of different levee materials as determined from conductivity measurements and drilling.

Site 3

P-wave First Arrivals

Compressional-wave data along the crest and toe were collected at site 3 in a fashion consistent with sites 1 and 2. Maintaining a consistent acquisition and processing format allowed direct comparisons of the different levee sites and location at each levee site (toe and crest) without introducing error associated with equalization techniques. Signal-to-noise ratio on compressional-wave first arrivals was high enough to characterize most of the arrivals as instantaneous. Model convergence and a good 2-D refraction-tomography V_p solution was easily accomplished in part due to the high quality of the first arrivals on P-wave data shot gathers along the crest (Figure 100a) and toe (Figure 100b) of the levee.

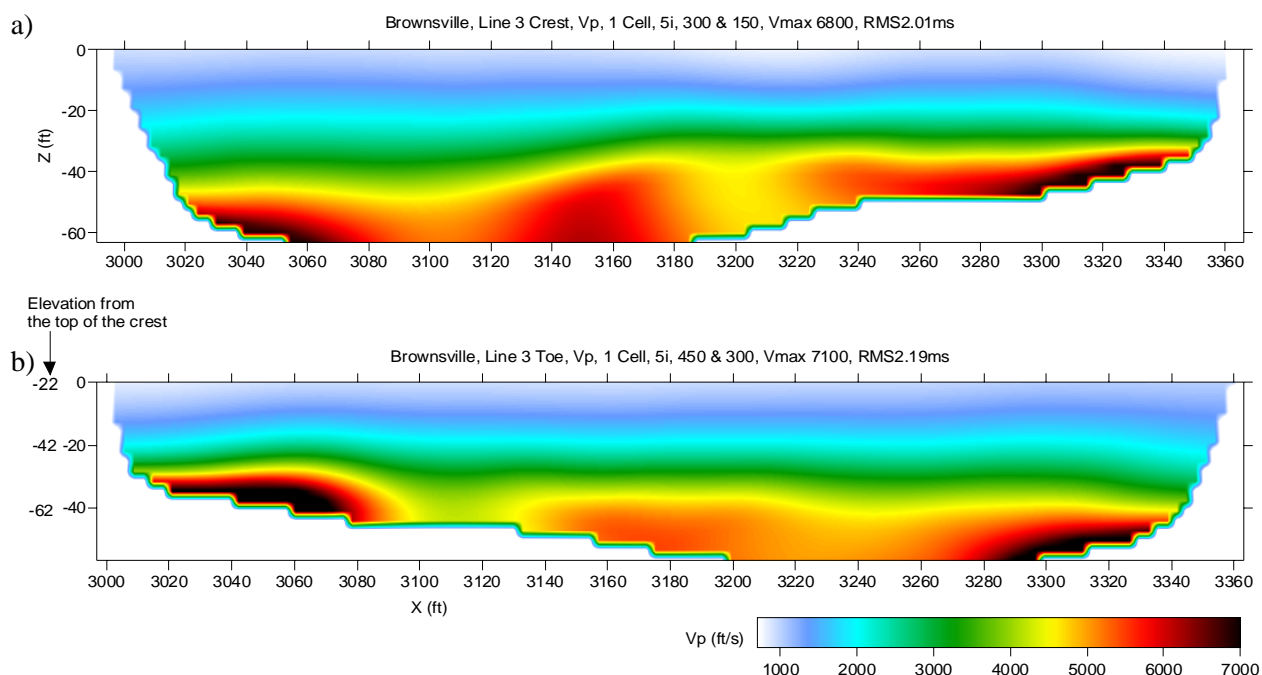


Figure 100. Line 3 P-wave velocity model estimates by analyzing P-wave-data first-arrival times using refraction-tomography software, a) at the crest of the levee, b) at the toe of the levee.

Crest-Toe Comparison

Ideally the compressional-wave data from toe and crest would result in near-identical velocity estimates from the native ground surface and deeper. However, several factors must be considered when making comparisons and contracting these data. First, the coupling and transmission characteristics of the levee will be significantly different than the toe. Second, with any inversion type processing, *a priori* information and non-uniqueness play a role in the final product. Finally, the velocity structure within the levee has the potential to alter the raypaths in the native materials, such that the toe and crest data sets actually have a less than expected overlap in sampled subsurface materials.

Similarity between the two data sets, which in principle sample the same materials, will be limited by differences in the near-surface properties. Simple differencing of these data sets will not provide beneficial results or gratifying conclusions. Changes in the material and therefore the raypaths between these two data sets most profoundly affect refraction tomography inversion, which is strongly nonunique, meaning that there is a wide range of equally possible solutions. Therefore, a unique solution

is not possible without abundant *a priori* information. This leaves two primary factors controlling the similarity between toe and crest data sets below the native ground surface—one is near-surface characteristics and the other is inversion non-uniqueness (Figure 100).

S-wave First Arrivals

Shear-wave data for line 3 possessed good quality first-arriving wavelets. At longer offsets the first arrivals are well pronounced, but their lack of unique character relative to the surface wave and merging with the guided wave raises some suspicion as to their likely propagation path and first-order mode. However, for purposes of our processing, the first arrivals were selected using the guide that direct and refracted body waves should be the first source-generated energy at the receiver. After first-arrivals were automatically selected and manually verified for all S-wave shot gathers collected along the crest of the levee, the arrival times and geometry information were fed into a 2-D refraction-tomography algorithm, which converged to a reasonable V_s solution (Figure 101).

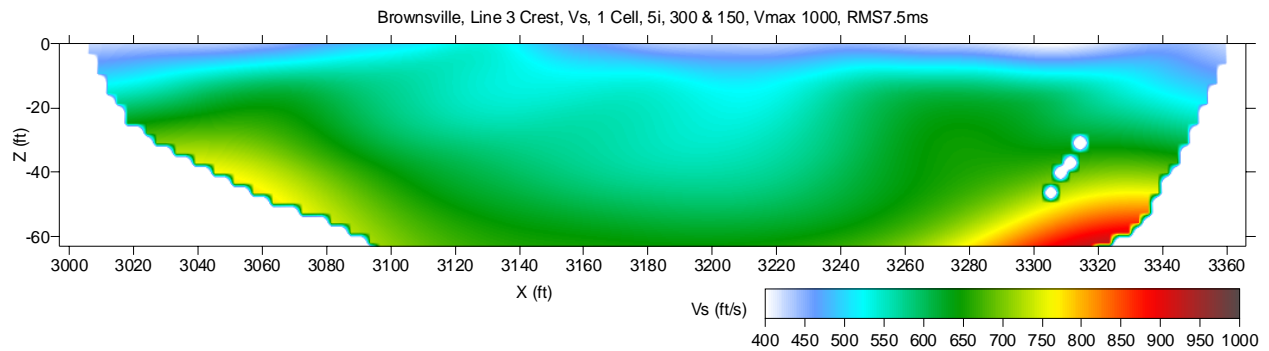


Figure 101. S-wave velocity model estimated for line 3 at the crest of the levee by analyzing S-wave-data first-arrival times using refraction-tomography software.

P-wave and S-wave V solutions

As a quality control measure, the velocity solutions from tomography analysis for both types of body waves were visually compared to appraise similarity of gross features. Differences are relatively pronounced and suggestive of changes in material properties that uniquely affect the two body-wave velocity values. In this unconsolidated environment the compressional-wave velocity of a sand, for example, will change more significantly as saturation changes than will the shear-wave velocity. Therefore, a saturated sand lens within a clay could easily possess a transition in compressional-wave velocity from low to high and shear-wave velocity from high to low. With these kinds of inverse relationships, it is not unexpected for gradients of the same material to be significantly different for the two wave types.

Rayleigh Wave

Crest

At this levee site, as with sites 1 and 2, surface-wave data recorded from the top of the levee lacked the higher-frequency components necessary for interrogating the body of the levee. Clearly our inability to generate and/or propagate high-frequency surface wave is not isolated to a particular site and therefore the limitation must be based in either the source, near-surface material, levee geometry, or some combination of the three. Although the fundamental mode of the surface wave lacked high frequencies (and thus no shallow V_s information), the MASW method still provided an accurate overall estimation of the V_s , between depths 25 ft and 80 ft at the crest of the levee (Figure 102).

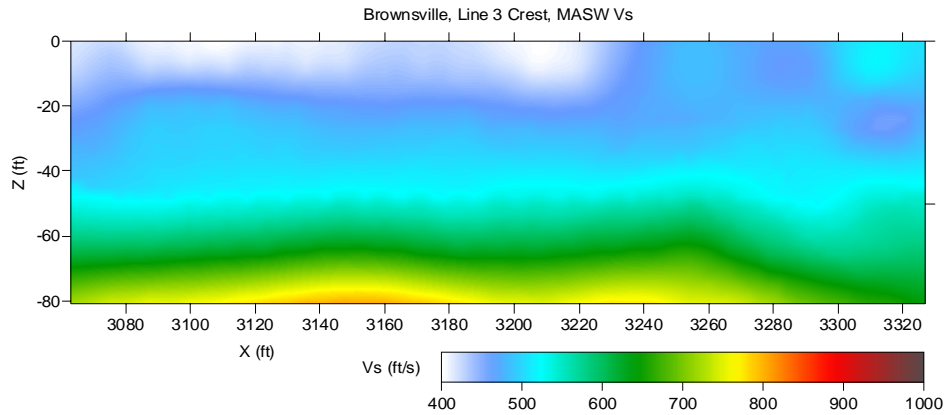


Figure 102. S-wave velocity model estimated for line 3 at the crest of the levee by analyzing P-wave-data surface-wave using the MASW method.

Crest-Toe Comparison

As a quality-control measure, comparison of the crest and toe data for each method were used to determine similarity. For MASW-determined Vs images at the toe and crest, the velocity ranges and general topography of velocity interfaces identified by rapid color change are very similar (Figure 103b, c). Compaction or removal of the shallow soil layer during construction likely changed the upper several feet beneath the present levee. Compounding that is the gravitational compaction that has taken place since placement of the levee materials. It is not surprising and is expected that the upper few feet at the toe is of slower velocity than its horizontal equivalent beneath the levee. With that understanding, comparisons demonstrate the consistency in the method and precision of the measurement process.

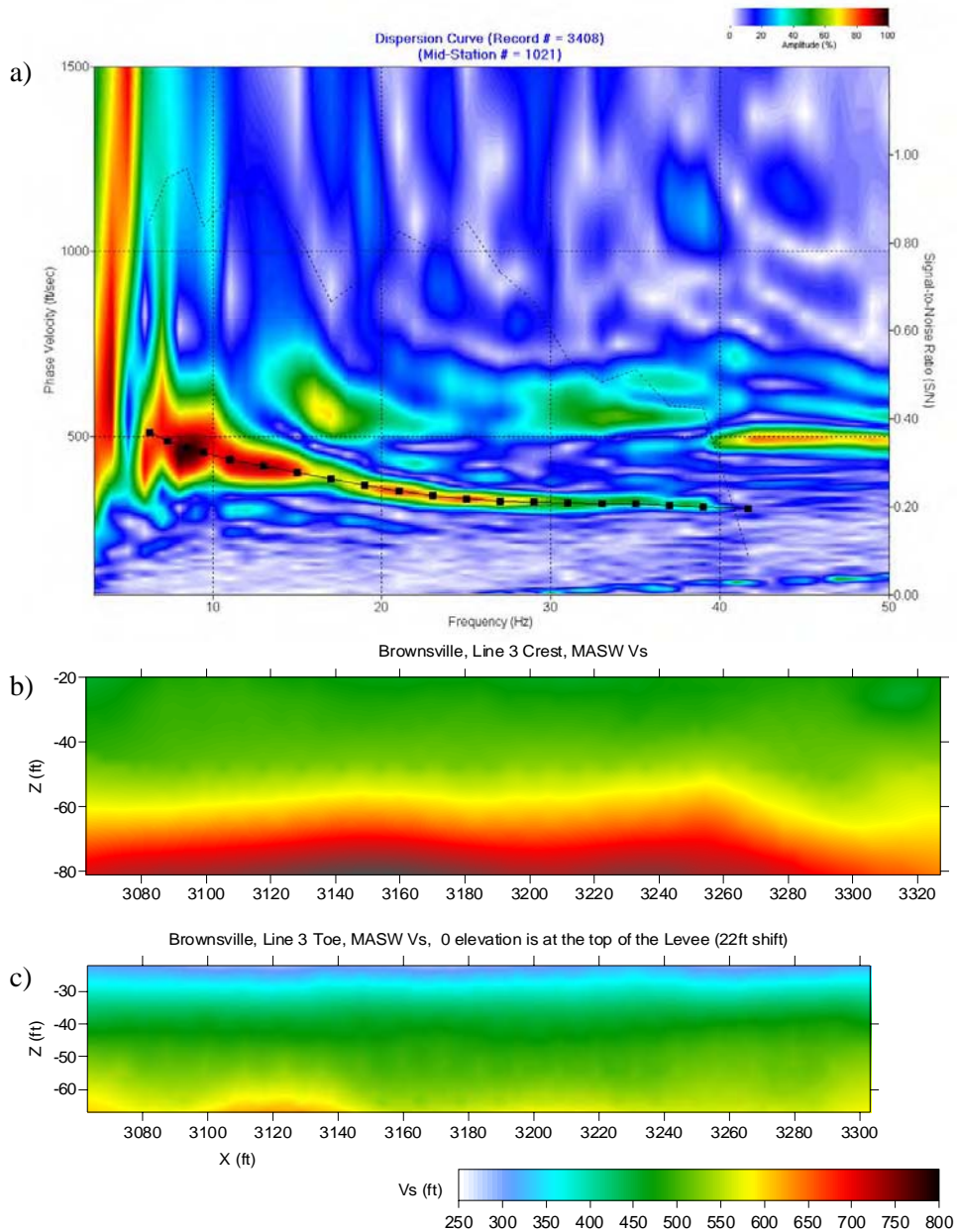


Figure 103. Line 3 S-wave velocity model estimates by analyzing P-wave-data surface-wave using the MASW method, a) Dispersion-curve analysis using the first 40 traces from shot record #3408, b) 2-D S-wave velocity model at the crest of the levee, c) 2-D S-wave velocity model at the toe of the levee.

Love Wave

A consistent theme at all sites seems to be the presence of a relatively wide range of frequencies within the surface-wave packet on S-wave data (Love wave). Assuming the same axiom that relates frequency to depth of penetration for Rayleigh waves is true for Love waves, then it can be stated with good confidence that Love waves were the only type of energy that provide V_s sampling within the levees. The technique for inverting Love waves is under development and therefore no depth estimations as a function of shear velocity can be assigned for these data. For that reason only dispersion-curve analysis was performed to locate anomalous zones. A 2-D Love-wave dispersion curve display was generated for the top of the levee (Figure 104). A gradient map was calculated and then filtered to emphasize potential anomalous zones (Figure 105).

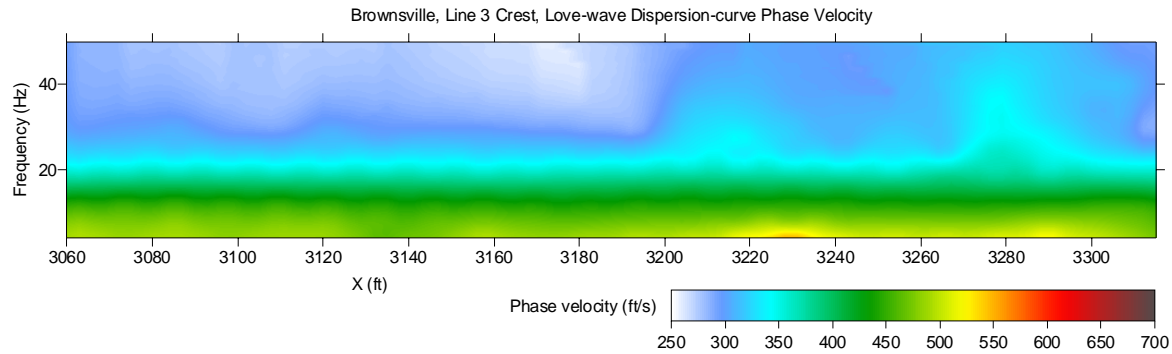


Figure 104. Love-wave dispersion-curve phase-velocity map estimated for line 3 by analyzing S-wave data.

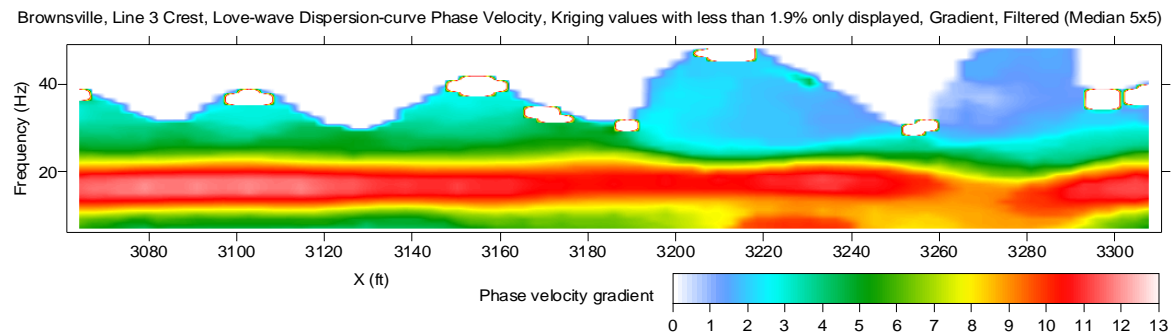


Figure 105. Love-wave dispersion-curve phase-velocity gradient map estimated for line 3 by analyzing S-wave data.

Site 4

P-wave First Arrivals

Compressional-wave data along the crest and toe were collected at site 4 in a fashion consistent with the previous three sites. Acquisition and processing methods and parameters were consistent for all sites to allow direct comparisons of the different levee sites and location at each levee site (toe and crest) without the need for equalization techniques. Signal-to-noise ratio on compressional-wave first arrivals was high enough to characterize most of the arrivals as instantaneous. Data quality was good with a strong apparent consistency in waveform and general velocity structure in comparison to data sets from other sites. Model convergence and a good 2-D refraction-tomography V_p solution was easily obtained in part due to the high quality of the first arrivals on P-wave data shot gathers along the crest (Figure 106).

S-wave First Arrivals

Shear-wave data is notorious for possessing narrower bandwidth and therefore more emergent first arrivals in comparison to equivalent compressional-wave data from a particular site. These characteristics were observed on shear-wave data from all sites occupied during this study. After both automatic

and manual first-arrival picking was complete, a 2-D refraction-tomography V_s solution was obtained for the data acquired along the crest (Figure 107). At this stage of this research project only crest data were inverted to a velocity profile because the characteristics of the toe data were extremely similar to the other sites and consistent with the crest information below the zone identified previously as related to basal compaction of the levee during and post-construction.

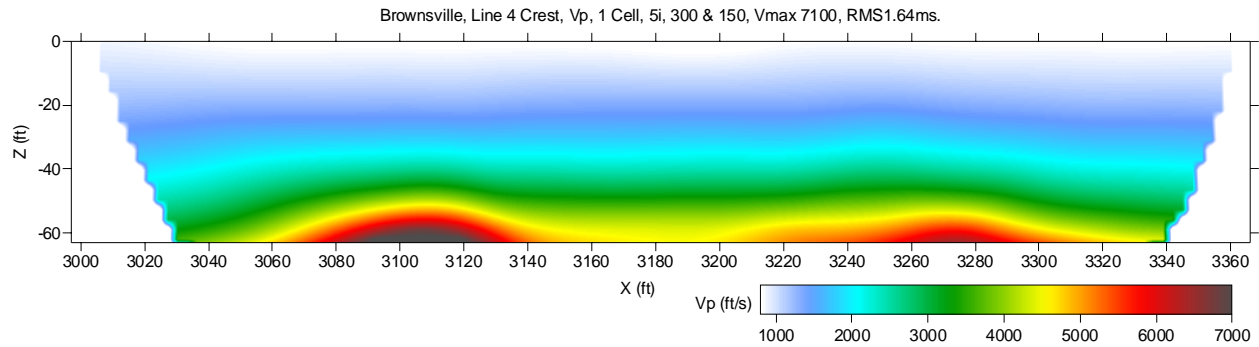


Figure 106. P-wave velocity model estimated for line 4 at the crest of the levee by analyzing S-wave-data first-arrival times using refraction-tomography software.

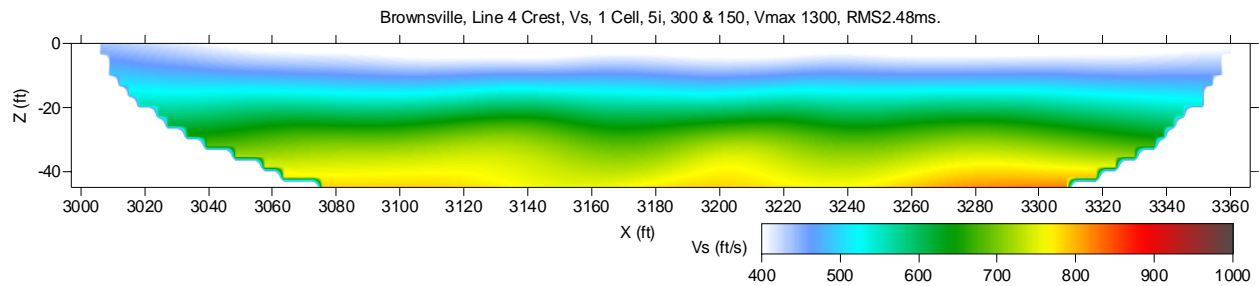


Figure 107. S-wave velocity model estimated for line 4 at the crest of the levee by analyzing S-wave-data first-arrival times using refraction-tomography software.

Rayleigh Wave

As with all the levee sites investigated during this study, Rayleigh-style surface waves did not possess the necessary broad spectrum of energy, likely as a result of either levee geometry or near-surface conditions. With the consistent lack of higher-frequency fundamental-mode surface-wave energy (and thus no Vs information within the levee itself), the MASW method was limited to providing estimations of the Vs from depths between 25 and 65 ft below the crest of the levee (Figure 108). “Bulls-eye” features or velocity undulations appearing in a very cyclic wave pattern above -10 ft are artifacts of the image interpolation algorithm.

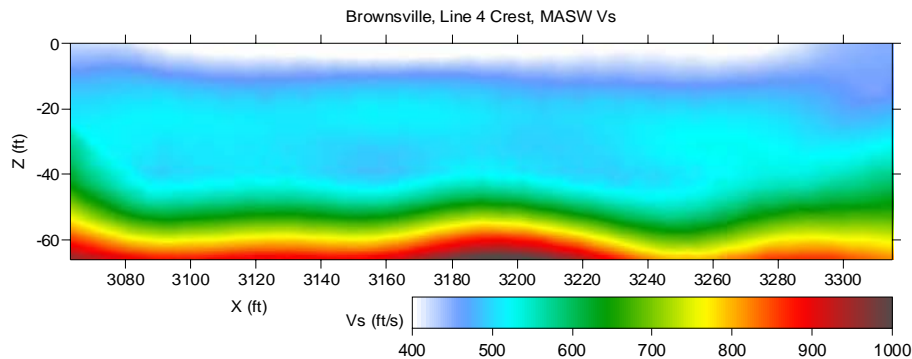


Figure 108. S-wave velocity model estimated for line 4 at the crest of the levee by analyzing P-wave-data surface-wave using the MASW method.

Love Wave

As with the other sites discussed so far, the presence of a relatively wide range of frequencies within the surface-wave packet on S-wave data (Love wave) is encouraging and may indicate information about the upper 15 ft at these sites might be rendered from seismic data after all. Assuming the same axiom that relates frequency to depth of penetration for Rayleigh waves is true for Love waves, then it can be stated with good confidence that Love waves appear to be the only type of seismic energy tested on this levee that have the potential to provide Vs sampling within the levees. The technique for inverting Love waves is under development and therefore no depth estimations as a function of shear velocity can be assigned for these data. For that reason only dispersion-curve analysis was performed to locate anomalous zones. A 2-D Love-wave dispersion curve was calculated from data collected along the top of the levee (Figure 109). A gradient map for these data was calculated and filtered to emphasize potential anomalous zones (Figure 110). Using a gradient map in this fashion assumes that significant lateral changes in velocity are not consistent with construction practices for levees.

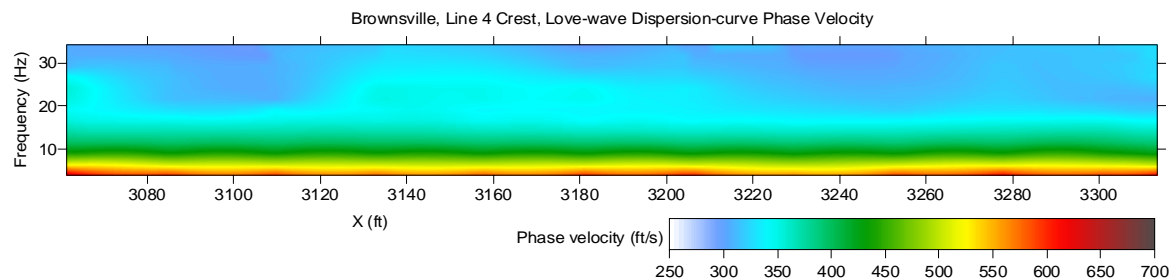


Figure 109. Love-wave dispersion-curve phase-velocity map estimated for line 4 by analyzing S-wave data.

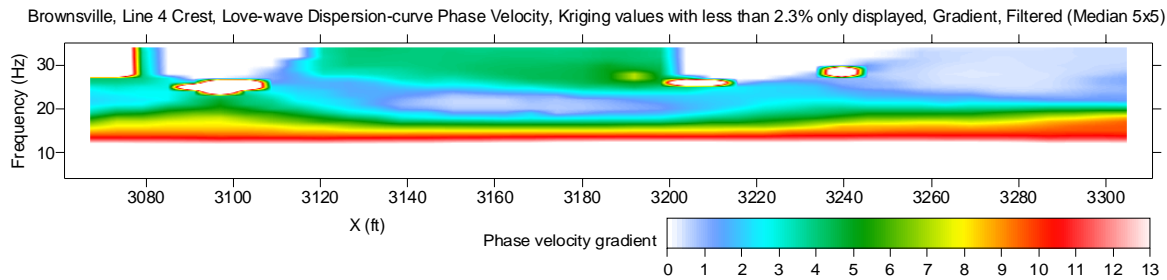


Figure 110. Love-wave dispersion-curve phase-velocity gradient map estimated for line 4 by analyzing S-wave data.

Site 5

P-wave First Arrivals

Compressional-wave data along the crest and toe were collected at site 5 in a fashion consistent with the previous four sites. Acquisition and processing methods and parameters were consistent for all sites to allow direct comparison of the different levee sites and locations at each levee site (toe and crest) without the need for equalization techniques. Signal-to-noise ratio on compressional-wave first arrivals was high enough to characterize most of the arrivals as instantaneous. Data quality was good with a strong apparent consistency in waveform and general velocity structure in comparison to data sets from other sites. Sites 4 and 5 were on younger levees (more recent construction methods and more uniform, less expansive clay composition) with a much more consistent velocity structure and therefore a more consistent first-arrival pattern. Model convergence and a good 2-D refraction-tomography Vp solution was easily obtained, in part due to the high quality of the first arrivals on P-wave data shot gathers acquired along the levee crest (Figure 111).

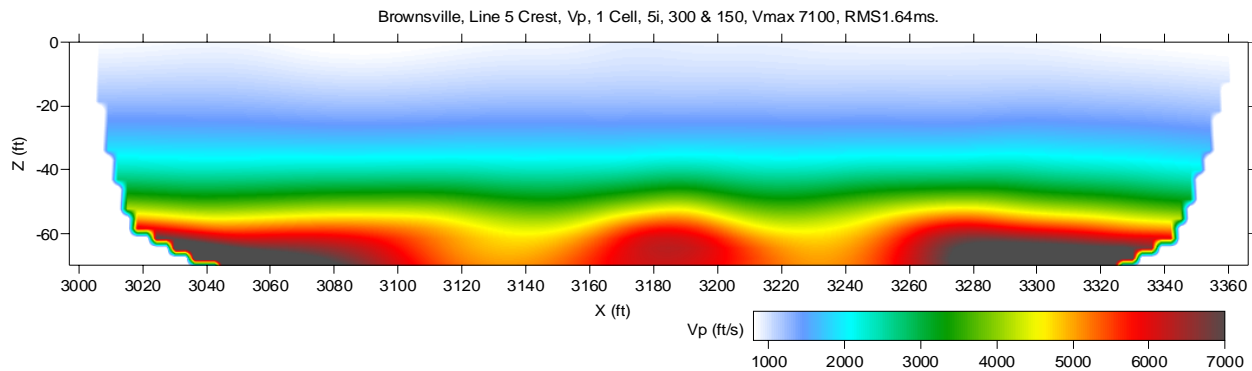


Figure 111. P-wave velocity model estimated for line 5 at the crest of the levee by analyzing S-wave-data first-arrival times using refraction-tomography software.

S-wave First Arrivals

Regardless of the much stiffer material properties measured in borehole samples of the levee at site 5, the shear-wave data possess a narrower bandwidth and therefore more emergent first arrivals than their equivalent compressional-wave data. As previously noted, these characteristics can be observed on shear-wave data from all sites occupied during this study. After completion of both automatic and manual first-arrival picking, a 2-D refraction-tomography Vs solution was obtained for the data acquired along the crest (Figure 112). At this stage of this research project, only crest data were inverted to a velocity profile because the characteristics of the toe data were extremely similar to the other sites and consistent with the crest information below the zone identified previously as related to basal compaction of the levee during and post-construction.

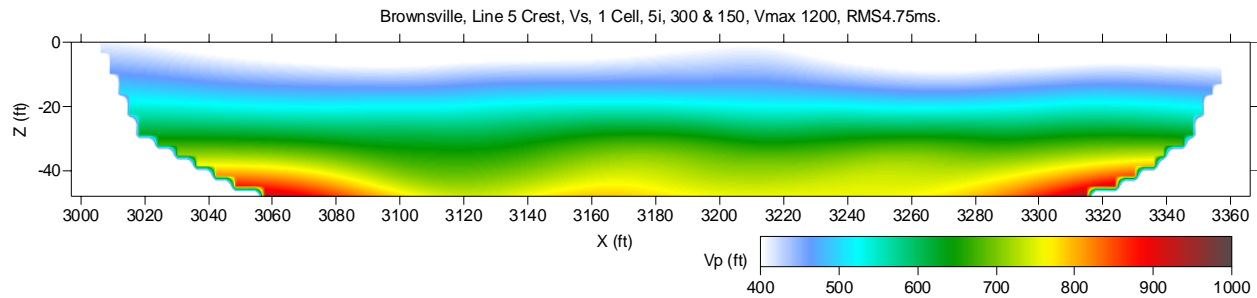


Figure 112. S-wave velocity model estimated for line 5 at the crest of the levee by analyzing S-wave-data first-arrival times using refraction-tomography software.

Rayleigh Wave

As with all the other levee sites investigated as part of this study, Rayleigh-style surface waves at site 5 did not possess the necessary frequency range to fully sample the depth range of primary interest. This ineffectiveness was likely the result of either levee geometry or near-surface conditions. With the consistent lack of higher-frequency fundamental-mode surface-wave energy (and thus no Vs information within the levee itself), the MASW method was limited to providing estimations of the Vs from depths between 25 ft and 65 ft below the crest of the levee (Figure 113).

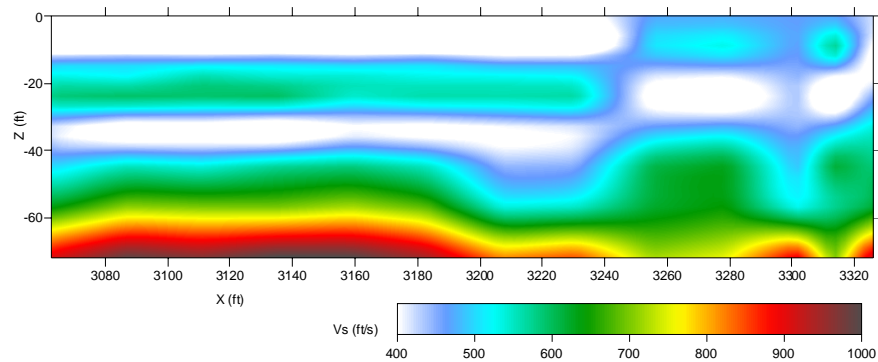


Figure 113. S-wave velocity model estimated for line 5 at the crest of the levee by analyzing P-wave-data surface-wave using MASW method.

Love Wave

A relatively wide range of frequencies within the surface-wave packet on S-wave data (Love wave) provided significant encouragement in evaluating various seismic energy modes for characterizing the upper 15 ft at sites like these around this area. Assuming the same axiom that relates frequency to depth of penetration for Rayleigh waves is true for Love waves, it can be stated with good confidence that Love waves appear to be the only type of seismic energy tested on this levee system that has the potential to measure Vs distribution within the levees. The technique for inverting Love waves is under development and therefore no depth estimations as a function of shear velocity can be assigned for these data. For that reason only dispersion-curve analysis was performed to locate anomalous zones. A 2-D Love-wave dispersion curve was calculated from data collected along the top of the levee (Figure 114). A gradient map for these data was calculated and filtered to emphasize potential anomalous zones (Figure 115). Using a gradient map in this fashion assumes that significant lateral changes in velocity are not consistent with construction practices for levees.

Other Processing

JARS P-wave Tomography

The JARS method was developed to overcome the wide range of equally possible solutions for the inverse refraction-tomography problem. It uses an abundant amount of *a priori* information from the

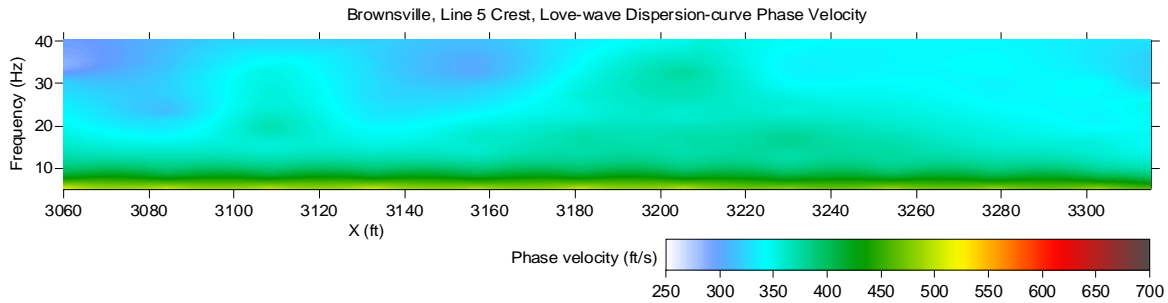


Figure 114. Love-wave dispersion-curve phase-velocity map estimated for line 5 by analyzing S-wave data.

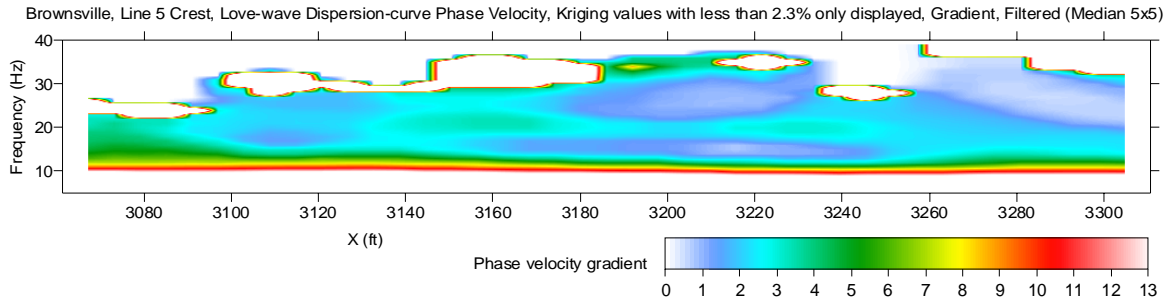


Figure 115. Love-wave dispersion-curve phase-velocity gradient map estimated for line 5 by analyzing S-wave data.

MASW method as a reference for selecting one of the many possible refraction-tomography solutions as an initial model. The JARS method was proposed as a superior first-arrival methodology for application to the crest of the levees. However, with the lack of higher-frequency fundamental-mode surface-wave energy, the method was severely limited by the lack of V_s information in the top 20-25 ft—the actual levee core—thereby eliminating any improvement in the initial refraction model within the key depth range of interest.

At the Toe of the Levee

At the toe of the levees the JARS method was applied with a great deal of success because MASW at the toe provided a wide enough range of V_s values throughout the upper 50 ft to define an initial model (Figure 116a). This success was due in large part to the richness of the high-frequency fundamental-mode surface-wave energy recorded in the relatively undisturbed material beneath the toe lines. Using the MASW results, a JARS V_p solution for the toe at site 2 with good convergence was formulated (Figure 116b). The MASW V_s results at the toe for site 3 did not possess sufficient depth coverage to fully develop the initial model at that site (Figure 102). Fortunately, the MASW V_s results for the crest at site 3 had the deeper information missing on the toe V_s field and by appending the V_s results from the crest onto the toe cross section (Figure 103b), a sufficiently encompassing range of *a priori* information was available to appropriately feed the JARS method (Figure 117a). Using a V_s model constructed in that fashion provided for a good JARS V_p solution for the toe at site 3 (Figure 117b). Incorporating this JARS V_p solution as the initial model for the standard P-wave refraction tomography inversion solution (Figure 100b) demonstrates that both solutions are possible to the inverse refraction tomography problem (their RMS error is very small: 2.19 and 2.17 ms) and a consistent overall nature. This comparison exemplifies how uniquely different equally possible refraction solutions may be from each other for a single site using the same input data. Still, because the JARS method chooses a solution based on *a priori* information obtained from MASW, while the standard refraction-tomography solution does not use any *a priori* information in selecting a solution, it is reasonable to suggest the JARS solution is likely closer to the truth. Furthermore, the JARS solution looks more realistic from geologic perspective for this site.

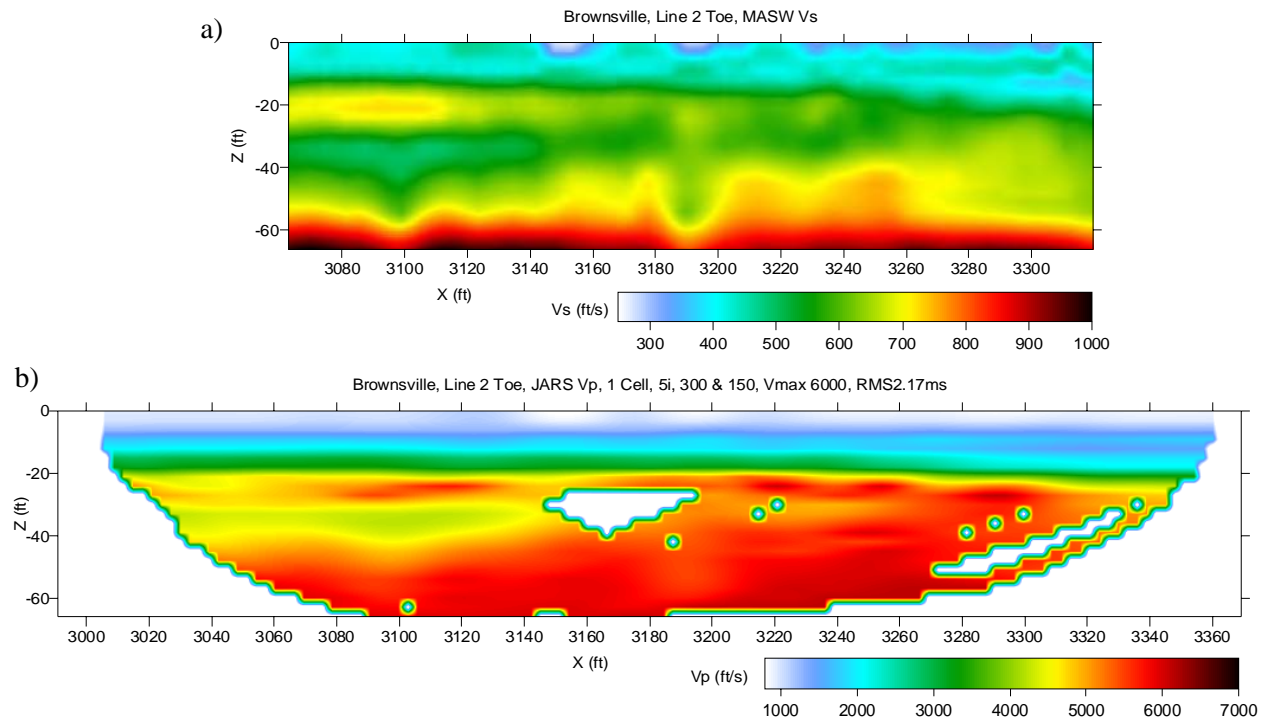


Figure 116. Application of JARS method at the toe of line 2, a) S-wave velocity model estimated at the toe of the levee by analyzing P-wave-data surface-wave using the MASW method, b) JARS P-wave velocity model estimated by analyzing P-wave-data first-arrival times and using a reference P-wave velocity model derived from the S-wave velocity model.

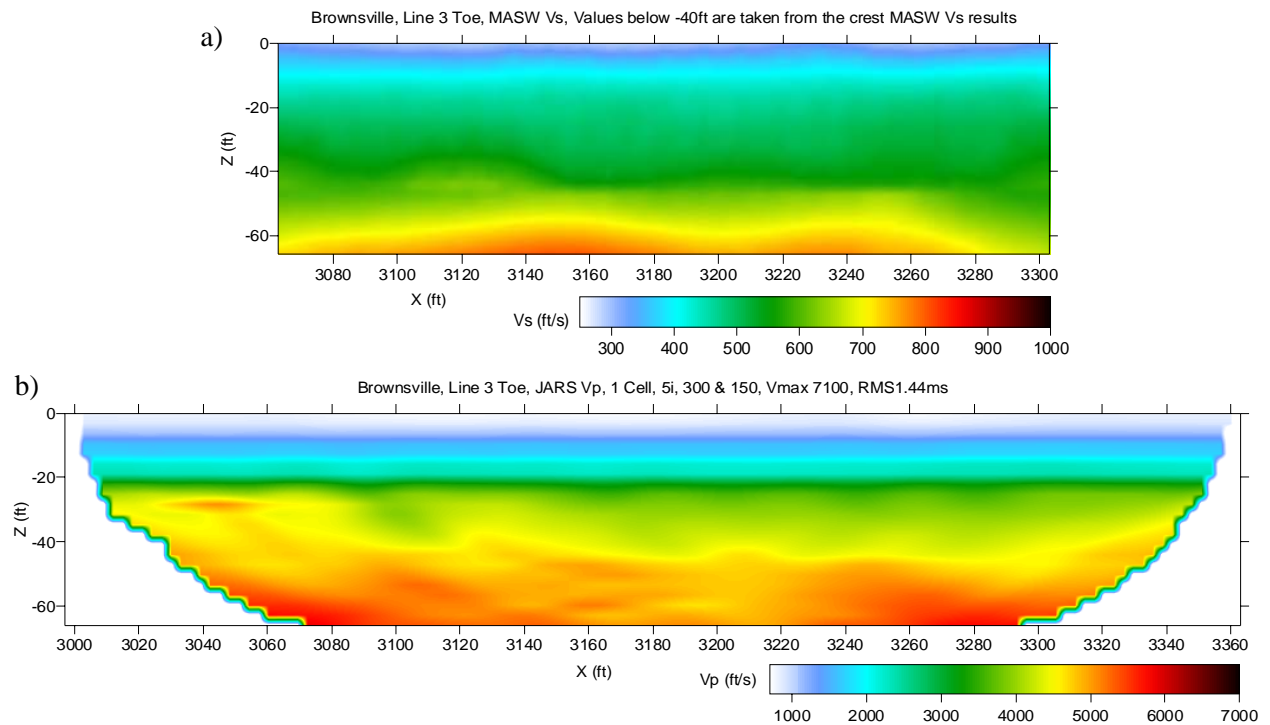


Figure 117. Application of JARS method at the toe of line 3, a) S-wave velocity model estimated at the toe of the levee by analyzing P-wave-data surface-wave using the MASW method, b) JARS P-wave velocity model estimated by analyzing P-wave-data first-arrival times and using a reference P-wave velocity model derived from the S-wave velocity model.

At the Crest of the Levee

Even though MASW did not successfully produce a velocity image of the upper 20 ft beneath the crest profile, an attempt to apply the JARS method at the crest of the levee was made using the reliable Vs data from the MASW analysis with extrapolation into the no-data zone. This extrapolation of deeper Vs information into the no-data zone within the levee was accomplished using Kriging (a very reliable geostatistical method). Because the Vs model generated by the MASW method is only used as an initial model, this extrapolation, even though not an accurate representation of the levee materials, does provide a starting point for the iterative inversion process used by the JARS method. Using the expanded Vs data set, a JARS solution was obtained for line 1 (Figure 118). As with any iterative inversion technique, many possible solutions exist for a data set; the one provided here represents the most likely considering all *a priori* data. Even though this solution honors all *a priori* data and has an RMS error of only 1.55 ms (meaning the data and model are an excellent fit), and therefore represents a possible solution, it does not appear realistic considering the known internal structural characteristics of the levees in this area. This excellent fit to the data—but a resultant unrealistic solution—suggests our attempt to interpolate into shallow areas without measured values was not only unreliable, but the estimates were sufficiently far from the “truth” that even with multiple iterations beyond the initial model, this starting point was sufficiently distant from the true values so that the real solution was outside the bounds of the method.

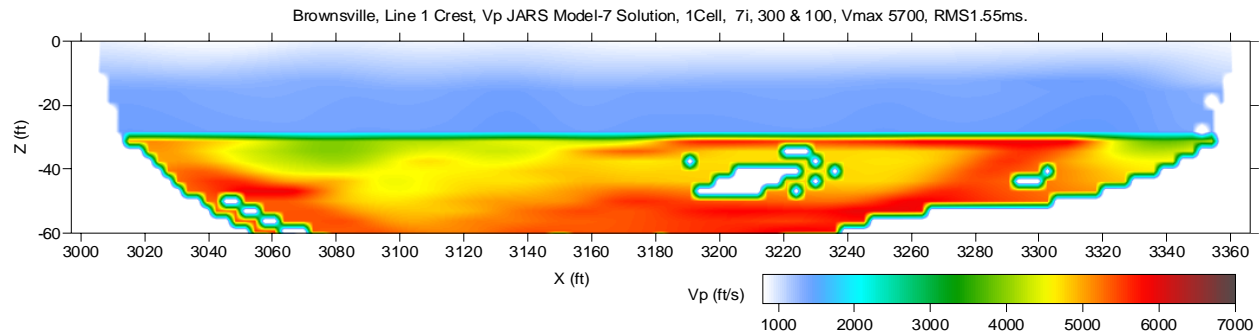


Figure 118. Application of JARS method at the crest of the levee of line 1 estimating a P-wave velocity model by analyzing P-wave-data first-arrival times and using a reference P-wave velocity model derived from the S-wave velocity model.

Refraction tomography is a well proven and effective way to estimate compressional-wave velocity structure of the earth from first-arriving seismic energy. However, like any inversion method, the results are only as reliable as the input data and the volume and redundancy of that data. Key to any inversion is the initial model. To demonstrate the wide range of possible refraction-tomography solutions with these data the JARS Vp solution (Figure 118) can be compared to the standard refraction-tomography solution for the crest at site 1 (Figure 119). Although both are possible, neither of these solutions are considered to be likely due to a lack of abundant *a priori* information.

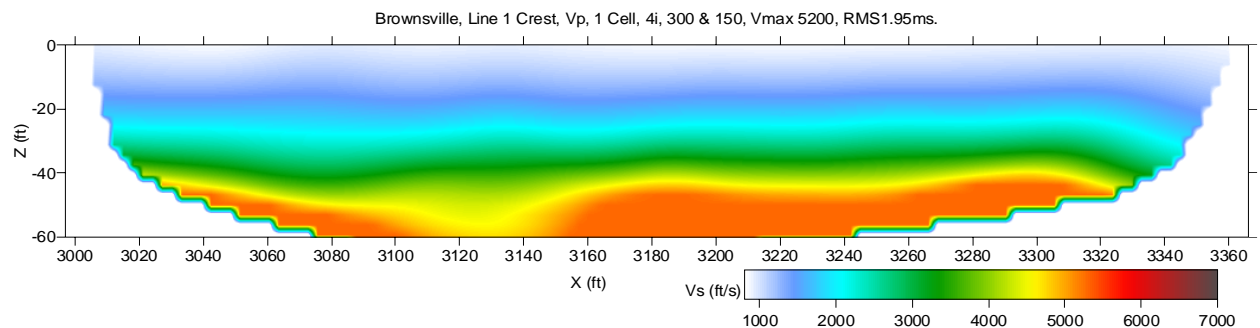


Figure 119. P-wave velocity model estimated at the crest of the levee of line 1 by analyzing P-wave-data first-arrival times using refraction-tomography software.

Discussion of Data and Processing at Each Site: Trip #2

Site 1

P-wave First-arrival

Data from the second trip possess notably different seismic characteristics than those observed on data acquired about a year previously during the first trip. Spectra were broader and waveforms were much more impulsive, supporting a higher signal-to-noise ratio (Figure 120, compare to Figure 44, p. 30). This difference can only be attributed to the near-surface materials. Acquisition and processing methods, equipment, and parameters were as near identical as possible for both surveys. After inquiring, the most likely reason for this difference is saturation of near-surface sediments. During the fall months a significantly larger volume of rain fell than in the same time period throughout most of the previous decade. These data were acquired in part to confirm that the change in near-surface velocities observed at site 2 were consistent for the area and not specific to site 2.

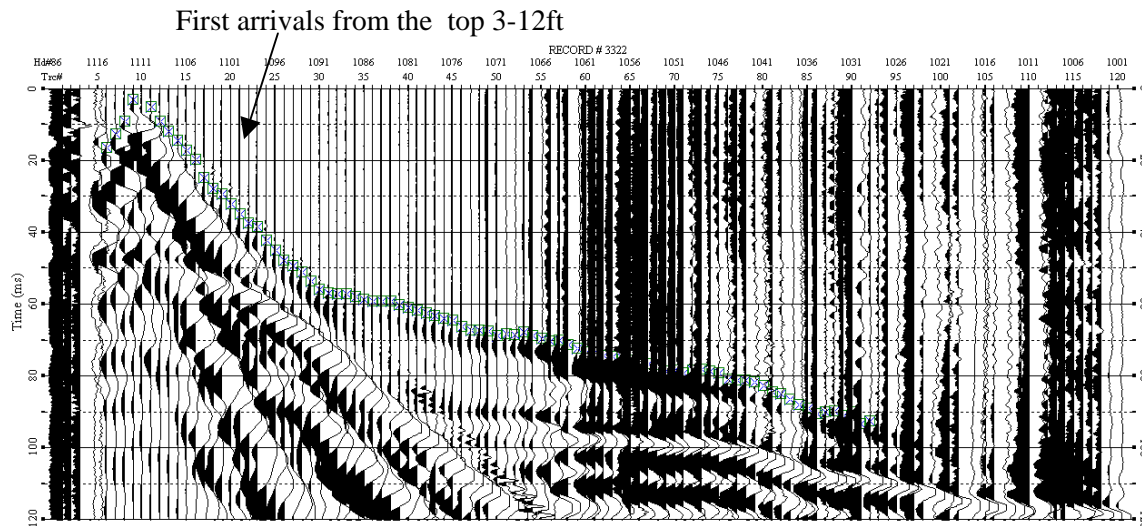


Figure 120. Estimation of first-arrivals times on a P-wave seismic data with source located at station 1111 (horizontal coordinate at 3333 ft) at site 1 in 2004.

Refraction-tomography V_p analysis from the 2003 and 2004 seismic data sets resulted in V_p images that were extremely similar with respect to the overall velocity structure and associated variability in materials as evidenced by changes in velocity (Figure 121). Considering the clear difference in seismic character, a better estimate of possible changes in the V_p properties between the 2003 and 2004 surveys was necessary. Therefore, a velocity-increment map with respect to the 2003 V_p measurement was calculated to more closely identify changes in velocity between the two survey dates (Figure 121c). A velocity increase between 3 and 8% is evident for most of the top 5-8 ft and about 3% at 30-ft depths, with the exception of the 3130-3180 ft offset range where the velocity decreases around 8-10%.

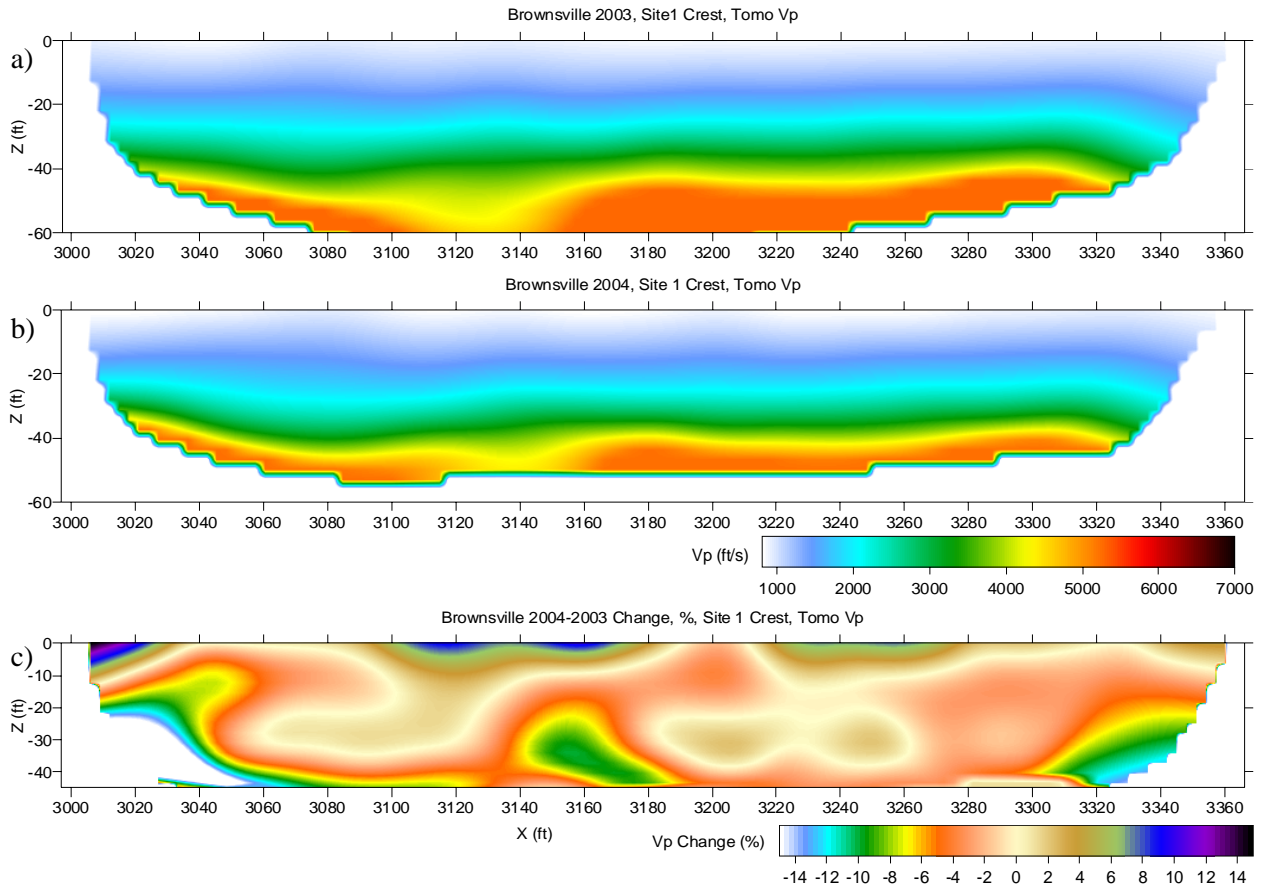


Figure 121. P-wave velocity models estimated at the crest of the levee at site 1 analyzing P-wave-data first-arrival times using refraction-tomography software, a) P-wave velocity model obtained from the seismic data acquired in 2003, b) P-wave velocity model obtained from the seismic data acquired in 2004, c) difference between the P-wave velocity models obtained in 2003 and 2004.

Rayleigh Wave

With the change in near-surface seismic characteristics came a marked improvement in the bandwidth of the surface-wave data as well. This improvement was most clearly seen in the increased high-frequency components of the fundamental-mode Rayleigh-wave energy. The availability of a wide range of both low- and high-frequency fundamental-mode energy in the dispersion curves from the 2004 seismic data provided a greatly improved and detailed V_s image of the levee (Figure 122a). The difference is extremely evident when compared directly to the V_s image from the 2003 seismic data (Figure 122b).

This success of MASW at site 1 in calculating the V_s using surface waves provides a great deal of optimism that the near-surface conditions were the limiting factor during 2003 and not the geometry of the levee. With this observation comes the realization that it might still be possible to use MASW as a tool for estimating V_s within levees susceptible to changes in stiffness due to long-term or seasonal changes in core-moisture content. Reconnaissance surveys designed to identify areas with reduced shear velocity, and therefore reduced rigidity, could be susceptible to internal erosion during high-water events.

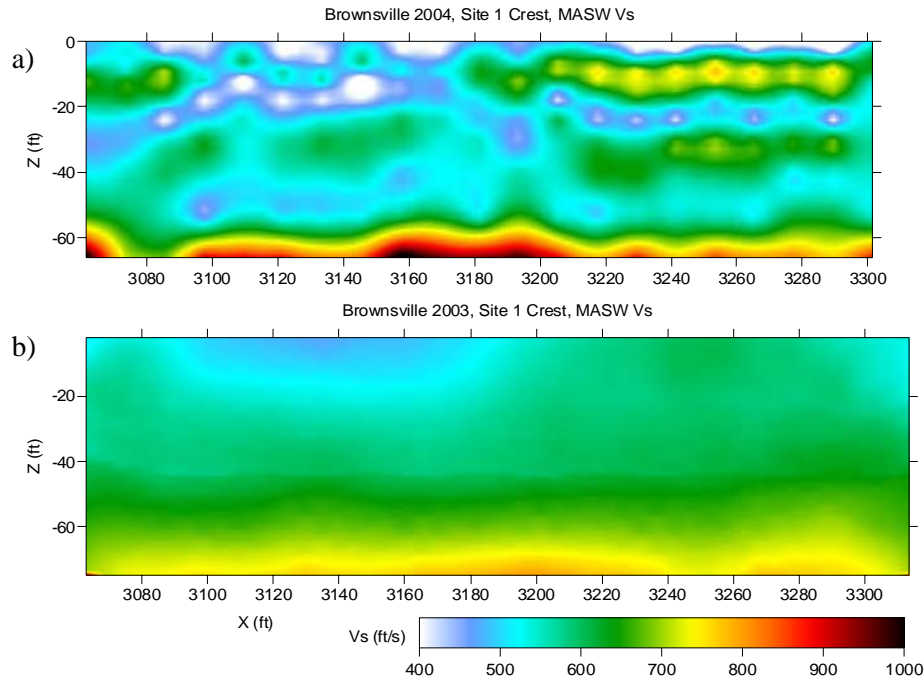


Figure 122. S-wave velocity models estimated at the crest of the levee at site 1 by analyzing P-wave-data surface-wave using MASW method acquired in, a) S-wave velocity model obtained from the seismic data acquired in 2004, b) S-wave velocity model obtained from the seismic data acquired in 2003.

Site 2

P-wave First Arrival

The lion's share of seismic testing during the 2004 component of the study was undertaken at site 2. Site 2 was the location of the ponding experiment designed to evaluate the potential of the levee to absorb water during a high-water event, allowing internal erosion of the core, such that failure could result. Seven surveys throughout the multi-day test were acquired, each with compressional and shear recorded along two profiles, one along the south edge of the crest nearest the pond and one along the north side. First-arrivals were picked on all seismic data automatically and then manually edited prior to population of the database. A 2-D refraction tomography V_p solution was obtained for all seven time slices both on the south line (Figure 123a-123g) and on the north line (Figure 124a-124g). Refraction-tomography V_p images of the south and north lines do not appear to suggest compressional-wave velocity is terribly sensitive to material changes that occurred in this segment due to infiltration of water. Based on these data alone, it is also possible that the skin layer covering the core acted to repel any water from making its way into the levee, and therefore no changes in V_p simply means no moisture penetrated the skin layer.

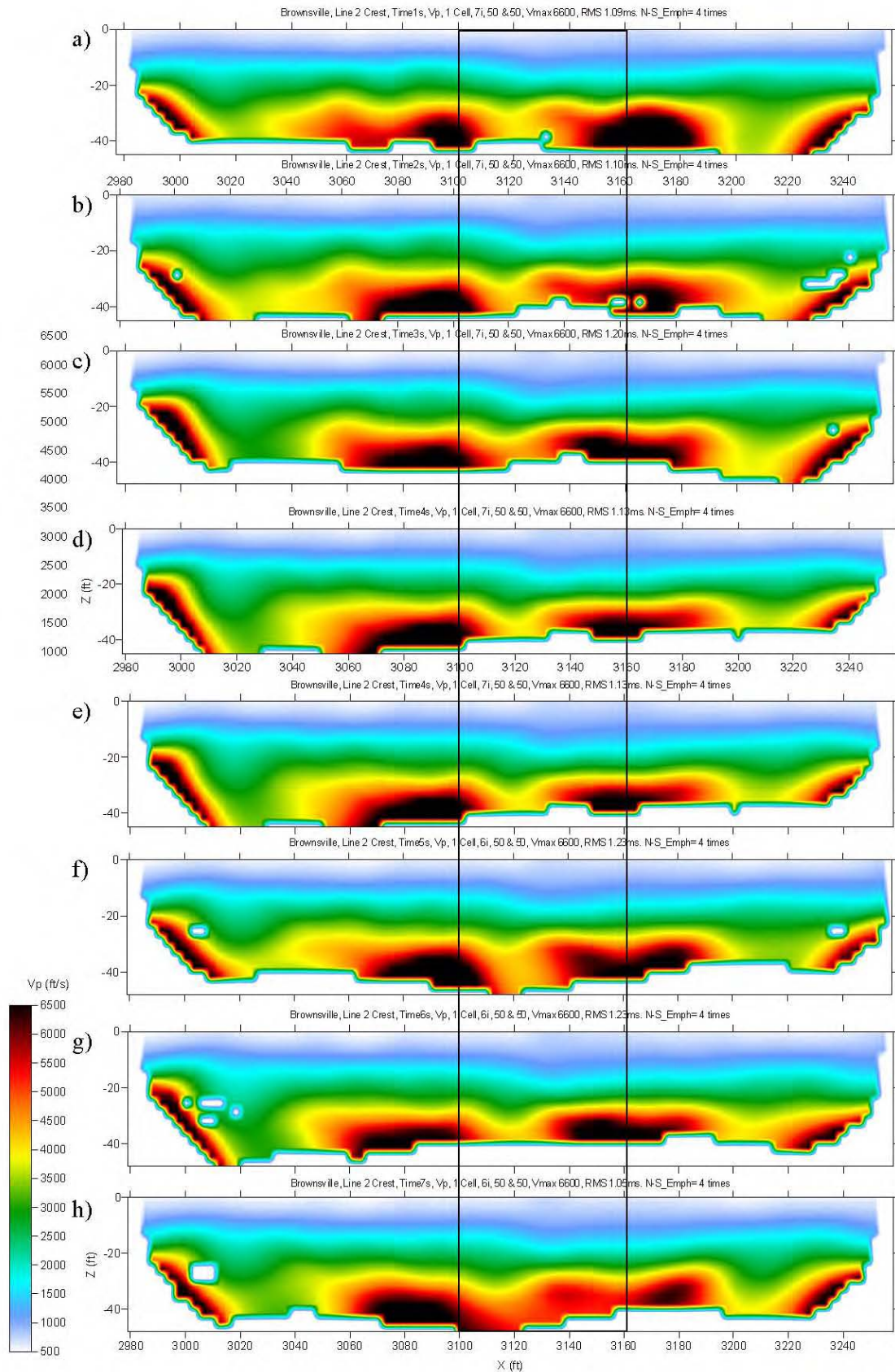


Figure 123. Refraction-tomography p-wave velocity models estimated at the south edge of the crest on site 2 by analyzing first-arrival times estimated from P-wave data a) base survey and at the following times after beginning of ponding: b) 24 hours, c) 36 hours, d) 48 hours, e) 60 hours, f) 72 hours, and g) 84 hours.

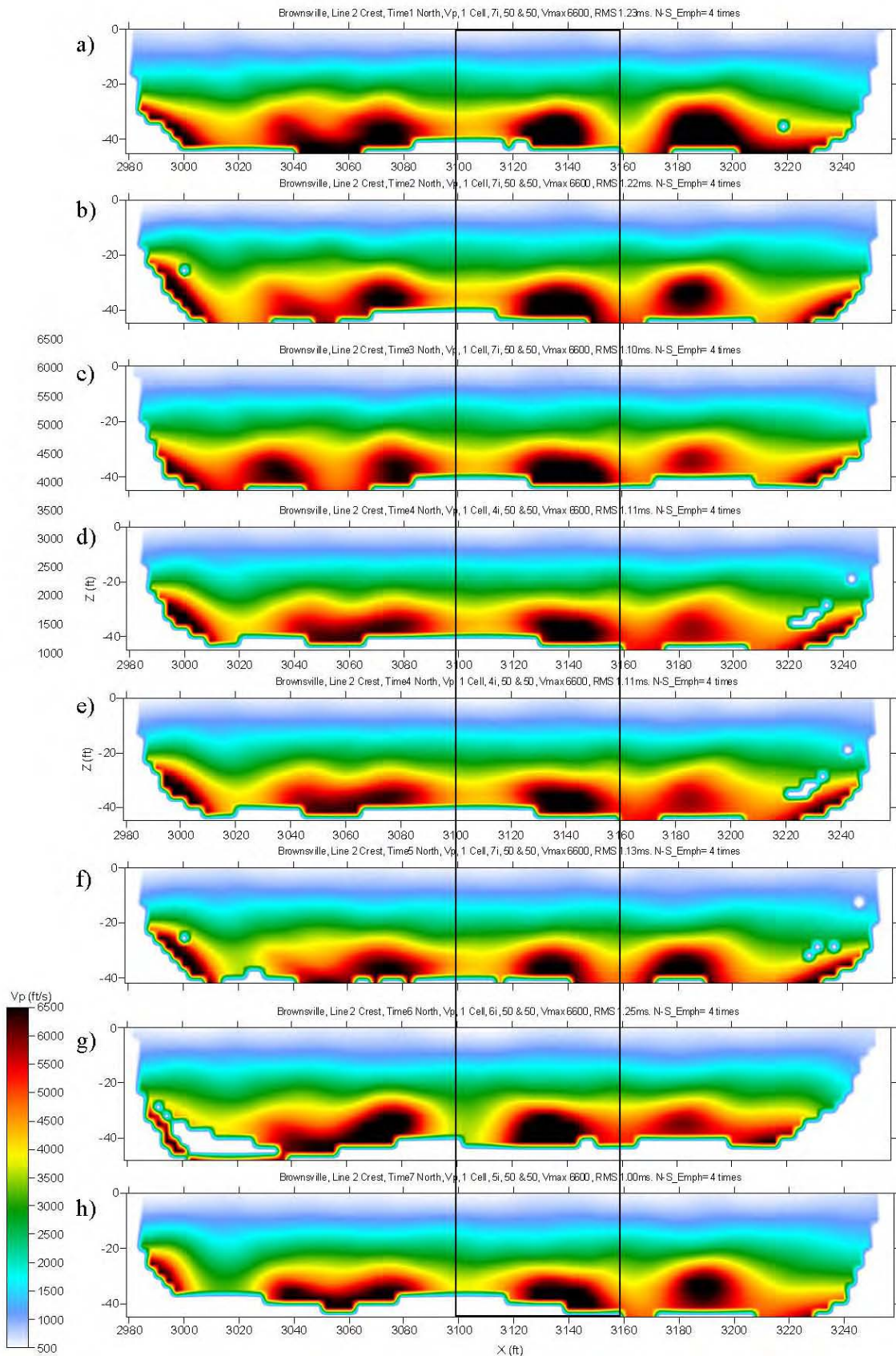


Figure 124. Refraction-tomography P-wave velocity models estimated at the north edge of the crest on site 2 by analyzing first-arrival times estimated from P-wave data a) base survey and at the following times after beginning of ponding: b) 24 hours, c) 36 hours, d) 48 hours, e) 60 hours, f) 72 hours, and g) 84 hours.

To better estimate possible changes in the Vp properties, velocity-increment maps with respect to the base-line Vp measurement were calculated (Figure 125). An increase in velocity is evident for the top 5 ft along the crest adjacent to the ponding experiment (3060-3160 ft) for time slices 2-4. Because the water had not reached the crest yet at the time of those surveys, it is most likely this increase in velocity is due to the multiple pass with the hammer and plate compacting the near-surface sediments. It was not until time slice 5 that the pool height reached maximum and changes in material properties in the upper 5 ft were possible as a result of the presence of water. Further Vp increases at time slices 5-7 at locations 3120-3140 ft could well be due to the presence of water against the sides of the levee.

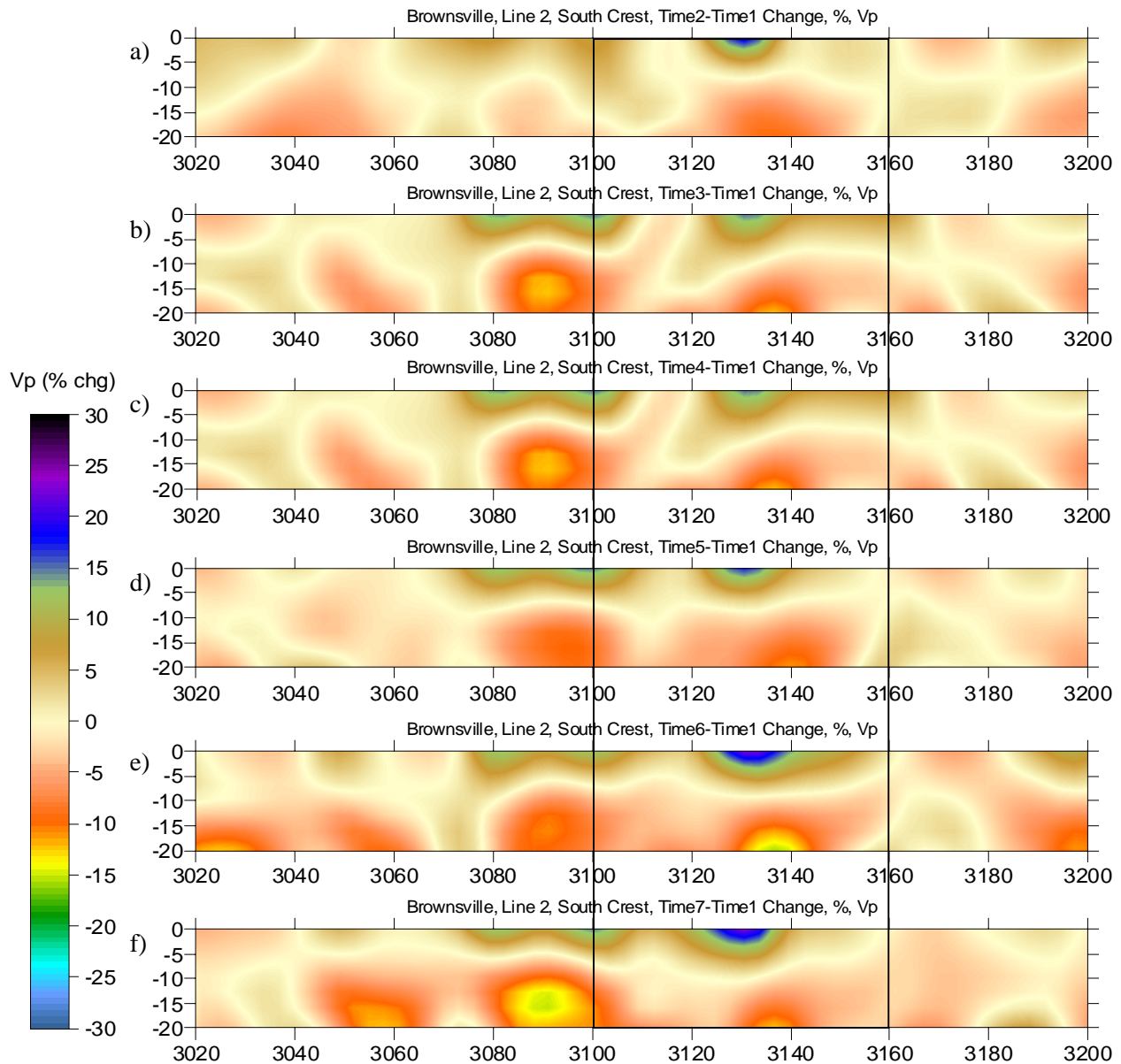


Figure 125. Refraction-tomography P-wave velocity-model increments with respect to the base survey estimated at the south edge of the crest at site 2 at the following times after beginning of ponding: b) 24 hours, c) 36 hours, d) 48 hours, e) 60 hours, f) 72 hours, and g) 84 hours.

S-wave First Arrival Analysis

A shear-wave shot gather possessed greater signal-to-noise and more impulsive first arrivals than those observed on previous surveys at this site. For each compressional-wave survey (seven in all) an equivalent shear-wave survey was acquired. With the success of MASW to calculate the Vs for the near surface, especially the upper 10 ft or so of the levee, the shear-wave data have not been fully processed. However, with the much improved quality of the Rayleigh-wave and shear-wave data sets, Vs calculated from refraction-tomography using shear-wave data will be an excellent way to evaluate the accuracy of both methods in this setting. With the data being collected in transverse mode, both polarities of shear energy were recorded, which should provide the opportunity to improve signal-to-noise by canceling a significant amount of the source-generated and mode-converted compressional-wave energy.

Rayleigh Wave

Compressional-wave shot gathers from the seismic data acquired along the levee crest were analyzed for dispersive surface-wave energy using the MASW method. In contrast with the 2003 data set (Figure 53, p. 35), it was possible to pick a wide range of frequencies and phase velocities from fundamental-mode dispersion curves (Figure 126).

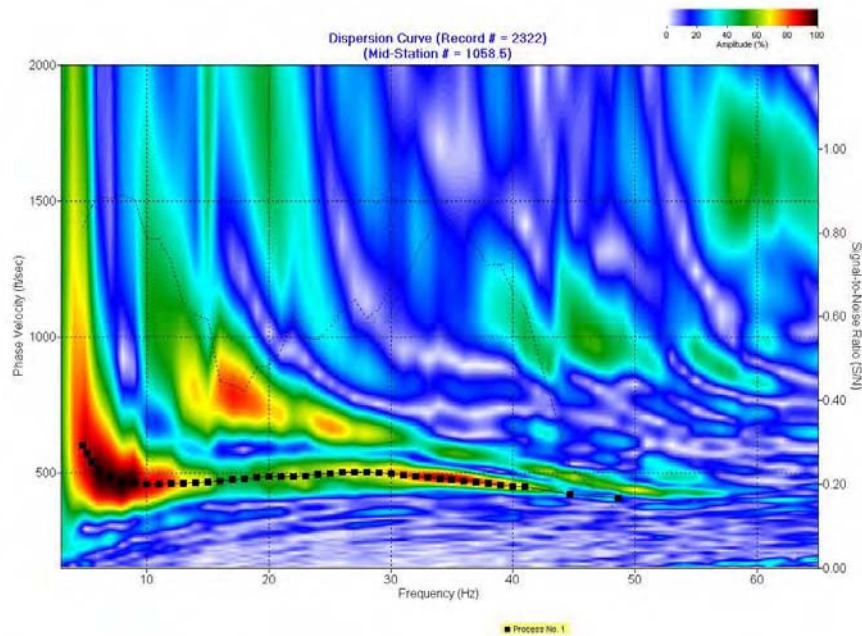


Figure 126. Dispersion-curve analysis of P-wave-data surface-wave using the first 40 traces from shot record #2322.

MASW Vs data calculated along the south seismic line for all seven time slices are of excellent quality and provide a consistent and logical progression of velocity change within the levee (Figure 127a-127g). As well, MASW Vs data were calculated for data from the north seismic line at each of the seven time slices (Figure 128b-128g). An interesting lack of lower-frequency surface-wave energy was observed in seismic data from the north side of the levee crest for the first or baseline survey prior to ponding on the south. This lack of low-frequency energy is still unexplainable, but it did prohibit the generation of a Vs profile for the baseline or time zero slice (would have been Figure 128a).

Love Wave

As with the shear-wave refraction tomography, no analysis was done to evaluate the Love wave energy on shear-wave data collected along the crest during the ponding experiment. The data are available and will be analyzed once technology exists to exploit the dispersive characteristics of the Love wave and invert for Vs.

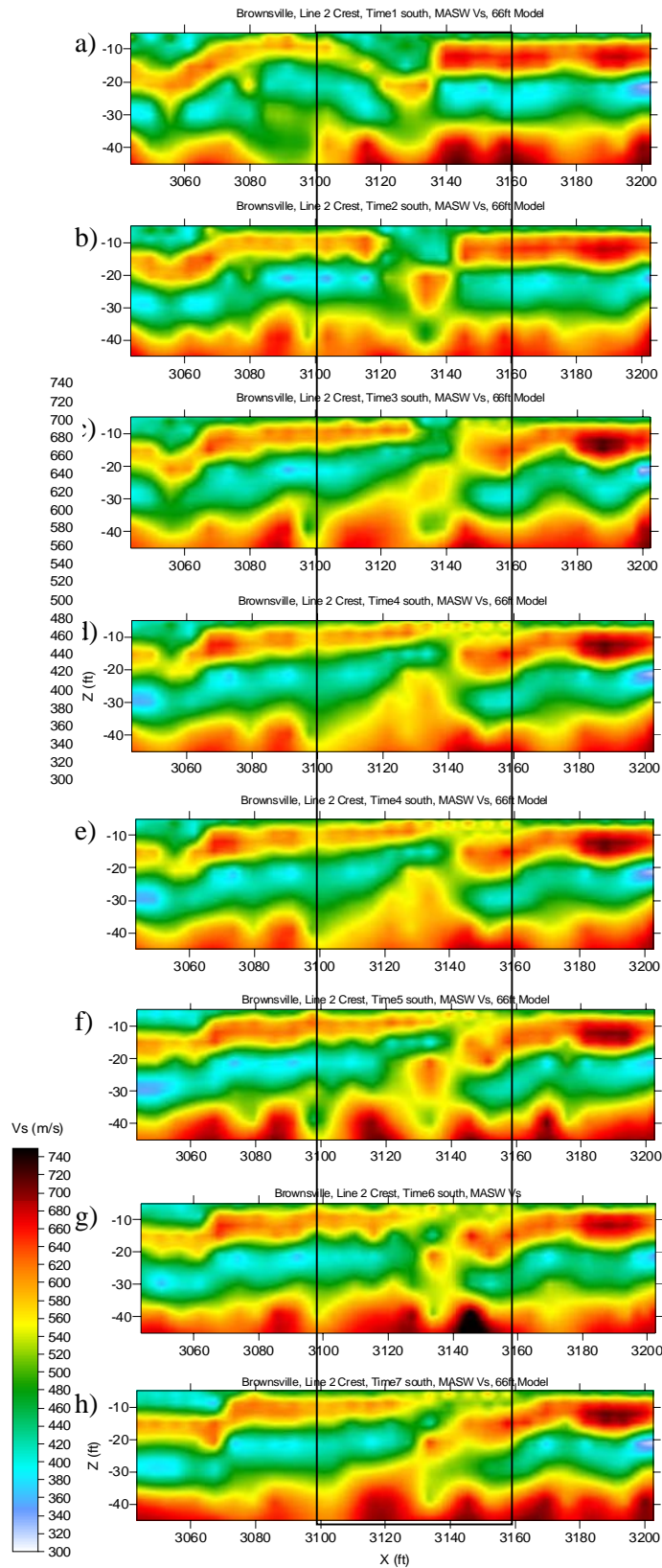


Figure 127. MASW S-wave velocity models estimated at the south edge of the crest on site 2 by analyzing surface wave from P-wave data a) base survey and at the following times after beginning of ponding: b) 24 hours, c) 36 hours, d) 48 hours, e) 60 hours, f) 72 hours, and g) 84 hours.

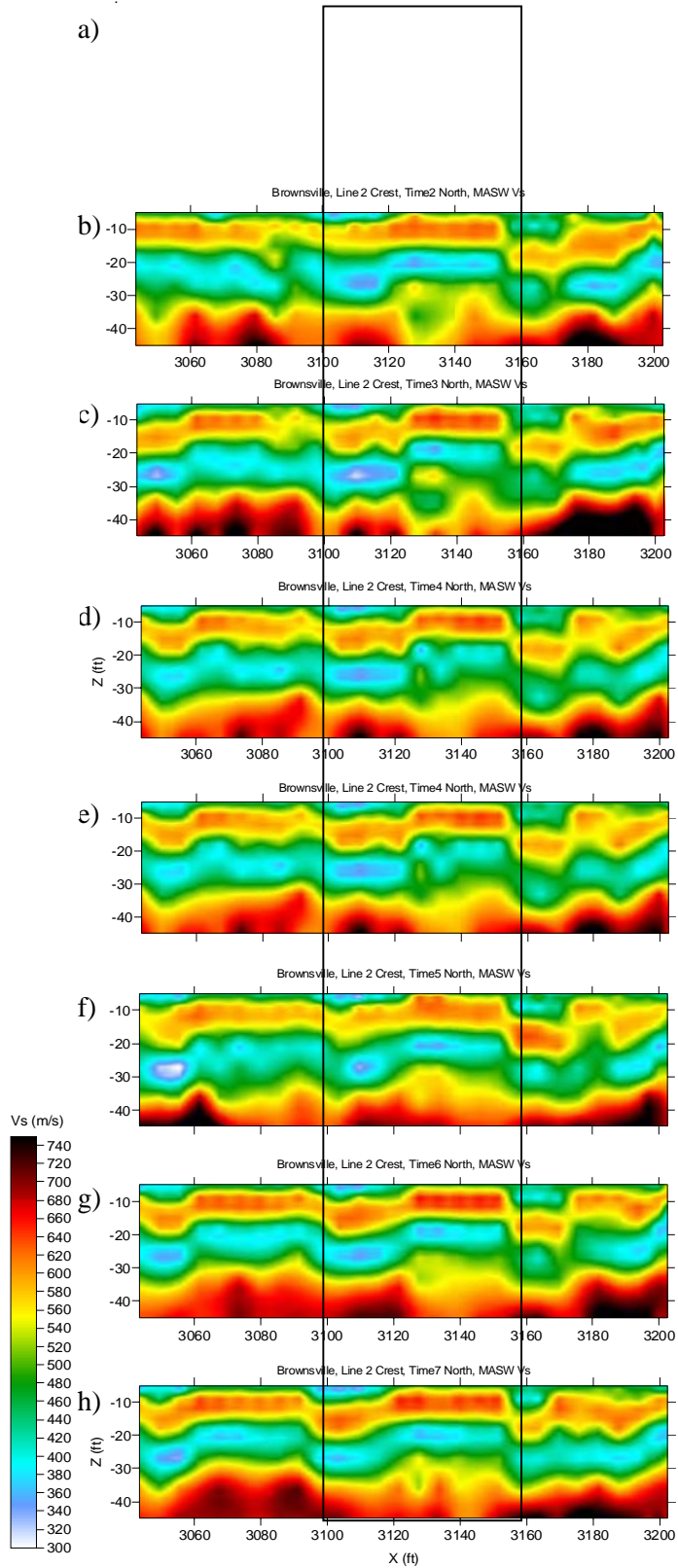


Figure 128. MASW S-wave velocity models estimated at the north edge of the crest on site 2 by analyzing surface wave from P-wave data a) base survey and at the following times after beginning of ponding: b) 24 hours, c) 36 hours, 4) 48 hours, e) 60 hours, f) 72 hours, and g) 84 hours.

Site 4

P-wave First Arrival

Compressional-wave data were recorded at site 4 to allow comparison and evaluation of any relative changes in velocity that could be related to changes in the near surface, possibly related to increased precipitation as speculated to be the cause of reduced water infiltration into the levee during the ponding experiments and the observed increase in seismic velocity. Data were acquired in a fashion as consistent with the 2003 trip as possible, with data processing matched for both data sets to avoid any parameters or operations that might be unique to either data set. Based on field analysis, a slight increase in velocity consistent with that observed at sites 1 and 2 was also observed at site 4.

Rayleigh Wave

Improvements in the bandwidth in the surface-wave energy were sufficient to allow calculation of the fundamental-mode dispersion curve for energy within the levee. With the availability of a wide range of both low- and high-frequency fundamental-mode energy, the dispersion curves from the 2004 seismic data provided a greatly improved and detailed V_s image of the levee. The difference is evident when compared directly to the V_s image from the 2003 seismic data.

This success of MASW at site 4 calculating the V_s using surface waves compounds the optimism that near-surface conditions were the limiting factor during 2003 and not the geometry of the levee. As noted previously, with this observation comes the realization that it is likely that MASW could be used as a tool for estimating V_s within levees susceptible to changes in stiffness due to long-term or seasonal changes in core-moisture content.

6—RESULTS/DISCUSSION

These investigations targeted seismic velocities, both absolute and relative (changes). Seismic velocities of levee materials were estimated and compared both site to site and within specific sites. A unique study of surface-wave phase velocity was conducted observing phase variations in the expected (for consistent material characteristics) uniform wavetrain at and near resonance (resonance in this case is controlled by levee height and surface-wave velocity of the materials: wavelength). This surface-wave study was conducted in hopes of identifying anomalous zones where changes in phase velocity might be indicative of reduced or increased material strength. Seismic velocities were measured based on travel time between adjacent sets of receivers.

Compressional-wave velocities were for the most part within a “reasonable” range for this setting; however, shear-wave velocities were estimated to be significantly higher than expected based on both levee materials and equivalent compressional-wave velocities. Shear velocities were consistently measured with a V_p/V_s ratio around 2, which is generally more characteristic of consolidated rocks. Ratios for unconsolidated fill materials such as these are generally expected to fall in the 3 to 5 range. This higher than expected ratio could result from measuring mode-converted shear rather than the primary direct shear arrival. It is also possible this higher than expected shear velocity could be real and related to these earth materials and the mechanical compaction used to construct these levees.

Estimates of shear velocity using both refraction tomography and slope intercept methods provided shear velocities that were unrealistically high and with offset dependent arrival patterns extremely consistent with the faster compressional-wave arrivals. Calculating shear-wave velocity from inverted surface waves was strongly dependent on bandwidth and percentage of higher-mode energy recorded. During the first survey ground conditions were not conducive to producing and/or recording broadband surface waves. Therefore, no confident shear-wave velocity sections were produced. On the second trip near-surface conditions had sufficiently changed to allow sufficient broadband surface wave that a 2-D shear wave profile could be produced for the levee core.

Velocity anomalies within the levee were detected at each of the three Retamal levee sites. Distribution and range of values for these anomalies are consistent with variations in material types used during construction and the construction processes itself. It is not clear that velocity information alone will be sufficient to identify areas with a high density of cracks, which could be present as a result of the dewatering during drought of the expansive clays used in some places during core construction. However, it does seem likely that reduction in the material stiffness of the levee core could be used to identify failure risk areas with a relatively high resolution. Discontinuities in the levees associated with cracks seem to interfere with the otherwise uniform propagation of surface waves through the levee. These disturbances, once fully understood, could provide relatively accurate locations of weak zones within the core material.

Problems and pitfalls associated with using seismic techniques to estimate velocities intended to help characterize levee competence do exist and require significant attention to detail and understanding of the seismic wavefield arrival patterns (t-x) and significance of the spectral properties of each mode. In particular, mode converted shear-wave energy can lead to completely incorrect conclusion. Interpreting the propagation irregularities in surface-wave energy is not clearly understood and therefore not yet ready for use as a routine tool in interrogating levees. It must also be kept in mind that the geometry of the levee and the proximity of its basal contact with native earth can result in refracted first arrivals dominating the majority of close-offset traces where direct waves are normally expected.

Infiltration of water into the levee skin was identified on seismic data during the ponding experiment conducted during the second site visit at site #2 (oxbow lake site). Notable changes in both compressional and shear velocity can be associated with the infiltration of water dammed against the south levee face. Compressional-wave data suggest percolation of water into the native river valley sediments beneath the levee. Shear-wave velocity change was rapid, occurring at the very beginning of the simulation, and was isolated to one area within the pond. The isolated nature of the infiltration on the shear data could be related to a fracture/crack system opened as a result of the years of drought and dewatering of the core. An alternate possibility is a possible material inconsistency resulting from construction practices and locally mined core material.

7—CONCLUSIONS

Rapid, precise seismic methods for identifying areas worthy of further investigation could be developed for specific levee geometries and construction materials. Monitoring is by far the most confident and accurate application for seismic techniques on levees. Consideration must be given for changes in skin conditions due to seasonal variations in moisture. At the five sites studied on the Retamal and Main levees, LRGV compressional-wave velocity estimations were most accurate for all conditions using refraction tomography. Shear-wave velocity survey data were contaminated with mode-converted energy and therefore difficult to use to estimate material characteristics. Changes in near-surface conditions between the first and second survey resulted in an increase in recorded surface-wave bandwidth and, therefore, reasonably confident shear-wave velocity estimations within the levee. This change in surface conditions did not seem to change the arrival patterns observed on data recorded to capture first-order shear-wave first arrivals.

Considering the observations from the ponding experiment and five-site study, it is clear that the seismic tool can be used during flood events to detect more permeable areas where infiltration is active and the potential exists for failure. The most effective use of this tool would be as a monitoring system, where a baseline survey is acquired for all suspect areas; then, during a flood event, repeat surveys are run using differencing techniques to detect weak points pre-failure. Complications from mode conversions and near-surface dependent propagation characteristics will limit the use of this tool in some settings until

more advanced processing capabilities have been developed. Clearly, more information is present in the seismic wavefield than we currently have the capability to meaningfully extract. Optimized future use of this tool will depend to some degree on acquisition of baseline data sets that will allow full wavefield processing once the methods have been fully developed. Current research in these areas is active and incrementally moving forward with providing solution to many problems encountered in this study.

8—REFERENCES

- Batzle, M., D. Han, and J. Castagna, 1999, Fluids and frequency dependent seismic velocity of rocks [Exp. Abs.]: Soc. Explor. Geophys., p. 5-8.
- Berryman, J.G., P.A. Berge, and B.P. Bonner, 1999, Role of λ -diagrams in estimating porosity and saturation from seismic velocities [Exp. Abs.]: Soc. Explor. Geophys., p. 176-179.
- Chiu, S.K.L., E.R. Kanasevich, and S. Phadke, 1986, Three-dimensional determination of structure and velocity by seismic tomography: *Geophysics*, v. 51, p. 1559-1571.
- Clement, W.P., S. Cardimona, A.L. Endres, and K. Kadinsky-Cade, 1997, Site characterization at the Groundwater Remediation Field Laboratory: *Leading Edge*, v. 16, p. 1617-1621.
- Cottin, J.F., P. Deletie, H. Jacquet-Francillon, J. Lakshmanan, Y. Lemoine, and M. Sanchez, 1986, Curved ray seismic tomography—Application to the Grand Etang Dam (Reunion Island): *First Break*, v. 4, no. 7, p. 25-30.
- Gaffran, Peter, 1999, WAC Bennett Dam Sinkhole Investigation Geophysics Report, Report MEP401, November.
- Glover, R.H., 1959, Techniques used in interpreting seismic data in Kansas: In *Symposium on Geophysics in Kansas*, ed. W.W. Hambleton. Kansas Geological Survey Bulletin 137, p. 225-240.
- Goforth, T., and C. Hayward, 1992, Seismic reflection investigations of a bedrock surface buried under alluvium: *Geophysics*, v. 57, p. 1217-1227.
- Guo, T., and L. Liu, 1999, Non-intrusive evaluation of submarine tunnel foundation using dynamic high-frequency surface wave prospecting: Proceedings of the Symposium on the Application of Geophysics to Engineering and Environmental Problems (SAGEEP 1999), Oakland, Calif., March 14-18, p. 67-74.
- Haeni, F.P., 1978, Computer modeling of ground-water availability in the Pootatuck River valley, Newtown, Connecticut, with a section on quality of water by Elinor H. Handman: U.S. Geological Survey Water Resources Investigations Open-file Report 83-4221.
- Haeni, F.P., 1986, Application of continuous seismic reflection methods to hydrologic studies: *Ground Water*, v. 24, p. 23-31.
- Hunter, J.A., S.E. Pullan, R.A. Burns, R.M. Gagne, and R.L. Good, 1984, Shallow seismic reflection mapping of the overburden-bedrock interface with the engineering seismograph—Some simple techniques: *Geophysics*, v.49, p.1381-1385.
- Ivanov, J.M., C.B. Park, R.D. Miller, and J. Xia, 2000, Mapping Poisson's ratio of unconsolidated materials from a joint analysis of surface-wave and refraction events: Proceedings of the Symposium on the Application of Geophysics to Engineering and Environmental Problems (SAGEEP 2000), Arlington, Va., February 20-24.
- Ivanov, J., 2002, JASR – Joint analysis of surface waves and refractions. Ph.D. dissertation, University of Kansas.
- Ivanov, J., R.D. Miller, J. Xia, and D.W. Steeples, 2005, The inverse problem of refraction traveltimes, part II: Quantifying refraction nonuniqueness using a three-layer model: *Pure and Applied Geophysics*, v. 162, n. 3, p. 461-477.
- Jongerijs, P., and K. Helbig, 1988, Onshore high-resolution seismic profiling applied to sedimentology: *Geophysics*, v. 53, p. 1276-1283.
- Kilty, K.T., and A.L. Lange, 1990, Acoustic tomography in shallow geophysical exploration using a transform reconstruction: Soc. Explor. Geophys. Investigations in Geophysics no. 5, S.H. Ward, ed., *Volume 3: Geotechnical*, p. 23-35.
- Knapp, R.W., and D.W. Steeples, 1986, High-resolution common-depth-point, seismic-reflection profiling: Field acquisition parameter design: *Geophysics*, v. 51, p. 283-294.
- Lankston, R.W., 1990, High-resolution refraction seismic data acquisition and interpretation: Soc. Explor. Geophys. Investigations in Geophysics no. 5, Stan H. Ward, ed., *Volume 1: Review and Tutorial*, p. 45-73.
- Lanz, E., H.R. Maurer, and A.G. Green, 1998, Refraction tomography over a buried waste disposal site, *Geophysics*, v. 63, p. 1414-1433.
- Lytle, R.J., and K.A. Dines, 1980, Iterative ray tracing between boreholes for underground image reconstruction: *Inst. Electr. Electron. Eng. Trans. Geosci. Remote Sensing*, v. GE-18, p. 234-240.
- Michaels, P., 1999, Use of engineering geophysics in the design of highway passing lanes: Proceedings of the Symposium on the Application of Geophysics to Engineering and Environmental Problems (SAGEEP 1999), Oakland, Calif., March 14-18, p. 179-187.
- Miller, R.D., D.W. Steeples, and M. Brannan, 1989, Mapping a bedrock surface under dry alluvium with shallow seismic reflections: *Geophysics*, v. 54, p. 1528-1534.

- Miller, R.D., D.W. Steeples, and P.B. Myers, 1990, Shallow seismic-reflection survey across the Meers fault, Oklahoma: *GSA Bulletin*, v. 102, p. 18-25.
- Miller, R.D., and D.W. Steeples, 1991, Detecting voids in a 0.6-m coal seam, 7 m deep, using seismic reflection: *Geo-exploration*, Elsevier Science Publishers B.V., Amsterdam, The Netherlands, v. 28, p. 109-119.
- Miller, R.D., N.L. Anderson, H.R. Feldman, and E.K. Franseen, 1995, Vertical resolution of a seismic survey in stratigraphic sequences less than 100 m deep in Southeastern Kansas: *Geophysics*, v. 60, p. 423-430.
- Miller R.D., and J. Xia, 1999, Using MASW to map bedrock in Olathe, Kansas: Kansas Geological Survey Open-file Report 99-9.
- Miller, R.D., J. Xia, C.B. Park, and J.M. Ivanov, 1999, Multichannel analysis of surface waves to map bedrock: *Leading Edge*, v. 18, n. 12, p. 1392-1396.
- Miller, R.D., T.S. Anderson, J.C. Davis, D.W. Steeples, and M.L. Moran, 2001, 3-D characterization of seismic properties at the Smart Weapons Test Range, YPG: Proceedings of the Military Sensing Symposium on Battlefield Seismic and Acoustic Sensing, October 23-25, Laurel, Maryland, Published on CD.
- Mooney, H.M., 1981, Handbook of engineering geophysics: Bison Instruments, Inc.
- Nazarian, S., K.H. Stokoe II, and W.R. Hudson, 1983, Use of spectral analysis of surface waves method for determination of moduli and thicknesses of pavement systems: Transportation Research Record No. 930, p. 38-45.
- Palmer, D., 1981, An introduction to the generalized reciprocal method of seismic refraction interpretation: *Geophysics*, v. 46, p. 1508-1518.
- Park, C.B., R.D. Miller, D.W. Steeples, and R.A. Black, 1996, Swept impact seismic technique (SIST): *Geophysics*, v. 61, p. 1789-1803.
- Park, C.B., R.D. Miller, and J. Xia, 1999, Multichannel analysis of surface waves (MASW): *Geophysics*, v. 64, p.800-808.
- Peterson, J.E., B.N.P. Paulsson, and T.A. McEvelly, 1985, Applications of algebraic reconstruction techniques to cross-hole data: *Geophysics*, v. 53, p. 1284-1294.
- Pullan, S.E., and J.A. Hunter, 1990, Delineation of buried bedrock valleys using the optimum offset shallow seismic reflection technique: Soc. Explor. Geophys. Investigations in Geophysics no. 5, S.H. Ward, ed., *Volume 3: Geotechnical*, p. 75-87.
- Redpath, B.B., 1973, Seismic refraction exploration for engineering site investigations, NTIS AD-768710.
- Sander, J.E., 1978, The blind zone in seismic ground-water exploration: *Ground Water*, v. 165, p. 394-397.
- Schepers, R., 1975, A seismic reflection method for solving engineering problems: *Journal of Geophysics*, v. 41, p. 267-284.
- Schneider, W.A., Jr., K.A. Ranzinger, A.H. Balch, and C. Kruse, 1992, A dynamic programming approach to first arrival traveltimes computation in media with arbitrarily distributed velocities: *Geophysics*, v. 57, p. 39-50.
- Scott, J.H., 1973, Seismic refraction modeling by computer, *Geophysics*, v. 38, p. 271-284.
- Scott, J.H., 1977, SIPT—A seismic refraction inverse modeling program for timeshare terminal computer systems: U.S. Geological Survey Open-file Report 77-365.
- Shtivelman, V., U. Frieslander, E. Zilberman, and R. Amit, 1998, Mapping shallow faults at the Evrona playa site using high-resolution reflection method: *Geophysics*, v. 63, p. 1257-1264.
- Soske, J.L., 1954, The blind zone problem in engineering geophysics: *Geophysics*, v. 24, p. 359-365.
- Steeple, D.W., and R.D. Miller, 1990, Seismic reflection methods applied to engineering, environmental, and groundwater problems: Soc. Explor. Geophys. Investigations in Geophysics no. 5, S.H. Ward, ed., *Volume 1: Review and Tutorial*, p. 1-30.
- Steeple, D.W., C.M. Schmeissner, and B.K. Macy, 1995, The evolution of shallow seismic methods: *Journal of Environmental and Engineering Geophysics*, v. 0, n. 1, p. 15-24 (invited paper).
- Steinhart, J.S., and R.P. Meyer, 1961, Explosion studies of continental structure: Carnegie Institution of Washington Publication 622.
- Stokoe II, K.H., S.G. Wright, J.A. Bay, and J.M. Roësset, 1994, Characterization of geotechnical sites by SASW method: in *Geophysical Characterization of Sites*, ISSMFE Technical Committee #10, ed. R.D. Woods, Oxford Publishers, New Delhi.
- Xia, J., R.D. Miller, and C.B. Park, 1999, Estimation of near-surface velocity by inversion of Rayleigh waves: *Geophysics*, v. 64, p. 691-700.
- Xia, J., R.D. Miller, C.B. Park, J.A. Hunter, J.B. Harris, and J. Ivanov, 2002, Comparing shear-wave velocity profiles from multichannel analysis of surface wave with borehole measurements: *Soil Dynamics and Earthquake Engineering*, v. 22, n. 3, p. 181-190.
- Yilmaz, O., 1987, Seismic data processing; S.M. Doherty, ed.; in Series: Investigations in Geophysics, no. 2, E.B. Neitzel, series ed.: Soc. Explor. Geophys.

Appendix F

Report on SP Surveys

Self-Potential Monitoring of Seepage Flow

Levee Ponding Field Test

Retamal Levee, San Juan, TX, November 8 - 16, 2004

Prepared for:

U.S. Army Corps of Engineers
ERDC-WES
3909 Halls Ferry Road
Vicksburg, MS 39180

Prepared by:

Robert F. Corwin, Ph.D.
Consulting Geophysicist
406 Sea View Drive
El Cerrito, CA 94530
(510) 527-2081

April 28, 2005

CONTENTS

	<u>page</u>
1.0 SUMMARY	1
2.0 INTRODUCTION	1
3.0 DATA ACQUISITION	1
4.0 MONITORING RESULTS	3
4.1 Time Series Plots	3
4.1.1 Description of Time Series Plots	3
4.1.2 Analysis of Time Series Plots	4
4.2 Spatial Profile Plots	6
5.0 CONCLUSIONS AND RECOMMENDATIONS	7
REFERENCES	8

TABLES

Table 1. Summary of SP Monitoring Data Files
Table 2. Wiring Color Code
Table 3. Example of Combined Logging Configuration File
Table 4. Example of Individual Logger Configuration File
Table 5. Pond Water Elevation and Geophysical Measurement Schedule

FIGURES

Figure 1. Sketch of Pond Test Site (from Dunbar et al., 2004)
Figure 2. SP Monitoring Electrode Layout
Figure 3. Sketch of Data Acquisition Arrangement
Figure 4. Example SP Monitoring Data File
Figure 5. SP Monitoring Data for Line C (Upstream Face)
Figure 6. SP Monitoring Data for Line D (Upstream Crest)
Figure 7. SP Monitoring Data for Line A (Downstream Crest)
Figure 8. SP Monitoring Data for Line B (Downstream Face)
Figure 9. SP Profile Plots for Lines A, B, C, and D, 03:43, 8 November (Before Filling)
Figure 10. SP Profile Plots for Lines A, B, C, and D, 00:59:48, 12 November (Pond Full, Elev. 93.7 ft)
Figure 11. SP Difference Profiles for Lines A, B, C, and D (Pond Full - Pond Empty)

APPENDIXES

Appendix 1. Trip Report: Levee Ponding Field Test, Retamal Levee, San Juan, TX, 8 to 16 November 2004 (Dunbar et al., 22 November 2004)
Appendix 2. SP Data Files and Plots

1.0 SUMMARY

Self-potential (SP) data can be used to help detect subsurface seepage flow. An SP monitoring system was installed on Retamal Levee, San Juan, Texas in November 2004 as part of a geophysical investigation conducted in conjunction with a ponding field test. SP measurements were made during the course of the test as the water level within the pond was raised and lowered. The SP data were of good quality, and showed no obvious evidence for the development of either uniform or concentrated seepage flow within the levee.

2.0 INTRODUCTION

This report presents a brief summary of the results of an SP monitoring investigation performed as part of a levee ponding field test conducted between 8 and 16 November, 2004 on a section of Retamal Levee, San Juan, Texas. The background and purposes of the ponding test are described in Dunbar et al. (2003) and in Dunbar et al. (2004), which is included as Appendix 1 of this report. The SP method and its application to seepage flow investigations in impoundment structures such as dams and levees are described in Corwin (1989, 1990a, 1990b).

The major objective of the SP monitoring component of this project was to help determine the location and nature of any seepage flow occurring in response to water impoundment within the section of the levee downstream of the pond. As described in the references above, seepage flow typically generates SP anomalies that show negative polarity associated with the upstream portion of the seepage flow path and positive polarity associated with the downstream portion. Analysis of the shape and wavelength of the SP anomalies can help to determine the depth and configuration of seepage flow paths. If sufficient supporting information is available (electrical resistivity, hydraulic conductivity, SP coupling coefficients, and geologic structure), estimates of seepage flow rates also can be made from the SP data. Because no significant SP anomalies were observed during the course of this test, no estimates of seepage depth or flow rate were performed for this report.

In addition to the SP monitoring, the ponding test included measurements of water conductivity and of the electrical resistivity of the levee soils. Changes in the electrical resistivity values can indicate corresponding changes in water saturation values related to the development of seepage flow. Also, the water conductivity and electrical resistivity values influence the SP data. Therefore some preliminary results of the resistivity monitoring and water conductivity measurements are discussed in this report.

The directional terms "riverside (R/S)" and "landside (L/S)" typically are used for levee orientation. For consistency with interpretation nomenclature developed for dam seepage analysis, this report uses the corresponding dam orientation terms "upstream (U/S)" and "downstream (D/S)".

3.0 DATA ACQUISITION

The SP monitoring was conducted using an array of 84 measuring electrodes. The electrodes were FARWEST Model SP-150, which use a plaster filling material saturated with copper-copper sulfate electrolyte. These electrodes are designed for stable, long-term measurement of SP values for corrosion monitoring and other applications.

The general layout of the SP and resistivity monitoring lines is shown on Figure 1 (from Dunbar et al., 2004). Specific electrode locations are shown on Figure 2. Nominal electrode separation was 2.5 feet (this value is incorrectly listed as 2 feet on Figure 3 of Dunbar et al., 2004). The electrodes for each line were connected to a cable running to the data logger for that line. For Line A, each electrode was connected to an individual conductor that extended all the way to the data logger. The conductors were bundled

together, and each conductor was labeled with a tag at the data logger input. For Lines B, C, and D, the individual conductors were spliced to a multiconductor cable (Carol # C4075, 20-conductor) that extended to the data loggers. The color code for these three cables is shown on Table 2. All splices were waterproofed to allow direct burial or water submersion.

As shown in Figures 2 and 3 of Dunbar et al., 2004, the electrodes were installed in trenches dug to a depth of about 1 foot and were covered with paper plates and soil to protect them from sun and direct rainfall. The soil in which the electrodes were buried was moist and contained significant clay content. Measured electrode contact resistance was low, of the order of 1 Kohm, resulting in relatively rapid electrode stabilization and low intrinsic electrode noise levels (see below).

Figure 3 shows a sketch of the data acquisition (DAQ) system. Each of the four electrode cables was connected to the input module of a Fluke Model 2620A 21-channel data logger. For each cable, electrode 1 was connected to channel 1 of the logger, electrode 2 to channel 2, etc. Channel 0 of each logger was connected to one of the auxiliary electrodes E1, E2, or E4 as shown on Figures 2 and 3.

The base station for all the measurements was electrode E3, located 160 ft east of electrode A20 as shown on Figure 2. This electrode was connected to the common input of all four data loggers. The common inputs for all 21 channels were connected together within each of the input modules.

The data loggers were controlled through a serial connection to the DAQ computer. Use of a port combiner as shown on Figure 3 allowed a single computer to control all four loggers. DAQ control was performed by QuickBasic program MLTHYDRA, loaded onto the hard drive of the computer. A copy of the code was provided to USACE. The data file names, scanning intervals, and other DAQ parameters were set by configuration files MONITOR.CFG and HYDRA[1-2-3-4].CFG. Copies of these files were provided to USACE. Examples of the configuration files are shown on Tables 3 and 4.

The computer was programmed to scan each of the four loggers in sequence and to write the measured data from each logger to a separate file. Data file names were specified in the HYDRA[1-2-3-4].CFG files and were automatically incremented each time the maximum number of readings had been made. For the example of Table 4, the first data set was written to file LINEA001.MON, the second to file LINEA002.MON, etc. The scanning interval was set at two minutes, and each scan took a few seconds. Four individual data files, one for each logger, were written every two minutes; and each file comprised 360 scans. Thus each data file spanned an interval of (2 X 360) minutes, or 12 hours.

A portion of a representative data file is shown on Figure 4. The first column is the line number of the reading. This number started at 1 and incremented continuously throughout the monitoring process, providing a plotting parameter independent of the date or time. The second column is the time of day in H:M:S format, and the third is time of day in decimal format. The following columns are the measured SP values for data channels V0 - V20 in millivolts (mV).

The SP monitoring files are listed in Tables 1A and 1B. Monitoring was initiated on a computer labeled "Laptop-1" at 11:03 on 6 November 2004, with data written to files LINEA001.MON, LINEB001.MON, LINEC001.MON, and LINED001.MON (Table 1A). On 10 November, DAQ was switched to a computer labeled "Laptop-2", with data written to files LBAKA001.MON, LBAKB001.MON, LBAKC001.MON, and LBAKD001.MON (Table 1B). As shown on Table 1B, the line numbers were re-started when the DAQ computer was changed. All of the *.MON files were stored on the hard drives of the respective computers, and were backed up on disk by USACE personnel on site.

4.0 MONITORING RESULTS

As described in Corwin (1989, 1990a, 1990b), the expected SP response to seepage flow comprises negative variations associated with areas of seepage inflow and positive variations associated with areas of seepage outflow. If the seepage is concentrated along one or more individual paths, this type of response should be observed at the monitoring electrodes closest to each path.

In this report, the monitored SP data are displayed both as time series and as spatial profiles. The time series plots (Figures 5 - 8) span the SP monitoring period from 6 through 16 November 2004, and show SP profiles for selected electrodes. The spatial profiles (Figures 9 - 11) show SP profiles for all the electrodes along a single monitoring line (A, B, C, or D) at a given instant of time. Additional time series plots and spatial profiles are shown in Appendix 2 of this report. This appendix was prepared by Ms. Sarah Jackson, working directly for USACE

4.1 Time Series Plots

4.1.1 Description of Time Series Plots

Figures 5, 6, 7, and 8 show SP time series plots in upstream-to-downstream sequence (Lines C, D, A, and B respectively). Each of these plots also includes a profile of the pond water surface elevation. Table 5 shows the general schedule of pond filling/emptying and SP - DC geophysical operations.

Figure 4 shows the format of the data files from which the SP plots were generated. For plotting purposes, the data files for "Laptop-1" and "Laptop-2" were combined into a single file at about line 2910 (the end of the "Laptop-1" files), so the line numbers (column A on the data files, line header labeled "N") were transformed to a continuous sequence from line 1 to about line 7161.

Note on Figure 4 that a number of the data lines show readings that deviate strongly from the average values in the column. These are readings that were affected by the DC resistivity data transmission, and are not usable for the SP analysis. Also, if retained, the density of these affected readings made it very difficult to observe the desired longer-term SP data trends indicative of seepage development. An effort was made to remove these affected readings from the SP data files before plotting. This involved manually deleting each of the several hundred affected data lines from the plotted files A_13.DAT through D_13.DAT. The listing below shows the number of readings that were deleted from each file.

Data File	A 13	B 13	C 13	D 13
Orig. no. of file lines	7161	7162	7162	7162
Final no. lines in file	6419	6350	6411	6352
No. of lines deleted	742	812	751	810

As is evident on the plots, a number of data spikes escaped this editing process, but their density is not great enough to obscure the general longer-term SP trends of interest.

For the time series plots shown in Appendix 2, removal of the affected lines was accomplished by clipping the displayed values for each data column to a maximum and minimum value. This is a much faster process than line-by-line deletion, but valid SP readings also may be lost using this process. However, the main long-term trends of primary interest for this investigation generally are still preserved in these plots.

For Figures 5 - 8, profiles for electrodes from the following five electrodes are shown:

Electrode	V1	V5	V10	V15	V20
Dist. from West end of pond (ft)	0	12.5	25.0	37.5	47.5

As listed in Table 1C, additional profiles for electrodes E1 (8 ft west of A1) and E2 (10 ft east of A20) also are plotted on Figure 7 (Line A; downstream crest). This set of electrodes was chosen to provide an evenly-spaced sampling distribution across each of the four monitoring lines while avoiding excessive detail on the plots. The SP effects of a significant path of concentrated seepage flow should be visible at this 12.5 ft spacing, although some detail may be lost for a shallow path exhibiting a short-wavelength anomaly. Time profile plots for the remaining electrodes, shown in Appendix 2, can be used to fill in the details of any such short-wavelength spatial variations.

4.1.2 Analysis of Time Series Plots

Long-term readings of SP monitoring electrodes typically stabilize within a few hours to a day after installation. Following stabilization, the intrinsic short-term (reading-to-reading) electrode noise level in the low-resistivity soil at this site would not be expected to exceed a few tenths of a mV. Therefore, if there were no disturbances from outside effects, the plots of Figures 5 - 8 would consist of a series of almost flat, level, parallel lines.

As noted above, the typical SP signature of seepage flow is a negative variation above the upstream portion of the flow path, transitioning to positive values along the downstream portion of the path. If the seepage path is laterally concentrated, the strongest negative and positive variations generally will be centered approximately above the area of greatest flow. For the monitoring arrangement used for this test, this type of variation would appear on the time profile plots as a developing negative trend, deviating from the surrounding parallel profiles, for the plot of the monitoring electrode above the inflow area on the upstream monitoring lines (C and D). The amplitude of the variation would be expected to correlate with the seepage flow rate (although there may be a phase lag between pond elevation changes and seepage flow rates within the embankment). A corresponding positive deviation from the general parallel trend would be seen at the electrodes above the downstream portion of the flow path (Lines A and B). These seepage-related variations would be superimposed on the other sources of SP variations described below.

Aside from seepage effects, the major expected sources of external SP variations are diurnal temperature variations and telluric voltages generated by geomagnetic activity. Temperature variations are responsible for the approximate 24-hour periodicity of up to (+/-) a few mV amplitude visible on all the profiles. These temperature-related variations could have been reduced by burying the electrodes deeper, but this would have made it difficult to remove the electrodes following completion of the test. Although prominent, these temperature-induced variations should not obscure longer-term seepage-related trends of the type described above.

Because the amplitude of SP variations caused by both telluric activity and seepage flow is affected by the electrical resistivity of the embankment, the results of the resistivity monitoring tests are briefly summarized below. This information was obtained from preliminary measured and inverted resistivity sections provided by USACE. Measured pond water resistivity was about 5.9 ohm-m (see Table 5).

Resistivity monitoring line no.	Location	Approx. avg. elev. (ft)	Approx. resistivity range (ohm-m)
1	U/S Crest (@ SP Line D)	95.5	5-10
2	D/S Face (@ SP Line B)	90	5-15
3	D/S Toe	86	5-20

The listed resistivities are those observed for the bulk of the embankment. These values are relatively low, and suggest that the soil is clay-rich. It would be expected that the amplitude of SP variations caused by

telluric activity ("noise" for this investigation) and seepage flow ("signal" for this investigation) would be correspondingly low compared with levels measured in higher-resistivity environments.

Comparison of resistivity profile sections measured on 10-11 November (when filling of the pond had just begun) with those measured on 16 November (when the pond surface elevation was about 86 ft and was decreasing rapidly) showed remarkably little change. This suggests that water saturation levels within the embankment changed very little during the course of the test, implying that little or no uniform or concentrated seepage flow entered the embankment during the test period. This also implies that the SP readings were not affected by changes of embankment resistivity during the course of the test.

An extremely powerful magnetic storm occurred between 7 and 12 November, reaching planetary magnetic Kp index readings of 9 on November 8 through 10 (storms of this intensity generally occur only once or twice a year during this portion of the solar cycle). The effects of this storm are clearly evident on Figures 5 - 8 as a higher short-period noise level for the SP readings during the period of 7 - 12 November compared with those after 12 November. This is especially evident on the generally quieter downstream lines (A and B). The large SP deviations on 7 November probably are due to a combination of magnetic storm onset and electrode stabilization effects.

Based on the preceding discussion, results from each of the monitoring lines are briefly described below in upstream-to-downstream order.

Line C (upstream face; Figure 5). The most notable feature of these profiles is the large positive jump that occurred on 10 November. This was caused by submersion of the electrodes beneath the water surface, and the resulting saturation of the soil, when the pond elevation reached Line C at an elevation of 90.7 ft. Positive differences of several mV are typical of SP readings between unsaturated soil (e.g., at the base station) and fully saturated soil. Because the soil remained saturated, the readings stayed positive even after the surface elevation dropped below 90.7 ft on 14 November.

The positive offset for electrode C5 on 10 November is larger than that for the other profiles. This probably was due to differing soil conditions at this station. The positive spike on this profile on 15 November was not seen on the adjacent electrodes (C4 and C6) or on Line D, so its localized nature does not indicate any significant seepage activity.

In general, the monitored data for Line C do not seem to indicate development of significant uniform or concentrated seepage flow within the embankment in response to the filling of the pond. There does appear to be a small overall negative trend of the profiles between 10 and 16 November. As discussed later, this could indicate some degree of uniform seepage flow beneath the base of the embankment.

Line D (upstream crest; Figure 6). The profiles for this line show no correlation with water elevation that would indicate development of uniform seepage flow through the embankment. With the exception of the temperature and magnetic storm effects described previously, the profiles remain generally parallel and show no indication of the development of concentrated seepage.

Line A (downstream crest; Figure 7). In addition to the five profiles shown on the other plots (X = 0, 12.5, 25, 37.5, and 47.5 ft), Figure 7 shows profiles for electrodes E1 (X = -8 ft) and E2 (X = 57.5 ft). The profiles for X = -8, 0, 12.5, and 25 ft remain relatively flat and parallel throughout the entire monitoring period. The three profiles at the eastern end of this line (X = 37.5, 47.5, and 57.5 ft) show considerable variation before 10 November, but then appear to "settle in" before the pond reaches maximum elevation. In general, the profiles for Line A show no correlation with water elevation that would indicate development of uniform seepage flow through the embankment, nor do they show any indication of the development of concentrated seepage.

Line B (downstream face; Figure 8). The profiles for this line show little variation and remain generally parallel throughout the entire monitoring period. They show no correlation with water elevation that would indicate development of uniform seepage flow through the embankment, nor do they show any indication of the development of concentrated seepage. The general overall positive trend of the profiles with time on Line B mirrors the overall negative trend seen on upstream face Line C, and could indicate some degree of deep, uniform seepage flow at the base of or beneath the embankment.

4.2 Spatial Profile Plots

Figures 9 - 11 show profile plots for all the electrodes on each of the four monitoring lines. Times and elevations for these plots are listed below.

Figure	9	10	11
Date(s) (Nov. 2004)	8	12	(12-8)
Time	03: 43	00: 59	-
Water Elevation (ft)	82. 2 (empty)	93. 7 (max.)	(max. - empty)

Figure 9 shows data taken with the pond empty, before filling of the pond had started. Figure 10 shows data taken with the pond at its maximum elevation (93.7 ft), just before draining began. Figure 11 shows the differences between the profiles of Figures 10 and 9.

For the empty-pond condition, the profiles of Figure 9 would be expected to be essentially level and to show point-to-point variations of (+/-) a few mV, corresponding to the geologic noise level at this site. With the exception of one point (Line A, X = 35.0 ft), this appears to be the case. The deviation at this electrode probably was due to poor soil contact at the time of installation, as this electrode appeared to "settle in" later. The average offset level for the four profiles is about +5 mV with respect to the survey base electrode E3.

Due to scheduling considerations, the SP monitoring was terminated before the pond was fully emptied (pond elevation was about 86 ft when SP monitoring ended at 14:49 on 16 November). Therefore it is not possible to perform before-and-after comparisons of SP data with the pond empty.

With the pond full, any seepage flow through the embankment would be expected to affect the SP profiles. Uniform seepage through the body of the embankment would be expected to produce uniform negative shifts of the base levels of the upstream lines (C and D) and positive shifts of the downstream lines (A and B). Concentrated seepage would be expected to produce a negative variation centered at one or more electrodes above the seepage inflow area, with a corresponding positive variation above the downstream portion of the flow path.

No evidence of either of these effects is observed on the full-pond profiles of Figure 10. On Figure 10, the profiles for Lines A, B, and D are similar to those on Figure 9, with the average offset with respect to the base electrode remaining at about +5 mV. The spike at X = 35.0 ft on Line A is gone. As discussed previously, the positive shift of about +7 mV for the profile of Line C was due to submergence of the electrodes and consequent saturation of the soil. The higher point-to-point noise level on Line C, compared with that seen on Figure 9, probably was due to localized differences in the response of the electrodes to increasing soil saturation levels. In general, there is no obvious sign of a laterally-restricted negative-upstream - positive-downstream pattern that would indicate a path of concentrated seepage flow.

The difference profiles of Figure 11 provide another way of observing possible SP changes between empty and full pond conditions. The difference profiles for Lines A, B, and D show an average base shift of close to zero, indicating little or no uniform seepage flow through the embankment. The positive spike

at X = 35.0 ft on Line A is due to the deviation at the time of installation rather than any change due to seepage flow. Taken together, the four difference profiles show no obvious pattern of laterally-restricted negative-upstream - positive-downstream variations that would indicate the development of a path of concentrated seepage flow.

The data shown on Figures 9 - 11 show profile "snapshots" at only two points of time. Additional profile plots were provided in a preliminary field report delivered to USACE on 23 November 2004; and a set of profile plots, listed below, is included in Appendix 2.

Profile Plots Included in Appendix 2

Date (Nov. 2004)	8	9	10	11	12	14	16
Time	1000	0200	0200	2300	0200	0200	0200
Water El ev. (ft)	82. 2	84. 6	88. 3	93. 7	93. 7	91. 7	88. 2

These additional profile plots appear similar to those discussed above, showing no consistent SP variations characteristic of either uniform or concentrated seepage flow during the course of filling or emptying the pond.

5.0 CONCLUSIONS AND RECOMMENDATIONS

The SP monitoring system was installed successfully and operated as designed, with no significant problems. The monitored data showed generally low levels of both geologic and time-varying noise, as expected in the low-resistivity soil characteristic of this site. A powerful magnetic storm that occurred during the initial portion of the program increased the short-period noise level, but did not obscure longer-period trends that would be associated with seepage-generated SP variations.

The SP data were inspected in the form of both time series (plots of individual electrode readings vs. time) and spatial profiles (plots of the readings for all the electrodes along a given monitoring line at a single point of time). None of the data showed any obvious indication of the development of either uniform or concentrated seepage flow within the embankment in response to changing water levels within the pond. These results suggest that the embankment soil was of very low permeability, and that there were no cracks or other features that allowed significant water flow through the embankment.

Any SP signals generated by seepage flow in this low-resistivity soil would be expected to be of small amplitude. It is possible that such signals were present in the data but were not detected. Thus it is important to examine all the available geophysical and geotechnical information from this investigation to confirm the SP interpretation.

It would be interesting to repeat a test of this type on a levee constructed of coarser-grained soils. All the SP equipment and software used for this test were retained by USACE, and only the Hydra data loggers would have to be provided to complete the instrumentation. If the test is repeated, it would be helpful to install the electrodes several days before beginning the test to allow establishment of baseline levels; and to continue the monitoring for a few days following emptying of the pond.

REFERENCES

- Brown, B.P., and Dunbar, J.B., 2004, Assessment of Foundation Systems, Rio Grande Levees - An Update: FastTimes (EEGS), v. 9, no. 4, Winter 2004, p. 15-19.
- Corwin, R.F., 1989, Development of self-potential interpretation techniques for seepage detection: Technical Report REMR-GT-6, no.3, U.S. Army Corps of Engineers, U.S. Army Engineer Waterways Experiment Station.
- Corwin, R.F., 1990a, The self-potential method for environmental and engineering applications: Geotechnical and environmental geophysics, Vol. I, S.H. Ward, ed., Soc. Explor. Geophys., Tulsa, OK, p. 127-145.
- Corwin, R.F., 1990b, Applications of the self-potential method for engineering and environmental investigations: Proceedings of the Symposium on the Application of Geophysics to Engineering and Environmental Problems (SAGEEP), EEGS, Englewood, CO, p. 107-120.
- Dunbar, J., Llopis, J., and Smith, E., 2004, Trip Report: Levee Ponding Field Test, Retamal Levee, San Juan, TX, 8 to 16 November 2004: Report prepared for ERDC-WES, 22 Nov. 2004.
- Dunbar, J.B., Stefanov, J.E., Bishop, M.J., Peyman-Dove, L., Llopis, J.L., and Ballard, R.F., 2003, An Integrated Approach for Assessment of Levees in the Lower Rio Grande Valley: Presented at SAGEEP Annual Meeting, 2003.

TABLES

TABLE 1

SUMMARY OF SP MONITORING DATA FILES

A. FILES FROM LAPTOP #1

FILENAME (*MON)	DATE (NOV. 2004)	START TIME	END TIME	START LINE	END LINE	SIZE (KB)
LINE[ABCD]001	06	1103	2335	1	360	78.5
LINE[ABCD]002	06	2337	2359	361	372	3.0
LINE[ABCD]003	07	0001	1205	373	732	78.5
LINE[ABCD]004	07	1207	0001	733	1089	77.9
LINE[ABCD]005	08	0003	1202	1090	1449	78.5
LINE[ABCD]006	08	1204	0001	1450	1808	78.3
LINE[ABCD]007	09	0003	1201	1809	2168	78.5
LINE[ABCD]008	09	1203	0000	2169	2525	78.1
LINE[ABCD]009	10	0000	1200	2526	2885	78.5
LINE[ABCD]010	10	1200	1253	2886	2911	6.0

B. FILES FROM LAPTOP #2

FILENAME (*MON)	DATE (NOV. 2004)	START TIME	END TIME	START LINE	END LINE	SIZE (KB)
LBAK[ABCD]001	10	1419	2400	1	291	63.5
LBAK[ABCD]002	11	0000	1200	292	651	78.5
LBAK[ABCD]003	11	1200	2400	652	1010	78.2
LBAK[ABCD]004	12	0000	1200	1011	1370	78.5
LBAK[ABCD]005	12	1200	2400	1371	1658	63.0
LBAK[ABCD]006	13	0000	1200	1659	2018	78.5
LBAK[ABCD]007	13	1200	2400	2019	2378	78.5
LBAK[ABCD]008	14	0000	1200	2379	2738	78.5
LBAK[ABCD]009	14	1200	2400	2739	3097	78.2
LBAK[ABCD]010	15	0000	1200	3098	3457	78.5
LBAK[ABCD]011	15	1200	2400	3458	3816	78.2
LBAK[ABCD]012	16	0000	1218	3817	4176	78.6
LBAK[ABCD]013	16	1220	1449	4177	4251	16.6

C. DATA FILES FOR FIGURES 5 - 8

FIGURE	FILE (*.GRF)	COMBINED FILES	PLOT FILE	PLOTTED ELECTRODES
5	C_LINE	LINE_C*. MON + LBAKC*. MON	C_13. DAT	C1 C5 C10 C15 C20
6	D_LINE	LINE_D*. MON + LBAKD*. MON	D_13. DAT	D1 D5 D10 D15 D20
7	A_LINE	LINE_A*. MON + LBAKA*. MON	A_13. DAT	E1 A1 A5 A10 A15 A20 E2
8	B_LINE	LINE_B*. MON + LBAKB*. MON	B_13. DAT	B1 B5 B10 B15 B20

TABLE 2
WIRING COLOR CODE
(Cables B, C, and D)

Notes:

- * Commons shorted together in input module connector and connected to front panel common input (see Figure 3)
- * Cable: Carol C4075 (20-conductor, 22 AWG)
- * Electrode number corresponds to data logger channel and data file column (i.e., electrode no. 1 is connected to logger channel 1 and recorded as V1, etc.)

<u>COLOR CODE</u>		
electrode no.	Main color	stripe color

1	black	none
2	white	none
3	red	none
4	green	none
5	orange	none
6	blue	none
7	white	black
8	red	black
9	green	black
10	orange	black
11	blue	black
12	black	white
13	red	white
14	green	white
15	blue	white
16	black	red
17	white	red
18	orange	red
19	blue	red
20	red	green

TABLE 3

EXAMPLE OF COMBINED LOGGING CONFIGURATION FILE
(MONITOR.CFG)

Configuration file for SP Monitoring

4 Number of Hydras
hydra1.cfg Filename of first Hydra
hydra2.cfg Filename of second Hydra
hydra3.cfg Filename of third Hydra
hydra4.cfg Filename of fourth Hydra
120 Number of seconds between scans, min=30, max=600
RATE 0 Command string to set hydra rate, RATE 0 is slow, RATE 1 is fast
360 Number of lines per file, 500 lines is about 110K bytes
0 Starting Xmin for graph (minutes)
30 Starting Xmax for graph (minutes)
30 Value to increment x-axis by when xmax is exceeded (minutes)
-200 Starting Ymin for graph (mV)
200 Starting Ymax for graph (mV)

TABLE 4

EXAMPLE OF INDIVIDUAL LOGGER CONFIGURATION FILE
(HYDRA1.CFG)

Hydra Configuration file for SP Monitoring

```
FUNC 0,VDC,2      Channel setup commands
FUNC 1,VDC,2      Channels are 0 to 20. Use OFF to turn off a
FUNC 2,VDC,2      channel (delete the 2 when off). Use VDC
FUNC 3,VDC,2      to set volts DC. 2 is for 2 -ranging.
FUNC 4,VDC,2      Fixed ranges are: 300mV, 3000 mV, 30 V, 300 V.
FUNC 5,VDC,2      Enter ranges as: 1 , 2 , 3 , 4 .
FUNC 6,VDC,2      See page 4-32 in Hydra manual
FUNC 7,VDC,2
FUNC 8,VDC,2
FUNC 9,VDC,2
FUNC 10,VDC,2
FUNC 11,VDC,2
FUNC 12,VDC,2
FUNC 13,VDC,2
FUNC 14,VDC,2
FUNC 15,VDC,2
FUNC 16,VDC,2
FUNC 17,VDC,2
FUNC 18,VDC,2
FUNC 19,VDC,2
FUNC 20,VDC,2      End of channel command entries
Enter on the next line the first data file header ----->|
HYDRA 1 LINE A CABLE A D/S CREST
Enter on the next line the second data file header ----->|
SCAN INTERVAL 120 SEC 360 LINES/FILE SLOW RATE 3 V RANGE
LINEA      SP voltage file name, 5 characters only, no extension
```

TABLE 5

POND WATER ELEVATION AND GEOPHYSICAL MEASUREMENT SCHEDULE

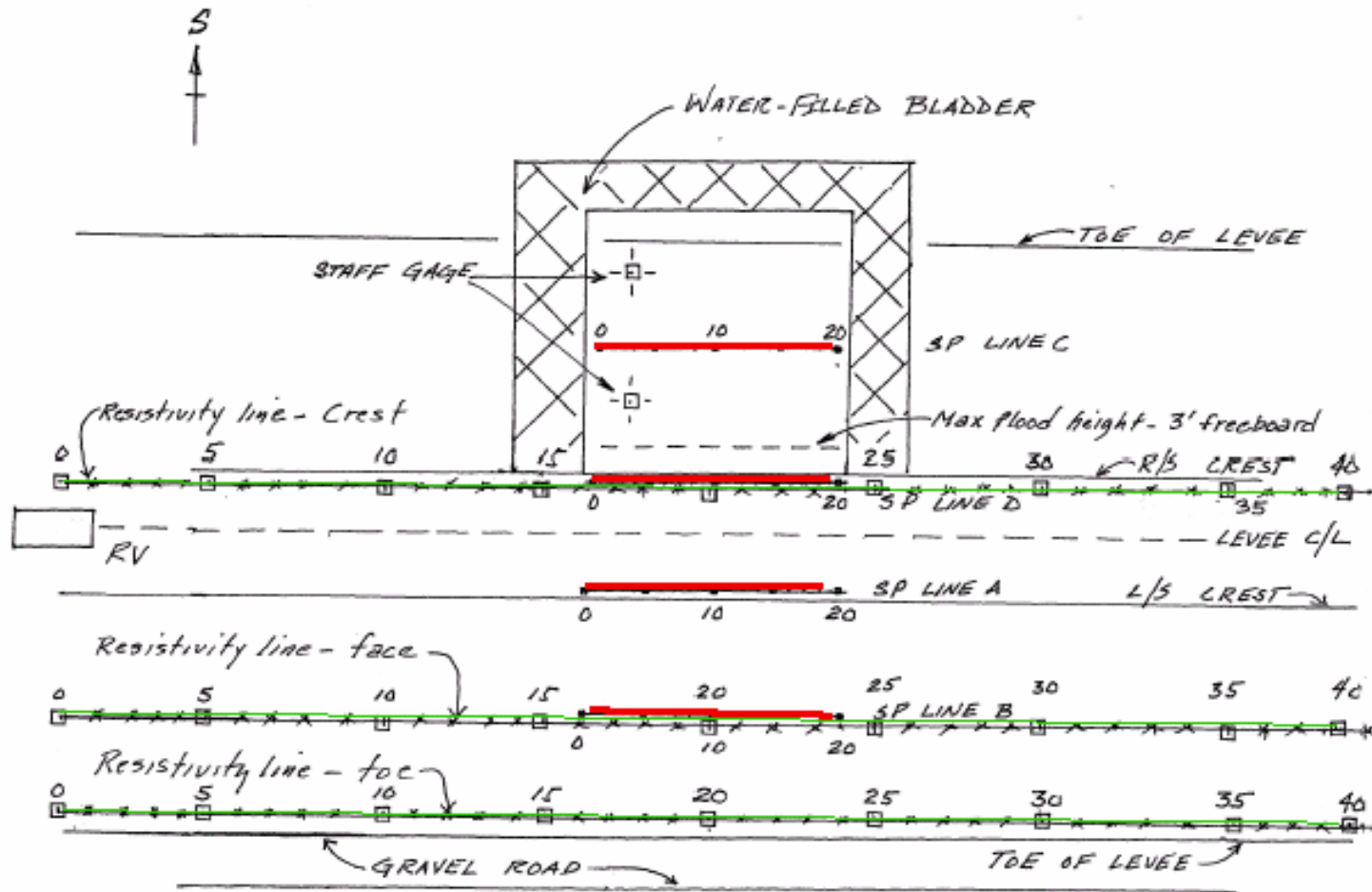
Date (Nov. 2004)	Time	Operation
6	11:03	Begin SP monitoring
8	10:00	Begin filling pond (base elevation 82.2 ft)
8	-	Begin DC resistivity monitoring
11	12:00	At maximum pond water elevation (93.7 ft)
12	02:00	Begin lowering pond water level
16	14:49	End SP monitoring (pond elevation 86.3 ft)
16	-	End DC resistivity monitoring
17	04:00	Pond empty (base elevation 82.2 ft)

Water Conductivity Data (8 November 2004)

Time	Water Elev. (ft NGVD)	Conductivity (mS/cm)	Temperature (deg. C)	Salinity (ppt)	Resistivity (ohm-m)
13:00	83.3	1.7	23.5	-	5.9
14:00	83.5	1.7	23.5	0.9	5.9
15:00	83.7	1.7	23.5	0.9	5.9
16:00	83.8	1.7	23.6	0.9	5.9

FIGURES

(From Dunbar et al., 2004)



F-19

Figure 1. Sketch of pond test site showing position of pond, riverside (R/S) of levee. View is facing south. SP lines are highlighted red and labeled A, B, C, and D. Resistivity lines are highlighted green and are located on R/S crest, and landside (L/S) face and toe of levee.

F-20

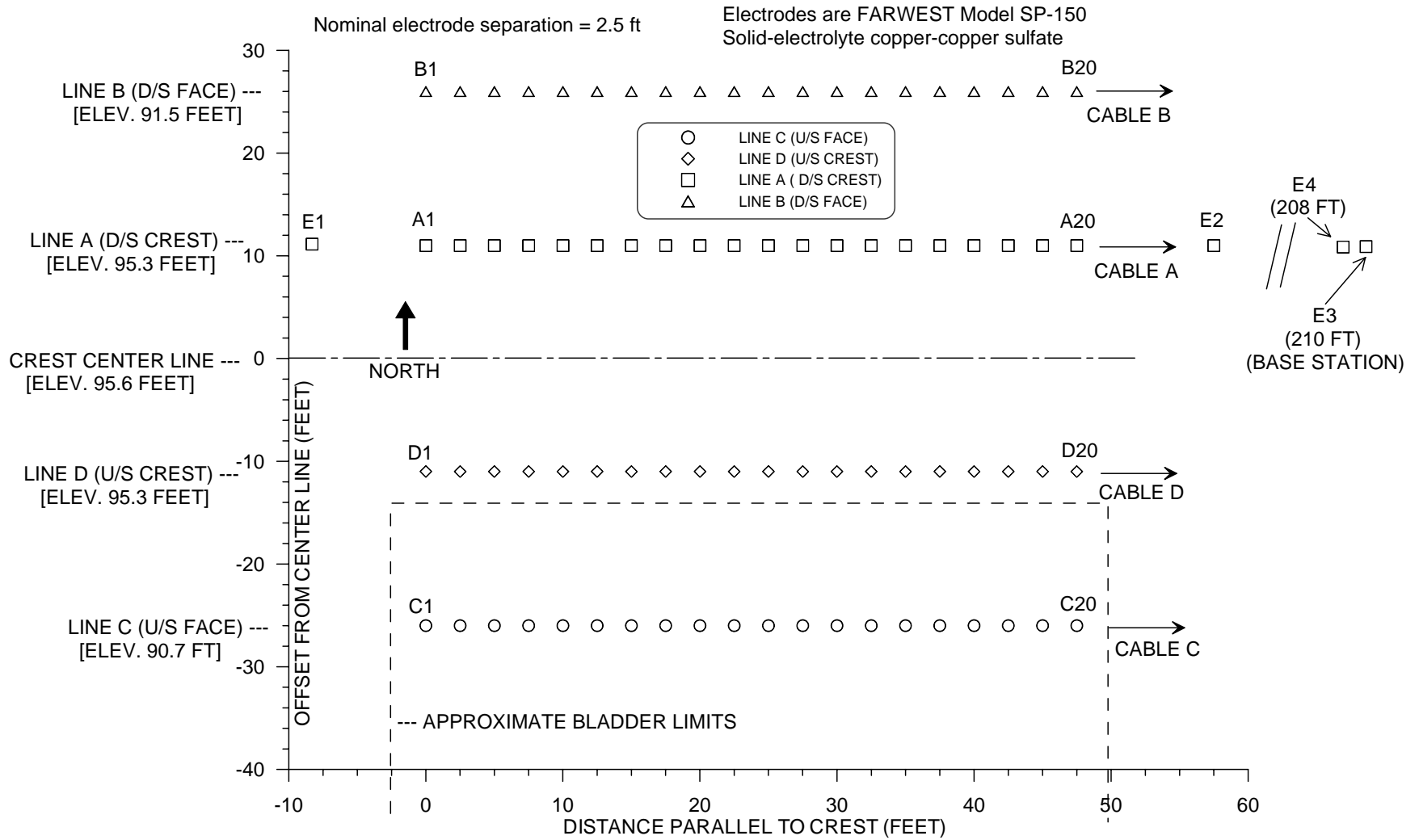


Figure 2. SP Monitoring Electrode Layout

HYDRA 1 LINE A CABLE A D/S CREST																							
SCAN INTERVAL 120 SEC 360 LINES/FILE SLOW RATE 3 V RANGE																							
LINE#006.MON Date: 11-08-2004 Time: 12:02:43 Rate= 120 sec/scan																							
N	TIME(N)	HOURS	V 0	V 1	V 2	V 3	V 4	V 5	V 6	V 7	V 8	V 9	V10	V11	V12	V13	V14	V15	V16	V17	V18	V19	V20
1450	12:04:20	12.0724	5.20	6.90	5.00	5.60	5.20	5.10	7.30	3.90	4.60	5.50	6.90	4.70	6.20	3.90	1.80	-2.60	5.00	4.40	3.00	6.50	1.40
1451	12:06:20	12.1057	5.20	6.80	5.10	5.00	4.60	4.50	7.20	4.50	4.60	5.10	7.00	5.10	6.10	3.40	2.00	-2.20	5.10	4.40	3.00	6.50	1.40
1452	12:08:20	12.1391	5.20	6.80	5.10	5.00	4.60	4.50	7.10	4.50	4.70	5.10	6.90	5.90	7.00	3.80	2.20	-1.90	5.10	4.10	3.00	6.80	1.30
1453	12:10:20	12.1724	5.20	6.80	5.10	5.00	4.60	4.50	7.20	4.50	4.60	5.00	6.90	5.10	6.10	3.50	2.00	-2.20	5.10	4.40	3.00	6.50	1.50
1454	12:12:20	12.2058	5.20	6.80	5.10	5.00	4.60	4.50	7.20	4.50	4.70	5.00	6.90	5.10	6.10	3.50	2.00	-2.20	5.10	4.40	3.00	6.50	1.40
1455	12:14:20	12.2391	5.20	6.70	5.10	5.10	4.60	4.50	7.10	4.50	4.60	5.00	6.90	5.10	6.10	3.50	2.00	-2.10	5.10	4.40	3.10	6.50	1.40
1456	12:16:20	12.2724	5.10	6.80	5.10	5.10	4.70	4.50	7.20	4.50	4.70	5.00	6.90	5.10	6.10	3.50	2.00	-2.10	5.10	4.40	3.10	6.50	1.40
1457	12:18:20	12.3058	5.10	6.70	5.10	5.10	4.60	4.40	7.10	4.40	4.60	5.00	6.90	5.00	6.10	3.40	2.00	-2.10	5.10	4.40	3.10	6.50	1.40
1458	12:20:20	12.3391	5.10	6.70	5.10	5.00	4.60	4.40	7.10	4.40	4.60	5.00	6.90	5.00	6.10	3.40	2.00	-2.10	5.10	4.40	3.00	6.50	1.40
1459	12:22:20	12.3724	5.10	6.70	5.00	5.00	4.60	4.40	7.10	4.50	4.50	5.00	6.90	5.10	6.00	3.40	2.00	-2.20	-3.30	-10.80	-16.40	-13.10	-17.30
1460	12:24:20	12.4058	22.90	27.20	-15.00	-13.10	25.60	22.00	-13.80	-7.80	26.50	19.90	6.90	5.10	6.10	3.40	2.00	-2.10	5.10	4.50	3.00	6.50	1.40
1461	12:26:20	12.4391	5.10	6.70	5.10	5.00	4.60	4.40	7.10	4.40	4.50	5.00	6.90	5.00	6.00	3.40	2.00	-2.10	5.10	4.40	3.00	6.50	1.40
1462	12:28:20	12.4725	5.10	6.70	5.10	-7.20	-11.10	-15.40	-13.10	-15.30	26.90	24.10	-16.20	-8.90	30.70	14.20	-23.50	-9.50	32.40	18.20	3.00	6.50	1.40
1463	12:30:20	12.5058	5.00	6.60	5.00	5.00	4.60	4.40	7.00	4.30	4.50	4.90	6.80	5.00	6.00	3.30	2.00	-2.10	5.10	4.40	3.00	6.40	1.40
1464	12:32:20	12.5391	5.00	6.60	5.10	5.00	4.60	4.40	7.00	4.40	4.50	4.90	6.80	5.00	6.00	3.40	1.90	-2.10	5.10	4.40	3.00	6.50	1.30
1465	12:34:20	12.5725	5.00	6.70	5.10	5.00	4.60	4.40	7.00	4.40	4.50	4.90	6.80	5.00	6.00	3.40	1.90	-2.00	5.10	4.40	3.00	6.50	1.40
1466	12:36:20	12.6058	5.10	6.70	5.10	5.00	4.60	4.40	7.00	4.40	4.50	4.90	6.80	5.00	6.00	3.40	1.90	-2.00	5.10	4.50	3.00	6.50	1.40
1467	12:38:20	12.6391	5.10	6.70	5.10	5.00	4.60	4.40	7.00	4.30	4.50	4.90	6.80	5.00	6.00	3.30	2.00	-2.00	5.10	4.50	3.00	6.50	1.50
1468	12:40:20	12.6725	10.80	-11.70	3.20	25.00	13.80	4.30	7.00	4.40	4.50	4.90	6.80	5.00	5.90	3.30	1.90	-1.90	5.10	4.40	3.00	6.50	1.40
1469	12:42:20	12.7058	5.00	6.70	5.10	5.00	4.70	4.40	7.00	4.40	4.60	4.90	6.50	2.50	-23.80	-35.50	-41.80	-52.00	-22.00	64.70	25.10	-55.30	-5.20
1470	12:44:20	12.7391	5.00	6.70	5.10	5.00	4.60	4.40	7.00	4.30	4.50	4.90	6.80	5.00	5.90	3.40	1.90	-1.90	5.10	4.50	3.00	6.50	1.40
1471	12:46:20	12.7725	5.10	6.60	5.10	5.00	4.70	4.40	7.00	3.80	-2.30	-41.00	-47.10	-47.60	-51.20	-18.90	49.90	7.20	-10.40	4.80	-15.70	10.70	46.00
1472	12:48:20	12.8058	5.10	6.70	5.10	5.00	4.70	4.40	7.00	4.30	4.50	4.90	6.80	5.00	5.90	3.40	1.90	-1.80	5.20	4.50	3.00	6.50	1.40
1473	12:50:20	12.8392	5.00	6.60	5.10	5.00	4.70	4.40	7.00	4.30	4.60	5.70	19.90	50.70	55.00	55.80	56.20	-4.50	-48.70	11.50	42.90	-9.70	-36.50
1474	12:52:20	12.8725	5.10	6.70	5.10	5.00	4.70	4.40	7.00	4.40	4.50	4.90	6.80	5.00	6.00	3.40	2.00	-1.80	5.20	4.50	3.00	6.50	1.50
1475	12:54:20	12.9058	5.10	6.70	5.10	5.00	4.70	4.40	7.00	4.30	4.60	4.90	6.80	4.90	5.90	3.30	2.00	-1.80	5.20	4.50	3.00	6.50	1.50
1476	12:56:20	12.9392	5.00	6.70	5.20	5.00	4.70	4.40	7.00	4.30	4.50	4.90	6.70	5.00	5.90	3.40	2.00	-1.80	5.20	4.50	3.00	6.50	1.50
1477	12:58:21	12.9725	5.00	6.70	5.10	5.00	4.70	4.40	7.00	4.30	4.50	4.90	6.80	4.90	5.90	3.40	2.00	-1.70	5.20	4.50	3.00	6.50	1.40
1478	13:00:21	13.0058	5.10	6.60	5.10	5.00	5.10	22.50	39.20	44.30	40.10	39.20	-9.50	-28.50	25.10	28.70	-20.10	-26.50	27.30	23.90	-17.50	-10.80	1.40
1479	13:02:21	13.0392	5.00	6.70	5.10	5.00	4.70	4.40	7.00	4.30	4.50	4.90	6.70	5.00	5.90	3.40	2.00	-1.70	5.20	4.50	3.00	6.50	1.50
1480	13:04:21	13.0725	5.00	6.60	5.20	5.00	4.70	4.40	7.00	4.30	4.50	4.90	6.60	5.70	6.50	4.00	2.20	-2.40	5.00	5.10	3.00	6.00	1.50
1481	13:06:21	13.1058	5.00	6.70	5.10	5.10	4.70	4.40	7.00	4.30	4.50	4.90	6.80	4.90	5.90	3.40	1.90	-1.70	5.20	4.50	3.00	6.50	1.50
1482	13:08:21	13.1392	5.10	6.70	5.20	5.00	4.80	4.40	7.00	4.30	4.50	4.90	6.80	4.90	5.90	3.40	1.90	-1.70	5.30	4.50	3.00	6.50	1.50
1483	13:10:21	13.1725	5.00	6.70	5.20	5.00	4.80	4.40	7.00	4.30	4.60	4.90	6.70	5.00	5.90	3.40	2.00	-1.70	5.30	4.50	3.00	6.50	1.40
1484	13:12:21	13.2059	5.00	6.60	5.10	5.00	4.80	4.40	7.00	4.20	4.50	4.90	6.70	5.00	5.90	3.30	2.00	-1.70	5.30	4.50	3.00	6.50	1.40
1485	13:14:21	13.2392	5.00	6.60	5.20	5.00	4.80	4.40	7.00	4.20	4.60	4.90	6.70	4.90	5.90	3.30	2.00	-1.70	5.30	4.50	3.00	6.50	1.50
1486	13:16:21	13.2725	5.00	6.60	5.20	5.00	4.70	4.40	7.00	4.30	4.50	4.90	6.70	4.90	5.90	3.30	2.00	-1.70	5.20	4.50	3.00	6.50	1.40
1487	13:18:21	13.3059	5.00	6.60	5.10	5.00	4.70	4.40	7.00	4.30	4.60	4.90	6.80	4.90	5.80	3.40	2.00	-1.60	5.30	4.50	3.00	6.50	1.50
1488	13:20:21	13.3392	5.00	6.60	5.10	5.00	4.70	4.40	7.00	4.30	4.50	4.90	6.70	5.00	5.90	3.30	2.00	-1.60	5.30	4.50	2.90	6.50	1.50
1489	13:22:21	13.3725	5.00	6.60	5.20	5.00	4.80	4.40	6.90	4.30	4.50	4.80	6.70	4.90	5.90	3.40	1.90	-1.60	5.30	4.50	2.90	6.50	1.50
1490	13:24:21	13.4059	4.90	6.50	5.10	5.00	4.70	4.40	6.90	4.20	4.50	4.90	6.70	4.90	5.80	3.30	1.90	-1.60	5.30	4.50	2.90	6.50	1.40
1491	13:26:21	13.4392	4.90	6.50	5.10	5.00	4.70	4.30	6.90	4.20	4.50	4.90	6.70	4.90	5.80	3.30	1.90	-1.60	5.20	4.50	2.90	6.50	1.40
1492	13:28:21	13.4725	4.90	6.60	5.10	5.00	4.70	4.40	6.90	4.20	4.50	4.90	6.60	4.90	5.80	3.30	2.00	-1.60	5.30	4.50	2.90	6.50	1.40
1493	13:30:21	13.5059	4.90	6.50	5.10	5.00	4.70	4.30	7.00	4.20	4.50	4.90	6.60	4.90	5.80	3.40	1.90	-1.60	5.20	4.50	2.90	6.50	1.40
1494	13:32:21	13.5392	5.00	6.50	5.20	5.00	4.70	4.40	6.90	4.20	4.50	4.80	6.60	4.90	5.80	3.30	1.90	-1.60	5.20	4.50	2.90	6.50	1.40
1495	13:34:21	13.5726	4.90	6.50	5.10	5.00	4.70	4.40	6.90	4.20	4.50	4.80	6.60	4.80	5.80	3.30	1.90	-1.60	5.30	4.50	2.90	6.50	1.50
1496	13:36:21	13.6059	4.90	6.50	5.10	5.00	4.70	4.30	6.90	4.10	4.40	4.80	6.60	4.80	5.70	3.30	1.90	-1.60	5.20	4.50	2.90	6.50	1.40
1497	13:38:21	13.6392	4.90	6.50	5.10	5.00	4.70	4.30	6.90	4.20	4.40	4.80	6.60	4.80	5.70	3.30	1.90	-1.60	5.30	4.50	2.90	6.50	1.40
1498	13:40:21	13.6726	4.80	6.50	5.10	4.90	4.70	4.20	6.90	4.10	4.40	4.80	6.50	4.80	5.70	3.30	1.90	-1.60	5.30	4.50	2.90	6.50	1.30
1499	13:42:21	13.7059	4.90	6.50	5.10	4.90	4.70	4.30	6.90	4.10	4.40	4.80	6.50	4.80	5.70	3.30	1.90	-1.60	5.20	4.50	2.90	6.50	1.40
1500	13:44:21	13.7392	4.90	6.50	5.10	5.00	4.70	4.30	6.80	4.10	4.40	4.80	6.60	4.80	5.60	3.20	1.80	-1.60	5.30	4.50	2.90	6.50	1.40
1501	13:46:21	13.7726	4.90	6.50	5.10	4.90	4.60	4.30	6.80	4.10	4.40	4.80	6.50	4.80	5.70	3.20	1.90	-1.60	5.30	4.50	2.90	6.50	1.30
1502	13:48:21	13.8059	4.90	6.50	5.10	4.90	4.70	4.40															

F-23

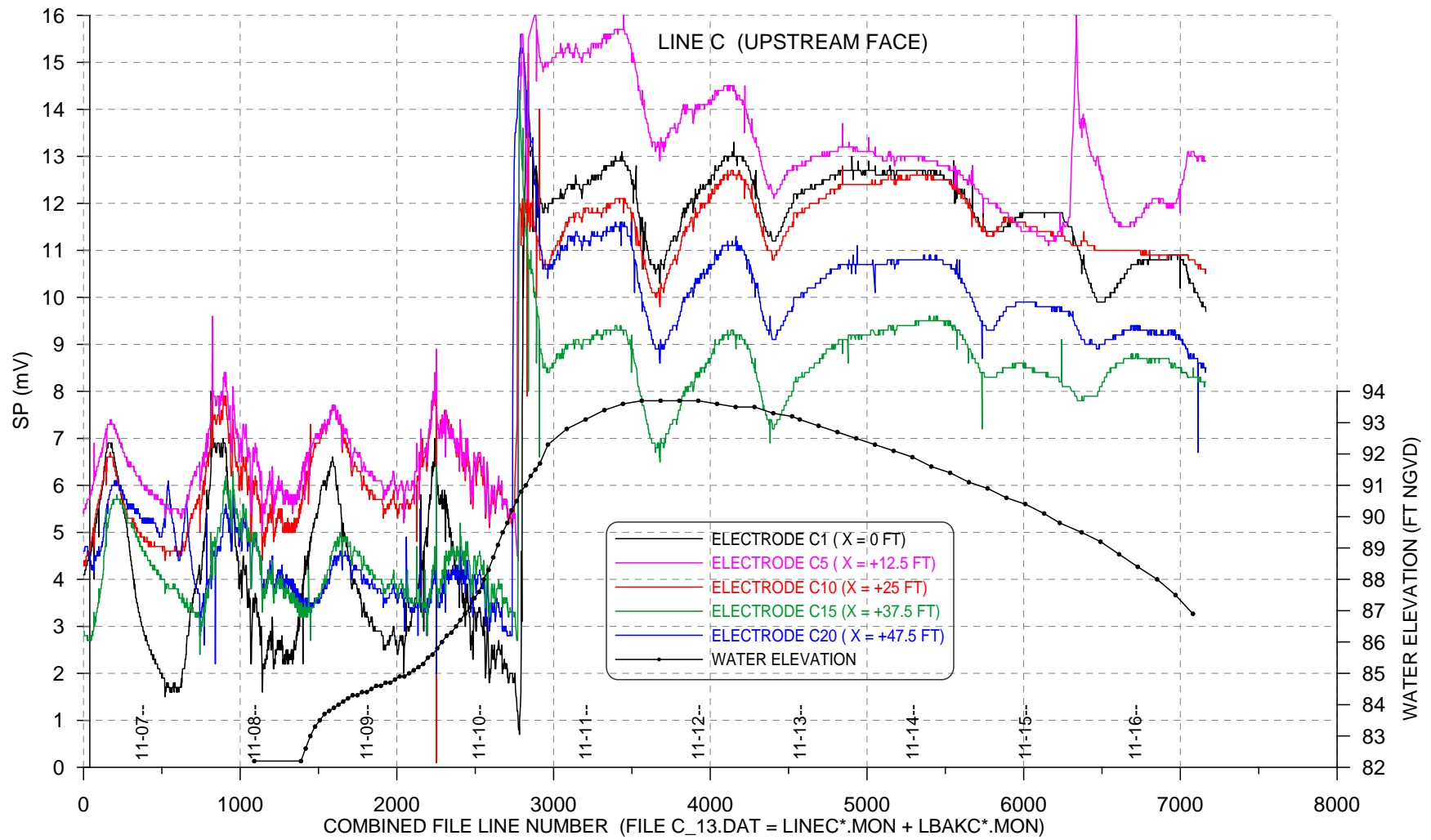


Figure 5. SP Monitoring Data for Line C (Upstream Face)

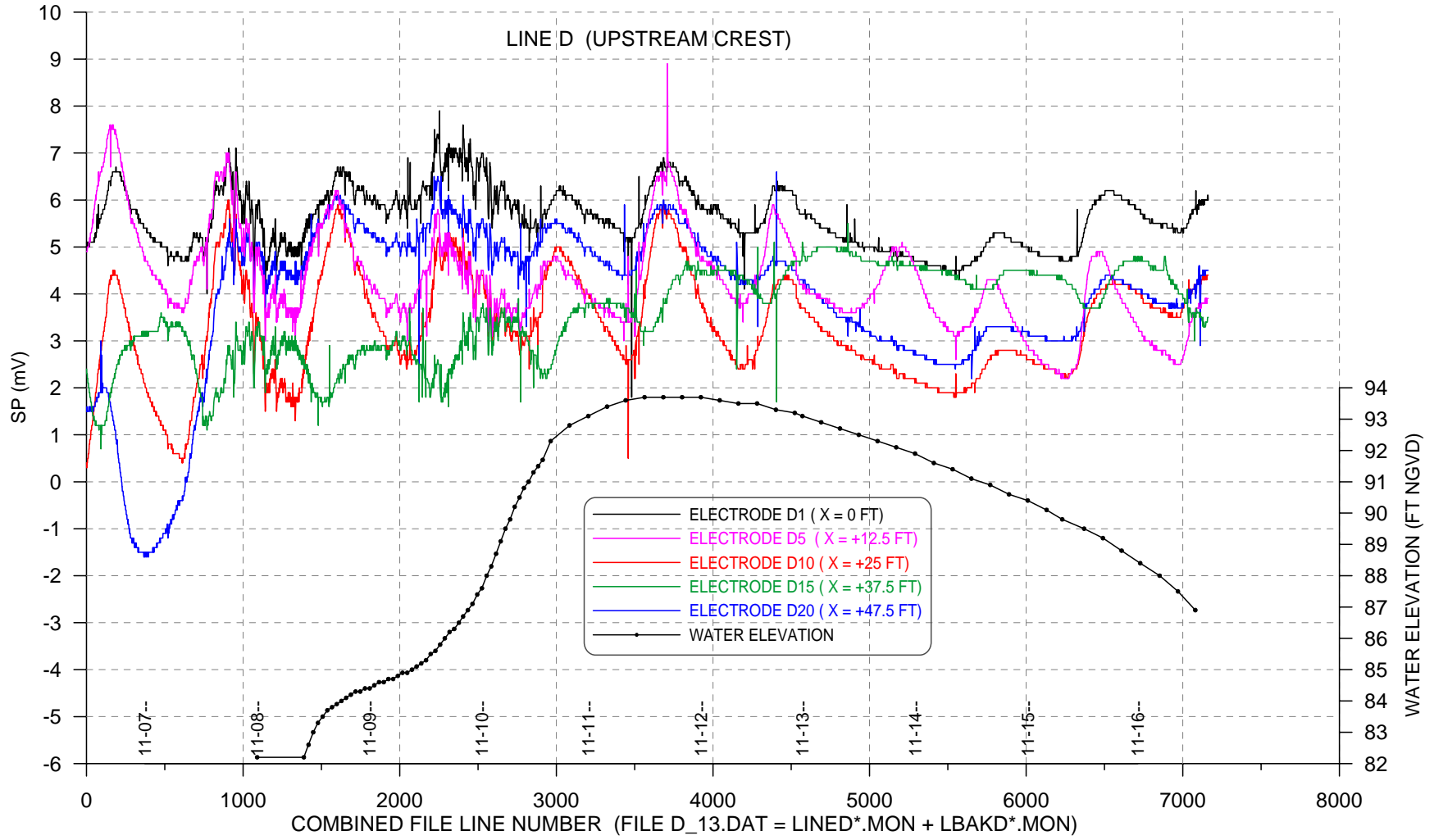


Figure 6. SP Monitoring Data for Line D (Upstream Crest)

F-25

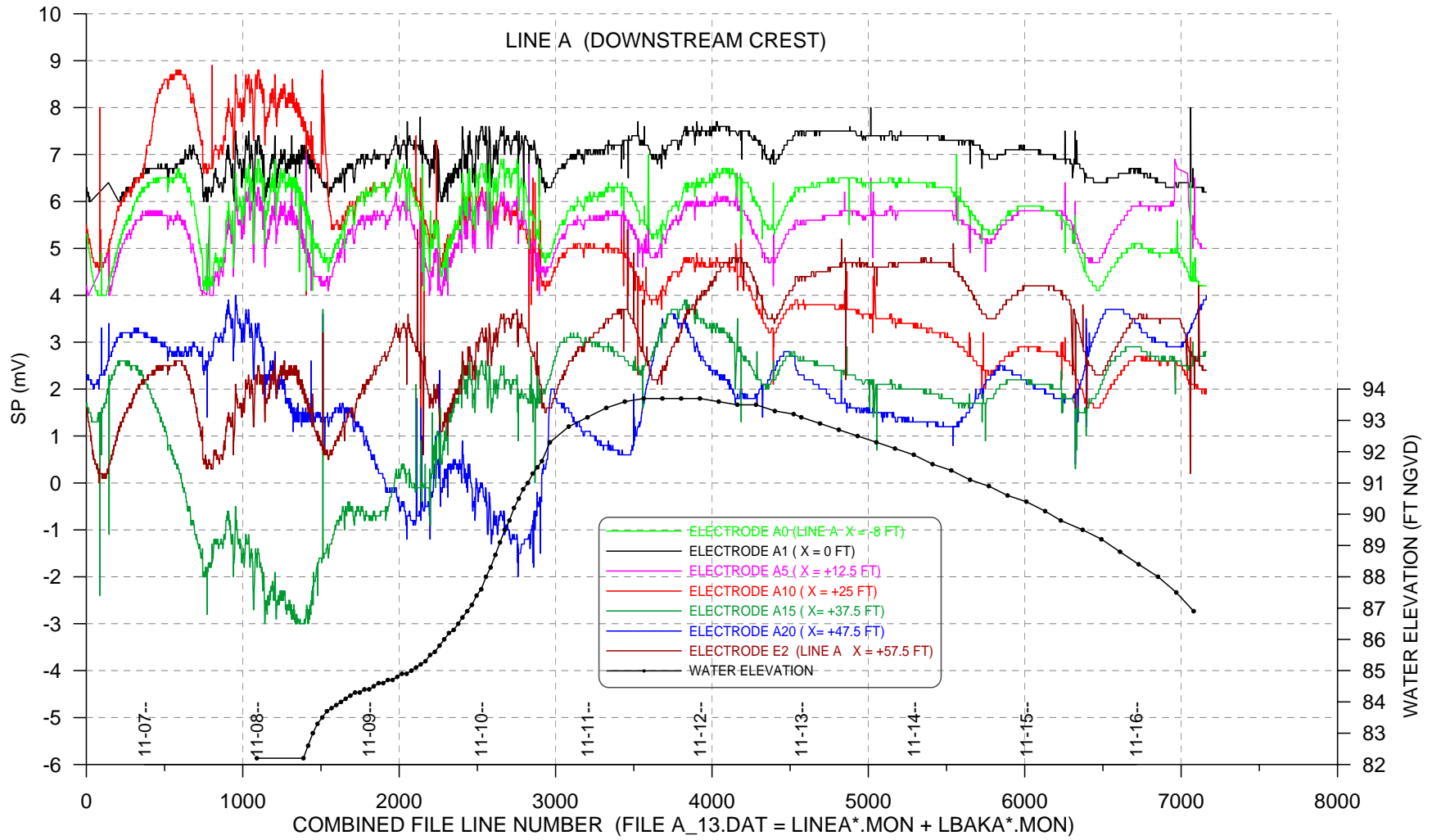


Figure 7. SP Monitoring Data for Line A (Downstream Crest)

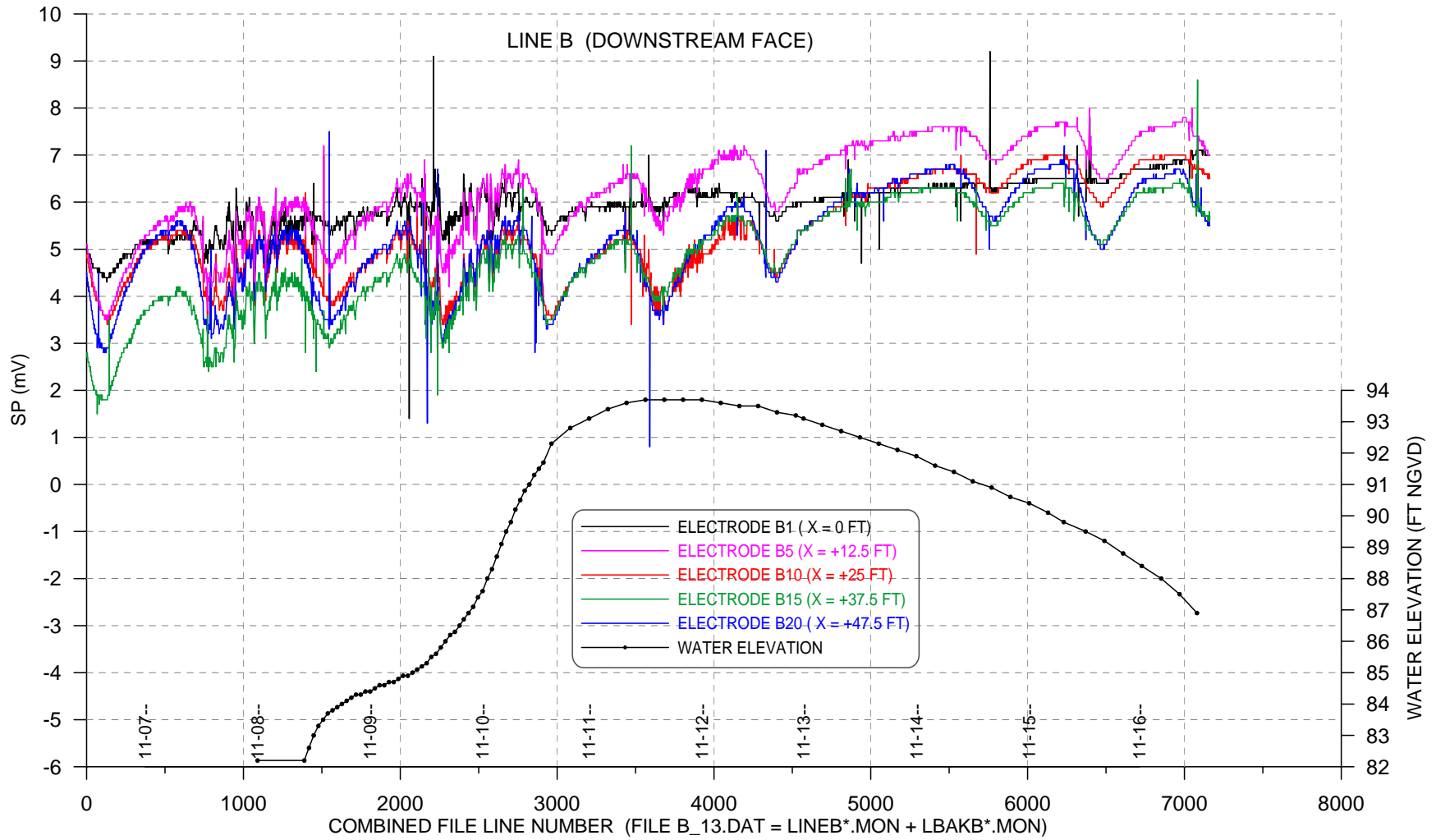


Figure 8. SP Monitoring Data for Line B (Downstream Face)

F-27

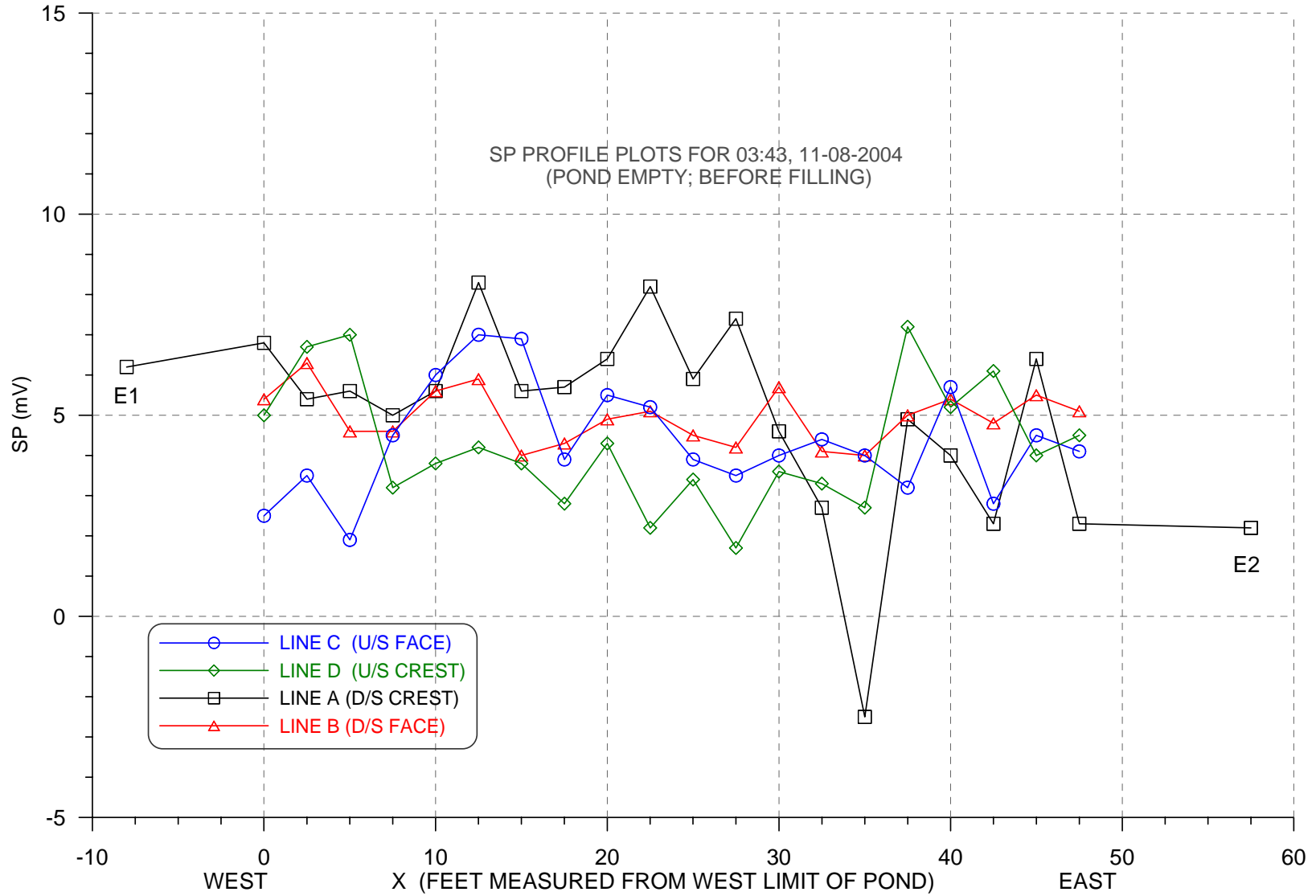


Figure 9. SP Profile Plots With Pond Empty (Before Filling)

F-28

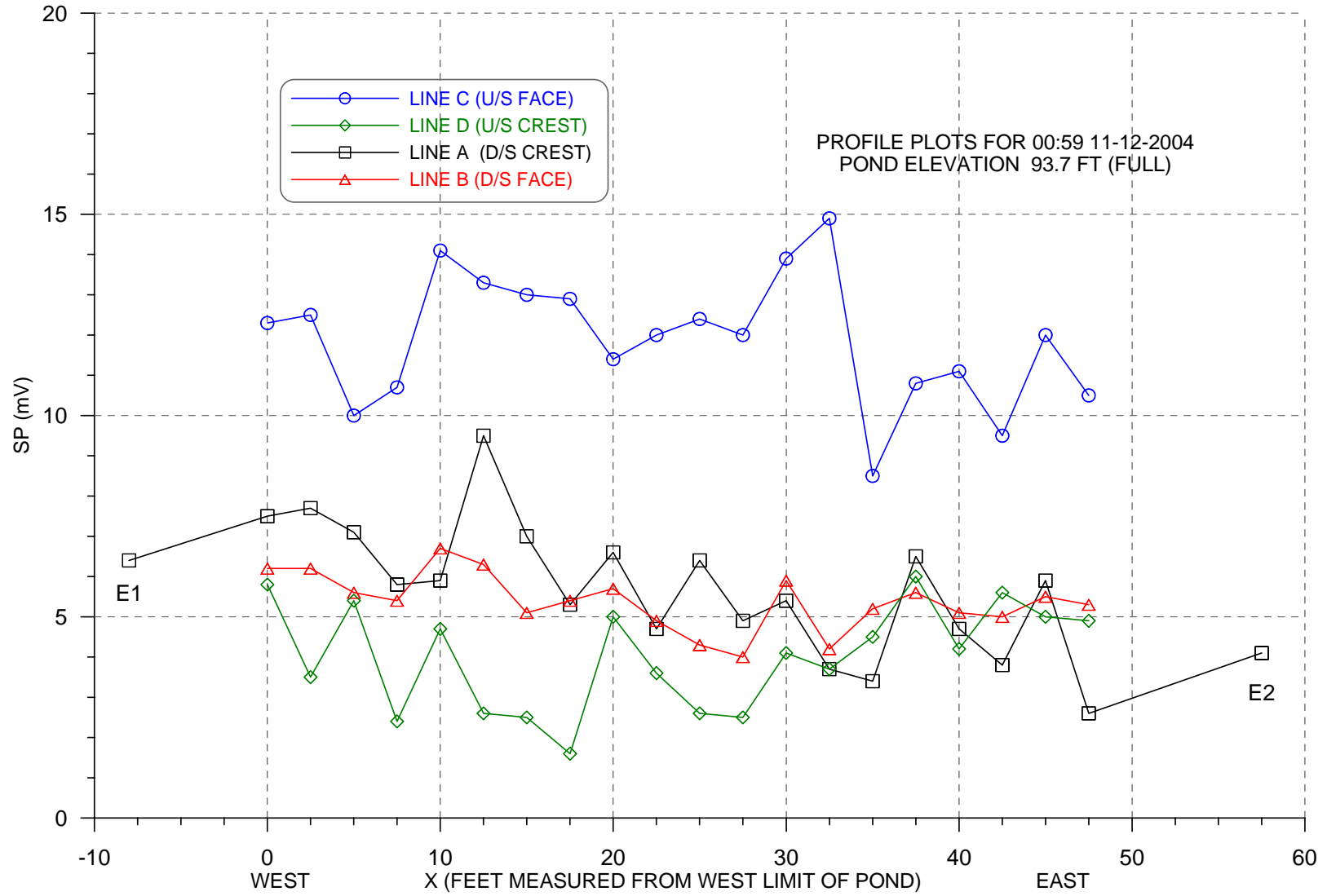


Figure 10. SP Profile Plots With Pond Full (Elevation 93.7 ft)

F-29

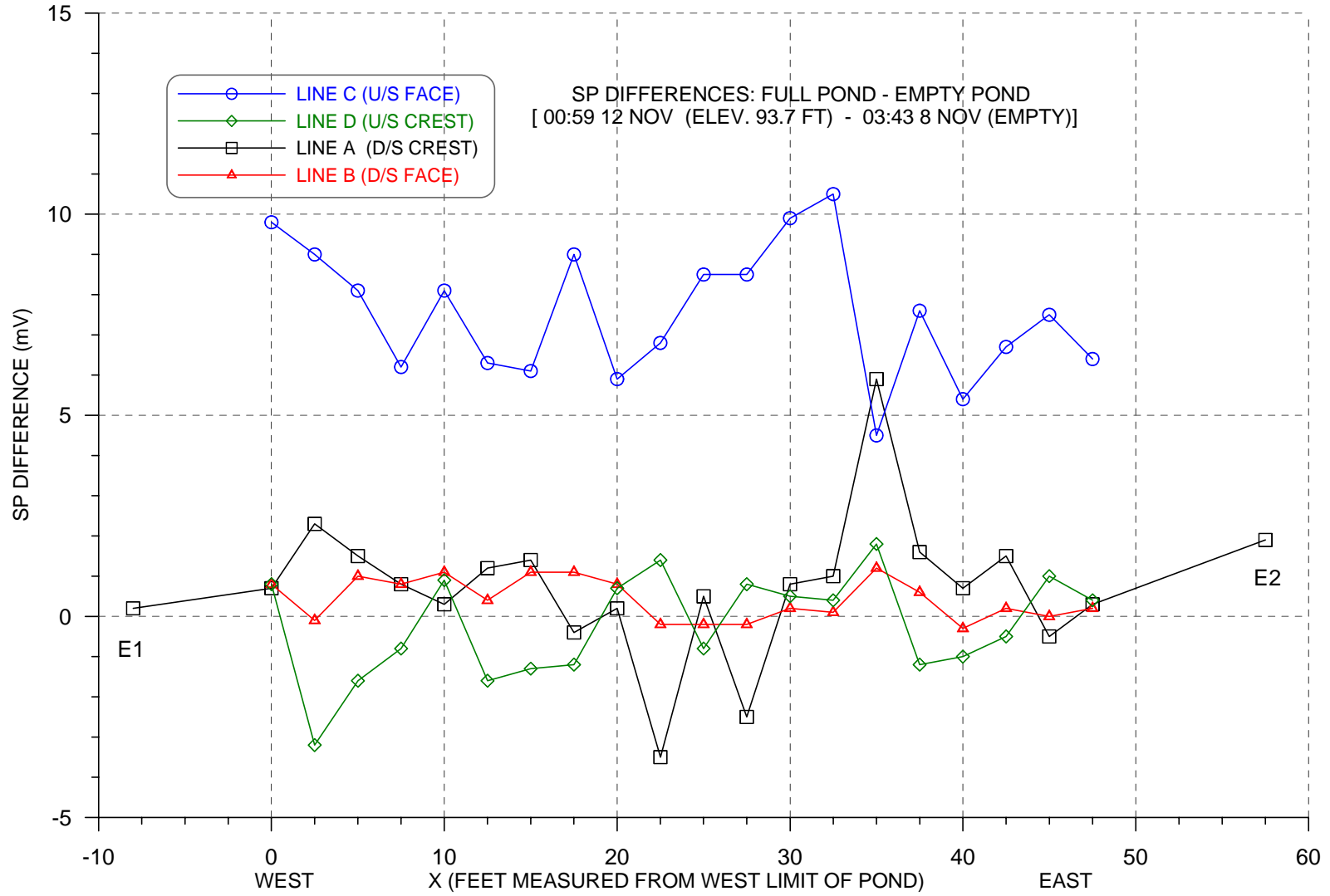
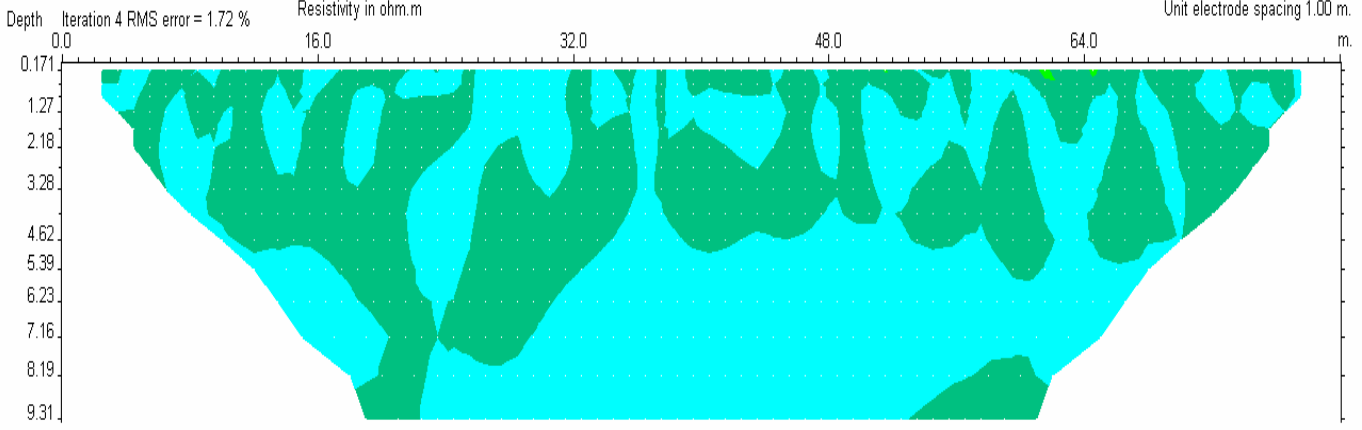
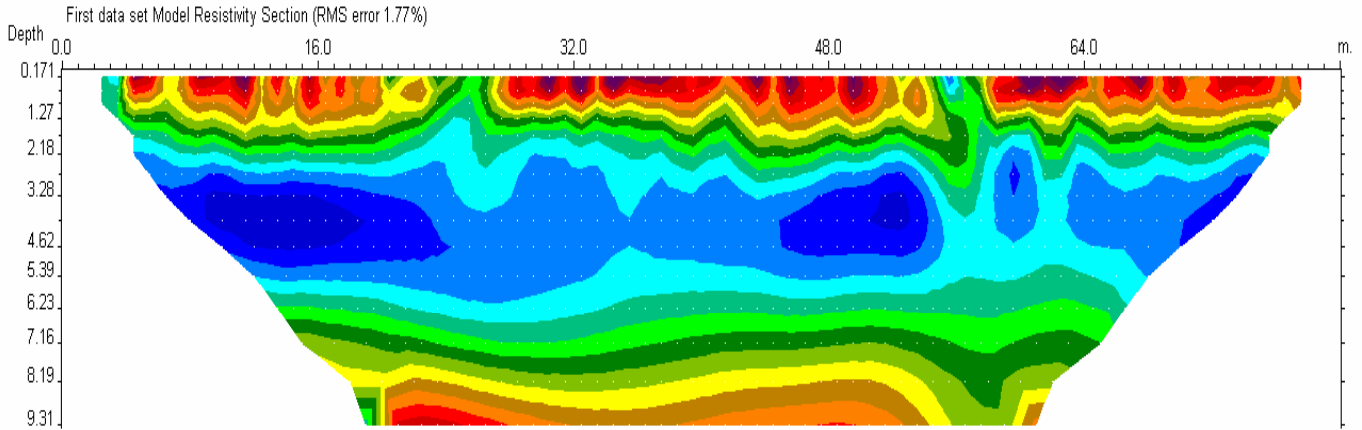
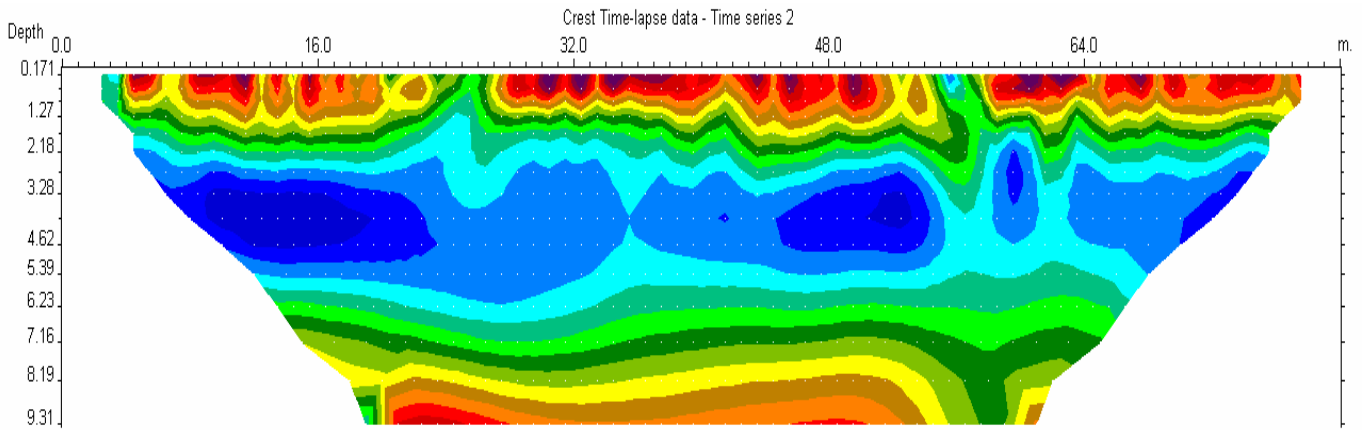


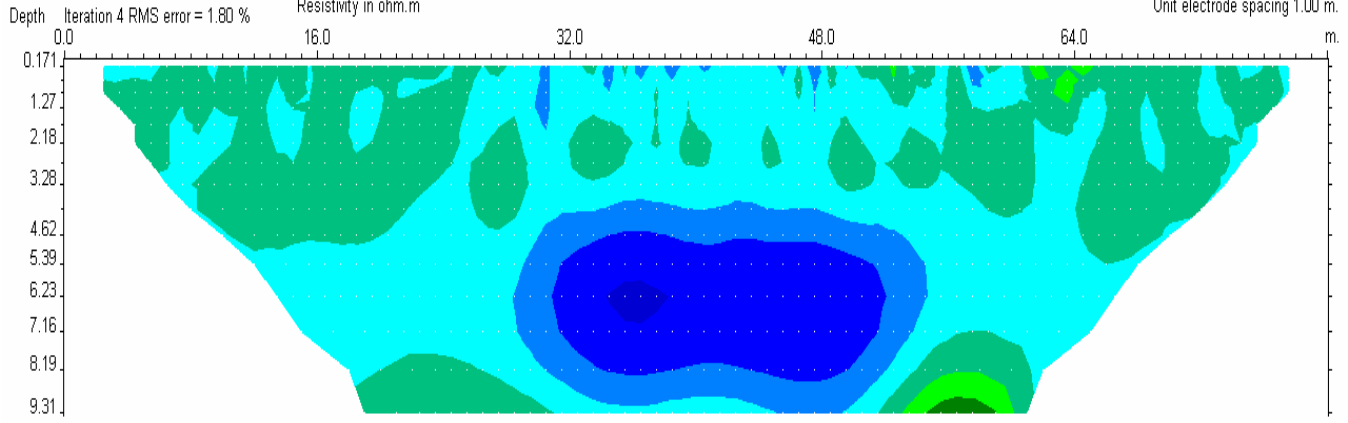
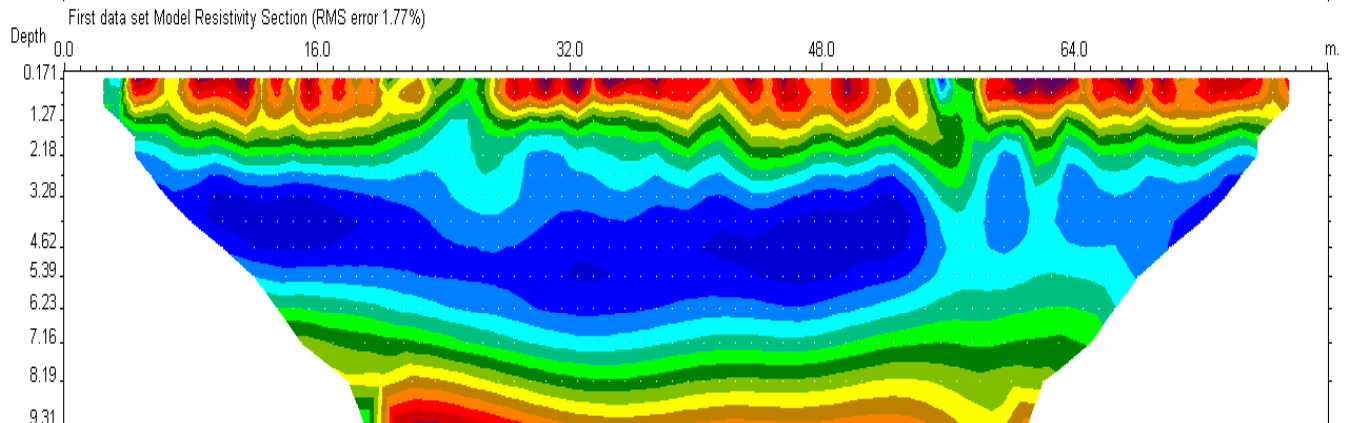
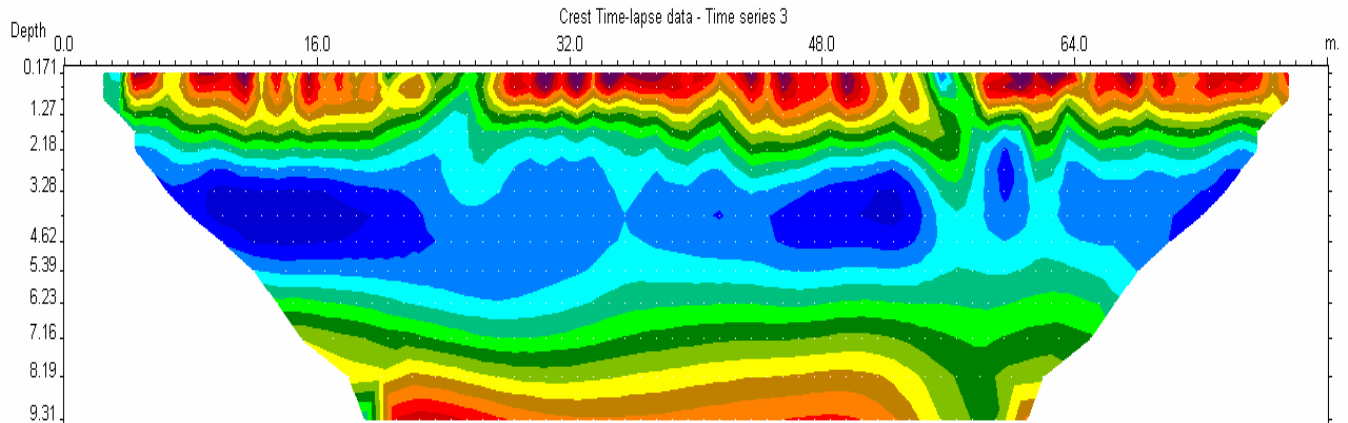
Figure 11. SP Difference Profile Plots [Full Pond (Elevation 93.7 ft) - Empty Pond]

Appendix G

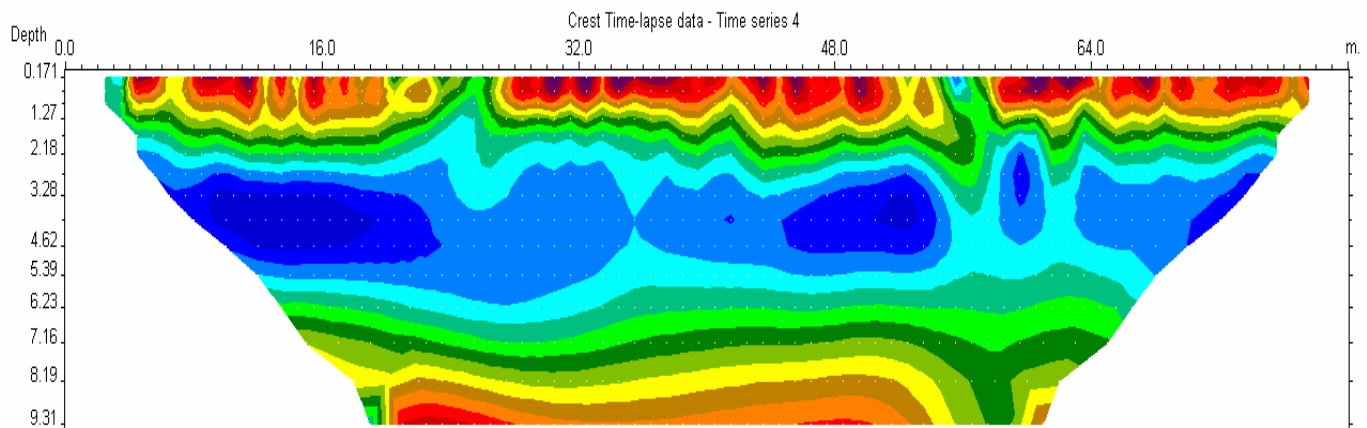
Resistivity Time Plots for Levee Crest, Face, and Toe



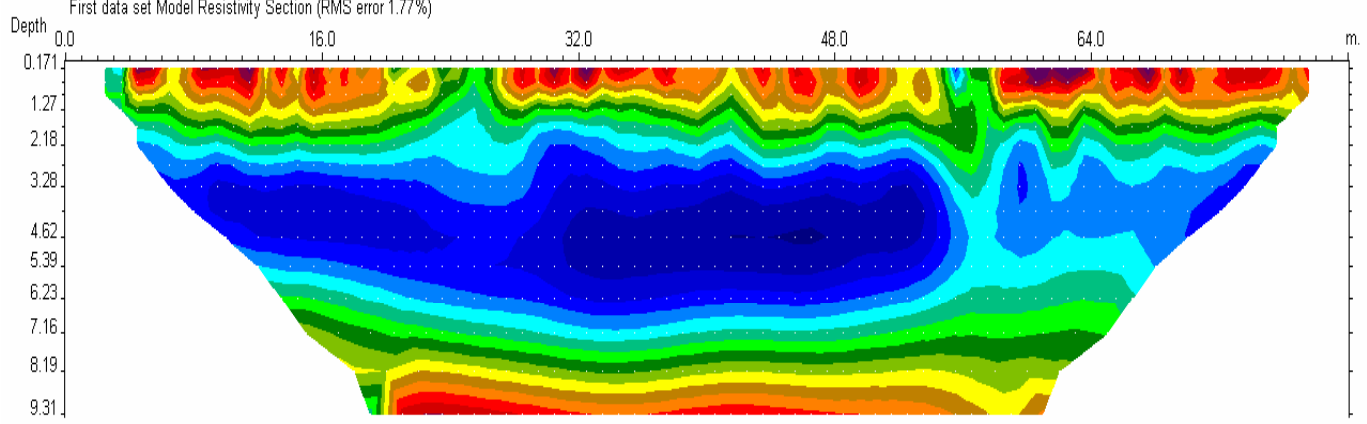
Crest, Time 2 = 31 hrs 15 min after start of test (time 1 = start of test)



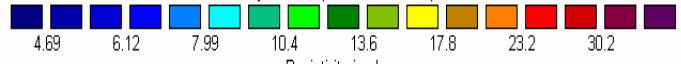
Crest, Time 3 = 53 hrs 15 min after start of test



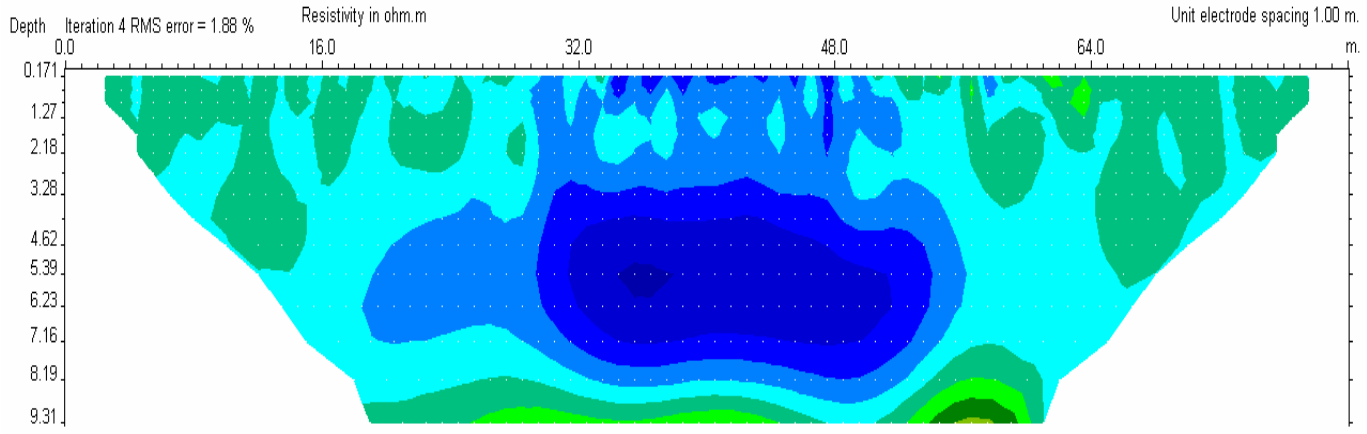
First data set Model Resistivity Section (RMS error 1.77%)



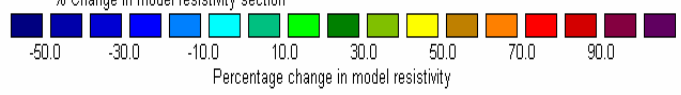
Second data set Model Resistivity Section (RMS error 1.88%)



Resistivity in ohm.m



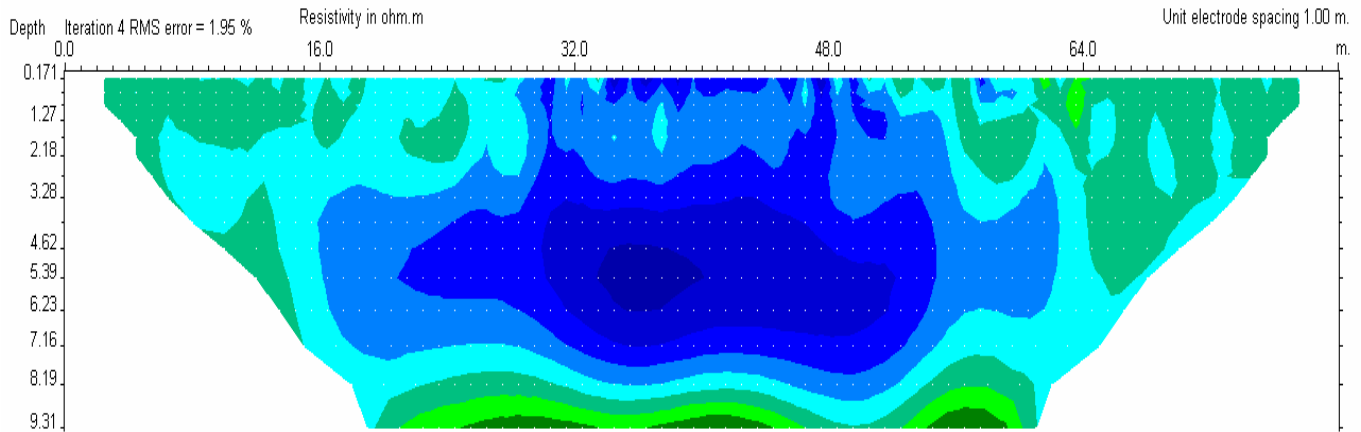
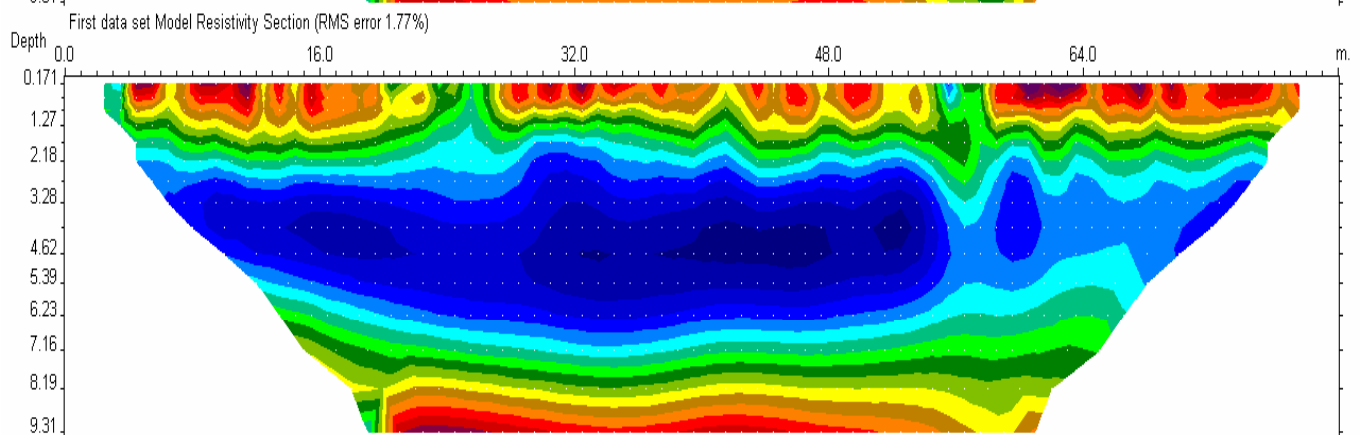
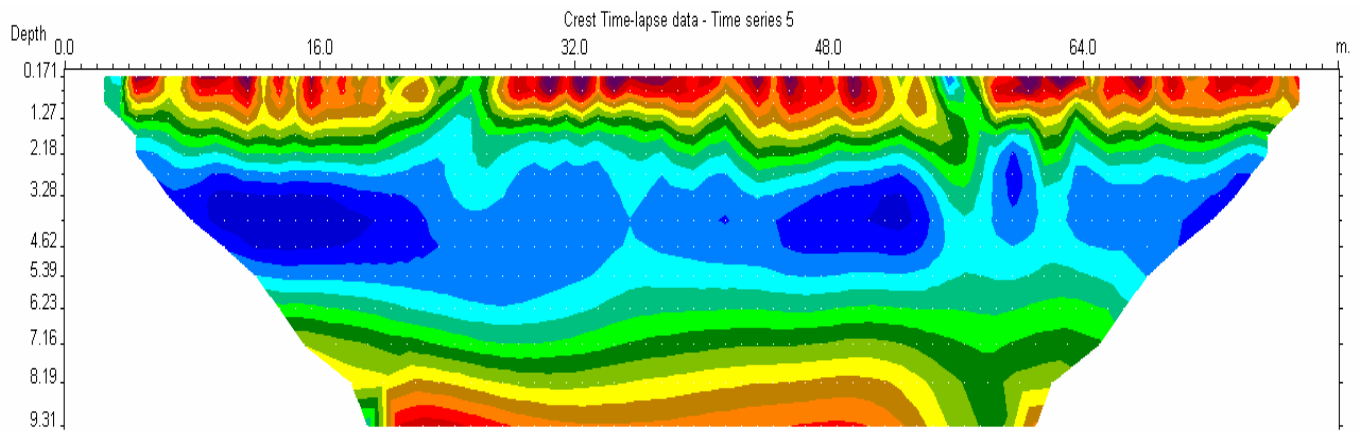
% Change in model resistivity section



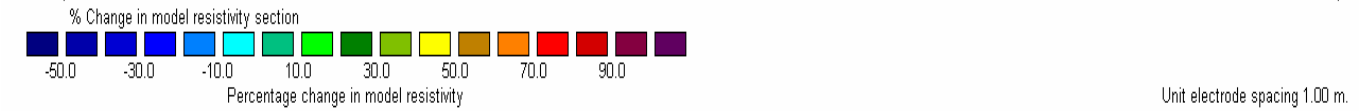
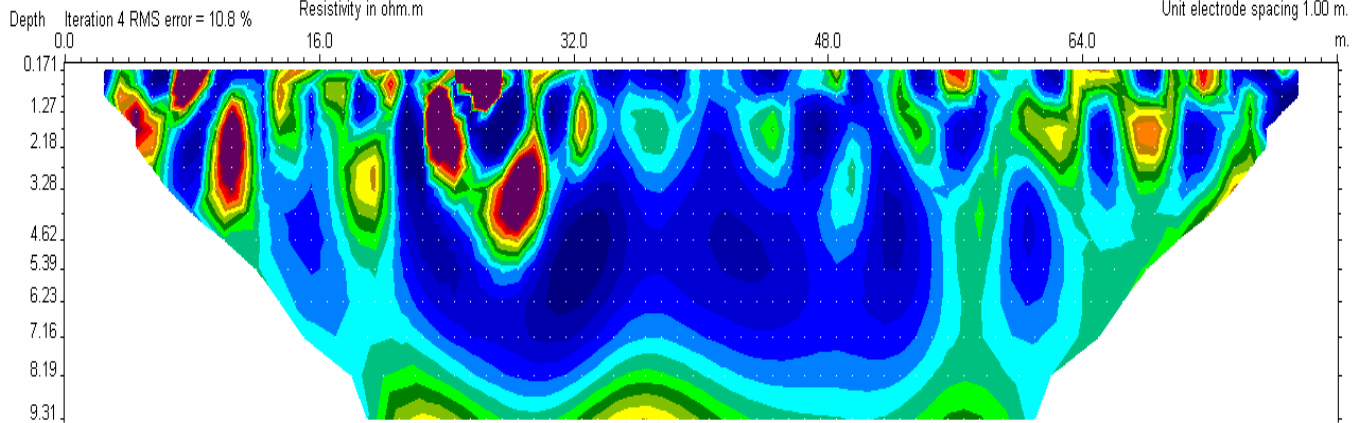
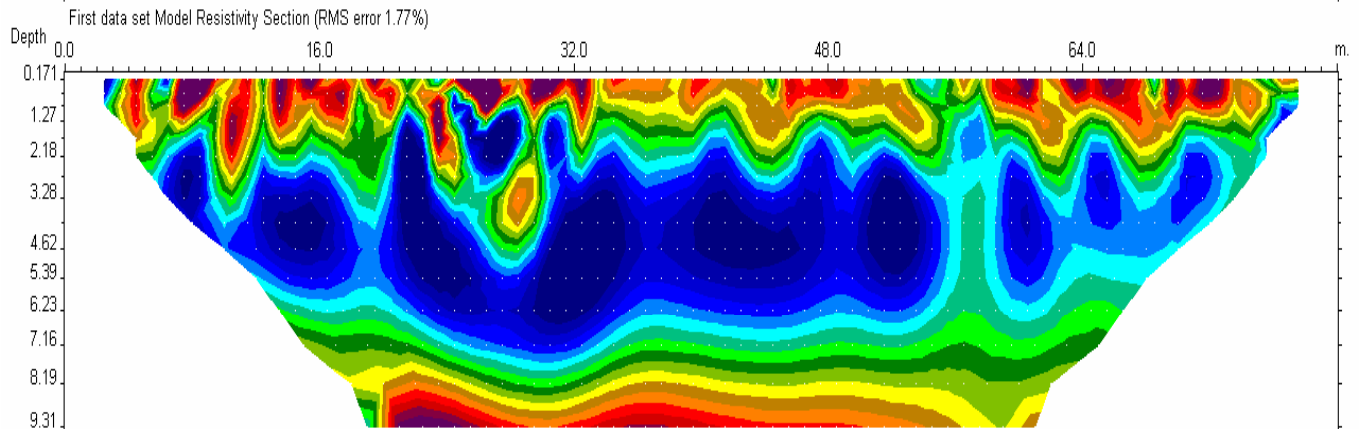
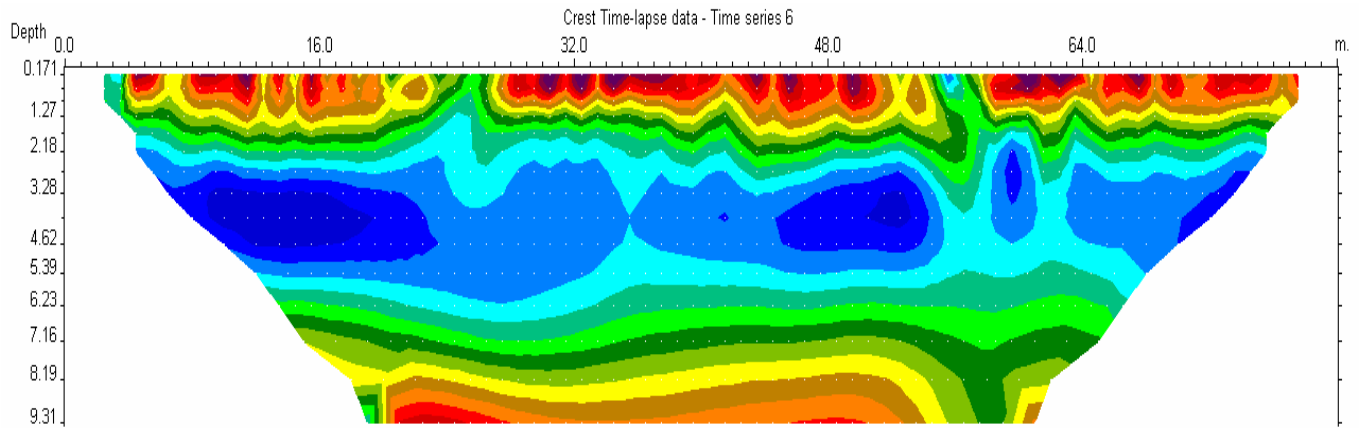
Unit electrode spacing 1.00 m.

Unit electrode spacing 1.00 m.

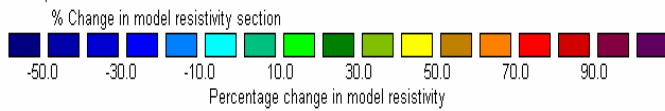
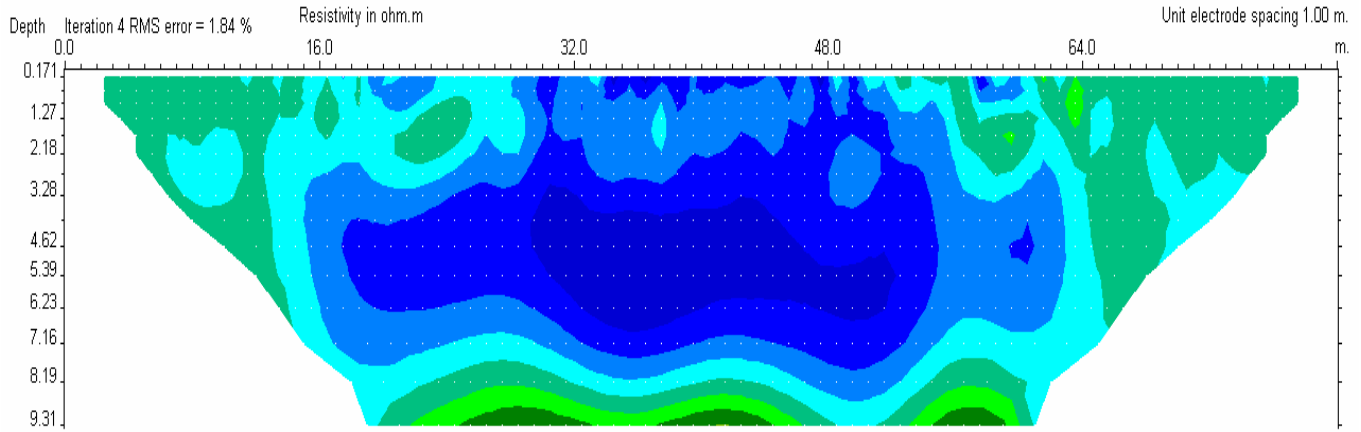
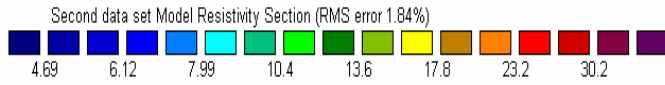
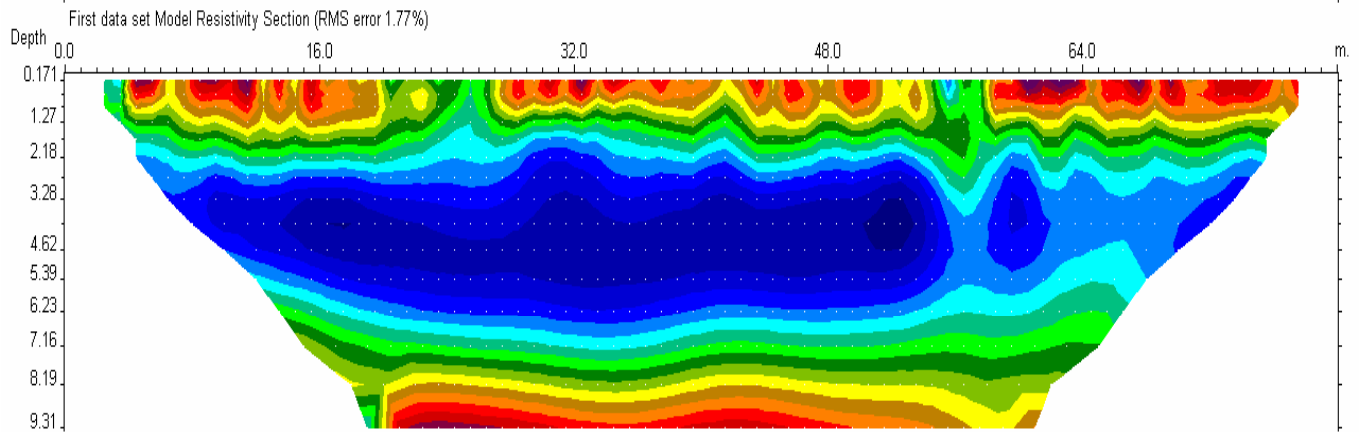
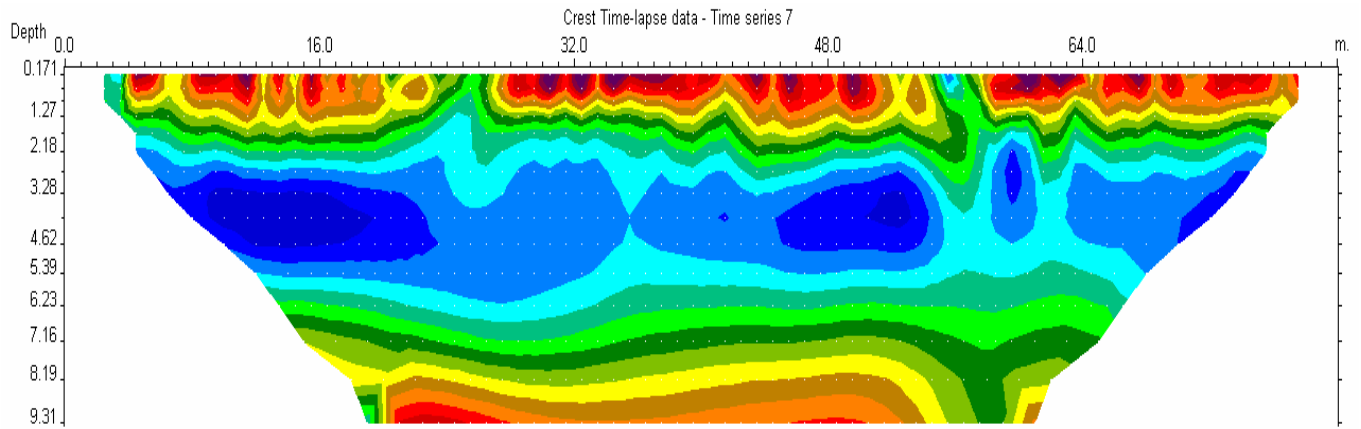
Crest, Time 4 = 71 hrs 55 min after start of test



Crest, Time 5 = 103 hrs 17 min after start of test



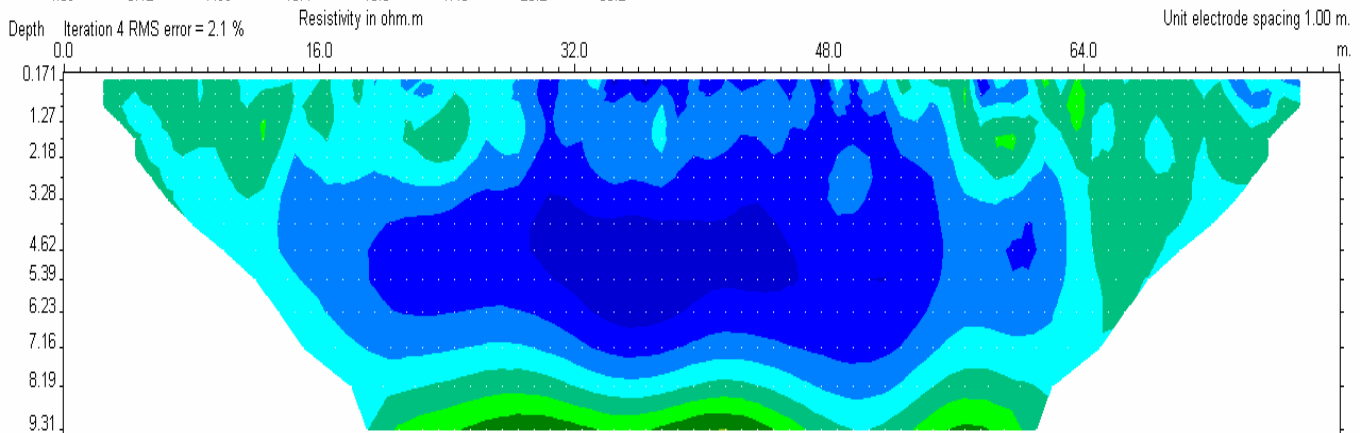
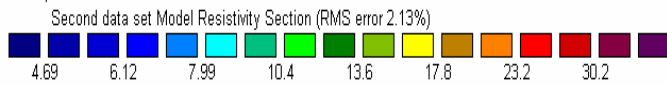
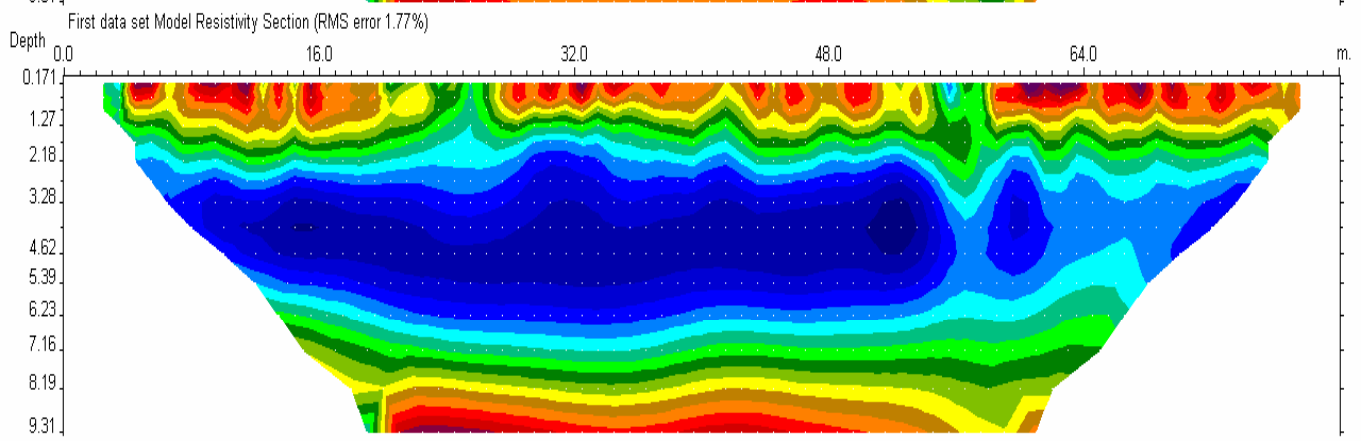
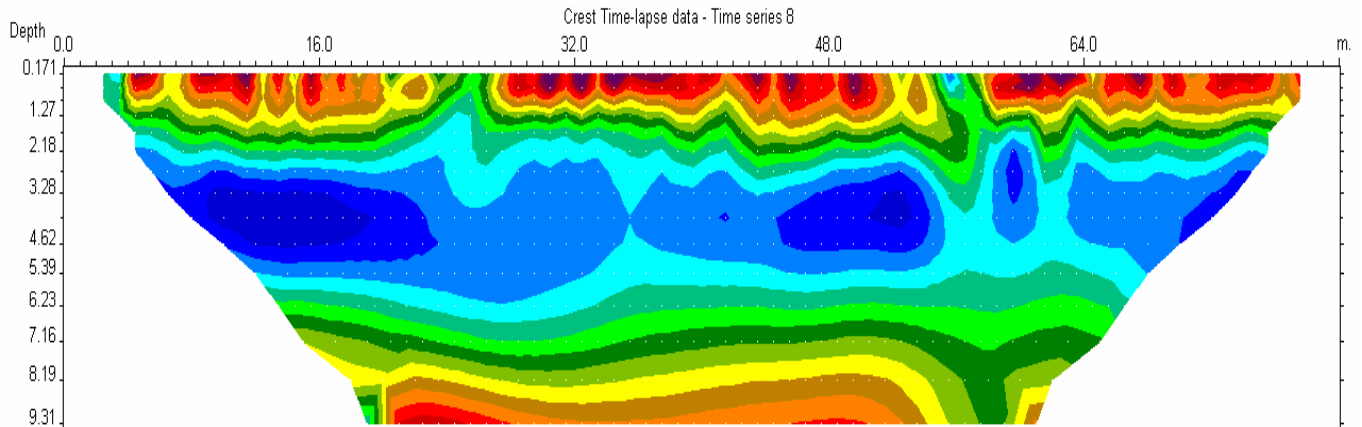
Crest, Time 6 = 120 hrs 36 min after start of test



Unit electrode spacing 1.00 m.

Unit electrode spacing 1.00 m.

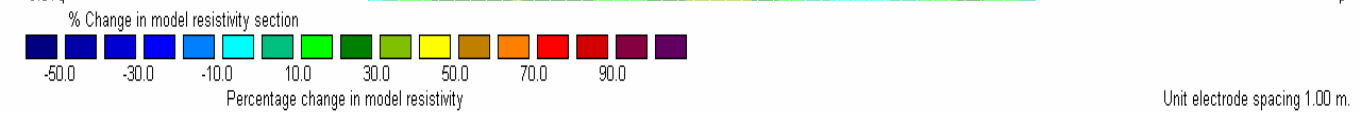
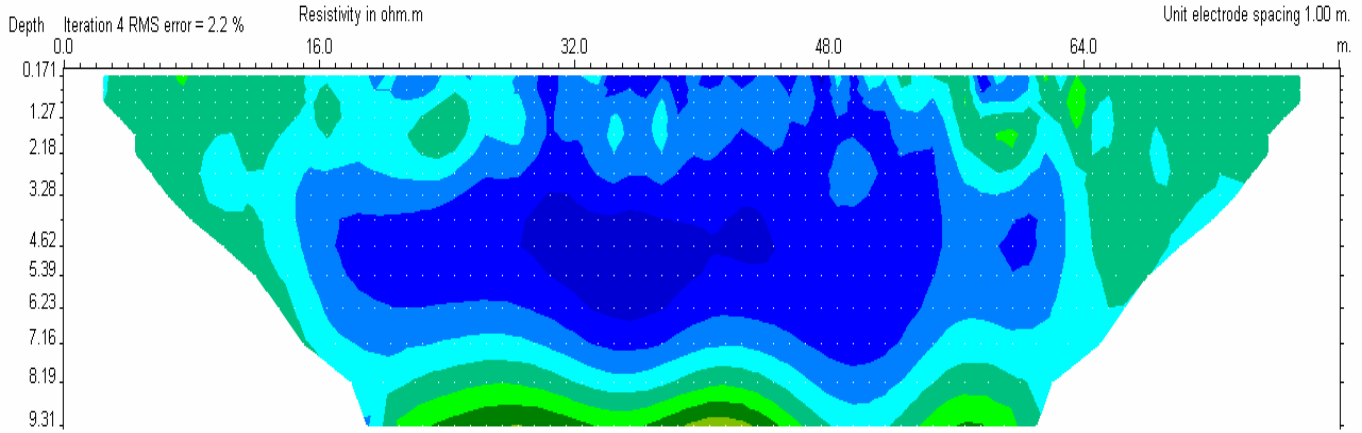
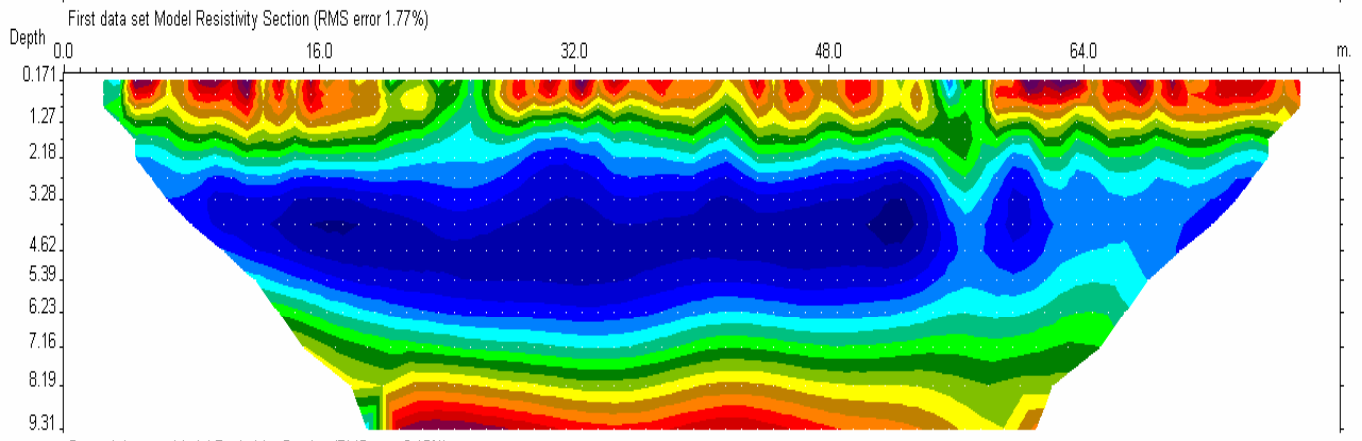
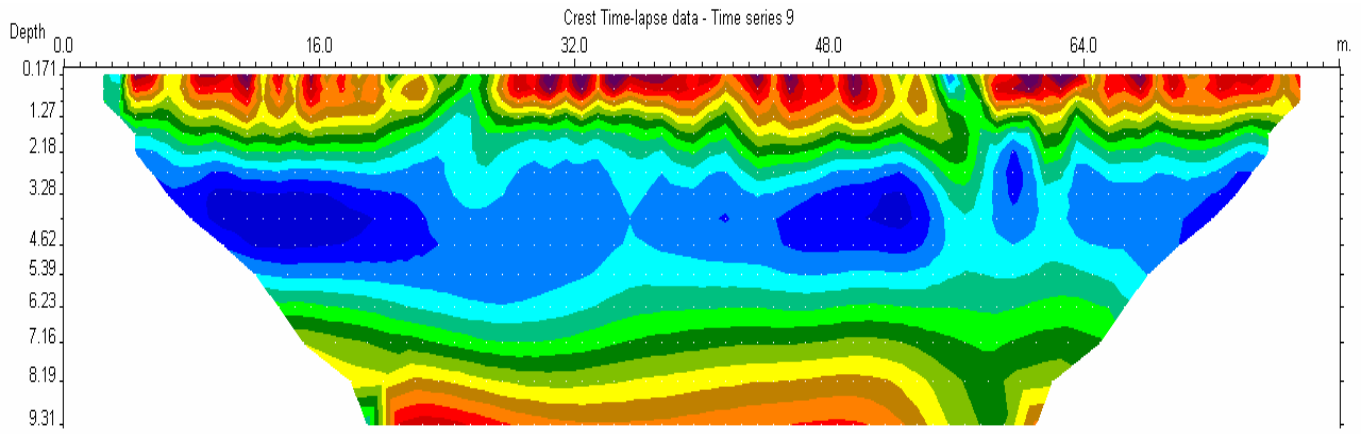
Crest, Time 7 = 150 hrs 50 min after start of test



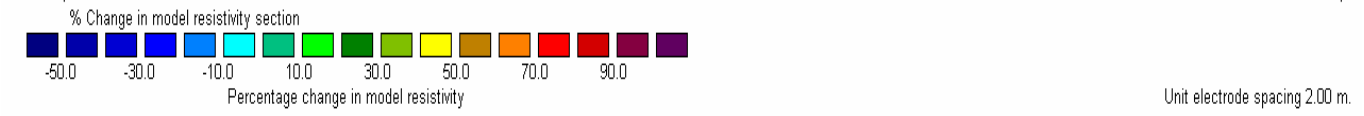
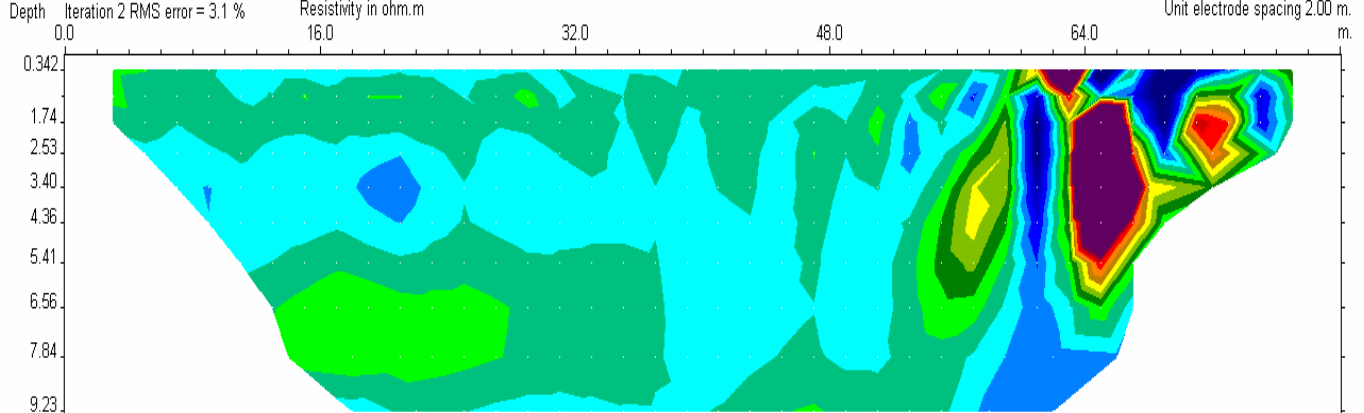
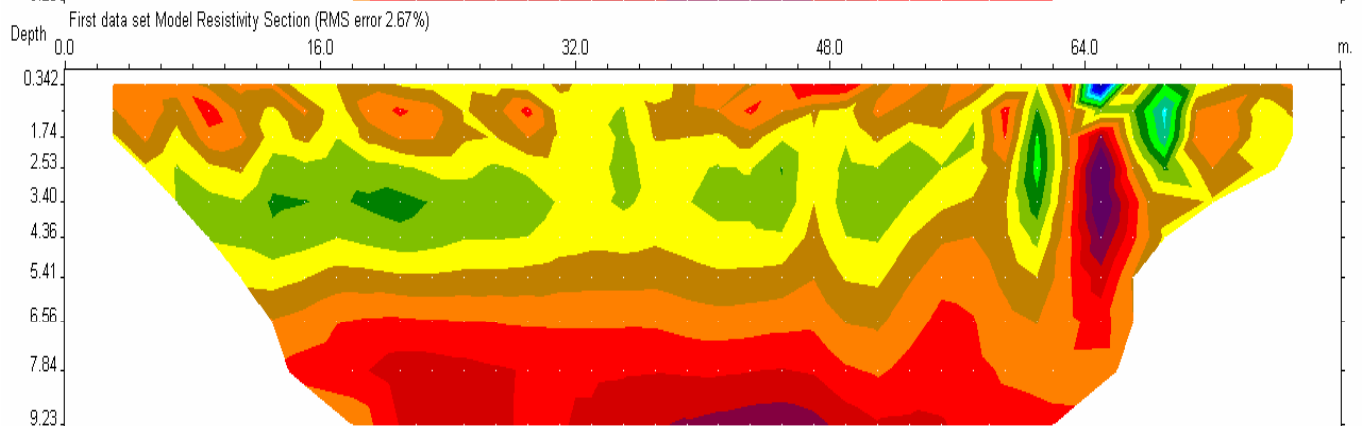
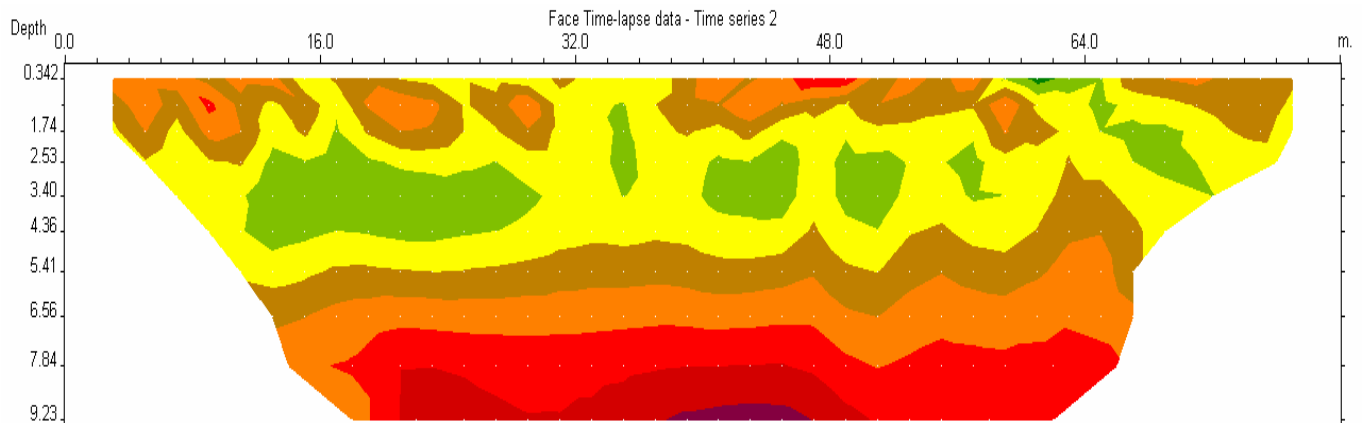
Unit electrode spacing 1.00 m.

Unit electrode spacing 1.00 m.

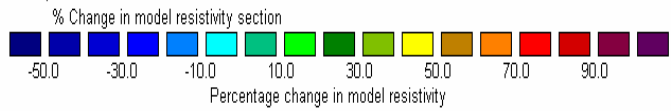
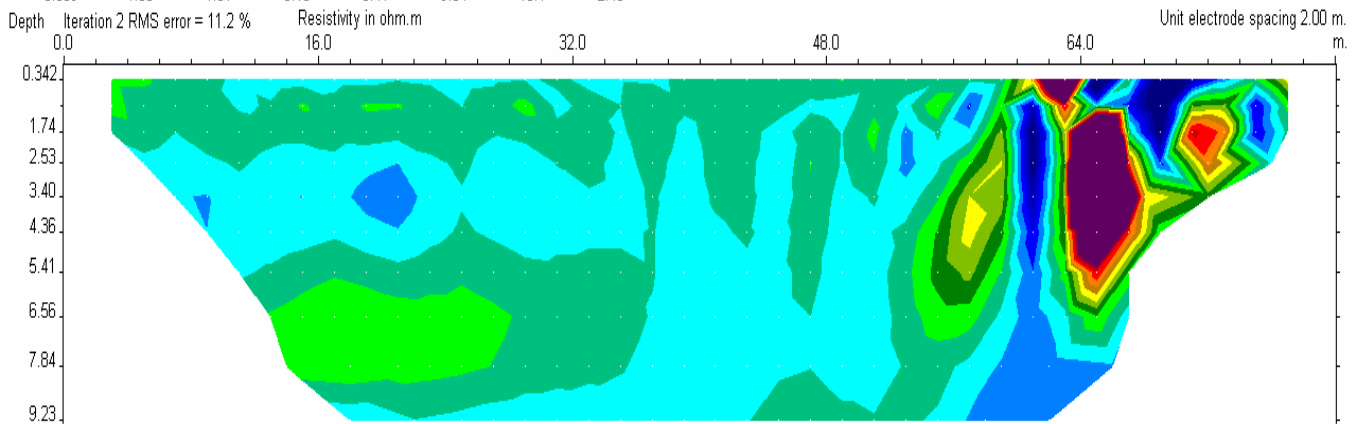
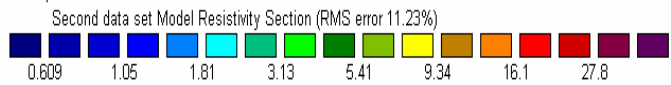
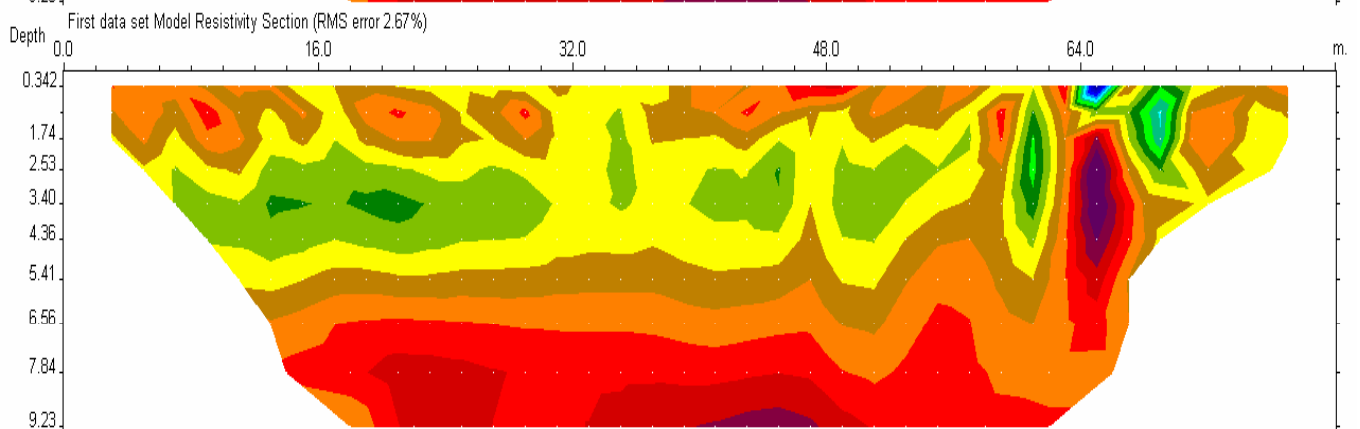
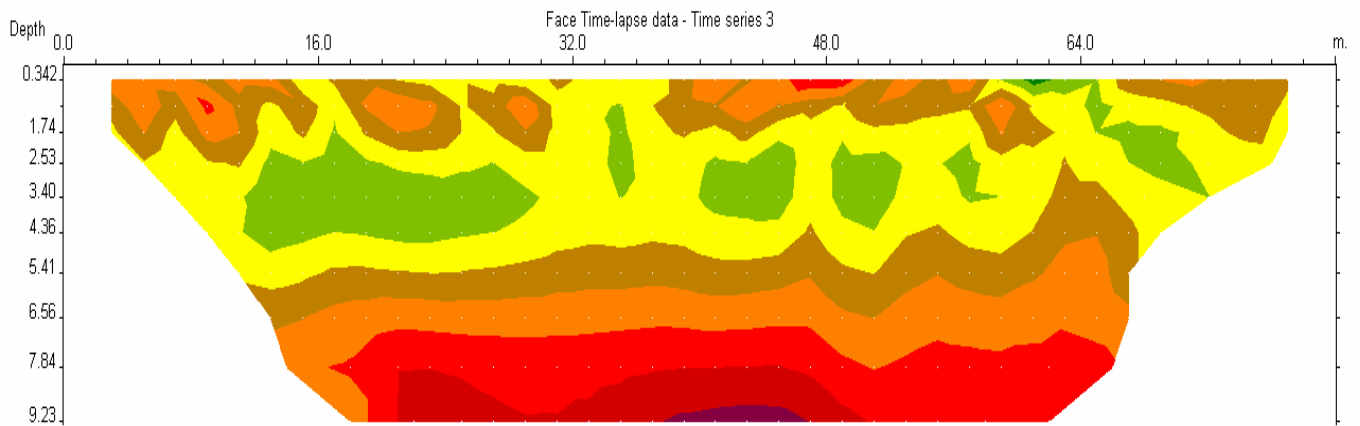
Crest, Time 8 = 167 hrs 19 min after start of test



Crest, Time 9 = 193 hrs 40 min after start of test

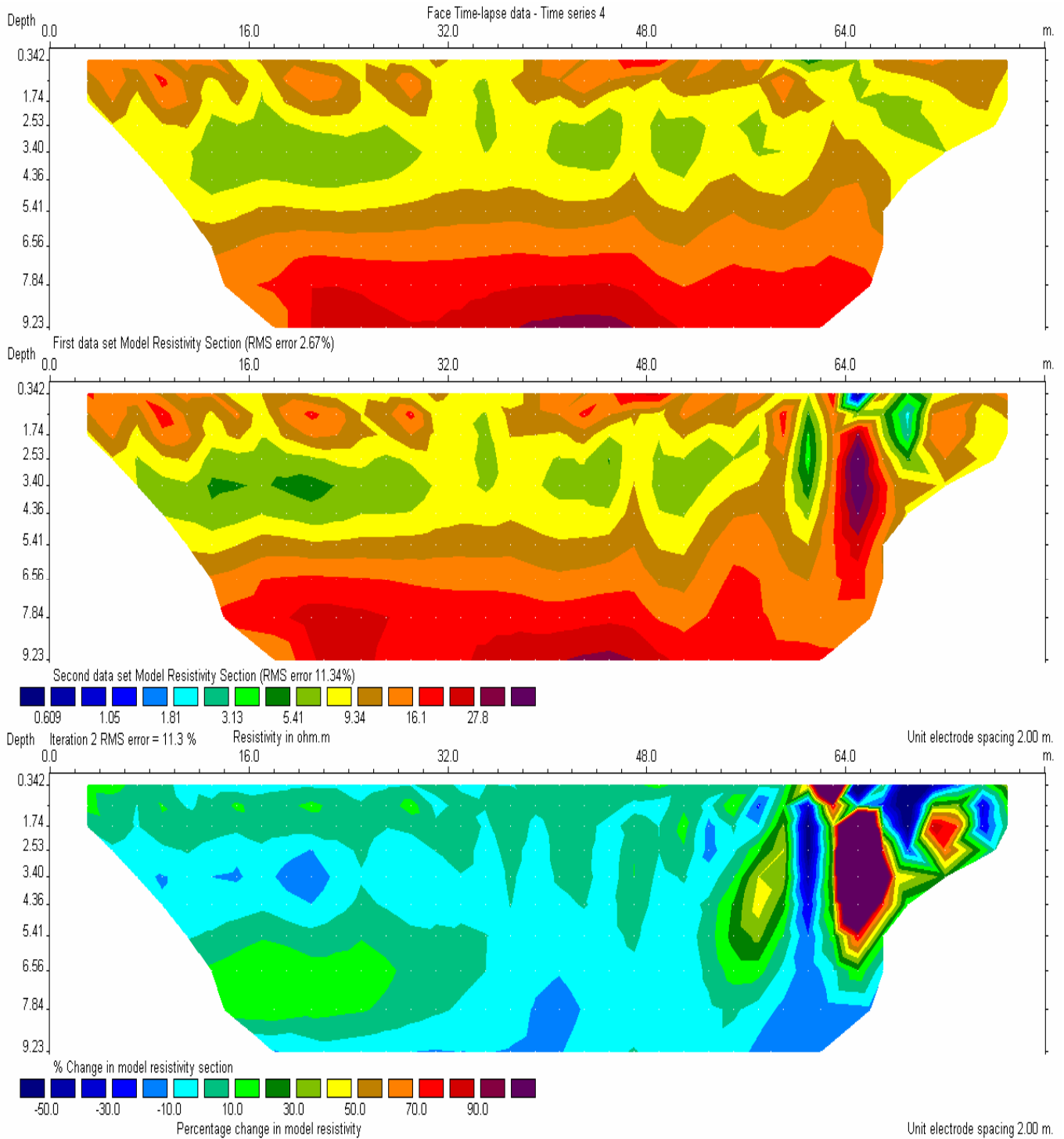


Face, Time 2 = 32 hrs 58 min after start of test (time 1 = start of test)

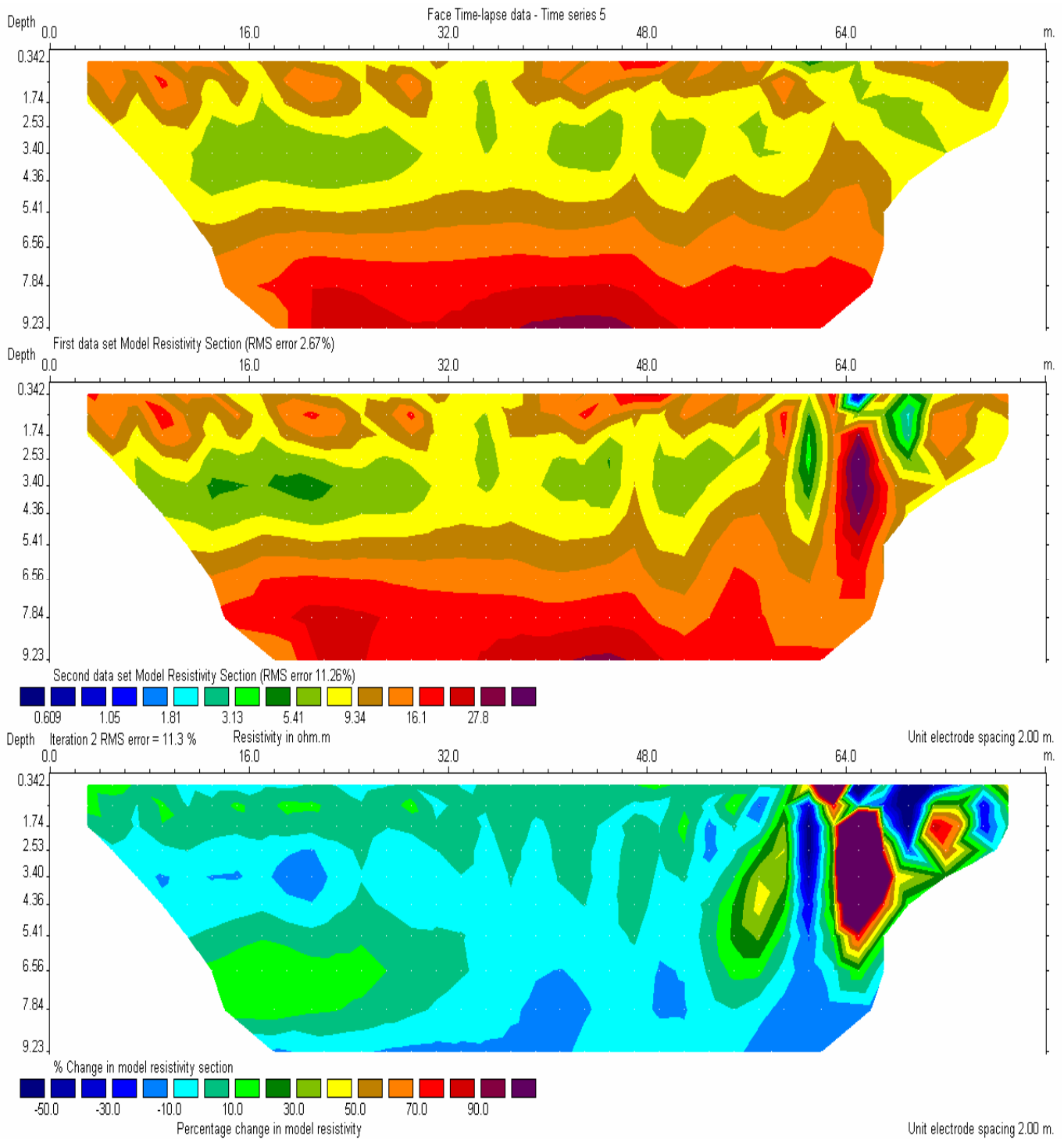


Unit electrode spacing 2.00 m.

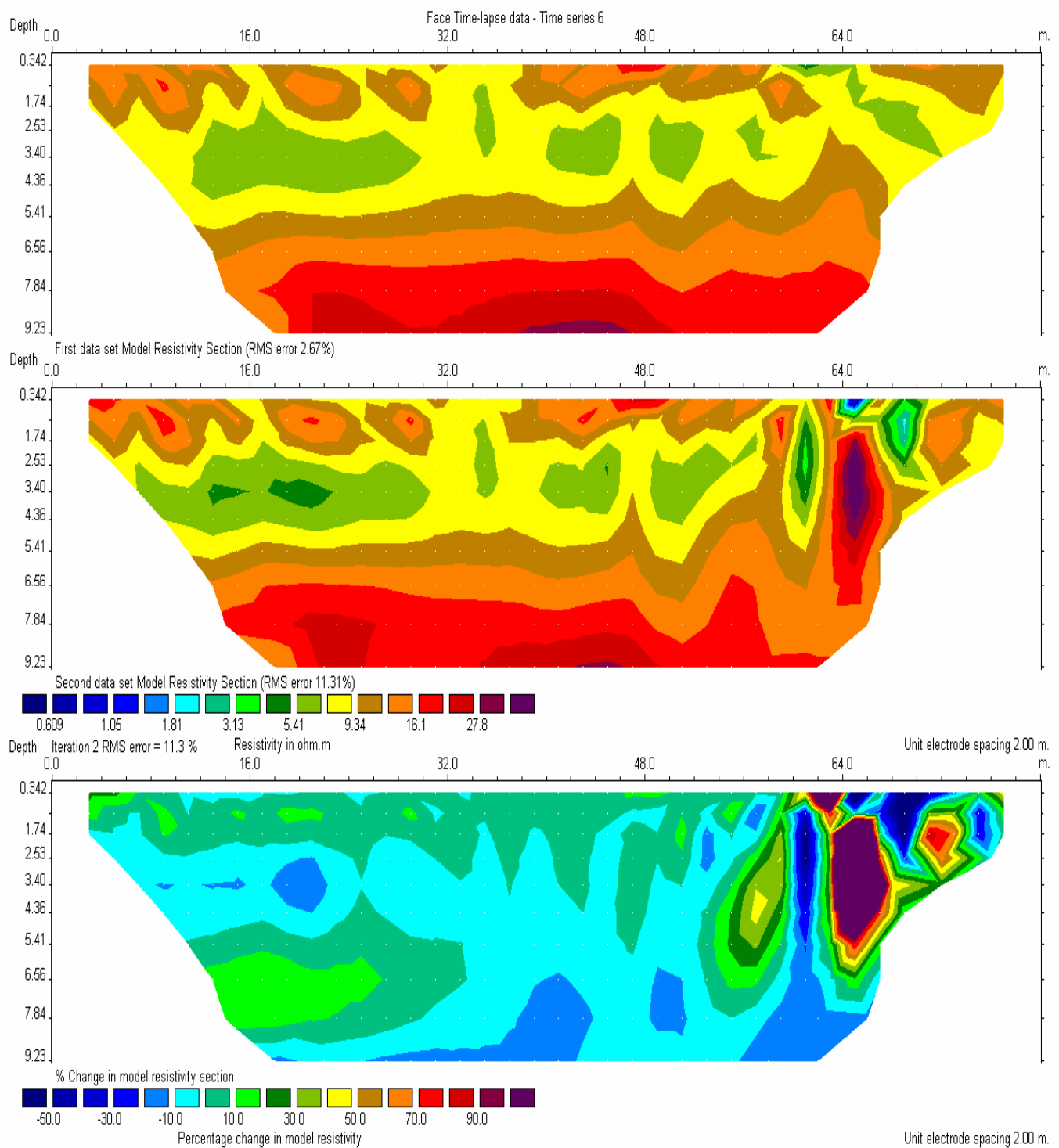
Face, Time 3 = 52 hrs 44 min after start of test



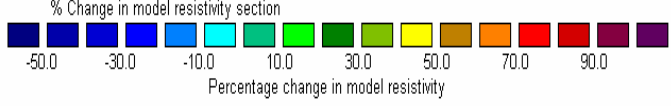
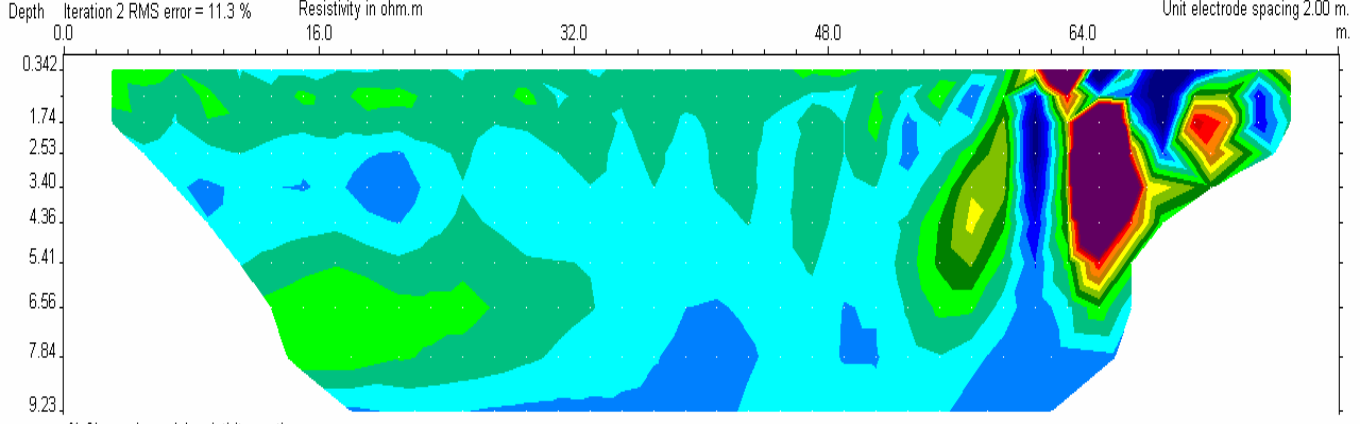
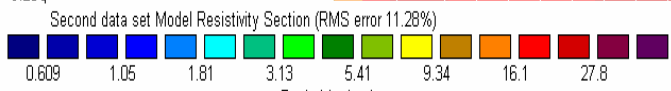
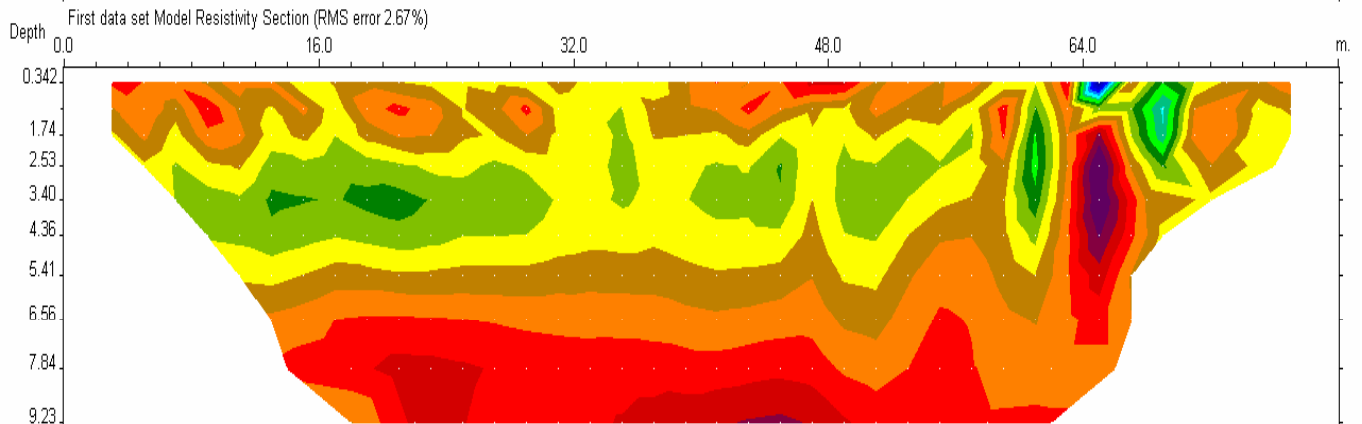
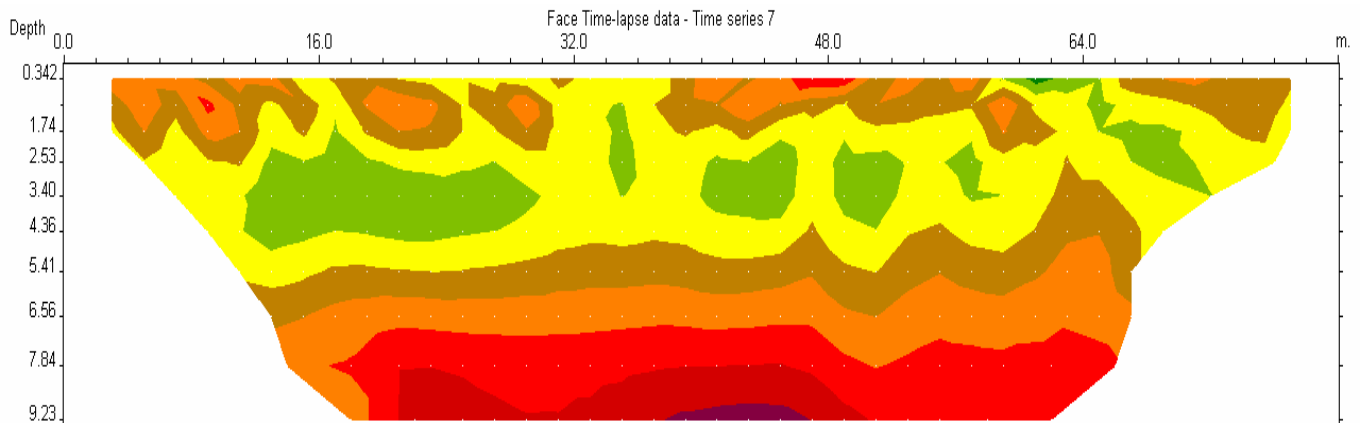
Face, Time 4 = 74 hrs 55 min after start of test



Face, Time 5 = 99 hrs 31 min after start of test



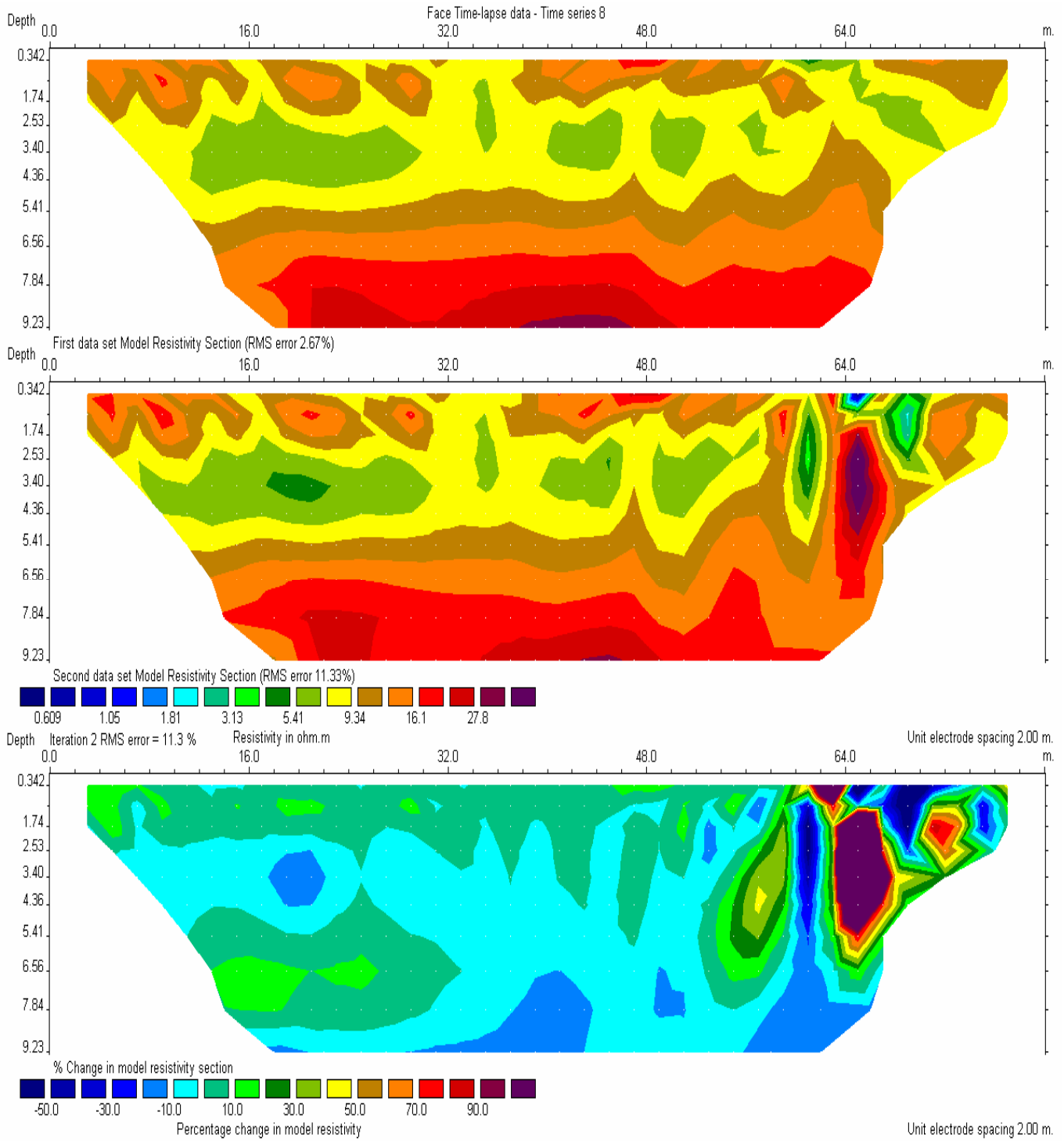
Face, Time 6 = 124 hrs 13 min after start of test



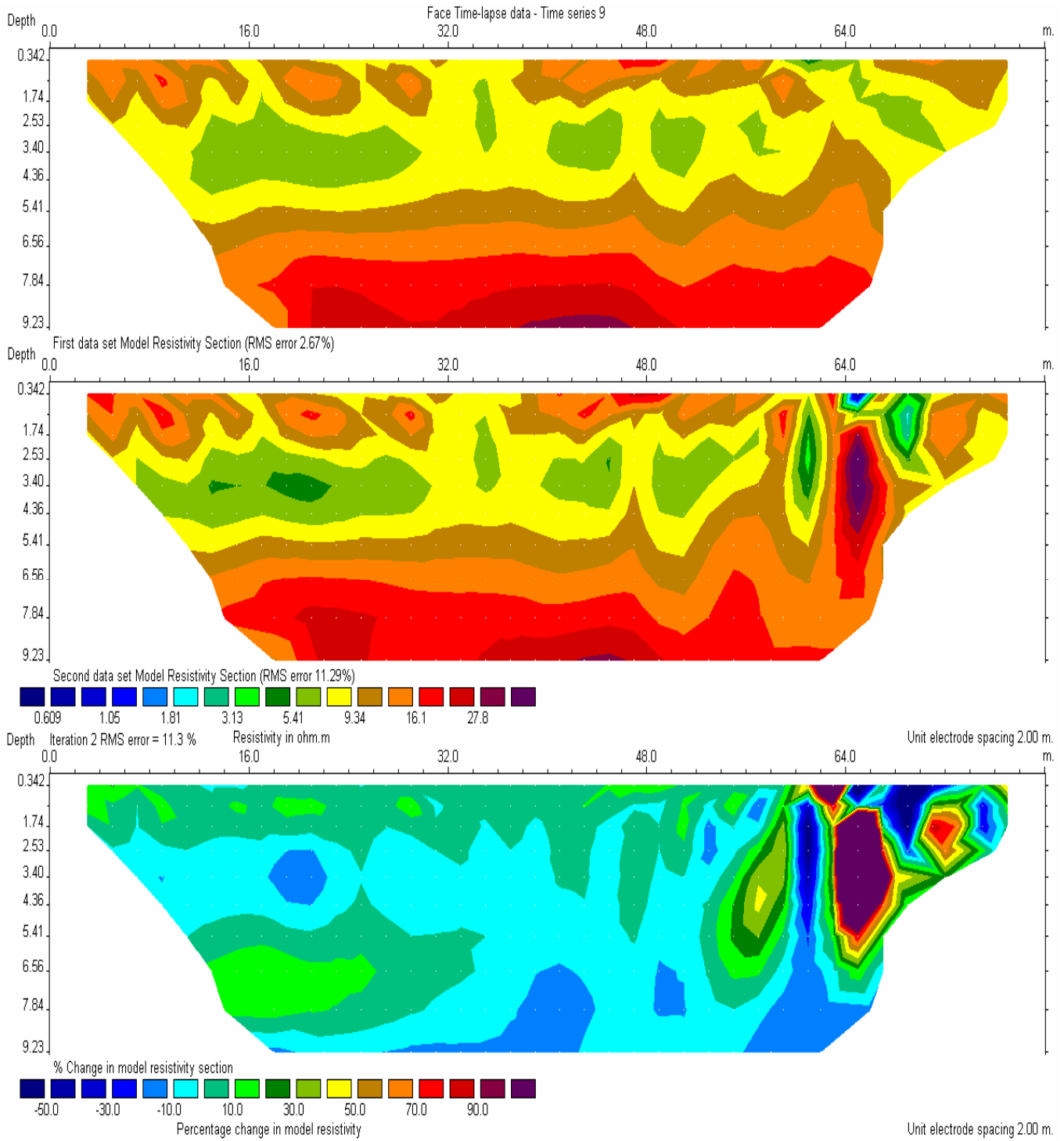
Unit electrode spacing 2.00 m.

Unit electrode spacing 2.00 m.

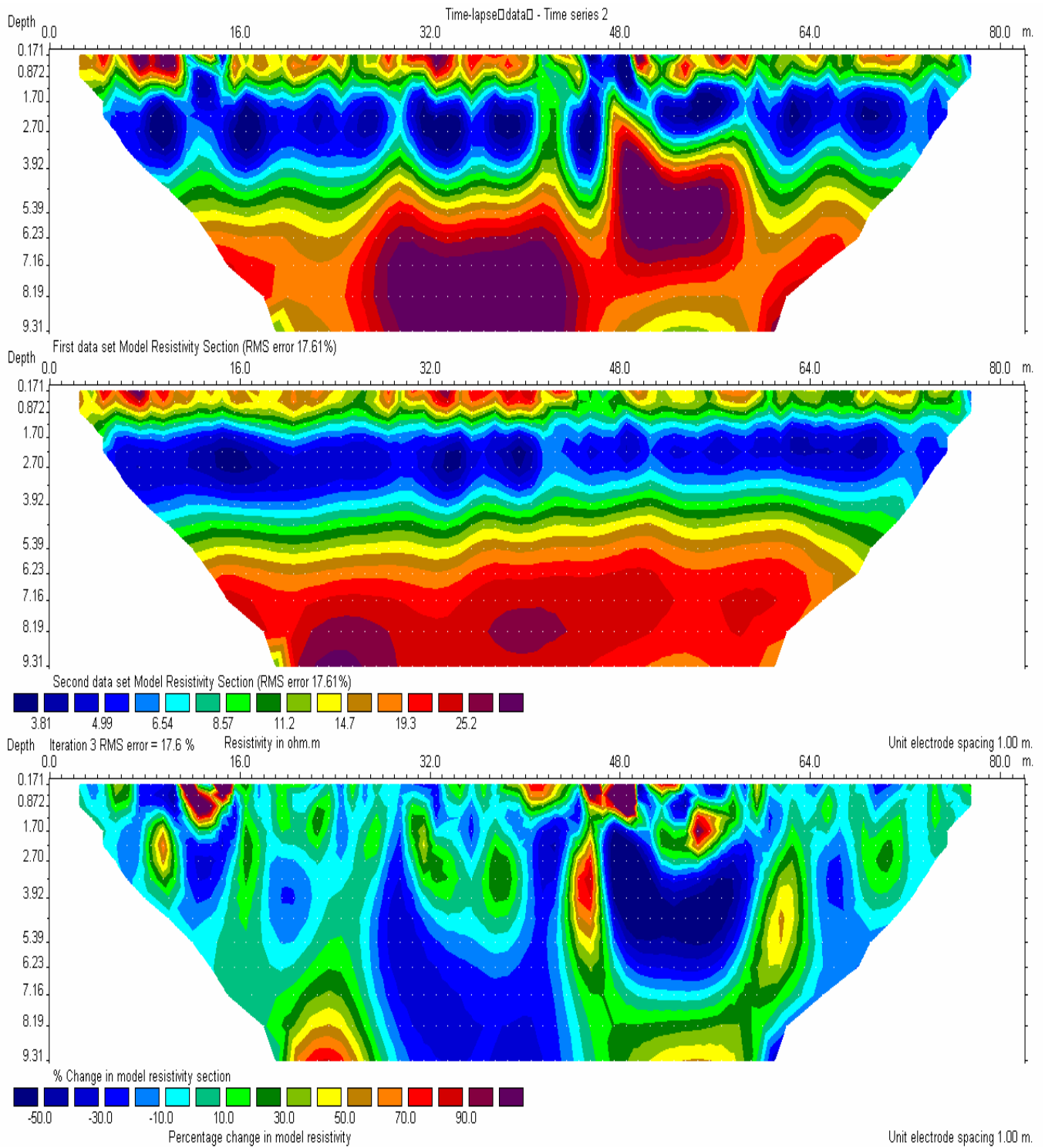
Face, Time 7 = 148 hrs 01 min after start of test



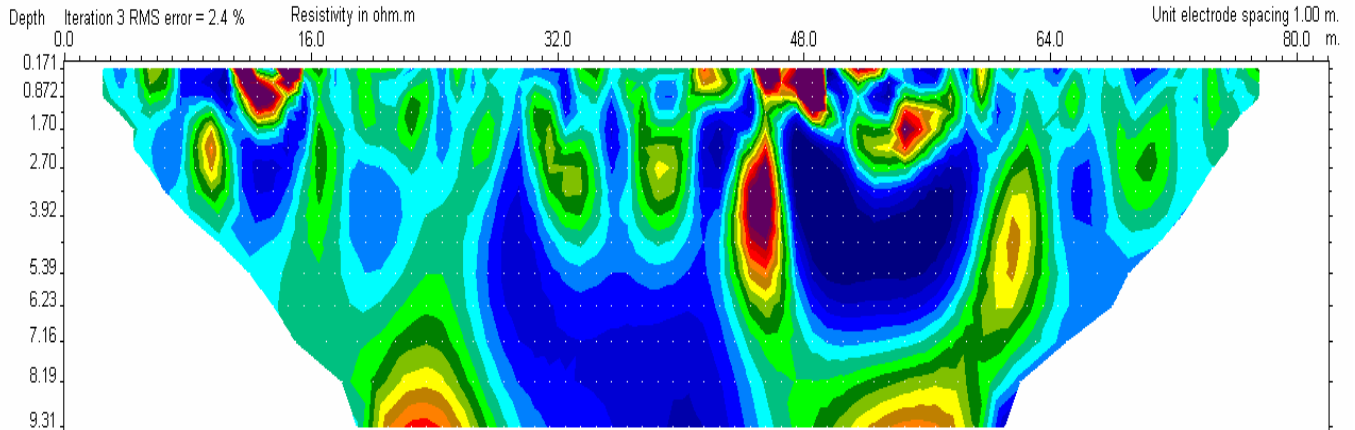
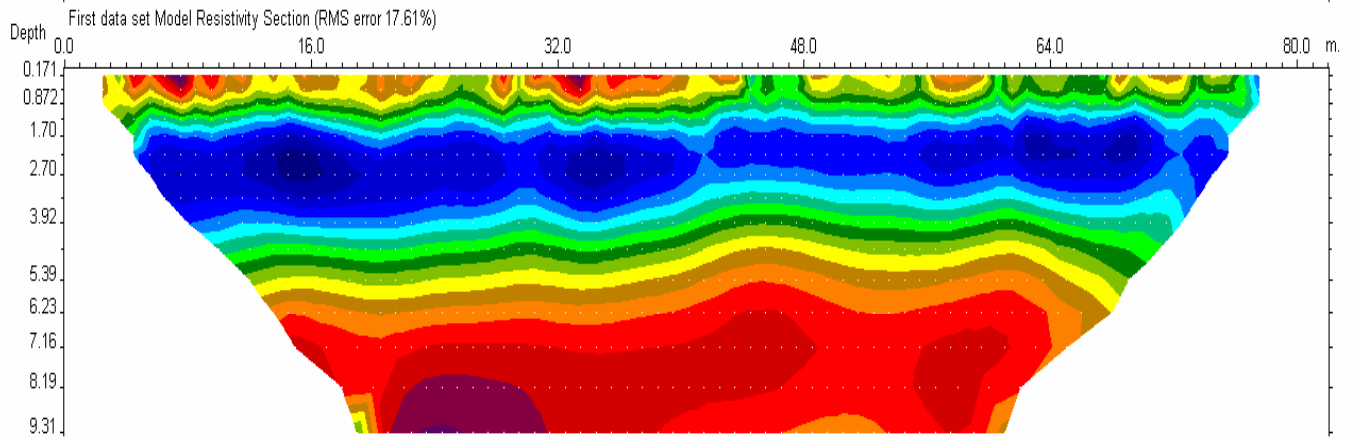
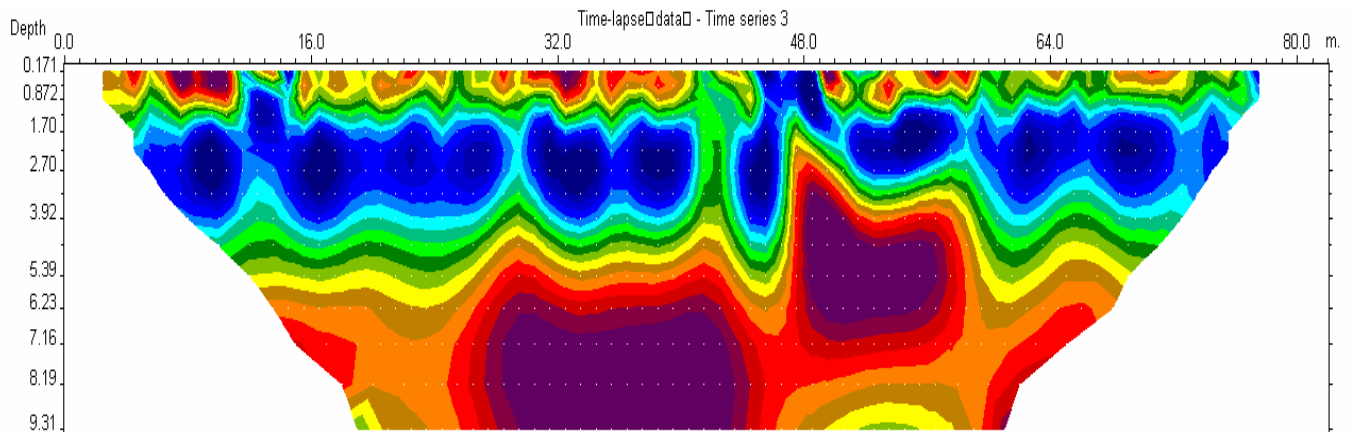
Face, Time 8 = 169 hrs 41 min after start of test



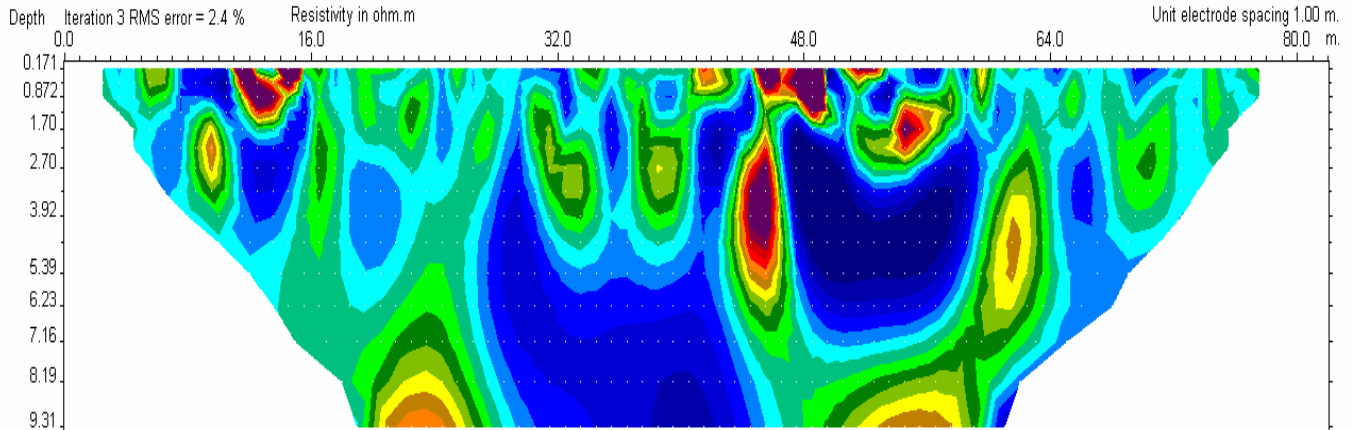
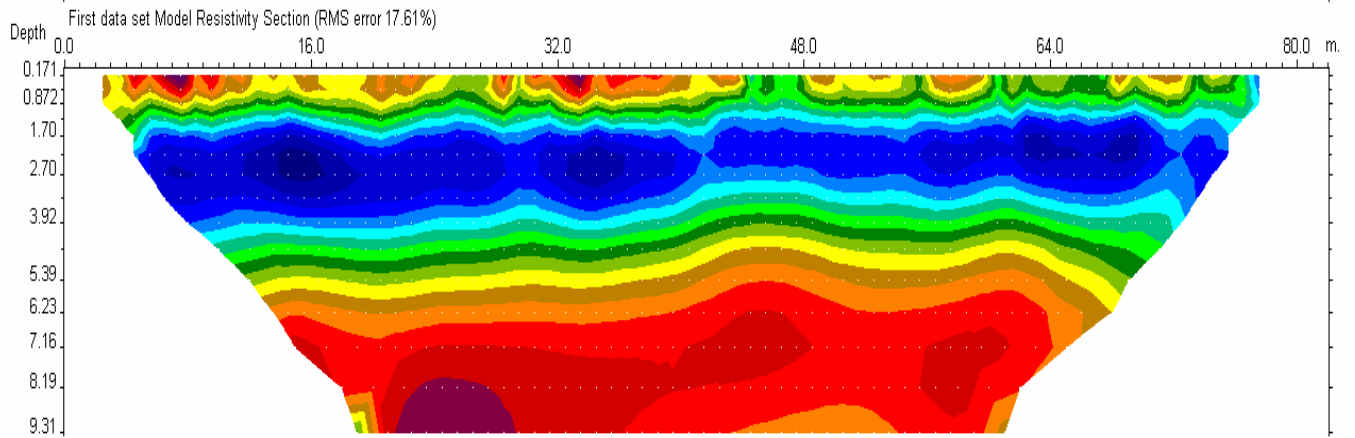
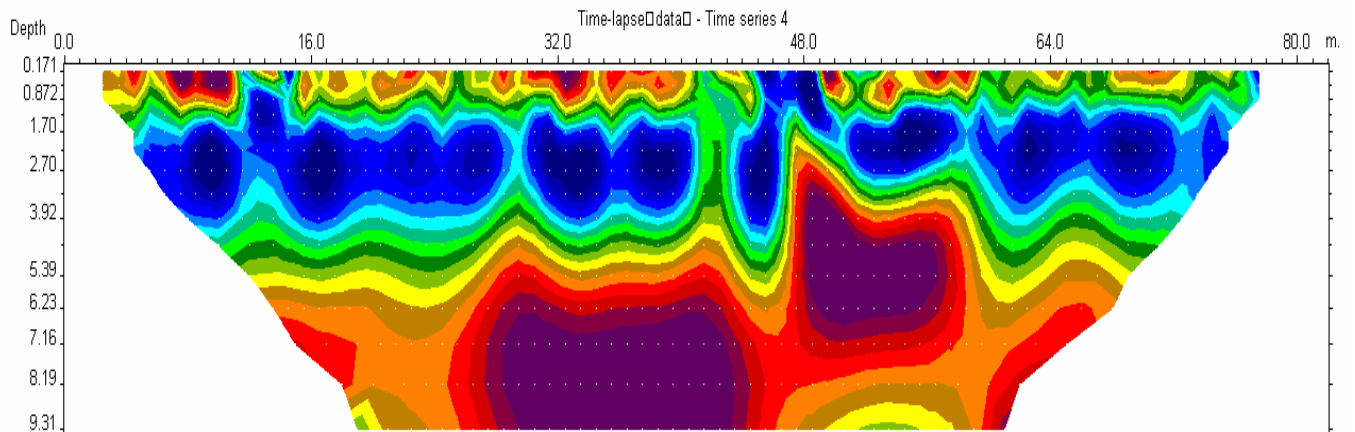
Face, Time 9 = 195 hrs 39 min after start of test



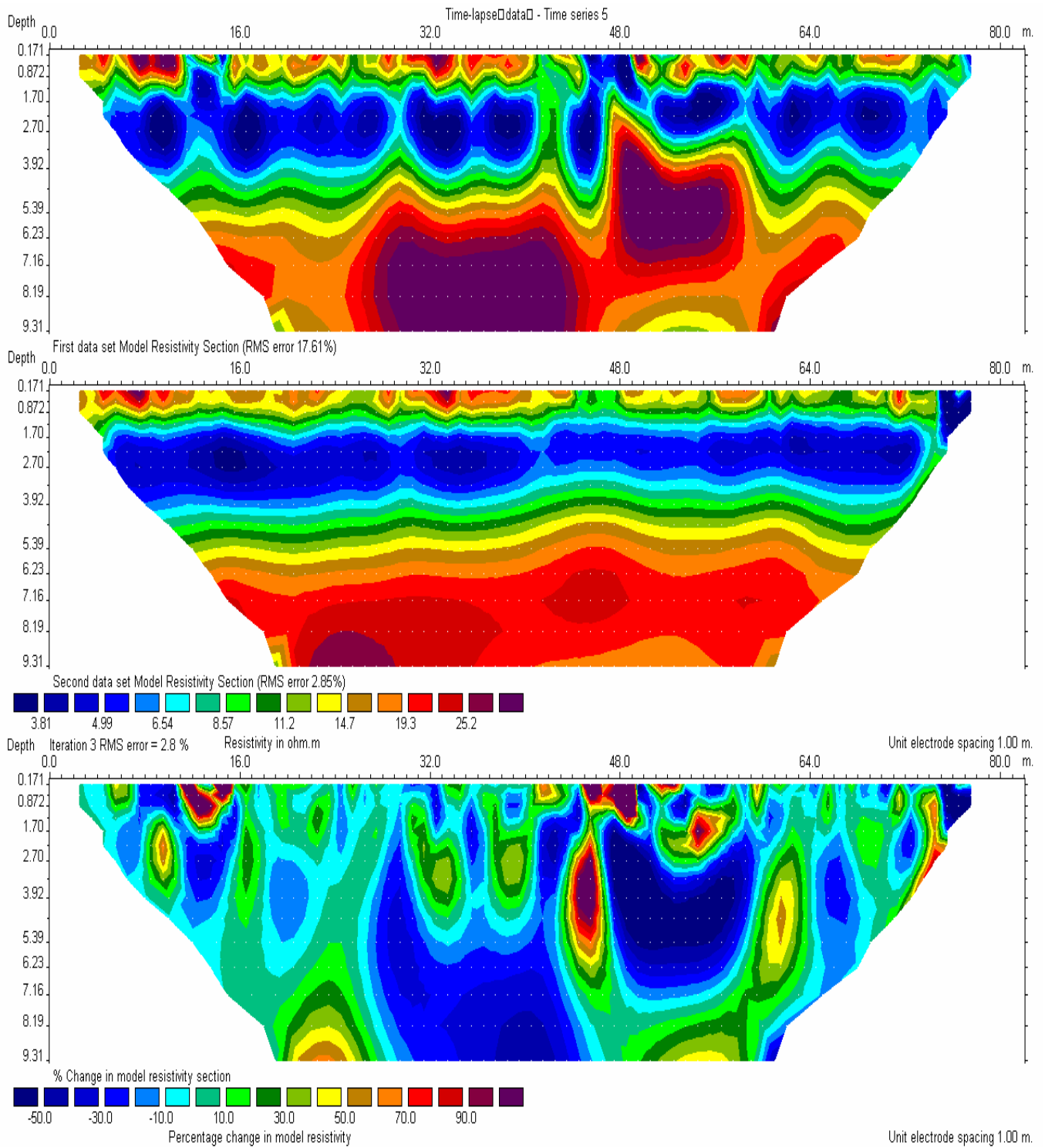
Toe, Time 2 = 32 hrs and 20 min after start of test (time 1= start of test)



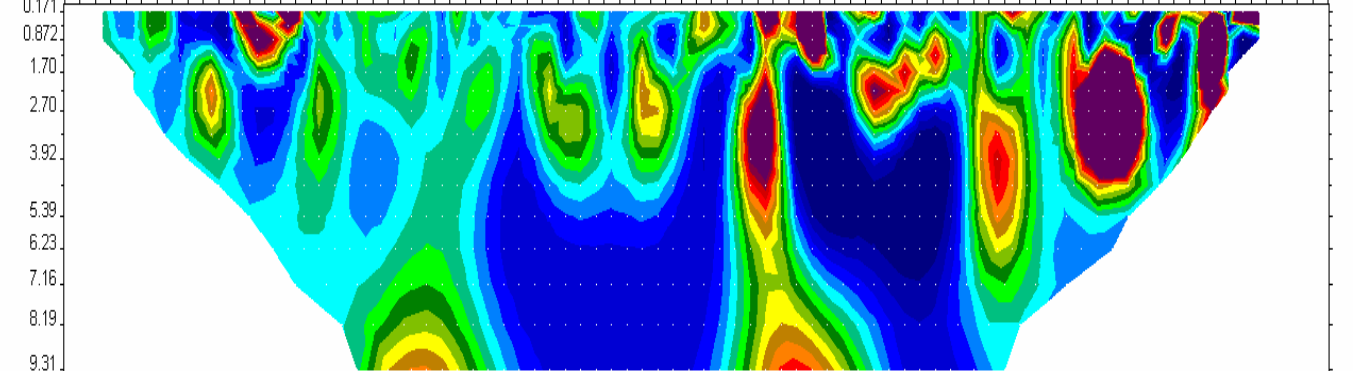
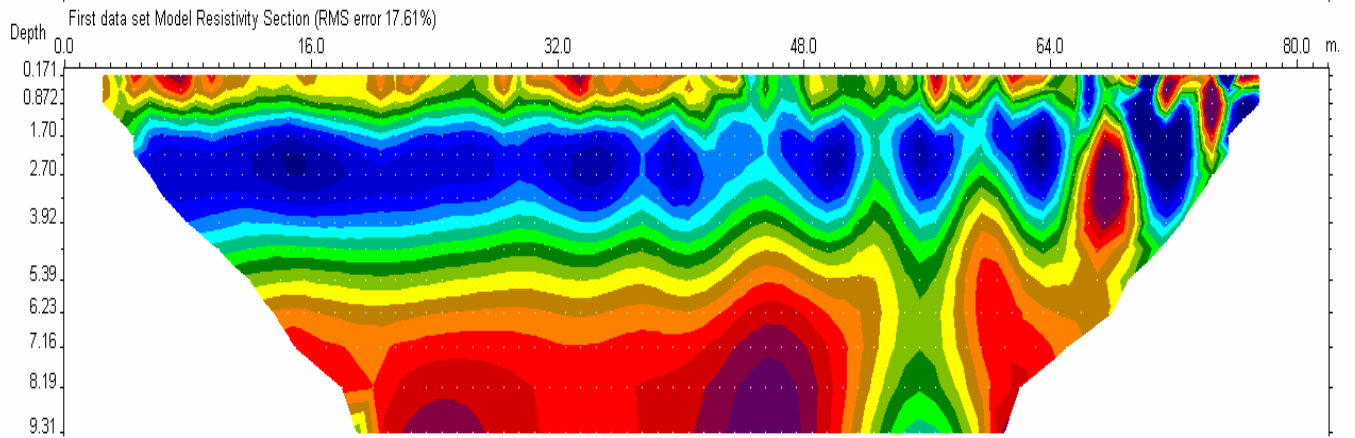
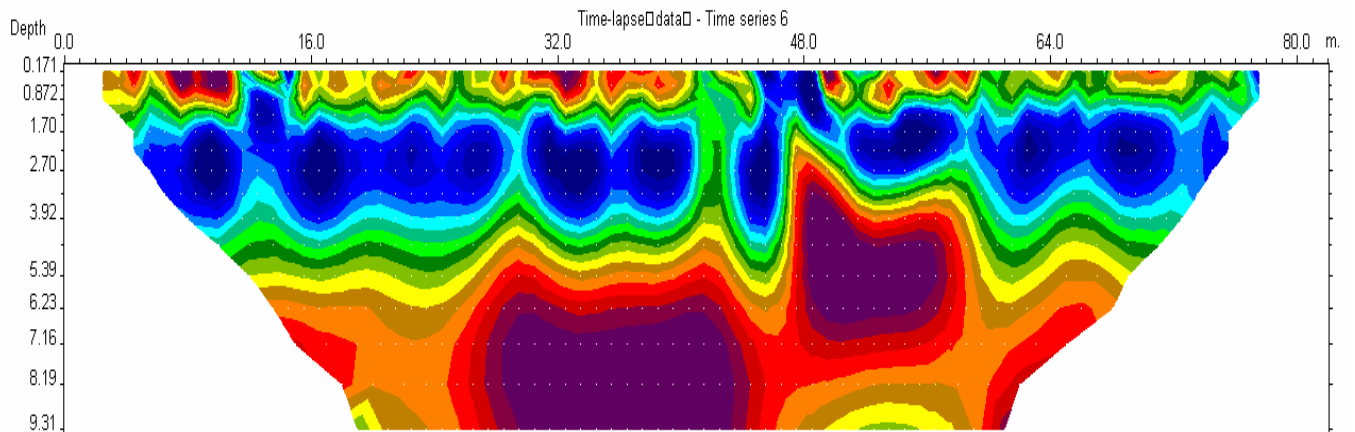
Toe, Time 3 = 46 hrs and 59 min after start of test



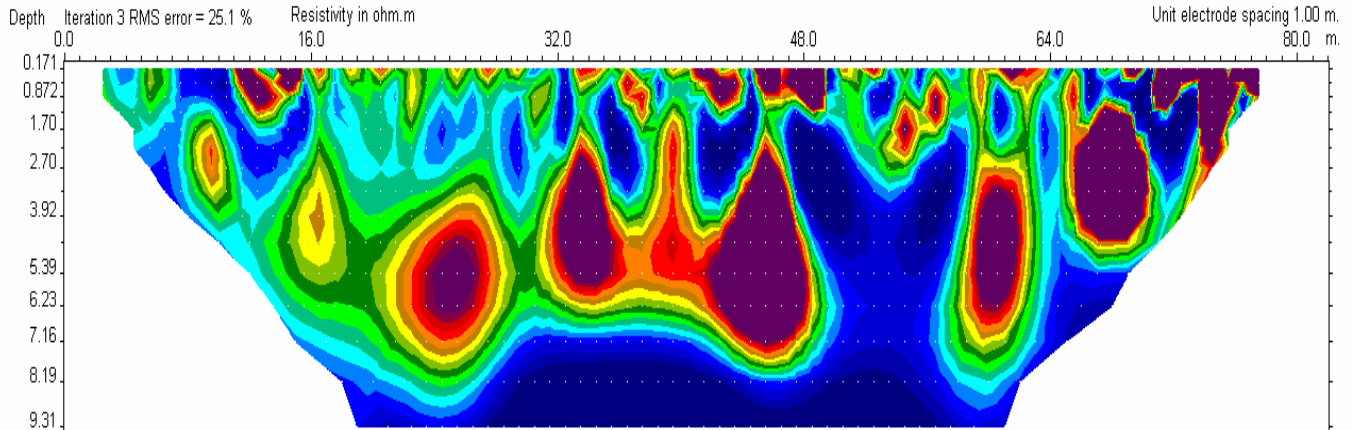
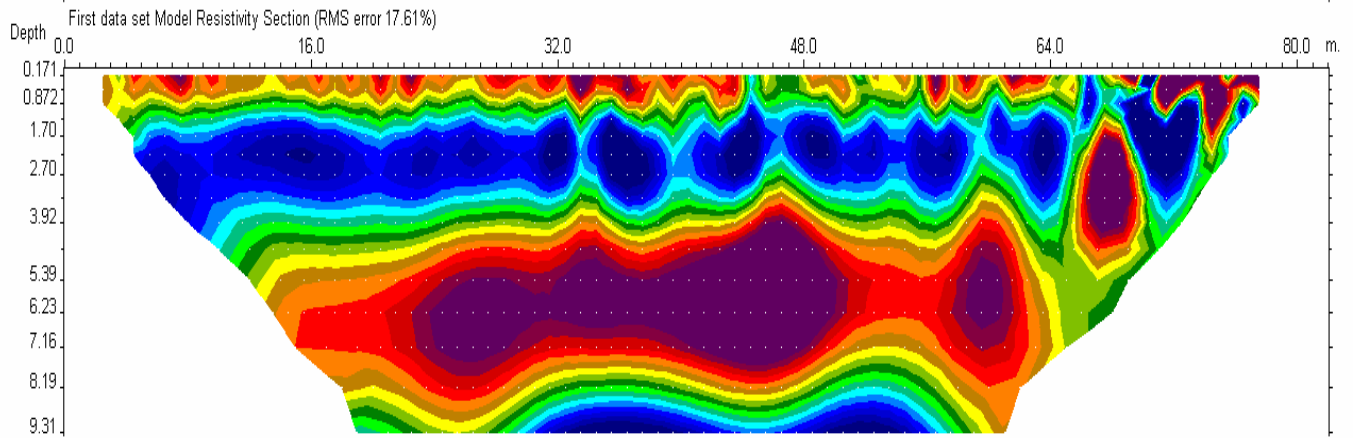
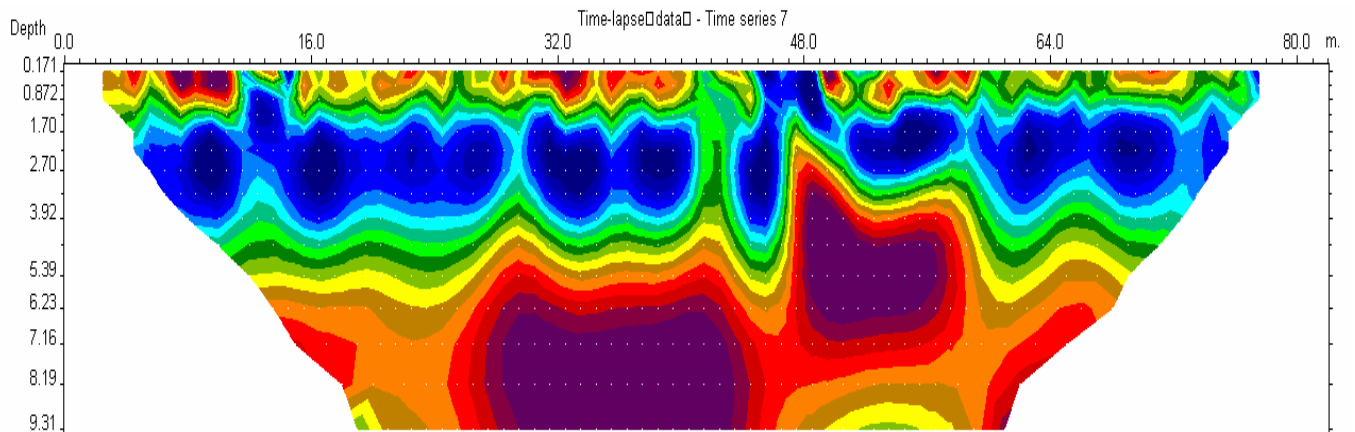
Toe, Time 4 = 75 hrs and 44 min after start of test



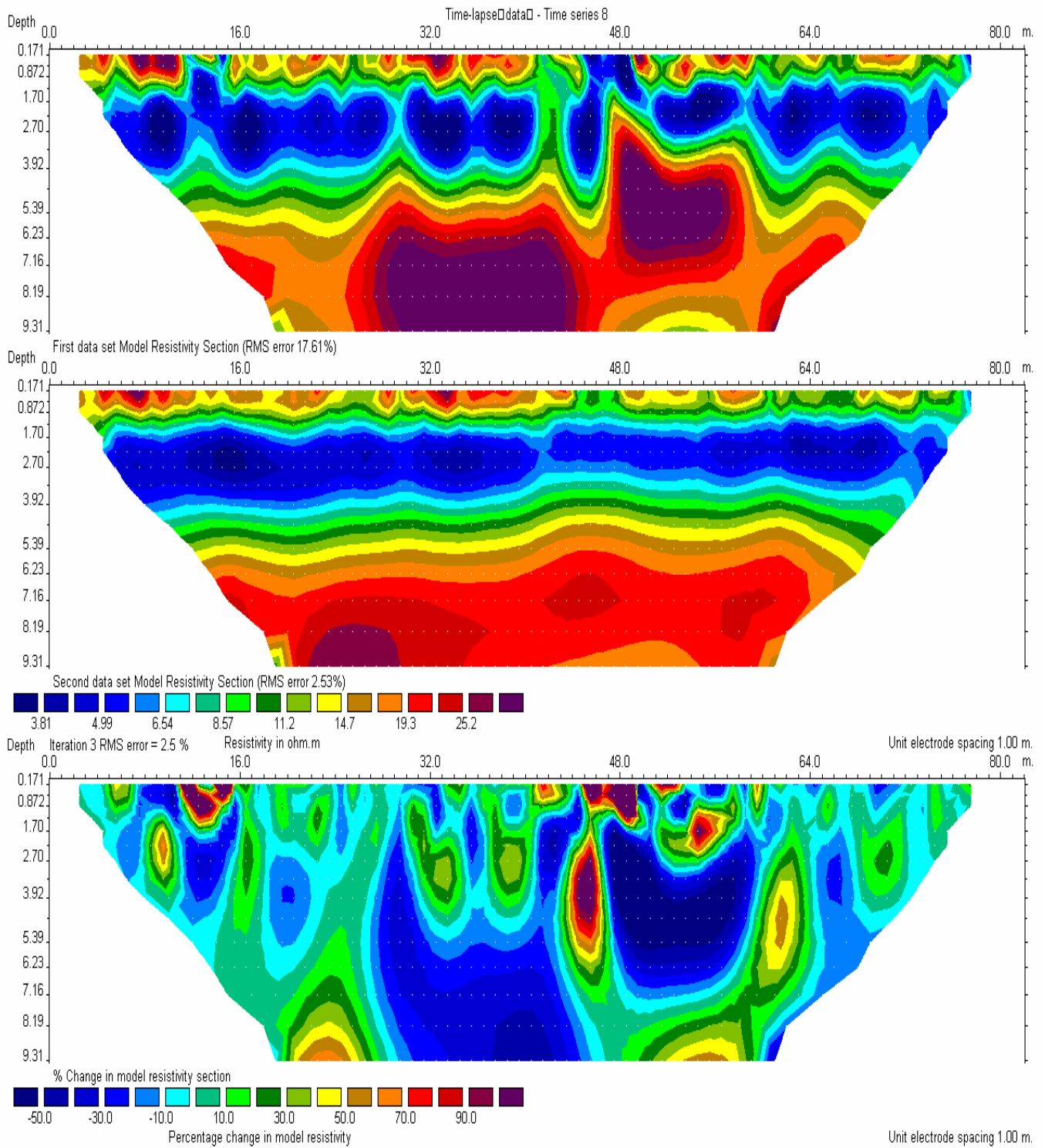
Toe, Time 5 = 95 hrs and 48 min after start of test



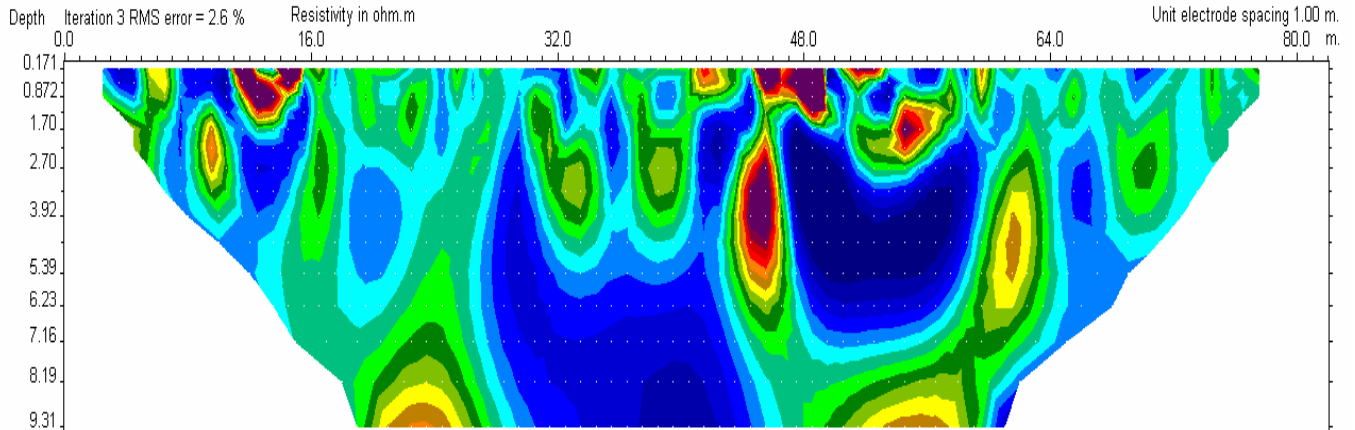
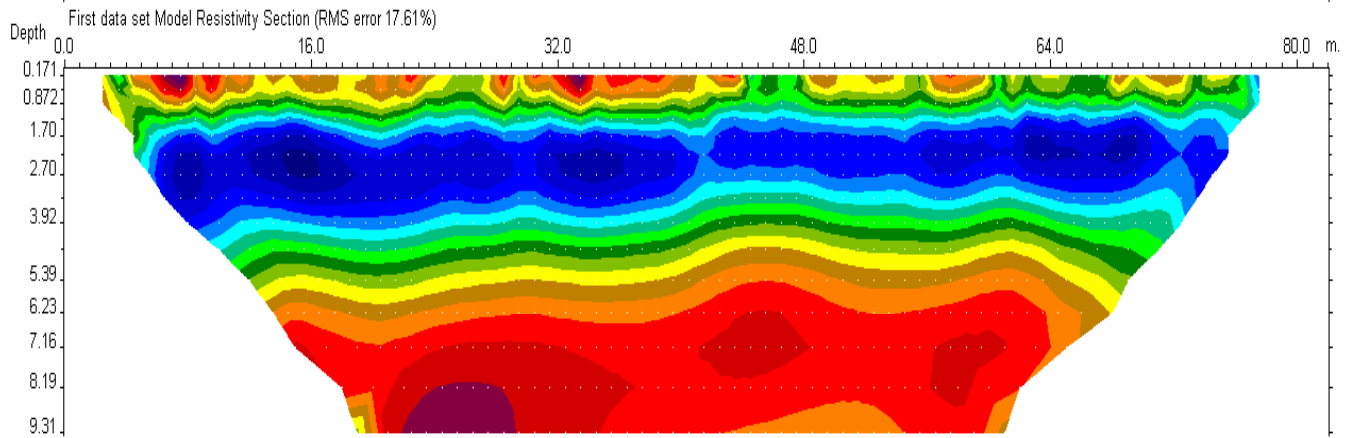
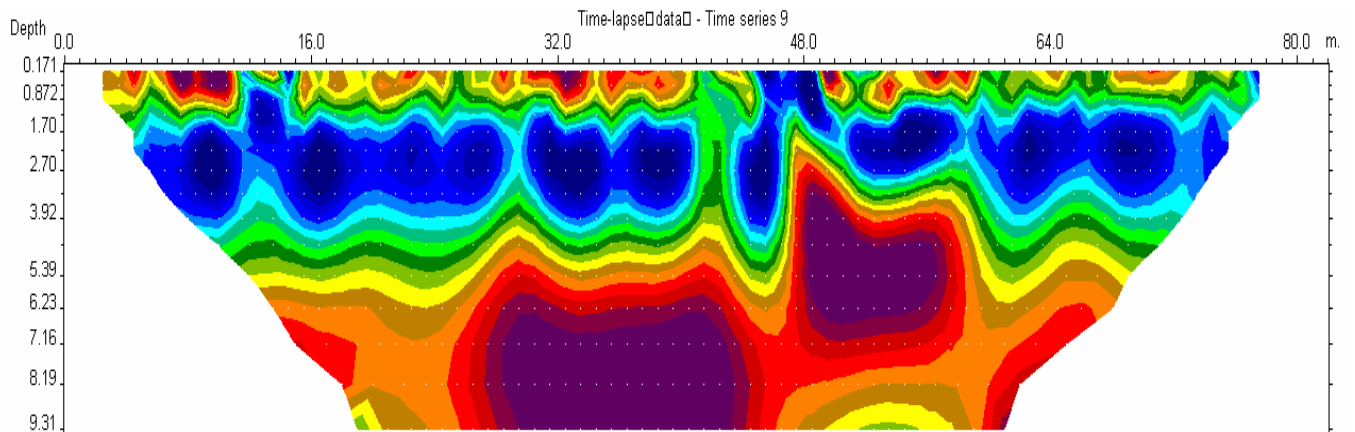
Toe, Time 6 = 127 hrs and 53 min after start of test



Toe, Time 7 = 145 hrs and 37 min after start of test



Toe, Time 8 = 171 hrs and 43 min after start of test



Toe, Time 9 = 191 hrs and 47 min after start of test

REPORT DOCUMENTATION PAGE

Form Approved
OMB No. 0704-0188

Public reporting burden for this collection of information is estimated to average 1 hour per response, including the time for reviewing instructions, searching existing data sources, gathering and maintaining the data needed, and completing and reviewing this collection of information. Send comments regarding this burden estimate or any other aspect of this collection of information, including suggestions for reducing this burden to Department of Defense, Washington Headquarters Services, Directorate for Information Operations and Reports (0704-0188), 1215 Jefferson Davis Highway, Suite 1204, Arlington, VA 22202-4302. Respondents should be aware that notwithstanding any other provision of law, no person shall be subject to any penalty for failing to comply with a collection of information if it does not display a currently valid OMB control number. **PLEASE DO NOT RETURN YOUR FORM TO THE ABOVE ADDRESS.**

1. REPORT DATE (DD-MM-YYYY) January 2007		2. REPORT TYPE Report 5 of a series		3. DATES COVERED (From - To)	
4. TITLE AND SUBTITLE Condition Assessment of Levees, U.S. Section of the International Boundary and Water Commission; Report 5, Flood Simulation Study of Retamal Levee, Lower Rio Grande Valley, Texas, Using Seismic and Electrical Geophysical Models				5a. CONTRACT NUMBER	
				5b. GRANT NUMBER	
				5c. PROGRAM ELEMENT NUMBER	
6. AUTHOR(S) Joseph B. Dunbar, José L. Llopis, George L. Sills, Eric W. Smith, Rick D. Miller, Julian Ivanov, and Robert F. Corwin				5d. PROJECT NUMBER	
				5e. TASK NUMBER	
				5f. WORK UNIT NUMBER	
7. PERFORMING ORGANIZATION NAME(S) AND ADDRESS(ES) U.S. Army Engineer Research and Development Center Geotechnical and Structures Laboratory 3909 Halls Ferry Road, Vicksburg, MS 39180-6199; Kansas Geological Survey, 1930 Constant Avenue, Lawrence, KS 66047; SP Surveys, 406 Sea View Drive, El Cerrito, CA 94530				8. PERFORMING ORGANIZATION REPORT NUMBER ERDC TR-03-4	
12. DISTRIBUTION / AVAILABILITY STATEMENT Approved for public release; distribution is unlimited.				10. SPONSOR/MONITOR'S ACRONYM(S)	
				11. SPONSOR/MONITOR'S REPORT NUMBER(S)	
13. SUPPLEMENTARY NOTES					
14. ABSTRACT In November 2004, a team from the U.S. Army Engineer Research and Development Center conducted a ponding test on a reach of the Retamal levee in the Lower Rio Grande Valley to simulate performance of the levee during a flood event. The work was performed for and with the assistance of the International Boundary and Water Commission, U.S. Section, on a levee reach with a significant number of surface cracks. Surface cracking of the levee was caused primarily by drought conditions as they affected expansive clay soils where total annual rainfall, in south Texas, was less than 20 in. (0.5 m) for several years between 1998 and 2003. Geophysical monitoring of the levee provided important information about levee performance during a maximum flood event and measured changes in moisture in clay soils in the levee. Various types of state-of-the-art electrical and seismic methods were appraised to monitor seepage caused by floodwater ponded against the levee. Seismic methods are especially attractive for levee screening, as velocity data from shear and body waves correlate directly to engineering properties that measure shear strength of soils. Seismic data indicated the higher rainfall in 2004 positively affected the core of the levee. Measurable increases in the seismic velocity of both body and shear waves were observed in 2004, compared with conditions in 2003, near the end of the drought period. Velocity values prior to the flood test in 2003 were much lower, likely caused by a levee core that was internally cracked and caused slower P- and S-wave velocities. (Continued)					
15. SUBJECT TERMS Condition assessment Electrical		Flood simulation Geophysics Geotechnical	Levees Lower Rio Grande Valley Resistivity	Self-potential Seismic	
16. SECURITY CLASSIFICATION OF:			17. LIMITATION OF ABSTRACT	18. NUMBER OF PAGES 332	19a. NAME OF RESPONSIBLE PERSON
a. REPORT UNCLASSIFIED	b. ABSTRACT UNCLASSIFIED	c. THIS PAGE UNCLASSIFIED			19b. TELEPHONE NUMBER (include area code)

14. (Concluded)

Shear-wave velocity measured by multi-channel analysis of surface waves increased slightly and was the property most significantly affected by the increased water content, and the material property most sensitive to changes occurring during the levee-ponding experiment. Electrical methods were valuable for monitoring changes in soil moisture and possible seepage through the levee and the foundation. Self-potential surveys indicate that there was no measurable seepage through internal cracks in the levee or the foundation. Instead, electrical resistivity measurements identify a gradual change in soil moisture in the levee from a wetting front. This front increased soil conductivity along the riverside levee crest, but did not extend much beyond the landside crest or midslope. Surveys were performed using ground penetrating radar but did not penetrate beyond 1 to 2 m because of the soil conductivity. Results of the field testing of a flood event against the Retamal levee are favorable from an engineering perspective. The levee performed as designed, without any through-seepage or piping.